Ecosystem Status Report 2026

EASTERN BERING SEA



Edited by:
Elizabeth Siddon
Auke Bay Laboratories, Alaska Fisheries Science Center, NOAA Fisheries
17109 Pt. Lena Loop Road, Juneau, AK 99801

With contributions from:
Grant Adams, Don Anderson, Alex Andrews III, Daniel Auerbach, Kelia Axler, Kerim Aydin, Diana Baetscher, Sunny Bak-Hospital, Steve Barbeaux, Cheryl Barnes, Lewis Barnett, Sonia Batten, Jessica Beck, Shaun W. Bell, Emily Bowers, Mike Brosnahan, Thaddaeus Buser, Matt W. Callahan, Chelsea Campbell, Jack Carroll, Patricia Chambers, Maggie Chan, Patrick Charapata, Wei Cheng, Craig Chythlook, Bryan Cormack, Jessica Cross, Curry Cunningham, Alex De Robertis, Lukas DeFilippo, Andrew Dimond, Lia Domke, Diloola Erickson, Evangeline Fachon, Thomas Farrugia, Erin Fedewa, Emily Fergusson, Sarah Gaichas, Jeanette C. Gann, Sabrina Garcia, Tom Gelatt, Ben Gray, Colleen E. Harpold, Shannon Hennessey, Kirstin K. Holsman, Kathrine Howard, Jim Ianelli, Nicholas Jacuk, Kelly Kearney, Julie Keister, Esther Kennedy, David G. Kimmel, Trond Kristiansen, Carey Kuhn, Gulce Kurtay, Jesse Lamb, Ben Laurel, Caroline Lawrence, Dustin Colson Leaning, Kimberly Ledger, Elizabeth Lee, Kathi Lefebvre, Emily Lemagie, Justin Leon, Cory Lescher, Aaron Lestenkof, Mike Levine, Mike Litzow, Josh London, W. Christopher Long, Brandyn Lucca, Katie Luxa, Andrew Magel, Jacek Maselko, Ryan M. McCabe, Elizabeth McHuron, Dallas Melovidov, Paul Melovidov, Todd Miller, Natalie Monacci, Calvin W. Mordy, Jacqueline Muehlbauer, Franz Mueter, Zoe Munson, Jim Murphy, Janessa Newman, Jens M. Nielsen, Kaitlyn O'Brien, Clare Ostle, Johanna Page, Melanie M. Paquin, Mrunmayee Pathare, Robert Pickart, Darren Pilcher, Cody Pinger, Drew Porter, Steven Porter, Bianca Prohaska, Rolf Ream, Patrick Ressler, Jonathan Reum, Jon Richar, Erin Richmond, Lauren A. Rogers, Sean Rohan, Matthew Rustand, Erik Schoen, Gay Sheffield, Kalei Shotwell, Elizabeth Siddon, Jim Simon, Kevin Siwicke, Adam H. Spear, Phyllis J. Stabeno, Jeremy Sterling, Raphaela Stimmelmayr, Michelle Stratton, Anna Sulc, Florence Sullivan, Rob Suryan, Hillary Thalmann, Rick Thoman, Cathy Tide, Rod Towell, Cooper Van Vranken, Terese Vicente, Vanessa von Biela, Muyin Wang, George A. Whitehouse, Megan Williams, Michael Williams, Stephani Zador, and Tonya Zeppelin

Reviewed by:
The Bering Sea and Aleutian Islands Groundfish Plan Team
November 20, 2026
North Pacific Fishery Management Council
1007 West 3rd Ave., Suite 400
Anchorage, AK 99501

Support for the assembly and editing of this document was provided jointly by NOAA Fisheries and the NOAA National Ecosystem Assessment Program (NEAP?). This document is NOAA NEAP program contribution #2026_XXX.

Citing the complete report:
Siddon, E. 2026. Ecosystem Status Report 2026: Eastern Bering Sea, Stock Assessment and Fishery Evaluation Report, North Pacific Fishery Management Council, 1007 West 3rd Ave., Suite 400, Anchorage, Alaska 99501.

Citing the Ecosystem Assessment:
Siddon, E. 2026. Ecosystem Assessment. In: Siddon, E. 2026. Ecosystem Status Report 2026: Eastern Bering Sea, Stock Assessment and Fishery Evaluation Report, North Pacific Fishery Management Council, 1007 West 3rd Ave., Suite 400, Anchorage, Alaska 99501.

Citing an individual contribution:
Contributor name(s), 2026. Contribution title. In: Siddon, E. 2026. Ecosystem Status Report 2026: Eastern Bering Sea, Stock Assessment and Fishery Evaluation Report, North Pacific Fishery Management Council, 1007 West 3rd Ave., Suite 400, Anchorage, Alaska 99501.

Citing information within a Synthesis section:
Contributor name(s), 2026. Sub-section heading. In: Synthesis section. In: Siddon, E. 2026. Ecosystem Status Report 2026: Eastern Bering Sea, Stock Assessment and Fishery Evaluation Report, North Pacific Fishery Management Council, 1007 West 3rd Ave., Suite 400, Anchorage, Alaska 99501.

Do not use or distribute any information of graphics from this Report without direct permission from individual contributors and/or the Ecosystem Status Report lead editor.

QR code for NOAA Alaska Fisheries Science Center's Ecosystem Status Reports webpage[1]. Time series from the report cards are also available[2].

[1] https://www.fisheries.noaa.gov/alaska/ecosystems/ecosystem-status-reports-gulf-alaska-bering-sea-and-aleutian-islands

[2] https://alaskaesr.psmfc.org

2026 Contributing Partners



Purpose of the Ecosystem Status Reports

This document is intended to provide the North Pacific Fishery Management Council (NPFMC), including its Scientific and Statistical Committee (SSC) and Advisory Panel (AP), with information on ecosystem status and trends. It follows the same annual schedule and review process as groundfish stock assessments, and is made available to the Council at the annual December meeting when Alaska's federal groundfish harvest recommendations are finalized.

Ecosystem Status Reports (ESRs) include indicators developed and contributed by scientists and fishery managers at NOAA, other U.S. federal and state agencies, academic institutions, tribes, nonprofits, and other sources. The ecosystem information in this report will be presented to the Groundfish and Crab plan teams in their annual September and November meetings, presentations to the Council in their annual October and December meetings, and submission of the final report to the Council in December (see Figure 1).

The SSC is the primary audience for this report, as final acceptable biological catch (ABCs) is determined by the SSC, based on biological and environmental scientific information through the stock assessment and Tier process[3],[4]. Total allowable catch (TAC) may be set lower than the ABCs due to biological and socioeconomic information. Thus, the ESRs are also presented to the AP and Council to provide ecosystem context to inform TAC as well as other Council decisions. Additional background can be found in the Appendix (p. 312). Outside the annual harvest specification cycle, the Alaska Region and NPFMC use ESRs to support National Environmental Policy Act assessments for regulatory and plan amendments, discussion papers, protected species analyses, responses to constituency inquiries, and policy write-ups.

ESRs and Ecosystem and Socioeconomic Profiles (ESPs) are complementary documents that allow for incorporating ecosystem information into stock-specific Risk Tables (Dorn, 2020) and thereby directly considering ecosystem dynamics in management decisions (i.e., EBFM). Both documents inform the SSC's ABC and overfishing limit (OFL) recommendations, as well as for the Council's final TAC determination for groundfish and crab. ESRs provide ecosystem status and trends annually for three Large Marine Ecosystems: the Eastern Bering Sea, Aleutian Islands, and the Gulf of Alaska. ESRs include assessments that reflect ecosystem components ranging from physical oceanography up through the food web. ESPs are both a process and a product and serve as a proving ground to identify key ecosystem and socioeconomic indicators within the stock assessment model and are presented as appendices in high priority stock assessments (see current list of available ESPs in Figure 1).

[3] https://www.npfmc.org/wp-content/PDFdocuments/fmp/GOA/GOAfmp.pdf
[4] https://www.npfmc.org/wp-content/PDFdocuments/fmp/BSAI/BSAIfmp.pdf

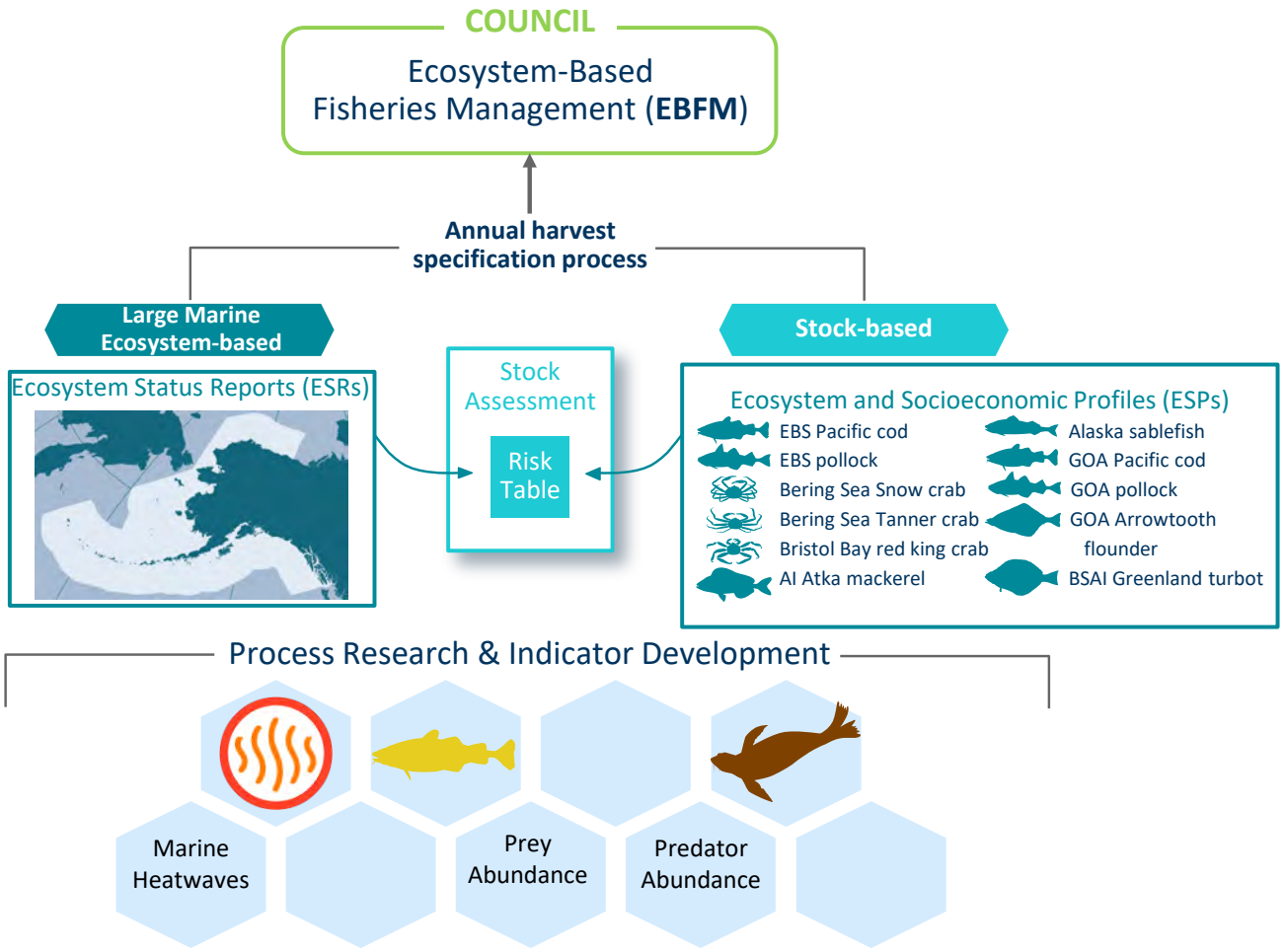
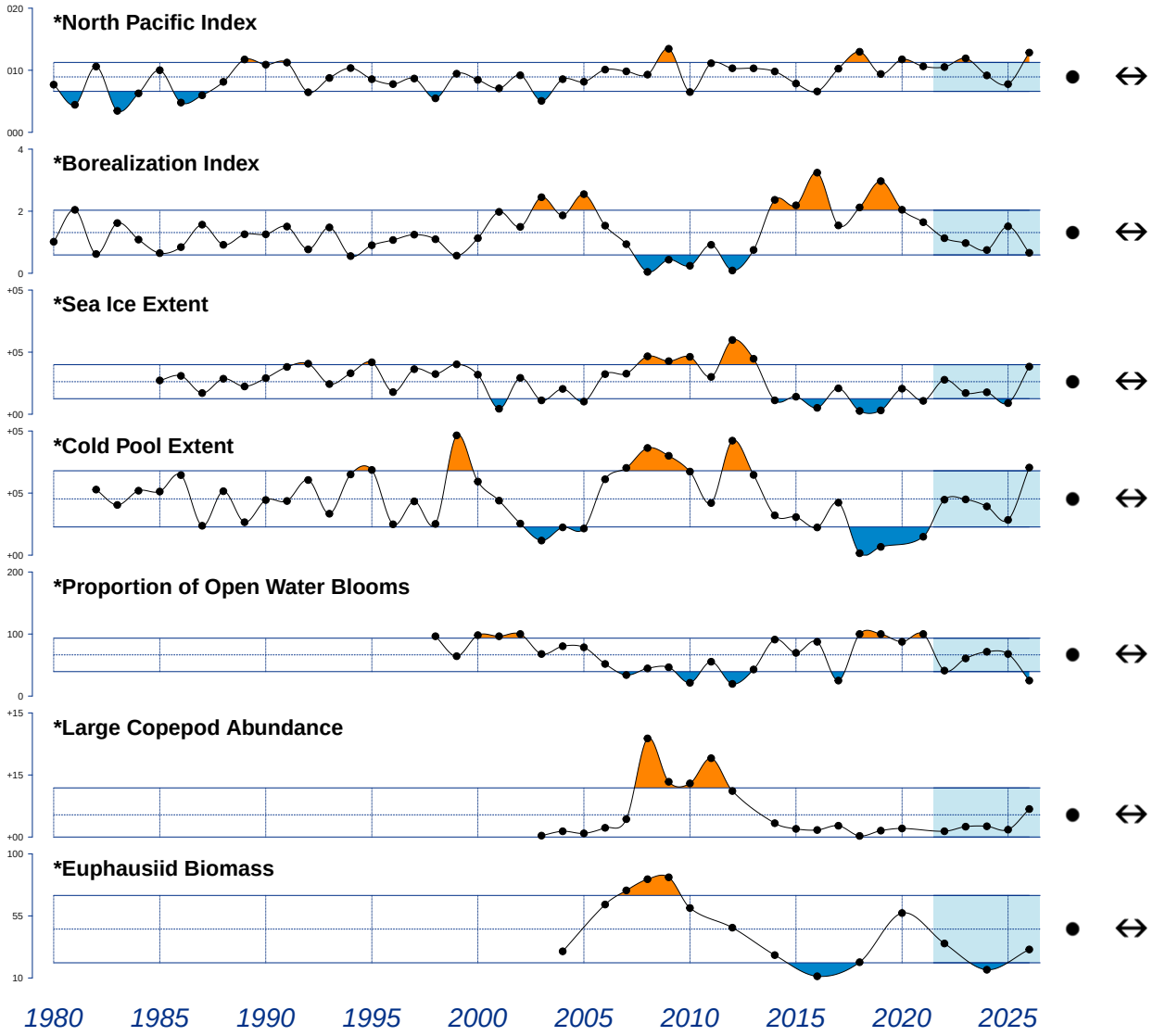


Figure 1: Ecosystem information mapping to support Ecosystem-Based Fisheries Management through Alaska's annual harvest specification process. The 'honeycomb' on the bottom shows examples of ecosystem indicators that are provided to Ecosystem Status Reports (ESRs) at the Large Marine Ecosystem (LME) scale and/or to Ecosystem and Socioeconomic Profiles (ESPs) at the stock-based level.

Southeastern Bering Sea 2026 Report Card



2022–2026 Mean

- 1 s.d. above mean
- 1 s.d. below mean
- within 1 s.d. of mean
- X fewer than 2 data points

2022–2026 Trend

- increase by 1 s.d. over time window
- decrease by 1 s.d. over time window
- ↔ change <1 s.d. over window
- X fewer than 3 data points

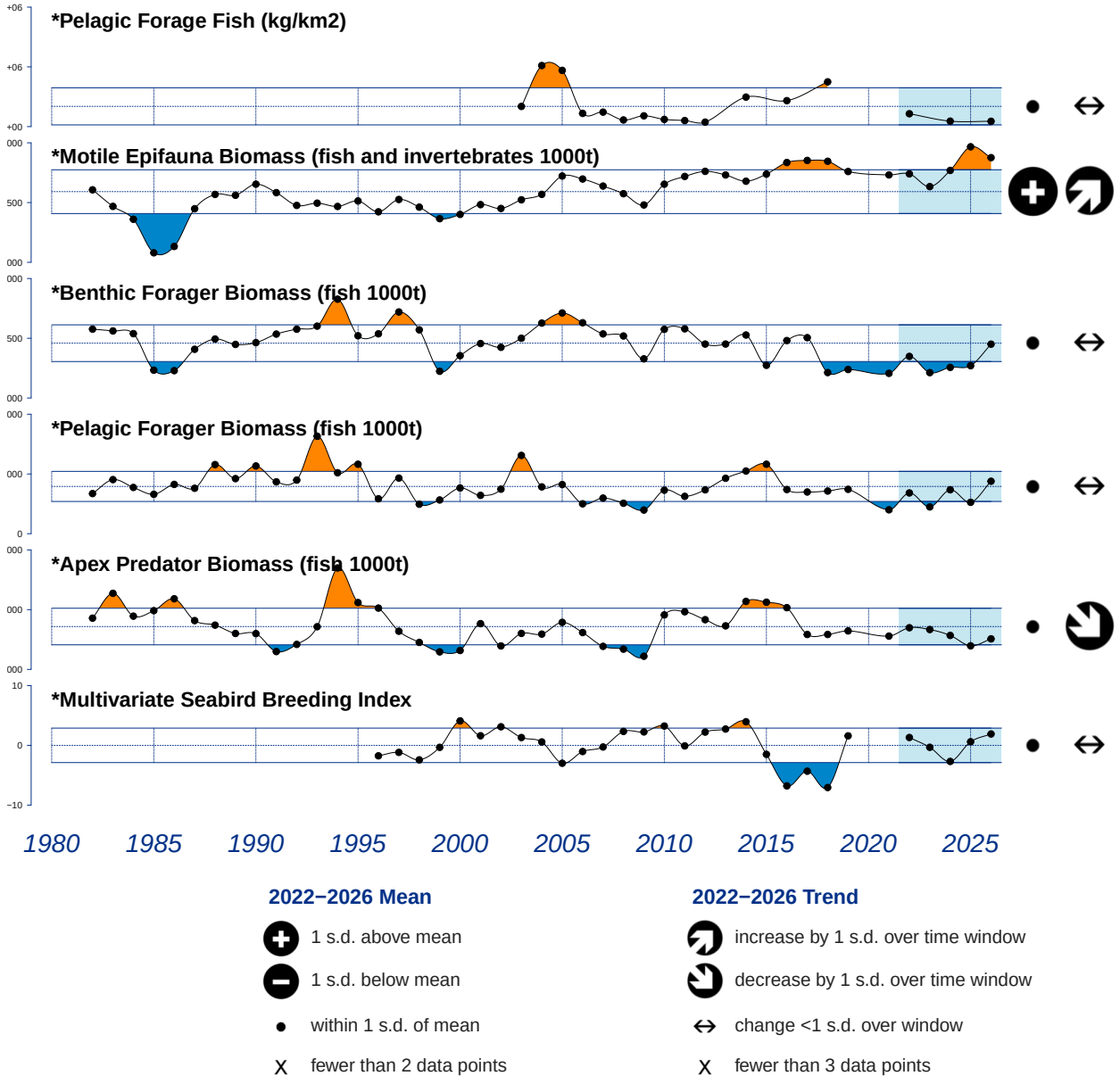


Figure 2: 2026 Southeastern Bering Sea report card; see text for indicator descriptions.
*indicates time series updated with 2026 data.

For more information on individual Report Card indicators, please see 'Description of the Report Card indicators' (p. 320 and p. 325). For more information on the methods for plotting the Report Card indicators, please see 'Methods Description for the Report Card Indicators' (p. 327).
* indicates Report Card information updated with 2026 data.

- *The **North Pacific Index (NPI)** effectively represents the state of the Aleutian Low Pressure System. Above average (below average) winter (Nov-Mar) NPI values imply a weak (strong) Aleutian Low and generally calmer (stormier) conditions. Contrast to the previous two winters (2024, 2025) which had near normal conditions, the **2026 winter NPI had a large positive anomaly** at 3.76 hPa, an indication of a weak Aleutian Low in the region (Figure 25). This may have partially contributed to the highly variable ice edge during January and February 2026, and the exceptional southward expansion of sea ice extent in March and April.
- *The updated median annual **borealization index** describes the transition from an Arctic physical state supporting a cold-adapted species assemblage to a subarctic (boreal) physical state supporting a warm-adapted assemblage. Arctic-like conditions occurred between 2007-2013, while boreal conditions dominated during the warm, low-ice years of 2014-2021. Following the 2018–2019 marine heatwave, the index returned to values near the timeseries mean and is **currently slightly below average in 2026** indicating a cooler physical state.
- *The mean **sea-ice extent** over the southeastern Bering Sea shelf (south of 60°N) was **above the long-term mean** (1985-2024) in 2026 (ice year defined as 1 Sept to Aug 31). Seasonal sea-ice extent has implications for the cold pool, spring bloom strength and timing, and bottom-up productivity.
- *The spatial **extent of the <2°C cold pool** in the eastern Bering Sea (EBS), as measured during the bottom trawl survey (Jun-Aug; including strata 82 and 90; 1982-2026), **was above the time series average in 2026**. The 2026 extent (282,325 km^2) was **~150% larger than in 2025**, representing the fifth-largest cold pool in the survey timeseries.
- *The **proportion of open water blooms** in the southeastern Bering Sea (south of 60°N) was 25% during 2026, similar to 2017, and **just below -1SD below the timeseries mean** (1998-2026). A higher proportion of ice-associated blooms is correlated with higher abundances of large zooplankton (Hunt et al., 2011).
- *The **abundance of large copepods** (predominantly *Calanus* spp.) as measured during August/September along the 70 m isobath over the southeastern shelf, peaked in 2008 and 2012 during cold years, but remained below the timeseries mean (2000-2024) between 2014-2025. The abundance of large copepods **increased in 2026 to just above the timeseries mean**.
- *An acoustic estimate of **euphausiid biomass** increased from 2015 through 2020, then declined to the second-lowest value in the time series in 2024, then **increased but remained below the timeseries mean in 2026**.
- *The relative biomass of **pelagic forage fish** (i.e., age-0 pollock, age-0 Pacific cod, herring, capelin, rainbow smelt, saffron cod, and all species of juvenile salmonids) sampled by surface trawl over the southeastern Bering Sea shelf in late-summer (Aug-Sep; 2003-2026) peaked in 2005, was below the time series average in 2006-2012, was above average in 2014, 2016, and 2018, but dropped below the long-term mean in 2022 and was **the second lowest in the timeseries in 2026**. The trends are dominated by age-0 pollock, age-0 Pacific cod, juvenile sockeye salmon, Pacific herring, and capelin.

- *The biomass of **motile epifauna** measured during the standard bottom trawl survey (Jun-Aug; 1982-2026) in **2026 is down from 2025 but remains more than one standard deviation above the long-term mean**. Since 1995, brittle stars, sea stars, and other echinoderms have collectively accounted for more than 50% of the biomass in this guild. Brittle stars alone have accounted for more than 25% of motile epifauna biomass since 1996. Brittle star biomass peaked in 2016 and has since trended downward to 2026.

- *The biomass of **benthic foragers** measured during the standard bottom trawl survey (Jun-Aug; 1982-2026) **increased 21% from 2025 to 2026 and are nearly equal to their timeseries mean**. The increase in benthic foragers from 2025 to 2026 was driven by increases in the biomass indices of several flatfishes, including Alaska plaice, flathead sole, northern rock sole, yellowfin sole, and miscellaneous flatfishes.

- *The biomass of **pelagic foragers** measured during the standard bottom trawl survey (Jun-Aug; 1982-2026) **increased 67% from 2025 to 2026 and is above the timeseries mean**. The trend in the pelagic forager guild is largely driven by pollock who on average account for 69% of the biomass in this guild. In 2026, the index for pollock increased 58% from 2025. Among species of secondary importance, there were increases in capelin, sandlance, eulachon, Pacific herring, and jellyfish.

- *The biomass of **apex predators** measured during the standard bottom trawl survey (Jun-Aug; 1982-2026) **increased from 2025 to 2026 but is still below the timeseries mean**. The trend in the apex predator guild is largely driven by Pacific cod, whose index increased 17% from 2025 to 2026. Other apex predators with noteworthy increases in their index included Greenland turbot (driven by one large haul) and large sculpins (e.g., *Myoxocephalus* spp., yellow Irish Lord).

- *The **multivariate seabird breeding index** indicated that **seabird productivity was average or better** for cliff-nesting seabirds across the Pribilof Islands. Hatch dates were earlier or about average, and population counts were within the expected range for all species. These observations suggest that foraging conditions were largely favorable for seabirds this spring and summer.

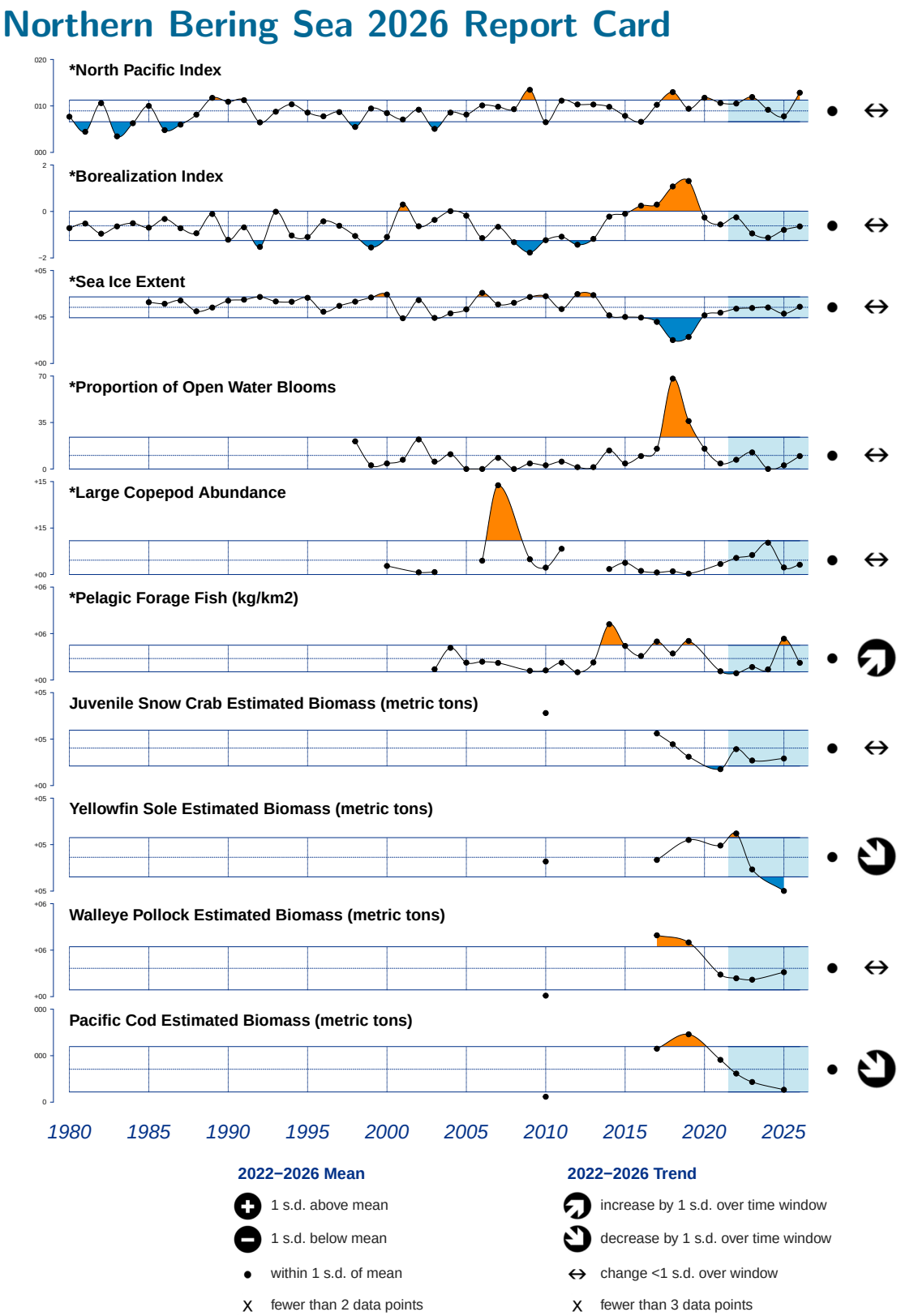


Figure 3: 2026 Northern Bering Sea report card; see text for indicator descriptions.
*indicates time series updated with 2026 data.

For more information on individual Report Card indicators, please see 'Description of the Report Card indicators' (p. 325). For more information on the methods for plotting the Report Card indicators, please see 'Methods Description for the Report Card Indicators' (p. 327).
* indicates Report Card information updated with 2026 data.

- *The **North Pacific Index (NPI)** effectively represents the state of the Aleutian Low Pressure System. Above average (below average) winter (Nov-Mar) NPI values imply a weak (strong) Aleutian Low and generally calmer (stormier) conditions. Contrast to the previous two winters (2024, 2025) which had near normal conditions, the **2026 winter NPI had a large positive anomaly** at 3.76 hPa, an indication of a weak Aleutian Low in the region (Figure 25). This may have partially contributed to the highly variable ice edge during January and February 2026, and the exceptional southward expansion of sea ice extent in March and April.

- *The updated median annual **borealization index** describes the transition from an Arctic physical state supporting a cold-adapted species assemblage to a subarctic (boreal) physical state supporting a warm-adapted assemblage. Borealization in the NBS has shown a multi-decadal increase over the timeseries despite high interannual variability. Following the peak during the 2018-2019 heatwave, the index has returned toward the long-term mean and is **currently slightly above average in 2026** indicating a warmer physical state.

- *The mean **sea-ice extent** over the northern Bering Sea shelf (north of 60°N) has generally been increasing since the timeseries low ice extent in 2018 (ice year defined as Sept 1 to Aug 31). Sea ice extent **was average in 2026**. Seasonal sea-ice extent has implications for the cold pool, spring bloom strength and timing, and bottom-up productivity.

- *The **proportion of open water blooms** in the northern Bering Sea (north of 60°N) was about 10% during 2026, which is **at the timeseries mean**. A higher proportion of ice-associated blooms is correlated with higher abundances of large zooplankton (Hunt et al., 2011).

- *The **abundance of large copepods** (predominantly *Calanus* spp.) as measured during August/September over the northern Bering Sea shelf, peaked in 2008 during a cold year, and was **near the time series mean** in 2026.

- *The relative biomass of **pelagic forage fish** (i.e., age-0 pollock, age-0 Pacific cod, herring, capelin, rainbow smelt, saffron cod, and all species of juvenile salmonids) sampled by surface trawl in late-summer (Aug-Sep; 2003-2026) peaked in 2014 and remained above average through 2019, dropped below the long-term mean in 2021-2024, reached $>+1$ SD above the mean in 2025 driven by age-0 pollock, then **decreased to the timeseries mean in 2026**.

- The biomass of **juvenile snow crab** measured during the northern Bering Sea bottom trawl survey (2010, 2017-2019, 2021-2023, 2025) has **declined throughout the time series and remains below the long term average**, showing only a slight increase in biomass from 2023 to 2025. The trend in juvenile snow crab biomass (combination of small male and immature female crab) reflects benthic production of the ecosystem and is a signal for future crab recruitment into the eastern Bering Sea.

- The biomass of **yellowfin sole** observed during the northern Bering Sea bottom trawl survey (2010, 2017, 2019, 2021-2023, 2025) peaked in 2022 and then **decreased to below -1 SD of the timeseries mean in 2025**. Trends in yellowfin sole biomass reflect relative predation pressure on small infaunal prey (e.g., polychaete worms, bivalves, small crustaceans).

- The biomass of **walleye pollock** observed during the northern Bering Sea bottom trawl survey (2010, 2017, 2019, 2021-2023, 2025) peaked from 2017-2019 and decreased through 2023. Biomass of pollock **increased to the timeseries mean in 2025**. Trends in pollock biomass reflect relative predation pressure on zooplankton and forage fish.
- The biomass of **Pacific cod** observed during the northern Bering Sea bottom trawl survey (2010, 2017, 2019, 2021-2023, 2025) peaked in 2019 and then **decreased through 2025**. Trends in Pacific cod biomass reflect relative predation pressure on forage fish and crab.

Ecosystem Assessment

Elizabeth Siddon
Auke Bay Laboratories, Alaska Fisheries Science Center, NOAA Fisheries
Contact: elizabeth.siddon@noaa.gov

Last updated: November 2026

Introduction

In recent decades, the eastern Bering Sea (EBS) transitioned from an ecosystem governed by inter-annual variability (1982-2000) into one that experienced multi-year stanzas of warm (2000-2005) and cold (2007-2013) conditions (Baker et al., 2020). In 2014, the EBS entered a warm period that was unprecedented in terms of magnitude and duration (Figure 42) and that persisted until 2021. This recent warm period included the near-absence of sea ice in the winters of 2017/2018 and 2018/2019 (Figure 31) and subsequent lack of cold pool in summers 2018 and 2019 (Figures 36 and 37) that had distinct impacts to the ecosystems of the southeastern (SEBS) and northern (NBS) Bering Sea shelves.

Beginning in about 2021, the eastern Bering Sea (EBS) exited the prolonged warm stanza and entered a more neutral thermal state that persisted into 2025. Over the past year (August 2025 - August 2026) many metrics, including sea surface temperature (e.g., Figures 43 and 54), depth-averaged temperature (Figure 50), wintertime sea ice extent (Figure 31) and thickness (Figures 34 and 35), and cool pool extent (Figures 36 and 37) show a rapid transition to cool thermal conditions. Currently, the broader North Pacific is experiencing a 'Very Strong' El Niño with warm anomalies predicted to reach the eastern Gulf of Alaska in winter 2026/2027, though conditions in the Bering Sea are governed more so by the Aleutian Low Pressure System (Figure 26) and regional wind dynamics (Figure 41).

This Assessment aims to synthesize recent biological metrics (e.g., zooplankton and fish dynamics) to characterize the eastern Bering Sea ecosystems in response to the near-average oceanographic conditions experienced between ∼2021-2025 followed by the abrupt transition to cooler conditions in 2026.

Oceanography

Between ∼2021-2025, both surface temperatures (SST) and bottom temperatures remained generally within ±1 standard deviation of historical climatological means (e.g., Figures 45 and 54), modulated by the near-neutral state of the Aleutian Low Index (ALI) (Figure 25). Beginning in early (Jan/Feb) 2026, an exceptionally weak winter Aleutian Low followed by strong north-to-south winds (Mar/Apr) drove rapid cooling and late-season sea ice expansion over the southeastern Bering Sea shelf, resulting in the largest sea ice extent since 2013 (Figure 2).

Spring 2026 surface and bottom waters were the coldest observed since 2012 (Figure 43). Depth-averaged water column temperatures at Mooring M2 remained more than 2°C below average through late summer (Figure 50). No marine heatwaves (based on SST) occurred in either the southeastern or northern Bering Sea during 2026 (Figure 53), and the cumulative annual SST anomaly for the southeastern Bering Sea reached its lowest point since prior to the extended warm stanza that began in 2014 (Figure 54). The spatial extent of the <2°C cold pool expanded to 282,325 km^2 (∼150% larger than in 2025), representing the fifth-largest cold pool in the 1982-2026 survey time series (Figures 2 and 36).

Seasonal sea ice and the resulting cold pool extent are defining features over the Bering Sea shelf. Combined, sea ice and the cold pool create thermal barriers, both horizontally (i.e., north/south) and vertically in the water column. Such thermal barriers affect the spatial distributions of crab and groundfish (e.g., Thorson et al., 2019; DeFilippo et al., 2023) that have subsequent direct (e.g., habitat expansion) and indirect (e.g., changes in predator/prey dynamics) impacts to managed stocks.

Primary and Secondary Productivity

Indicators of primary productivity (i.e., large diatoms, chlorophyll-a) were generally above average after 2022, including the percent of large chlorophyll >10 μm (Figure 62; last data measurement 2024). Large diatom abundance was above average in 2023 through 2025 (Figure 68; last data measurement 2025) and spring chlorophyll concentrations have generally been above average in the SEBS and NBS, especially in 2025 and 2026 (Figure 65). Combined, these indicators suggest productive, ice-associated blooms supporting good-quality food and efficient energy transfer to secondary consumers, though 2026 observations are limited.

The quantity and quality of secondary producers (i.e., copepods, euphausiids) had a lagged response to the end of the extended warm stanza. As thermal conditions cooled to average, secondary production took several years to rebound. In 2026, with an abrupt shift to cold conditions over the shelf, both the quantity and quality of secondary producers has improved. Copepod dynamics shift from spring to fall over the EBS shelf based on thermal conditions, phenology, and life cycles. In spring, small copepod abundances were above average since the onset of the recent warm stanza (2014) dropping to average in 2026. By fall, small copepod abundances remained largely above average during the warm stanza (2014-2020), decreasing to average in the more recent near-average thermal conditions (2022-2024), and dropping below 1 standard deviation below the timeseries mean in 2026. Fall large copepods remained below average since the onset of the recent warm stanza (2014) increasing to above average in 2026 for the first time since 2012 (see p. 122). Large copepod and euphausiid lipid content has increased since below-average levels in 2018 and 2022, respectively (Figure 76). Euphausiid abundance tends to increase with colder temperatures in the EBS (Ressler et al., 2014), with low summer (Figure 79) and late summer (Figure 81) abundances during the recent warm stanza. Like copepods, euphausiid abundance increased under cold thermal conditions in 2026. Combined, these indicators suggest good quantity and quality of prey resources for pelagic consumers.

Forage Fish

Forage fish dynamics vary with thermal regime, and can vary between the SEBS and NBS. However, capelin are generally more abundant in cooler conditions and herring in warmer conditions in both the SEBS and NBS (Andrews et al., 2015; Suryan et al., 2026, see p. 154). The delineation between the SEBS and NBS is often considered to be at 60°N latitude; this delineation is supported by broad-scale analyses of the physical oceanography and hydrography (Stabeno et al., 2012*a*; Baker et al., 2020) and zoogeography of the region (Sigler et al., 2017). Forage fish response to the shift to near-average thermal conditions followed the lagged response of zooplankton prey resources.

In the SEBS, capelin biomass has remained below average since 2014 and has not rebounded under cooler conditions since 2022 (Figure 102), contrary to expectations. Herring biomass has generally remained below average with the exception of above average biomass in 2018 (Figure 101). Age-0 pollock biomass was above average in the warm years of 2014-2018 and below average in the cooler years of 2022-2026 (Figure 95). Pollock condition (e.g., energy density) generally fluctuates in response to temperature-mediated processes, with below-average energy density during warm periods and above-average body condition during cold periods. However, age-0 pollock energy density remained below average during the near-average thermal conditions years of 2022-2025 (Figure 99), similarly following the lagged response of zooplankton and other forage fish species. In 2026 with the abrupt change to cold ocean temperatures, energy density was higher than average (Figure 99).

In the NBS, capelin biomass peaked in 2024, declined in 2025, and increased to average in 2026 while herring biomass has remained below average since 2021 with a slight increase in 2026. Age-0 pollock biomass peaked to a timeseries high in 2025 and returned to average abundance in 2026. Age-0 pollock body condition in the NBS is less variable than in the SEBS and is not coupled with regional thermal conditions. In 2026, age-0 pollock had low energy density and average weight (Figures 99 and 100).

In summary, for 2026, the SEBS showed low biomass of capelin, herring, and age-0 pollock with the exception of high energy density for age-0 pollock. Conversely, in the NBS, capelin and age-0 pollock were average while herring remained low. While these direct survey measurements reflect low pelagic forage abundance in 2026, it is important to note that the surveys capture a brief temporal window and are limited in their spatial extent. Indirect measures of forage fish by upper trophic level consumers (groundfish condition, Figure 120; seabirds, see p. 233; and fur seals, Figure 140) provide broader temporal and spatial integration of forage conditions and all show positive trends over the EBS shelf (see additional details below).

Salmon

Pacific salmon exhibit variable age structure and complex life cycles that span multiple habitats in the eastern Bering Sea and Gulf of Alaska, including river and freshwater habitats, therefore it can be challenging to disentangle the impacts of thermal conditions and predator/prey conditions on their population dynamics (see p. 175). However, signals of species-specific responses to the near-average temperature conditions have prevailed recently. Generally, juvenile salmon energy density was average to positive in the NBS (Figure 105) but remained low in the SEBS (Figure 106). For western Alaska chum salmon, which experienced steep declines following the 2018-2019 marine heatwave years driven by negative bottom-up processes (Farley Jr et al., 2024), have rebounded under the cooler conditions since 2022. After several years of above-average condition from 2021 through 2023 linked to cooler waters, NBS juvenile chum salmon had near-to-above-average energy density from 2024 to 2026 (Figure 105), alongside a drop to slightly below-average abundance in 2025-2026 following a large 2024 cohort (Figure 108). The abundance and energy density patterns in 2025-2026 are consistent with the near-average temperature and ecosystem conditions in recent years, and indicate neither evidence of severe adverse ecosystem conditions, nor strongly favorable conditions for chum salmon. For NBS juvenile Chinook salmon, severe low runs in 2022-2023 and depressed juvenile abundance through 2024 showed signs of recovery in 2025 with above-average energy density (Figure 105) and improved abundance (Figure 107). In 2026, juvenile abundance was slightly below average with near-average energy density, suggesting adult run sizes could improve over the next three to four years. Bristol Bay sockeye salmon runs peaked in 2021-2022 due to warm-water productivity, then tapered through 2025 as ocean temperatures cooled, though they remained above average. As cooler temperatures prevailed into 2026, adult returns continued to decline and more modest run sizes are expected in the next few years (Figure 110).

Groundfish

The expansion of the 2°C cold pool provided a thermal barrier and spatial separation between adult groundfish (e.g., pollock, Pacific cod) concentrated in the NW outer domain and juvenile habitat over the middle shelf. Cooler conditions generally result in reduced metabolic demands (Figures 124 and 125), increased pelagic productivity, and reduced top-down predation pressure (see p. 219) due to reduced spatial overlap. As thermal conditions transitioned from near-average to cool between 2022-2026, the abundance and condition (Figure 120) of many groundfish species over the SEBS shelf increased in 2026. The NOAA Fisheries standard bottom trawl survey showed increased biomass and fish condition across major groundfish species, including pollock, Pacific cod, and yellowfin sole, representing pelagic foragers, apex predators, and benthic foragers, respectively (Figures 2 and 120). Pollock diets were dominated by energy-rich oceanic copepods and euphausiids along the outer shelf, and spatial separation from juvenile pollock resulted in low levels of cannibalism on age-1 pollock (Figure 115). However, pollock was the largest proportion of Pacific cod diets for the first time since 2005 while snow and tanner crab consumption remained at a low level (Figure 116). Since 2018, Pacific cod processed for diets have been dominated by larger cod (i.e., fork lengths of 60+ cm) that have more piscivorous diets (see p. 201), contributing to the higher proportion of pollock in Pacific cod diets. Indirect measures of benthic prey resources were strongly positive, with motile epifauna (Figure 2), eelpouts (highest biomass since 1983; Figure 131), and poachers (highest since 2005; Figure 131) all remaining $>+1$ SD above time-series means. The groundfish community mean lifespan (Figure 145) and mean length (Figure 146) experienced minor downward dips coinciding with declining sablefish survey biomass (see p. 249). However, the groundfish community biomass stability index (Figure 147) remained well above its long-term historical mean, demonstrating ecosystem resilience to environmental perturbations.

Seabirds

Seabirds serve as key indicators of secondary productivity and shifts in prey availability that similarly affect commercial fish populations (see p. 233). On the Pribilof Islands, 2026 was a strong reproductive year overall across monitored species (Figure 137). On St. George Island, productivity remained near long-term averages for both plankton-eating species (such as least auklets) and fish-eating species. In contrast to earlier years, St. Paul Island experienced above-average reproductive success for murres, kittiwakes, and red-faced cormorants, reflecting favorable local foraging conditions and high chick survival. An unusual mortality event occurred on St. George Island in August 2025, predominantly affecting thick-billed murres, that was linked to a harmful algal bloom exposure (Figure 139). Population counts of thick-billed murres continued to be relatively stable in 2026, indicating no significant population level effect at the Pribilof breeding colonies following the 2025 HAB-related die-off (M. Rustand, pers. comm.). In 2026, overall beached bird carcass encounter rates returned to very low baseline levels across Bering Sea beaches, though localized mortality from paralytic shellfish toxicosis was confirmed during a seabird die-off on Round Island in August 2026.

Northern Fur Seals

In 2025 and 2026, northern fur seals on St. Paul Island recorded below-average maternal foraging trip durations. Maternal trip duration reached a timeseries low in 2026 indicating favorable feeding conditions within 120-150 km of the rookeries over the outer and middle shelf. These shorter foraging trips facilitated more frequent nursing and resulted in above-average female pup masses, especially at St. Paul Island (Figure 140). Northern fur seal diets were dominated by pelagic forage species, with diets in 2025 and preliminary diet data from 2026 dominated by Pacific herring and pollock (predominantly age-0) (Figures 20 and 141). Fur seal mortalities from saxitoxin were reported in 2025, indicating observed blooms of *Alexandrium catenella* that produce saxitoxin were transferred into the upper trophic levels of the eastern Bering Sea food web (see p. 267).

Emerging Stressors

We track emerging stressors like ocean acidification (OA) and harmful algal blooms (HABs) to better understand dynamics and potential impacts to the EBS ecosystem. In 2026, modeled bottom water pH and aragonite saturation state reached shelf-wide minimums across the 1993-2026 time series (Figure 150), driven by strong freshwater runoff and carbon loading near the Yukon River delta (Figure 148) alongside thermal solubility effects from cooler bottom temperatures. Consequently, the spatial footprint of corrosive bottom waters expanded across the middle and outer shelf, though shallow inner shelf waters in Bristol Bay remained relatively well-buffered (Figure 148). Crab stocks are likely the most vulnerable to negative impacts of OA, with corrosive bottom waters negatively impacting growth, shell hardening, and survival. Red king crab may be more impacted than snow crab that appear more resilient. The 'hotspot' of low pH in Norton Sound in 2026 was documented in the Norton Sound red king crab Risk Table, though not directly related to a recommendation to reduce the ABC from maximum permissible. A dense and widespread *Alexandrium* bloom developed in the southeastern Bering Sea for the third consecutive year (see p. 262), reaching concerning cell concentrations by late August 2026. These *Alexandrium* blooms produce neurotoxic saxitoxin that transfers up marine food webs (see p. 267), causing the confirmed toxicosis die-off in seabirds on Round Island in August 2026 after previously causing northern fur seal mortalities in 2024 and 2025. However, overall cooler thermal conditions in 2026 likely contributed to a slight decrease in overall bloom events compared to recent warm years.

Looking Ahead

Looking ahead to 2027, oceanographic models indicate a very strong El Niño strengthening in the tropical Pacific (Figure 24), which is expected to drive warm surface anomalies across the North Pacific and Gulf of Alaska. However, any developing warmth over the eastern Bering Sea shelf will overlay the cool thermal conditions (Figure 54), expansive cold pool (Figures 36 and 37), and absence of marine heatwaves (Figure 53) experienced in 2026. Furthermore, the ecosystem is currently supported by strong pelagic and benthic productivity, including energy-dense zooplankton (Figure 76) and abundant benthic epifauna (Figure 2), which fostered above-average body condition across major groundfish stocks (Figure 120). This positive condition baseline and low thermal stress provide a resilient buffer against potential food web disruptions if warming from the El Niño reaches the EBS ecosystem.

Contents

Eastern Bering Sea 2026 Contributing Partners **2**

Purpose of the Ecosystem Status Reports **4**

Southeastern Bering Sea 2026 Report Card **6**

Northern Bering Sea 2026 Report Card **10**

Ecosystem Assessment **13**

Ecosystem Indicators **31**

Noteworthy Topics 31

†*Introducing MOM6 to the Alaska regional modeling framework 31

†*Eastern Bering Sea Walleye Pollock Early Survival Pathways 42

†*Oceanography On Deck: Industry-driven data collection to fill spatial and temporal information gaps 52

†Imaging FlowCytobot: Phytoplankton, Lower Trophic Dynamics, and Survey Modernization 57

†DNA metabarcoding of northern fur seal scats improves species-level prey identification and tests scalability of efficient data generation 62

†*A Spatially Resolved Borealization Index for the Bering Sea 64

Ecosystem Status Indicators 67

Physical Environment 67

*1. Alaska-Wide Trends 69

(a) Climate Overview 69

(b) Regional Summaries . . . 78
†*2. Eastern Bering Sea Trends . . . 79
(a) Sea Ice . . . 79
(b) Cold Pool Extent . . . 85
(c) Surface Winds and Air Temperatures . . . 89
(d) Sea Surface and Bottom Temperatures . . . 92
Habitat . . . 107
*Eastern and Northern Bering Sea – Structural Epifauna . . . 107
Primary Production . . . 112
†Surface Phosphate Concentrations and Mixed Layer Depth Correlate with Larger Phytoplankton in the Eastern Bering Sea . . . 112
*Spring Satellite Chlorophyll-a Concentrations . . . 115
Zooplankton . . . 119
Continuous Plankton Recorder Data from the Eastern Bering Sea . . . 119
*Current and Historical Trends for Zooplankton in the Bering Sea . . . 122
*Lipid Content of Copepods and Euphausiids in the Bering Sea . . . 129
†*Summer Eastern Bering Sea Euphausiids ('Krill') . . . 132
†*Late Summer Eastern Bering Sea Euphausiids ('Krill') . . . 139
Jellyfish . . . 142
*Eastern and Northern Bering Sea – Jellyfishes . . . 142
*Jellyfish from Surface Trawl Surveys, 2004-2026 . . . 144
Ichthyoplankton . . . 147
*Abundance and Distribution of Larval Fishes in the Southeastern Bering Sea 2012-2026 . . . 147
*Morphometric Condition of Walleye Pollock Larvae . . . 150
Forage Fish . . . 154
*Forage Fish Dynamics in the Eastern Bering Sea . . . 154
†Mapping Fish Distributions in the NBS Using eDNA . . . 162
*Age-0 Pollock and Pacific Cod from Surface Trawl Surveys, 2003-2026 . . . 165

*Vertical Distribution of Age-0 Pollock in the Southeastern Bering Sea 168

*Fall Condition of Young-Of-The-Year Walleye Pollock in the Northern and Southeastern Bering Sea, 2002-2026 170

*Pacific Herring and Capelin from Surface Trawl Surveys, 2003-2026 173

Salmon 175

*Salmon Summary and Synthesis 175

*Southern Bering Sea Nearshore Juvenile Salmon Survey, 2024-2026 177

*Juvenile Salmon Condition Trends in the Eastern Bering Sea 181

*Northern Bering Sea Juvenile Salmon Abundance Indices 184

*Temporal Trend in the Annual Inshore Run Size of Bristol Bay Sockeye Salmon (*Oncorhynchus nerka*) 188

*Trends in Alaska Commercial Salmon Catch – Bering Sea 191

†*Synthesizing Indicators of Yukon and Kuskokwim Salmon Health and Abundance for a 2027 Outlook 194

Groundfish 201

*Summer Food Habits of Walleye Pollock and Pacific Cod 201

*Eastern and Northern Bering Sea Groundfish Condition 205

*Patterns in Foraging and Energetics of Bering Sea Walleye Pollock, Pacific Cod, and Pacific Halibut 213

†*Bering Sea Multispecies Model (CNRG) Estimates of Time-Varying Natural Mortality 219

Benthic Communities and Non-target Fish Species 224

*Eastern and Northern Bering Sea – Miscellaneous Benthic Fauna 224

†Diet-based Indicators of Benthic Fauna 229

*Eastern Bering Sea Commercial Crab Stock Biomass Indices 230

Seabirds 233

*Integrated Seabird Information 233

Marine Mammals 240

†*Integrated Marine Mammal Information 240

*Marine Mammal Strandings 244

Ecosystem or Community Indicators . . . 249
*Mean Lifespan of the Fish Community . . . 249
*Mean Length of the Fish Community . . . 251
*Stability of Fish Biomass . . . 253
Emerging Stressors . . . 256
*Ocean Acidification . . . 256
*Harmful Algal Blooms . . . 262
*ECOHAB: Harmful Algal Bloom (HAB) Toxins in Arctic Food Webs . . . 267
Discards and Non-Target Catch . . . 270
*Time Trends in Groundfish Discards . . . 270
Time Trends in Non-Target Species Catch . . . 274
Seabird Bycatch Estimates in the Eastern Bering Sea, 2016-2025 . . . 275
Sustainability . . . 284
*Fish Stock Sustainability Index – Bering Sea and Aleutian Islands . . . 284

References **288**

Appendix **312**

*History of the Ecosystem Status Reports . . . 312
*Responses to SSC Comments From December 2024 . . . 316
*Responses to Crab Plan Team Comments from September 2025 . . . 317
*Responses to Joint Groundfish Plan Team Comments from September 2025 . . . 318
*Responses to SSC Comments From October 2025 . . . 318
*Responses to Joint Groundfish Plan Team Comments from September 2026 . . . 319
*Responses to Crab Plan Team Comments from September 2026 . . . 319
*Responses to SSC Comments From October 2026 . . . 319
*Description of the SEBS Report Card Indicators . . . 320
*Description of the NBS Report Card Indicators . . . 325
Methods Description for the Report Card Plots . . . 327

† indicates new or significantly revised Ecosystem Status Indicator contribution
* indicates Ecosystem Status Indicator contribution updated with 2026 data

List of Tables

1 Primary forcing datasets used for Alaska region hindcasts. 34

2 Skill metrics used in the MOM6 study. 36

3 Standardized ecosystem framework. 44

4 Mean size, temperature, condition ratio, and stations classified in poor condition in the SEBS. 151

5 Hypothesized mechanism table for ecosystem linkages included in the forage fish DSEM. 160

6 eDNA detection frequencies of four fish species in the NBS, 2023 and 2024. 164

7 Salmon and forage fish catch from the southern Bering Sea juvenile salmon survey, 2024-2026. 179

8 Potential processes reflected in high or low RFR under different conditions. 214

9 Reported marine mammal strandings between January 1, 2022 and September 30, 2026. 248

10 Estimated seabird bycatch in southeastern Bering Sea groundfish and halibut fisheries. . 278

11 Estimated seabird bycatch in northern Bering Sea groundfish and halibut fisheries. . . . 279

12 Estimated seabird bycatch outside the ESR ecoregions. 283

13 BSAI FSSI stocks under NPFMC jurisdiction updated through June 2026. 287

14 Composition of foraging guilds in the eastern Bering Sea. 323

List of Figures

1 Ecosystem information mapping to support EBFM in Alaska. 5

2 2026 Southeastern Bering Sea Report Card. 7

3 2026 Northern Bering Sea Report Card. 10

4 Map of the MOM6-NEP and ROMS Bering 10K model domains. 33

5 State variables in the BEST$_N PZ and COBALT v3 biogeochemical models$. 35

6 Skill metrics for MOM6-NEP hindcast simulation bottom temperature. 38

7 Skill metrics for MOM6-NEP hindcast simulation surface temperature. 39

8 Skill metrics for ROMS Bering10K hindcast simulation bottom temperature. 40

9 Skill metrics for ROMS Bering10K hindcast simulation surface temperature. 41

10 Pollock Workshop conceptual model building: Recruitment in the Bering Sea. 43

11 Quantitative linkages among variables driving early survival pathways of pollock. 45

12 Observed and estimated values for variables in the DSEM. 50

Hypothesized mechanism table for pollock early survival pathways. 51

13 The Oceanography On Deck observing system. 53

14 Cold pool formation measured by OOD network vessels. 54

15 Map of subsurface temperature profile locations. 55

16 Example portal display of publicly available oceanographic data. 56

17 Conceptual model of lower trophic dynamics across environmental stanzas, 2003-2018. . 58

18 Imaging FlowCytobot and inset image of phytoplankton cells. 60

19 Phytoplankton images overlaid onto station map for the spring mooring survey during 2015. 61

20 Prey species in northern fur seal diets. 62

21 Relative proportions of DNA metabarcoding sequencing reads for northern fur seal diets. 63
22 Spatially resolved borealization index for the Bering Sea. 66
23 Geographic regions of interest across the North Pacific and Arctic. 70
24 Time series of three commonly used oceanic indices. 71
25 Time series of three indices related to winter atmospheric patterns. 72
26 Map of SLP in 2026 relative to climatatology. 73
27 Monthly sea surface temperature (SST) anomalies and surface winds. 74
28 Seasonal sea level pressure (SLP) anomalies and mean winds. 75
29 Predicted SST anomalies from the National Multi-Model Ensemble. 77
30 Early (15 Oct-15 Dec) mean sea-ice extent in the Bering Sea. 79
31 Mean sea ice extent in the Bering Sea, 1979/1980 - 2025/2026. 80
32 Daily ice extent in the Bering Sea. 81
33 Map of six areas within which sea ice thickness was calculated. 82
34 Sea-ice thickness in the Bering Sea. 83
35 Sea-ice thickness in the Bering Sea. 84
36 Cold pool extent in the EBS as measured during the EBS bottom trawl survey. 86
37 Cold pool extent in the EBS as estimated by the MOM6-NEP hindcast. 87
38 Summer clustering. 88
39 Winter (Nov-Mar) average north-south wind speed anomaly in the Bering Sea, 1949-2026. 89
40 Map showing the section chosen to evaluate along- and cross-shelf wind components. . . 90
41 Along shelf and cross shelf wind components. 91
42 St. Paul air temperature anomalies. 92
43 Average surface and near-bottom temperatures during the spring EcoFOCI survey (2012-2026). 93
44 Maps of near-bottom temperatures during the spring EcoFOCI survey (2012-2026). . . . 94
45 Summer surface and bottom temperatures during the bottom trawl survey, 1982-2026. . 95
46 Maps of bottom temperatures from the EBS and NBS bottom trawl surveys. 96
47 Average surface and near-bottom temperatures during the NBEST survey (2022-2026). . 97
48 Maps of near-bottom temperatures during the NBEST survey (2022-2026). 98

49 Temperature measured at M2 during summer 2026. 99

50 Depth-averaged temperature (°C) at M2. 100

51 Map of longline survey sites on the Bering Sea shelf break, 2009-2026. 101

52 Bottom temperatures from longline surveys in the Bering Sea. 101

53 MHWs in the northern and southeastern Bering Sea since September 2023. 102

54 Cumulative annual SST anomalies. 103

55 Seasonal mean SSTs for each year. 104

56 Map of the eastern Bering Sea domains. 105

57 Mean daily SST and mean weekly bottom temperature by domain. 106

58 Biomass of structural epifauna from the EBS shelf bottom trawl survey, 1982-2026. . . . 108

59 Biomass of structural epifauna by EBS shelf bottom trawl survey strata, 1982-2026. . . 109

60 Biomass of structural epifauna from the NBS bottom trawl survey, 2010-2025. 110

61 Biomass of structural epifauna by NBS bottom trawl survey strata, 2010-2025. 111

62 Surface phosphate and large chlorophyll over the middle domain in the EBS. 113

63 Phosphate, salinity, and MLD as predictors of large chlorophyll. 114

64 Map of regions used for satellite Chl-a analyses. 116

65 Average spring Chl-a concentrations in the eastern Bering Sea. 117

66 Peak spring bloom timing in 4 SEBS regions and at mooring M2. 118

67 Location of Continuous Plankton Recorder data. 120

68 Annual anomalies from Continuous Plankton Recorder data. 121

69 Maps of RZA estimates from the spring 70 m isobath/spring larval survey. 123

70 Timeseries of RZA abundance estimates for spring. 124

71 Maps of RZA estimates from the fall age-0 (BASIS) survey. 125

72 Maps of RZA estimates from the fall 70 m isobath survey. 125

73 Timeseries of RZA abundance estimates for summer/fall. 126

74 Maps of RZA estimates from the northern Bering Sea survey. 127

75 Timeseries of RZA abundance estimates in the northern Bering Sea. 128

76 Lipid content of large copepods and euphausiids in the EBS. 131

77 Relative effect of methodological changes to acoustic data. 133
78 Time series comparison of methodological changes to acoustic data. 136
79 Estimates of average krill density from EBS summer acoustic-trawl surveys. 137
80 Maps of krill backscatter estimates in the EBS summer acoustic-trawl surveys. 138
81 Late summer abundance estimates of euphausiids in the eastern Bering Sea. 141
82 Biomass of jellyfish from the EBS shelf bottom trawl survey, 1982-2026. 143
83 Biomass of jellyfish by EBS shelf bottom trawl survey strata, 1982-2026. 143
84 Biomass of jellyfishes from the NBS bottom trawl survey, 2010-2025. 144
85 Biomass of jellyfishes by NBS bottom trawl survey strata, 2010-2025. 144
86 Biomass of jellyfish in surface waters during late summer, 2004-2026. 146
87 Maps of larval catch for five taxa during spring ichthyoplankton surveys, 2012-2026. . . 148
88 Estimates of mean larval and egg catch from spring ichthyoplankton surveys, 2012-2026. 149
89 Mean condition ratio and location of pollock larvae in the SEBS. 152
90 Mean water temperature in the upper 40m of the water column in the SEBS. 153
91 Mean standard length of pollock larvae in the SEBS. 153
92 Quantitative linkages among variables driving forage fish dynamics in the EBS. 156
93 Ecosystem variables included in the forage fish DSEM. 159
94 eDNA detection frequencies of four fish species in the NBS, 2023-2024. 163
95 Biomass of age-0 pollock in surface waters during late summer, 2003-2026. 166
96 Biomass of age-0 Pacific cod in surface waters during late summer, 2003-2026. 167
97 Map of age-0 pollock distribution in surface waters in 2026. 167
98 Annual mean depth of age-0 pollock in the southeastern Bering Sea. 169
99 Energy density of YOY pollock in the NBS and SEBS. 171
100 Annual length-weight residuals of YOY pollock in the NBS and SEBS. 172
101 Biomass of herring in surface waters during late summer, 2003-2026. 173
102 Biomass of capelin in surface waters during late summer, 2003-2026. 174
103 Southern Bering Sea juvenile salmon survey stations, 2026. 178
104 CPUE of juvenile salmon caught in the southern Bering Sea juvenile salmon survey, 2024-2026. 180

105 Energy density anomalies of juvenile salmon in the NBS, 2002-2026. 182
106 Energy density anomalies of juvenile salmon in the SEBS, 2006-2024. 183
107 Juvenile Chinook salmon abundance estimates in the NBS, 2003-2026. 185
108 Juvenile chum salmon abundance index for the Upper Yukon River (fall), 2003-2026. . . 186
109 Juvenile pink salmon abundance index in the NBS, 2003-2026. 187
110 Annual Bristol Bay sockeye salmon inshore run size 1963-2026. 188
111 Annual Bristol Bay sockeye salmon inshore run size 1963-2026 by fishing district. 190
112 Alaska statewide commercial salmon catches. 192
113 Commercial salmon catches in the eastern Bering Sea. 192
114 2027 outlook for Yukon and Kuskokwim salmon. 200
115 Diet composition of walleye pollock in the eastern Bering Sea. 201
116 Diet composition of Pacific cod in the eastern Bering Sea. 202
117 Daily consumption rate of snow crab by Pacific cod. 202
118 Carapace width of snow crab and *Chionoecetes* spp. in Pacific cod stomachs, 1987-2026. 203
119 Bottom trawl survey strata and station locations in the EBS and NBS. 205
120 Condition of groundfish collected during the EBS bottom trawl survey. 208
121 Length-weight residuals by survey stratum for groundfish species in the EBS. 209
122 Condition of groundfish collected during the NBS bottom trawl survey. 210
123 Length-weight residuals by survey stratum for groundfish species in the NBS. 211
124 Bioenergetic diet indices for juvenile groundfish in the EBS. 216
125 Bioenergetic diet indices for adult groundfish in the EBS. 217
126 Bioenergetic (potential) scope for growth for fish in recent years. 218
127 Total mortality for age-1 pollock, P. cod, and arrowtooth flounder. 221
128 CNRG model estimates of annual predation mortality. 222
129 CNRG model estimates of annual pollock biomass consumed by cannibalistic conspecifics. 223
130 CNRG annual estimates of combined prey biomass consumed by all predators in the model. 223
131 Biomass of benthic fauna from the EBS shelf bottom trawl survey, 1982-2026. 225
132 Biomass of benthic fauna by EBS shelf bottom trawl survey strata, 1982-2026. 226

133 Biomass of benthic fauna from the NBS bottom trawl survey, 2010-2025. 227
134 Biomass of benthic fauna by NBS bottom trawl survey strata, 2010-2025. 228
135 Annual abundance anomalies for key benthic invertebrate functional groups and species. 229
136 Biomass of commercial crab stocks from the bottom trawl survey, 1998-2026. 232
137 Reproductive success of seabirds at St. George and St. Paul Islands, 1996-2026. 235
138 Month-averaged beached bird abundance. 237
139 Species composition of carcasses from August 2025 seabird die-off event. 238
140 Northern fur seal maternal trip duration and female pup mass. 242
141 Northern fur seal prey occurrence. 243
142 Northern fur seal pup production and annual growth rates. 244
143 Reported cetacean strandings Sept 1, 2024 through Sept 30, 2026. 246
144 Reported pinniped strandings Sept 1, 2024 through Sept 30, 2026. 246
145 Mean lifespan of the eastern Bering Sea demersal fish community. 249
146 Mean length of the fish community, 1982-2026. 251
147 Stability of the groundfish biomass in the eastern Bering Sea. 253
148 Maps of summer 2026 modeled bottom water pH. 257
149 Timeseries of July-Sept modeled pH and Ω_{arag} undersaturation indices. 258
150 Timeseries of annualized July-Sept modeled average bottom water Ω_{arag} and pH. 258
151 Timeseries comparison of pH and Ω_{arag} from MOM6-COBALT-NEP10k and ROMS Bering10K. 260
152 Spatial map comparisons of pH from ROMS Bering10K and MOM6-COBALT-NEP10k. 260
153 Timeseries pH and Ω_{arag} undersaturation indices from MOM6-COBALT-NEP10k and ROMS Bering10K. 261
154 Tracks of IFCBs deployed during 2026. 263
155 Tracks of IFCBs deployed in the eastern Bering Sea in 2026. 265
156 Map of *Alexandrium* cell concentrations in the SEBS August 2026. 266
157 Algal toxins and accumulated heat flux. 268
158 Deaths of Northern Fur Seals linked to saxitoxin poisoning. 269
159 Total biomass and percent of total catch biomass of FMP groundfish discards. 271

160 Total biomass of FMP groundfish discarded in the EBS by sector and week, 2021-2026. . 272

161 Total catch of non-target species in EBS groundfish fisheries (2011-2025). 275

162 Estimated seabird bycatch by region, 2016-2025. 277

163 Estimated albatross bycatch by region, 2016-2025. 280

164 Fish Stock Sustainability Index for Alaska from 2006 through 2026. 285

165 Fish Stock Sustainability Index for the BSAI from 2006 through 2026. 286

166 The IEA (integrated ecosystem assessment) process. 315

Ecosystem Indicators

Noteworthy Topics

Here we present items that are new or noteworthy and of potential interest to fisheries managers.

Introducing MOM6 to the Alaska regional modeling framework

Between 2024 and 2025, the regional modeling team at NOAA Fisheries Alaska Fisheries Science Center and OAR Pacific Marine Environmental Laboratory transitioned our operational regional model work from our previous Bering Sea-only Bering10K ROMS model (Kearney et al., 2020) to the new Modular Ocean Model version 6 Northeast Pacific (MOM6-COBALT-NEP10k) model (Drenkard et al., 2025). This transition is part of the Changing Ecosystem and Fisheries Initiative (CEFI), which aims to provide operational regional model support for fisheries management across US coastal waters.

This document provides some context for how this transition may impact model-informed products presented to fisheries management decision-makers. It highlights key differences between the ROMS Bering10K and MOM6-NEP10k models in the Bering Sea region. It also provides a baseline assessment of the MOM6-NEP model skill across all three Alaska management regions relative to the groundfish survey datasets that are commonly used in stock assessments and supporting material (e.g., ESRs, ESPs, Risk Tables).

Model Configurations

Model Frameworks

The Regional Ocean Modeling System (ROMS) and Modular Ocean Model version 6 (MOM6) are two different numerical ocean models. Both models are mature, widely-used primitive equation models that simulate the physical dynamics of the ocean. Each model has its own strengths and weaknesses; the current migration to MOM6 is primarily motivated by pragmatic reasons. The MOM6 framework is not inherently better than ROMS, but the cohesive, national NOAA-wide support associated with the CEFI program supports more rapid and comprehensive development, which in turn produces more skillful and stable model implementations than our previous region-specific efforts.

Spatial configurations

The MOM6-NEP domain (Figure 4a, blue) covers the northeast Pacific region, extending from the Chukchi Sea in the north to the Baja Peninsula in the south, and is designed to support marine resource management across the Bering Sea and Aleutian Islands, Gulf of Alaska, and California Current ecosystems. This larger spatial extent is the most obvious advantage that this newer model offers over the previously-used ROMS Bering10K model (Figure 4a, red), which was developed with a focus on the Bering Sea region only[5]. By spanning all three Alaska ecosystems, as well as coastal ecosystems along the west coast of the US and Canada, the model is able to cohesively simulate the relevant environmental processes throughout the region and model transboundary processes across ecosystems, management regions, and national boundaries.

The MOM6-NEP10k and ROMS Bering10K model grids share similar 10-km horizontal resolutions, but their vertical configurations differ significantly. The ROMS model used a terrain-following (sigma) coordinate system with 30 vertical layers. While well-suited to resolving coastal dynamics across the shelf, this coordinate system suffered from one key weakness: it requires bathymetric smoothing to avoid steep topological slopes that could otherwise produce false pressure gradients and spurious circulation patterns. The bathymetric smoothing primarily affected the outer shelf region in the Bering Sea, which was poorly represented within the Bering10K model. The MOM6 model includes a novel internal vertical coordinate scheme that allows one to use a more flexible set of coordinates while resolving realistic bathymetry across shelf, slope, and basin regions. The MOM6-NEP implementation uses 75 z* vertical levels (i.e., near-constant geopotential surfaces that deform slightly in response to dynamic sea surface height), with layer thickness ranging from 2 m at the surface to 250 m at depth. The resulting differences in bathymetry and vertical resolution are depicted in Figures 4b and 4c.

Temporal Coverage

The ROMS Bering10K simulation[6] that was presented for semi-operational use from 2020-2024 simulated the period of 1970-2024. The MOM6-NEP10k model covers a shorter timespan, running from 1993 to the present. This temporal coverage reflects the extent of the reanalysis datasets that are used to drive the simulations.

No single reanalysis dataset covers the entirety of the modern groundfish survey record in Alaska (1982-present). For the ROMS Bering10k hindcast, we opted to concatenate three different forcing products to achieve a longer "continuous" simulation. This was possible due to the focus on a shallow shelf region that is relatively isolated from the model's oceanic boundaries, and we attempted to minimize the influence of the transition by placing the most disruptive shift in the mid-1990's, a period with less prominent sub-decadal variability. But we note that evidence of the forcing dataset transitions were noticeable in certain analyses, e.g. a small drift in carbonate system values and step-like discontinuities in deep basin nutrients. Given its larger spatial footprint and cross-ecosystem focus, those transitional artifacts would have been more prominent and problematic in the MOM6-NEP10k model should a similar stitching-together of forcing be attempted; therefore, the regional MOM6 hindcast simulations are currently limited to the extent of the parent ocean-forcing dataset (1993-present, Table 1). We anticipate an alternative MOM6-NEP10k simulation to be available in the coming year that may be able to fill the pre-1991 period that can be of interest in the Alaska region.

[5] A separate ROMS implementation for the northeast Pacific was also developed and used for Gulf of Alaska-focused simulations. However, this model implementation was never updated operationally to inform the GOA ESR, so we do not include it in this comparison.

[6] In public datasets, this is nicknamed the B10K-K20P19_CORECFS simulation, reflecting the primary citations documenting its source code (Kearney et al., 2020; Pilcher et al., 2019) and the forcing datasets it used (CORE/CFSR/CFSv2-OA concatenation).

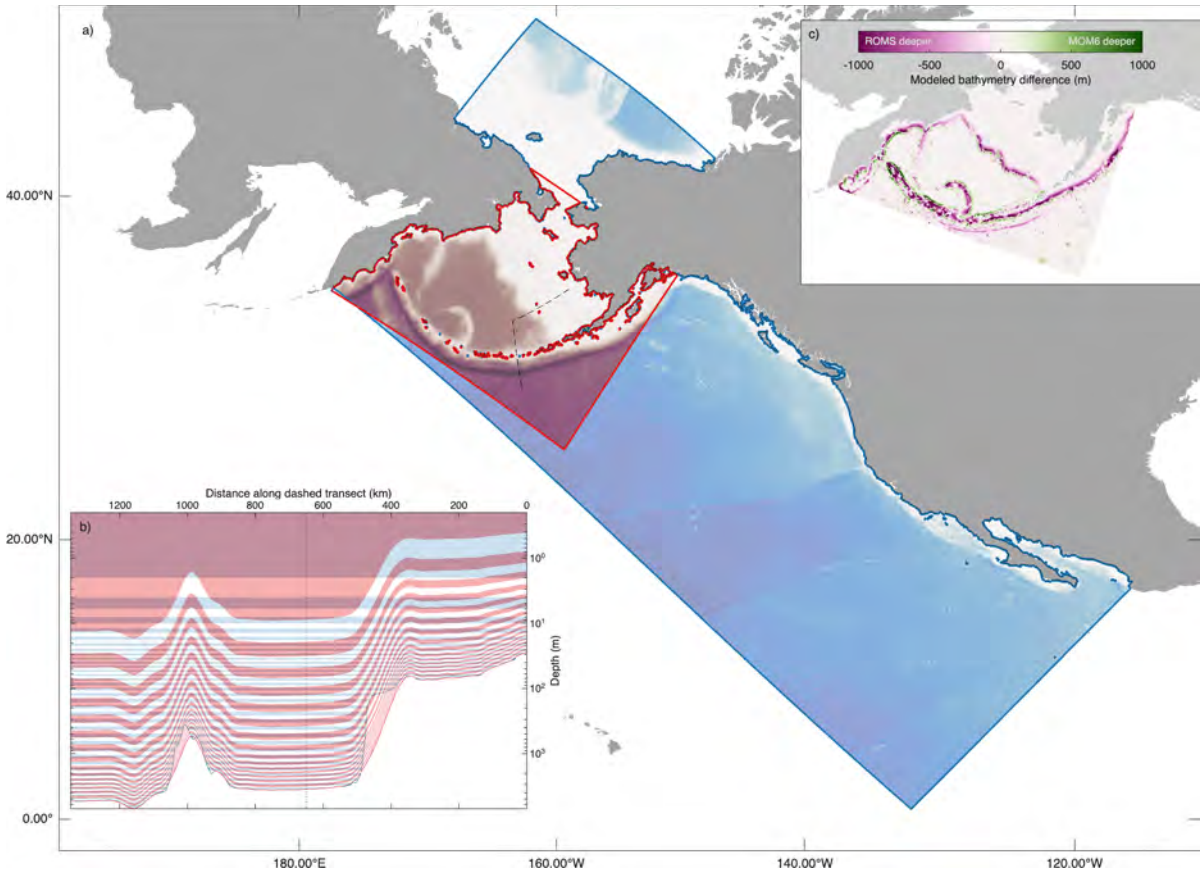


Figure 4: a) Map of the MOM6-NEP (blue) and ROMS Bering 10K (red) model domains extent and bathymetry, b) depth layers, depicted in logarithmic vertical space, for each model along the dashed transect in the map; vertical dashed line indicates the location of the transect angle, and c) bathymetry differences between the two models.

Biogeochemistry

The ROMS and MOM6 regional models each include their own biogeochemical components to represent nutrient cycling and plankton dynamics. While this report focuses on the physical dynamics within the models, Figure 5 depicts the high-level differences between the two models' state variables. Preliminary validation of biogeochemical tracers suggests that neither ROMS' BEST_NPZ model nor MOM6's COBALTv3 clearly outperforms the other in the subarctic regions. The COBALT model skillfully simulates first-order patterns in primary and secondary production throughout the domain but may need further refinement to fully capture subarctic dynamics of interest, such as the sharp onset of the diatom-driven spring bloom in the Bering Sea. The MOM6-COBALT biogeochemical configuration is an area of active development and we expect continued progress over the next several releases.

[7]The CFSv2 operational analysis data product extends beyond this point, but near-real-time public distribution ceased in early 2025, preventing its use for near-real-time updates of our model.

Table 1: Primary atmospheric and ocean forcing datasets used for Alaska region hindcasts.

Abbreviation	**Full name**	**Reference**	**Component**	**Extent**	**Used for**
COREv2	Common Ocean Reference Experiment, version 2	Large and Yeager, 2009	atmosphere	1948-2009	ROMS Bering10K, 1970-1994
CFSR	Climate Forecast System Reanalysis	Saha et al., 2010	atmosphere, ocean	1979-March 2011	ROMS Bering10K, 1995-March 2011
CFSv2-OA	Climate Forecast System Operational Analysis	Saha et al., 2014	atmosphere, ocean	April 2011-2024[7]	ROMS Bering10K, April 2011-2024
ERA5	European Centre for Medium-Range Weather Forecasts Reanalysis 5	Hersbach et al., 2020	atmosphere	1940-present	MOM6-NEP10k, 1993-present
GLORYS12	1/12° Global Ocean Physics Reanalysis	Lellouche et al., 2021	ocean	1993-present	MOM6-NEP10k, 1993-present

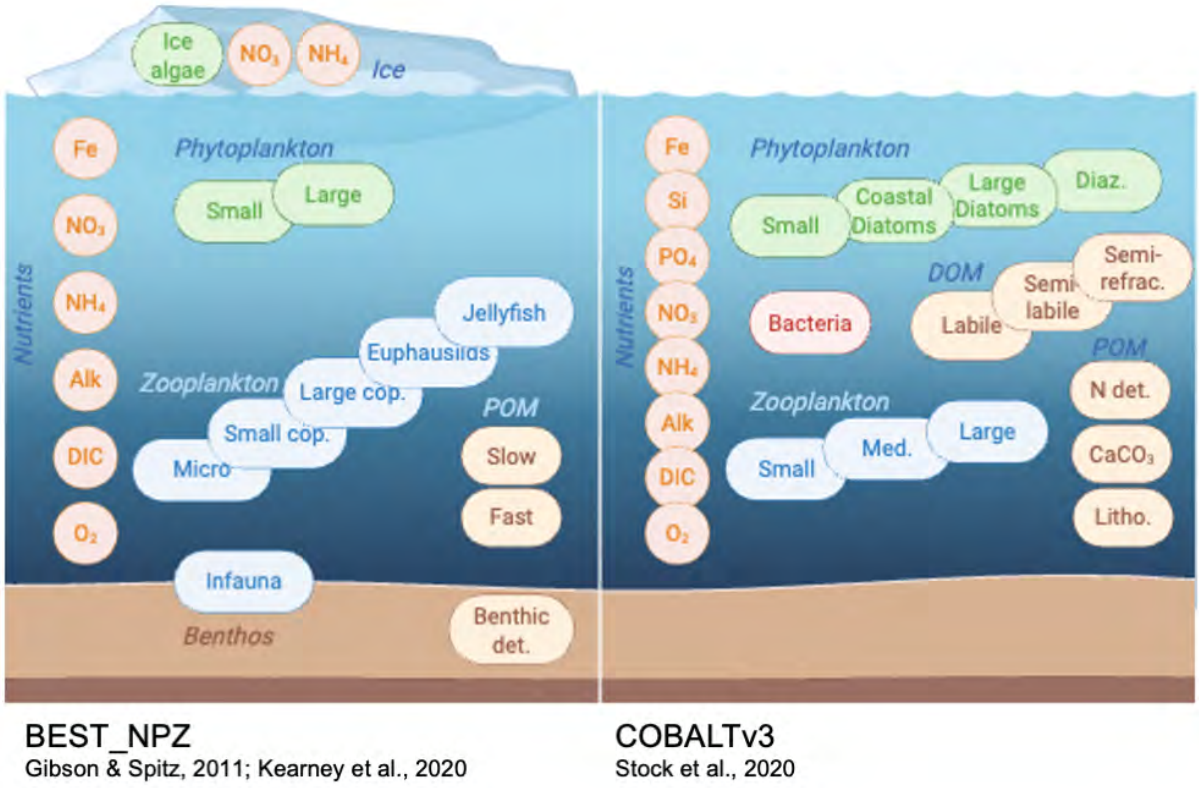


Figure 5: Schematic of state variables in the BEST_NPZ and COBALTv3 biogeochemical models.

Skill Assessment Versus Survey: Surface and Bottom Temperature

The temperature data collected during the annual Bering Sea and biannual northern Bering Sea, Gulf of Alaska, and Aleutian Island groundfish surveys serve as our primary model validation datasets. They provide both spatial and temporal (interannual across summer) resolution of surface and bottom temperature, and are a primary data source for many assessment calculations, so confirming that a model is able to capture similar patterns in environmental variability is a first step to using regional models in this context.

For these skill assessments, we matched each survey datapoint with the closest model output point in space and time. We then calculated a variety of skill metrics (Table 2) that assess how well each of the models capture the spatiotemporal variability of temperature seen in the surveys. For this report, we assess skill using the stratified sampling polygon geometry used for the surveys themselves; this spatial scale provides a high-level overview of performance across broad regions. Data points were grouped based on the strata polygon in which they were collected, then statistics were applied to each group.

Table 2: Skill metrics used in this study. The variables r_i and m_i indicate observation and model points, respectively; $\bar{r}$ and $\bar{m}$ are means over the grouping and σ_r and σ_m are standard deviations; n is the total number of points in the grouping.

Metric	**Definition**	**Interpretation**
Bias	$\bar{m} - \bar{r}$	Measures offset in the mean.
Centered root mean squared difference	$\sqrt{\frac{1}{n}\sum_{i=1}^{n}\left[(m_i - \bar{m}) - (r_i - \bar{r})\right]^2}$	Also referred to as unbiased RMSD, measures difference between unbiased model and observation.
Linear correlation coefficient	$\frac{\sum_{i=1}^{n}(m_i - \bar{m})(r_i - \bar{r})}{\sigma_m \sigma_r}$	Range: -1 to 1, measures covariability between model and observations, but not bias.
Model efficiency	$\frac{\sum_{i=1}^{n}(r_i - \bar{r})^2 - \sum_{i=1}^{n}(m_i - r_i)^2}{\sum_{i=1}^{n}(r_i - \bar{r})^2}$	Measures model skill relative to mean of the observations. Near 1 indicates high skill, $0 =$ same skill as mean of observations, < 0 worse than mean of observations.
Normalized standard deviation	$\frac{\sigma_m}{\sigma_r}$	Measures under- (< 1) or over- (> 1) estimation of variability.

In the Bering Sea region, the MOM6-NEP hindcast simulation (Figures 6 and 7) performs more skillfully than the Bering10K ROMS hindcast simulation (Figures 8 and 9) across almost all quantitative measures. Patterns of bias in bottom temperature are similar between the two models. Both models tend to run a little cool in the south and warm in the north, with a shoreward bias in the placement of the inner front that results in a warm bias at the surface and a cool bias at depth for the inner domain region. Surface temperature bias, however, is much improved throughout the rest of the southeastern shelf region in MOM6-NEP relative to Bering10K ROMS, primarily reflecting better resolution of mixed layer depth (which was consistently too shallow in the ROMS configuration, trapping heat in a too-thin layer and leading to a positive bias) and seasonal stratification and destratification processes. MOM6-NEP model efficiency is high across the southeastern shelf, suggesting skillful replication of interannual temperature variability, though a normalized standard deviation of 0.85 in bottom temperature shows it underestimates the amplitude of interannual variability at depth. We note improvement in skill metrics along the outer shelf region in MOM6-NEP relative to ROMS Bering10K due to MOM6-NEP's significantly more realistic bathymetry. There are still small regions along the slope, in the vicinity of Zemchug and Pribilof Canyons, where year-to-year variability is poorly captured, but the majority of the shelf is well-characterized in this regard.

Northern Bering Sea statistics should be considered with caution since the region has only been surveyed in 7 years total, with one of those years (2023) at a lower spatial density and one (2025) outside the ROMS Bering10K temporal limits. We present these statistics here but are intentionally avoiding any further interpretation of the results at this time.

In the Gulf of Alaska and Aleutian Islands, the MOM6-NEP configuration clearly outperforms the ROMS Bering10K hindcast, but that is to be expected given that the ROMS model was never intended to be used in these regions and therefore little effort was made to reduce boundary artifacts outside the Bering Sea region. The MOM6-NEP model shows a cool bias in bottom temperature and a warm bias in surface temperature, possibly stemming from an overestimation of sea surface height variability that could impact downwelling intensity. Model efficiency for bottom temperature in the southeast Gulf of Alaska and western Aleutian Islands is negative, but this primarily reflects the low interannual variability in these regions rather than a systematic model deficiency. Further model refinement is in progress to better capture patterns of flow through the Aleutian Passes and their impact on advection and mixing. Given the scale of topological variability in this region relative to the 10-km model resolution, we caution against overinterpretation of the skill metrics in this region.

Contributed by
Kelly Kearney
Alaska Fisheries Science Center, NOAA Fisheries, Seattle, WA
Wei Cheng
NOAA/Pacific Marine Environmental Laboratory, Seattle, WA

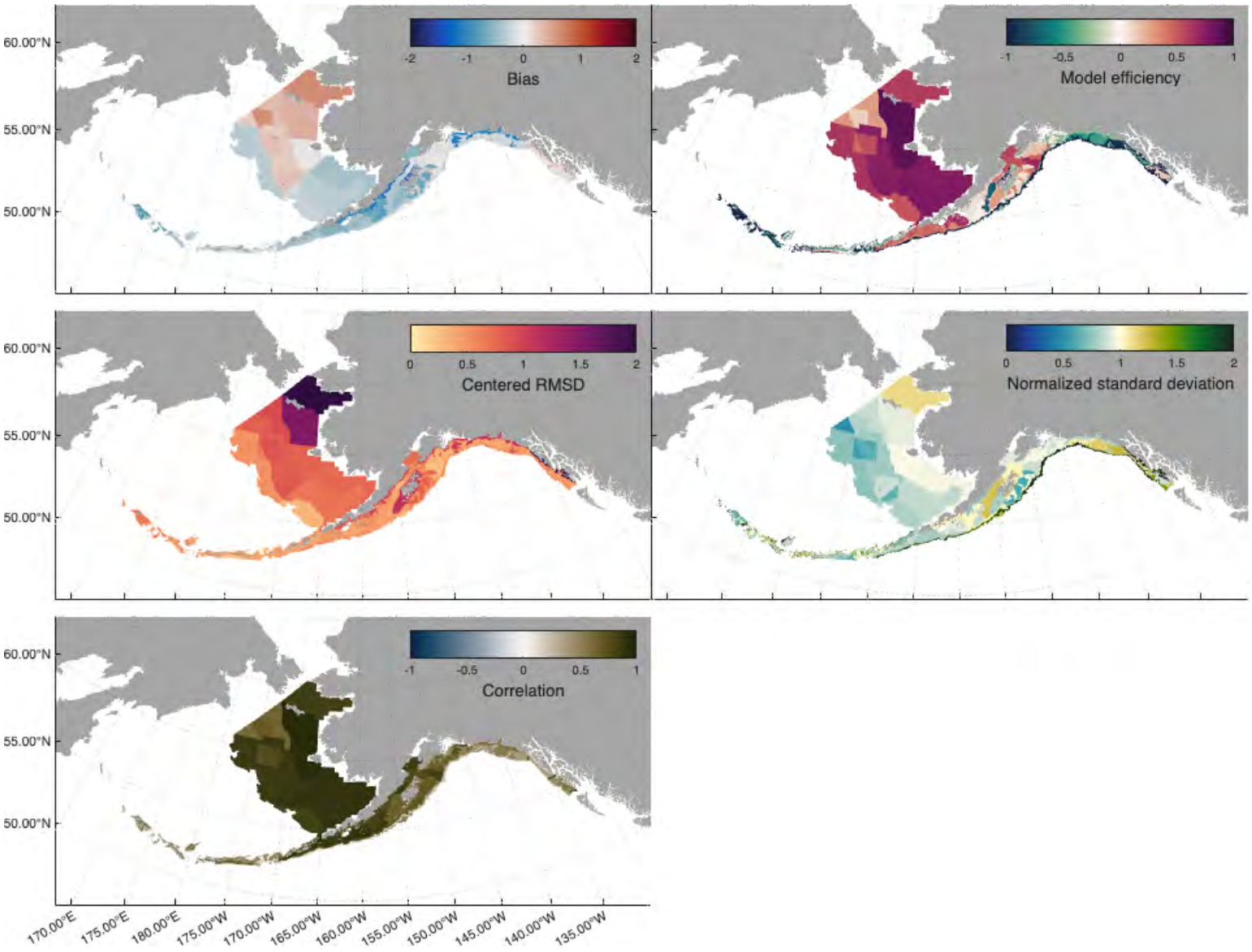


Figure 6: Map of skill metrics for the MOM6-NEP hindcast simulation bottom temperature.

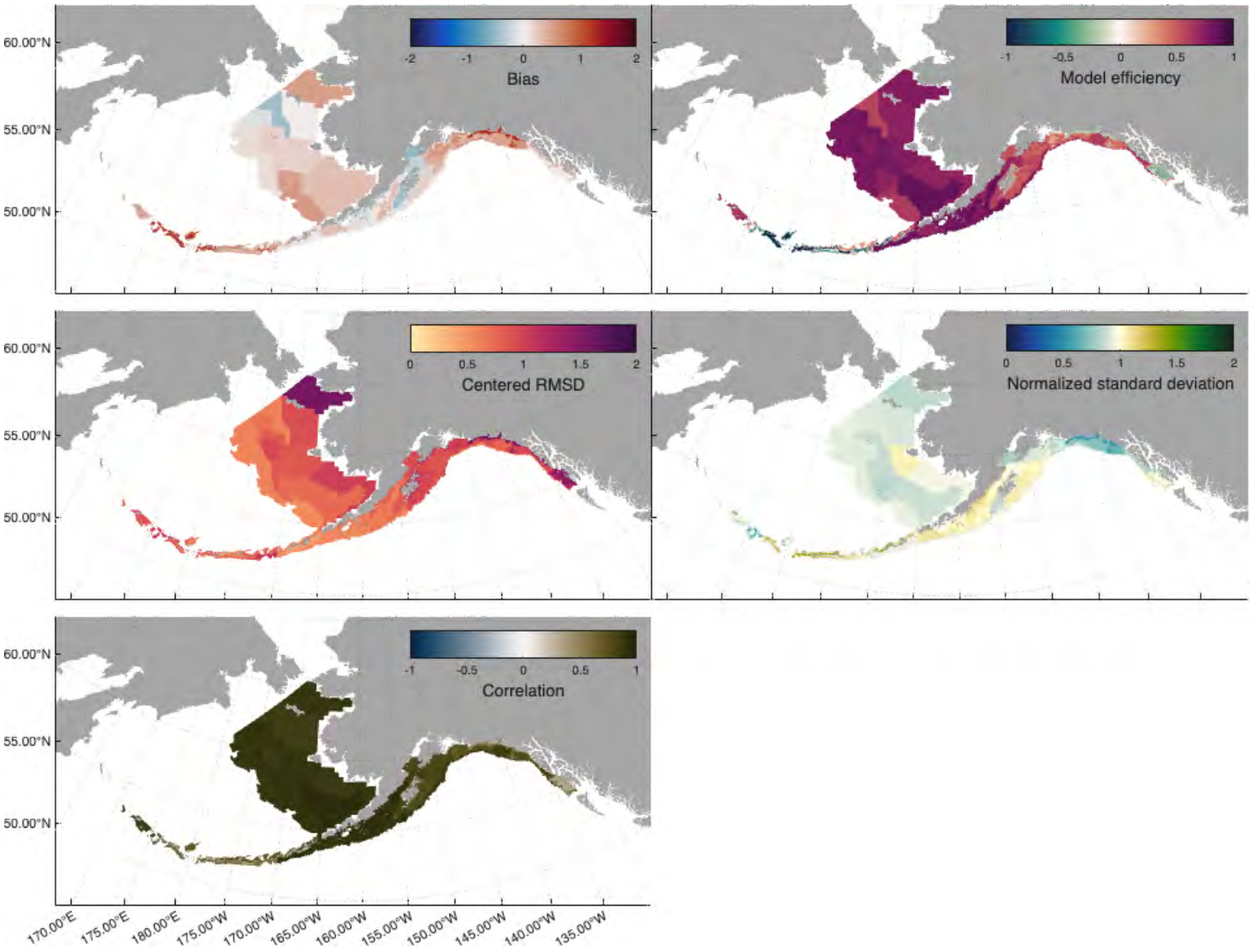


Figure 7: Map of skill metrics for the MOM6-NEP hindcast simulation surface temperature.

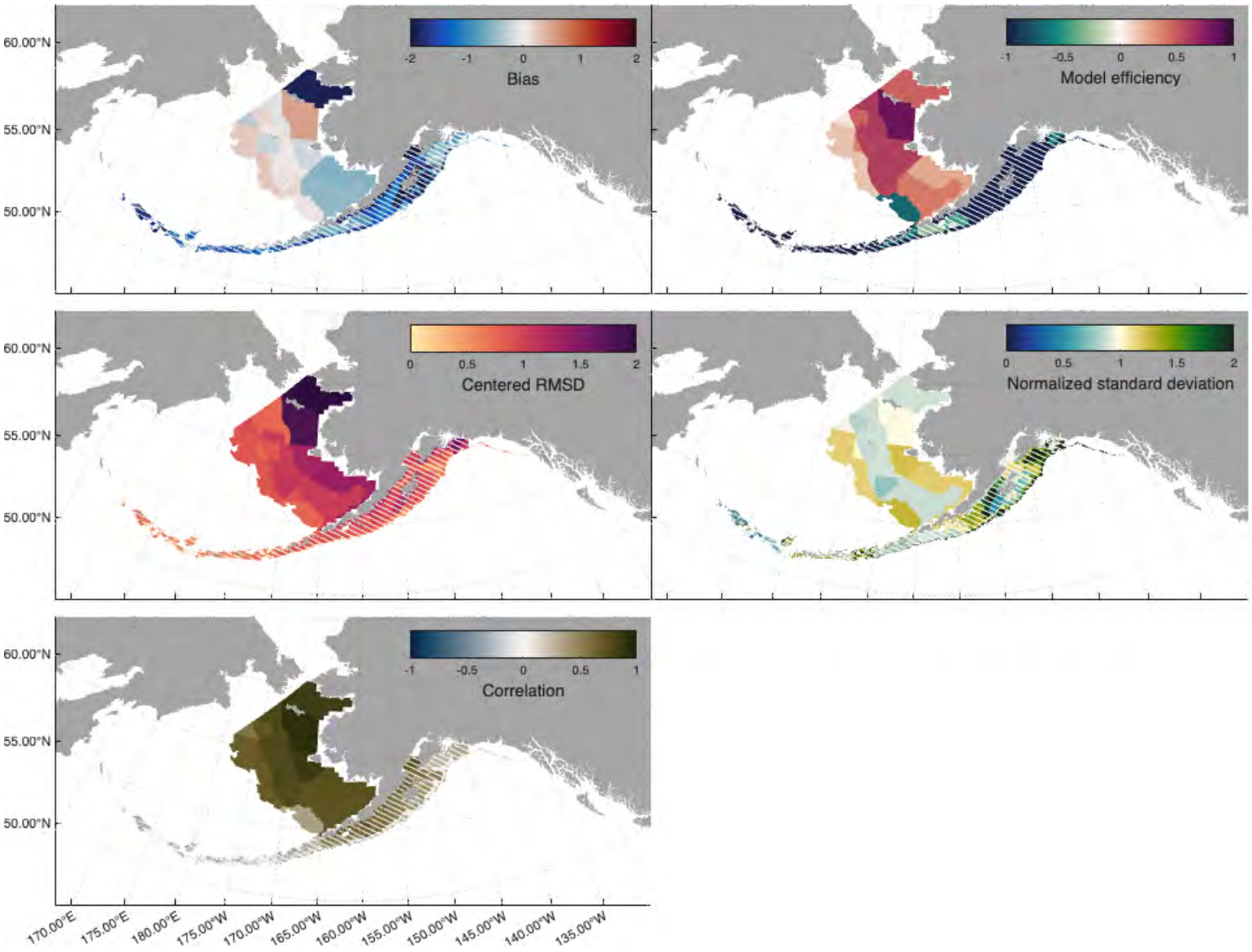


Figure 8: Map of skill metrics for the ROMS Bering10K hindcast simulation bottom temperature. White-hatched regions indicate portions of the model domain that were outside the target region for which the model was developed (and thus not expected to capture realistic variation in water properties).

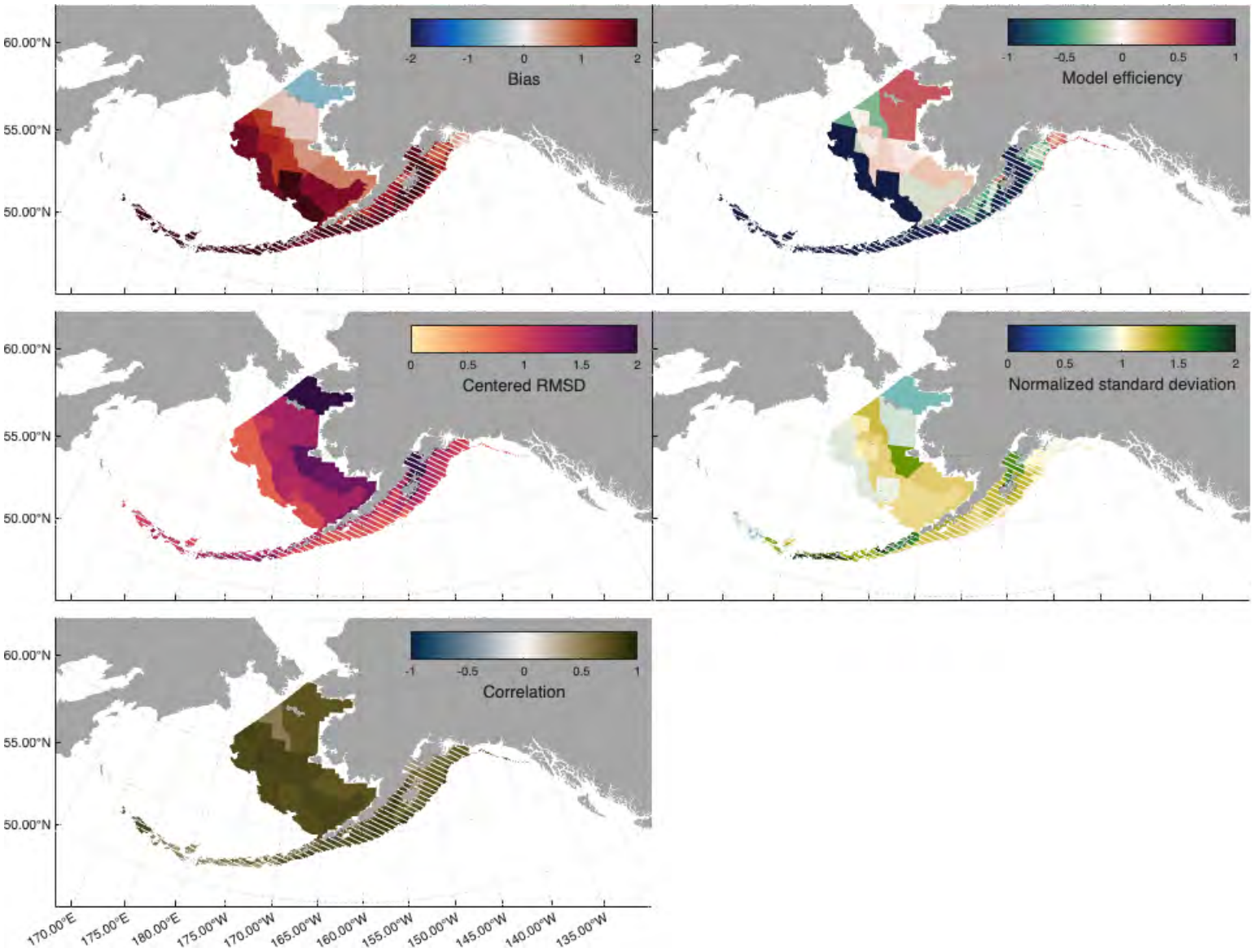


Figure 9: Map of skill metrics for the ROMS Bering10K hindcast simulation surface temperature. White-hatched regions indicate portions of the model domain that were outside the target region for which the model was developed (and thus not expected to capture realistic variation in water properties).

Eastern Bering Sea Walleye Pollock Early Survival Pathways

Background

Juvenile walleye pollock are important prey for fish, marine mammals, and seabirds across the eastern Bering Sea (EBS) ecosystem. Tracking age-0 and age-1 abundance and the processes connecting these stages helps interpret changes in forage availability for the Ecosystem Status Report. Understanding early-life survival pathways informs recruitment dynamics and may help explain recruitment variation and improve assessment estimates and forecasts, providing a foundation for development of an Ecosystem and Socioeconomic Profile (ESP) and for exploring links between ecosystem processes and assessment parameters using dynamic structural equation models (DSEMs). Responding to a December 2024 request by the Scientific and Statistical Committee (SSC)[8], this effort supports (1) evaluation of hypotheses about age-0 survival and forage availability and (2) development of a broader ESP and future ecosystem-linked assessment research.

Causal Development & Application Framework

Conceptual Model & Directed Acyclic Graph (DAG) Construction

The development of the Directed Acyclic Graph (DAG) for juvenile pollock relies on decades of process studies conducted by researchers at NOAA Fisheries Alaska Fisheries Science Center (AFSC) and an extensive body of published literature focused on understanding early life history and recruitment dynamics of age-0 pollock in the EBS. In January 2025, AFSC convened a dedicated Pollock Workshop bringing together subject-matter experts (SMEs) to map out key drivers influencing EBS recruitment (Monnahan et al., 2026; Figure 10). While the workshop produced a broad conceptual model of recruitment, the DAG developed here draws on a subset of that model, focusing on the hypothesized mechanisms affecting survival to age 1 (circled portion of conceptual diagram in Figure 10).

Standardized Framework & Subject Matter Expert Integration

In 2025-2026, the AFSC Ecosystem Refresh Team (J. Keister, L. Rogers, E. Siddon, R. Suryan, and S. Zador) developed a framework that maps ecosystem metrics (e.g., temperature, fish condition, predator abundance) against time-varying parameters in single-species stock assessments (e.g., growth, mortality, recruitment) (Table 3) to identify ecosystem information needed to understand each stock-specific demographic process. The framework organizes subject-matter expertise and can serve as the starting point for multiple management products (i.e., Risk Tables, ESPs, ecosystem-linked assessments). This standardized framework provides a structure for reviewing expert knowledge about environmental and biological processes, mechanistic hypotheses, and empirical data availability. The framework also draws on methods developed through the AFSC causal modeling reading group and workshop series, which aim to establish a standardized process across AFSC for applying quantitative causal modeling tools to managed species.

[8] https://meetings.npfmc.org/CommentReview/DownloadFile?p=dc61bc73-be5c-492f-89b3-a723ea14311d.pdf&fileName=SSC%20Report%20Dec%202024_FINAL.pdf

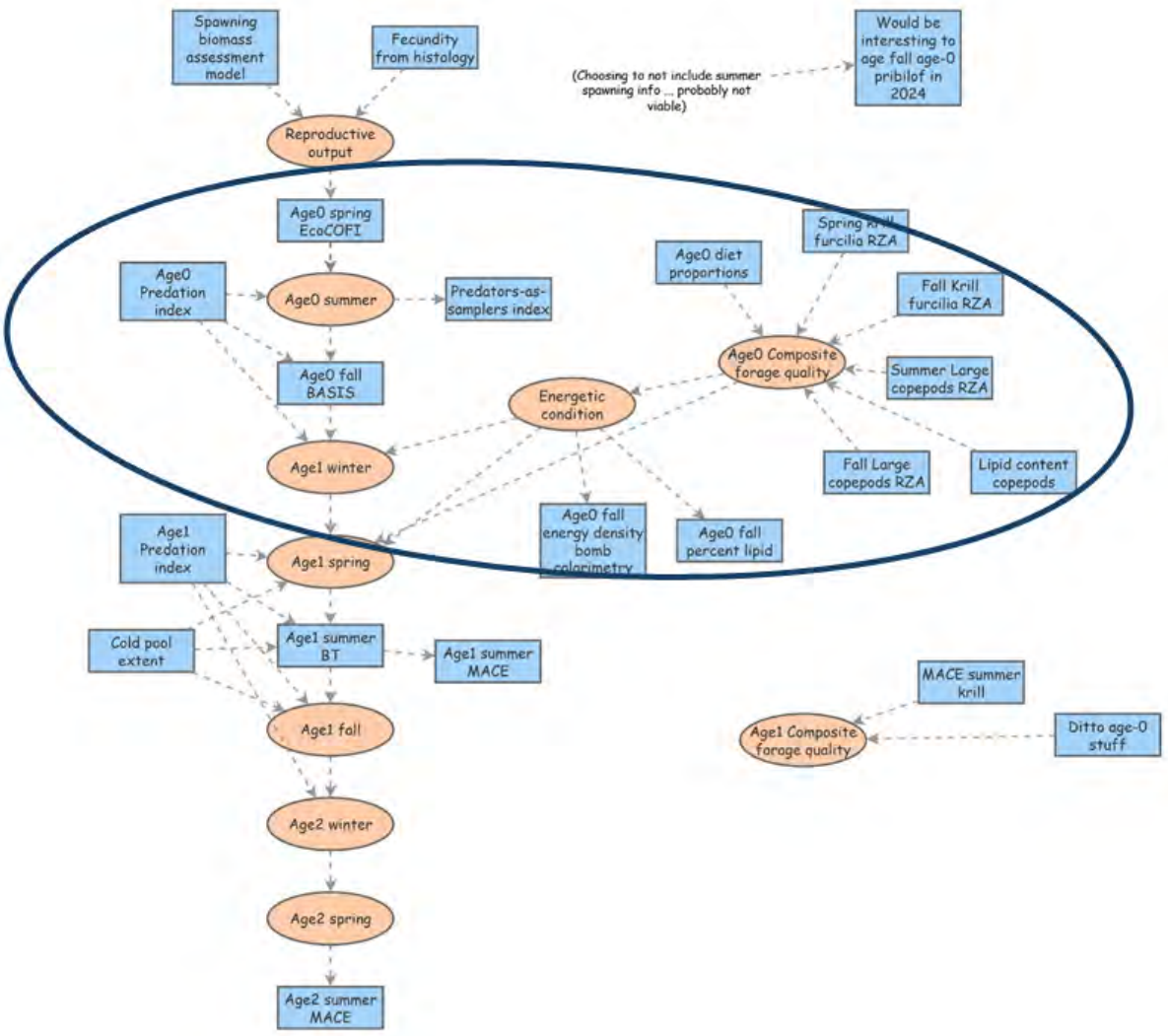


Figure 10: Pollock Workshop conceptual model building: Recruitment in the Bering Sea. AFSC Participants: A. Andrews, L. Copeman, L. Domke, K. Holsman, D. Kimmel, M. Levine, S. Neidetcher, and J. Thorson. Circled portion of full conceptual diagram addressed in this Early Survival Pathways model.

Dual Analytical Applications

The resulting DAG framework supports two complementary applications under development within fisheries management:

1. External Application (e.g., ESRs): Serves as an external synthesis tool to track ecosystem-level dynamics, evaluating how early-life processes relate to age-0 & 1 abundance and prey availability for fish, seabirds, and marine mammals.

2. Internal Application (i.e., Stock Assessments): Functions internally within the stock assessment model – specifically integrating Dynamic Structural Equation Modeling (DSEM) – to explicitly evaluate whether incorporating hypothesized environmental and biological linkages improves estimates, forecasts, and uncertainty characterization in specific stock assessment model parameters.

Table 3: Standardized ecosystem framework developed to prioritize ecosystem science for use in ecosystem-based fisheries management (EBFM) at the Alaska Fisheries Science Center.

	Growth	Mortality	Catchability	Recruitment	Distribution
Temperature					
Adult fish condition					
Adult fish diet					
Prey abundance and quality					
Age-0 (-1, -2) abundance					
Predator abundance					
Competitor abundance					

In this external application of DSEM, the specified structure is based on the following design choices (see the mechanism table for more information):

1. We include the physical variable of sea ice ("Sea ice extent") and hypothesize that greater sea ice extent contributes to a larger cold pool extent ("Cold Pool Extent"; Stabeno and Bell, 2019), cooler sea surface temperatures ("Sea Surface Temperature"; Hunt et al., 2002), and a lower proportion of open-water-associated phytoplankton blooms ("Percent Open Water Blooms"; Nielsen et al., 2024; Eisner et al., 2016; Sigler et al., 2014).

2. A higher proportion of ice-associated blooms (lower "Percent Open Water Blooms") is hypothesized to result in a higher abundance of pelagic secondary consumers in the summer and fall, in particular large lipid-rich copepods ("Summer Large Copepods "; Kimmel et al., 2018; Coyle et al., 2008).

3. Higher abundances of pelagic secondary consumers are hypothesized to contribute to higher juvenile (age-0) pollock energy density ("Energy Density"; Heintz et al., 2013; Eisner et al., 2020).

4. Higher juvenile (age-0) pollock energy density is hypothesized to result in higher overwinter survival and age-1 abundance ("Age 1 Pollock"; Siddon et al., 2013).

5. We include several sources of predation mortality (e.g., "Adult Pollock", "Pacific Cod", "Arrowtooth Flounder") and hypothesize that higher predator abundances reduce survival and abundance of age-1 pollock (Mueter and Litzow, 2008; Holsman et al., 2024; Hunt Jr et al., 2025).

We fit this model by including links from physical drivers (sea ice extent, SST) to bloom type (percent open water blooms) to zooplankton indices (spring small copepods, summer large copepods, and euphausiids) as indicators of secondary productivity and prey availability for age-0 pollock. All measures of secondary productivity were linked through juvenile (age-0) pollock energy density as a hypothesized component of the pathway to age-1 abundance (Figure 11).

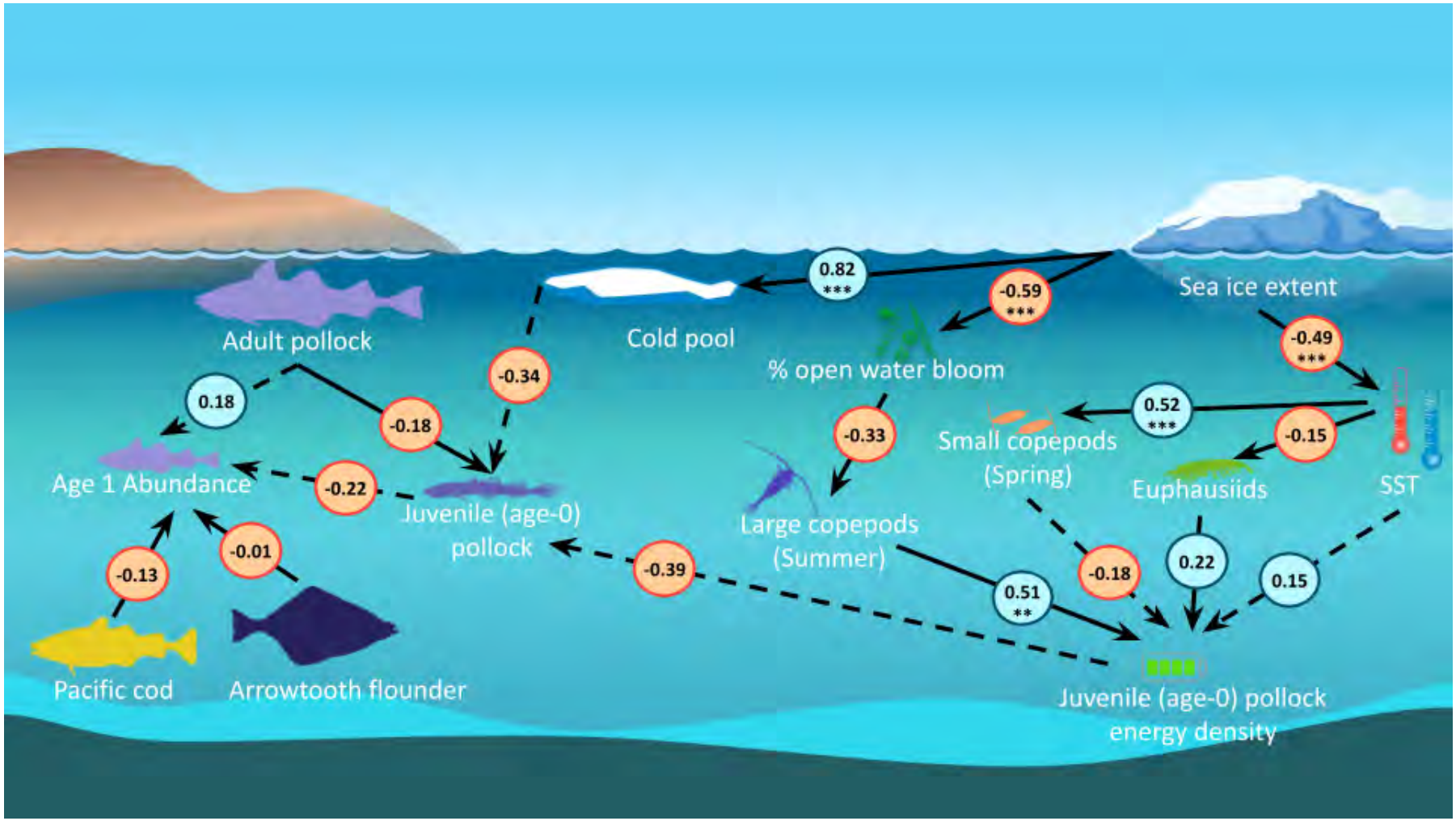


Figure 11: A path diagram showing estimated quantitative linkages among ecosystem variables. Arrows correspond to hypothesized relationships, where an arrow pointing from X to Y indicates that a change in X is estimated to cause a change in Y. For each listed coefficient we include the significance value with stars where * <0.1, ** <0.05, *** <0.01. The sign of the causal relationship with dashed lines is opposite from our *a priori* expectation (see hypothesized mechanism table below). We also estimated additional independent and identically distributed (IID) and first-order autocorrelation for each variable. Figure courtesy of Lia Domke, AFSC.

Results

We fit the full Dynamic Structural Equation Model (DSEM) for pollock alongside alternative model configurations and evaluated the models using Akaike information criterion (AIC) and reduction in variance. A staged model evaluation indicated that the lowest AIC occurred prior to incorporating the final hypothesized linkages leading to age-1 pollock – specifically, excluding the direct pathways from juvenile (age-0) pollock energy density to age-1 and links representing predation pressure on age-1 fish. This pattern suggests that, while the current DAG provides stronger support for some environmental and lower-trophic links associated with age-0 pollock dynamics, data gaps or relationships between the age-0 and age-1 stages remain unresolved in the model.

In terms of model performance, the fitted framework yielded a 52% variance reduction relative to an Independent and Identically Distributed (IID) model for age-0 juveniles. Variance reduction for age-1 pollock was 7%. In Leave-Future-Out (LFO) cross-validation, the model generated larger forecast errors than an autoregressive (AR1) model for age-0 pollock and slightly larger errors than both IID and AR1 models for age-1 pollock. Possible contributors to these forecast errors include limited empirical observations of age-0 juveniles and the influence of the large 2018 year class.

Despite these predictive limitations, model estimates of age-1 pollock abundance indicate slightly elevated abundance in the most recent years over average recruitment which is used in the stock assessment model (Ianelli et al., 2024). Specifically, estimated age-1 abundance is 8% above average in 2025 and 4.5% above average in 2026.

Discussion

This effort represents a first step toward evaluating hypotheses about age-0 survival and forage availability for the ecosystem. The DAG was developed using subject matter expertise, after which data acquisition and analysis were initiated. The next step will be to share model results with SMEs and refine the DAG and review the suitability of the source series.

Some fitted coefficients were consistent with a priori hypotheses; others differed in sign or had weak statistical support. Specifically, (i) links between sea ice extent and cold pool, percent open water blooms, and sea surface temperature, (ii) the link between sea surface temperature and spring small copepods, and (iii) the link between summer large copepods and energy density met the nominal p-value thresholds shown in Figure 11. The first set of links represent physical and biological oceanographic conditions driven by sea ice extent. Sea ice is a known determinant of EBS shelf dynamics. The second link supports the physical oceanographic connection between winter sea ice conditions and a metric of spring secondary productivity. Finally, the third link is consistent with process research suggesting that the abundance of large, lipid-rich copepods in summer and fall contributes to higher energy density of age-0 pollock (e.g., Eisner et al., 2020).

Several of the model results were either inconclusive or contrary to expectations. Most notably, (i) the link between energy density and juvenile (age-0) pollock and (ii) links driving age-1 pollock abundance. It was hypothesized that higher energy density would result in higher abundance of juvenile (age-0) pollock (i.e., positive direction; better condition would lead to higher survival), but the model estimated a negative relationship where higher energy density is associated with lower age-0 biomass. Similarly, it was hypothesized that a higher abundance of adult pollock would have a negative effect on age-1 abundance through cannibalism, but the model estimated a positive relationship. Lastly, it was hypothesized that a higher abundance of juvenile (age-0) pollock would result in a higher abundance of age-1 pollock the following year (i.e., positive direction; lag=1), but the model estimated a negative relationship where a higher age-0 biomass was associated with lower age-1 abundance.

Several explanations warrant evaluation for these unexpected results, including (i) data limitations, such as changes in underlying survey extents, (ii) short available time series (Figure 12), and (iii) missing or misspecified interactions (for example, accounting for density dependence or shifts in spatial overlap).

Implications
Age-0 pollock are an important component of the EBS food web, transferring energy from lower trophic levels directly to predatory groundfish, seabirds, and marine mammals. Their abundance, size, energetic condition, and spatial availability can influence survival, reproductive success, and foraging dynamics across these higher-trophic predators throughout the shelf ecosystem.

Data sources
List of all data sources available for evaluation in the external DSEM approach. Several indicators were initially removed from the full DAG due to convergence issues and low confidence in the hypothesized relationship (e.g., jellyfish, bottom temperature, chlorophyll-a, small copepods summer, large copepods spring, larval pollock abundance).
*indicates the data source is also a Report Card indicator, with further details available in the 'Description of the Report Card indicators' on p. 320

***Sea Ice Extent:** The Bering Sea ice year is defined as 1 August–31 July. Annual sea ice extent was calculated using NSIDC monthly sea ice concentration (SIC) data at a 25 km resolution with a 0.15 concentration threshold. Data courtesy of Sunny Hospital (shospital@nexusdatasolutions.com)

***Proportion of Open Water Blooms:** The timing of ice retreat and bloom peak was used to estimate bloom type, which differentiates between open-water blooms (i.e., ice retreat occurred $\geq$21 days prior to bloom peak) and ice-associated blooms (i.e., ice retreat occurred $<$21 days prior to bloom peak) for each year (Perrette et al., 2011). Timing of sea-ice retreat was determined as the date when ice coverage remained below 15% based on the 15-day running mean of the daily sea-ice fraction data. Bloom peak timing was estimated using standardized merged ocean color satellite data of 8-day satellite chlorophyll-a (chl-a, μg/L) at a 4 km-resolution from the Hermes GlobColour website covering the years 1998-2026. Data courtesy of Matt Callahan (Matt.Callahan@noaa.gov)

***Cold Pool Extent:** Area of the cold pool in the eastern Bering Sea (EBS) shelf bottom trawl survey area (including strata 82 and 90) from 1982-2026. The cold pool is defined as the area of the EBS continental shelf with bottom temperature $<$2°C, in square kilometers (km^2). Data courtesy of Sean Rohan (Sean.Rohan@noaa.gov)

Sea Surface Temperature and Bottom Temperature: Annual mean surface and bottom temperatures were calculated from spatially interpolated measurements collected during NOAA-AFSC's summer bottom trawl surveys of the EBS shelf (1982-2026, except 2020). Data courtesy of Sean Rohan (Sean.Rohan@noaa.gov)

Chlorophyll-a: Annual estimates of phytoplankton biomass in the surface layer of the south middle shelf region (Figure 64) were calculated as the average spring (Apr-Jun) chlorophyll-a concentrations (Chl-a, ng mL^{-1}) using ocean color data, a measure of surface phytoplankton concentration, obtained from the European Space Agency Climate Change Initiative Ocean Colour Product (OC-CCI19) and covering the years 1998-2026. Data courtesy of Jeanette Gann (Jeanette.Gann@noaa.gov)

Spring Small Copepods and Spring Large Copepods: Small copepods (*Acartia* spp., *Pseudocalanus* spp., and *Oithona* spp.) were quantified from the 153 μm mesh, 20 cm bongo net samples and large copepods were quantified from the 505 μm mesh, 60 cm diameter net during two spring surveys: 70-m

isobath survey and the spring larval survey over the southern Bering Sea shelf. Data courtesy of David Kimmel (David.Kimmel@noaa.gov)

Summer Small Copepods and *Summer Large Copepods: Small and large copepods were quantified during two summer surveys: the fall age-0 survey and fall 70 m-isobath survey. Data courtesy of David Kimmel (David.Kimmel@noaa.gov)

***Euphausiids:** An estimate of euphausiid biomass was determined by multifrequency acoustic backscatter and midwater trawl data collected during biennial pollock surveys in krill areal density in units of wet weight (g/m^2). Data are restricted to the southeastern Bering Sea south of 60°N. Data courtesy of Mike Levine (Mike.Levine@noaa.gov)

Jellyfish: The biomass for jellyfishes (Scyphozoa, but primarily *Chrysaora melanaster*) was calculated from the eastern Bering Sea shelf bottom trawl survey. The index (biomass in kilotons) and confidence intervals were estimated by fitting a multivariate random effects model (REM) to stratum-level design-based time series calculated from the summer bottom trawl survey catch and effort data. Data courtesy of Thaddaeus Buser (Thaddaeus.Buser@noaa.gov)

Larval Pollock Abundance: Estimates of larval abundance (mean number per 10 m^2) from spring (May/June) ichthyoplankton surveys conducted by EcoFOCI. Data courtesy of Lauren Rogers (Lauren.Rogers@noaa.gov)

Juvenile Age-0 Pollock Biomass: Fish were sampled using a surface trawl net towed in the upper 25 m during the fall (Aug/Sept) EMA Eastern Bering Sea Juvenile Fish Fall (BASIS) survey in the southeastern Bering Sea (south of 60°N). Annual indices of relative biomass were estimated using a single-species spatio-temporal model with the sdmTMB package version 1.1.0. Data courtesy of Lia Domke (Lia.Domke@noaa.gov)

Energy Density: Mean annual age-0 pollock energy density (kJ/g dry mass) in the southeastern Bering Sea from 2002-2025. Data courtesy of Johanna Page (Johanna.Vollenweider@noaa.gov)

Adult Pollock, Pacific Cod, and Arrowtooth Flounder: The estimated biomass index (metric tons) sampled during the eastern Bering Sea shelf bottom trawl survey from 1982-2026. Data courtesy of Sean Rohan (Sean.Rohan@noaa.gov)

Age-1 Pollock: Age-1 abundance estimates from the 2024 Assessment of Eastern Bering Sea Walleye Pollock (Ianelli et al., 2024). Data courtesy of Jim Ianelli (Jim.Ianelli@noaa.gov)

Contributed by
Elizabeth Siddon and Kalei Shotwell
Alaska Fisheries Science Center, NOAA Fisheries, Juneau, AK
Jim Ianelli
Alaska Fisheries Science Center, NOAA Fisheries, Seattle, WA

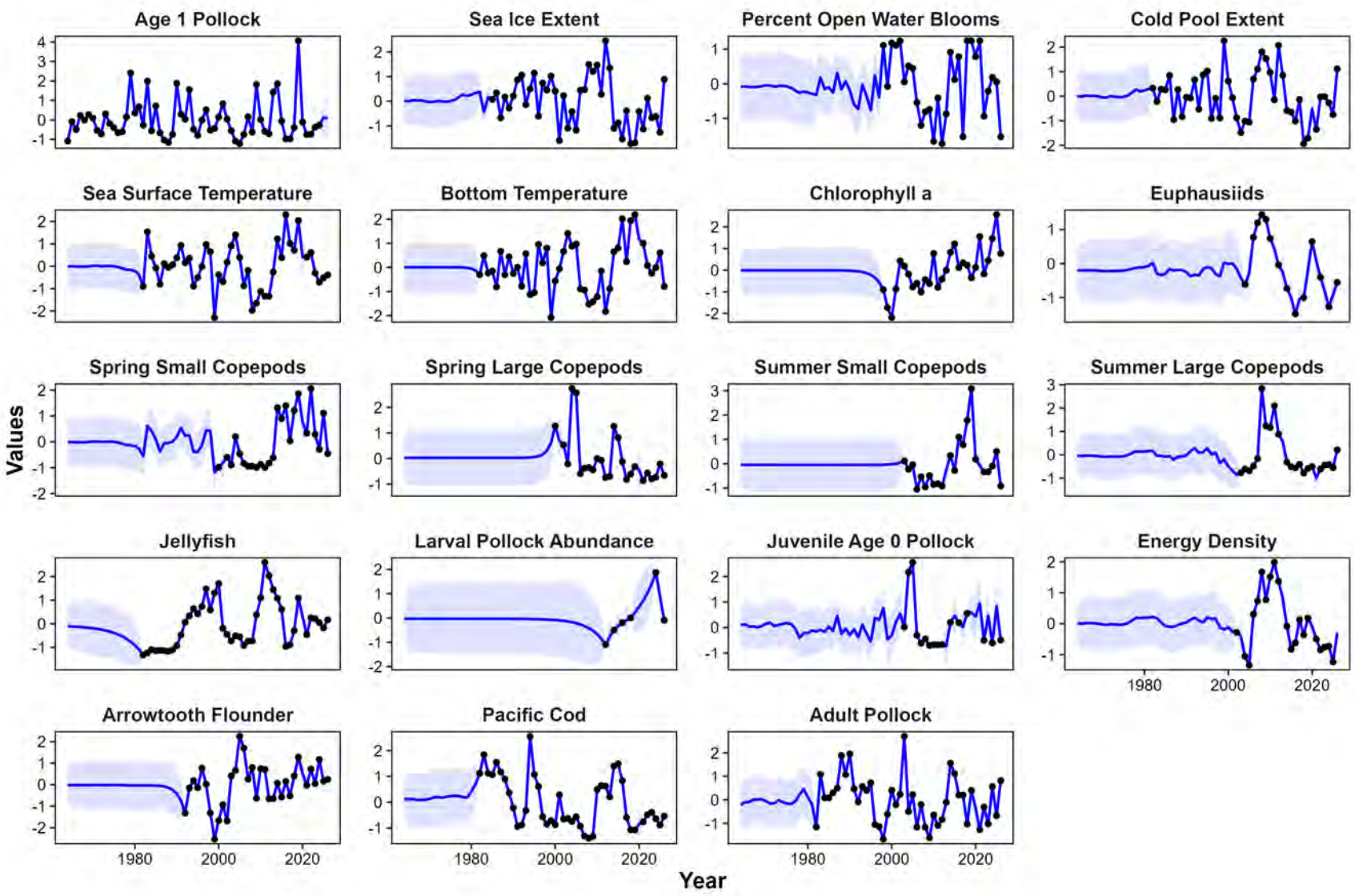


Figure 12: Time series showing observed (blue dot) and estimated (blue lines with a shaded uncertainty band) value for each ecosystem variable included in the Dynamic Structural Equation Model. The model treats supplied observations as exact, such that estimates (lines) are equal to observations (dots) when observations are available in a given year. See list of data sources below.

Hypothesized mechanism table for pollock early survival pathways. Each row represents an arrow where we include the lag and hypothesized effect sign for the relationship based on literature. We provide the data availability and our assessed confidence in said relationship.

Driver	**Causal Hypothesis**	**Lag(s)**	**Hypothesized Effect Sign**	**Data Availability & Caveats**	**Relationship Confidence (L,M,H)**	**Reference(s)**
Sea Ice Extent	Higher sea ice extent in winter leads to larger cold pool	0	Positive	Annual index available by SEBS, NBS, or EBS combined.	H	Stabeno & Bell 2019
Cold Pool Extent	Larger cold pool in summer leads to higher age-0 survival; less cannibalism via spatial mismatch	0	Positive	Annual cold pool index available from BTS or MOM6; Age-0 abundance is estimate from BASIS survey (intermittent years)	H	Mueter & Litzow 2008; Hunt Jr et al. 2025
Sea Surface Temperature	Higher sea ice extent in preceding winter leads to cooler SSTs the following summer	0	Negative	Annual index available from surveys or MOM6	H	Hunt et al. 2002
Percent Open Water Blooms	Higher sea ice extent leads to lower % open water blooms	0	Negative	Annual index available as SEBS or NBS	H	Nielsen in 2024 ESR Report Cards (Siddon 2024)
Primary Production	% open water blooms: higher proportion of ice-associated blooms (lower proportion of open water blooms) are correlated with higher abundances of large zooplankton	0	Negative	Annual index available as SEBS or NBS	M	Hunt et al., 2011
Spr Small Copepods	Warm years result in larger abundances of small copepods in the spring	0	Positive	Abundance of small copepods from spring mooring (when pollock are larval/early juv) is available most years 2000–present	H	Hunt et al. 2002
Spr Small Copepods	Small copepods are prey for larval and early juvenile pollock in Spring	0	Positive	Abundance of small copepods from spring mooring (when pollock are larval/early juv) is available most years 2000–present	H	Kimmel et al., 2024
Summer Large Copepods	Large copepods are prey for late juvenile pollock in Fall and support higher over-winter survival and recruitment to age-3	0	Positive	Abundance of large copepods from Fall BASIS (when pollock are late juv) is available, but intermittent. Data can be augmented by Fall mooring data	H	Eisner et al. 2020
Euphausiids	Euphausiid abundance is higher in colder years	0	Negative	Acoustic estimate available in even years	H	Hunt et al., 2016
Euphausiids	Euphausiids are alternative (to large copepods) high quality prey for late juvenile pollock in Fall	0	Positive	Acoustic estimate available in even years	H	Hunt Jr et al. 2025
Energy Density	Late juvenile pollock ED is higher in cold years	0	Negative	Age-0 pollock ED from Fall BASIS is available, but intermittent	M	Heintz et al., 2013
Age-0 Pollock	Higher ED in late juvenile pollock leads to higher overwinter survival to age-1	1	Positive	Age-0 pollock ED from Fall BASIS is available, but intermittent	H	Heintz et al., 2013; Siddon et al., 2013
Larval pollock	Larval abundance in spring can indicate good year class	0	Positive	Estimate of larval abundance in 5 years (2012, 2014, 2016, 2018, and 2024; expect to receive 2026 any day)	L	"Ongoing research is focused on the importance of larval [dynamics] for eventual recruitment success."
Cannibalism	Higher cold pool, less cannibalism due to spatial mismatch = higher age-0 survival	0	Positive	Annual index of adult pollock diets from BTS	H	Mueter & Litzow 2008; Hunt Jr et al. 2025
Predation	Higher abundance of predators leads to lower abundance of age-1 pollock	0	Negative	Annual indices of predator abundance from BTS	H	Holsman et al., 2024

Oceanography On Deck: Industry-driven data collection fills spatial & temporal information gaps

Background

Fishing vessel-based ocean observation is gaining traction around the globe as a viable method to collect reliable subsurface ocean observations at scale in the shelf and coastal ocean regions that are both most difficult to observe and most relevant to society for their ecological and economic value. The Fishing Vessel Ocean Observing Network (FVON) – a global consortium of research institutions, NGOs, and private companies – was recognized by the Global Ocean Observing System (GOOS) in 2024 as an emerging observing network to support existing operational observation systems such as the ARGO float program (Van Vranken et al., 2023). Traditional cruise based ocean observations provide sparse and often seasonally skewed data collection, while commercial fishing activities cover the broad shelf and coastal areas across different seasons, making fishing vessel-based ocean observing a mechanism to fill these spatial and temporal data gaps (Van Vranken et al., 2020). Significant improvements to regional ocean model performance when assimilating these data streams are well documented (Kerry et al., 2024; de Souza and Costa, 2026).

System Description

Ruggedized instruments are mounted directly on fishing gear such as trawls, pots, traps, and longlines (Figure 13a). They operate autonomously after installation, requiring no crew action, no changes to fishing practices, and no maintenance during the season. These instruments use a compact temperature-depth logger with temperature accuracy better than ± 0.05°C, a resolution of 0.001°C, a one-second response time, depth accuracy within 0.5% of the depth rating (1000 m), and two years of battery life and calibration. When gear is retrieved on deck, the instrument automatically transfers its data via Bluetooth to a deck unit mounted on the wheelhouse (Figure 13b), where the data is relayed to the cloud via the vessel's satellite Wi-Fi. Prior to data release, automated quality control based on QARTOD and ARGO practice, as well as a growing set of QC tests specific to fishing-gear deployment, are applied to data (Martinelli et al., 2026). Quality-controlled data are published to an ERDDAP server[9] and to regional portals, depending on network-specific data-sharing agreements, and are passed to the U.S. National Data Buoy Center, which routes them to the WMO Global Telecommunication System (GTS). The operational target is fifteen minutes from the instrument surfacing at the end of a fishing operation to the observation being available to off-vessel users. Figure 13c shows the resulting pathway.

Bering Sea Network

In 2025, the North Pacific Research Board awarded Ocean Data Network Inc. (ODN), Alaska Bering Sea Crabbers (ABSC), and the Alaska Marine Community Coalition (AMCC) a grant to establish a fishing-vessel-based ocean observation network covering the southeastern and northern Bering Sea, hereafter referred to as Oceanography On Deck (OOD). The impetus for OOD was initial challenges in understanding the marine heatwave of 2018-2019 when the eastern Bering Sea snow crab population collapsed and the fishery closed (Szuwalski et al., 2023). Bottom temperature and the extent of the cold pool are the stated variables governing the Bering Sea ecosystem (Stabeno and Bell, 2019; Rohan et al., 2022), and the observational record is thin outside the seasonal survey windows. A recent skill assessment of the ROMS Bering10K regional model reported a shelf-wide summer bottom-temperature bias of 0.06°C and high correlation across most of the shelf, but stated validation was "primarily limited to the summer months," historical sampling lacked winter and spring observations, and CTD coverage was "highly skewed toward a few well-sampled transect lines" (Kearney et al., 2025).

[9] `https://erddap.fvon.org`

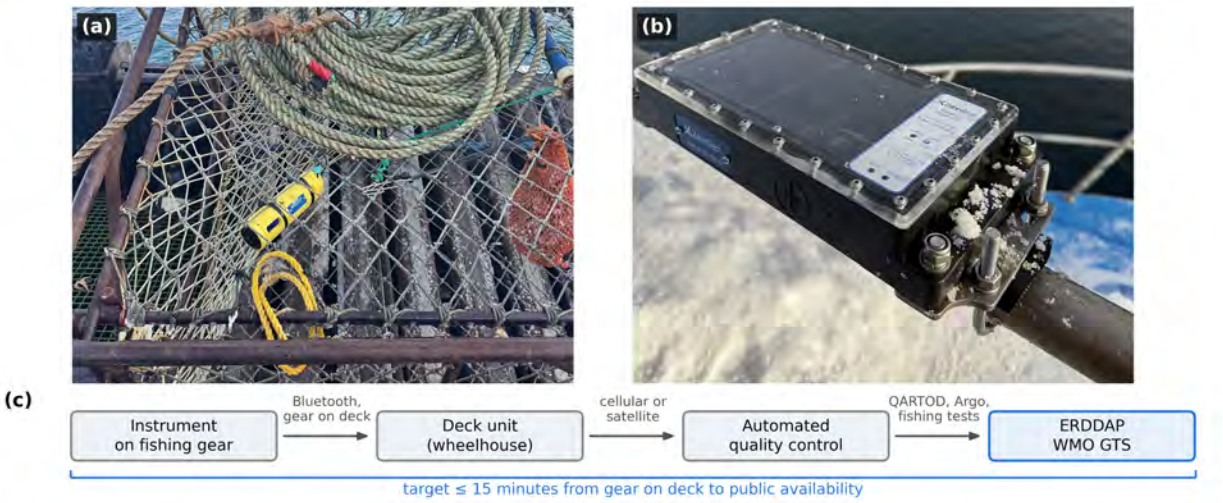


Figure 13: The observing system. (a) A temperature–depth instrument secured inside a crab pot. (b) A deck unit mounted on a wheelhouse roof. (c) The data pathway from instrument to data repositories and the GTS.

Applications

Spatial and Temporal Expansion of Observations

OOD is providing broader spatiotemporal subsurface temperature data coverage than traditional research cruises permit, and this spring was able to observe the formation of the cold pool in real time (Figure 14). The OOD network has succeeded in achieving consistent, year round data collection because it is purposefully built across multiple fleets and gear types (longline, pot, pelagic trawl, and non-pelagic trawl) that target different species across seasons. Since installations began in the fall of 2025 the network has collected over 8,000 temperature profiles and counting (Figure 15), making OOD by far the largest near real-time subsurface observing network within Alaska's Exclusive Economic Zone. Further, this network is a uniquely complementary component to existing ocean observations in the region because it captures temporal and spatial data gaps such as the winter months when surveys are not in operation and nearshore regions where these surveys cannot sample.

Industry Uptake

The OOD project has received support from participating fleets and captains, who are given real-time access to their own vessel data in the wheelhouse via ODN's web portal (Figure 16). This allows them to see bottom temperatures haul by haul to inform their fishing strategy, resulting in bait and fuel savings and reduced time at sea, improving operational efficiency and safety, and, in some cases, even aiding bycatch avoidance by building mental models of species' temperature ranges. One longline captain described the system this way: "I use it on a daily basis to check the temperatures where I am fishing... When I am doing exploratory sets, I am setting across a range of areas in the Bering Sea and then noting the temperatures I see and the catch I get. From this, I can deduce the temperature that the cod are liking and whether I am going in the direction of too hot or too cold and what direction I want to go for my next set." Such enthusiasm from industry has led vessels outside the project to inquire about how to get involved in the OOD network or, in some cases, even to purchase their own equipment because of the value it can bring in informing their fishing strategy.

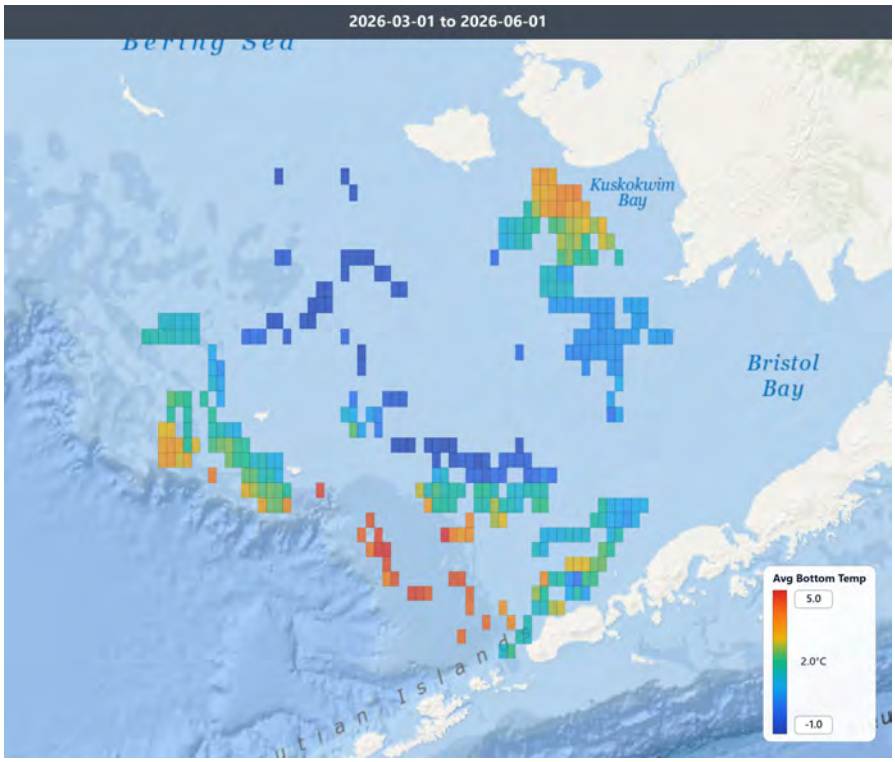


Figure 14: Cold pool formation measured by Oceanography On Deck network vessels in the eastern Bering Sea between 3-1-2026 and 6-1-2026.

Data Flow and MOM6 Validation Effort

Currently, OOD data is reaching the GTS for ingestion into global ocean models. Data sharing beyond the GTS has been an ongoing co-design process with the participating fleets. Public data release will take the form of Convention for Data Management standard-format profiles on a six-week delay, with no vessel, instrument, or deck-unit identifiers as well as spatial auto-deletion rules removing data in defined areas per request from specific vessels. Potential data users whose application is compromised by those constraints may request additional access, but this will require discussion and approval between OOD project staff and participating fleets to ensure data will not be used in any unintended or malicious manner. Initial discussions with ocean modelers at AFSC indicate that this data set will be a valuable tool for validating and improving regional model (MOM6-NEP) simulations. In particular, it will add much-needed spatial and temporal coverage to water column temperature sources outside of the well-sampled summer months, allowing better constraint of the seasonal evolution of temperature across the shelf.

Conclusion

The Bering Sea ecosystem is changing seasonally and interannually and survey schedules are seasonally limited. A network built on fishing vessels already operating in the shelf in every season is a practical way to increase monitoring to keep both fishermen and fisheries managers informed on seasonal trends in water column and bottom temperature. The OOD network is a paradigm shift for ocean observing in Alaska, with many avenues for expansion, from adding oceanographic parameters to extending coverage to neighboring regions. Furthermore, this collaboration is mutually beneficial to fleets, scientists, and resource managers, while giving the fishing industry an opportunity to contribute meaningfully to fisheries management strategies.

Contributed by
Jack Carroll
Ocean Data Network, Portland, ME
Cooper Van Vranken
Ocean Data Network and Fishing Vessel Ocean Observing Network, Portland ME
Kelly Kearney
Alaska Fisheries Science Center, NOAA Fisheries, Seattle, WA
Wei Cheng
NOAA/Pacific Marine Environmental Laboratory, Seattle, WA
Cory Lescher
Alaska Bering Sea Crabbers, Anchorage, AK
Michelle Stratton
Alaska Marine Community Coalition, Anchorage, AK
Dustin Colson Leaning
Environmental Defense Fund and Fishing Vessel Ocean Observing Network, Boston, MA
Elizabeth Siddon
Alaska Fisheries Science Center, NOAA Fisheries, Juneau, AK

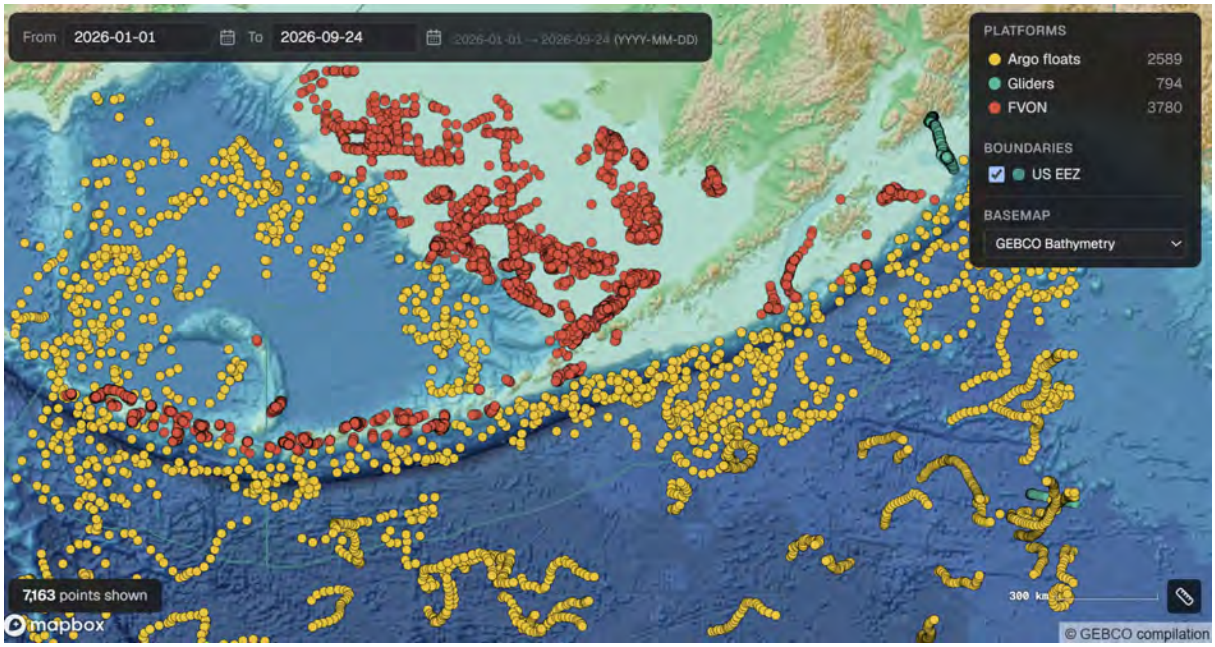


Figure 15: Map showing subsurface temperature profile locations available in near real-time. Red dots are profiles collected by vessels participating in the Oceanography On Deck project, and yellow points are Argo profiles. Note the fishing vessel collected data fills in the shelf and coastal gap left by the Argo float network which largely falls outside of EEZs.



Figure 16: Example portal display of publicly available data from a research vessel operating in the North Atlantic. This data is only available in this format to the captains of the participating vessels. `https://portal.oceandata.net/en/jakup_sverri`.

Imaging FlowCytobot: Phytoplankton, Lower Trophic Dynamics, and Survey Modernization

Background

Due to the ephemeral nature of phytoplankton in natural environments and the time-consuming nature of traditional microscopy methods for identification, understanding the mechanistic links between primary and secondary production in the eastern Bering Sea (EBS) has been challenging to measure. Typical measurements of phytoplankton use standing stock as a proxy, and can be calculated using chlorophyll (Chl-a) concentration derived from laboratory analyses, in-situ instrumentation, or irradiance and color imaging measurements including satellite analyses (Campbell et al., 2002; Polovina and Howell, 2005). However, estimates based on total Chl-a can be biased by the presence of chloroplast-containing microzooplankton (Stoecker et al., 2014), and do not detect taxonomic or functional changes in the phytoplankton community, such as cell size (many small-celled taxa may yield the same Chl-a biomass as fewer large cells), structure, or energy storage products. Different phytoplankton taxa contain differing energy storage products like lipids and starches, which are held in different ratios among species, and vary with environmental conditions, including nutrient availability (e.g., Moal et al., 1987; Metting Jr, 1996; Dickman et al., 2008). For example, diatoms are particularly lipid rich because they have lipid storage vacuoles only possible in large sized cells (Baird, 2022). Nutritional composition can also change within a given taxon based on environmental conditions and growth stage (e.g., Jónasdóttir, 2019). Thus, total phytoplankton biomass as measured via Chl-a concentration may obscure ecologically important trends in phytoplankton communities that impact energy and nutritional flows in marine food webs.

Phytoplankton communities represent the biological manifestation of physical and chemical conditions (water column stability, temperature, light, nutrients), such that the base of the food web is heavily influenced by seasonal and inter-annual changes in environmental conditions (e.g., Winder and Sommer, 2012; Xiao et al., 2019).

Environmental variation in the EBS is known to cause shifts in phytoplankton abundance, taxonomic composition, and/or size structure, with likely nutritional consequences for copepods that rely on phytoplankton as a significant food source (e.g., Meyer et al., 2002; Falk-Petersen et al., 2009; Liu et al., 2016).

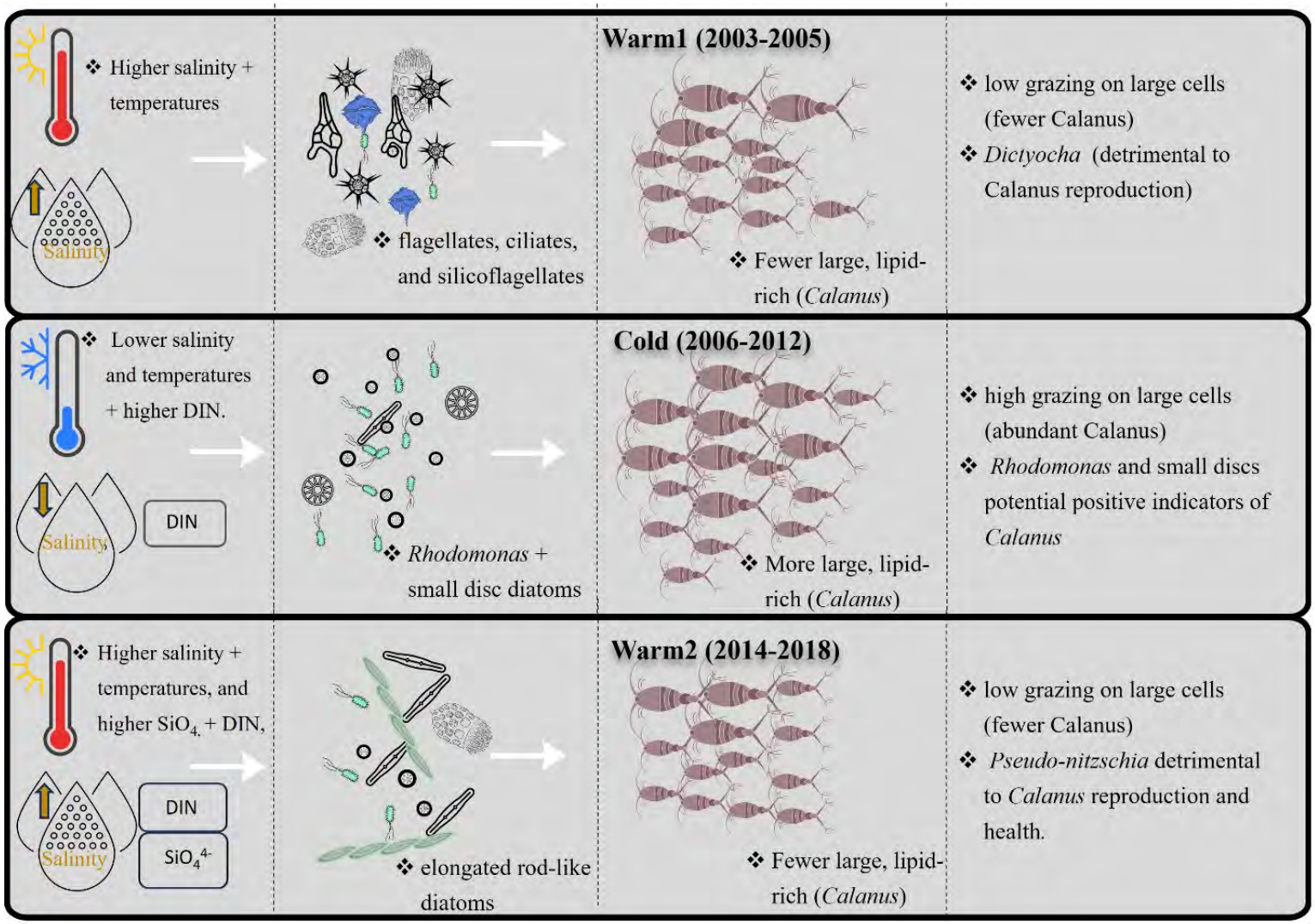


Figure 17: Conceptual model depicting potential bottom-up and top-down lower trophic dynamics in different environmental stanzas from 2003-2018 (Gann et al., 2026).

Large crustacean zooplankton constitute a critical trophic link between microplankton (phytoplankton, mesoplankton, and microzooplankton) communities and higher trophic-level species such as fish, birds, and whales. In Alaskan marine ecosystems, commercially harvested and forage fishes feed heavily on large lipid-rich zooplankton like copepods and euphausiids (e.g., Coyle et al., 2011; Strasburger et al., 2014; Bouchard and Fortier, 2020). Gann et al., 2026 observed 3 distinct environmental stanzas over a 15-year period (2003-2018) in the southeastern Bering Sea that correlated with phytoplankton communities and shared links to *Calanus* copepods through phytoplankton size and specific taxa (Figure 17). This study utilized traditional and time consuming microscopy techniques for phytoplankton identification. A more efficient method of monitoring phytoplankton populations, for example via new imaging techniques, allows for improved understanding of mechanistic relationships between environmental conditions, phytoplankton, and zooplankton within the lower trophic food web.

Imaging FlowCytobot

The IFCB is an in-situ submersible instrument that captures images of particles, such as phytoplankton, in aquatic environments (Olson et al., 2017, Figure 18). It uses laser-induced fluorescence and light scattering to detect particles within the size range of $<$10-150μm. Due to its fluorescence-based triggering features, it can differentiate between chlorophyll-containing and non-chlorophyll containing particles[10]. With its self-contained design and remote data access capabilities, the IFCB can be deployed on oceanographic research cruises, moored platforms, or in laboratories, efficiently providing detailed information on phytoplankton communities.

The IFCB, with its internal microscope and automated imaging system is used in conjunction with artificial intelligence (AI) and machine learning (ML) to quickly classify phytoplankton taxa in multiple samples and extract metrics such as cell biovolume and surface area. Development of algorithms to process image data using a curated phytoplankton image library tailored for Alaska's large marine ecosystems (LMEs) has led to significant improvements in community characterization, and routines are currently being optimized for data uploads to the cloud for near-real time access to data from shore-based facilities.

Applications

Lower Trophic Dynamics

Because of the difficulties in using Chl-a as a proxy for available food, it often fails to reliably correlate with abundance and productivity of individual fish stocks, even for lower trophic-level early life stages (e.g., Marsh et al., 2020). Using the IFCB for improved temporal and spatial coverage in phytoplankton communities in conjunction with other variables (temperature, salinity, nutrients and when available zooplankton community composition), can significantly improve our understanding of these lower trophic relationships by using phytoplankton taxonomic groups as proxies for nutritional availability based on their correlations with key fatty acids (Gann et al., in prep) and thus potentially improve on forecast models for recruitment of young fish feeding at lower trophic levels. Additionally, while IFCB configurations are generally optimized for phytoplankton detection, the capture of larger particles can also provide opportunities to investigate meroplankton communities, particularly when high densities of early larval life stages are present (Fachon et al., 2025).

Harmful Algal Blooms

Additionally, harmful algal blooms (HABs) are an increasing concern in Alaska's LMEs, and IFCBs can help with detection and monitoring of potential HAB species (Fachon et al., 2025; Lefebvre et al., 2025*a*) in addition to ground-truthing remote sensing methods like hyperspectral cameras on drones,

[10]McLane Research Laboratories, Inc, `https://mclanelabs.com/imaging-flowcytobot`



Figure 18: McLane Laboratories Imaging FlowCytobot with case and inset of binned images of phytoplankton cells.

or satellite imaging systems using color data to differentiate broad categories of taxa (Lange et al., 2025). By increasing our monitoring footprint with continuous flow-through ship-board monitoring and individual sample analyses, the IFCB has helped modernize survey operations, groundtruth satellite algorithms, and improve our ability to monitor Alaska's LMEs (Figure 19).

Collaborations

Phytoplankton monitoring in Alaska has undergone a significant upgrade over the past couple of years through the use of multiple Imaging FlowCytobots (IFCBs), and a collaborative network including the Alaska Fisheries Science Center, Alaska Ocean Observing System, and Woods Hole Oceanographic Institution. Through these networks, image libraries and model updates are shared for Alaska's LMEs that will help improve accuracy of the AI/ML models and lessen the need for human in the loop (HIL) intervention of models (though will not completely eliminate the need for HIL). Additionally, monthly meetings during the spring, summer, and fall field seasons, combined with email updates and notifications, allow for frequent communications between stakeholders in Alaska through the Alaska Harmful Algal Bloom network (AHAB[11]).

[11] `https://ahab.aoos.org/`

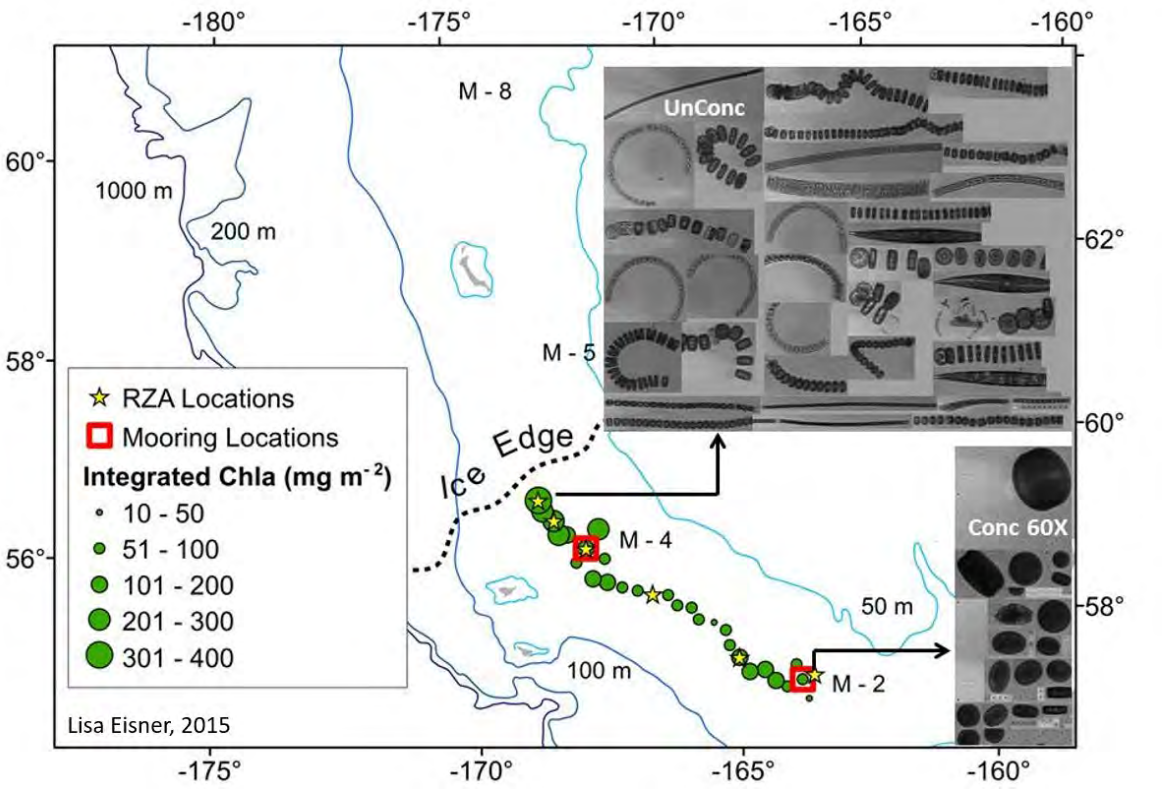


Figure 19: Phytoplankton images overlaid onto station map for the spring mooring survey during 2015 that traveled close to the ice edge. Red boxes show mooring sites for M-2 and M-4, while arrows from green station locations depict image bin examples from those locations.

Contributed by
Jeanette Gann
Alaska Fisheries Science Center, NOAA Fisheries, Juneau, AK
Gulce Kurtay and Calvin Mordy
Cooperative Institute for Climate, Ocean, and Ecosystem Studies,
University of Washington, Seattle, WA
Pacific Marine Environmental Laboratory, Seattle, WA
Jens Nielsen
Cooperative Institute for Climate, Ocean, and Ecosystem Studies,
University of Washington, Seattle, WA
Alaska Fisheries Science Center, NOAA Fisheries, Seattle, WA
Thomas Farrugia
Alaska Ocean Observing System
Evie Fachon, Mrunmayee Pathare, and Mike Brosnahan
Woods Hole Oceanographic Institute

DNA metabarcoding of northern fur seal scats improves species-level prey identification and tests scalability of efficient data generation

Northern fur seal (*Callorhinus ursinus*) diet analysis for 2025 was conducted using two methods: hard parts analysis, in which fish bones, otoliths, and squid beaks recovered from scat and spew samples are identified to the highest possible taxonomic resolution (see p. 240), and DNA metabarcoding of scat samples, which relies on amplifying genetic material from fish prey.

DNA metabarcoding offers advantages over traditional hard parts analysis in that it provides a more efficient and scalable method to generate diet information, which can allow data to be produced on an annual timeline and used in ecosystem analyses. Another key benefit is that DNA-based data can provide species-level resolution for many primary prey items, including differentiating among multiple salmon species and separating walleye pollock from Pacific cod, both of which can be challenging with hard parts. DNA may also improve detections of fish prey with delicate hard parts that do not survive digestion.

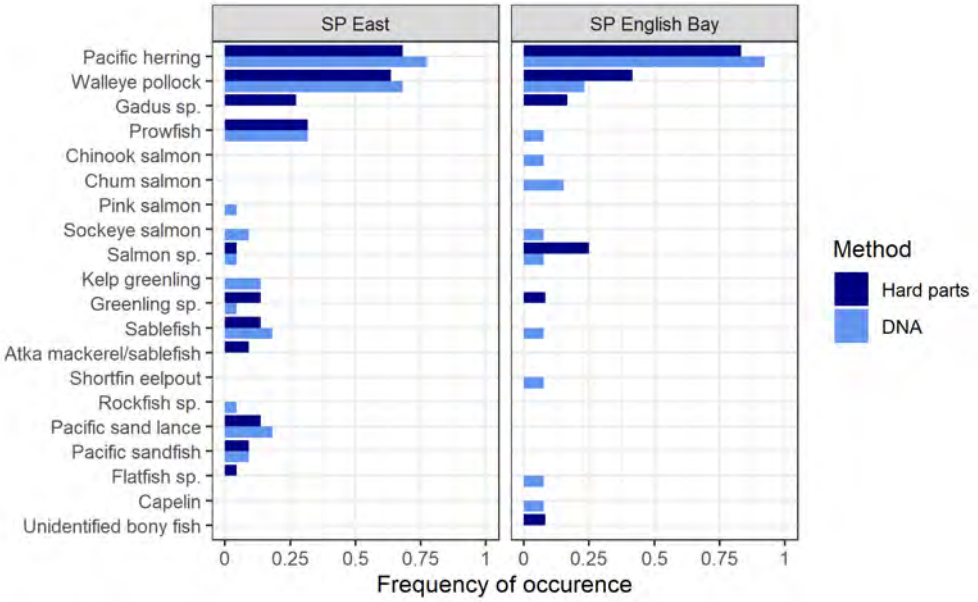


Figure 20: Frequency of occurrence of prey species in northern fur seal diets collected on St. Paul Island and identified using DNA metabarcoding and/or prey hard parts. These data include 23 scats from SP East and 13 from SP English Bay.

A subset of scats collected from two northern fur seal rookery complexes (St. Paul East and St. Paul English Bay) in 2025 were analyzed for both hard parts and DNA. Two subsamples per scat were collected and preserved for DNA analysis. Three technical PCR lab replicates for DNA metabarcoding were generated from each of the subsamples, providing six combined replicates per scat to improve confidence in prey identification. Prey taxa in 23 scats from East and 13 scats from English Bay were successfully identified using one or both methods. Of these samples, two scats did not contain identifiable hard parts, but could be analyzed with DNA, while one sample contained hard parts, but did not meet minimum quality criteria for retention in the DNA dataset. Thirteen samples that did not

contain identifiable hard parts similarly did not contain DNA of sufficient quantity/quality for analysis.

The major prey constituents were consistent between the hard parts analysis and the DNA metabarcoding data, with Pacific herring and walleye pollock representing the dominant prey items in diets across rookery complexes (Figure 20). Prowfish, sablefish, and greenling all represent more common prey constituents in East rookeries compared to English Bay, also consistent with hard parts results.

Highlighting the improvements in species-level resolution compared to hard parts, chum, pink, sockeye, and Chinook salmon all appeared in one or more scats in the DNA data. Additionally, the metabarcoding data suggest that most of the *Gadus* spp. hard parts belong to walleye pollock rather than Pacific cod.

Although the metabarcoding data provides relative proportions of DNA for the prey items in the sample (Figure 21), additional research is being conducted to understand the digestion rates of different prey species and how that might influence our understanding of the relative quantity of each prey. Despite this caveat, the metabarcoding data suggest that more of the scats from English Bay rookeries were dominated by herring, whereas animals from the East rookeries included more walleye pollock and prowfish. One East rookery scat included a large amount of Pacific sandfish and another Pacific sand lance (Figure 21).

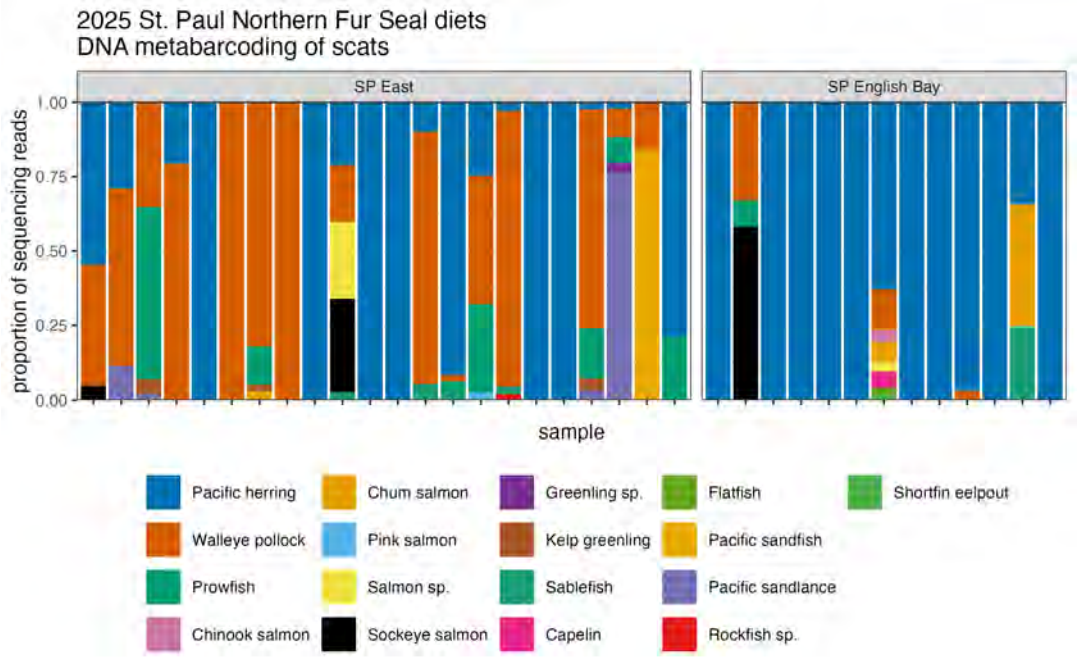


Figure 21: Relative proportions of DNA metabarcoding sequencing reads per prey item averaged across two scat subsamples and three technical lab replicates. Each bar represents one scat.

Contributed by
Diana Baetscher
Auke Bay Laboratories, Alaska Fisheries Science Center, NOAA Fisheries, Juneau, AK
Tonya Zeppelin and Katie Luxa
Marine Mammal Laboratory, Alaska Fisheries Science Center, NOAA Fisheries, Seattle, WA

A Spatially Resolved Borealization Index for the Bering Sea

Borealization, the transition from an Arctic physical state supporting a cold-adapted species assemblage to a subarctic (boreal) state supporting a warm-adapted assemblage, was previously quantified for the southeastern Bering Sea using Dynamic Factor Analysis (DFA). DFA is a dimension-reduction technique that models multiple short, non-stationary time series as linear combinations of shared latent trends. However, applying standard DFA across broad, oceanographically dynamic systems like the Bering Sea implicitly assumes the study area behaves as a single spatially homogeneous unit, masking sub-regional differences, localized hotspots, and persistent Arctic refugia. We therefore extended the framework to a Spatial Dynamic Factor Analysis (SDFA), enabling evaluation of spatiotemporal trends in borealization across the full U.S. Bering Sea and management sub-regions of interest.

We evaluated physical variables previously linked to Arctic-subarctic ecosystem shifts including water temperature (summer surface and bottom values), sea ice cover (Jan-Feb and Mar-Apr), salinity (summer bottom values), and open-water duration (number of days between ice retreat – ice cover <0.15 – and fall freeze up) alongside one biological variable: peak spring phytoplankton bloom timing. While the original index included more biological variables (e.g., zooplankton and groundfish community composition) to evaluate the 2019-2021 snow crab collapse, we removed those biological components here. This ensures the index is broadly applicable across diverse management contexts and prevents circularity when used as a predictor in downstream ecological models. Bloom timing was retained to represent lower trophic level phenology. Each variable was extracted for the months, seasons, and depth layers most relevant to its ecological role, providing an annual snapshot of the water column. All variables were standardized prior to analysis so that the resultant spatial latent factor and corresponding loadings were unitless.

The SDFA considered a single spatial latent factor (representing borealization) tracking transitions in Arctic/boreal ecotones from 1958 to 2026 (Figure 22a displays spatial patterns for 2019-2026). Variables associated with Arctic conditions loaded negatively, while those associated with boreal conditions loaded positively (Figure 22b). To summarize temporal trends, we calculated the annual median index across the full U.S. Bering Sea domain and within the Eastern (EBS) and Northern (NBS) Bering Sea management sub-regions (Figure 22c, d). To evaluate spatial trends, we fit a spatially varying coefficient model estimating the linear trend in the index at each location (expressed as change per decade) to identify localized borealization hotspots and refugia (Figure 22e).

The spatial patterns in the index tracked well-documented events, with the end of the 2018-2019 marine heatwave shown here as an example (Figure 22a). By 2026, the median index for the Bering Sea (0.29) was lower than its 1958-2026 mean (0.61). This differed between subregions: the EBS median (0.66) was lower than its long-term mean (1.19), whereas the NBS median (-0.75) remained slightly higher than its long-term mean (-0.96; Figure 22c, d). Over the full 69-year record, however, the median index increased across the entire domain and in both subregions, with a faster rate of increase in the NBS than in the EBS (Figure 22c, d). Hotspots of persistent, multi-decadal borealization were concentrated in the NBS and along the inner domain of the EBS (Figure 22e). In contrast, across the EBS middle domain, where the cold pool typically forms, the 95% confidence interval on the decadal trend included zero, indicating no significant multi-decadal trend and identifying a potential Arctic refugium.

Contributed by
Kaitlyn O'Brien
College of Fisheries and Ocean Sciences, University of Alaska Fairbanks, Juneau, AK
Mike Litzow
Alaska Coastal Observations and Research, Kodiak, AK
Franz Mueter
College of Fisheries and Ocean Sciences, University of Alaska Fairbanks, Juneau, AK
Erin Fedewa
Alaska Fisheries Science Center, NOAA Fisheries, Kodiak, AK
David Kimmel
Alaska Fisheries Science Center, NOAA Fisheries, Seattle, WA
Trond Kristiansen
Farallon Institute for Advanced Ecosystem Research, Petaluma, CA
Jens Nielsen
Cooperative Institute for Climate, Ocean, and Ecosystem Studies,
University of Washington, Seattle, WA
Alaska Fisheries Science Center, NOAA Fisheries, Seattle, WA
Emily Ryznar
Alaska Fisheries Science Center, NOAA Fisheries, Kodiak, AK

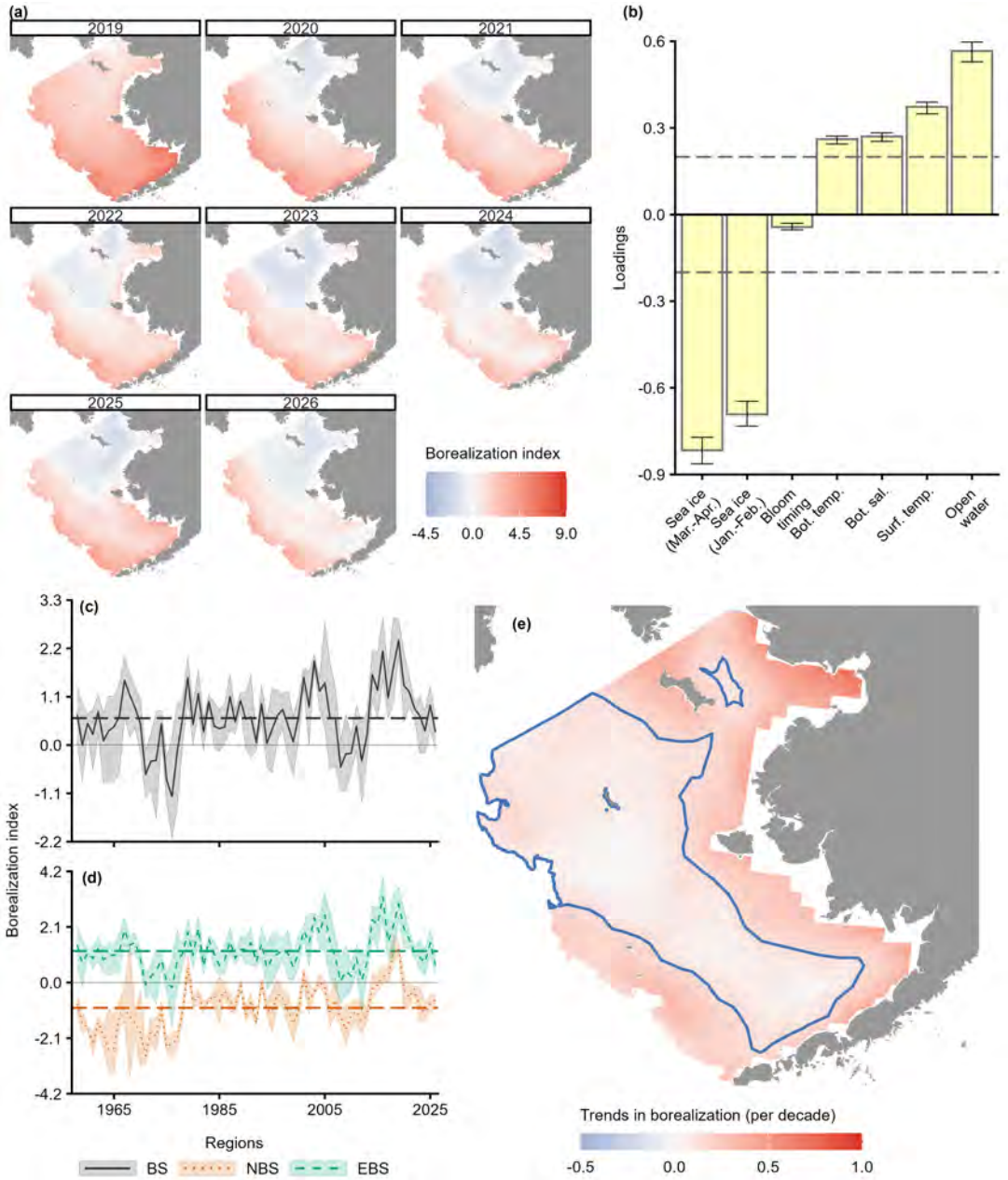


Figure 22: Results from a Spatial Dynamic Factor Analysis (SDFA) of borealization in the Bering Sea. (a) Annual latent spatial factor from the SDFA (1958-2026) for the most recent 8 years, where smaller values (blue) indicate more Arctic-like conditions and larger values (red) indicate more boreal conditions. (b) Variable loadings for each of the seven input variables in the SDFA, arranged from most negative to most positive. Dashed lines indicate the ± 0.2 threshold, above which variables are considered to have a relatively strong influence on the spatial factor. Negative loadings denote variables with an inverse spatial relationship to the borealization index. (c) Annual median borealization index for the full spatial domain (solid line) with respective 95% confidence intervals (shaded) derived from sampling of the joint precision matrix. Grey dashed line indicates the long-term average for the full spatial domain. (d) Regional median borealization index for the Northern Bering Sea (NBS; orange dotted) and Eastern Bering Sea (EBS; green dashed) with respective 95% CIs and long-term averages (dashed horizontal lines). In both panels (c) and (d) a horizontal grey line at 0 was included as a visual reference. (e) Spatial trends in borealization, expressed as the slope per decade, where warmer colors indicate increasing borealization over the temporal domain examined. The blue outlined polygons enclose locations where the 95% CI of the spatially varying coefficient includes zero and may act as an Arctic refugium.

Ecosystem Status Indicators

Physical Environment

This section provides an overview of physical oceanographic variables and contains contributions from (in alphabetical order):

Kelia Axler - Resource Assessment and Conservation Engineering Division, Alaska Fisheries Science Center, NOAA Fisheries, Seattle, WA
Lewis Barnett - Resource Assessment and Conservation Engineering Division, Alaska Fisheries Science Center, NOAA Fisheries, Seattle, WA
Shaun W. Bell - NOAA Pacific Marine Environmental Lab, Seattle, WA
Matt Callahan - Pacific States Marine Fisheries Commission, Juneau, AK
Tyler Hennon - University of Alaska Fairbanks, College of Fisheries and Ocean Sciences, Fairbanks, AK
Kelly Kearney - Resource Assessment and Conservation Engineering Division, Alaska Fisheries Science Center, NOAA Fisheries, Seattle, WA
Emily Lemagie - NOAA Pacific Marine Environmental Lab, Seattle, WA
Ryan M. McCabe - NOAA Pacific Marine Environmental Lab, Seattle, WA
Jim Overland - NOAA Pacific Marine Environmental Lab, Seattle, WA
Lauren Rogers - Resource Assessment and Conservation Engineering Division, Alaska Fisheries Science Center, NOAA Fisheries, Seattle, WA
Sean Rohan - Resource Assessment and Conservation Engineering Division, Alaska Fisheries Science Center, NOAA Fisheries, Seattle, WA
Kevin Siwicke - Auke Bay Laboratories, Alaska Fisheries Science Center, NOAA Fisheries, Juneau, AK
Phyllis Stabeno - NOAA Pacific Marine Environmental Lab, Seattle, WA
Rick Thoman - University of Alaska Fairbanks, International Arctic Research Center, Alaska Center for Climate Assessment and Policy, Fairbanks, AK
Muyin Wang - University of Washington, Cooperative Institute for Climate, Ocean, and Ecosystem Studies and NOAA Pacific Marine Environmental Lab, Seattle, WA

Last updated: October 2026

Outline

1. Alaska-wide Trends
    (a) Climate Overview
    (b) Regional Highlights
2. Eastern Bering Sea Trends
    (a) Sea Ice
    (b) Cold Pool
    (c) Surface Winds and Air Temperatures
    (d) Sea Surface and Bottom Temperatures

Summary
Beginning in about 2021, the eastern Bering Sea (EBS) exited the prolonged warm stanza and entered a more neutral thermal state that persisted into 2025. Over the past year (August 2025 - August 2026) many metrics, including sea surface temperature (e.g., Figures 43 and 54), depth-averaged temperature (Figure 50), wintertime sea ice extent (Figure 31) and thickness (Figures 34 and 35), and cool pool extent (Figures 36 and 37) show a rapid transition to cool thermal conditions.

Climate:
The North Pacific climate state in 2025-2026 was marked by a transition from weak La Niña to a strengthening El Niño in the tropical Pacific, while the Pacific Decadal Oscillation (PDO) remained strongly negative (Figure 24). During winter (Jan-Feb), the Aleutian Low Pressure System was exceptionally weak, resulting in a strongly negative Aleutian Low Index (ALI) (Figure 25). This weak low pressure system resulted in reduced winter storminess (Figure 26). In spring (Mar-Apr) strong, persistent north-to-south wind anomalies across the Bering Sea resulted in rapid sea ice expansion (Figure 27). Along the shelf break, winds from March through July favored off-shelf Ekman transport (Figure 41).

Sea Ice:
The temporal evolution of sea ice extent in the Bering Sea (Figure 32) resembled recent winters through February. Sea ice was largely below average until early March when a rapid increase brought sea ice as far south as the Aleutian Islands and into Bristol Bay, the highest sea ice extent since 2013 (Figure 2). A 6-week period of above average ice extent occurred between March and April. Sea ice retreated quickly beginning in mid April and by late April ice extent was below average. In 2026 sea ice thickness in most regions of the Bering Sea was slightly above to above average (Figures 34 and 35). In the western Bering Sea (Gulf of Anadyr), ice thickness has decreased since 2021 while in the Bering Strait ice thickness has increased since 2019 and been above average 2021-2026 (Figure 34b). Over the southern Bering Sea ice thickness was the highest since 2013 (Figure 35a).

Sea Surface Temperature and Cold Pool:
Providing a stark contrast to recent warm years, spring 2026 surface and bottom waters were the coldest observed since 2012 (Figure 43). Depth-averaged water column temperatures at Mooring M2 remained more than 2°C below average through late summer (Figure 50). No marine heatwaves (based on SST) occurred in either the southeastern or northern Bering Sea during 2026 (Figure 53), and the cumulative annual SST anomaly for the southeastern Bering Sea reached its lowest point since prior to the extended warm stanza that began in 2014 (Figure 54). The spatial extent of the <2°C cold pool expanded to 282,325 km^2 (~150% larger than in 2025), representing the fifth-largest cold pool in the 1982-2026 survey time series (Figures 2 and 36).

Ocean Forecasts:
For projections into 2027, the National Multi-Model Ensemble (NMME) forecasts project SST anomalies over the EBS shelf (Figure 29) to remain near or slightly below (-0.25°C to -0.5°C) historical means, strongly conditioned by seasonal sea ice cover. In contrast, warm anomalies (≥1°C above normal) are forecast to persist in the central/western North Pacific and western Bering Sea, while the Gulf of Alaska is expected to experience increasing warm surface anomalies in response to the 'Very Strong' Niño event.

1. Alaska-Wide Trends

(a) Climate Overview

Contributed by Emily Lemagie, *emily.lemagie@noaa.gov*, and Shaun Bell

Sea surface temperatures (SST) and sea ice data from the NOAA High-resolution Blended Analysis of Daily SST and Ice (OI SST V2[12]), along with 10-m wind data from the ERA5 Reanalysis[13] from September 2025 - August 2026 are described across eight regions of the North Pacific Ocean and U.S. Arctic (Figure 23). Note the transition this year to the ERA5 Reanalysis from the National Centers for Environmental Prediction (NCEP) due to data availability; the conclusions in this report are not impacted by the change.

State of the North Pacific Ocean

Contributed by Emily Lemagie, *emily.lemagie@noaa.gov*, and Muyin Wang

Strong positive SST anomalies have dominated the mid-latitudes of the global oceans this summer. As these anomalies increase in the eastern equatorial Pacific, El Niño conditions have strengthened (Figure 24). The latest update from the NOAA Climate Program Center is for a 90% chance of a very strong El Niño this coming autumn through winter. As El Niño reaches peak strength and the impacts expand northward, warm anomalies are expected to strengthen in the Gulf of Alaska, where ocean forecasts from the NOAA Physical Sciences Laboratory projects a 50% chance of reaching marine heatwave threshold by winter. Despite warm ocean conditions to the south, the continuing negative pattern of the PDO suggests that a warm major sea ice loss event over the Bering Sea is unlikely in the near future due to ocean-atmosphere interactions

[12] https://psl.noaa.gov/data
[13] https://cds.climate.copernicus.eu/datasets/reanalysis-era5-land

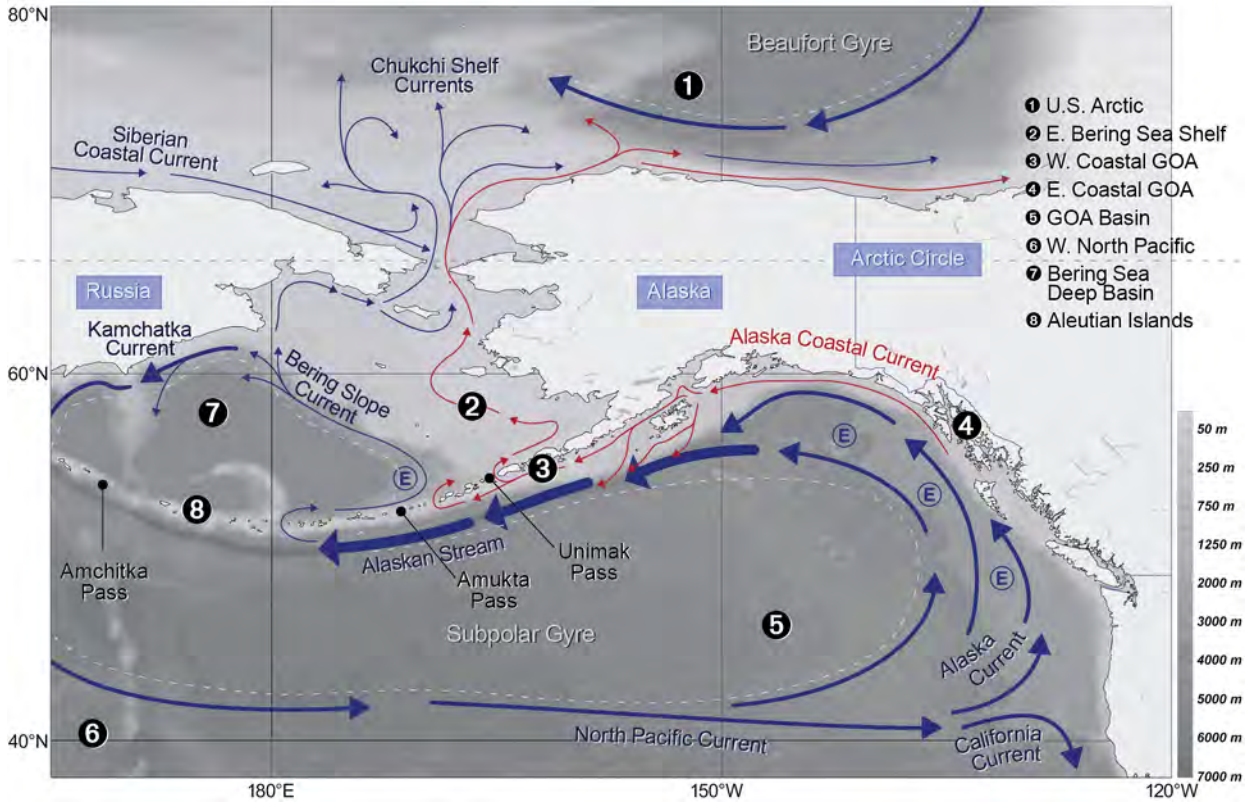


Figure 23: Geographic regions of interest, ocean bathymetry, and mean currents across the North Pacific and U.S. Arctic. Circled "E" denote eddies. Figure courtesy of Sarah Battle, PMEL.

The Aleutian Low is the dominant feature of the atmospheric pressure system in the North Pacific during winter (Dec - Mar), which develops and strengthens seasonally between the Beaufort high and North Pacific high pressure regions. The intensity and position of the Aleutian Low can significantly impact storm tracks, ocean circulation, and weather across the North Pacific, driving the extent of sea ice cover in the Bering Sea. Motivated by work from (Rodionov and Overland, 2005), we defined the Aleutian Low Index (ALI) as the areas where sea level pressure (SLP) is less than or equals to 1000hPa in the North Pacific region (40 - 60°N, and 160°E - 160°W). Aleutian Low is a statistical low, which exists in winter only. We computed the monthly Aleutian Low Index, and then averaged for the winter mean (January and February). A 30-yr climatology (1991-2020) mean is removed from the index.

A stronger Aleutian Low means the Bering Sea tends to be warm, stormy, and have less ice. This past winter, the Aleutian Low was extremely weak (Figures 25, 26). This reduced the poleward advection of warm air masses over the eastern North Pacific and the southward advection of Arctic air masses over the Bering Sea. Winter air temperature anomalies were cool over much of Alaska, except along the northern coast, while warm air temperature anomalies spanned the Russian continent and most of the North Pacific west of the dateline. This contrast marks a departure from the previous three winters, when above-average temperatures were anchored over Alaska and neighboring regions experienced far greater variability. In spring, the steep pressure gradient between the high pressure to the north and low pressure systems moving across the Aleutian Islands and Gulf of Alaska drove strong southward winds, bringing cold air and sea ice across the Bering Sea and rapid cooling into the North Pacific.

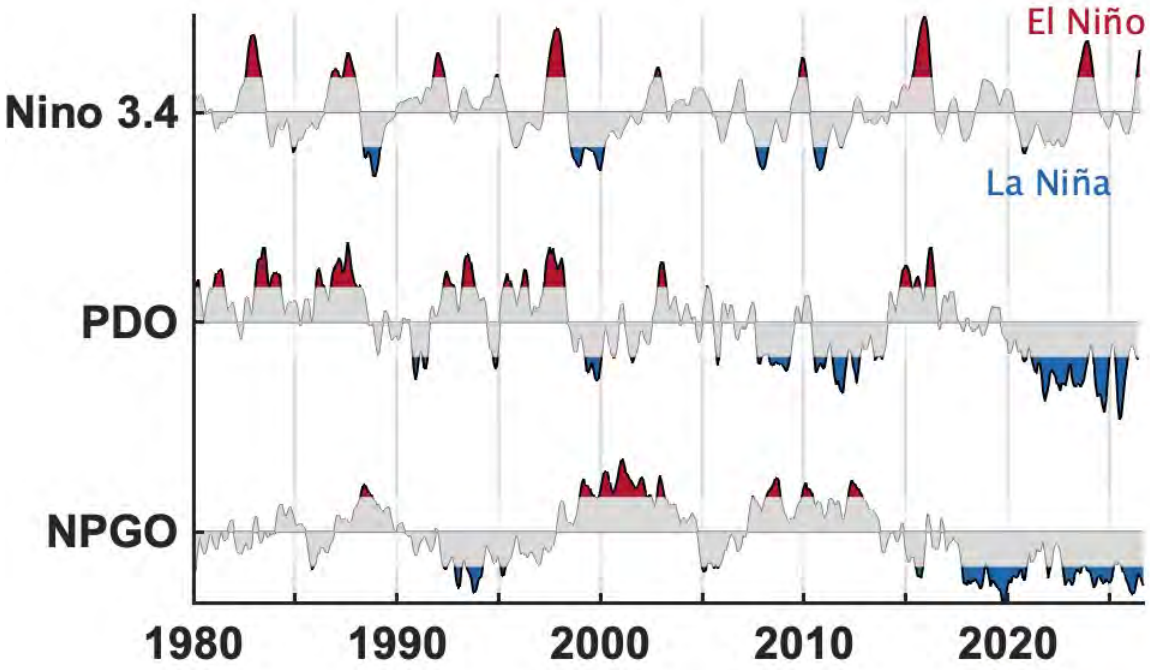


Figure 24: Time series of three commonly used oceanic indices related to the Alaska marine ecosystem, including the NINO3.4 index for the state of the El Niño/Southern Oscillation, the Pacific Decadal Oscillation (PDO) index, and the North Pacific Gyre Oscillation (NPGO) index, from 1980 to present. Each monthly index is normalized using a 30-year climatology from 1991-2020 and smoothed using a 3-month running mean. Red and blue shading indicates positive and negative values outside of one standard deviation, respectively. Lighter shaded areas are within one standard deviation of the 30-year climatology. Additional information on these indices can be found on the NOAA Physical Sciences Laboratory website.

Seasonal SST and Sea Level Pressure (SLP)

Contributed by Emily Lemagie, *emily.lemagie@noaa.gov*, and Shaun Bell

From Autumn 2025, surface temperatures were 1-2°C above average across much of the Alaska region (Figure 27). Over winter there was above average sea ice advance, and by spring this reached the greatest maximum sea ice extent across the Bering Sea since 2013. The advance of sea ice and of cold air masses over this period resulted in cool anomalies over the southeastern Bering Sea shelf that have persisted through the summer. However in the North Pacific and Bering Sea basins, positive SST anomalies have persisted (Figure 27). The weak Aleutian Low in winter and development of a strong Beaufort High pressure system in the spring and summer contributed to the strong wind-driven ice advection and reduced coastal current heat transport between the Gulf of Alaska and the Bering Sea shelf (Figure 28).

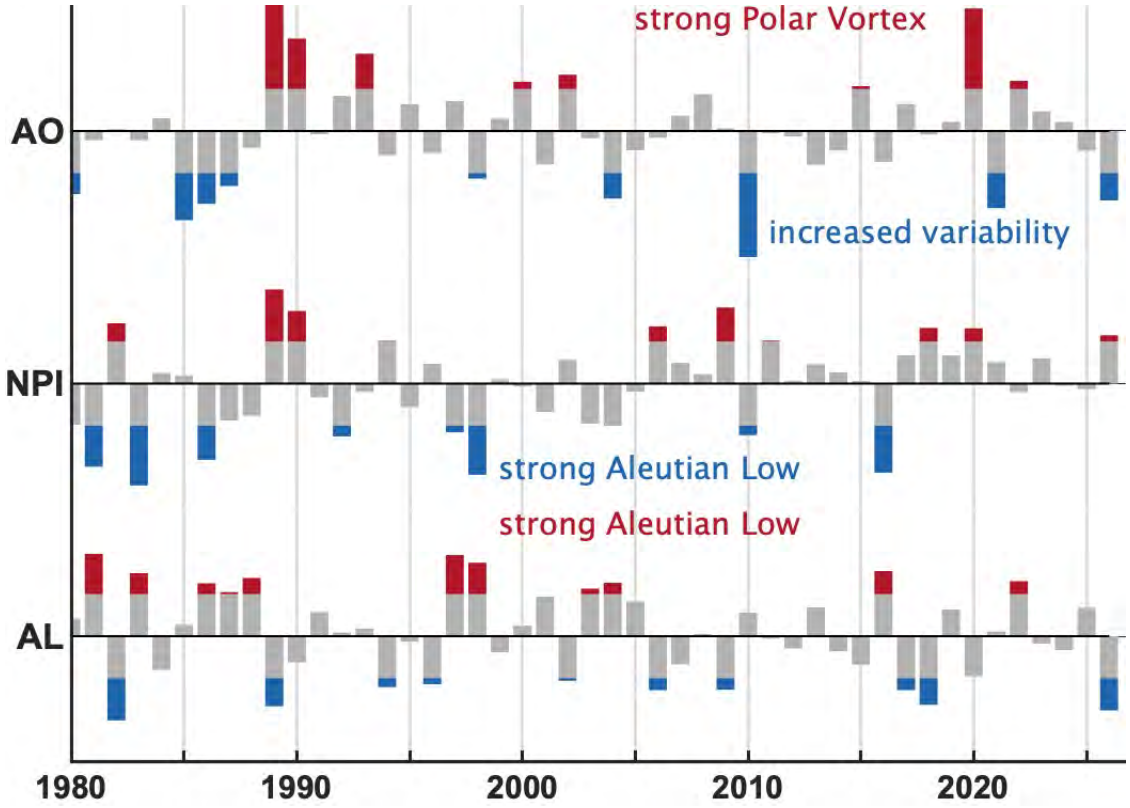


Figure 25: Time series of three indices related to winter atmospheric patterns, including the Arctic Oscillation (AO), North Pacific Index (NPI), and Aleutian Low index (AL) from 1980 to present. The AO and NPI indices are averaged over the winter period from November to March, while the Aleutian Low index is calculated as averaged over the months of January and February. The NPI and AL are normalized using a 30-year climatology from 1991-2020. Red and blue shading indicates positive and negative values, respectively, outside of a threshold value (AO $= \pm 1$) or of one standard deviation from the mean (NPI and AL). Additional information on these indices can be found on the NOAA Physical Sciences Laboratory website.

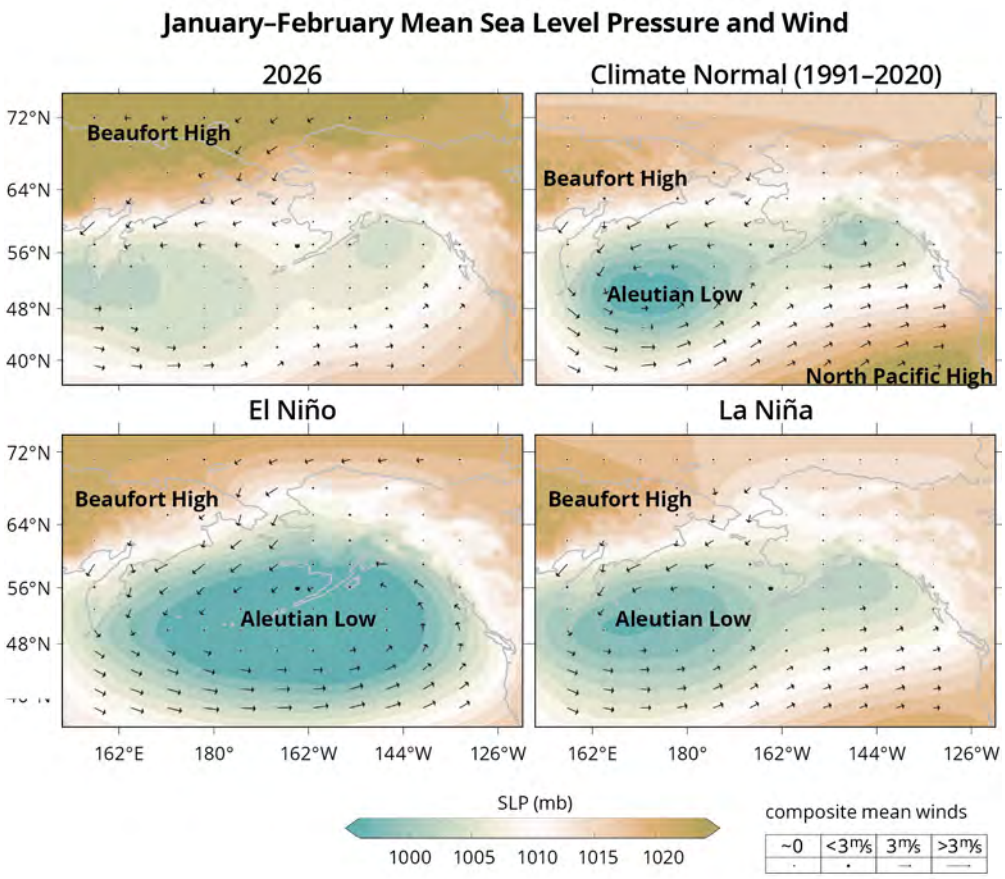


Figure 26: Top row: Mean January-February sea level pressure (SLP) and surface wind patterns in 2026, from the climatological mean (1991-2020). For reference, January-February SLP composite mean patterns for positive (El Niño) and negative (La Niña) Nino3.4 conditions are also shown.

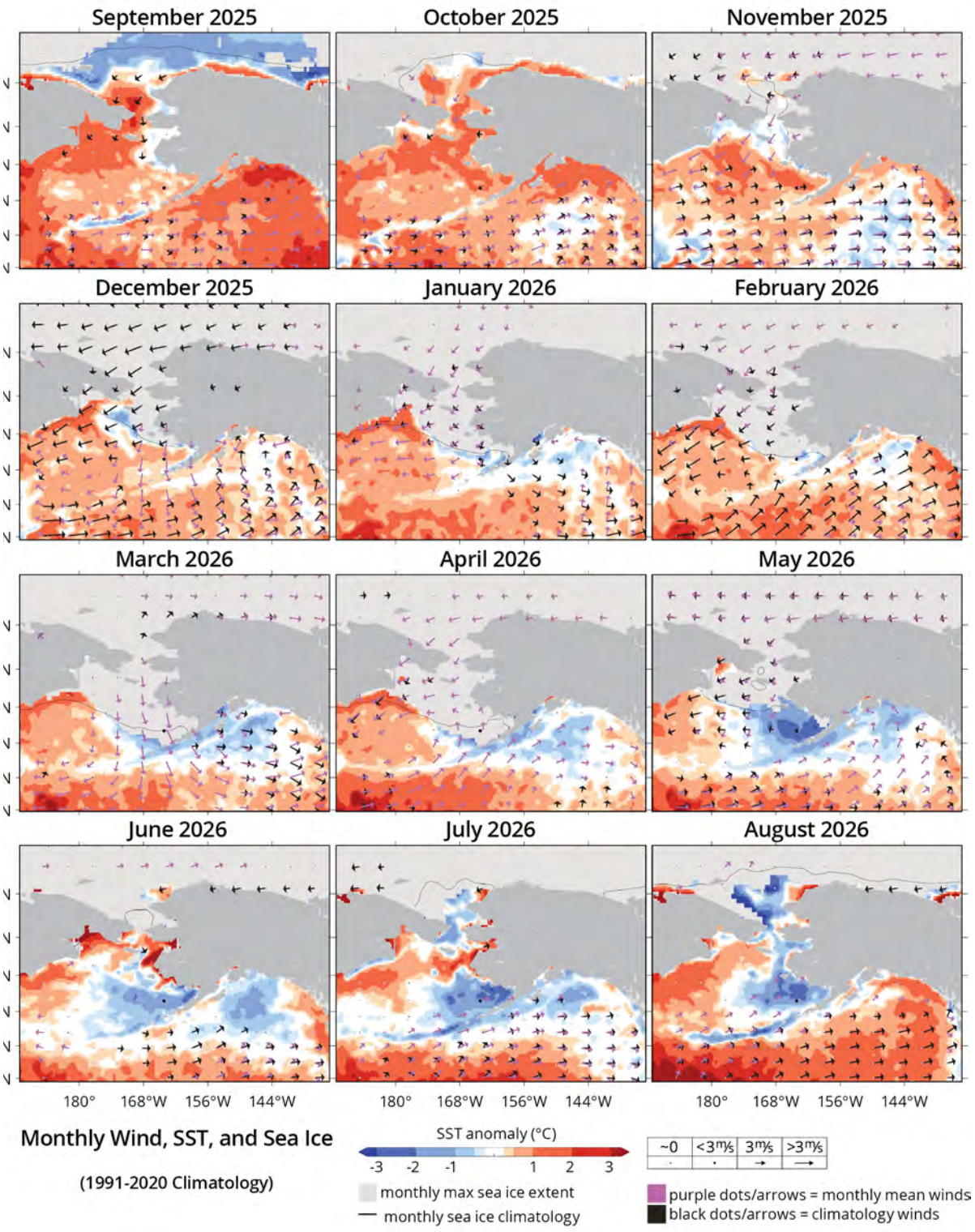


Figure 27: Monthly mean maps of sea surface temperature (SST) anomalies and surface winds. Monthly climatological winds (black) are compared to monthly mean winds (purple). The climatological period is from 1991-2020. SST data are from the NOAA High-resolution Blended Analysis of Daily SST and Ice (OISST) available from NOAA's Physical Sciences Laboratory[12], and 10-m wind data are from the ERA5 Reanalysis available from the Copernicus Climate Change Service[13]. Figure design courtesy of Sarah Battle, PMEL.

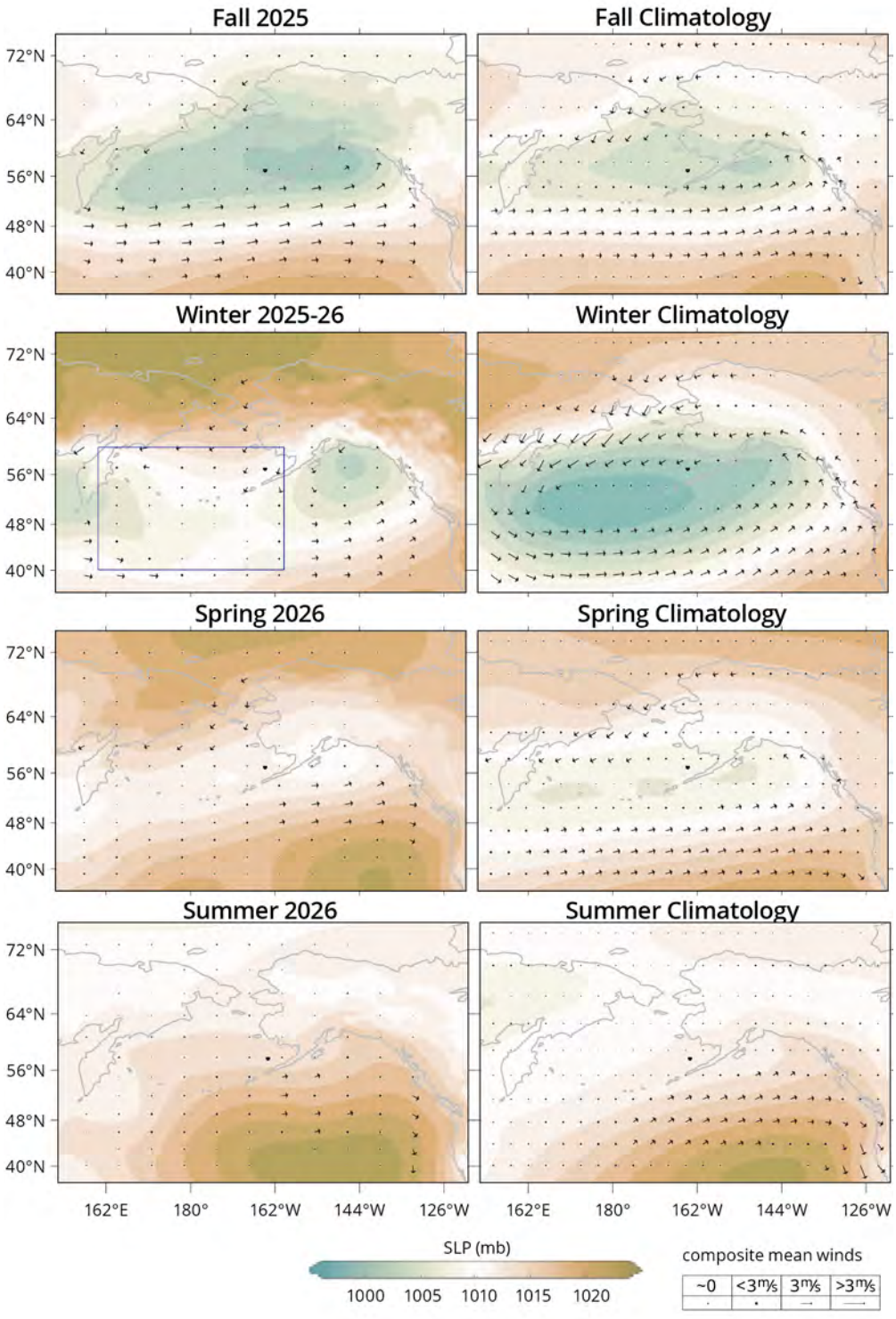


Figure 28: Left: Seasonal SLP and mean winds for autumn (Sep-Nov 2025), winter (Dec 2024-Feb 2025), spring (Mar-May 2025), and summer (Jun-Aug 2025). Right: climatologies of seasonal mean SLP and wind calculated from 1991-2020. The blue box over the winter panel corresponds with the region over which the Aleutian Low climate index is calculated (Figure 25). Data are from ERA5 Reanalysis available from the Copernicus Climate Change Service[13].

Model Prediction Summary

Contributed by Emily Lemagie, *emily.lemagie@noaa.gov*

Seasonal predictions of SST anomalies from the National Multi-Model Ensemble (NMME) are shown in Figure 29. An ensemble approach incorporating different models is particularly appropriate for seasonal and interannual predictions. The NMME represents the average of eight climate models. The uncertainties and errors in the predictions from any single climate model can be substantial. More detail on the NMME, and predictions of other variables, are available at the NCEP website[14]. A description of the probability forecasts can be found on the NOAA NMME website[15]. This probability forecast combines predictions from 79 model ensembles and divides the outcomes into three equal groups: Above normal, Below normal, and Near normal. Map contours highlight a specific category whenever a clear consensus emerges: Above (A) or Below (B) is shown if at least 38% of models favor that outcome while fewer than 33% favor the opposite. If Near Normal is also high (over 33%), the Above or Below forecast still takes priority. Near Normal (N) is shown only when more than 38% of models predict average conditions and both Above and Below remain under 33%. White areas indicate uncertainty where no single category dominates—either because model votes are split evenly across all three outcomes, or because models are conflicting heavily between Above and Below.

Surface temperatures are projected to be below - but within 0.5°C - of the historical mean temperature over the eastern Bering Sea shelf. However, the winter and spring forecasts are highly dependent on seasonal sea ice coverage. Warm surface ocean temperatures $\geq$1°C above typical are likely to persist over the central and western North Pacific and the western Bering Sea. Gulf of Alaska temperature anomalies are projected to increase over time, with greater warmth along the coast, particularly in the eastern coastal Gulf of Alaska, through spring 2026. This pattern is consistent with a lagged response to the ongoing El Niño in the tropical Pacific. In the eastern north Pacific basin, south of the Gulf of Alaska, near-normal or slightly below average surface temperatures are forecast. There is high model agreement across the ensemble member forecasts, particularly in the western and central North Pacific and in the Gulf of Alaska.

[14] `http://www.cpc.ncep.noaa.gov/products/NMME`

[15] `https://www.cpc.ncep.noaa.gov/products/NMME/NMME_PROB_descr.html`

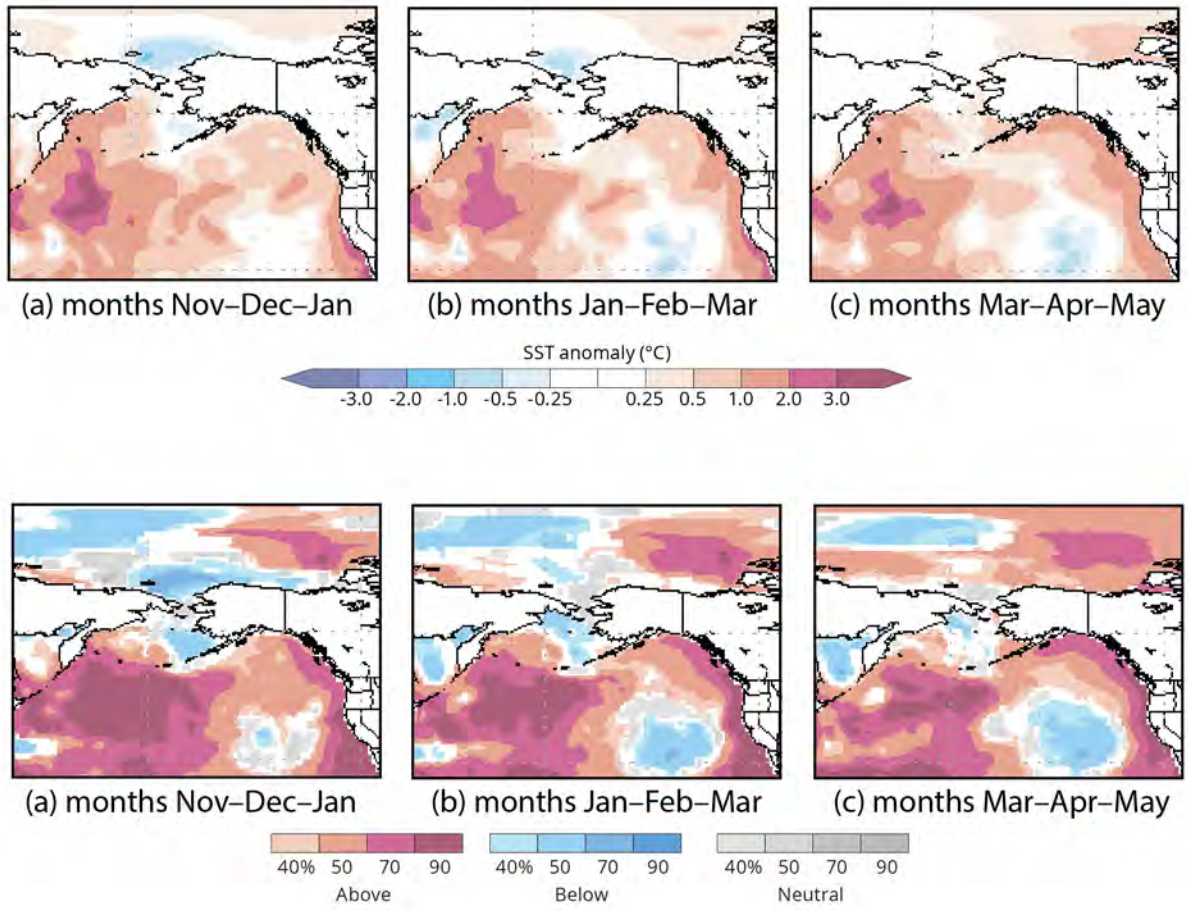


Figure 29: Predicted SST anomalies (top) and corresponding forecast probabilities from the NMME model for Nov-Dec-Jan (1-month lead) for the 2026-2027 season, Jan-Feb-Mar (3-month lead), and Mar-Apr-May (5-month lead) 2027.

(b) Regional Summaries

Contributed by Emily Lemagie, *emily.lemagie@noaa.gov*

U.S. Arctic

The near-average and slightly above average sea ice extent on the North Slope and over the Chukchi Sea since October 2025 contrasted the relative lack of sea ice coverage on the far side of the Arctic basin. The sea ice conditions in the Laptev, Kara, and Barents Sea and along eastern Greenland were far below normal. Arctic-wide, the annual maximum extent (reached March 15, 2026) was the lowest in the 47-year satellite record, and this summer the July sea ice extent was the 6th lowest on record. Meanwhile, mean winds predominantly stronger than average and southward through the Bering Strait helped to deliver cool air and sea ice into the Bering Sea (Figure 27). Following the local sea ice retreat, late summer surface temperature anomalies in 2026 were negative in parts of the Chukchi Sea, but warm surface anomalies have persisted along the bays and coastal waters in northern Alaska.

Bering Sea Deep Basin

Above average surface temperature anomalies ~1-2°C persisted across the Bering Sea basin since autumn 2025, similar to the conditions since autumn 2024 (Figure 27). Through much of the last year, winds were weaker than average over the basin. In particular, due to the extremely weak Aleutian Low pressure over winter, there was less advection of cool air from northern latitudes (Figure 28). Transport of heat from lower latitudes via the Alaska Stream that feeds the Bering Slope and Kamchatka current (e.g., Figure 23) and from warm air temperature anomalies over the region likely contributed to the above average basin surface temperatures. The slightly below-average sea ice extent this winter near Cape Navarin - where the Bering Slope current becomes the Kamchatka current - was likely due to the warm current melting the ice along the leading edge.

Eastern Bering Sea Shelf

In autumn 2025, the eastern Bering shelf surface temperatures were 1-2°C above average (Figure 27). In November, southward winds through the Bering Strait began to cool the northern Bering sea shelf and advect sea ice southward. The sea ice extent as it advanced over the shelf from November through February was near-average, varying in association with the prevailing winds. In March and April, a six week period of anomalous southward winds drove a rapid expansion of sea ice southward, passing the long-term M2 mooring site, and extending into Bristol Bay and to the Aleutian Islands. This resulted in the greatest local sea ice coverage at M2 since 2017, and the greatest maximum sea ice extent across the Bering Sea since 2013. This rapid late-season expansion was followed by a rapid retreat in mid-April. However, the sea ice was present long enough to cool the waters of the southeastern Bering Sea shelf, and temperatures cooler than 2°C below average have persisted through the summer 2026.

Aleutian Islands

Since 2020, strong SST anomalies and subsurface warming has persisted over the central North Pacific Ocean, captured by ocean indices such as the PDO and marine heatwave statistics (Figure 24). Weaker, but largely persistent warm anomalies have also spanned much of the Aleutian Islands, particularly in the west, and Bering Sea basin. Anomalous spring and summer winds disrupted typical atmospheric and oceanic heat transport, driving cooler ocean temperatures eastward across the archipelago. Sea surface temperatures dropped below the marine heatwave threshold in mid-summer across the western and central Aleutians. However, moving into fall, marine heatwave conditions have reemerged as subsurface warmth mixes to the surface.

2. Eastern Bering Sea Trends

(a) Sea Ice

Early Season Ice Extent

Contributed by Rick Thoman, *rthoman@alaska.edu*

The presence or absence of early sea ice in the Bering Sea is important because, at least during the passive microwave era, nearly all ice in the Bering Sea is first year ice, therefore Bering Sea ice thickness is related to both the air temperature and the age of the ice.

Early season (Oct 15 - Dec 15) ice extent in 2026 was higher than most years since 2013 except for 2022's very high values, and lower than any year prior to 2000. Over the 48 year period of record, early season mean sea ice extent has decreased (Figure 30).

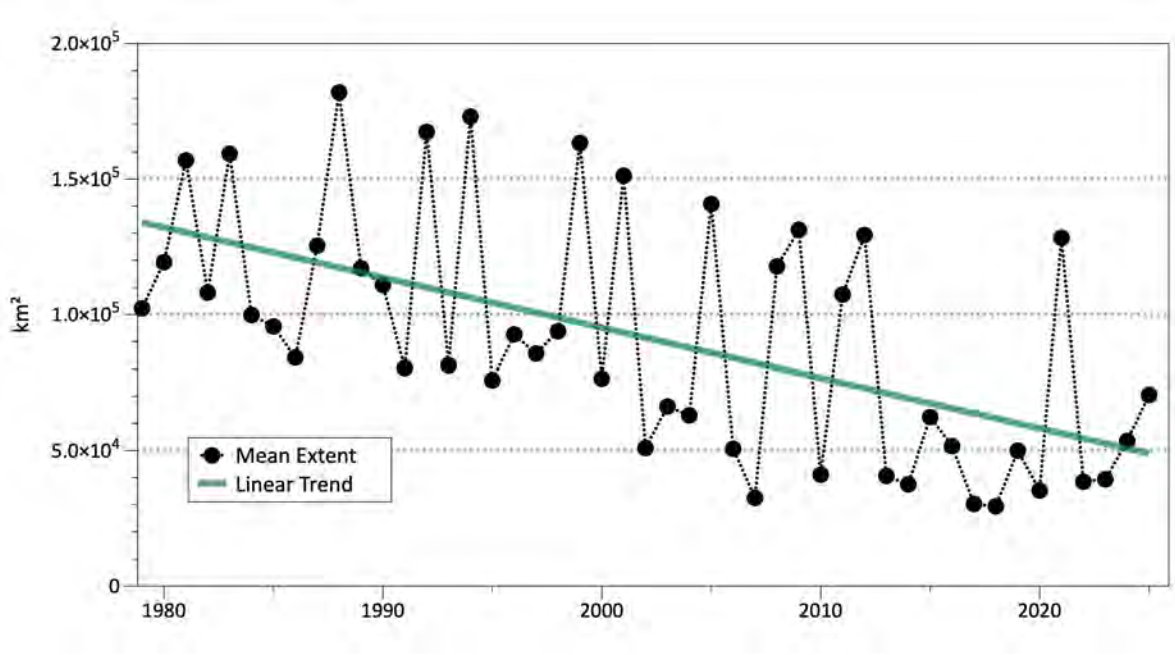


Figure 30: Early (15 Oct-15 Dec) mean sea-ice extent in the Bering Sea, 1979-2025.

Annual Bering Sea Ice Extent

Contributed by Rick Thoman, *rthoman@alaska.edu*

The Bering Sea has historically been ice-free in the middle and late summer, with ice developing during the second half of October. To account for this seasonal cycle, the Bering Sea ice year is defined as 1 August to 31 July. Bering Sea ice extent data are from the National Snow and Ice Center's Sea Ice Index, version 3 (Fetterer et al., 2017), and use the Sea Ice Index definition of the Bering Sea (effectively south of the line from Cape Prince of Wales to East Cape, Russia).

Annual mean daily sea ice extent in the Bering Sea has declined overall and interannual variability has increased significantly since the mid-1990s (Figure 31). The 2025-2026 average ice extent was higher than every year since 2013 except for 2022's very high value. While a significant recovery from the extreme 2017-2018 and 2018-2019 seasons, the 12-month average extent was similar to what were considered "low stanza" years prior to 2010. **Note:** The current season is based on preliminary data and slight changes usually occur in extent values after final processing.

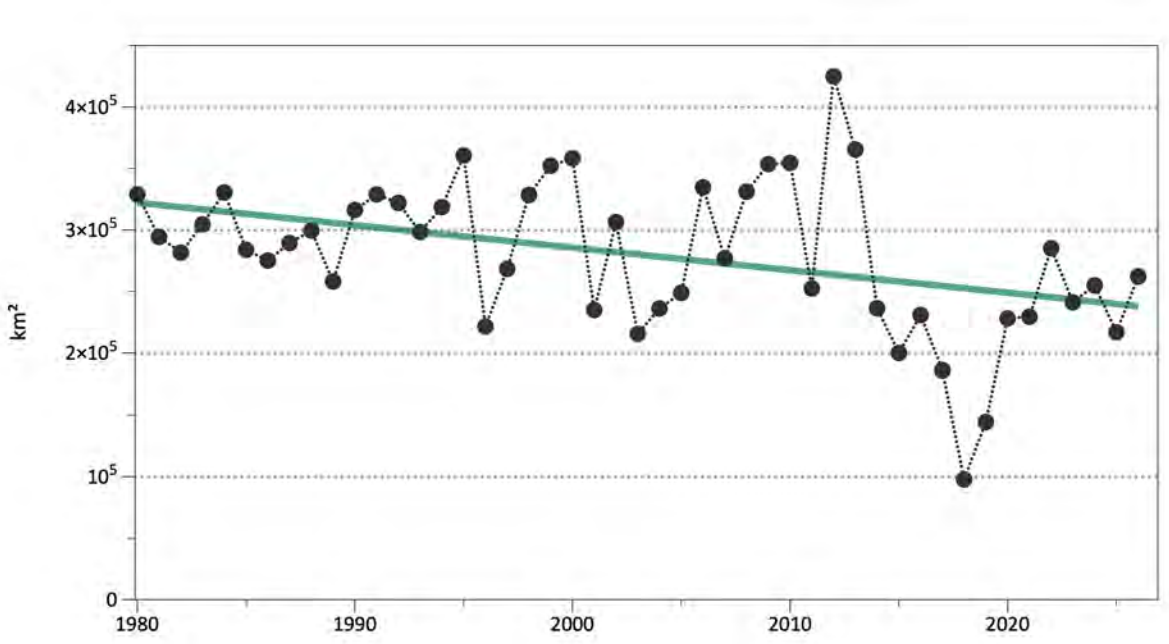


Figure 31: Mean sea ice extent in the Bering Sea from 1 August to 31 July, 1979/1980 - 2025/2026.

Bering Sea Daily Ice Extent

Contributed by Rick Thoman, *rthoman@alaska.edu*

Tracking the seasonal progression and retreat of sea ice highlights the interactive roles of water temperature (i.e., warmth in the system) and winds (Figure 32). Sea ice extent was largely below average until early March 2026 when a dramatic increase in ice extent brought sea ice as far south as the Aleutian Islands and into Bristol Bay. A 6-week period of above average ice extent occurred between March and April. Sea ice retreated quickly beginning in mid April and by late April ice extent was below average.

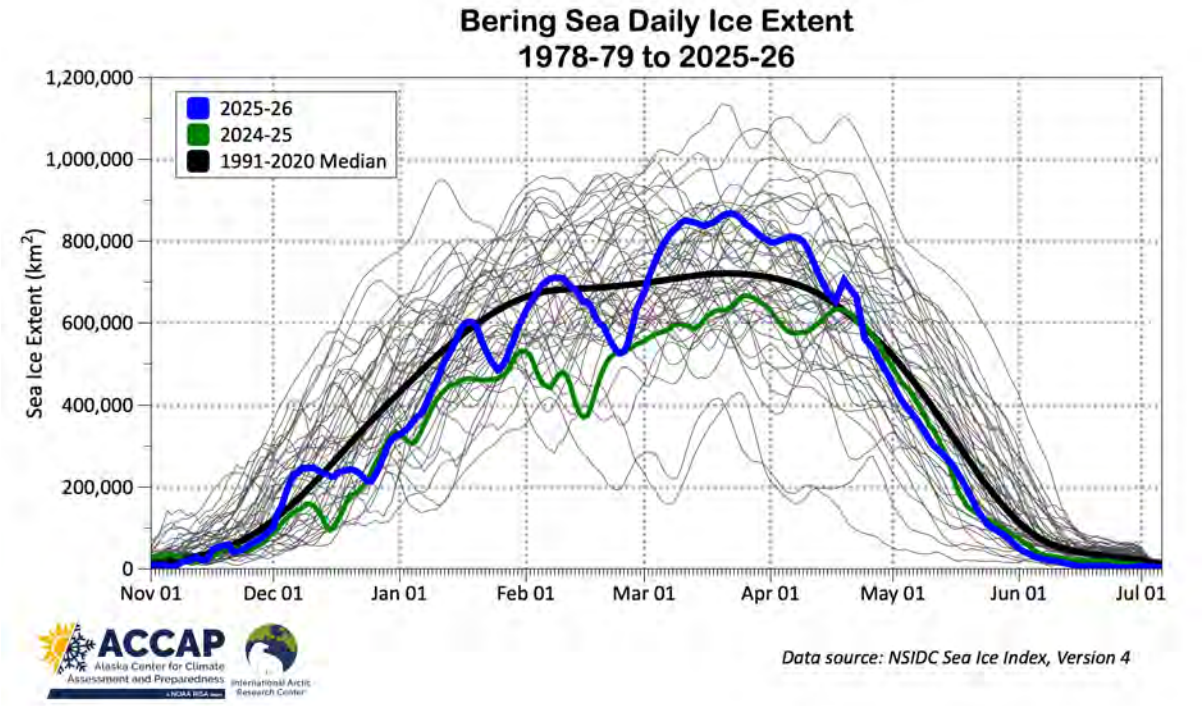


Figure 32: Daily ice extent in the Bering Sea. The most recent year (2023-2024) is shown in blue, 2022-2023 in green, and the historical median in black. Individual years in the time series are shown in gray.

Sea Ice Thickness

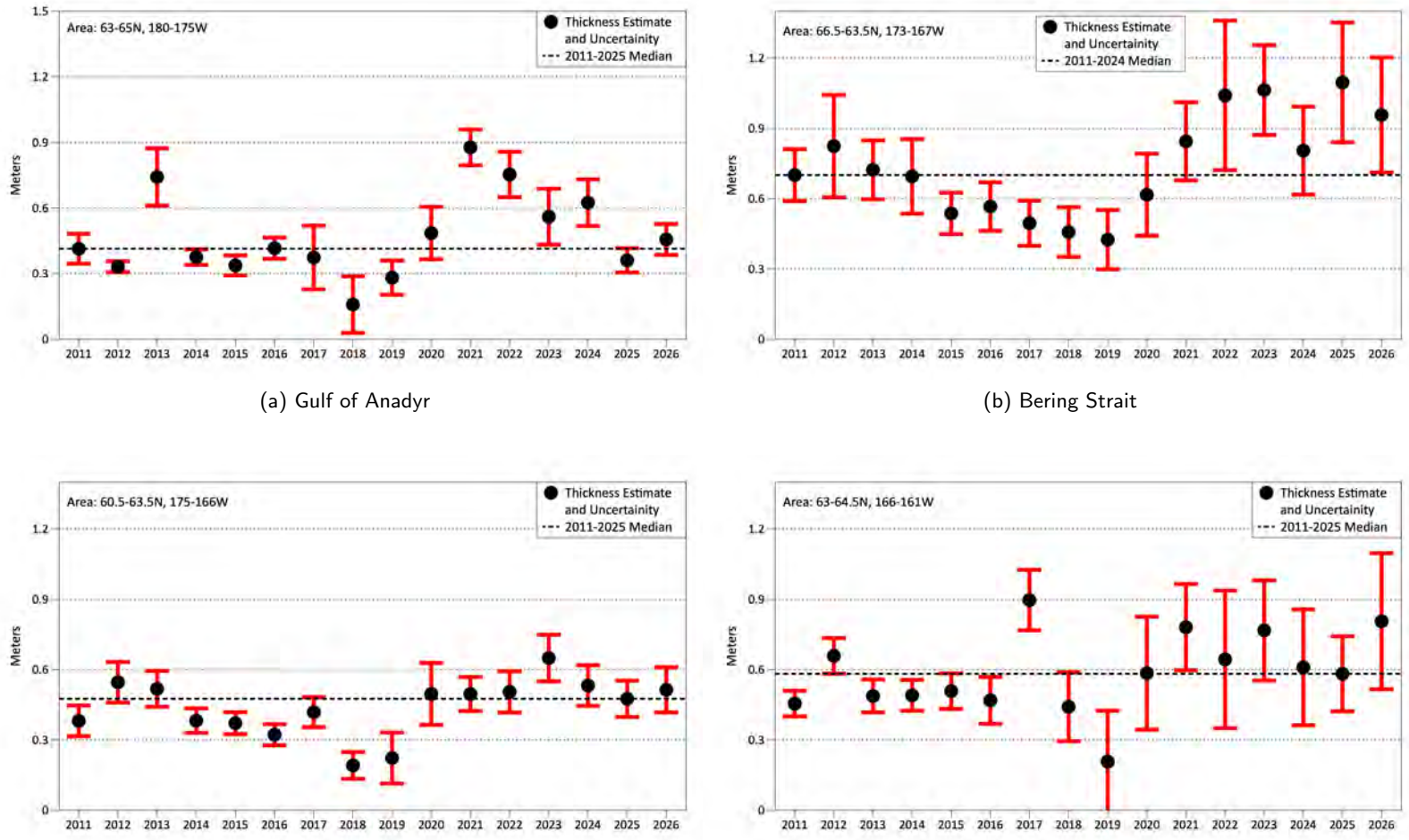
Contributed by Rick Thoman, *rthoman@alaska.edu*

Ice thickness is evaluated at six regions (Figure 33) in the Bering Sea from March 15-21, as this is generally the week with the greatest areal extent of sea ice. This year's report uses version 3.0 of the combined CryoSat-2/SMOS sea ice thickness from the Alfred Wegener Institute. There are only very minor differences from version 2.05 that was used last year.

In 2026 sea ice thickness in most regions was slightly above to above average (timeseries 2011-2026). In the western Bering Sea (Gulf of Anadyr), ice thickness has decreased since a timeseries maximum in 2021 to slightly above average in 2026 (Figure 34a). Ice thickness in Bering Strait was below average 2015-2019 and increased to above average 2021-2026 (Figure 34b). Ice thickness in the northern Bering Sea (Figure 34c) was below average 2014-2019 and increased to average or above average 2020-2026. Ice thickness in Norton Sound was above average and thicker than every year in the timeseries except 2017 (Figure 34d). Over the southern Bering Sea (Figure 35a) ice thickness was the highest since 2013. While ice thickness in Bristol Bay is more variable interannually, 2026 ice was slightly thicker than 2024 and 2025 (Figure 35b).



Figure 33: Map showing the six areas over the Bering Sea within which sea ice thickness indices were calculated: Gulf of Anadyr (Bering W), Bering Strait, Norton Sound (Bering E), St. Lawrence Island to St. Matthew Island (Bering NC), St. Matthew Island to St. Paul Island (Bering S), and Bristol Bay (Bering SE).



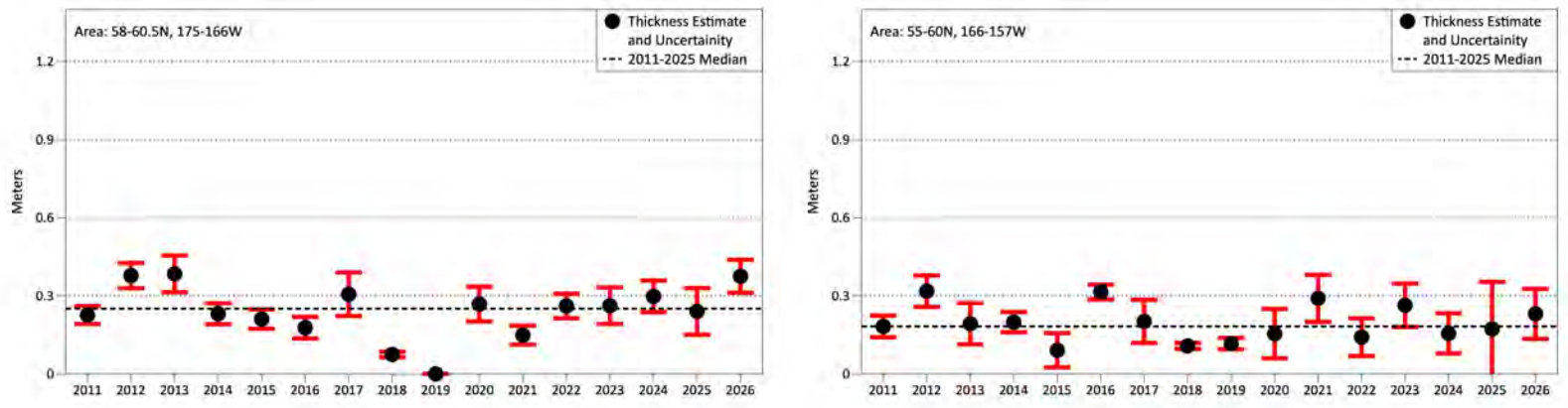
(a) Gulf of Anadyr

(b) Bering Strait

(c) St. Lawrence Island to St. Matthew Island

(d) Norton Sound

Figure 34: Sea-ice thickness in the Bering Sea for (a) Gulf of Anadyr, (b) Bering Strait, (c) St. Lawrence Island to St. Matthew Island, and (d) Norton Sound. Source: Alfred Wegener Institute. Details on how uncertainty in sea-ice thickness was quantified are available at: `https://www.meereisportal.de/en`.



(a) St. Matthew Island to St. Paul Island

(b) Bristol Bay

Figure 35: Sea-ice thickness in the Bering Sea for (a) St. Matthew Island to St. Paul Island and (b) Bristol Bay. Source: Alfred Wegener Institute. Details on how uncertainty in sea-ice thickness was quantified are available at: `https://www.meereisportal.de/en`.

(b) Cold Pool Extent

Cold Pool Extent - AFSC Bottom Trawl Survey

Contributed by Sean Rohan, *sean.rohan@noaa.gov*, and Lewis Barnett

The cold pool extent (waters <2°C) in 2026 was 282,325 km^2, 150% larger than in 2025 and the fifth largest in the 1982-2026 survey time series (Figures 2 and 36). The extent of the ≤0°C isotherm (71,925 km^2), which is considered a more important temperature barrier for subarctic fishes than 2°C, was the largest since 2013 and 12th largest in the time series. The coldest temperatures, represented by the extent of <-1°C isotherm (16,275 km^2) was 39% smaller than in 2023 and 69% smaller than the average extent during the 2006-2013 cold stanza.

Cold Pool Extent - ROMS

Contributed by Kelly Kearney, *kelly.kearney@noaa.gov*

The most recent MOM6-NEP near-real-time hindcast extension, which runs through Aug 14, 2026, was used to analyze the seasonal evolution of surface and bottom temperature in the eastern Bering Sea.

Winter 2026 conditions in the Bering Sea began very close to the long-term mean across the entire shelf. Then in March 2026, the southeastern shelf region cooled due to rapid sea ice advance, with surface and bottom temperatures dropping approximately 0.4°C and 1.16°C, respectively, below average (Figures not shown). As ice retreated in spring, surface temperatures in the southeastern region moved toward average values, but bottom temperatures remained below average, closely tracking the persistence signal from late April/early May. The 2°C cold pool peaked at near-average in April, but decreased more slowly than the average, staying above the mean through August. The EBS °C cold pool index peaked well above the median in mid-April. However, this less than 0°C water rapidly diminished in May, reaching below the mean by mid June. In the northern Bering Sea, bottom temperatures remained near average throughout the year, while surface temperatures were warmer than average (and warmer than the conditions predicted by persistence alone).

In 2026, a smaller than average summer 0°C cold pool but larger than average 2°C cold pool can be seen in the July bottom temperature maps (Figure 37). The closest analog year from the hindcast suite (1993-2025) with this summer pattern of cold conditions in the southeastern region but neutral to warm conditions in the northern Bering Sea in the summer months is 2007 (Figure 38).

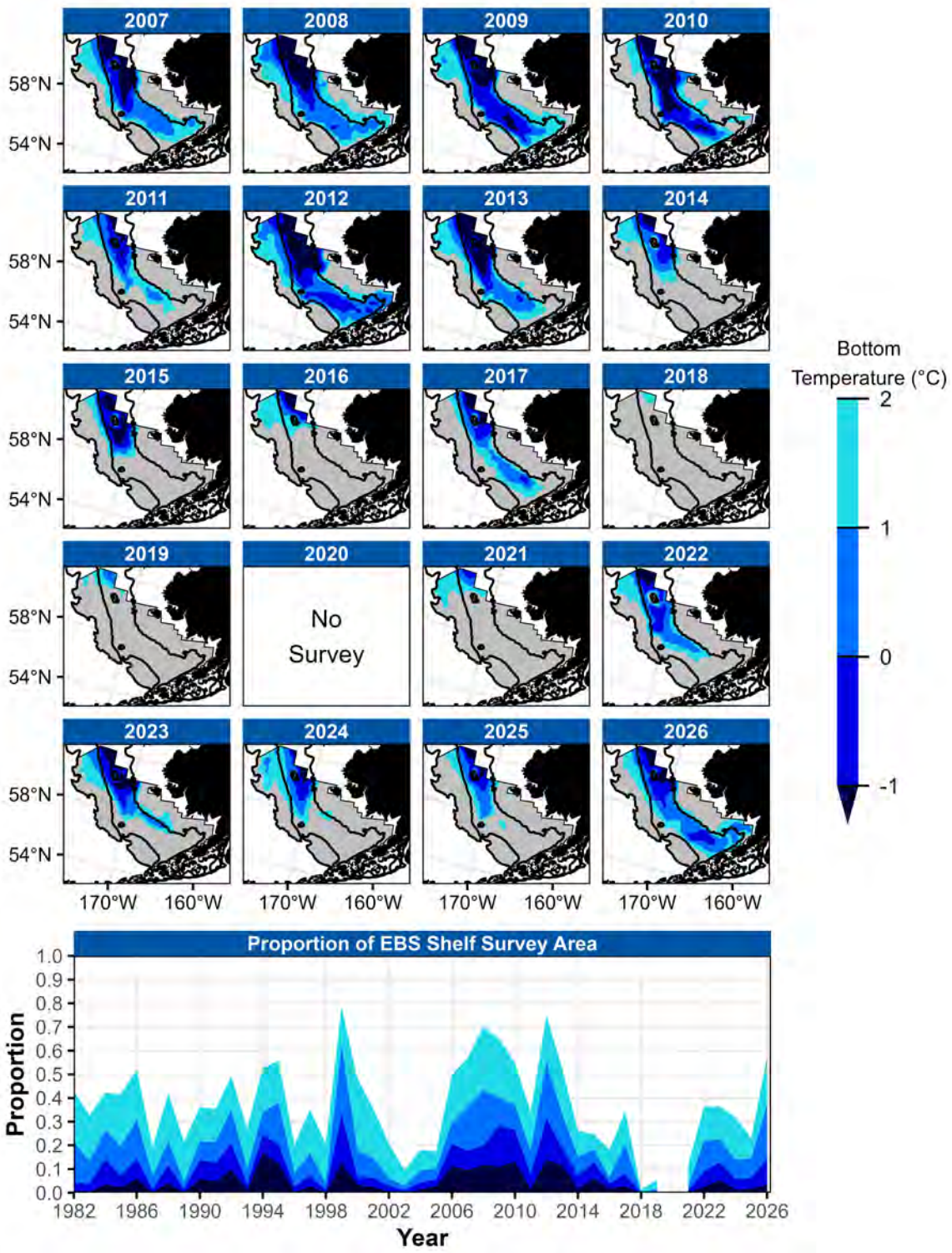


Figure 36: Cold pool extent in the eastern Bering Sea (EBS), as measured using observations from the EBS bottom trawl survey. Upper panels: Maps of cold pool extent in the EBS shelf survey area from 2007-2026. Lower panel: Extent of the cold pool in proportion to the total EBS shelf survey area from 1982-2026. Fill colors denote bottom temperatures $\leq$2°C, $\leq$1°C, $\leq$0°C, and $\leq$-1°C.

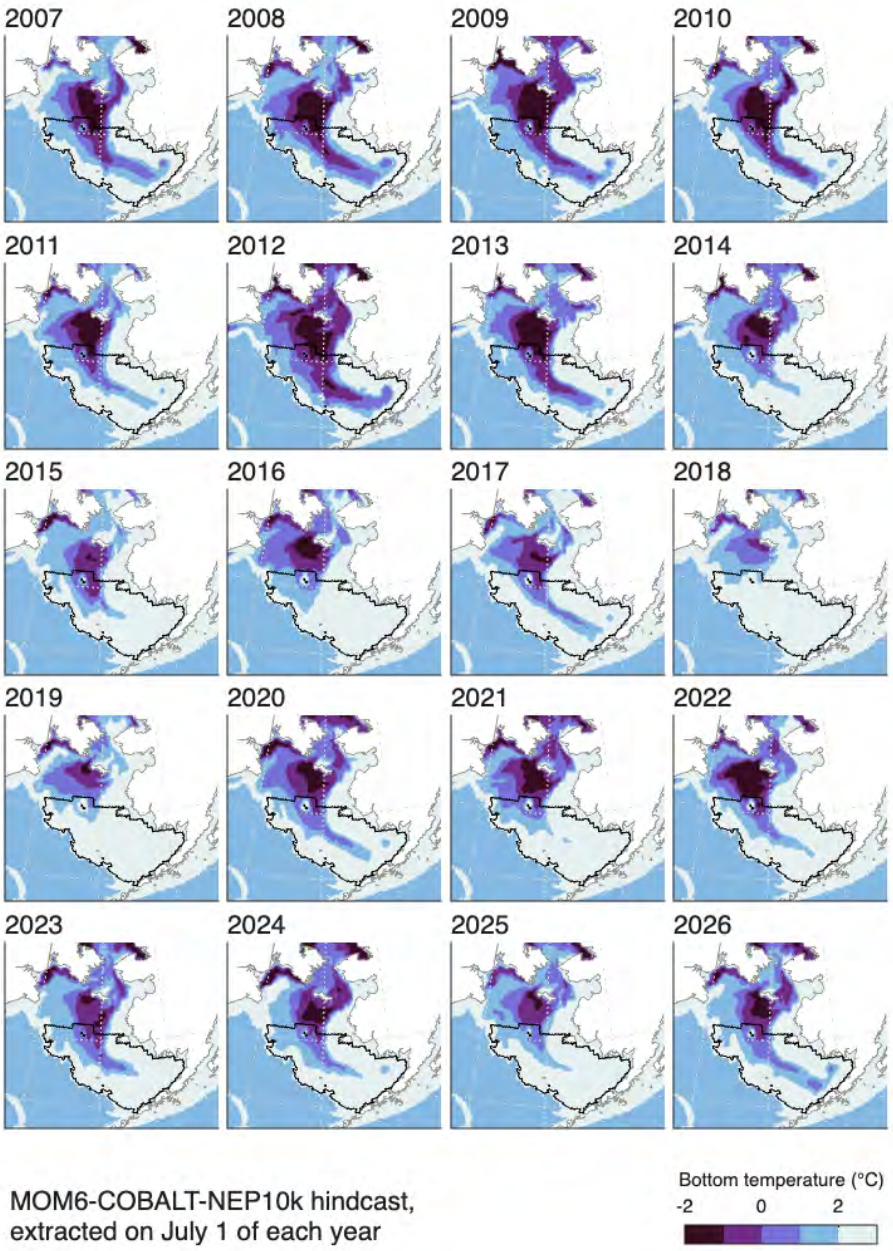


Figure 37: MOM6-NEP hindcast, extracted on July 1 of each year, for the Bering Sea, 2007-2026. The black outline denotes the standard bottom trawl survey grid.

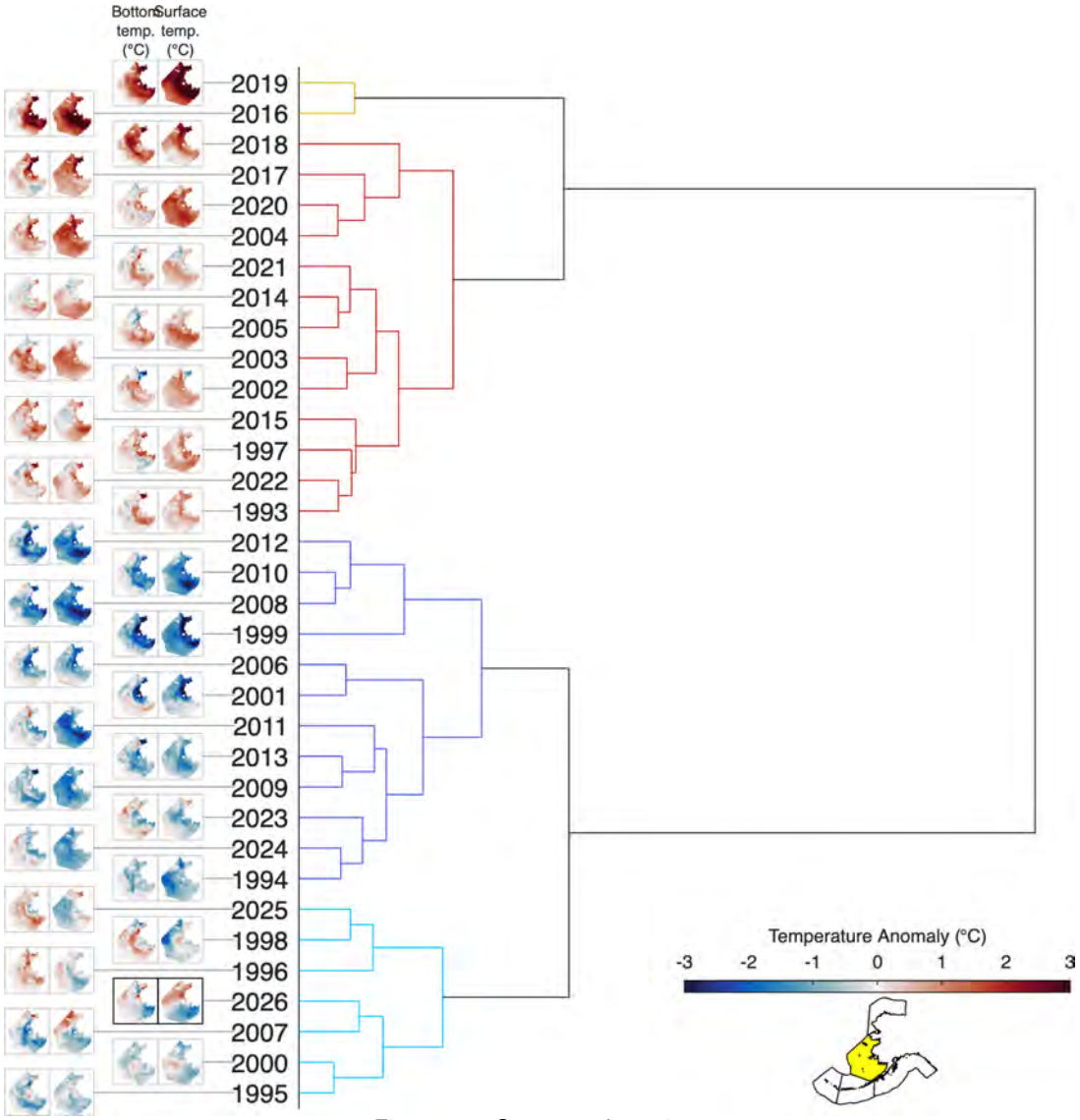


Figure 38: Summer clustering.

(c) Surface Winds and Air Temperatures

Winter Wind Speed and Direction

Contributed by Rick Thoman, *rthoman@alaska.edu*

The average winter (Nov-Mar) wind speed categorizes years as having prevailing north winds or south winds. No long-term trend is exhibited, although winters ending in 2018 and 2019 were among 10 years with the strongest south winds, which contributed to low sea ice extent in those years. The north-south component of the low level wind for the 2025-2026 winter was above average (north winds prevailed) (Figure 39). Winds from the north contributed to sea ice advance in early January and early March 2026 (Figure 32).

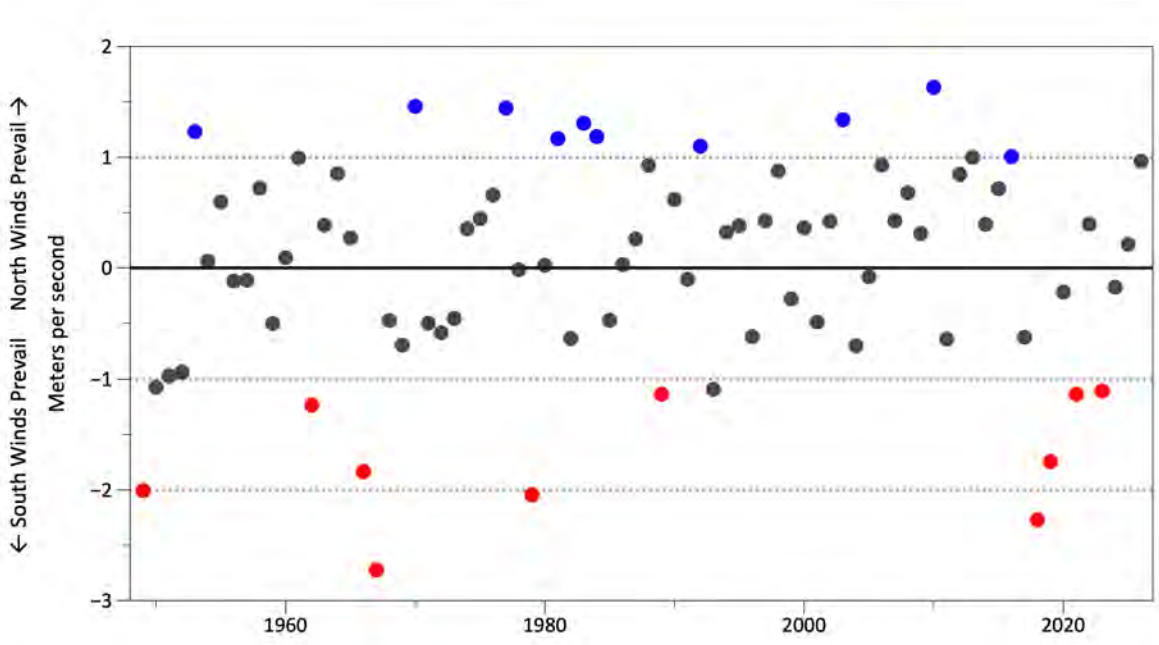


Figure 39: Winter (Nov-Mar) average north-south wind speed anomaly in the Bering Sea, 1949-2026. Red dots denote five years with strongest south winds, blue dots the five strongest north winds. **Note:** the north-south (meridional) component of the wind is plotted inverse to meteorological convention with south to north as negative values and north to south as positive values. Source: NCEP/NCAR reanalysis.

Winds at the Shelf Break

Contributed by Tyler Hennon, *tdhennon@alaska.edu*

ERA5 wind reanalysis was used to look at the along- and cross-slope wind components along the Bering shelf break. Monthly averages of the meridional and zonal 10 m wind data dating back to January 1980 are interpolated to a transect approximating the shelf break (Figure 40) and wind vectors are rotated into along- and cross-shelf components.

The average annual cycle (from 1991-2020) is stronger for the cross-shelf component than along-shelf (Figure 41). Generally, the Ekman transport associated with cross-shelf winds will be parallel to the shelf break, and could either inhibit or enhance near surface transport associated with the current along the shelf break. Winds oriented along the shelf break will either favor on- or off-shelf transport. Measurements taken at the M2 mooring show that the Ekman layer is no deeper than 30-40 meters from May-October (Noel Pelland, pers comm). This suggests the cross-shelf transport driven by winds is unlikely to directly drive upwelling or downwelling at the shelf break, as the water is substantially deeper there (∼200 m). However, the Ekman transport associated with surface wind stress may still be informative to understanding egg and larval dispersal (e.g., crab or groundfish) in the upper ocean.

While in both 2025 and 2026 the cross-shelfbreak winds were within the nominal normal range (20-80%), there were noteworthy trends in the along-shelfbreak winds. In 2025, winds were anomalously (outside the 20-80% band) favorable to off-shelf Ekman transport between March and April, reversing to become anomalously favorable to on-shelf Ekman transports in the middle of summer (June/July). In 2026, the winds were anomalously favorable to off-shore Ekman transport from March to June, except for a brief reversal toward on-shelf favorable Ekman transports (Figure 41).

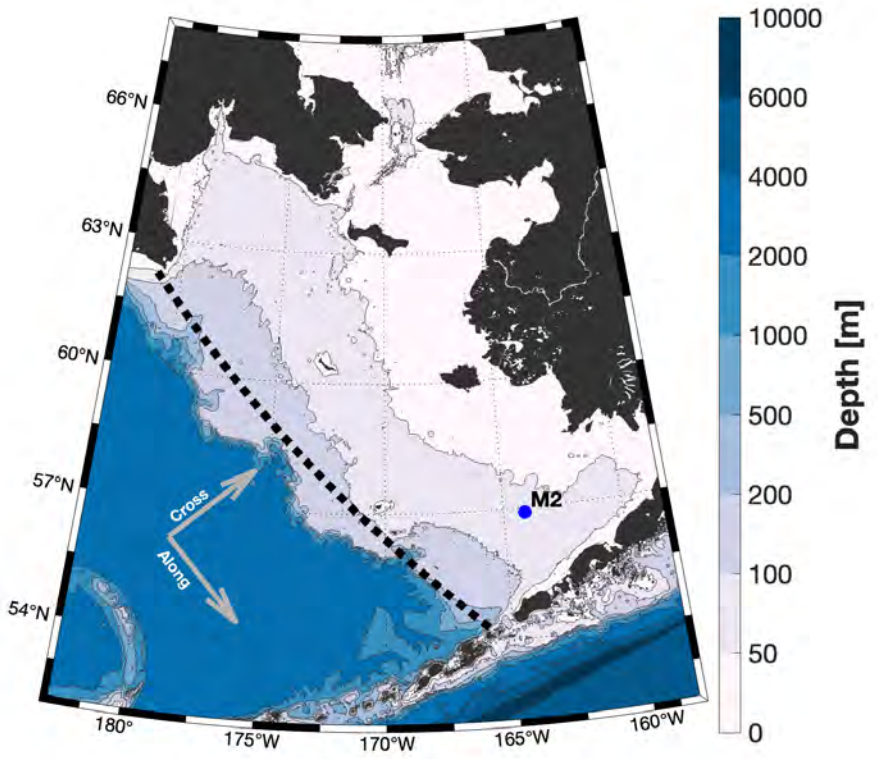


Figure 40: The dashed black line shows the section chosen to evaluate along-shelf and cross-shelf wind components in the Bering Sea. Annotation arrows show the direction used to define positive cross- and along-shelf components of wind. The blue dot shows the location of the M2 mooring.

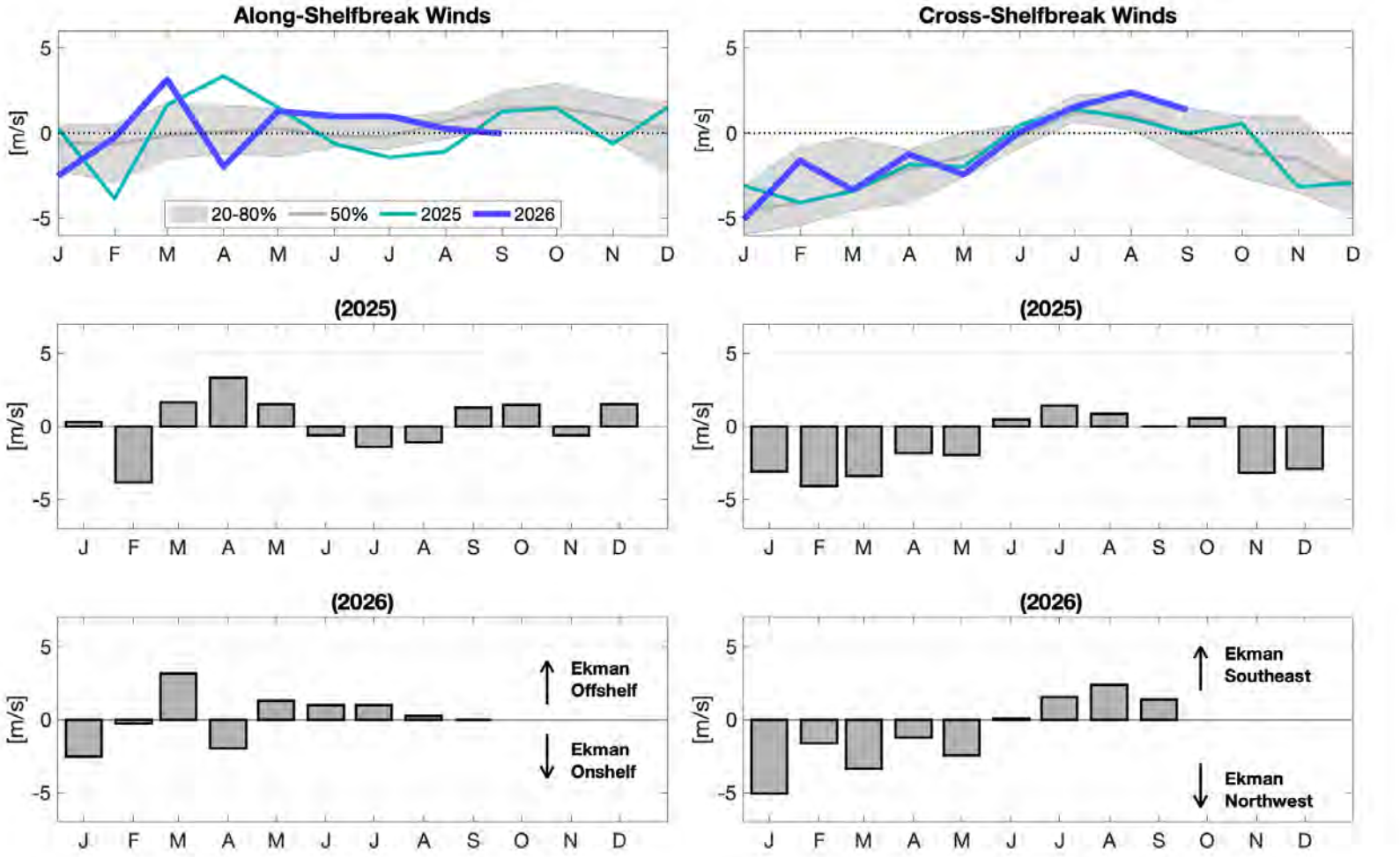


Figure 41: Along-shelf (left set of panels) and cross-shelf (right set of panels) wind components averaged along the dashed line in Figure 40. Top panels show the climatological median (thick gray line) and range spanning the 20th to 80th percentiles (shaded region), the 2025 monthly averages (teal) and 2026 monthly averages through September (blue). Middle panels and bottom panels show only averages for 2025 and 2026, respectively. Annotations for how along- and cross-shelfbreak winds affect expected Ekman transport are shown in the bottom panels.

St. Paul Air Temperature Anomalies

Contributed by James Overland, *james.e.overland@noaa.gov*, and Muyin Wang

Monthly surface air temperature anomalies at St. Paul Island (WMO ID 25713) are shown in Figure 42. The anomaly is computed relative to the 1991-2020 period mean based on GISSTemp V4[16].

A linear trend of 0.50°C/decade has been observed at St. Paul Island since 1981. Although temperature anomalies have remained predominantly positive since spring 2014, their magnitudes have generally decreased in recent years. Since the beginning of 2020, temperatures have fallen below the historical mean (defined as 1991-2020 average) in only five winter months: November 2021, January 2022, December 2023, and January and March 2026. Notably, March 2026 marked the first month during this period in which the temperature anomaly fell more than 1.5 standard deviations below the historical mean.

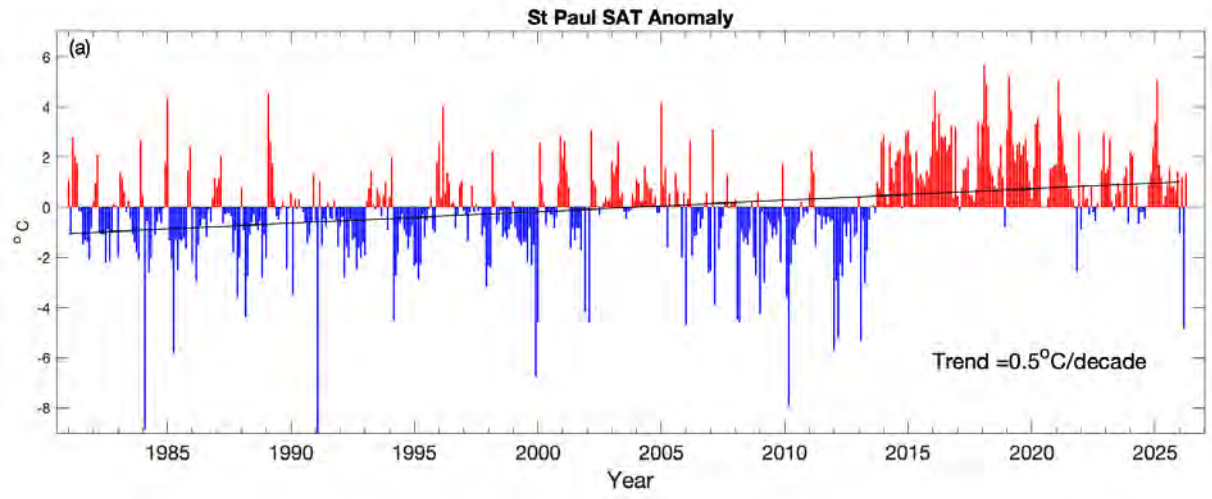


Figure 42: St. Paul air temperature anomalies updated to April 2026.

(d) Sea Surface and Bottom Temperatures

Spring Temperatures

Contributed by Kelia Axler, *kelia.axler@noaa.gov*, and Lauren Rogers

NOAA-Alaska Fisheries Science Center's EcoFOCI program conducts biennial surveys in spring (May-June) in the eastern Bering Sea (EBS), targeting early life stages of fishes and their zooplankton prey. At each sampling station, a bongo net array is towed obliquely from surface to 300 meters or to 10 meters off bottom in shallower waters. Attached to the wire above the bongo frame is a Seabird FastCAT profiler which measures temperature, salinity, and depth. Up casts were processed and used to generate maps and time series of temperatures at the surface (1-5 m) and at maximum gear depth (within 10 m of seafloor) using the custom R package FastrCAT[17]. While surveys have been ongoing for multiple

[16]Data are obtained from `https://data.giss.nasa.gov/gistemp/data_v4.html`

[17]`https://github.com/Copepoda/FastrCAT`.

decades, time series are provided here for the six most recent surveys with similar survey extent and timing (2012-2026). Surveys did not take place in 2020 and 2022. The 2026 spring EcoFOCI survey was conducted from May 5-19th, roughly two weeks earlier than normal, and with a reduced station grid.

Overall, the EBS shelf experienced a return to colder than average spring conditions that closely mirror those of 2012 (Figure 43). Temperatures across the consistently sampled core region averaged 1.32 $\pm$ 1.29°C at the surface (top 5 m) and 0.94 $\pm$ 1.8°C near the bottom (within 10 m of the seafloor). Providing a stark contrast to recent warm years, spring 2026 surface and bottom waters were 5.5°C and 3.6°C cooler on average, respectively, than the anomalously warm conditions observed in 2016. Spatially, the warmest bottom temperatures were found near Unimak Pass and in deeper waters near the shelf break, while the coolest temperatures were observed in shallower shelf waters near the 70-m isobath (Figure 44). However, given the earlier than usual timing of this year's survey, these initially cool conditions may not persist, and above average warming could still emerge as the summer progresses.

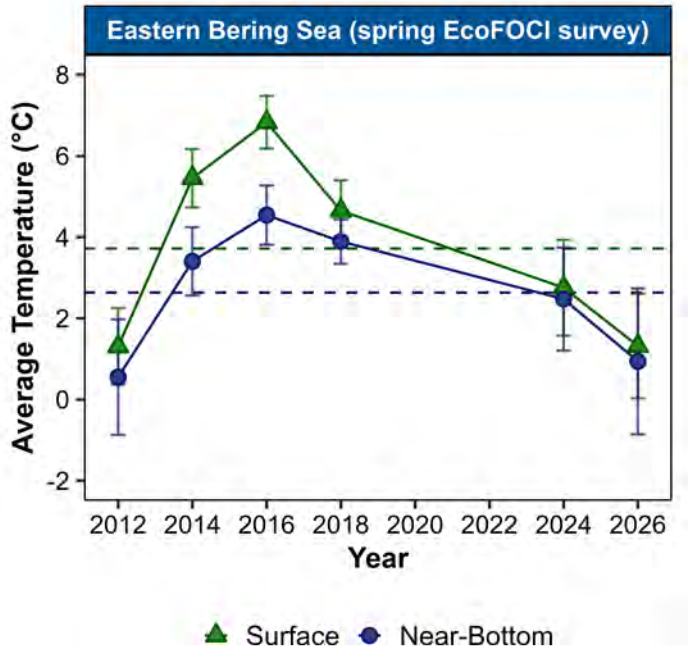


Figure 43: Average spring surface (green triangles; 1-5 m) and near-bottom (blue circles; within 10 m of seafloor) temperatures (°C; $\pm$ mean standard deviation) on the eastern Bering Sea shelf based on data collected within a consistently sampled core region (red polygon in Figure 44) from 2012-2026. Dashed lines represent the time series mean.

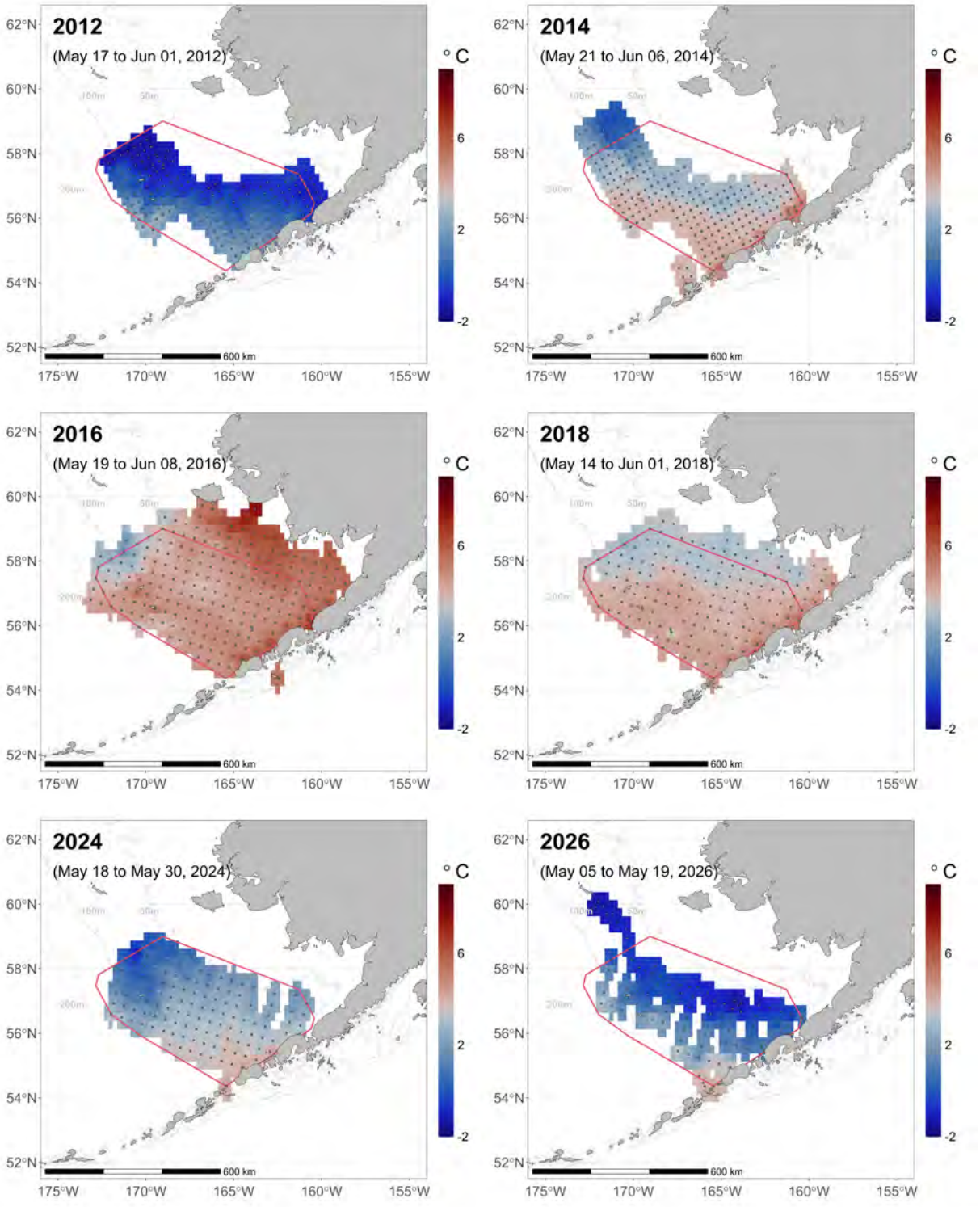


Figure 44: Near-bottom temperatures (°C) during the biennial spring EcoFOCI survey from 2012-2026. The blue points show the sampled stations, and the red polygon delineates the core region of sampling. Note that survey coverage in 2026 was two weeks earlier and lower overall due to reduced ship time.

Summer Temperatures

Contributed by Sean Rohan, *sean.rohan@noaa.gov*, and Lewis Barnett

Annual mean surface and bottom temperatures were calculated from spatially interpolated measurements collected during NOAA-AFSC's summer bottom trawl surveys of the EBS shelf (1982-2026, except 2020) and NBS (2010, 2017, 2019, 2021-2023, 2025). Temperature interpolation was conducted using ordinary kriging with Stein's parameterization of the Matérn semivariogram model (Rohan et al., 2022). Code, figures, and data products presented in this contribution are provided in the *coldpool* R package version 3.3-1.

In the EBS, the mean surface temperature (6.23°C) was 0.5°C cooler than the time series average and 0.15°C warmer than in 2025 (Figure 45). The 2026 mean bottom temperature (1.81°C) was below average (2.49°C) and 1.21°C cooler than 2025. The cooler than average bottom temperatures in 2026 represents a return to cold conditions, with the lowest observed mean bottom temperature since 2013. Note: There are no NBS temperature updates in this year's contribution because the NBS bottom trawl survey was not conducted in 2026.

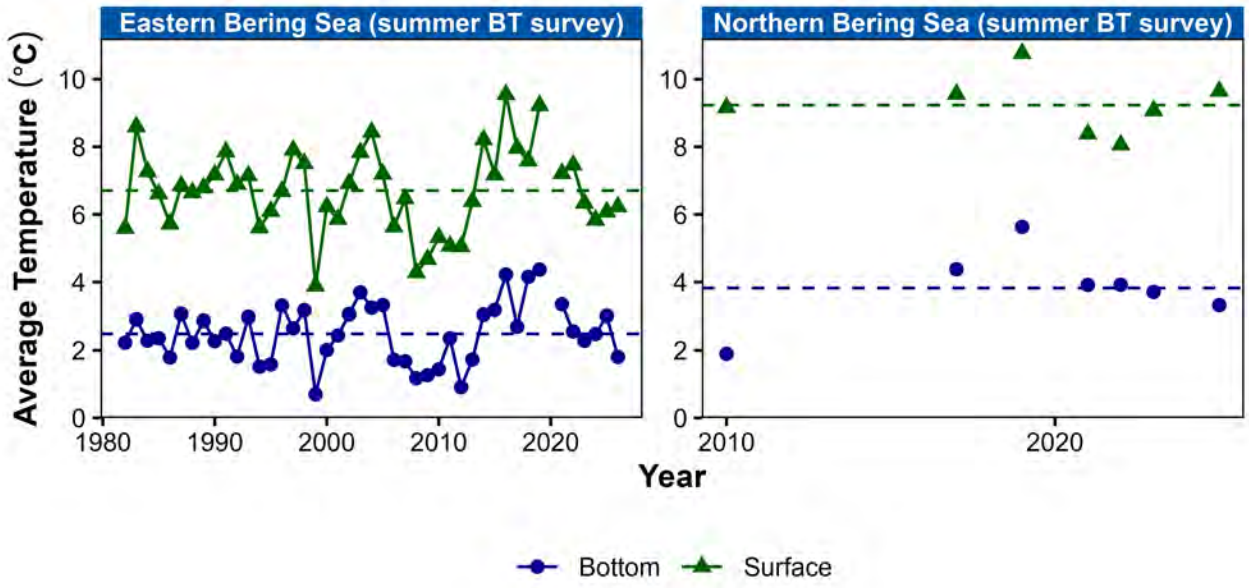


Figure 45: Average summer surface (green triangles) and bottom (blue circles) temperatures (°C) on the eastern Bering Sea shelf based on data collected during standardized summer bottom trawl surveys from 1982-2026. Dashed lines represent the time series mean. **Note:** There are no NBS temperature updates in this year's contribution because the NBS bottom trawl survey was not conducted in 2026.

In 2026, the cold pool extended into the inner domain (<50 m bottom depth) in Bristol Bay (Figure 46). The coldest bottom temperatures (<-1°C) were restricted to the northern portion of the middle shelf at latitudes greater than 60°N, similar to 2024 and 2025. The warmest bottom temperatures (6-7°C) were observed along the coast of the Alaska mainland near Nunivak Island.

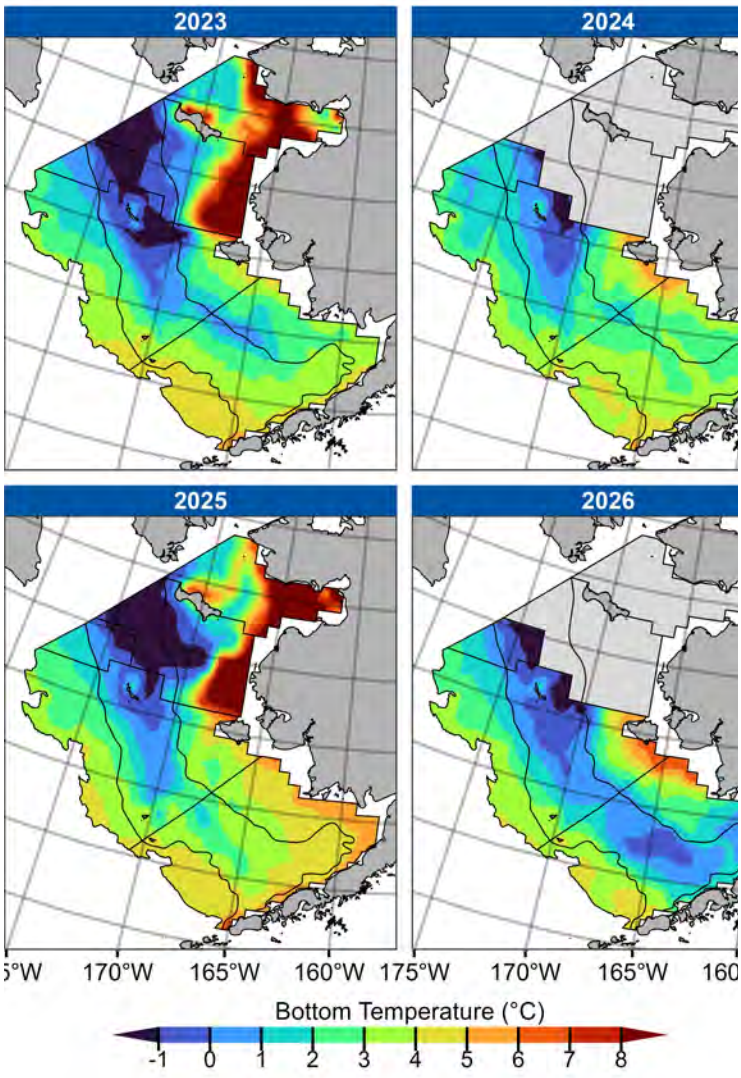


Figure 46: Contour maps of bottom temperatures from the 2023-2026 eastern Bering Sea shelf and northern Bering Sea bottom trawl surveys.

Late Summer Temperatures in the Northern Bering Sea

Contributed by Kelia Axler, *kelia.axler@noaa.gov*, and Lauren Rogers

Since 2002, the Northern Bering Sea Ecosystem and Surface Trawl (NBEST) survey has provided multi-disciplinary annual data on oceanographic conditions, zooplankton, fish, shrimp, and juvenile crab, within the northern Bering Sea (NBS) coastal region (60°N-66.5°N) in the late summer to early fall (August-September). In 2026, this research was supported by NOAA, ADFG, Alaska Sustainable Salmon Fund, and the North Pacific Research Board. At each sampling station, a bongo net array is towed obliquely from surface to 5 meters off bottom. Attached to the wire above the bongo frame is a Seabird FastCAT profiler which measures temperature, salinity, and depth. Up casts were processed and used to generate maps and time series of temperatures at the surface (1-5 m) and at maximum gear depth

(within 10 m of seafloor) using the custom R package FastrCAT[17]. While surveys have been ongoing for multiple decades, time series are provided here for the five most recent surveys (2022-2026).

On average, the NBS shelf was characterized by warm surface waters during the 2026 survey period alongside the coolest bottom temperatures observed in the five-year time series (Figure 47). Temperatures across the consistently sampled NBS standard core region averaged 9.06 $\pm$ 1.18°C at the surface (top 5 m) and 5.41 $\pm$ 4.37°C near the bottom (within 5 m of the seafloor). Over the 2022-2026 time series, surface temperatures have exhibited some interannual variability without a clear trend (ranging from 7.47°C in 2024 to 9.25°C in 2025), whereas near-bottom temperatures remained consistently warm (5.85 - 6.71°C) from 2022 to 2025 before dropping sharply to a five-year low in 2026. Spatially, the warmest bottom temperatures were found in shallow nearshore waters and Norton Sound where the water column was often fully mixed, while the coolest temperatures remained constrained to deeper waters southwest of St. Lawrence Island near the 50-m and 100-m isobaths, where strong vertical temperature stratification was observed (Figure 48). The cold-pool, defined as bottom-temperatures below 2°C, extended further to the east into shallower waters in 2026 compared to recent years. As late summer transitions into fall, autumnal storm events and wind-driven vertical mixing are expected to erode the pronounced thermal stratification across the shallow NBS shelf.

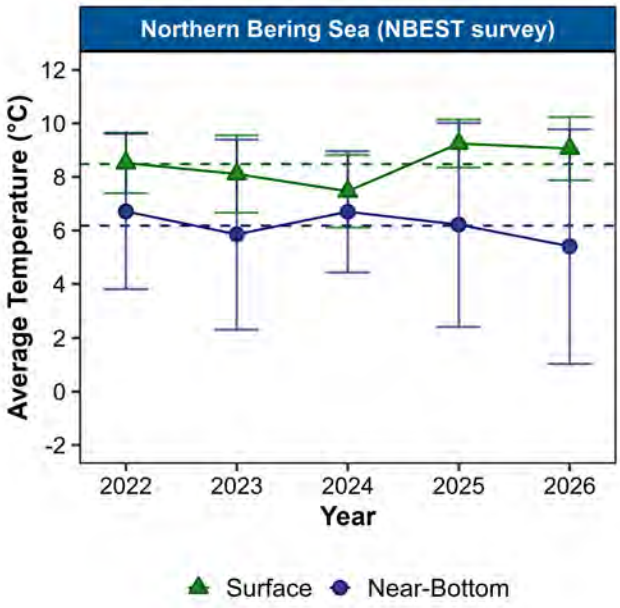


Figure 47: Average late summer surface (green triangles; 1-5 m) and near-bottom (blue circles; within 10 m of seafloor) temperatures (°C; $\pm$ mean standard deviation) on the Northern Bering Sea shelf based on data collected within a consistently sampled core region (red polygon in Figure 48) from 2022-2026. Dashed lines represent the time series mean.

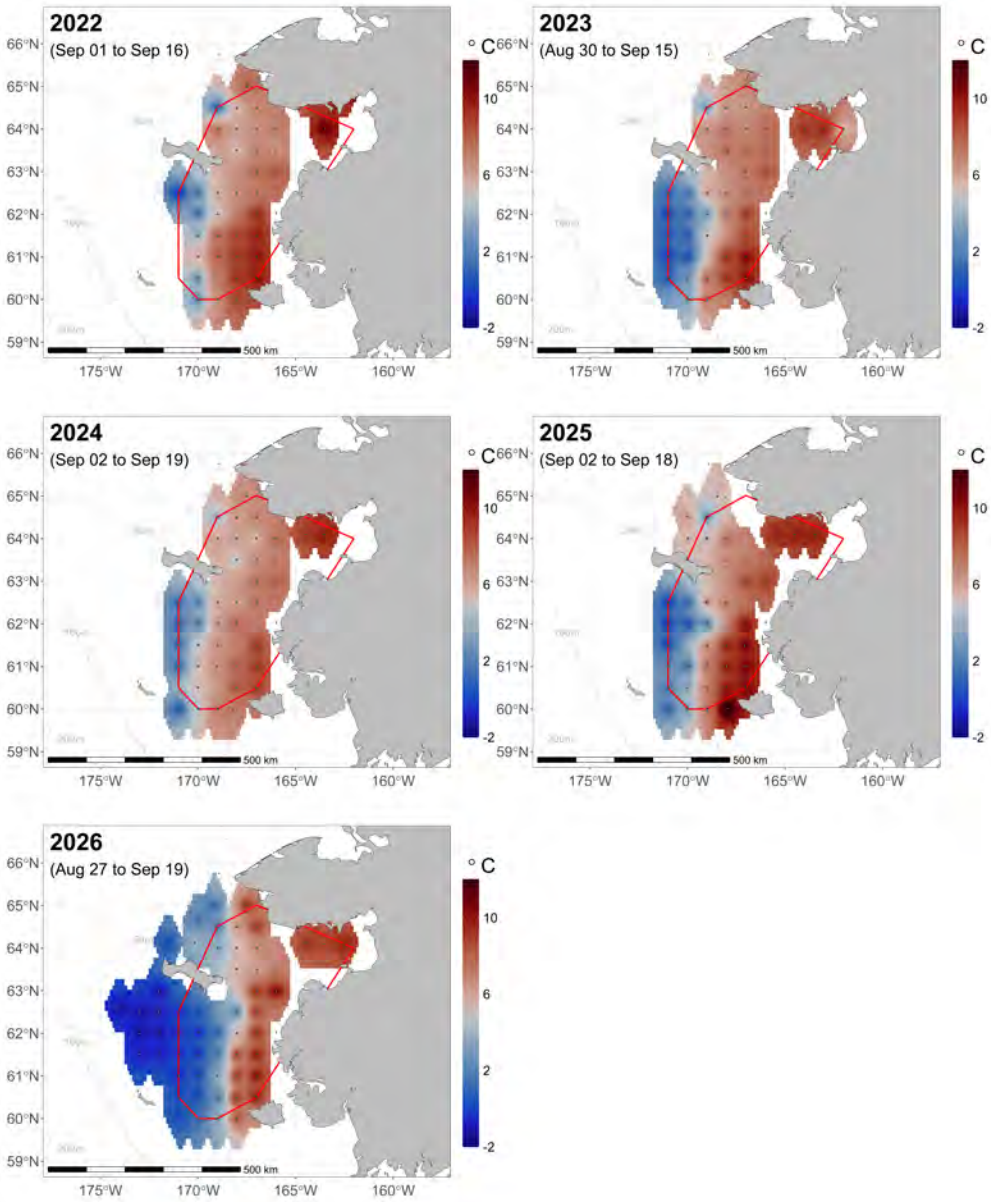


Figure 48: Near-bottom temperatures (°C) during the annual NBEST surveys from 2022-2026. The blue points show the sampled stations, and the red polygon delineates the core region of sampling.

Water Column Temperature at Mooring M2

Contributed by Ryan M. McCabe, *ryan.mccabe@noaa.gov*, Shaun W. Bell, and Phyllis J. Stabeno

The M2 mooring records temperature at a number of depths throughout the water column (02 m; Figure 49). In 2026, sea ice was extensive, covering M2 for ∼6 weeks and was comparable in extent to the ice coverage of 2012. It retreated from the mooring site in mid-April. The surface mixed layer was particularly thin (<13 m) through most of June and only deepened to its typical 20 m in mid-July. Because of the thin surface mixed layer, warming in June was rapid with three distinct thermal layers forming.

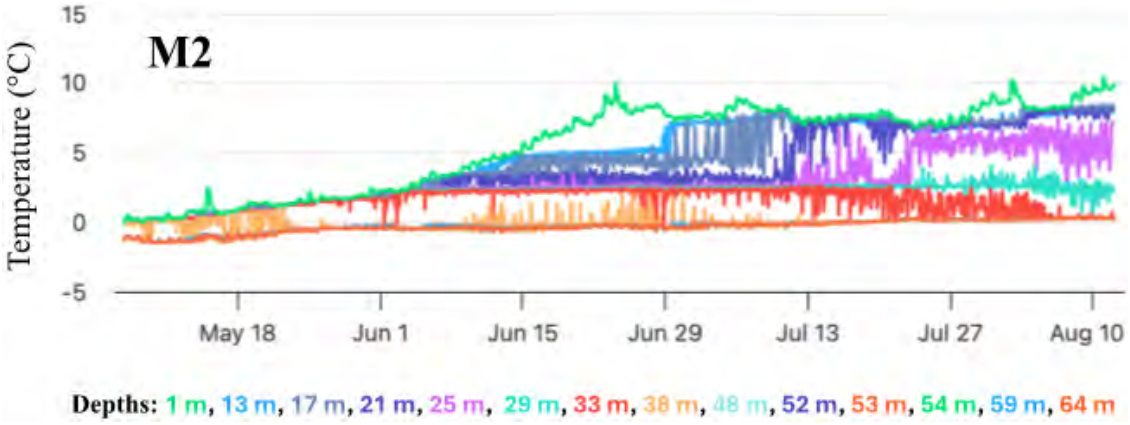


Figure 49: Mooring M2 temperature (°C) time series spanning May-August 2026 at 14 different depths ranging from 1 m to 64 m.

Using the data from Figure 49, the depth-averaged temperature was calculated (Figure 50). For historical context, the depth-averaged temperature in 2019 was one of the warmest in the 32-year time series and 2012 was the coldest. In winter 2026, the depth-averaged temperature was as cold as in 2012, nearly 3°C below the historical average. Maximum sea-ice extent in 2026 was also similar to the extent in 2012, however, ice retreated from the M2 site about a month earlier than in 2012. This accelerated ice retreat helps to explain why the average water column temperature warmed more quickly in 2026 compared to 2012. Despite this warming, the depth-averaged temperature remained more than 2°C below the historical average in July and August 2026.

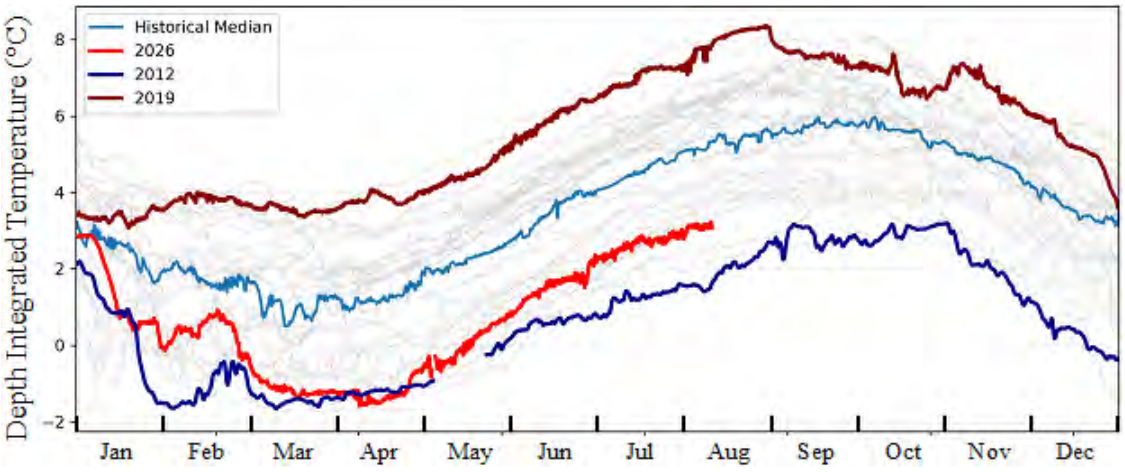


Figure 50: Depth-averaged temperature (°C) at M2 for 2026 (red) relative to prior years, with the historical median temperature (light blue), the record cold year of 2012 (dark blue), and the very warm year of 2019 (dark red) highlighted for comparison.

Bottom Temperatures Along the Shelf Break

Contributed by Kevin Siwicke, *kevin.siwicke@noaa.gov*

Since 2005 bottom temperatures have been measured during the EBS longline survey, generally in early June. Thermistors are mounted to longline equipment, and remain on the bottom for several hours before recovery. Longline surveys were conducted on the Bering shelf break every odd year from 2005 to 2023, and following survey changes, every even year going forward beginning in 2026. The index is the average from 1-m increments in the water column from 246 m to 255 m, and the bottom depths at these locations ranged between about 250 m and 800 m (Figure 51).

Trends

Though the period of record is relatively short for the Bering Sea shelf break, the bottom temperature averaged across all EBS stations during the last six survey years (between 2015 and 2026) are markedly higher than from 2009 to 2013 (Figure 52). While the water temperatures $\leq$200 m across the EBS have seen a relaxation from the most recent warm stanza, the trends in the slightly deeper longline survey data may suggest that vertical stratification has decoupled the deeper water from shallower processes, allowing the relatively warm conditions to persist.

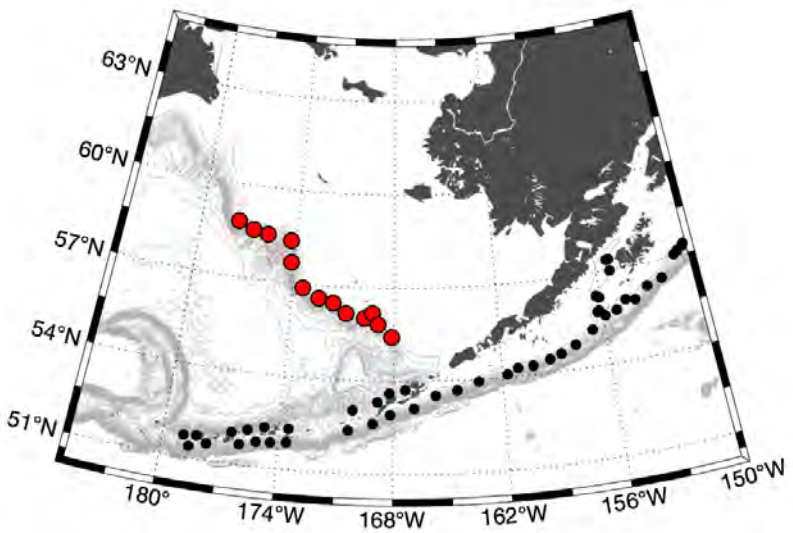


Figure 51: Map of longline survey sites (red circles) on the Bering Sea shelf break, 2009-2026. Black circles show locations of other longline sites across the Aleutian Islands and western Gulf of Alaska.

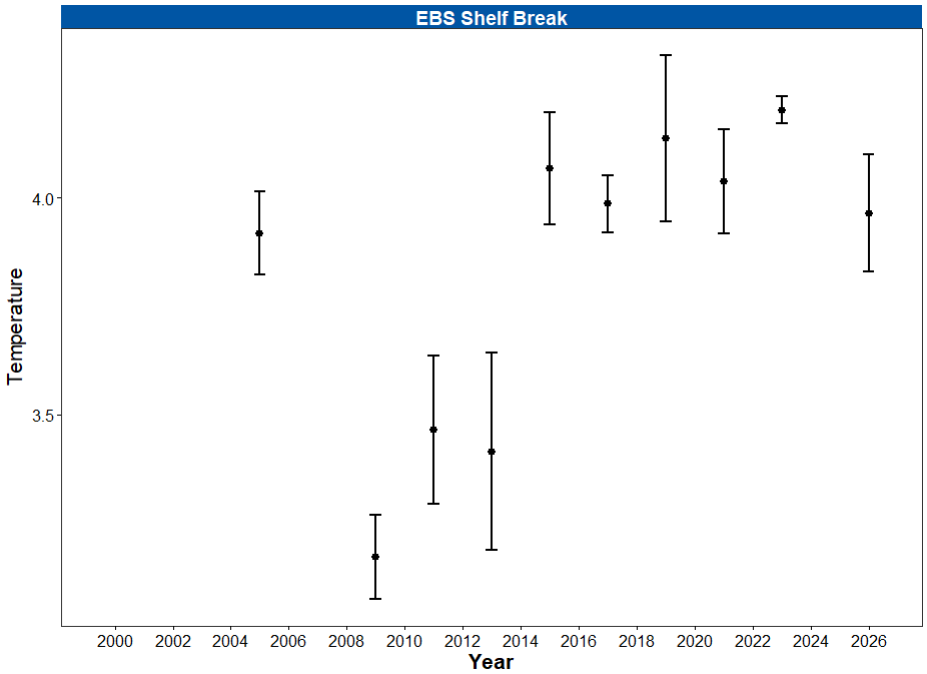


Figure 52: Bottom temperatures averaged across all longline surveys in the Bering Sea (red circles in Figure 51).

Bering Sea SST anomalies

Marine Heatwave Index

Contributed by Emily Lemagie, *emily.lemagie@noaa.gov*, and Matt Callahan

Satellite SST data (source: NOAA Coral Reef Watch Program) were accessed via the Alaska Fisheries Information Network (AKFIN). Daily data were averaged within the southeastern (south of 60°N) and northern (605.75°N) Bering Sea shelf (10-200 m depth). Detailed methods are available online[18].

There were no marine heatwaves (MHWs) in 2026 (Figure 53). Northern Bering Sea temperatures increased rapidly through the summer, with temperatures near the MHW threshold for much of the season. Below average winter surface temperature anomalies prevailed in early spring over the southeastern Bering Sea; following this early-season set-up temperatures remained near or below average with no MHWs in 2026. **Note:** this MHW index is based on SST, which is strongly influenced by sea ice and stratification in the Bering Sea, particularly over the middle shelf where surface and bottom temperature dynamics can be decoupled much of the year (Ladd and Stabeno, 2012). Bottom temperature in the Bering Sea is an important ecosystem indicator (Stabeno and Bell, 2019).

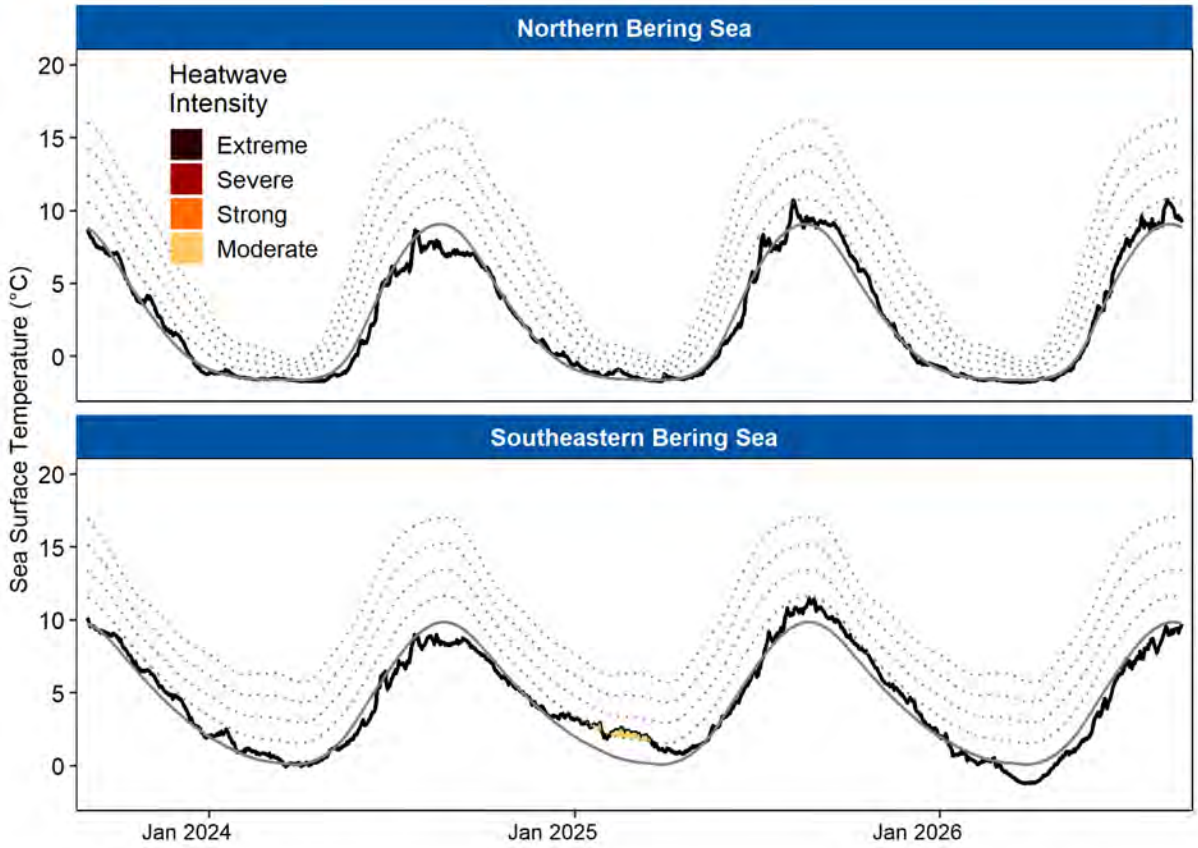


Figure 53: Marine heatwaves in the northern and southeastern Bering Sea since September 2023. The smoothed solid black line represents the baseline average temperature (i.e., climatology) for each day during the 30-yr baseline period (1 Jan 1991 to 31 Dec 2020). The jagged solid black line is the observed (satellite-derived) SST for each day. Dotted lines illustrate thresholds for increasing MHW intensity categories (moderate, strong, severe, extreme). Colored portions indicate periods during which MHW occurred, with intensity increasing as colors darken.

[18] `https://github.com/MattCallahan-NOAA/ESR/tree/main/SST/EBS`

Annual and Seasonal SST Trends

In the northern Bering Sea, the cumulative SST anomaly for 2026 was positive whereas the southeastern Bering Sea SST anomaly for 2026 was lower than it has been since before the extended warm period that began in 2014 (Figure 54), particularly in spring 2026 (Figure 55). Thermal conditions since 2022 have been within 1 standard deviation; cumulative thermal exposure impacts the ecology of these systems through metabolic rates, prey demands, and growth rates. Seasonal thermal conditions have also been within one standard deviation of historical temperatures, except that the cold temperatures this spring were about 1 standard deviation below the historical mean over the southeastern Bering Sea shelf (Figure 55).

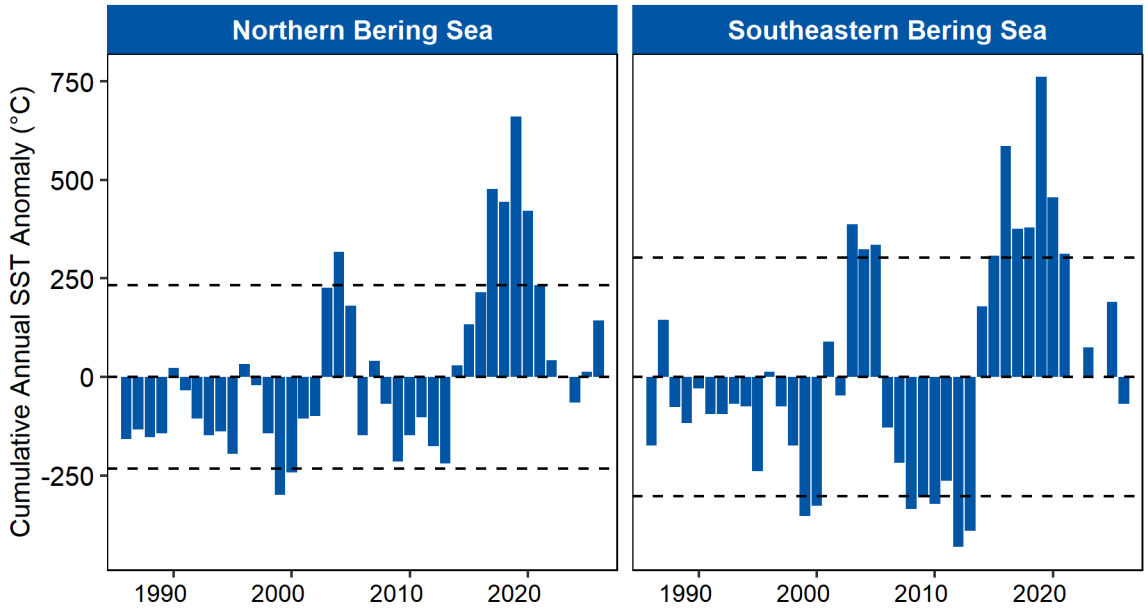


Figure 54: Cumulative annual SST anomalies (sum of daily temperatures). Horizontal lines are ±1 standard deviation from the mean during the 30-yr baseline period (1 Jan 1991 to 31 Dec 2020).

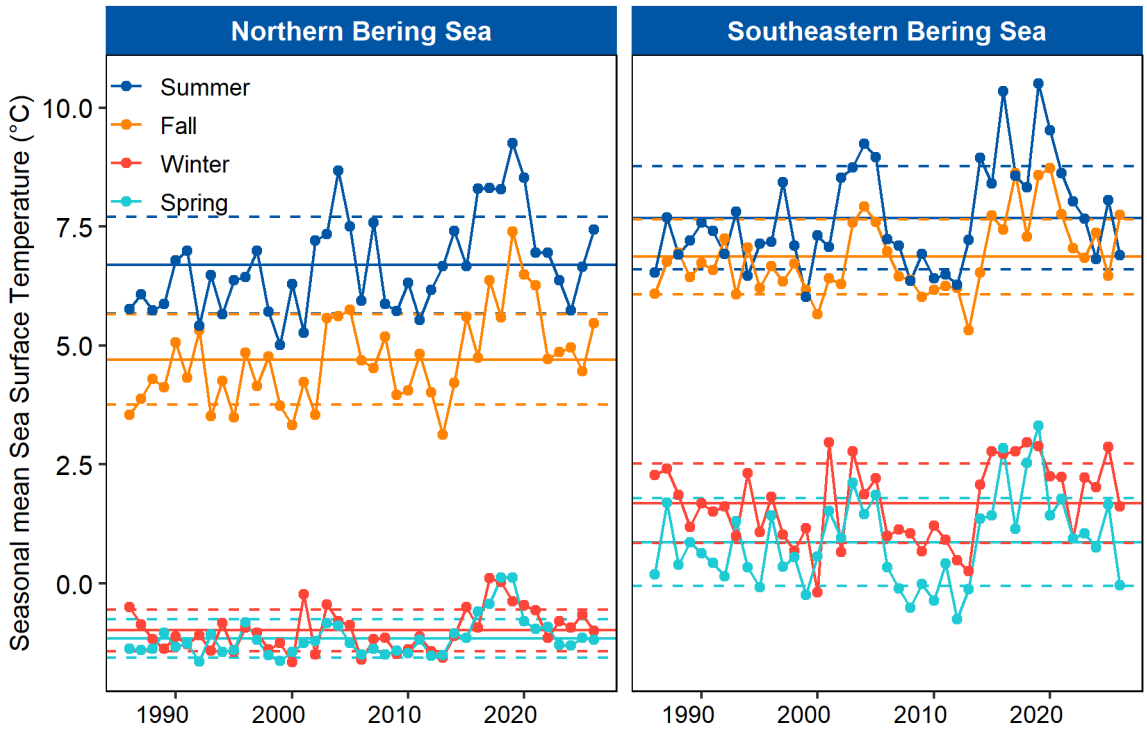


Figure 55: Seasonal mean SSTs for each year: fall 2025 (Sep-Nov), winter 2025/2026 (Dec-Feb), spring 2026 (Mar-May), and summer 2026 (Jun-Aug). Horizontal dashed lines are ±1 standard deviation from the seasonal mean for all years (horizontal solid line). Negative values are due to sea surface temperatures below zero.

Bering Sea SST and Bottom Temperature Trends

Contributed by Emily Lemagie, *emily.lemagie@noaa.gov*, Matt Callahan, and Kelly Kearney

Estimates of bottom temperature are derived from the Northeast Pacific Modular Ocean Model (MOM6) hindcast simulation, which was extended to the near-present, using reanalysis-based input forcing. This hindcast simulation now extends from Jan 1, 1993 to Dec 31, 2025, with a near-real-time extension through Aug 16, 2026.

Thermal conditions over the northern and southeastern Bering Sea shelves have been near-normal since 2022 (Figure 54). Between September 2025 and August 2026, exceptions to near-normal or cool thermal conditions include a relatively warm autumn in 2025 across all domains. Rapid winter cooling resulted in near-normal to cooler than average temperatures across all domains of the SEBS in 2026. In the NBS, surface temperatures warmed rapidly in late summer 2026, resulting in above average anomalies (but not exceeding the MHW threshold), particularly over the middle shelf (Figure 57).

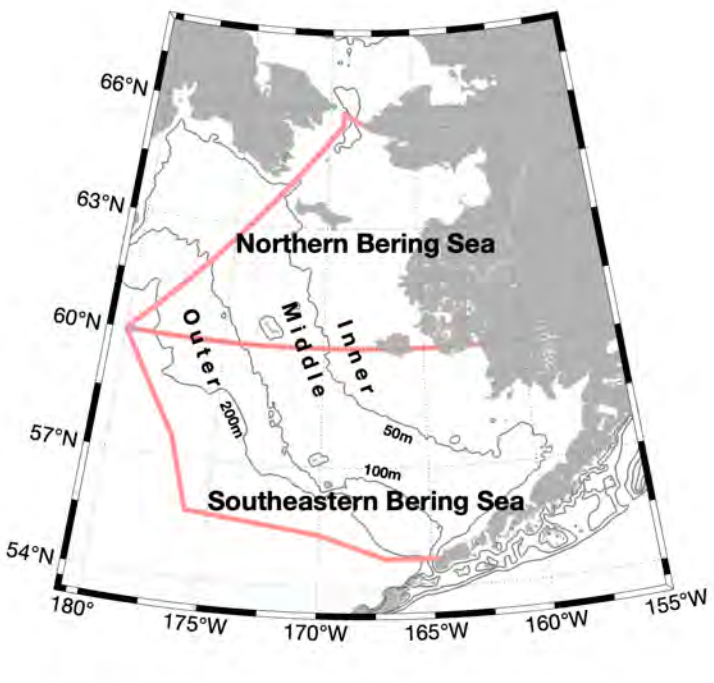


Figure 56: Map of the eastern Bering Sea domains. The inner (<50 m isobaths), middle (50-100 m isobaths), and outer (100-200 m isoboaths) domains are shown. The southeastern and northern Bering Sea are delineated at 60°N.

Similar to SST, MOM6-estimated bottom temperatures in the NBS and SEBS began the 2026 winter season near mean or slightly warmer than average conditions. However, in March, rapid ice advance dropped bottom temperatures below the mean, where they remained (closely tracking the persistence signal) through the summer months. Spatially, the cold anomalies were strongest in the Bristol Bay region (SEBS inner and middle shelves) with the outer EBS shelf near neutral, whereas the northern Bering sea anomalies were more spatially patchy, with warm anomalies in Norton Sound and in the west but cold anomalies in between.

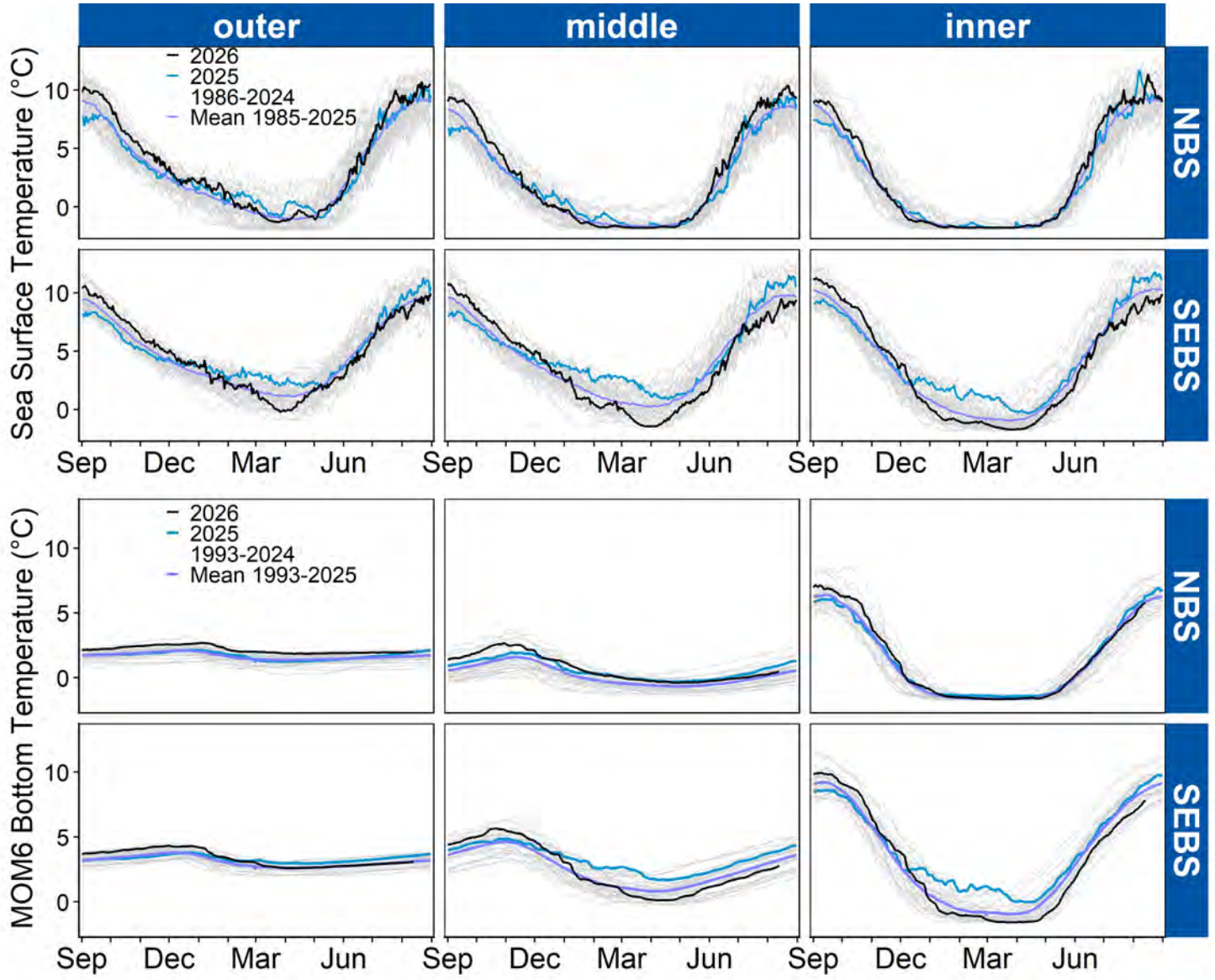


Figure 57: Top 2 rows: Mean daily SST for the northern (NBS) and southeastern (SEBS) outer, middle, and inner shelf domains. Bottom 2 rows: Mean weekly bottom temperature for the NBS and SEBS outer, middle, and inner shelf domains. The most recent year (2025-2026; through August 2026) is shown in black, 2024-2025 is shown in blue, and the historical mean is shown in purple. Individual years in the time series are shown in light gray.

Habitat

Eastern and Northern Bering Sea – Structural Epifauna

Contributed by Thaddaeus Buser
Groundfish Assessment Program, Resource Assessment and Conservation Engineering Division,
Alaska Fisheries Science Center, NOAA Fisheries, Seattle, WA
Contact: thaddaeus.buser@noaa.gov
Last updated: September 2026

Description of indicator: Groups considered to be structural epifauna include: sea pens, corals, anemones, and sponges. Corals are rarely encountered in the eastern Bering Sea so they were not included here. For each group, biomass indices were updated for 2026 from the eastern Bering Sea shelf survey. Since 1982, the RACE Groundfish Assessment Program (GAP) and Shellfish Assessment Program (SAP) have conducted annual fishery-independent summer bottom trawl surveys on the EBS shelf using standardized trawl gear and methods. Biomass index trends from the survey are likely to reflect changes in the abundance of species and life history stages that are available to the survey, especially if trends are sustained over time.

Regional and stratum indices of abundance (biomass in kilotons) and confidence intervals were estimated for each taxonomic group by fitting a multivariate random effects model (REM) to stratum-level design-based abundance index time series calculated from AFSC summer bottom trawl survey catch and effort data. Indices were calculated for the standardized survey time series (EBS: 1982-2026, NBS: 2010-2025). Design-based indices of abundance were calculated using the gapindex R package (Oyafuso, 2025) and REM were fitted to survey time series using the rema R package (Sullivan and Balstad, 2022). Code and data used to produce these indicators are provided in the esrindex R package and repository (Rohan, 2025).

Status and trends:
Eastern Bering Sea:
Sponges have undergone cyclical variability in abundance throughout the time series (Figure 58). The biomass of sponges (Porifera) in 2026 remains >1 standard deviation below the time series average, which is a continuation of the extremely low biomass level observed since 2021. Similarly low biomass was also observed intermittently early in the time series, 1984-1992. Whether the current period of low sponge biomass represents a temporary phase or is in fact a new normal remains to be seen. Sponges have primarily been observed in Stratum 30, the southern middle shelf, at 50–100m bottom depth (Figure 59).

The biomass of sea anemones (Actiniaria) has been above average from 2022-2026, similar to 2010-2015. The recent period of above-average biomass contrasts with the period of near-average biomass observed from 2016-2021. Sea anemones are regularly encountered in all EBS survey strata, except Stratum 20, the inner shelf (<50m) north-northwest of Kuskokwim Bay, near Nunivak Island.

Sea pen (Pennatulacea) biomass has increased since 2019 and has remained above the time series average since 2019. The 2026 estimate is >1 standard deviation from the time series mean, similar to recent estimates in 2023 and 2025. Sea pens are most abundant on the outer shelf (100-200m bottom depth) in Strata 50 and 60.

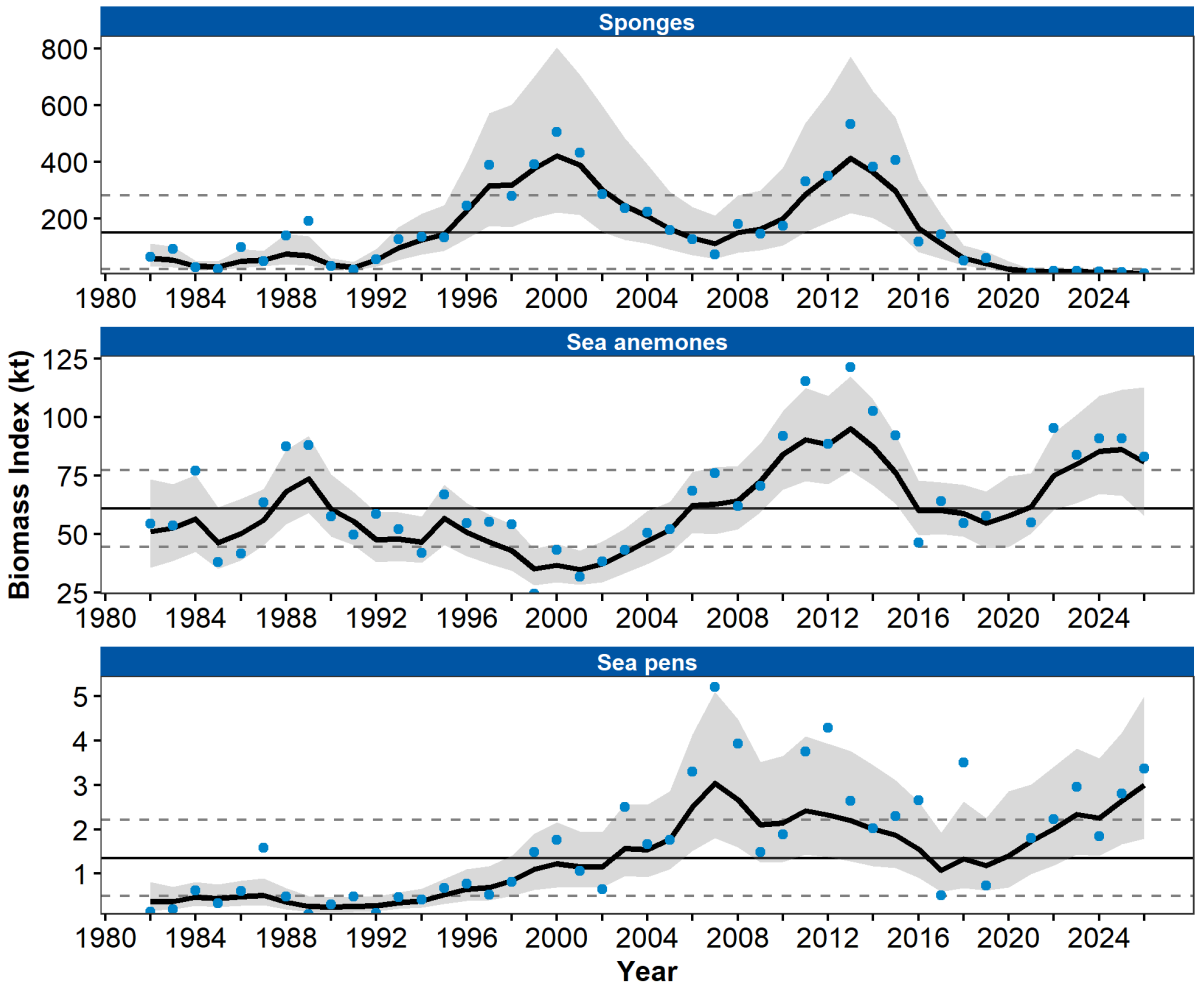


Figure 58: Biomass index of structural epifauna (sponges, sea anemones, and sea pens; kilotons) estimated from AFSC/RACE summer bottom trawl surveys of the eastern Bering Sea continental shelf from 1982 to 2026. Panels show the observed survey biomass index mean (blue points), random effects model fitted mean (solid black line), 95% confidence interval (gray shading), overall time series mean (solid gray line), and horizontal dashed gray lines representing one standard deviation from the mean.

Northern Bering Sea:

The Northern Bering Sea was not sampled in 2026, results from the 2025 survey are presented here. The estimated biomass of sponges in the NBS is highly variable across the time series, with high relative biomass in 2010, 2017, 2022, and 2023 and low relative biomass in 2019 and 2021 (Figure 60). The 2025 estimate is >1 standard deviation above the overall time series mean, but the broad 95% confidence interval on this estimate shows that any interpretation of this estimate should be made with appropriate caution. Sponges are predominantly encountered in stratum 71 (Figure 61).

The biomass estimates of sea anemones are relatively consistent across the time series except for that of 2022, which was much larger than all other years. The 2025 estimate is similar to that of 2023, which is approximately one standard deviation higher than the overall time series mean. Sea anemones are encountered throughout the survey area but are most abundant in stratum 71 (Figure 61).

Sea pens (Pennatulacea) are not encountered in the NBS and are therefore not reported here.

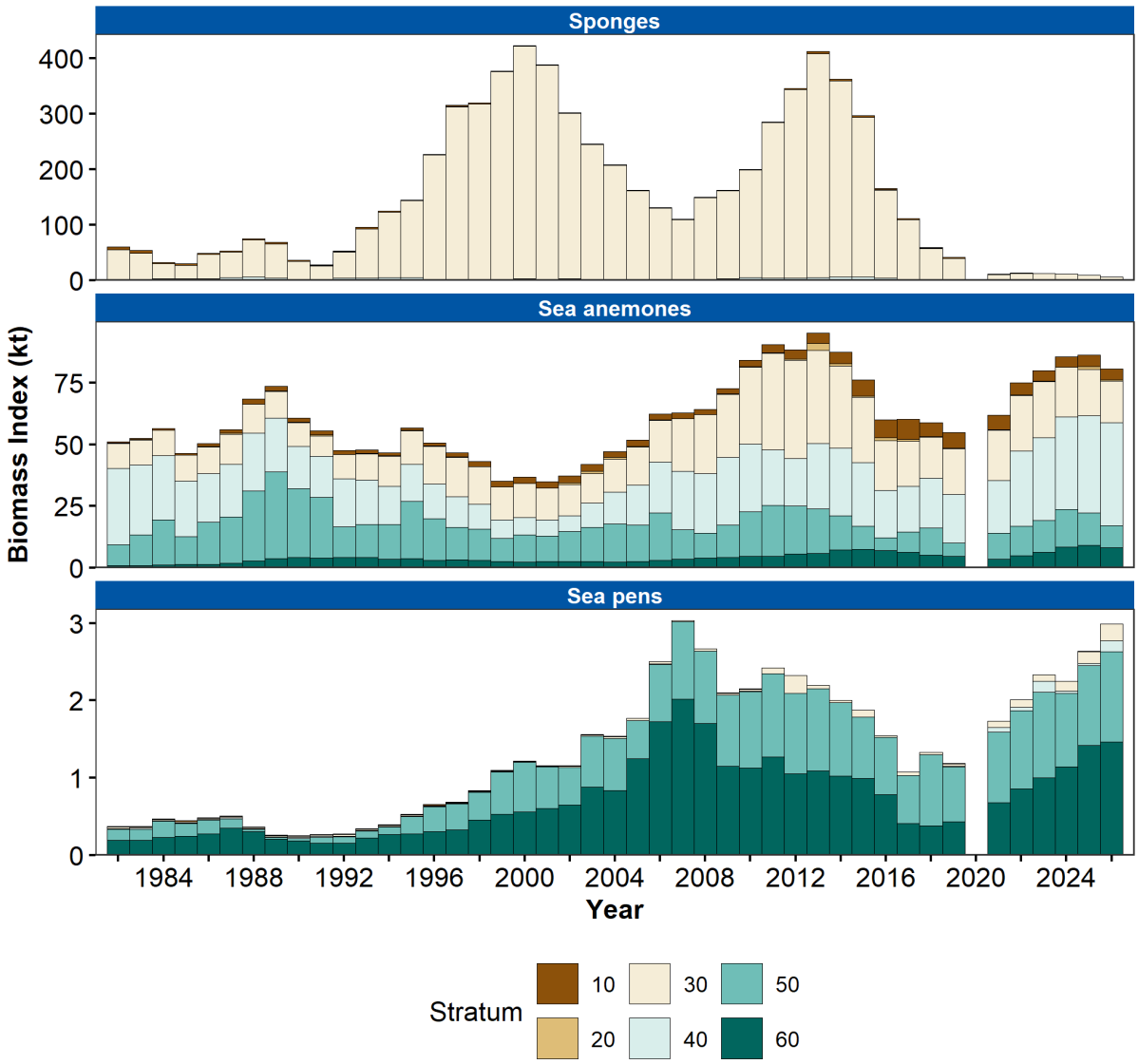


Figure 59: Biomass index of structural epifauna (sponges, sea anemones, and sea pens; kilotons) in eastern Bering Sea continental shelf survey strata 10-60 estimated from RACE Groundfish Assessment Program and Shellfish Assessment Program summer bottom trawl survey data from 1982 to 2026.

Factors influencing observed trends: Further research in several areas would facilitate the interpretation of structural epifauna trends including systematics and taxonomy of Bering Sea shelf invertebrates, better characterization of survey gear efficiency, and the life history characteristics of the epibenthic organisms captured by the survey trawl.

Implications: Structural epifauna are utilized as habitat by commercial groundfish species in Alaska (Rooper et al., 2019), although associations of fish species with epifauna on the Bering Sea shelf are not well understood. Sponges can be extremely long-lived and have slow recovery times from disturbance, meaning they may be vulnerable to impacts from fishing gear (Malecha and Heifetz, 2017; Montero-Serra et al., 2018). However, very little is known about the longevity and growth rates of most sponge taxa in Alaska. Generally, sponge longevity increases with depth (Stone et al., 2019). Understanding

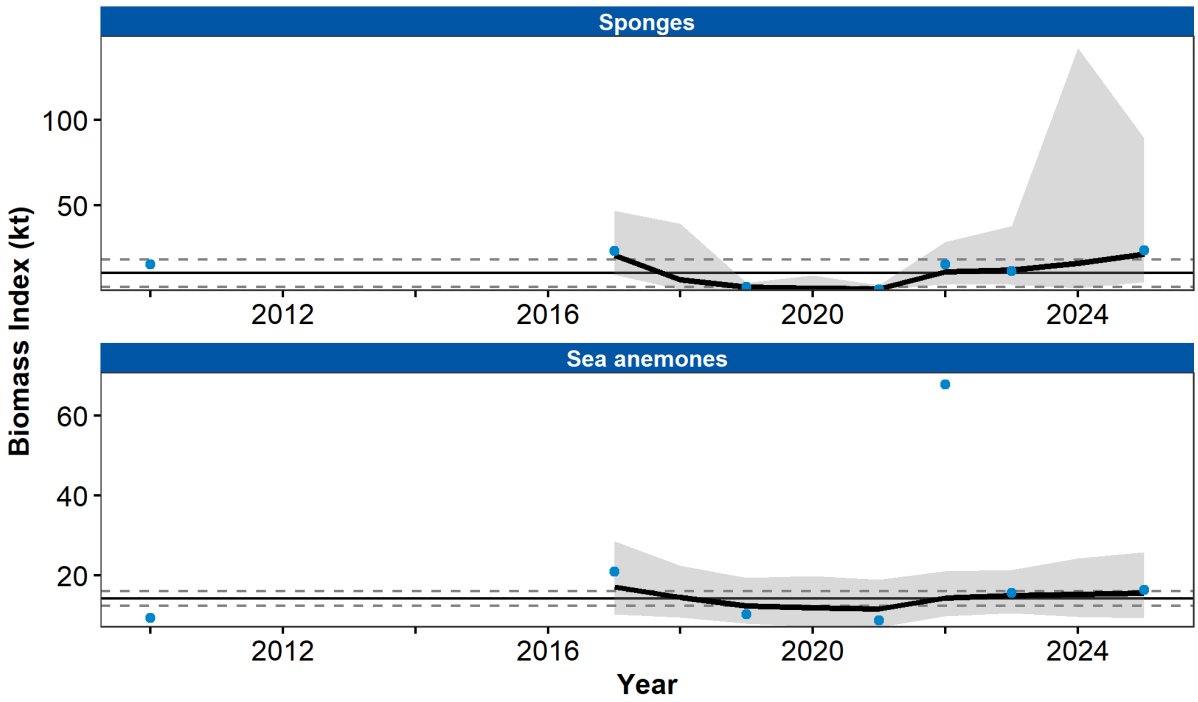


Figure 60: Biomass index of structural epifauna (sponges, sea anemones, and sea pens; kilotons) estimated from AFSC/RACE summer bottom trawl surveys of the northern Bering Sea from 2010 to 2025. Panels show the observed survey biomass index mean (blue points), random effects model fitted mean (solid black line), 95% confidence interval (gray shading), overall time series mean (solid gray line), and horizontal dashed gray lines representing one standard deviation from the mean.

the trends as well as the distribution patterns of structural epifauna is important for modeling habitat to develop spatial management plans for protecting habitat, understanding fishing gear impacts, and predicting responses to future climate change (Rooper et al., 2016). More research on the eastern Bering Sea shelf will be needed to determine if there are definitive links between sponge abundance and these factors.

Research priorities: The bottom trawl survey uses standardized survey protocols aimed at ensuring consistent sampling efficiency. However, additional research is needed to better characterize the catchability and selectivity of structural epifauna groups by the bottom trawl survey.

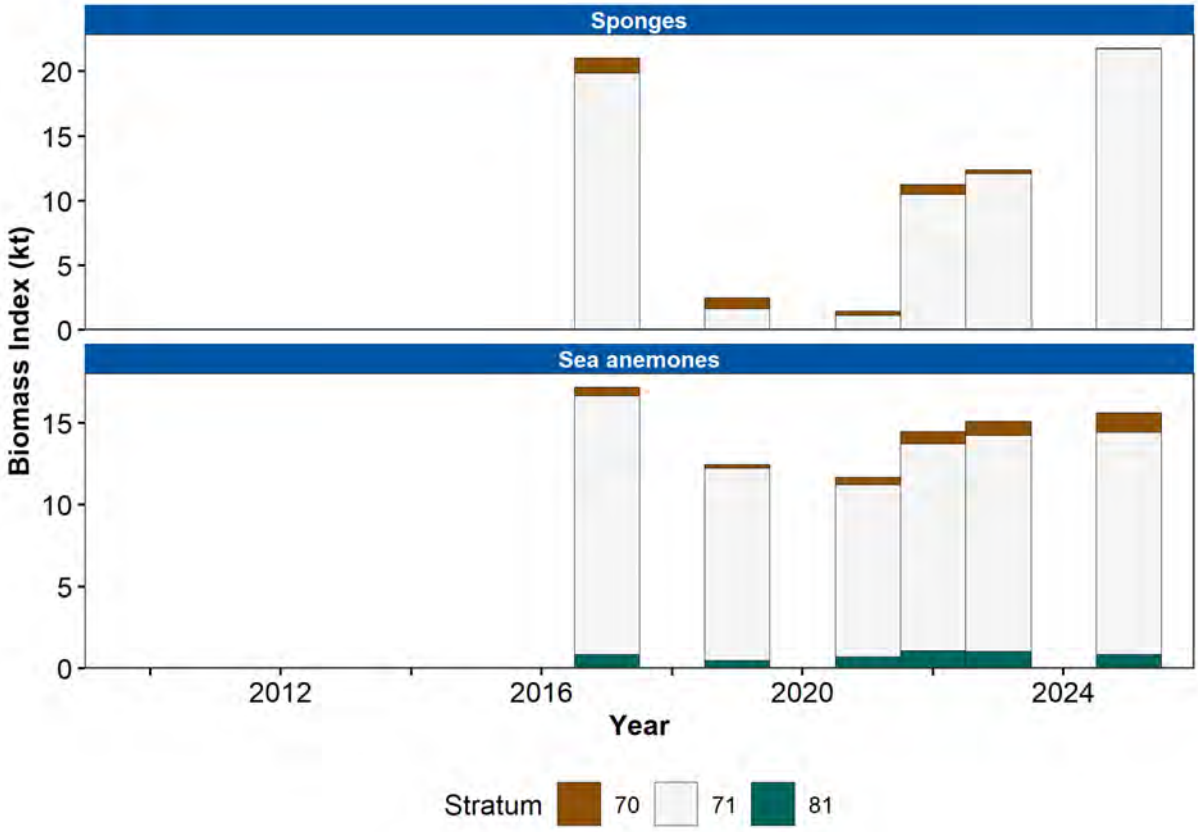


Figure 61: Biomass index of structural epifauna (sponges and sea anemones; kilotons) in northern Bering Sea survey strata 70, 71, and 81, estimated from RACE Groundfish Assessment Program and Shellfish Assessment Program summer bottom trawl survey data from 2010 to 2025.

Primary Production

Surface Phosphate Concentrations and Mixed Layer Depth Correlate with Larger Phytoplankton in the Eastern Bering Sea

Contributed by Jeanette C. Gann
Auke Bay Laboratories, Alaska Fisheries Science Center, NOAA Fisheries, Juneau, AK
Contact: Jeanette.Gann@noaa.gov
Last updated: September 2026

Description of indicator: We viewed dissolved phosphate (PO_4) concentrations (μM), salinity (PSU), and percent large size fraction of chlorophyll a (LrgChl, $>10\mu$m/ total chlorophyll a) representing large phytoplankton above the mixed layer depth (MLD) over the middle domain (Bering Sea Integrated Ecosystem Research Project (BSIERP) regions 3 in the south and 13 in the north) during late summer/early fall, 2003-2025 in the eastern Bering Sea (EBS). Data was pooled for both regions, and mean values above the mixed layer depth were normalized for each year and used as a predictor of LrgChl in generalized additive models (GAMs).

Generally, nutrients above the surface mixed layer represent what is currently available for primary production at the end of summer (storm activity/wind mixing of deep nutrients to the surface tend to be lower during the summer, and surface nutrient stores are often depleted). Deeper MLD tend to indicate more recent storm activity and thus mixing of deep nutrients to the surface for replenished primary production. PO_4 has been recently observed as a potential limiting nutrient in ocean waters (Gerace et al., 2025). Here we use PO_4 as a proxy for available nutrients and investigate nutrients, salinity, and large phytoplankton in conjunction with MLD in the EBS.

Status and trends: Surface PO_4 and LrgChl concentrations vary from year to year over the eastern Bering Sea middle shelf. With the exception of a few years, deeper MLD ($>$28 m) generally corresponds with higher surface PO_4, and higher LrgChl above the long term mean (Figure 62). GAMs using PO_4 (at lower 75% of concentration range), salinity, and MLD as significant predictors of LrgChl explain about 20% of the variation (temperature was initially included, but not considered significant in the GAM) (Figure 63). Both PO_4 and MLD had positive significant ($P<0.05$) correlations with large phytoplankton, while salinity had a significant ($P<0.05$) negative correlation. The 2024 MLD over the middle domain was very deep during late summer ($>$30 m), and had both higher PO_4 and LrgChl than the overall mean.

Factors influencing observed trends: During summer, the strength and frequency of summer storm events and water column stratification will influence the depth of the mixed layer, and the amount of nutrients that are brought to surface waters from depth. Late summer concentrations of PO_4 at the surface may serve as an indicator of a limiting nutrient for phytoplankton growth, with higher concentrations seen during windy years (deeper MLD), and low concentrations seen when storm activity is minimal (shallower MLD) (Eisner et al., 2016). Accordingly, years with higher percentages of large chlorophyll a (estimate of larger phytoplankton taxa) are associated with higher wind mixing (Eisner et al., 2016, 2017). Salinity has been noted to have significant negative correlations with phytoplankton abundance in other marine shelf ecosystems (Guo et al., 2014), and could be related to storm systems

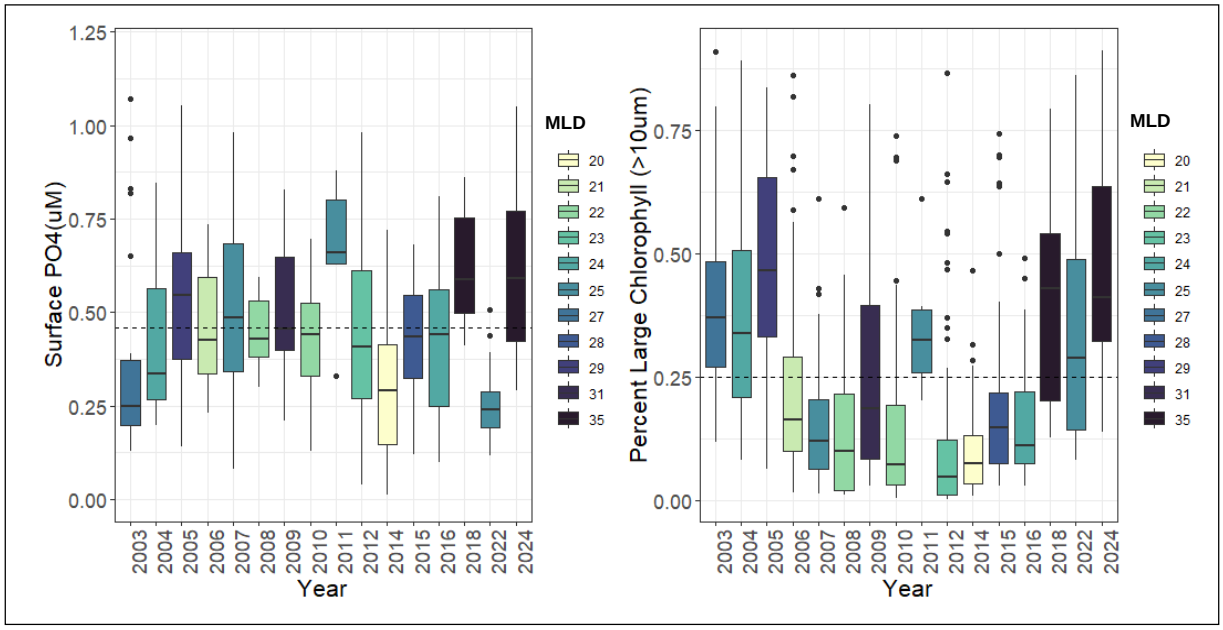


Figure 62: Boxplots of mean surface phosphate (PO_4, μM, left) and percent large chlorophyll greater than 10 μm in size (right) for each year over the middle domain in the eastern Bering Sea. Color fill is based on mixed layer depth (m), shown on the right. Boxplot horizontal lines depict median values, vertical whiskers show the first and 4th quartiles, dots are shown as outliers within each year, and the dashed horizontal line shows the time series mean for each variable.

mixing some rain into the upper water column.

Implications: Increased surface PO_4, large phytoplankton (LrgChl), and deeper MLDs imply an increase in summertime wind mixing events during 2024. Additionally, larger phytoplankton cells (like diatoms) are correlated with taxa that hold higher concentrations of key lipids like EPA and DHA. Thus the correlations showing higher percentages of large phytoplankton with deeper MLD, and higher PO_4 may indicate shorter food chains and more efficient energy flows to young and forage fish in the EBS. Diminished nutrient stores and shallower MLDs leading to lower production in the upper water column may directly affect food stores for higher trophic levels and lead to slowed growth of age-0 pollock and other forage fishes during summer and fall.

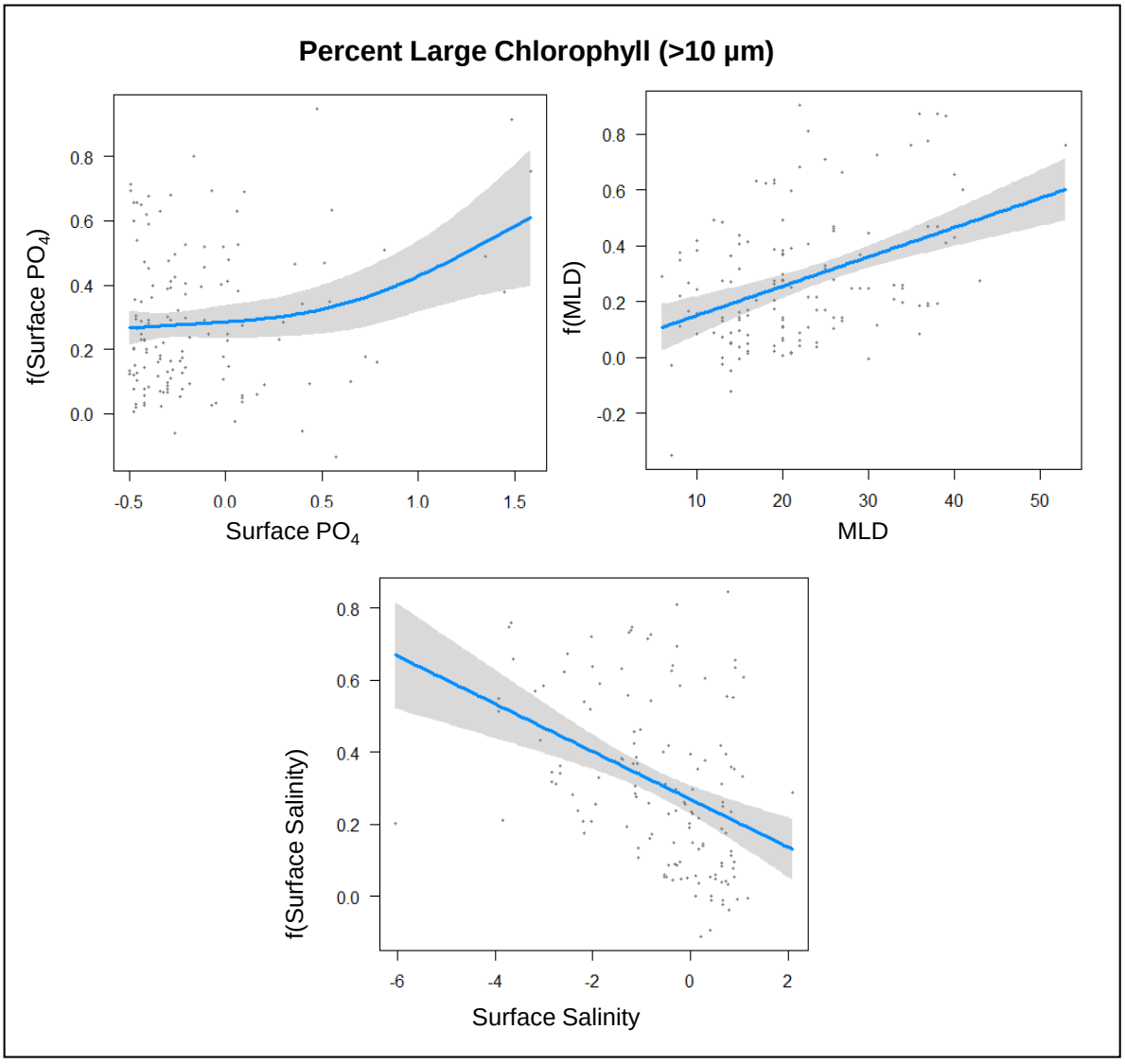


Figure 63: Generalized additive model visualizations for scaled mean; surface phosphate concentrations (PO_4), surface salinity, and mixed layer depth (MLD, in meters) as predictors of percent large chlorophyll above 10μm in size.

Spring Satellite Chlorophyll-a Concentrations

Contributed by Jeanette C. Gann[1], Matt W. Callahan[2], Jens M. Nielsen[3,4], Calvin W. Mordy[4,5], Shaun W. Bell[5], and Phyllis Stabeno[5]
[1]Auke Bay Laboratories, Alaska Fisheries Science Center, NOAA Fisheries, Juneau, AK
[2]Pacific States Marine Fisheries Commission - Alaska Fish Information Network
[3]Resource Assessment and Conservation Engineering Division, Alaska Fisheries Science Center, NOAA Fisheries, Seattle, WA
[4]Cooperative Institute for Climate, Ocean, and Ecosystem Studies (CICOES), University of Washington, Seattle, WA
[5]Pacific Marine Environmental Laboratory, NOAA Research, Seattle, WA

Contact: jeanette.gann@noaa.gov
Last updated: October 2026

Description of indicator: In subarctic systems like the eastern Bering Sea, the timing of the spring phytoplankton bloom can have large and long-lasting effects on biological production with subsequent impacts on higher trophic levels including commercial fish stocks (Platt et al., 2003). The fate of the spring bloom (pelagic grazing or sinking to benthos), and it's timing also impact benthic feeders in the Bering Sea (Hunt et al., 2002). Warm years with open water blooms tend to result in fewer large copepods and reduced pollock recruitment (Kimmel et al., 2018). Recent climatic changes in the Bering Sea have included reduced sea ice and warming ocean temperatures (Stabeno and Bell, 2019), with consequent changes to the food web (Duffy-Anderson et al., 2019). Understanding annual changes in spring phytoplankton biomass and peak timing dynamics are thus important metrics for depicting ecosystem changes.

Here we use ocean color data, a measure of surface phytoplankton concentration, obtained from the European Space agency Climate Change Initiative Ocean Colour Product (OC-CCI[19]) and covering the years 1998-2026. OC-CCI is a merged product that combines information from Visible-Infrared Imaging Radiometer Suite (VIIRS), MODerate resolution Imaging Spectroradiometer (MODIS), Sea-viewing Wide Field-of-view Sensor (SeaWiFS), and the Ocean and Land Color Instrument (OLCI), using 8-day composites at a 4 km x 4 km resolution.

We estimate the phytoplankton biomass in the surface layer via: 1) average spring (Apr-Jun) chlorophyll-a concentrations (Chl-a, ng mL^{-1}) and 2) peak timing of the spring bloom for major regions in the eastern Bering Sea. In the southeastern Bering Sea, sustained observations at the M2 mooring (56.9°N, -164.1°W) provide good representation of the south middle shelf biophysical conditions. Thus, the long-term Chl-a fluorescence mooring measurements, when available, were added as a comparison to the bloom peak timing estimates calculated from the satellite data.

We focus on the spring period as this is an important time for providing a large pulse of basal resources for post-winter zooplankton reproduction and growth of nauplii, and thus energy for higher trophic level species. The April-June time period was chosen as this period consistently includes the pelagic spring bloom peak. We further divided the eastern Bering Sea into 8 distinct regions split between approximately north and south of 60°N and defined by oceanographic fronts and water mass characteristics

[19]https://coastwatch.pfeg.noaa.gov/erddap/griddap/pmlEsaCCI60OceanColor8Day.html

based on Ortiz et al., 2012 (Figure 64). There are several advantages of satellite data, including high spatial and temporal coverage. However, these products are also limited to measurements within the surface ocean and also have missing data due to ice and cloud cover, particularly in high latitude systems such as the Bering Sea. We used 8-day composite data for the biomass estimates and timing estimates.

Spring bloom peak timing was estimated from data binned and averaged into ∼0.5° (56 km) latitude × 1° (47-65 km) longitude spatial grid cells. We then calculated the average and standard deviation of all estimated bloom peaks within a specific region, which allowed for calculation of variability for each of the 8 areas.

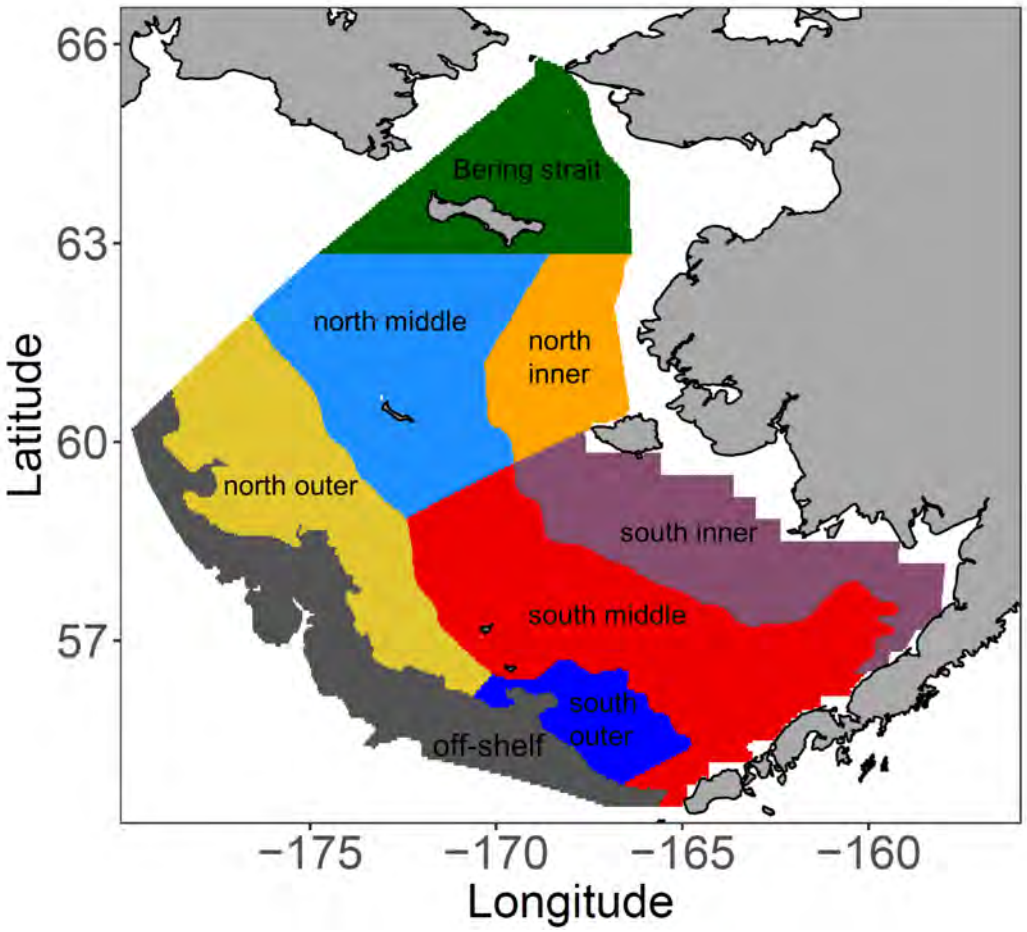


Figure 64: Map of the 8 shelf regions used for satellite Chl-a analyses: south inner (purple), south middle (red), south outer (dark blue), off-shelf (dark grey), north inner (orange), north middle (light blue), north outer (yellow), and the Bering Strait (dark green). Off-shelf denotes regions on the shelf break and slope deeper than 200 m Ortiz et al. (2012).

Status and trends: There was a high degree of interannual variability in satellite Chl-a from 1998-2026. All regions had above average values in 2026 relative to the long-term average. The highest Chl-a concentrations in the north were within the Bering Strait and the inner shelf regions, while the highest in the south were within the middle and outer shelves (Figure 65). Data coverage in the southern regions was generally good across all years, however further north, in some years data from April were particularly scarce due to extended ice coverage. Consequently, estimates in spring should be considered with caution during the years when coverage was limited.

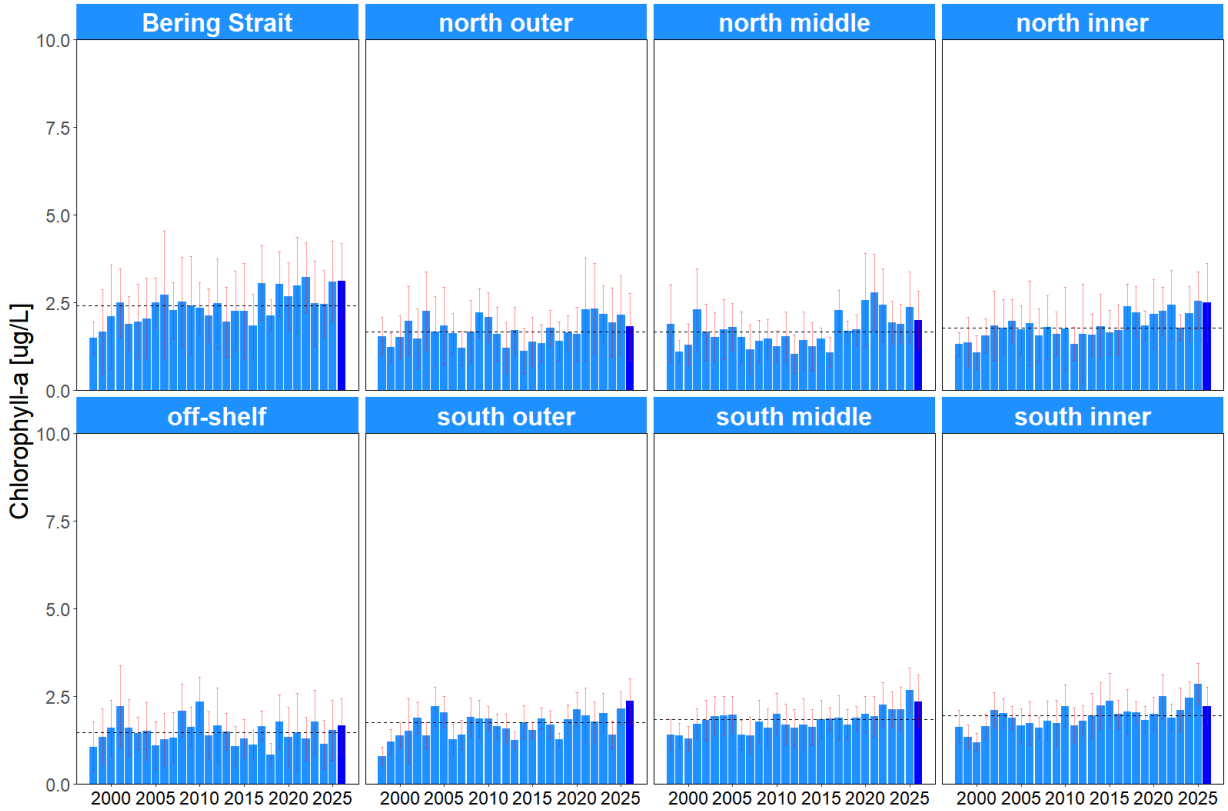


Figure 65: Average and standard deviation (SD) from spring (Apr-Jun) Chl-a concentrations for 8 regions in the Bering Sea. Dotted black line denotes the long-term (1998-2026) median for each region. Dark blue bar on the right represents 2026 values.

Analyses of the pelagic spring bloom peak timing suggest that 2026 was similar to the long-term mean in most regions except for south outer and the M2 mooring regions where timing was early according to satellite data but closer to the mean according to M2 data (Figure 66). Overall, annual timing estimates from 1998 to present from the M2 mooring align well with estimates based on satellite Chl-a at the mooring (0.5 lon x 0.5 lat box with M2 in the center), although differences between M2 and satellite data seem larger in 2026 than many other years. It's possible that this is due to a lack of M2 mooring data available before May 6 of this year. No bloom satellite peak estimates were done for the northern regions.

Factors influencing observed trends: Previous studies have highlighted the strong coupling between temperature and sea ice dynamics and spring bloom timing. For example, in the southern Bering Sea, ice present after mid-march commonly results in an early and prominent ice-associated bloom, while lack of ice normally results in a delayed open water bloom in mid- to late- May (Sigler et al., 2014). On the southern middle shelf, we observed an earlier spring bloom in the cold years of 2007-2012 (excluding 2009) and in the average years of 2013 and 2017. However, spring bloom timing varied considerably in recent warm years (2018-2021), suggesting that the timing of the bloom in those years was impacted by other factors besides simply ice retreat timing. Recent analyses suggest that in years when ice is not the driving factor, wind intensity influences bloom timing (Nielsen et al., 2024). In low ice years, variations in springtime winds influence the setup of stratification (e.g., higher winds can

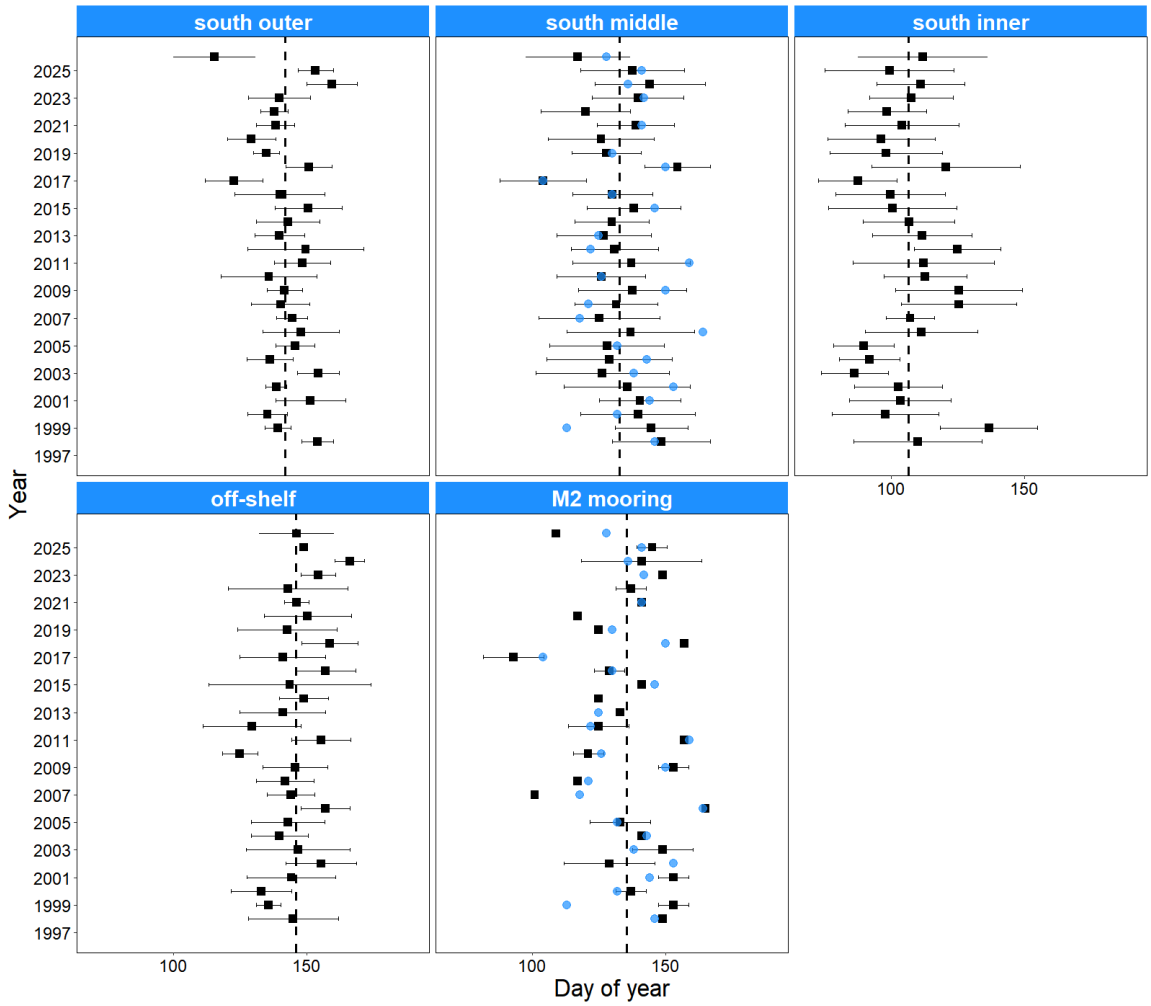


Figure 66: Average and SD of peak spring bloom timing estimated from areas within 4 southern regions in the Bering Sea. Blues dots are the mooring M2 fluorescence peak timing estimates, which are compared to both the south middle shelf data and specifically to satellite data near mooring M2.

delay stratification, Stabeno et al., 2016), which in turn affects light availability and the timing of the bloom. Analysis of Chl-a biomass, though informative in depicting spring bloom timing, does not directly provide information of primary productivity (growth rates) or underlying community composition, though biomass levels in spring generally align well with the timing of production peak estimates.

Implications: Our analyses show no significant long-term change in the bloom peak timing among low and high ice years combined for most of the southern Bering Sea (<60 °N). For the northern Bering Sea, bloom timing occurs earlier as ice retreat advances with warming (Waga et al., 2021), except in the years 2018-2019 when ice retreated so early that open water blooms formed in large areas in this region (Nielsen et al., 2024). Our analyses indicate spring 2026 Chl-a concentrations were average to high (time series 1998-2026) for all regions.

Zooplankton

Continuous Plankton Recorder Data from the Eastern Bering Sea

Contributed by Clare Ostle[1] and Sonia Batten[2]
[1]CPR Survey, The Marine Biological Association, The Laboratory, Citadel Hill, Plymouth, Devon, PL1 2PB, UK
[2]PICES, 4737 Vista View Cr, Nanaimo, BC, V9V 1N8, Canada
Contact: claost@mba.ac.uk
Last updated: July 2026

Description of indicator: Continuous Plankton Recorders (CPRs) have been deployed in the North Pacific routinely since 2000. Two transects are sampled seasonally, both originating in the Strait of Juan de Fuca, one sampled monthly (~April-September) which terminates in Cook Inlet, the second sampled three times per year (in spring, summer, and fall) which follows a great circle route across the Pacific, usually through the southern Bering Sea, before terminating in Asia. As well as this regular Pacific CPR sampling, the icebreaker the *Sir Wilfrid Laurier* (SWL) has now towed a CPR along a transect through the Bering Strait, and the western Chukchi and Beaufort Seas during the summer months since 2018.

We present CPR data from the eastern Bering Sea region (Figure 67) as the following indices: the abundance per sample of large diatoms (the CPR retains large, hard-shelled phytoplankton so while a proportion of the community is not sampled, the data are internally consistent and may reveal trends), mean copepod community size (see Richardson et al., 2006 for details but essentially the length of an adult female of each species is used to represent that species and an average length of all copepods sampled calculated) as an indicator of community composition, and mesozooplankton biomass (estimated from taxon-specific weights and abundance data). Annual anomaly time series of each index have been calculated using a standard z-score calculation: z-score = $(x - \mu)/\sigma$ where x is the value and μ is the mean, and σ is the standard deviation (Glover et al., 2011). Scores of zero are equal to the mean, positive scores signify values above the mean, and negative scores values below the mean.

Status and trends: Figure 68 shows that the large diatom abundance anomaly remained positive in 2025, for a third consecutive year, though it declined notably from the peak values recorded in 2023 and 2024. The copepod community size anomaly rose sharply in 2025 to one of the highest positive values in the time series, reversing the near-neutral anomalies seen from 2022 to 2024. The mean mesozooplankton biomass anomaly remained negative in 2025, consistent with the negative anomalies recorded in every year since 2021.

Factors influencing observed trends: As there are only 8 years of consistently sampled data it remains difficult to determine trends. The decline in diatom abundance in 2025 from its 2023-2024 peak did not coincide with any recovery in mesozooplankton biomass, which remained negative for a fifth consecutive year, continuing to run counter to the expectation that diatoms are typically good-quality food for mesozooplankton. Copepod community size increased sharply in 2025 after three years of near-neutral values, again showing no clear relationship with either the diatom or mesozooplankton biomass trends, consistent with the potential decoupling or species composition shifts noted previously. Analysis of summer CPR data in this region has revealed a general alternating pattern of high and low copepod size

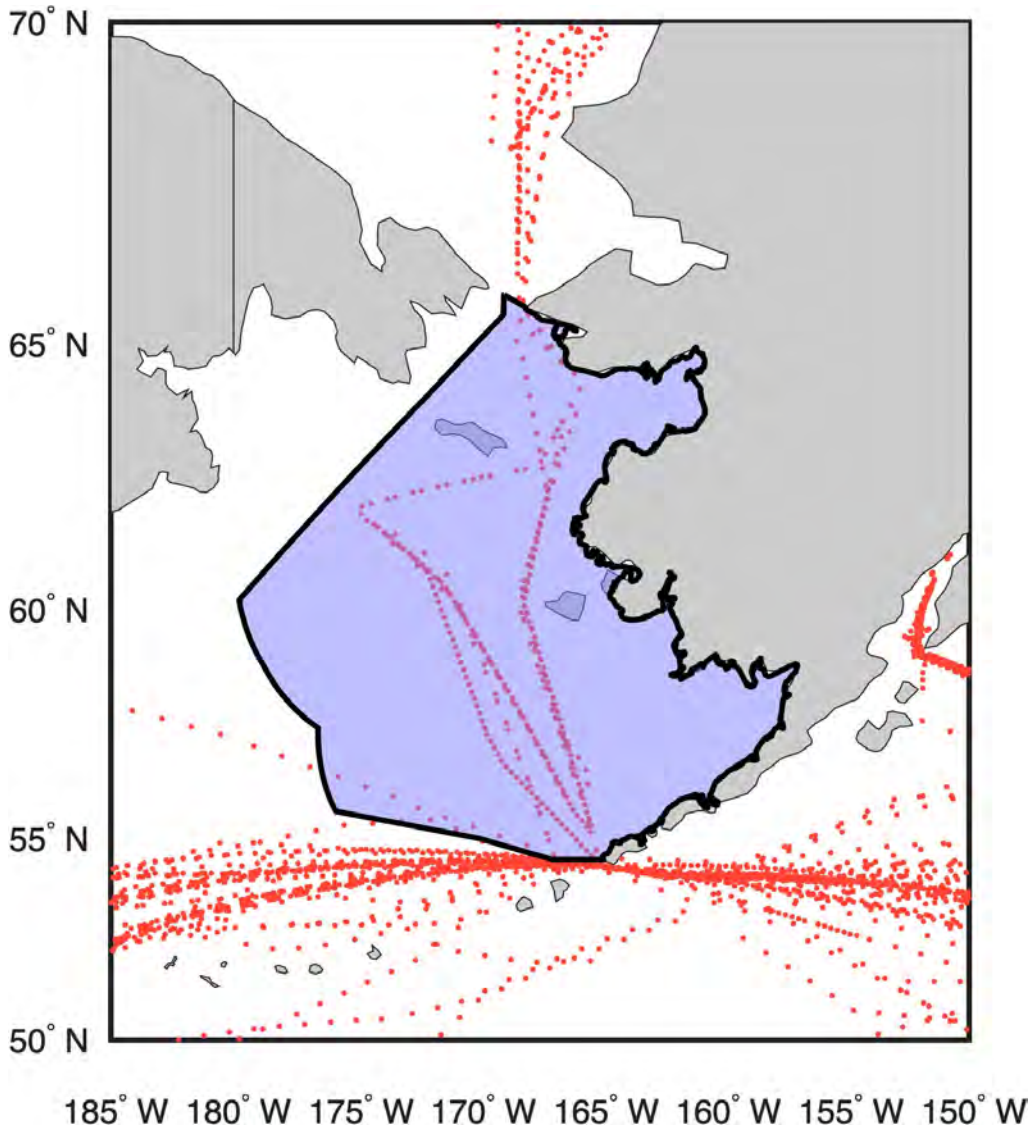


Figure 67: Location of Continuous Plankton Recorder data. The EBS region selected for analysis is shaded in purple. Red dots indicate actual sample positions and may overlay each other.

(indicated in Figure 68 by copepod community size), and the sharp 2025 increase is broadly consistent with that pattern continuing. This could be a similar finding to the analysis from Batten et al. (2018) which was carried out in the southern Bering Sea and Aleutian Islands and concluded that this was the result of a trophic cascade caused by maturing pink salmon present in the region. It should be noted though, that this trophic cascade is not reflected in the diatom abundance data in this region.

Implications: This region appears to be subjected to top-down influence as well as bottom up forcing by ocean climate, which is particularly challenging to interpret. Changes in community composition (e.g., abundance and composition of large diatoms, prey size as indexed by mean copepod community size) may reflect changes in the nutritional quality of the organism to their predators. Changes in abundance or biomass, together with size, influences availability of prey to predators.



Figure 68: Annual anomalies of three indices of lower trophic levels (see text for description and derivation) for the region shown in Figure 67.

Current and Historical Trends for Zooplankton in the Bering Sea

Contributed by David G. Kimmel[1], Colleen E. Harpold[1], Julie Keister[1], Jesse Lamb[1], James Murphy[2], Melanie M. Paquin[1], Steven Porter[1], Lauren A. Rogers[1], and Adam H. Spear[1]
[1]Resource Assessment and Conservation Engineering Division, Alaska Fisheries Science Center, NOAA Fisheries, Seattle, WA
[2]Auke Bay Laboratories, Alaska Fisheries Science Center, NOAA Fisheries, Juneau, AK
Contact: david.kimmel@noaa.gov
Last updated: September 2026

Description of indicator: NOAA's Alaska Fisheries Science Center (AFSC) implemented a Rapid Zooplankton Assessment (RZA) to provide leading indicator information on zooplankton abundance trends in Alaska's Large Marine Ecosystems in 2015 (Kimmel et al., 2025). The RZA is a rough count conducted at sea from paired 20/60 cm oblique bongo tows and provides a preliminary estimate of zooplankton abundance (Kimmel et al., 2025). The RZA uses standard zooplankton processing methods to enumerate zooplankton into three categories: small copepods <2 mm (example species: *Acartia* spp., *Oithona* spp., and *Pseudocalanus* spp.), large copepods >2 mm (example species: *Calanus* spp. and *Neocalanus* spp.), and euphausiids <15 mm (example species: *Thysanoessa* spp.). Small copepods were counted from the 153 μm mesh, 20 cm diameter net and large copepods and euphausiids were counted from the 505 μm mesh, 60 cm diameter net. Detailed taxonomic information on these groups is provided after laboratory processing has been completed (approximately one year post survey) and abundance indices are updated with laboratory processed counts in the following year. All current survey year zooplankton abundance estimates are derived from the RZA.

This year we have made changes to the zooplankton contribution. First, we are no longer reporting euphausiid abundances as we have developed an acoustic index for EcoFOCI surveys (see p. 139). This provides a more accurate abundance index for euphausiids moving forward as bongo net estimates are considered less reliable for abundance estimation due to net avoidance (Hunt et al., 2016). We made a minor change in the spatial mapping of the current year's RZA data to allow for better visual comparisons across surveys. We now report abundance estimates in log10 number m^2 for both taxonomic groups: small copepods < 2 mm and large copepods > 2 mm. This has the effect of keeping the scales more consistent from both within and between surveys, making maps easier to interpret as well as integrating abundances over the entire water column. Second, we have standardized the annual abundance indices for each coarse taxonomic group using spatiotemporal modeling (Shelton et al., 2014; Thorson et al., 2016). This approach better accounts for spatial and temporal variability arising from different spatial coverage and timing across years (Anderson et al., 2022). Using this approach, we were also able to expand the spatial area used to estimate the standardized, annual abundance index.

Standardized indices provide an area-weighted population index that predicts from a model covering a specified grid area and is therefore independent of sampling locations that vary annually. Modeling was performed using the sdmTMB package in R (Anderson et al., 2022) to develop the standardized, annual abundance indices. Prior work has demonstrated the effectiveness of spatiotemporal modeling for exploring the seasonal dynamics of the copepod *Calanus marshallae/glacialis* (*Calanus* spp. hereafter) in the Bering Sea (Thorson et al., 2020). Annual abundance indices were modeled using year as a factor and may or may not include a smooth day-of-year effect to account for shifts in sample collection times year to year. Day-of-year was standardized to day 135 (~15 May) for the spring index and day 258

(~15 September) for the summer/fall index. None of the annual indices for the northern Bering Sea required a day-of-year adjustment.

The spatial area used to estimate the spring and summer/fall indices for the Bering Sea was a combination of BSIERP regions: Alaska Peninsula, South Middle Shelf, Central Middle Shelf, and Saint Matthew (Ortiz et al., 2012). The spatial area used to estimate the northern Bering Sea indices was a spatial polygon called north Bering Sea strata of the AFSC Groundfish Survey[20]. Zooplankton data were modeled using the Tweedie distribution (to account for zeros and right-skewed distribution) or the lognormal distribution and included spatial random effects and spatiotemporal random effects (Anderson et al., 2022). The entire, area-weighted, summer abundance over 20 km^2 grid cells was then estimated for each zooplankton group and reported as an annual time-series.

We completed four surveys in the Bering Sea in 2026: the spring 70 m isobath/spring larval survey (May 2026), the fall age-0 survey (Bering Arctic Subarctic Integrated Survey; BASIS) (Aug/Sep 2026), the fall 70 m isobath survey (Aug/Sep 2026) and the northern Bering Sea survey (NBS, Aug/Sep 2026). We also show annual abundance time-series for each RZA taxa for both spring and summer/fall in the Bering Sea and a separate time-series for the north Bering Sea.

Status and trends:

Spring 70 m isobath/spring larval survey

The spring survey covered the middle shelf region northwards to approximately 60°N (Figure 69). Small and large copepods were less abundant along the 70 m isobath compared to abundances further offshore. The abundance index was near the long-term mean for small copepods in 2026 and represented a drop from the high abundances observed in abundance from the previous year (Figure 70, top). Large copepods remained below average, a trend that has continued since 2017 (Figure 70, bottom).

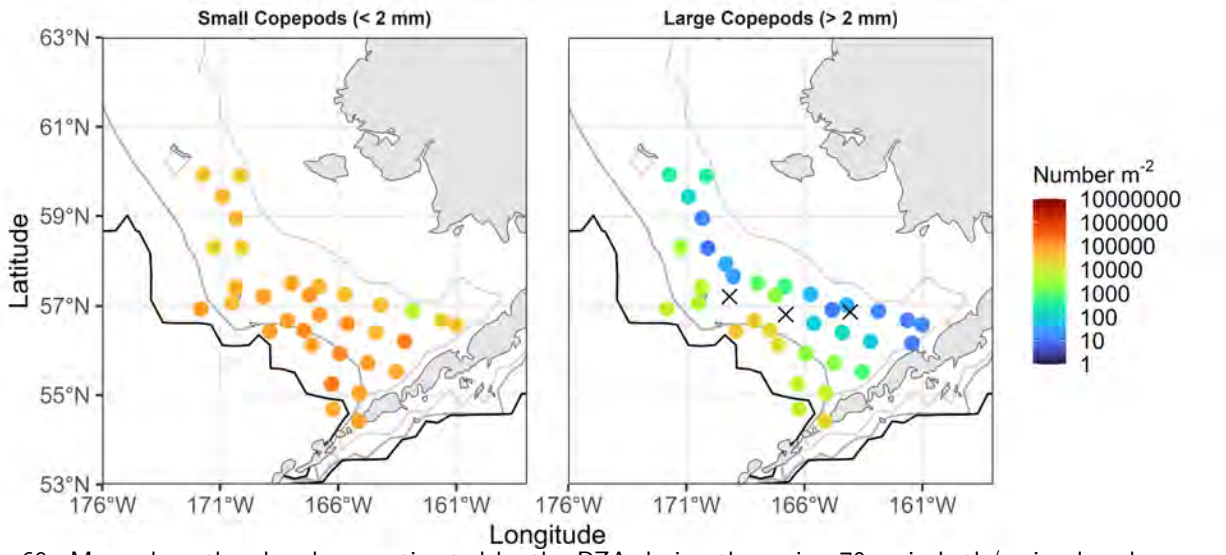


Figure 69: Maps show the abundance estimated by the RZA during the spring 70 m isobath/spring larval survey. X indicates a sample with abundance of zero individuals m^2. Bathymetry is shown by light gray (50 m), medium gray (100 m), and black (200 m) lines.

[20] https://github.com/afsc-gap-products/bering-sea-spatial

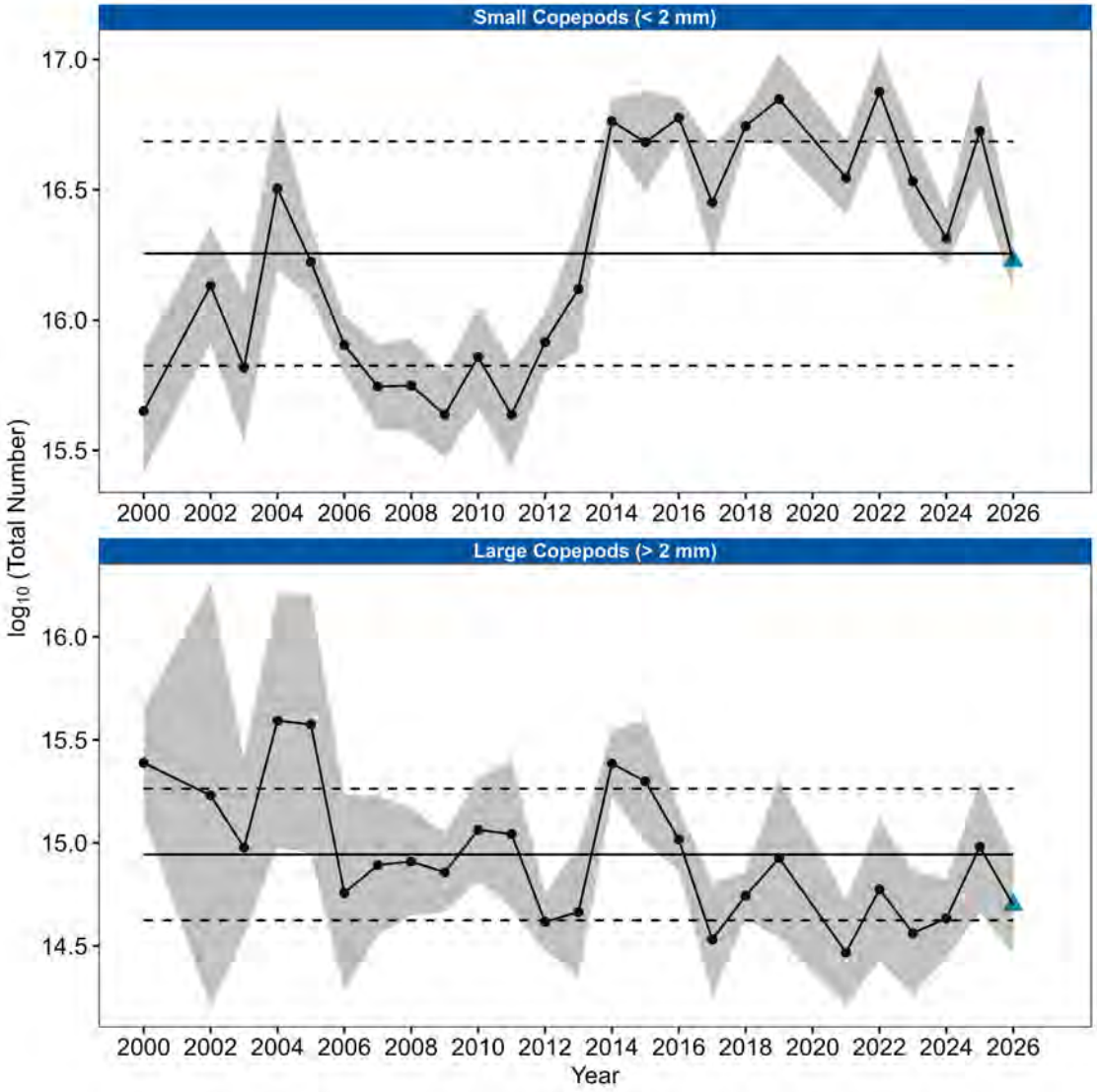


Figure 70: Standardized annual abundance indices for the spring on the Bering Sea middle shelf. Annual, area weighted abundance estimate (black circles), abundance estimate based on RZA data (blue triangle), upper and lower confidence intervals of the estimate (shaded area), mean abundance for the total data record (solid black line), and ± 1 standard deviation of the mean abundance for the total data record (dashed lines).

Fall age-0 survey and fall 70 m isobath survey

Small copepods during the fall age-0 survey (Figure 71, left) and fall 70 m isobath survey (Figure 72, left) were evenly distributed across the shelf and no spatial patterns were observed. Large copepod numbers were high across the shelf, with the lowest numbers observed in the south (Figures 71 and 72, right). Small copepod abundances were well below the long-term average and much lower than the extreme warm years of 2018 and 2019 when abundances were very high. Note that during the prolonged cold period from 2006-2013, small copepod abundances remained low (Figure 73, top). Large copepod abundances were above the long-term mean (Figure 73, bottom), rebounding from the recent period of low abundances that occurred from 2015-2025.

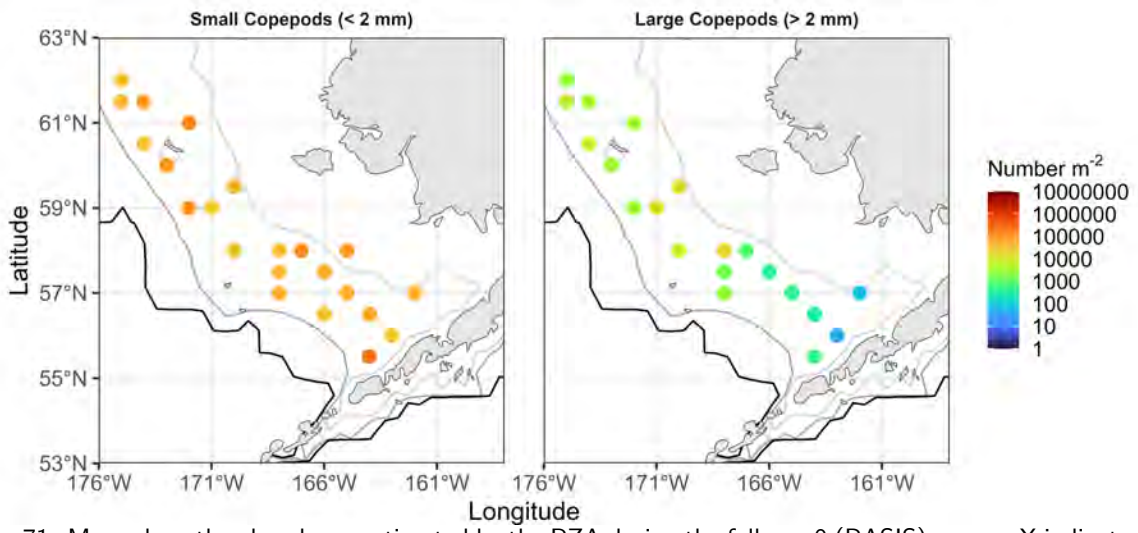


Figure 71: Maps show the abundance estimated by the RZA during the fall age-0 (BASIS) survey. X indicates a sample with abundance of zero individuals m^2. Bathymetry is shown by light gray (50 m), medium gray (100 m), and black (200 m) lines.

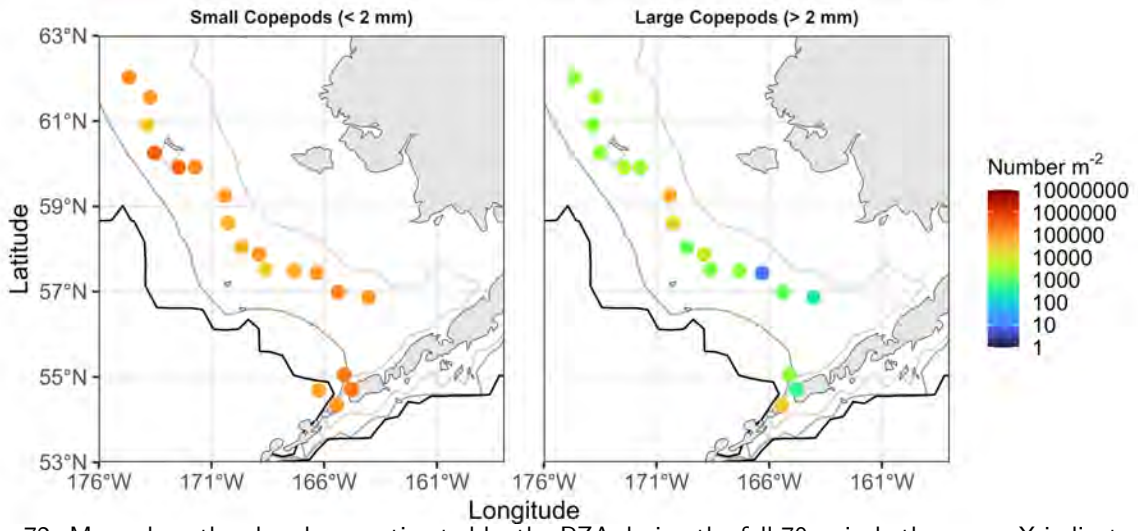


Figure 72: Maps show the abundance estimated by the RZA during the fall 70 m isobath survey. X indicates a sample with abundance of zero individuals m^2. Bathymetry is shown by light gray (50 m), medium gray (100 m), and black (200 m) lines.

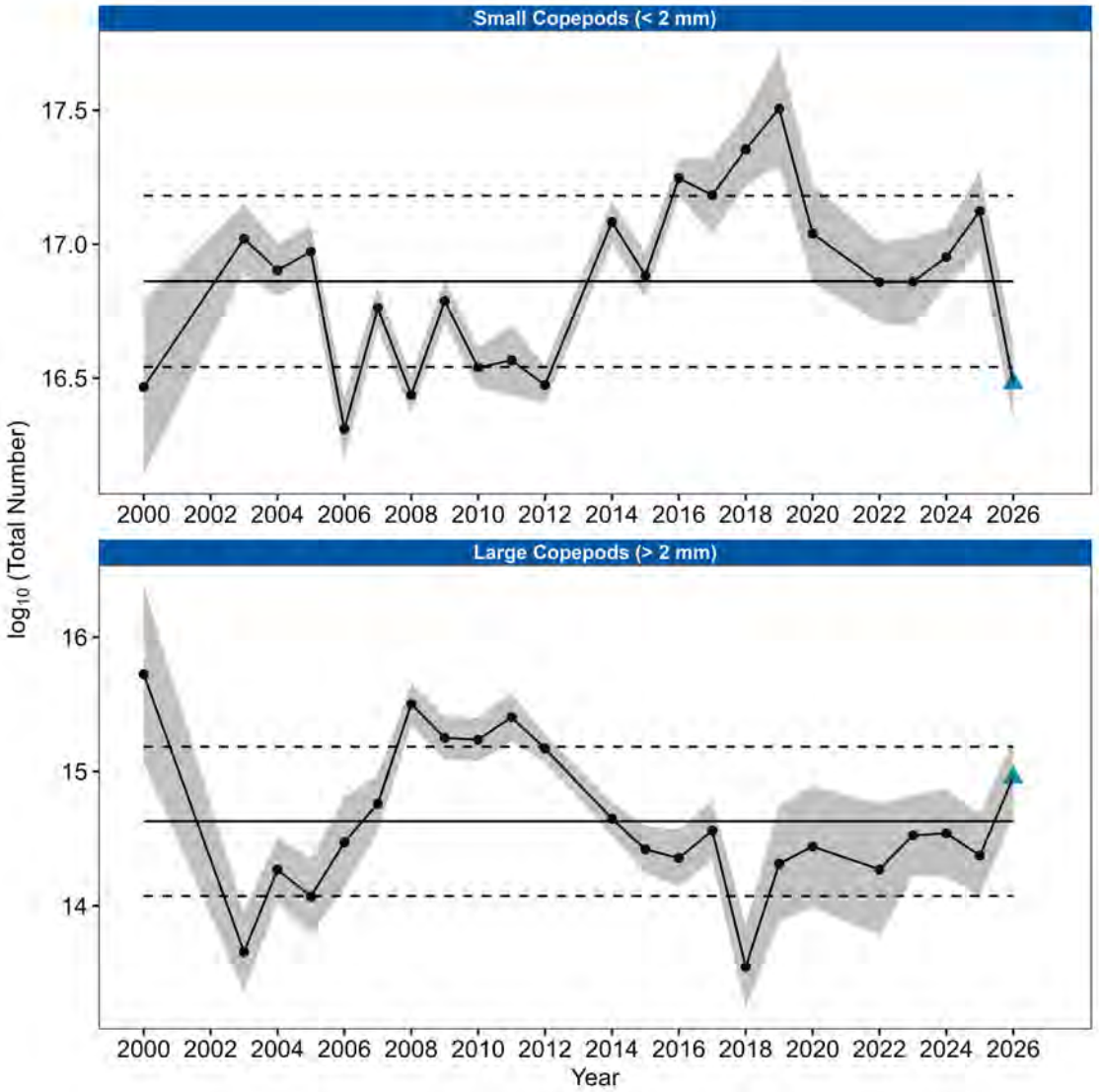


Figure 73: Standardized annual abundance indices for the summer/fall on the Bering Sea middle shelf. Annual, area weighted abundance estimate (black circles), abundance estimate based on RZA data (blue triangle), upper and lower confidence intervals of the estimate (shaded area), mean abundance for the total data record (solid black line), and ± 1 standard deviation of the mean abundance for the total data record (dashed lines).

Northern Bering Sea survey

Abundances of small copepods in the Northern Bering Sea were similar throughout the sampling grid (Figure 74, left). Large copepods were low in abundance along the inner shelf and abundances increased as the survey moved offshore (Figure 74, right). Both small and large copepods were near the long-term averages (Figure 75).

Factors influencing observed trends: Spring conditions in the Bering Sea produced very cold temperatures, particularly along the middle shelf. This resulted in a substantial decline in the average, small copepod abundance (Figure 70, top). Abundance of small copepods was still elevated relative to the cold years of 2006-2013 but did not achieve the highest values observed during the more recent warm years. This trend is primarily driven by temperature as small copepods have multiple generations

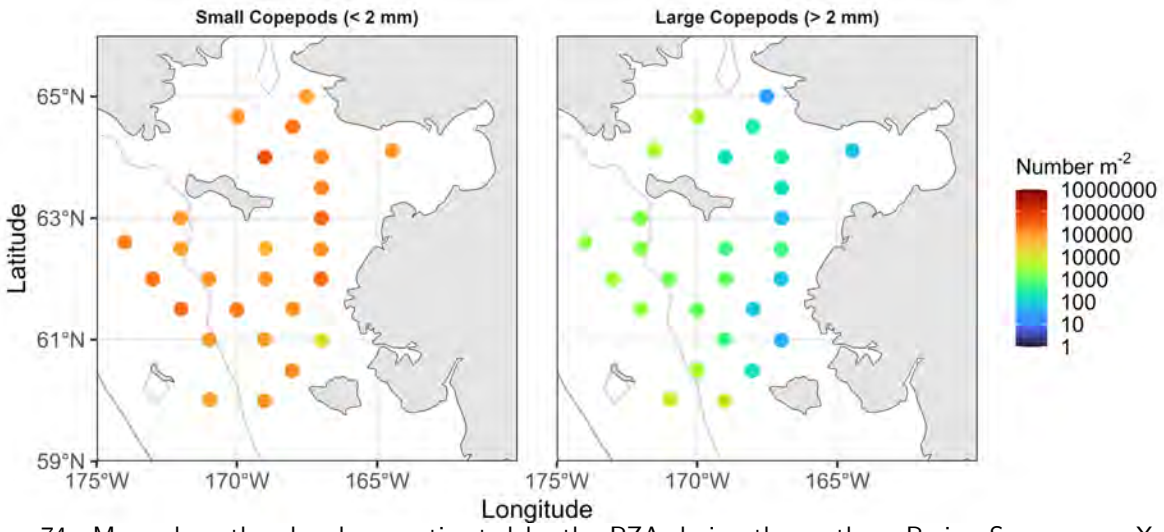


Figure 74: Maps show the abundance estimated by the RZA during the northern Bering Sea survey. X indicates a sample with abundance of zero individuals m^2. Bathymetry is shown by light gray (50 m) and medium gray (100 m) lines.

per year, faster turnover times, and metabolic rates that scale less dramatically with temperature than large copepods (Kiorboe and Sabatini, 1995). When temperatures are lower due to late ice retreat, small copepod numbers are expected to be reduced, and this prediction matches observations. Large copepods showed less variability during spring (Figure 70, bottom) and abundance remained slightly below average. Despite the below average abundance, conditions were favorable for the overwintering, large copepods (*Calanus* spp.) to produce a larger annual cohort. This prediction was based on the cold temperatures and late ice retreat observed in 2026.

Colder temperatures continued to impact small copepods into the late summer and fall, reducing their abundance to numbers not observed since the cold years of 2006-2013 (Figure 73, top). In contrast, large copepod abundance (primarily *Calanus* spp., but some *Neocalanus* spp. were also observed) was above average along the southeastern Bering Sea shelf for the first time since 2014 (Figure 73, bottom). The spatial gradient observed for large copepods is driven entirely by the presence of the cold pool resulting in the presence of *Calanus* spp. (Figures and 71 and 72, right). This sub-Arctic species requires cold pool conditions (Hunt et al., 2011; Eisner et al., 2017; Kimmel et al., 2018) to achieve higher abundances in fall and this is clearly seen in the time-series where the cold years of 2006-2013 had very high large copepod abundances in contrast with the low abundances observed since 2018. Therefore, an increase in large copepod abundance was expected and observed (Figure 73, bottom).

The small copepod numbers in the northern Bering Sea also declined in relation to colder conditions (Figure 75, top). Small copepod numbers are more variable in this survey as it samples the inner shelf more frequently and this area has higher abundances of small, neritic species as well as meroplankton (Kimmel et al., 2023). Large copepods showed a distinct inner shelf-outer shelf gradient and had numbers that were higher on the middle shelf, relative to the inner shelf (Figure 74, right). This is expected as *Calanus* spp. are located primarily on the middle shelf (Cooney and Coyle, 1982). In general, large copepod abundances remain at or near the long-term average during colder conditions (2006-2013) as was observed in 2026 (Figure 75, bottom) but drop significantly during warm periods as warm water penetrates the north Bering Sea (Kimmel et al., 2023).

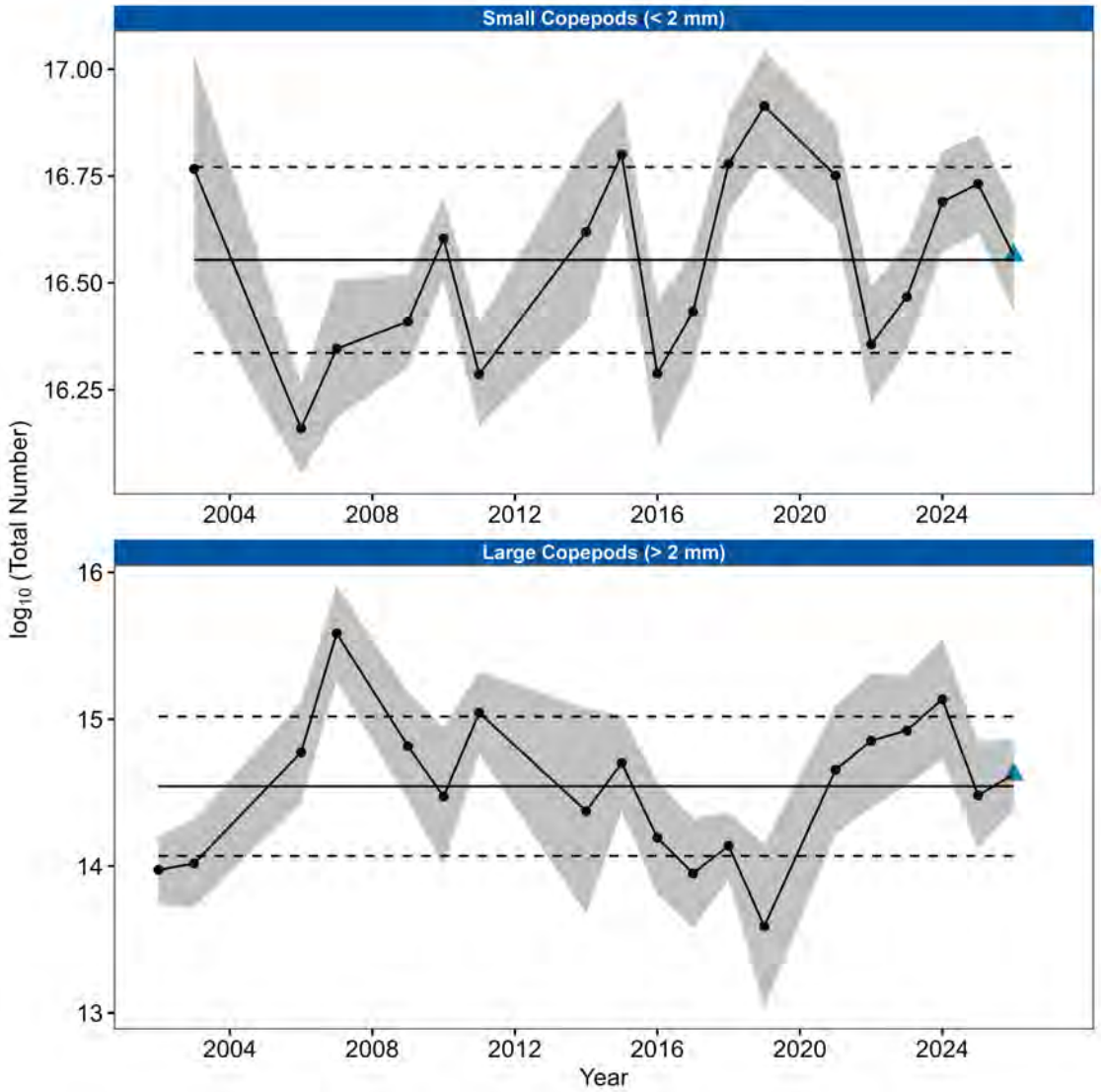


Figure 75: Standardized annual abundance indices for the northern Bering Sea. Annual, area weighted abundance estimate (black circles), abundance estimate based on RZA data (blue triangle), upper and lower confidence intervals of the estimate (shaded area), mean abundance for the total data record (solid black line), and ± 1 standard deviation of the mean abundance for the total data record (dashed lines).

Implications: Smaller copepods and their early life history stages (nauplii) form the prey base for larval to early juvenile pollock, as well as other fish species, during spring (Figures 69 and 70) on the eastern Bering Sea middle shelf. Small copepods were less plentiful during spring of 2026 compared to recent, warm years; however, these copepods and nauplii were still abundant, indicating adequate forage for larval and early juvenile fish. That said, as fish transition away from small copepods and nauplii to feed on larger prey during summer and fall, large copepods become a primary prey item (Strasburger et al., 2014). The highest abundances of large copepods were observed between 2006-2013, whereas recent abundances have been well below these in the southeastern Bering Sea (Figure 73, bottom). The higher abundance and broad distribution of large, lipid rich *Calanus* spp. observed in 2026 may indicate a better forage for age-0 pollock as the abundance of *Calanus* spp. has been linked to pollock abundances at age-3 (Eisner et al., 2020). There also appears to be adequate forage in the form of abundant, lipid-rich

Calanus spp. on the southeastern Bering Sea shelf in 2026 (Figures 71 - 73). Conditions in the northern Bering Sea were characterized by near long-term average abundances of both small and large copepods. This indicates that the warm, neritic waters of the Alaska Coastal Current remained nearshore and did not expand onto the middle shelf as was observed during the more recent warm period (Kimmel et al., 2023). This can be seen in the difference in abundance of large copepods between inner and middle shelves (Figure 74, right) and in the near average abundances of small copepods (Figure 75, top).

In summary, the 2026 zooplankton community for the Bering Sea matches recent observations during colder conditions. This suggests that larval fish in the early portion of the year experienced adequate forage and large copepods were present later in the year to act as lipid-rich forage for age-0 pollock and other planktivorous fishes. Assuming there is sufficient overlap with these large copepod prey, pollock may be better prepared to survive their first winter under 2026 conditions (Siddon et al., 2013).

Lipid Content of Copepods and Euphausiids in the Bering Sea

Contributed by Cody Pinger[1], Bryan Cormack[1], Colleen Harpold[2], Dave Kimmel[2], Jesse Lamb[2], Drew Porter[3], and Rob Suryan[1]
[1]Auke Bay Laboratories, Alaska Fisheries Science Center, NOAA Fisheries, Juneau, AK
[2]Resource Assessment and Conservation Engineering Division, Alaska Fisheries Science Center, NOAA Fisheries, Seattle, WA
[3]University of Alaska Fairbanks, College of Fisheries and Ocean Sciences, Juneau, AK
Contact: cody.pinger@noaa.gov
Last updated: October 2026

Description of indicator: Large copepods (*Calanus* spp.) and euphausiids are important prey for fishes in the Bering Sea, including age-0 walleye pollock (*Gadus chalcogrammus*), juvenile salmon (*Oncorhynchus* spp.), and capelin (*Mallotus catervarius*), because they provide a valuable source of dietary lipids (Heintz et al., 2013; Farley et al., 2016; Kimmel et al., 2018). Consumption of a high lipid diet prior to winter is important for age-0 fishes, as higher growth and lipid reserves can reduce starvation, mortality, and predation risk over prolonged winter months of low prey availability and quality. The lipid content of large copepods and adult euphausiids collected in early spring are at their seasonal lowest and show little variability, however samples from late summer/fall collections that are reflective of summer production vary annually and are therefore the focus of this indicator. This indicator provides insight into diet quality affecting the future health and recruitment success of age-0 fishes.

Mean annual lipid content of large copepods collected from the NMFS annual Northern Bering Sea Ecosystem and Surface Trawl Survey (NBEST) and both large copepods and adult euphausiids from the biennial Southeast Bering Sea (SEBS) survey grids occurring in late August and September are presented. Samples were collected by bongo net tows as part of the Rapid Zooplankton Assessment (RZA, Kimmel et al., 2025). Samples consisted of composites of 2-10 individuals, with copepods $>$2 mm (primarily stage IV and V *Calanus glacialis*) and for euphausiids $\geq$15 mm or the largest available individuals (primarily *Thysanoessa* spp. and *Euphausia* spp). Once picked from the RZA, zooplankton were blotted dry with a tissue and placed in glass vials, frozen, and transported to NOAA Auke Bay Laboratories immediately after the survey for analysis of lipid content. Lipid content was measured as a percent of total wet weight via the sulfo-phospho-vanillin (SPV) assay (Pinger et al., 2022).

Status and trends: This time series shows significant interannual variability in large copepod lipid content in the late summer/fall in the NBS and SEBS, and adult euphausiid lipid content in the SEBS (Figure 76). An ANOVA test revealed that the mean lipid values differed significantly between years for zooplankton in both ecosystems. The mean lipid content of large copepods surveyed across the NBS ecosystem in 2026 (13.6%) was higher and statistically different from the overall mean (10.38%, $p<0.05$). A Tukey multiple comparison of means test reveals that the mean lipid content of large copepods in the NBS in 2026 was significantly greater than heat wave years (2018 and 2019), as well as 2023 ($p<0.05$), but not different from 2024 or 2025 ($p>0.05$).

Similarly, the mean lipid content of large copepods in the SEBS in 2026 (18.8%) was slightly higher than the long-term mean (16.38%), but not statistically different ($p>0.05$). A Tukey multiple comparison of means test reveals that the mean lipid content of SEBS large copepods in 2026 was statistically greater than 2018 ($p<0.05$), during the heat wave, but not different from 2022 or 2024 ($p>0.05$).

Additionally, the mean lipid content of adult euphausiids in the SEBS in 2026 (10.7%) was higher than the long-term mean (8.99%), but not statistically different. A Tukey multiple comparison of means test reveals that the mean lipid content of SEBS adult euphausiids in 2026 was statistically greater than 2022 ($p<0.05$), but not different from 2024 ($p>0.05$).

Factors influencing observed trends: Large copepods and euphausiids store energy in the form of lipids for future use in survival, growth, and reproduction. The lipid content observed in this time series may be driven in part by water temperature, food availability (e.g., phytoplankton), competition, sea ice extent, and timing of sea ice retreat.

Implications: Large lipid-rich copepods are less abundant during warm years in the Bering Sea (Kimmel et al., 2023; Eisner et al., 2014). Our time series shows that large copepods also contain less lipid during warm years, suggesting there is less energy available at the base of the food web in these years. Data from 2023 suggest that temperature may not be the only factor influencing late summer/fall copepod lipid content. Other factors, such as food availability and quality, also play a key role. The mean lipid content of both large copepods and adult euphausiids in 2026 was slightly elevated compared to recent years, with copepod lipid content significantly higher than warm years. These results are consistent with greater cold pool extent and generally cooler conditions in the Bering Sea during 2026. This information, paired with an increase in large copepod abundance relative to recent years (see Figure 73 in 'Current and Historical Trends for Zooplankton in the Bering Sea' on p. 122 of this report), indicates above average diet quality for species that depend on this prey source.

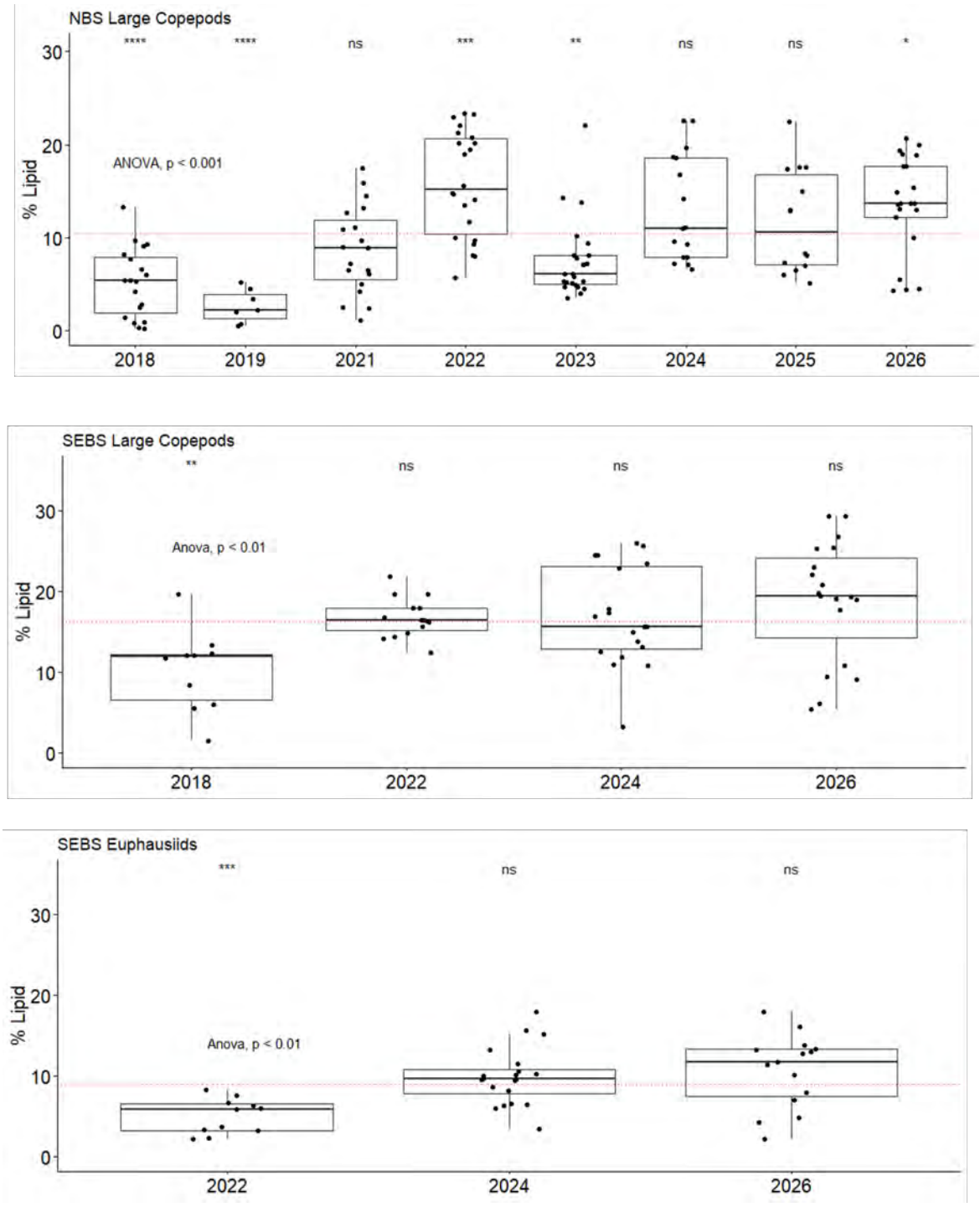


Figure 76: Annual and biennial lipid content (% lipid per wet mass) of zooplankton collected from the NBEST and SEBS surveys. The stars above each group indicate the significance of the difference of that group mean from the overall mean which is indicated by the horizontal red line. ns = no significant difference from the overall mean.

Summer Eastern Bering Sea Euphausiids ('Krill')

Contributed by Mike Levine[1], Alex De Robertis[1], Patrick Ressler[1], and Brandyn Lucca[2]
[1]Resource Assessment and Conservation Engineering Division, Alaska Fisheries Science Center, NOAA Fisheries, Seattle, WA
[2]Fisheries Collaborative Program, University of California - Santa Cruz
Contact: mike.levine@noaa.gov
Last updated: September 2026

Description of indicator: The Alaska Fisheries Science Center Midwater Assessment and Conservation Engineering (MACE) Program has produced a time series of euphausiid (primarily *Thysanoessa raschii* and *T. inermis*, hereafter referred to as krill) density since 2004 (Ressler et al., 2012; Levine and Ressler, 2024). This time series is based on data collected during biennial acoustic-trawl surveys of the EBS shelf. While these surveys are primarily designed to assess walleye pollock (*Gadus chalcogrammus*, hereafter referred to as pollock) distribution and abundance, the multifrequency acoustic data they collect at frequencies ranging from 18 to 200 kHz is useful for acoustically differentiating krill from other common midwater species groups. Backscatter from krill is stronger at higher frequencies than at lower frequencies, while backscatter from swim-bladdered fish species is not (Cochrane et al., 1991; Holliday and Pieper, 1995; De Robertis et al., 2010). This characteristic allows pairwise differences in backscattering strength at each combination of acoustic frequencies ("dB-differencing") to be compared to expected differences from trawl-verified samples dominated by krill, yielding estimates of acoustic backscatter attributed to krill (De Robertis et al., 2010; Ressler et al., 2012; Simonsen et al., 2016). Estimates of krill backscatter are then converted into estimates of krill abundance and biomass using three data sources: targeted trawl catches to determine the species and size composition of acoustically observed krill layers, models of the amount of backscatter reflected from individual krill based on their size composition (i.e., 'target strength', hereafter TS), and krill length-weight relationships.

In 2026, we are sharing two updates: an updated method which affects the existing (2004-2024) krill density time series (see **Updated method** below) and a preliminary estimate of krill density in the EBS during summer 2026 (see **Preliminary 2026 krill density and distribution** below).

Updated method
We were motivated to update our historical krill time series methods (Ressler et al., 2012) due to incremental improvements to acoustic data processing and krill identification techniques that have occurred since the methodology was first developed, a review of our use of krill trawl catch data to convert acoustic backscatter, and recent work which has improved estimates of krill TS in the EBS (Lucca et al., 2021). The updated method incorporated six changes to the acoustic krill identification process, three changes to the backscatter-to-density and -biomass conversion process, and one change to the index standardization process. Here, we provide a brief summary of these changes; for more detail, see Levine et al., 2026. To explore the magnitude of each change, we conducted a series of comparisons with the historical method, noting the relative effect of each change as well as the net effect compared to the historical timeseries. These comparisons indicated that updates to the backscatter to abundance and biomass conversion process had a much greater effect on abundance estimates than updates to the acoustic identification process or index standardization process (Figure 77).

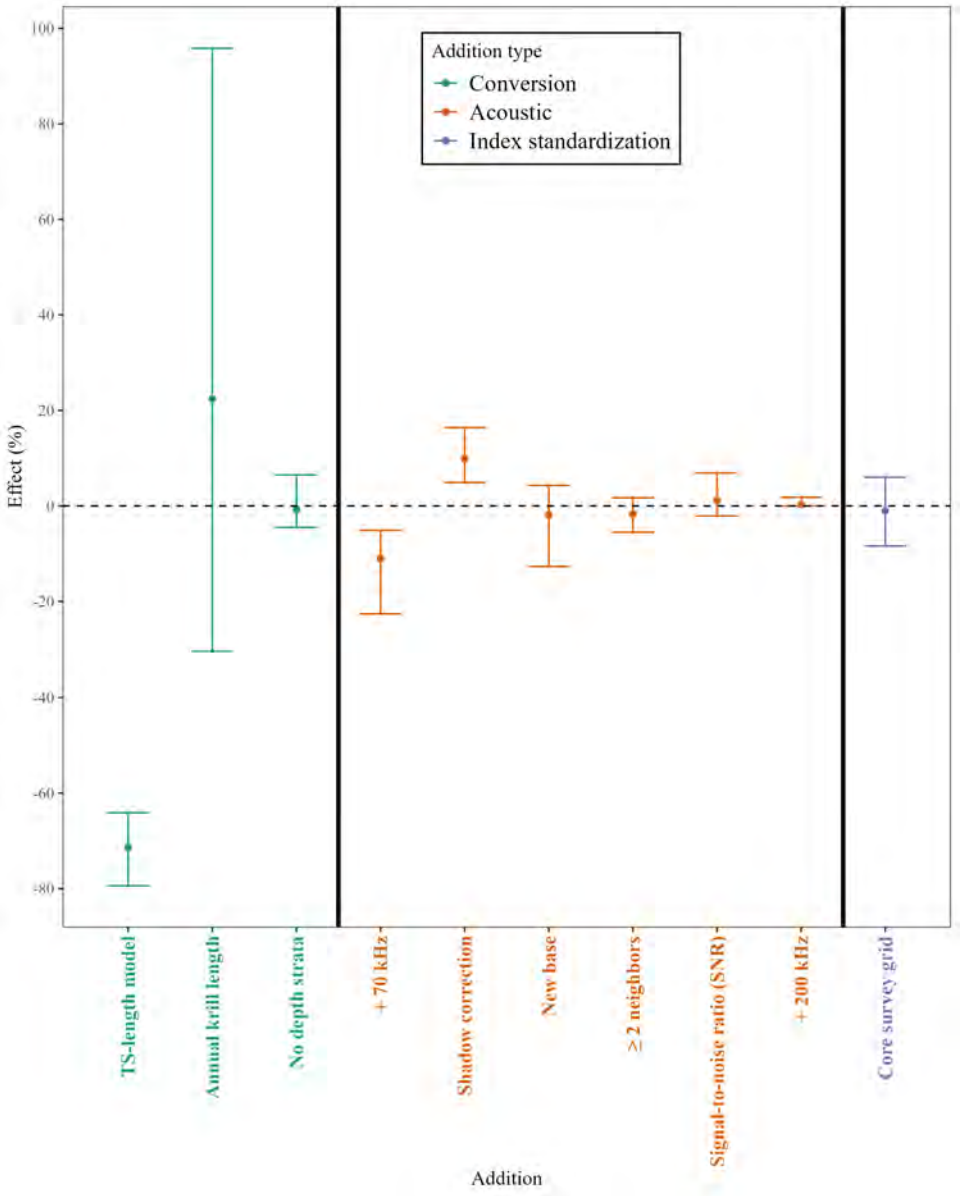


Figure 77: Relative effect of each methodological addition. Changes are reported as the mean percent change (points) and range (error bars) for each addition, in relation to an appropriate reference point (see Levine et al., 2026 for more detail).

Conversion from backscatter to density and biomass:

As compared to the large volume of acoustic data (collected over 2,500 - 5,000+ nautical miles (nmi) of transect line each survey year), the number of trawls used to sample the species and size composition of acoustically observed krill layers is comparatively low (mean of 10 trawls per year, ranging from 1 - 24 trawls per year). Given the limited trawl information available, the historical method used pooled multi-year averages of krill length to parameterize a single TS model for the EBS that included all observed krill species (i.e., the abundance estimates are not species-specific; Ressler et al., 2012; Levine and Ressler, 2024). However, pooling size and species composition among years may miss inter-annual and longer-term changes in species or size composition, including those driven by climate change (Mueter and Litzow, 2008; Michael et al., 2021; Rooper et al., 2021; Levine et al., 2023). Additionally, given that

the EBS krill time series now spans 20 years, there are more available krill length data to examine how the targeted krill trawl information should be used than when the historical method was established.

In terms of species composition, krill dominated Methot trawl catches, the majority of the species captured were *T. raschii* and *T. inermis*, and there was no evidence of a clear change in krill species composition over the time series. However, changes in annual mean krill length (average ∼19 mm, varying by ∼3.5 mm over the 2004-2024 dataset) were substantial despite low sample size and high variability. We therefore decided to use the annual mean krill length to apply krill TS models as opposed to using a long-term mean length. Using annual estimates of mean length produced krill density estimates that differed appreciably from those made using the historic method of pooling lengths across years. Mean survey-level krill density changed by an average of 22.4% over the survey years (range: -30.3% - 95.8%). In periods when krill were larger than the long-term mean length (including the years 2009-2014), the use of annual length estimates lowered density estimates relative to the historical method: estimates declined by 11.0% - 30.3% using annually estimated lengths as compared to using the long-term mean length because the estimated acoustic backscatter per krill increased. Conversely, in periods when krill were smaller in size (including the years 2016-2024), krill densities increased (2016-2024 estimates increased by 48.1% - 95.8%).

As compared to the Smith et al., 2013 TS model used in the historical approach, the updated TS model (Lucca et al., 2021) indicates that krill are stronger scatterers at all length classes. At the range of lengths observed in the 2004-2024 catch data (annual mean krill length 16.7 mm - 20.7 mm), this corresponds to a 4.5 dB - 6.9 dB increase in TS in the updated TS model as compared to the historical model. The increase in TS led to a corresponding decrease in krill density: as compared to the historical method, krill density declined on average by 71.3% (-79.4% - -64.1%) (Figure 77).

Acoustic identification of krill:
The impact of changes to the acoustic identification process were relatively small (Figure 77), but added meaningful improvements to the time series. For example, the addition of the 70 kHz frequency for multifrequency identification provided an additional, useful contrast in differentiating krill from pollock (De Robertis et al., 2010), resulting in more precise krill identification. Similarly, updates to the 'shadow correction', which estimates the effect of comparatively strong pollock 'shadowing' krill when both taxa co-occur and applies a backscatter correction proportional to the extent of the shadowing, removed a persistent low bias in the historical method and increased krill backscatter. Other changes integrated improvements in monitoring and mitigating for acoustic noise that have had negligible effects on the time series but could become important in future surveys. For example, we now provide methods that allow for the 200 kHz frequency to 'fill in' in cases where the 120 kHz is not available, and methods that assess acoustic noise at all frequencies (background noise at 18 and 38 kHz was assumed to be negligible).

Index standardization:
We standardized the time series survey area by limiting the survey domain to the core area which is sampled in all years. This makes the data more comparable across years; though it has little impact on the current time series (Figure 77), it could be more important if the survey spatial domain changes in the future.

Summary
The revised annual krill density and biomass estimates differ from those made using historical methods. This is due primarily to updates to the krill backscatter-to-density conversion process. While the historical and the updated krill methods produce similar estimates of krill backscatter (Figure 78a), the net effect of the various methodological changes (Figure 77) is that updated krill volumetric density, areal density, and wet weight time series are substantially lower than the historical versions (Figure 78b-d) in absolute terms, with the relative interannual pattern (e.g., 'high' and 'low' years) remaining mostly the same between the time series versions.

The sizeable effect of krill length estimates on the krill indices (Figure 77) highlights the importance of size composition data obtained from trawl sampling and the need to better quantify and characterize this uncertainty. To reduce this uncertainty, future surveys should sample krill in areas of high abundance throughout the entire survey area, either through trawls or through emerging optical (Levine et al., 2018; Svantemann et al., 2025) or acoustic (i.e., broadband acoustic measurements, Amakasu et al., 2017) methods. Increased biological sampling effort could allow for species-specific krill estimates to be produced in the EBS.

Updated method: data access:
Because krill density and distribution in the EBS is of interest to researchers working on ecosystem processes as well as those conducting analyses for ecosystem-based fisheries management efforts, we have shared the EBS krill time series in a publicly accessible repository. The MACE *KrillCommunication* repository[21] shares krill estimates from all EBS summer surveys from 2004-2026, including data from a 2020 survey that was conducted using Saildrone uncrewed surface vehicles (Levine and De Robertis, 2025).

The data are reported in units of krill backscatter (Nautical Area Scattering Coefficient, s_A, m^2 nmi^{-2}), krill volumetric density (individuals m^{-3}), krill areal density (individuals m^{-2}), and krill wet weight (g m^{-2}). We provide data at three spatial scales: totals per survey year (useful for ecosystem-scale interannual patterns), vertically integrated at 0.5 nmi horizontal resolution along acoustic transects (useful for 2-dimensional spatial krill distributions), and 0.5 nmi horizontal X 20 m vertical resolution (useful for both the horizontal and vertical distribution of krill). Additionally, we provide metadata and example scripts to allow researchers to more easily use this dataset. *KrillCommunication* is intended to be updated biennially as additional EBS summer surveys are conducted.

Preliminary 2026 krill density and distribution
Status and trends: Summertime euphausiid density increased in the eastern Bering sea from 2004 to 2010, then subsequently declined through 2016, when the lowest value in the time series was reported. Since 2016, abundance has been variable, with an increasing pattern from 2016 to 2020 followed by a decrease through 2024. The 2026 estimate (30.7 g m^{-2}) represents an increase as compared to 2024 but is not a remarkably high estimate in the time series (Figure 79). As in previous survey years, a high-density hotspot was observed in the southwest corner of the EBS shelf at bottom depths from 100-200 m (Figure 80). Additionally, relatively dense aggregations were observed along the eastern edge of the survey area in shallower (<100 m bottom depth) water; this is consistent with other relatively cool survey years (compare 2026 distribution to those in the relatively cool years of 2022 and 2024, for example, Figure 80).

[21] `https://github.com/noaa-afsc-mace/KrillCommunication`

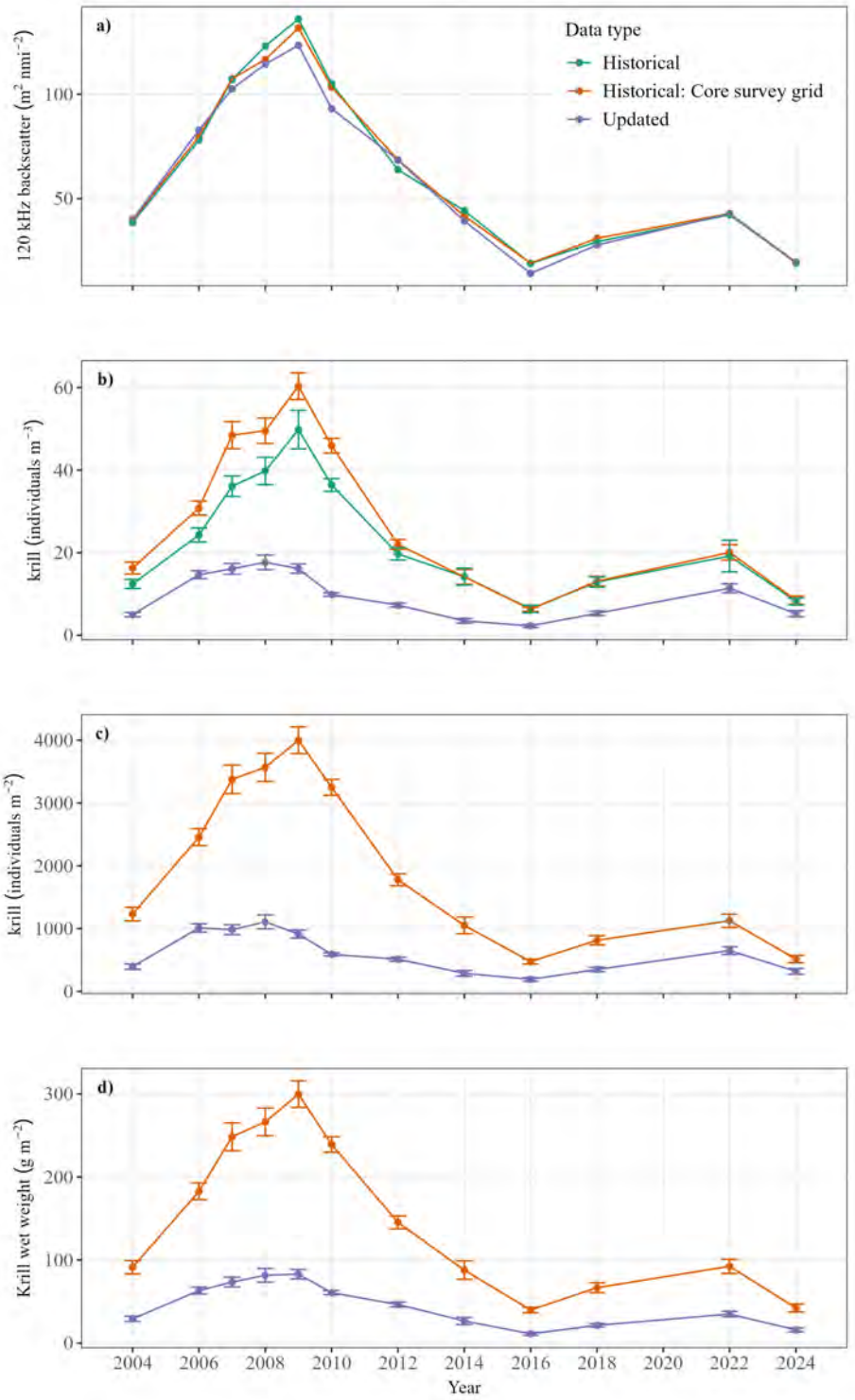


Figure 78: Time series comparison. "Historical" refers to estimates previously calculated using the historical processing method, "Historical: Core survey grid" refers to estimates generated using the historical method but re-calculated within a standard survey footprint, and "Updated" refers to estimates made using the updated processing method. Estimates are presented in units of a) krill backscatter (m^2 nmi^{-2}), b) krill volumetric density (m^{-3}), c) krill areal density (m^{-2}), and krill wet weight (g m^{-2}). Error bars represent 95% confidence intervals on units of density and wet weight calculated using a geostatistical estimate of sampling error. Note that "Historical" values were only available in units of backscatter and volumetric density (the values historically provided within Ecosystem Status Reports).

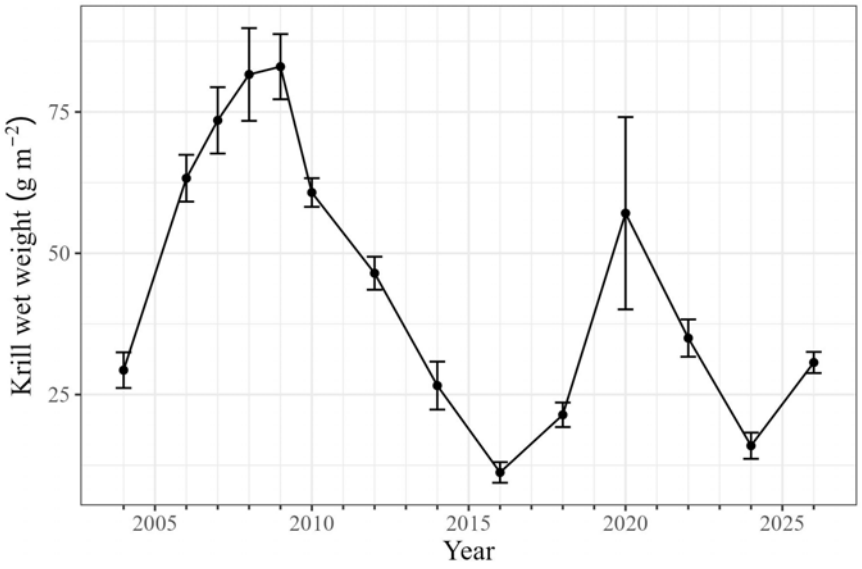


Figure 79: Acoustic estimates of average krill density (wet weight, g m^{-2}) from EBS summer acoustic-trawl surveys. Error bars are approximate 95% confidence intervals computed from one-dimensional geostatistical estimates of sampling error (Petitgas, 1993).

Factors influencing observed trends: Factors controlling annual changes in euphausiid abundance in the north Pacific are not well understood; possible candidates include bottom-up forcing by temperature and food supply, and top-down control through predation (Hunt et al., 2016). When factors including temperature, pollock abundance, primary production, and spatial location have been considered in spatially-explicit multiple regression models, temperature has been the best predictor, with increases in euphausiid abundance associated with cold temperatures in the eastern Bering Sea (Ressler et al., 2014), but not in the Gulf of Alaska (Simonsen et al., 2016). Observed temperatures in the summer of 2026 were moderately cold and a substantial cold pool was observed (McCarthy et al., in prep.). The biomass of eastern Bering Sea pollock (an abundant predator of euphausiids) has generally been above the historical mean over the past decade (Ianelli et al., 2024), though euphausiid abundance has not been strongly correlated with pollock biomass in multiple regression models of euphausiid biomass in either the eastern Bering Sea or the Gulf of Alaska (Ressler et al., 2014; Simonsen et al., 2016). Recent work comparing a diet-based index of krill abundance with these acoustic estimates (Reum et al., 2026) affirms the conclusion that increased krill abundance is associated with cold temperatures and conditions in the eastern Bering Sea (and conversely, low krill abundance is associated with warm conditions), and that the top-down effect of predation on krill abundance appears small.

Implications: Euphausiids are a major trophic link in the Eastern Bering Sea (EBS) ecosystem. Krill are a primary prey item for fishes including pollock (Brodeur et al., 2002; Lang et al., 2005; Reum et al., 2026), birds including short-tailed shearwaters (*Ardenna tenuirostris*; Hunt Jr et al., 2002; Nishizawa et al., 2017) and murres (*Uria* spp.; Decker and Hunt Jr, 1996), and fin (*Balaenoptera physalus*) and humpback (*Megaptera novaengliae*) whales (Witteveen et al., 2015).

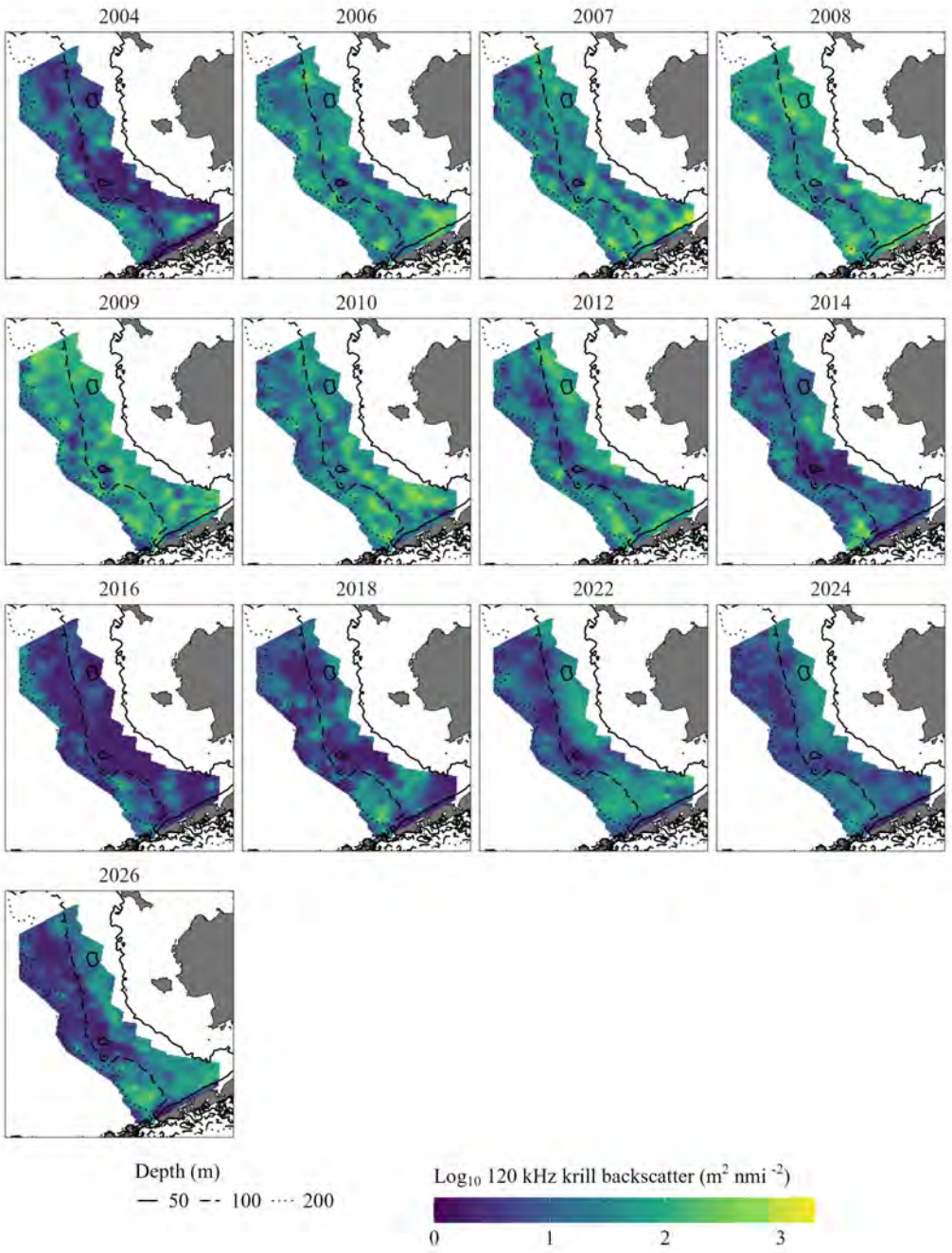


Figure 80: Distribution of krill backscatter (m^2 nmi^{-2}) estimates in the EBS acoustic-trawl survey time series. Values are interpolated using universal kriging (Pebesma, 2004) to make distributions easier to compare.

Late Summer Eastern Bering Sea Euphausiids ('Krill')

Contributed by Adam Spear, David Kimmel, Jesse Lamb, Mike Levine, Patrick Ressler
Resource Assessment and Conservation Engineering Division, Alaska Fisheries Science Center, NOAA Fisheries, Seattle, WA
Contact: Adam.Spear@noaa.gov
Last updated: September 2026

Description of indicator: Euphausiid abundance from the 2011-2026 Bering Sea late summer juvenile fish survey were estimated using acoustic and net sampling data. Euphausiid acoustic backscatter was identified using methods developed by Ressler et al., 2012, Simonsen et al., 2016, and updated by Levine et al., 2026 (see also p. 132). Euphausiid backscatter was integrated within 5 nautical mile (nmi) grid cells along the survey track line. Euphausiid length from several trawl samples were used to average length and species composition over the time series. These values were used to estimate the acoustic target strength of individual euphausiid using a Gulf of Alaska-specific target strength model (Lucca et al., 2021, as parameterized in Levine et al., 2026), allowing for conversion from backscatter to abundance (number m^{-3}).

Age-0 walleye pollock that are observed during our late summer juvenile fish survey are much stronger acoustic scatterers than euphausiids because they possess a swim bladder. During the late summer, the amount of fish backscatter can mask the relatively weak euphausiid backscatter, making the latter completely acoustically invisible over substantial portions of the surveyed area at times. Existing methods (Ressler et al., 2012; Levine et al., 2026) attempt to correct for this 'shadowing' by applying a correction to euphausiid backscatter in proportion to the degree of shadowing. However, these methods are not effective in areas where 100% of the euphausiid backscatter is likely to be shadowed.

A different approach to these large areas of 100% shadowing is needed. We propose that additional data from Bongo zooplankton net samples and a spatiotemporal model can be used to interpolate euphausiid densities in these problem areas. Bongo nets do not capture large euphausiids well due to net avoidance (Hunt et al., 2016), but most of the Bongo tows in this study were at night when avoidance is lower and euphausiid presence or absence can be determined more accurately. Bongo net tows from the same year located within 5 nmi of each acoustic interval were used to verify presence-absence of euphausiids in support of subsequent interpolation by a spatiotemporal model. Annual abundance indices were standardized with a spatiotemporal model (Shelton et al., 2014; Thorson et al., 2016) in the sdmTMB package in R (Anderson et al., 2022), which can predict density in gaps left by shadowing and reduces bias from uneven coverage among years. Through this method, we generated grid-based population indices that predict density over a continuous spatial area, resulting in metrics that reduce bias from sampling deficiencies. We fit a delta-lognormal model, estimating the probability of presence and the density when present. Both components had independent (IID) spatiotemporal random fields approximated with the SPDE method (Lindgren et al., 2011), year as a categorical factor, and survey day-of-year and bottom depth as linear covariates. Day-of year-was standardized to 248 ($\sim$September 5^{th}). The spatial area used for the index estimation was a combination of BSIERP regions: Alaska Peninsula, South Middle Shelf, Central Middle Shelf, and Saint Matthew (Ortiz et al., 2012).

Status and trends: Total euphausiid abundance increased from 2011 to a time-series peak in 2012, followed by a sharp decline through 2014 to reach the lowest reported value in 2016 (Figure 81). Since the 2016 low, total abundance has steadily increased across the subsequently surveyed years of 2022, 2024, and 2026. By 2026, the abundance index recovered to just above the long-term time-series mean.

Factors influencing observed trends: A recent study by Reum et al., 2026, using predator stomach contents, has confirmed previous findings (Ressler et al., 2014; Hunt et al., 2016) that euphausiid densities in the eastern Bering Sea respond negatively to increasing bottom temperatures. In addition to temperature, euphausiid distributions are positively associated with the spatial extent of the cold pool (Reum et al., 2026). The effect of the cold pool in the southeastern Bering Sea may be the result of cool, icy years enhancing euphausiid productivity due to the early timing of ice-associated phytoplankton blooms (Sigler et al., 2014, 2016; Reum et al., 2026). These findings align closely with the observed data reported here. The highest euphausiid abundances in the time series occurred during the cold years of 2011 and 2012 (see Figure 54). The change to unusually warm conditions coincided with a decline in 2014, then further dropping to the lowest recorded abundance in 2016. As bottom temperatures decreased to average levels in 2022 and 2024, the euphausiid density increased. Most recently, the return to cold conditions in 2026 resulted in continued population increases above the long-term mean.

Implications: This contribution represents ongoing research and is subject to change, particularly with regard to the new method we introduce for data-informed interpolation in substantial areas where euphausiid acoustic backscatter was obscured by fish backscatter. Knowledge of euphausiid abundance is relevant because both forage fish and juveniles of commercially important fish species use euphausiids as an important prey source, therefore information on their relative population size is useful to assess system productivity and standing stock. Trends in euphausiid distribution and abundance have been noted as a gap in our understanding of the ecosystem, therefore these metrics would be useful for both ecosystem-based fisheries management and system modeling. Due to their position in the food web linking primary producers to fish, shifts in euphausiid population sizes will impact the food web. These impacts would translate into population level effects beyond fish, including birds (Hunt Jr et al., 2002; Nishizawa et al., 2017), marine mammals, and humans.

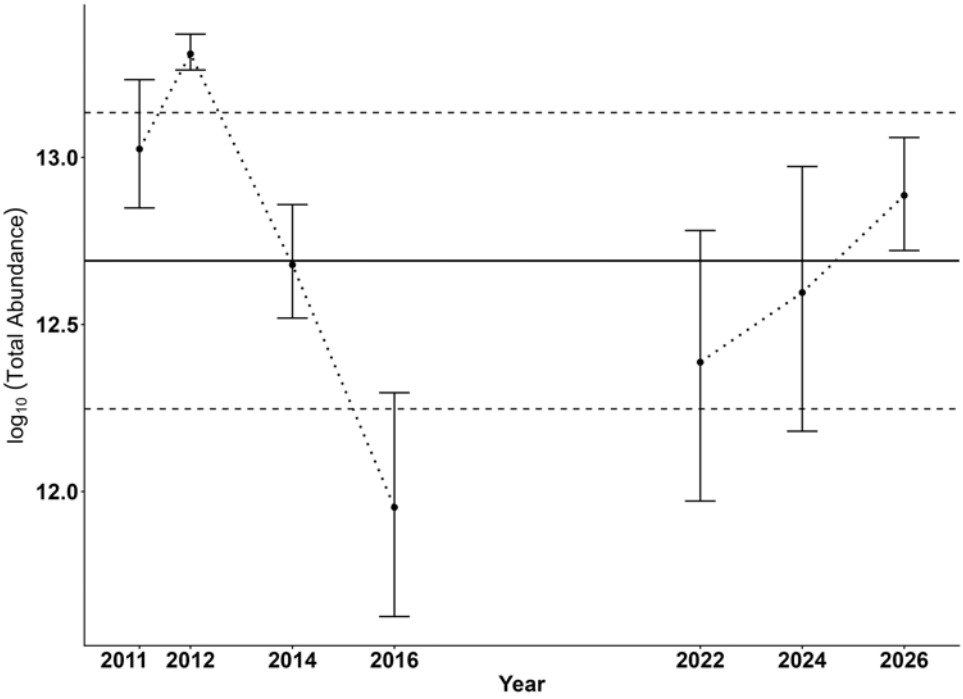


Figure 81: Late summer annual abundance estimates of euphausiids in the eastern Bering Sea survey region across sampled years (2011-2026). Black points denote the median annual estimated total abundance, and vertical error bars represent the 95% confidence intervals. The solid horizontal line indicates the overall time-series mean, while the upper and lower dashed horizontal lines represent ± 1 standard deviation from the mean.

Jellyfish

Eastern and Northern Bering Sea – Jellyfishes

Contributed by Thaddaeus Buser
Groundfish Assessment Program, Resource Assessment and Conservation Engineering Division,
Alaska Fisheries Science Center, NOAA Fisheries, Seattle, WA
Contact: thaddaeus.buser@noaa.gov
Last updated: September 2026

Description of indicator: The biomass index time series for jellyfishes (Scyphozoa, but primarily *Chrysaora melanaster*) was updated for 2026 from the eastern Bering Sea shelf and northern Bering Sea surveys. Since 1982, the RACE Groundfish Assessment Program (GAP) and Shellfish Assessment Program (SAP) have conducted annual fishery-independent summer bottom trawl surveys on the EBS shelf using standardized trawl gear and methods. Biomass index trends from the survey are likely to reflect changes in the abundance of species and life history stages that are available to the survey, especially if trends are sustained over time.

Regional and stratum indices of abundance (biomass in kilotons) and confidence intervals were estimated for jellyfish by fitting a multivariate random effects model (REM) to stratum-level design-based abundance index time series calculated from GAP summer bottom trawl survey catch and effort data. The index was calculated for the entire standardized survey time series (EBS: 1982-2026, NBS: 2010-2025). The design-based index of abundance were calculated using the gapindex R package (Oyafuso, 2025) and REM were fitted to survey time series using the rema R package (Sullivan and Balstad, 2022). Code and methods to calculate these indicators are provided in the esrindex R package and repository (Rohan, 2025).

Status and trends:
Eastern Bering Sea:
The abundance of jellyfishes in the eastern Bering Sea in 2026 was near (within 1 standard deviation) the time series mean and similar to estimates from the previous four years (2022-2025; Figure 82). While there has been relative stability in the biomass estimates since 2022, there is an apparent pattern of cyclical rise and fall in jellyfish abundance throughout the time series. The relatively low abundance estimated from 1982 to 1988 was followed by a period of increasing biomass throughout the 1990s. A second period of relatively low biomass from 2001 to 2008 was followed by a period with relatively high abundance from 2009 to 2015. Jellyfish occur throughout the survey area, but their biomass is highest in Strata 10 (southern inner shelf at bottom depth <50m), 30 (southern middle shelf at 50-100m), 40 (northern middle shelf at 50-100m), and 60 (northern outer shelf at 100-200m; Figure 83).

Northern Bering Sea:
The Northern Bering Sea was not sampled in 2026; results from the 2025 survey are presented here. The abundance of jellyfishes in 2025 is similar to what was estimated in 2023 and close to the time series mean (Figure 84). However, while an apparent pattern of cyclical rise and fall of jellyfish biomass index values exists in the EBS time series, gaps in sampling years across the northern Bering Sea time series makes identifying multi-year trends difficult. In 2025, jellyfish were found throughout the NBS and had roughly equal relative biomass in all three strata (Figure 85).

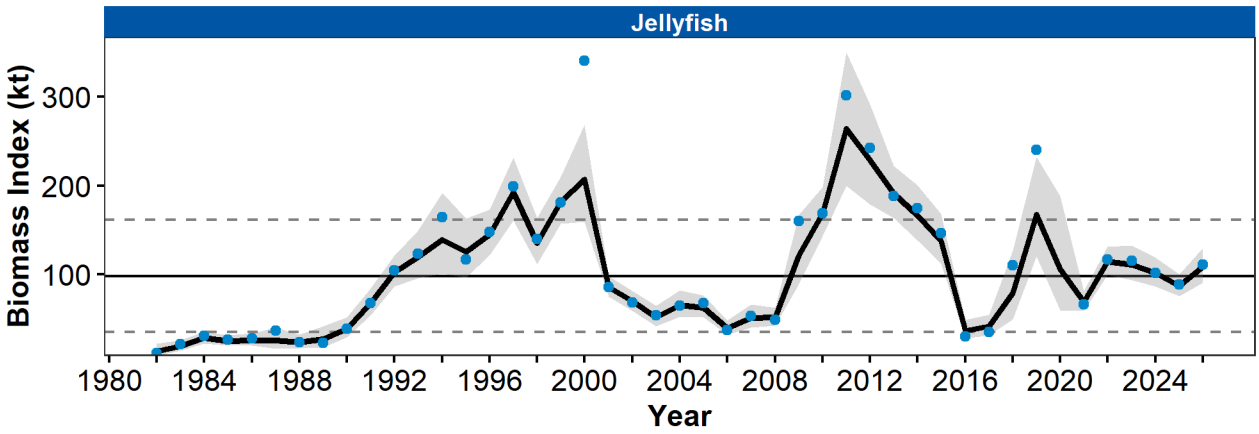


Figure 82: Biomass index of jellyfish (kilotons) from AFSC/RACE summer bottom trawl surveys of the eastern Bering Sea continental shelf from 1982 to 2026 showing the observed survey biomass index mean (blue points), random effects model fitted mean (solid black line), 95% confidence interval (gray shading), time series mean (solid gray line), and horizontal dashed gray lines representing one standard deviation from the mean.

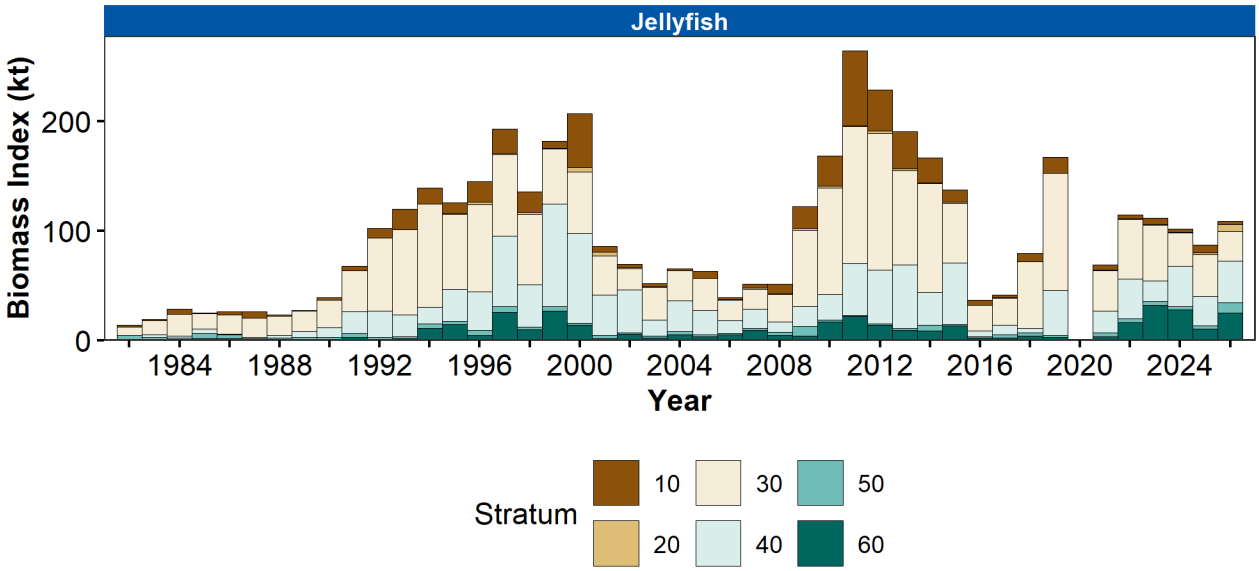


Figure 83: Biomass index of jellyfish (kilotons) in eastern Bering Sea survey strata 10-60 estimated from RACE Groundfish Assessment Program and Shellfish Assessment Program summer bottom trawl survey data from 1982 to 2026.

Factors influencing observed trends: Cyclic fluctuations in jellyfish abundance in the EBS are associated with jellyfish biomass during the preceding year and environmental and climatological factors, including the timing of sea ice retreat, sea surface temperature, wind mixing, and currents (Brodeur et al., 2008; Decker et al., 2023).

Implications: Jellyfishes are pelagic consumers of zooplankton, larval and juvenile fishes, and small forage fishes. At high levels of abundance, jellyfishes can limit fish productivity through competition

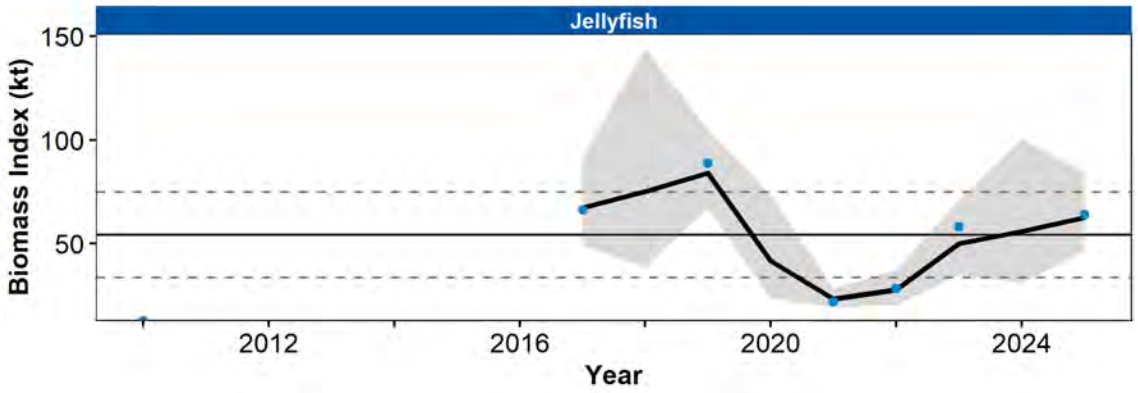


Figure 84: Biomass index of jellyfish (kilotons) estimated from AFSC/RACE summer bottom trawl surveys of the northern Bering sea from 2010 to 2025. Panels show the observed survey biomass index mean (blue points), random effects model fitted mean (solid black line), 95% confidence interval (gray shading), time series mean (solid gray line), and horizontal dashed gray lines representing one standard deviation from the mean.

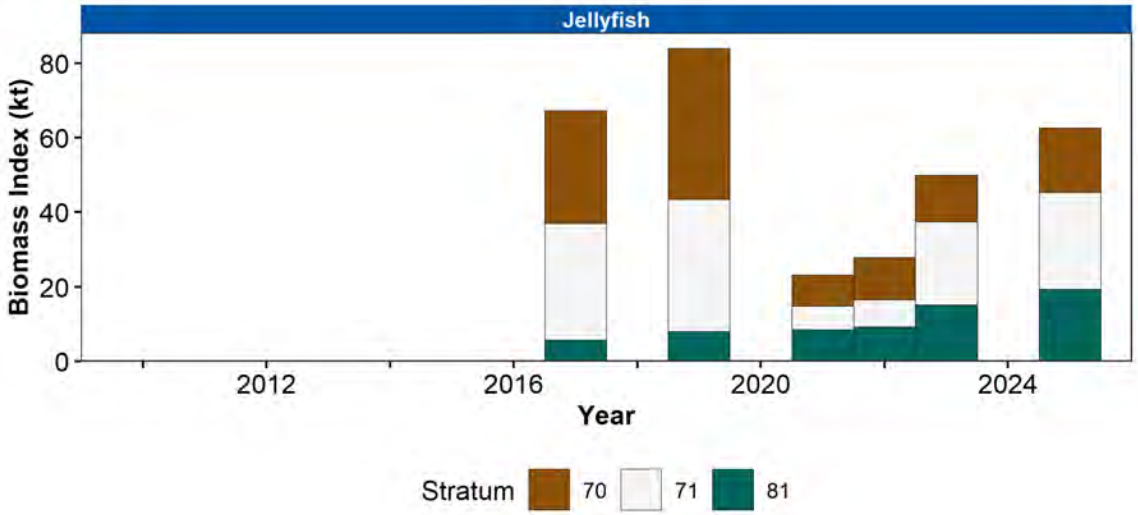


Figure 85: Biomass index of jellyfish (kilotons) in northern Bering Sea survey strata 70, 71, and 81, estimated from RACE Groundfish Assessment Program and Shellfish Assessment Program summer bottom trawl survey data from 2010 to 2025.

for prey and predation on larval fish (Purcell and Arai, 2001). ECOTRAN modeling suggests that the predominant jellyfish species in the EBS, *Chrysaora melanaster*, utilized 1% of consumer production over the middle shelf (51–100m) during a period of high abundance (2009-2014; Ruzicka et al., 2020). This level of consumption corresponds with roughly a quarter of production required to support predominant forage fish in the EBS (age-0 walleye pollock, age-0 Pacific cod, Pacific herring, and capelin; Ruzicka et al., 2020).

Research priorities: The bottom trawl survey uses standardized survey protocols aimed at ensuring consistent sampling efficiency. However, additional research is needed to better characterize the catchability and selectivity of jellyfish by the bottom trawl survey.

Jellyfish from Surface Trawl Surveys, 2004-2026

Contributed by Lia Domke, Alex Andrews, Andrew Dimond, Caroline Lawrence, and Jim Murphy
Auke Bay Laboratories, Alaska Fisheries Science Center, NOAA Fisheries, Juneau, AK
Contact: lia.domke@noaa.gov
Last updated: September 2026

Description of indicator: Annual indices of juvenile groundfish, forage fish, and jellyfish in surface waters were estimated from the Alaska Fisheries Science Centers' fall juvenile fish and ecosystem surface trawl surveys. In recent years, these integrated fisheries ecosystem surveys have been performed annually for the EMA Northern Bering Sea Ecosystem Surface Trawl (NBEST) Fall survey (2003-2007, 2009-2019, 2021-2026) and annually for the EMA Eastern Bering Sea Juvenile Fish (BASIS) Fall survey (2003-2012) before it shifted to biannual in 2016 (2016, 2018, 2022, 2024, 2026). Jellyfish sampling began in 2004. Primary fish caught and included in the forage fish species aggregate are age-0 Pacific cod (*Gadus macrocephalus*), age-0 pollock (*G. chalcogrammus*), capelin (*Mallotus villosus*), Pacific herring (*Clupea pallasii*), juvenile Chinook salmon (*Oncorhynchus tshawytscha*), juvenile sockeye salmon (*O. nerka*), juvenile chum salmon (*O. keta*), juvenile pink salmon (*O. gorbuscha*), juvenile coho salmon (*O. kisutch*), rainbow smelt (*Osmerus mordax*), and saffron cod (*Eleginus gracilis*). Primary jellyfish taxa include *Chrysaora melanaster*, *Cyanea* sp., *Aequorea* sp., *Aurelia labiata*, *Phacellophora camtschatica*, and *Staurophora mertensii*. Unidentified or non-dominant jellyfish species were included in the total jellyfish catch.

Pelagic fish and jellyfish were sampled using a trawl net towed in the upper 25 m. We estimated species biomass in the southeastern Bering Sea (SEBS) covering an area of 373,404 km^2 spanning south to north from 54.54° to 59.50° and west to east from -173.08° to -159.00°. For the northern Bering Sea (NBS) we defined spatial extent south to north from 59.97° to 65.50° and west to east from -176.00° to -161.50° covering an area of 197,868 km^2. A trawl was towed for approximately 30 minutes. Area swept was estimated from horizontal net opening and distance towed.

Methodological changes:
Methods were updated to estimate relative biomass using sdmTMB package version 1.1.0 in R software version 4.3.3 (Anderson et al., 2022) rather than density estimates from VAST. Similar to previous years we used spatial and spatio-temporal models to account for spatially unbalanced sampling and any residual spatial correlation in catch data to reduce bias in biomass indices. We estimated relative biomass for the survey area with models that included main effects of year and scaled day of year to account for changes in survey timing with an offset for effort (area swept). Spatial and spatio-temporal (with IID) random effects were included in all models except those where the spatial/spatio-temporal parameter decomposed to zero in which case it was removed. We fit log-linked tweedie or delta gamma models with encounter (binomial log-linked) and positive catch rate (gamma log-linked) components. We fit all index-standardization models to a high resolution mesh that remained computationally feasible, which for the northern Bering Sea was 200 knots and in the southern 95 knots (Ward and Anderson, 2025). All models passed typical model convergence "sanity" checks and had final gradients less than 0.0005.

Status and trends: During 2026, the estimated relative biomass of jellyfish in pelagic waters was reduced in the north relative to 2025, but still above the time series average. In the southeastern Bering Sea the index increased slightly from 2024, but remained below the long term average during late summer (Figure 86). Trends in jellyfish biomass were similar in the northern and southeastern Bering

Sea, except from 2012-2018. Trends in the north have been more variable with a time series maximum in 2018. In the south, relative jellyfish biomass peaked in 2014, but have remained low since 2022.

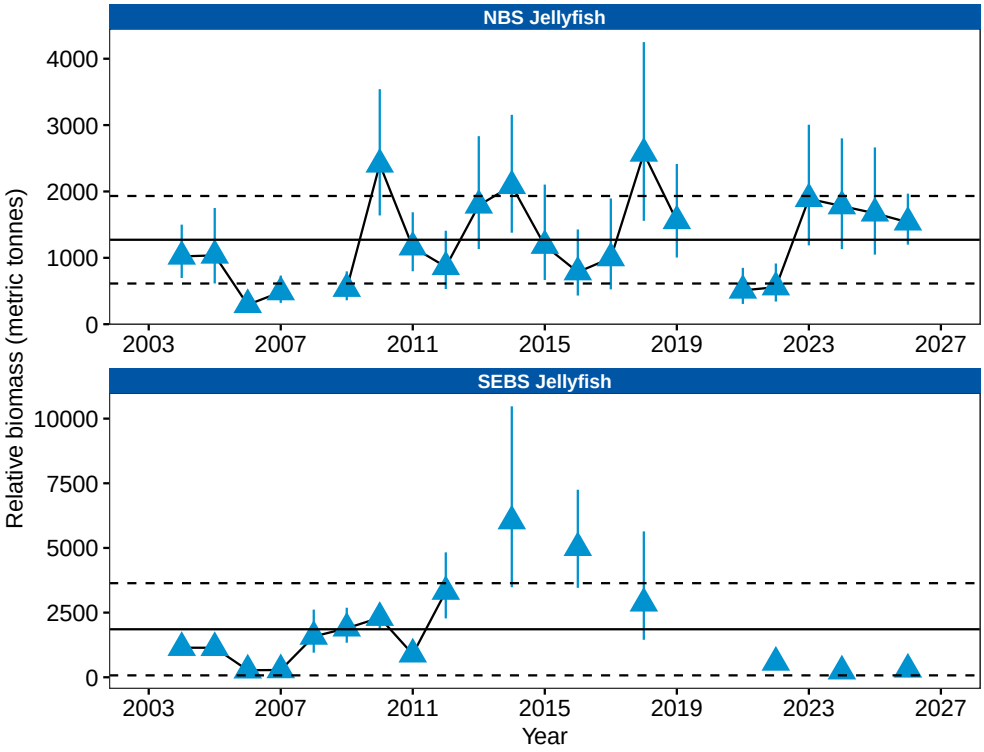


Figure 86: Estimated relative biomass (metric tonnes) of jellyfish in surface waters surveyed in the eastern Bering Sea during late summer, 2004-2026 in the north (upper panel) and southeastern (lower panel) Bering Sea. Solid line is the long term average with the dashed lines representing $\pm$ 1 standard deviation around the average.

Factors influencing observed trends: Jellyfish feed primarily on small fish and zooplankton and are influenced by oceanographic conditions such as sea ice and sea surface temperature (Suchman et al., 2008; Decker et al., 2023). Biomass of jellyfish were relatively high during warm years and low during cool years in the south. Similarly, in the north, biomass estimates were higher during warm years and lower in cool years, except for estimates that were above average during recent years (2023-2026) that cooled to average thermal conditions. In the south, overall low biomass of forage fish may represent low prey availability for jellyfish and may contribute to lower jellyfish production in 2022-2026. However in the NBS in 2023 and 2024, average thermal years, jellyfish estimates were high and forage fish biomass low (see Figure 3). In addition, the higher levels of jellyfish densities in the south in 2014 and 2016 corresponded with above average temperature and higher densities of age-0 pollock (see p. 165) and forage fish (Figure 2), prey items of jellyfish.

Implications: Jellyfish are competitors, predators, and can act as shelters for forage fishes. During 2026, the above average albeit declining biomass of jellyfish in the north may indicate favorable environmental conditions for the growth and survival of jellyfish and other species, while the below average biomass in the south may indicate less favorable conditions in the southeastern Bering Sea during late summer. As planktivores, high jellyfish biomass may potentially reduce plankton available for other planktivorous species such as forage fish (Ruzicka et al., 2020).

Ichthyoplankton

Abundance and Distribution of Larval Fishes in the Southeastern Bering Sea 2012-2026

Contributed by Lauren Rogers, Kelia Axler, Jesse Lamb, Melanie Paquin, and Steve Porter
Resource Assessment and Conservation Engineering Division, Alaska Fisheries Science Center, NOAA Fisheries, Seattle, WA
Contact: lauren.rogers@noaa.gov
Last updated: September 2026

Description of indicator: The southeastern Bering Sea shelf ichthyoplankton survey is conducted biannually in late spring (May) to assess the abundance and spatial distribution of early life stages of fishes. Ichthyoplankton (fish eggs and larvae) were sampled using a paired 60 cm bongo array with 505 μm mesh nets towed to 10 m off bottom or 300 meters maximum depth. A Sea-Bird FastCAT CTD was mounted above the bongo array to acquire gear depth, temperature, and salinity profiles. Larval fish abundance (number/10 m^2) for 2012-2024 was calculated from laboratory-processed and verified quantitative data, standardized by the volume of water filtered during a tow. Here we report on five commercially important fish species or taxonomic groups: Walleye pollock (*Gadus chalcogrammus*), Pacific Cod (*G. macrocephalus*), northern rock sole (*Lepidopsetta polyxystra*), southern rock sole (*L. bilineata*), and rockfish (*Sebastes* spp.). For the current survey year (2026) a Rapid Larval Assessment was conducted at sea, enabling provisional time-series updates in the year of collection. These data are subject to revision upon laboratory processing.

Mean larval abundance was estimated using spatial-temporal generalized linear mixed models with the R package sdmTMB (Anderson et al., 2022). A Tweedie error distribution was used, and the mean larval abundance was calculated over the standardized survey area outlined in Figure 87. In addition, model-derived estimates of pollock egg abundances (2012-2024) are shown for comparison of relative abundance between early life stages. Note, no surveys occurred in 2020 or 2022. The 2026 survey occurred approximately two weeks earlier than usual and with a reduced grid due to ship-time constraints.

Status and trends: Pollock were the most abundant larvae of the five taxa examined, and their estimated abundance increased from near the end of the last cold stanza (2012) through the warm stanza (2014, 2016, 2018), to a time-series maximum in 2024, decreasing again in 2026 (Figure 88). Pollock larvae were distributed across the shelf, with the highest abundances concentrated near the Pribilof Islands and the Alaska Peninsula (Figure 87). In contrast, the abundance of Pacific cod larvae was highest in 2012, yet declined and remained low, with 2024 and 2026 abundances the lowest of the time series. Pacific cod larvae were concentrated in the northwest portion of the survey grid in 2012, along the 100 m isobath in 2014, and patchily distributed near the Alaska Peninsula in more recent years. Northern rock sole larvae were most abundant in 2012 with abundances declining in 2014 and remaining low in subsequent years to the present. These larvae were distributed similarly to pollock, often present at pollock hotspots, albeit at lower densities. Southern rock sole larvae were the least abundant of all the species examined, with notable catches only in 2014, clustered east of the Pribilof Islands. Rockfish larvae have been relatively stable in abundance, with higher abundances in 2014 and 2026 compared to the other years. They were present on the outer domain primarily in waters deeper than 100 m; the high uncertainty in the 2026 estimate reflects limited sampling in that region this year.

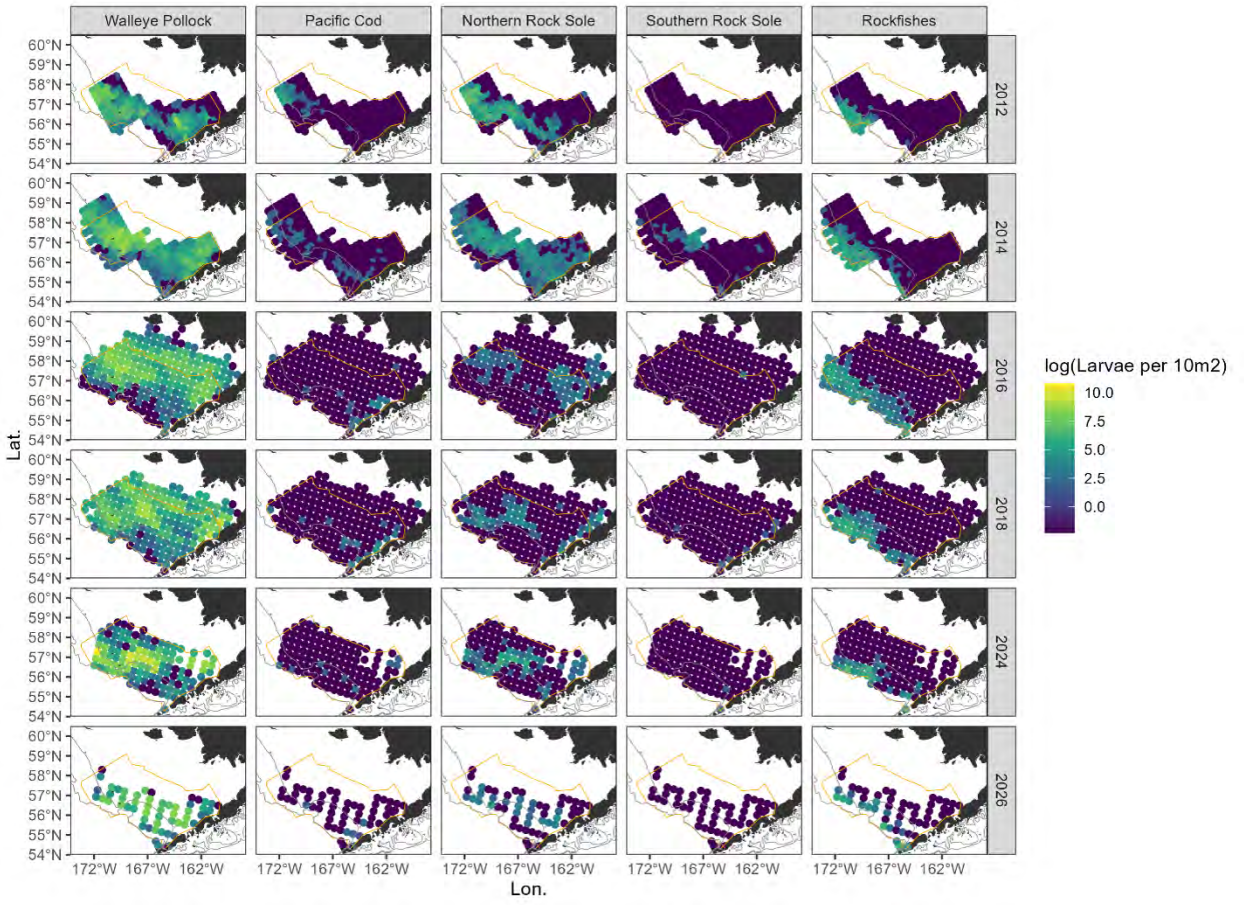


Figure 87: Distribution of larval catch per 10 m^2 on the SEBS shelf for five taxa during spring ichthyoplankton surveys, 2012-2026. Gray lines show the 100 m and 200 m isobaths, and the standardized index area is outlined in orange. Data from 2026 are provisional pending laboratory processing.

Factors influencing observed trends: Interannual variation in ocean temperature in early spring can shift phenology of fishes and the timing of the spring phytoplankton bloom that is important for the production of zooplankton prey for fish larvae (Nielsen et al., 2024; Sullaway et al., 2025; Rogers et al., 2026). This can lead to a temporal mismatch between fish larvae and their prey resulting in poor larval survival. In addition, temperature can affect the timing of spawning and rate of egg development, which can affect whether larvae are present in the study region during the survey. In 2012, larval pollock were relatively scarce, but eggs were abundant (Figure 88), indicating that hatching was relatively late during that cold year, at least partly explaining the low larval abundance observed in 2012. Due to the extensive cold pool and earlier than typical sampling in 2026, we might expect a significant portion of the population to still be in the egg stage, a hypothesis we can address with future quantitative identification of pollock eggs from 2026.

The time-series abundances for Pacific cod and northern rock sole showed a decline when conditions on the southeastern Bering Sea shelf changed from cold to warm. However, northern rock sole recruitment is typically higher in warmer years relative to cold years, a pattern which is linked to differential use of a

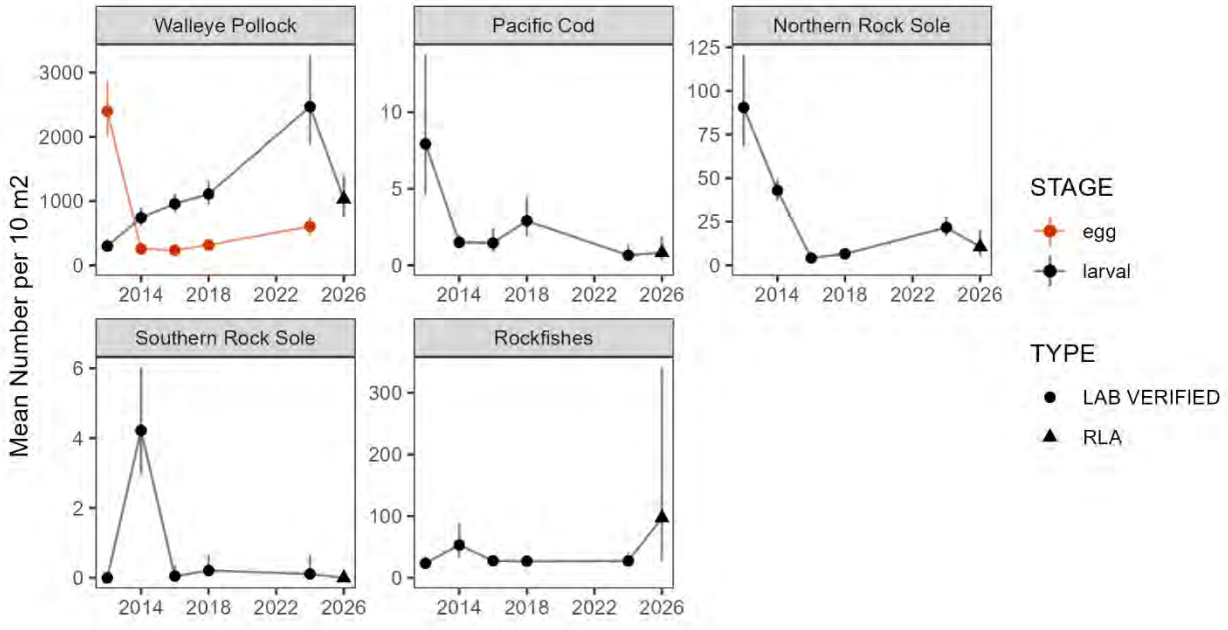


Figure 88: Estimates of mean abundances for larvae and eggs in the standardized area of the Bering Sea outlined in orange in Figure 87. Bars show 95% confidence intervals. In 2026, estimates were based on a Rapid Larval Assessment (RLA) conducted at sea and data are subject to revision upon laboratory processing.

northern nursery area (Cooper and Nichol, 2016), highlighting the importance of settlement processes for this stock. Southern rock sole is at the northernmost extent of its range in the Bering Sea and this may account for its low abundance.

Sample processing of 2024 specimens may have introduced some uncertainty into abundance estimates of pollock and Pacific cod. For 2024 samples, approximately 3% of all gadid larvae were unidentifiable to species (likely Pacific cod or pollock), and therefore excluded from abundance estimates. This adds a negligible amount of uncertainty to the pollock abundance estimate, but additional uncertainty for Pacific cod.

Implications: Ichthyoplankton surveys can provide early-warning indicators for ecosystem conditions, spawning phenology, and recruitment patterns in marine fishes. In 2026, pollock larval abundance was approximately average, northern rock sole and Pacific cod abundances were relatively low, rockfish larvae abundance was slightly higher than previous reporting years, while abundance for southern rock sole was similar to 2024. Ongoing research is focused on the importance of larval phenology, condition (see Porter et al. p. 150), geographic distribution, and overlap with zooplankton prey for eventual recruitment success.

Morphometric Condition of Walleye Pollock Larvae

Contributed by Steven Porter, Kelia Axler, Colleen Harpold, David Kimmel, Jesse Lamb, and Lauren Rogers
Resource Assessment and Conservation Engineering Division, Alaska Fisheries Science Center, NOAA Fisheries, Seattle, WA
Contact: steve.porter@noaa.gov
Last updated: August 2026

Description of indicator: The morphometric condition of walleye pollock larvae in the southeastern Bering Sea (SEBS) was assessed using the ratio of the body depth at anus (BDA) to standard length (SL). The BDA:SL ratio, hereafter called Condition Ratio (CR), was used to show the spatial distribution of larval condition. The CR is based on the observation that for two fish larvae of similar size, the larva in poorer condition is "skinnier" (smaller BDA) than the larva in better condition (larger BDA), resulting in a smaller CR. For Atlantic cod (*Gadus morhua*) larvae, CR was sensitive to environmental surroundings, including prey abundance (Koslow et al., 1985). The CR for pollock larvae was calibrated using fed (good condition) and starved (poor condition) larvae reared in the laboratory at 3° and 6°C (n=263). The CR of larvae in good condition (mean=0.0635 $\pm$ 0.0088, SL=5.96-11.17 mm) was significantly larger than the ratio of larvae in poor condition (mean=0.0525 $\pm$ 0.0053, SL=4.89-6.15 mm; t-Test, $p<0.001$). The mean ratio for larvae in good condition was used to classify the condition of Bering Sea larvae, with CRs $\geq$0.0635 indicating good condition and larvae in poor condition having smaller CRs. In May 2026, EcoFOCI conducted an ichthyoplankton survey in the SEBS that is run biennially. At each station, digital photographs were taken of up to 15 randomly selected pollock larvae collected from a 60 cm bongo net tow and larvae were measured using image analysis software. Mean ratio for larvae measured at a station was used to determine larval condition at that location.

Status and trends: Morphometric condition of pollock larvae (n=303) was assessed from 48 stations located across the SEBS in 2026 (Figure 89A), covering a similar area as 2024 (Figure 89B). In 2026, larvae in poor condition occurred from the Alaska Peninsula to near the Pribilof Islands, mostly in the inner and middle domains (Figure 89A). In 2024, nearly all the larvae in poor condition were found in the western most area sampled (Figure 89B). Pollock larvae were smaller and had lower CR in 2026 compared to 2024 (Table 4). Contributing to the smaller size larvae was that the 2026 survey occurred two weeks earlier than in 2024. Larvae in poor condition were found at 21% of stations in 2026 compared to 8% of stations in 2024 (Table 4).

Factors influencing observed trends: Results for the inner and middle domains for 2026 were combined because only two stations were sampled in the inner domain. The coldest temperatures occurred at the inshore stations, and this was the result of sea ice extending further south during late March and early April than has occurred in recent years (Figure 90). Water was colder in the inner and middle domains (0.5 $\pm$ 1.1°C; mean temperature in the upper 40m of the water column $\pm$ standard deviation, depth range where the majority of pollock larvae are located; Smart et al. (2013)) than in the outer domain (2.9 $\pm$ 0.7°C). The percentage of stations classified in poor condition in the inner and middle domains (17%) was greater than in the outer domain (4%). The largest CR occurred in the southeast near the shelf break where temperature was warmest (Figures 89A and 90). Larvae tended to increase in size from north to south (Figure 91), indicating colder water in the north may have slowed larval growth or delayed spawning. Large numbers of pollock eggs were observed in bongo net tows throughout the surveyed area in 2026, suggesting later hatching could have contributed to smaller size larvae.

Implications: Larval condition may indicate the likelihood of survival to later life stages (Theilacker et al., 1996). Pollock larvae in good condition are more likely to occur when water temperature in the Bering Sea is warmer than 3°C (Porter, 2025). Cold temperatures (<2°C) are associated with slower growth and decreased survival of pollock larvae (Koenker et al., 2018). In 2026, mean upper water column temperatures ranged from -0.2°C to 4.4°C at the stations where larval condition was assessed, and temperature was ≤3°C at many of those stations. Nearly all the stations classified in poor condition in 2024 occurred where water temperature was coldest (0.1°C to 2.1°C). Overall mean water temperature was 1.4°C colder in 2026 (Table 4), and that may have contributed to the higher proportion of stations classified in poor condition. Small-size copepods (<2mm) were distributed throughout the area surveyed and their abundance was average in 2026 (see p. 122), indicating there was sufficient prey for pollock larvae. As prey was adequate for larval feeding, the lower overall CR for larvae in 2026 may be due in part to cold temperatures adversely affecting larval swimming ability that impacted their foraging success (Moyano et al., 2016). Additionally, previous observations suggest that relatively warm water temperatures in the Bering Sea are beneficial for larval pollock survival (Hunt et al., 2011).

Table 4: Mean size of larvae assessed for condition, mean temperature in the upper 40m of the water column, mean condition ratio, and percentage of stations classified in poor condition in the southeastern Bering Sea for 2024 and 2026. SL = standard length; SD = standard deviation; CR = condition ratio.

Year	Number of Stations	SL (mm) ± SD	Temperature (°C) ± SD	CR ± SD	% Stations Poor Condition
2024	78	8.7 ± 2.0	2.6 ± 1.2	0.0798 ± 0.0142	8 (6/78)
2026	48	6.5 ± 1.6	1.2 ± 1.5	0.0727 ± 0.0120	21 (10/48)

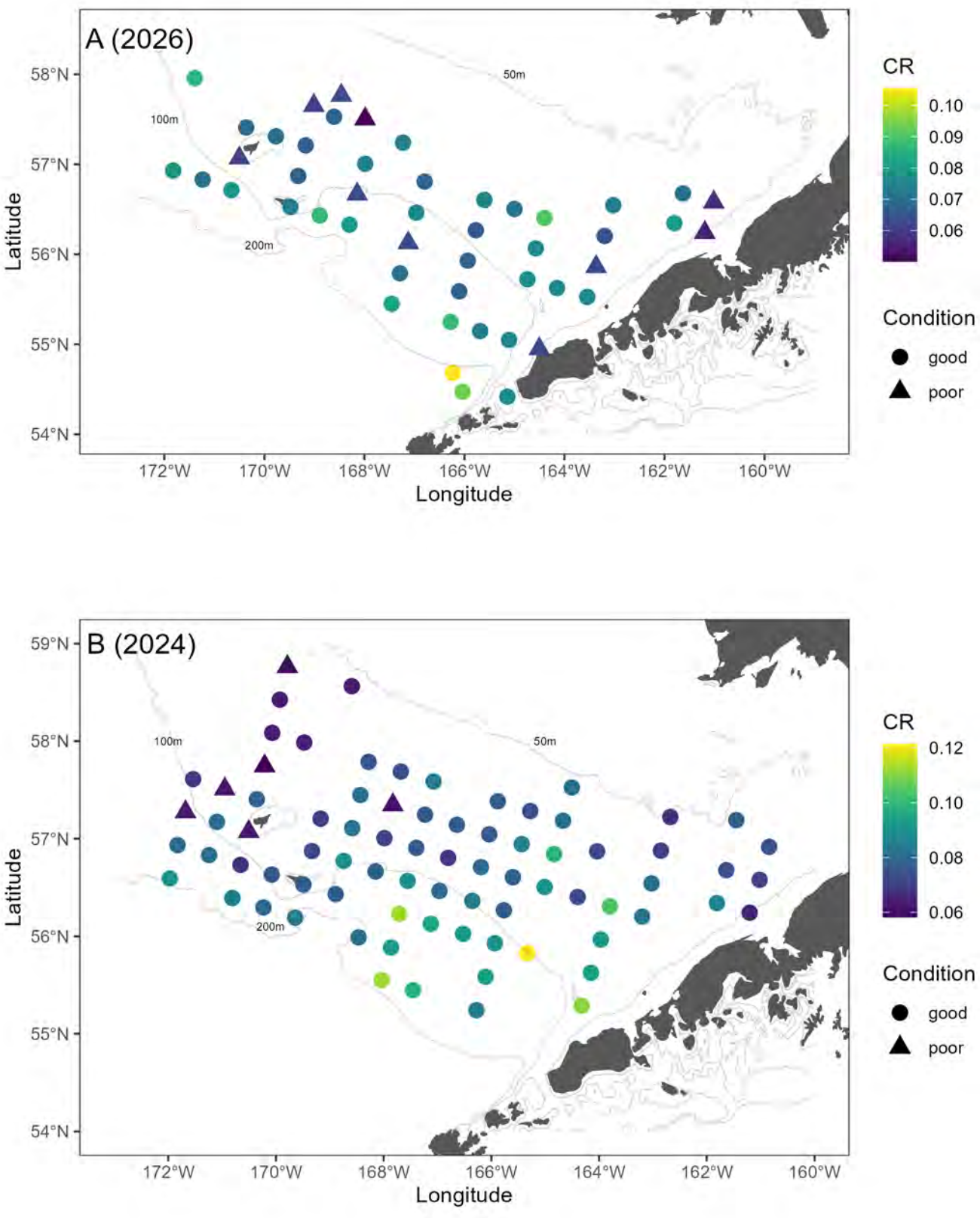


Figure 89: Mean condition ratio (CR) and location of pollock larvae in good or poor condition in the southeastern Bering Sea in (A) 2026 and (B) 2024. Mean CR was used to classify that location as having larvae in good or poor condition.

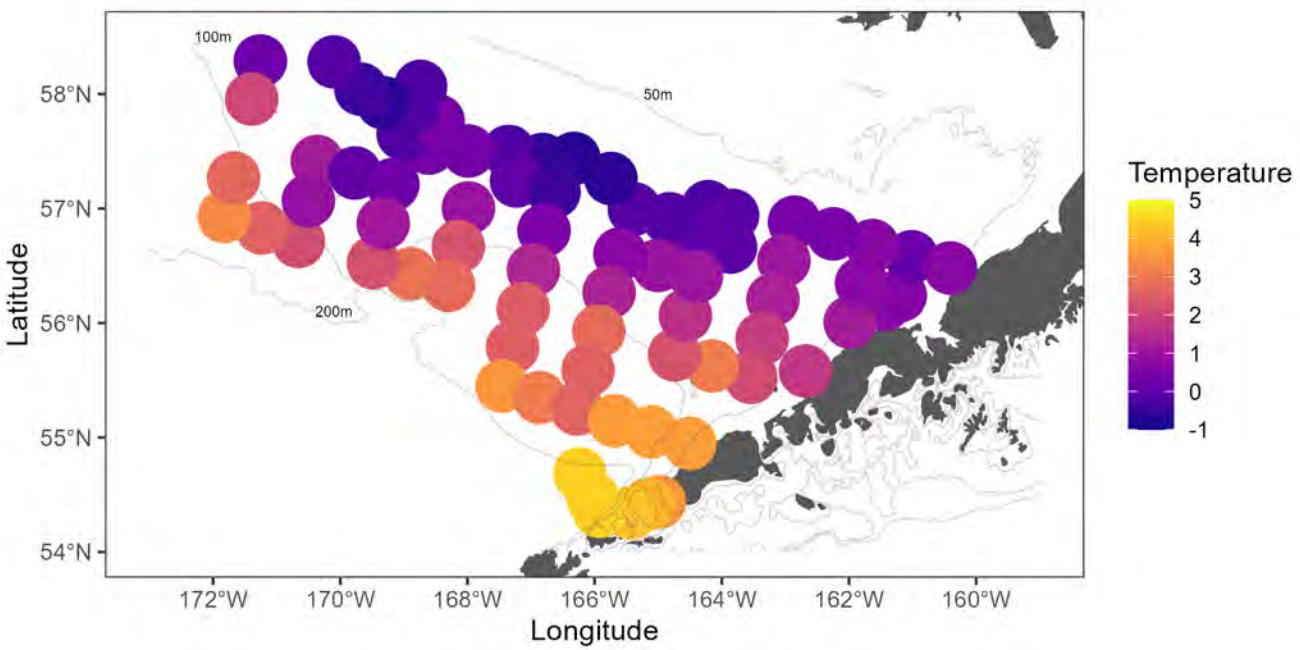


Figure 90: Mean water temperature in the upper 40m of the water column in the southeastern Bering Sea in 2026. That depth range is where a majority of pollock larvae are located (Smart et al., 2013).

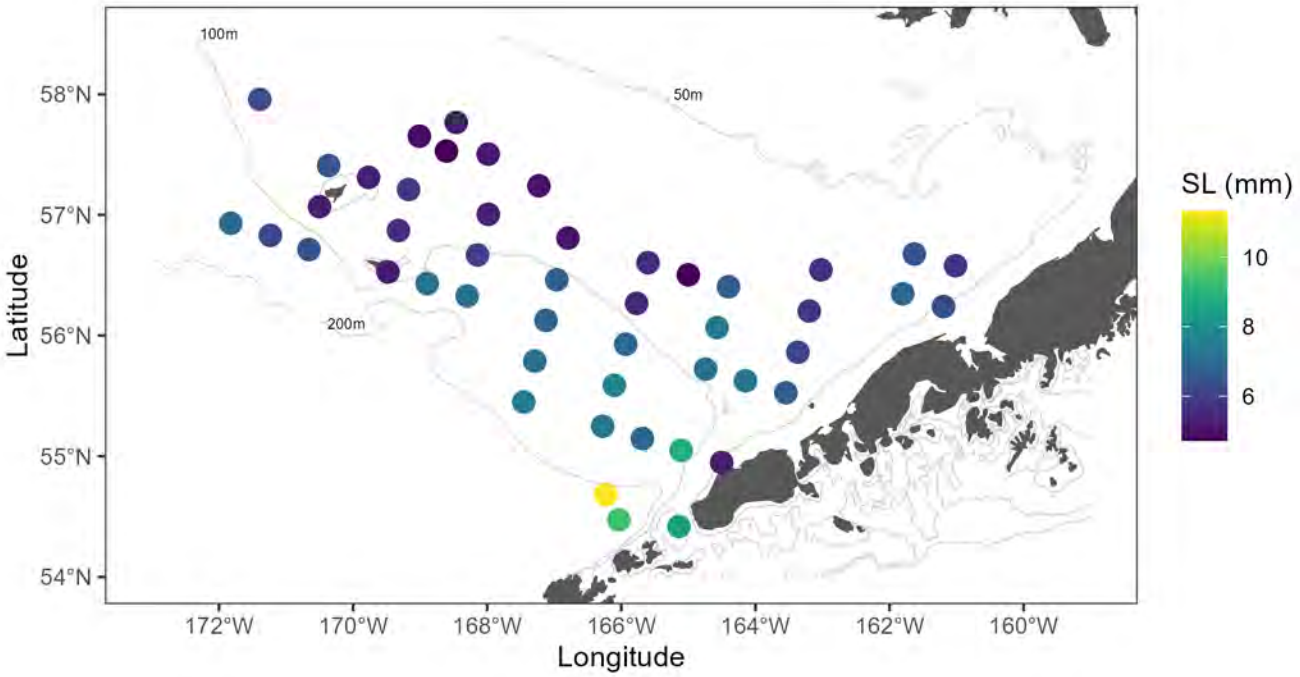


Figure 91: Mean standard length (mm) of pollock larvae assessed for condition in the southeastern Bering Sea in 2026.

Forage Fish

Forage Fish Dynamics in the Eastern Bering Sea

Contributed by Lia Domke[1], Elizabeth Siddon[1], Alex Andrews[1], Jeanette Gann[1], David Kimmel[2], and Mike Levine[2]
[1]Auke Bay Laboratories, Alaska Fisheries Science Center, NOAA Fisheries, Juneau, AK
[2]Resource Assessment and Conservation Engineering Division, Alaska Fisheries Science Center, NOAA Fisheries, Seattle, WA
Contact: Lia.domke@noaa.gov
Last updated: September 2026

Description of indicator: To improve understanding of ecosystem function, we developed a simplified conceptual model of mechanisms that influence forage fish dynamics in the southeastern Bering Sea. The goal of this exercise was to improve understanding of causal mechanisms influencing forage fish in the southeastern Bering Sea and provide an estimate of fall forage fish relative biomass in unsampled odd-years given springtime patterns in sea ice and phytoplankton. To accomplish these goals, we used a Dynamic Structural Equation Modeling approach (DSEM, Thorson et al., 2024). We developed a causal map of all links between the environment, primary production, secondary consumers, and forage fish thought to drive changes in forage fish biomass. Causal links can be thought of as hypotheses (outlined in the mechanisms table; Table 5) of the proposed driver of a variable in our causal map. This causal map represents the effects of a variable (exposure) on another (outcome) through a series of hypothesized mechanisms (arrows). We can then estimate the strength, direction, and significance of the effect of the exposure on an outcome. DSEM is a statistical framework designed for causal inference that allows ecological time series that may have missing values. DSEM can also address potential correlations and complementarity (i.e., trade-offs) among indicators.

In this species-specific application of DSEM, the specified structure is based upon the following design choices:

1. We include the physical variable of sea ice ("Sea ice extent") and assume greater sea ice extent results in a lower proportion of open-water-associated phytoplankton blooms ("Percent open water bloom") and greater proportion of early, ice-associated blooms (Nielsen et al., 2024; Eisner et al., 2016; Sigler et al., 2014; Hunt et al., 2011; Hare et al., 2007).

2. Whether the phytoplankton bloom is associated with open water (higher "Percent open water bloom") or sea ice (lower "Percent open water bloom") is hypothesized to cause changes in pelagic secondary consumers (e.g., summer euphausiids ["Euphausiids"] and fall zooplankton ["Small copepods" and "Large copepods"]). A higher proportion of ice-associated blooms is thought to result in higher abundance of pelagic secondary consumers in the summer and fall, in particular large lipid-rich copepods and euphausiids and to a lesser extent for small copepods (Coyle et al., 2008; Kimmel et al., 2018).

3. Large-bodied, lipid-rich copepods and euphausiids are characteristic of fish diets during years of enhanced fish abundance of all three fishes evaluated, as well as enhanced body condition in age-0 pollock (Heintz et al., 2013; Andrews et al., 2015). Small copepod species, while lower in lipids

compared to large copepods, may represent an alternative prey resource when large copepods are limited for forage fishes, in particular herring as generalist foragers (Andrews et al., 2015).

4. Euphausiids are assumed to drive changes in forage fishes including Pacific herring ("Herring"), capelin ("Capelin"), and juvenile gadids, including "Age-0 pollock" (Heintz et al., 2013; Andrews et al., 2015).

5. In addition to zooplankton, age-0 pollock were included as prey source for Pacific herring (Andrews et al., 2015). Increases in age-0 pollock are presumed to increase prey availability for herring, increasing survival and biomass during the fall surveys.

We fitted this model by including links from physical drivers (sea ice extent) to primary productivity (percent open water bloom) to zooplankton indices (small copepods, large copepods, and euphausiids) as a measure of secondary productivity and prey source for forage fishes. Every zooplankton group (small copepods, large copepods, and euphausiids) was linked to each forage species tested (herring, capelin, and age-0 pollock). In addition we included a link from age-0 pollock to herring (Figure 92).

Status and trends: The resulting DSEM model (Figure 92) provided estimated strength, direction, and significance of each linkage between variables. Some linkage directions were in line with prior expectations outlined in the causal hypotheses (Table 5). For example, increased sea ice extent resulted in a lower proportion of open water blooms, as predicted by other studies (Nielsen et al., 2024; Eisner et al., 2016; Sigler et al., 2014; Hunt et al., 2011; Hare et al., 2007). This relationship had a strong negative association and was statistically significant (p-value $<$0.001). Open water blooms, in turn, were positively associated with small copepods (p-value $<$0.001) and negatively associated with large copepods, also in agreement with the literature (Kimmel et al., 2018; Hunt et al., 2011; Coyle et al., 2008). Large copepods were more responsive than euphausiids to open-water blooms (i.e., had a stronger relationship), such that the ratio of euphausiids to large copepods is higher in warm than cold years (Figure 93). The model identified significant strong positive impacts of euphausiid density on herring biomass (p-value $<$0.001) which aligned with previous expectations (Andrews et al., 2015). Euphausiid contribution to herring diets has been shown to fluctuate with changing ocean temperatures (Andrews et al., 2015). The model estimated that small copepods were associated with increased herring biomass (p-value $<$0.001) while large copepods had a positive association with capelin. Capelin abundance and distribution has been found to vary significantly between warm and cool periods, with higher abundance and a larger proportion of large copepods in their diets in cold years than warm years (Suryan et al., 2026; Andrews et al., 2015). This supports the overall expectation that warm years (with low sea ice extent) have more open-water blooms, more small copepods, and more herring. Alternatively, cool years (with high sea ice extent) have fewer open-water blooms (more ice-associated blooms), more large copepods, and more capelin.

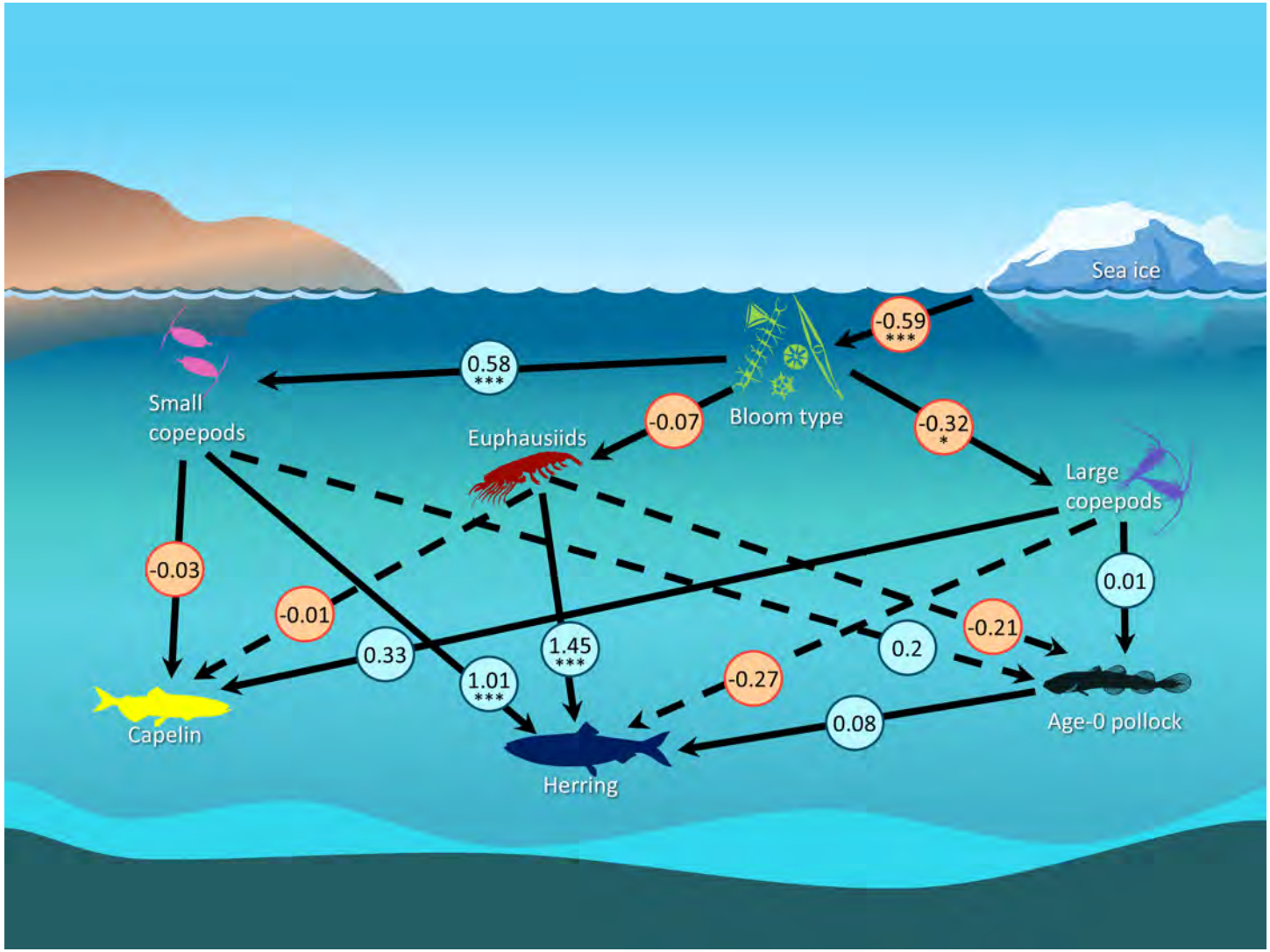


Figure 92: A path diagram showing estimated quantitative linkages among ecosystem variables. Arrows correspond to hypothesized relationships, where an arrow pointing from X to Y indicates that a change in X is estimated to cause a change in Y. The number listed in each arrow shows the estimated path coefficient, where e.g., the value of 1.01 from small copepods to herring indicates that a 10% increase in small copepod biomass is associated with a 10.1% increase in herring. For each listed coefficient we include the significance value with stars where * <0.1, ** <0.05, *** <0.01. The sign of the causal relationship with dashed lines is opposite from our *a priori* expectation (see Table 5). We also estimated additional first-order autocorrelation for each variable.

Several of the model results were contrary to expectations, however, most notably the lack of effect of large copepods on age-0 pollock dynamics. Much work has connected consumption of large copepods with better body condition and overwinter survival for age-0 pollock, so much so that the linkages have been an important component of the Oscillating Control Hypothesis (Buckley et al., 2016; Heintz et al., 2013; Siddon et al., 2013; Hunt et al., 2011). However, the weak positive association between small copepods and age-0 pollock may indicate an alternative prey source supporting moderate pollock biomass, although this would require further research. In this model we do not evaluate the connection between age-0 abundance or condition with overwinter survival to age-1 (see p. 42); therefore, we could be missing implications on later life-stages of pollock.

The lack of strong connections of euphausiids in this causal map was also unexpected. Percent open water bloom was insignificantly and only very weakly negatively associated with euphausiids. Generally, factors influencing euphausiid abundance in the EBS are not well understood but correlative research indicates temperature is a good predictor of abundance (Ressler et al., 2014). The extent of the EBS cold pool, a proxy for sea ice extent from the prior winter (Clement Kinney et al., 2022), also appears to influence euphausiid abundance on a location-specific basis, with euphausiid abundance in the eastern and southeastern Bering sea showing a strong relationship with cold pool extent (Reum et al., 2026). Because the DSEM model does not account for spatial variation, local-scale patterns in euphausiid abundance may be driven by temperature and the DSEM linkage may be weaker on a regional basis. Additionally, this index aggregates across all life stages and species of euphausiids potentially confounding any species-specific variability in the relationship between percent open water bloom and euphausiid density, weakening this linkage in the DSEM model.

The lack of strong effect of euphausiids on age-0 pollock was also unexpected. Euphausiids were negatively (-0.21), but insignificantly (p-value = 0.477) associated with age-0 pollock. Euphausiids are a major component of the diets of age-0 pollock in particular in cold years (Heintz et al., 2013; Coyle et al., 2011). Spatial and temporal mismatches of the summer euphausiid index and age-0 pollock may be related to the lack of effect.

Factors influencing observed trends: For forage fish species dynamics that have moderate to strong links in the causal map (i.e., capelin and herring), sea ice extent and its influence on primary productivity appears to alter the trophic pathways leading to each forage fish species. Spring time ice extent and bloom type sets up the primary productivity in the southeastern Bering Sea, with lower sea ice extent years associated with open-water blooms, and more abundant small copepods in late summer/fall. High abundance of small copepods and euphausiids are associated with a more abundant herring population than in high sea ice extent years. Conversely, in high sea ice extent years the phytoplankton bloom is ice-associated rather than open-water. This cooler year pattern is associated with more abundant populations of large copepods and increased capelin abundance.

Interestingly, we did not observe the expected ecosystem connections to age-0 pollock. Here, we represent the diversity of available prey as indices of three zooplankton groups: euphausiids, small and large copepods. In reality different life stages of these species and different species within these groups may be more important for age-0 pollock at different points of its life cycle (e.g., larval pollock consuming copepod eggs and small copepods like *Pseudocalanus* in the spring versus age-0 pollock consuming euphausiids or *Calanus* spp. in the fall among other species) and during different thermal regimes (Kimmel et al., 2018; Hunt et al., 2011). While this causal map primarily explored bottom-up drivers of forage fish and prey availability, competition and predation are unaccounted for in the model and could be contributing to the weak relationships. The large age-0 cohort in 2018 indicates that even in warm years without large copepod species (*Calanus* spp.) large age classes of pollock can be

produced (Hunt Jr et al., 2025).

In recent years due to spatial and temporal limitations of surveys, we are only representing even year trends in the southeastern Bering Sea during the late summer/fall. Therefore, odd-year trends, such as changes in available zooplankton related to trophic connections (Batten et al., 2018), are unaccounted for with these current data underlying the causal map and could be influencing forage biomass.

Implications: Forage fish, such as age-0 pollock, capelin, and herring, are a critical trophic link in the Bering Sea ecosystem. Exploring quantitative linkages among ecosystem drivers and forage fish biomass illustrates how environmental changes might affect the availability of different forage fish species for the broader ecosystem.

For species where we did not observe a strong mechanistic link (e.g., age-0 pollock), this could indicate a misspecified causal map, a gap in ecosystem understanding, or that the chosen indices representing the species and linkages are inaccurate.

Future Research: To understand the predictive capacity of this model and identify potential misspecification, additional diagnostic analyses such as leave-one-out and refitting the model while dropping recent years to assess stability in estimated parameters are needed. Depending on those results it may require iterative review of the current literature/mechanism table and re-fitting the causal map before attempting to use this model in predictive capacity.

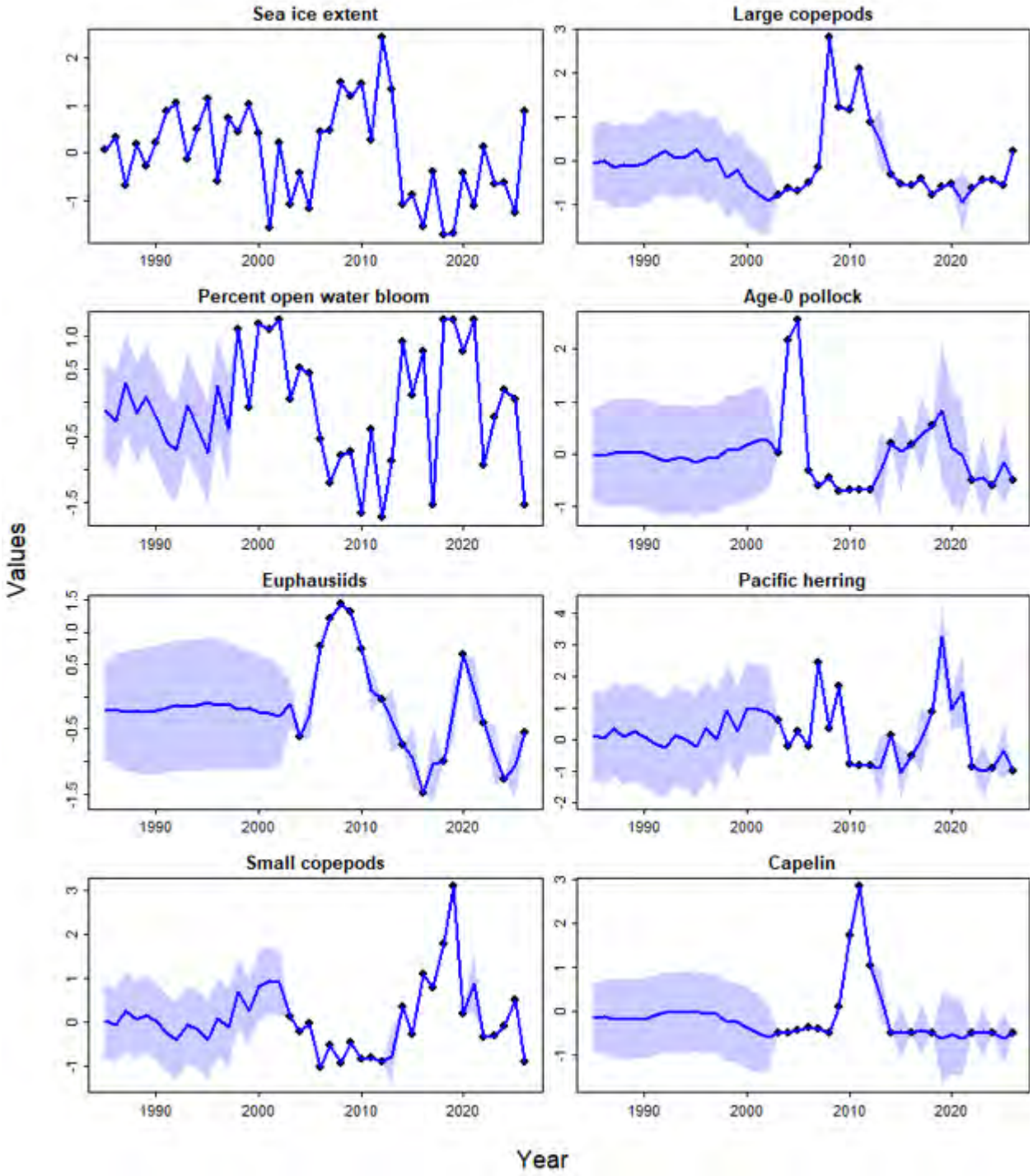


Figure 93: Values from a time series showing observed (blue dot) and estimated (blue lines with shaded region representing 95% confidence interval) value for each ecosystem variable included in the Dynamic Structural Equation Model. Note that the model is specified to exactly fit observations, such that estimates (lines) are equal to observations (dots) when observations are available in a given year. See list of data sources below.

Table 5: Hypothesized mechanism table for ecosystem linkages. Each row represents an arrow from an exposure to an outcome where we include the lag and hypothesized effect sign for the relationship based on literature (e.g., first row represents the effect of sea ice extent on phytoplankton blooms at a lag of 0 where we expect the effect to be negative based on Nielsen et al., 2024). We provide the data availability and our assessed confidence in said relationship.

Driver	**Causal Hypothesis**	**Lag(s)**	**Hypothesized Effect Sign**	**Data Availability and Caveats**	**Confidence (L,M,H)**	**References**
Sea ice	Greater sea ice extent decreases open-water during spring phytoplankton blooms.	0	Negative	Aggregated NSIDC monthly data at 25 km resolution	H	(Nielsen et al., 2024)
Percent open water (primary production)	Percent open-water decreases nutrient-rich ice-associated phytoplankton blooms.	0	Neg to Euphausiid Neg to Lg Copepods Pos to Sm Copepods	Annual index from satellite imagery	H	(Nielsen et al., 2024)
Sm Copepods	In the fall, higher proportion of small copepods indicates less available food for age-0 pollock, capelin, decreasing energy density and reducing survival thereby decreasing abundance. In warm years, small copepods provide an alternative prey resource in the absence of large copepods for herring.	0	Pos to Herring Neg to Capelin Neg to Pollock	Integrated from 70 m mooring and BASIS; RZA in recent years	M, M, M	(Coyle et al., 2011; Heintz et al., 2013; Sigler et al., 2016; Andrews et al., 2015)
Euphausiids (adults)	Increased adult abundance increases prey availability for herring and capelin. Increased adult abundance represents good conditions for other euphausiid age classes increasing prey availability for age-0 pollock during low large copepod years increasing age-0 pollock survival and abundance.	0	Pos to Herring Pos to Capelin Pos to Pollock	MACE biannual acoustic survey	L, L, L	(Heintz et al., 2013; Andrews et al., 2015; Hunt Jr et al., 2025)
Lg copepods	More lipid-rich large copepods increases survival and abundance of capelin, herring, pollock. Particularly for specialists age-0 pollock and capelin.	0	Pos to Herring Pos to Capelin Pos to Pollock	Integrated from 70 m mooring and BASIS; RZA in recent years	M, M, H	(Hunt et al., 2002, 2011; Andrews et al., 2015; Coyle et al., 2011)
A0 Pollock	Increased age-0 pollock increases prey availability for herring, increasing survival and abundance.	0	Pos to Herring	Biannual BASIS survey	L	(Andrews et al., 2015)

Data sources
*indicates the data source is also a Report Card indicator, with further details available in the 'Description of the Report Card indicators' on p. 320

***Sea Ice Extent:** The Bering Sea ice year is defined as 1 August–31 July. Annual sea ice extent was calculated using NSIDC monthly sea ice concentration (SIC) data at a 25 km resolution with a 0.15 concentration threshold. Due to the lag of the most recent data availability, the most current year extent was computed using the near real time data sea ice concentration while the extent of the previous years were computed using the Climate Data Record (CDR). Data courtesy of Sunny Hospital (shospital@nexusdatasolutions.com)

***Proportion of Open Water Blooms:** The timing of ice retreat and bloom peak was used to estimate bloom type, which differentiates between open-water blooms (i.e., ice retreat occurred $\geq$21 days prior to bloom peak) and ice-associated blooms (i.e., ice retreat occurred $<$21 days prior to bloom peak) for each year (Perrette et al., 2011). Timing of sea-ice retreat was determined as the date when ice coverage remained below 15% based on the 15-day running mean of the daily sea-ice fraction data. Bloom peak timing was estimated using standardized merged ocean color satellite data of 8-day satellite chlorophyll-a (chl-a, μg/L) at a 4 km-resolution from The Hermes GlobColour website covering the years 1998-2026. Data courtesy of Matt Callahan (Matt.Callahan@noaa.gov)

Small Copepods: Small copepods (*Acartia* spp., *Pseudocalanus* spp., and *Oithona* spp.) were quantified from 153μm mesh, 20 cm bongo net samples taken during two fall (Aug/Sept) surveys: EMA Eastern Bering Sea Juvenile Fish (BASIS) survey and 70m isobath mooring survey over the southern Bering Sea shelf (south of 60°N). Annual indices of relative biomass were estimated using spatio-temporal model with sdmTMB package. The current year value is an estimate of relative abundance derived from an at-sea Rapid Zooplankton Assessment (RZA). RZA abundance estimates may not closely match historical estimates of abundance as methods differ between laboratory processing and ship-board RZA. Data courtesy of David Kimmel (David.Kimmel@noaa.gov)

***Large Copepods:** Large copepods (predominantly *Calanus* spp.) were quantified from 505 μm mesh, 60 cm bongo net samples taken during two fall (Aug/Sept) surveys: EMA Eastern Bering Sea Juvenile Fish survey (BASIS) and 70-m isobath mooring survey over the southern Bering Sea shelf (south of 60°N). See small copepod methods. Data courtesy of David Kimmel (David.Kimmel@noaa.gov)

***Euphausiids:** An estimate of euphausiid biomass was determined by multifrequency acoustic backscatter and midwater trawl data collected during biennial pollock surveys in krill areal density in units of wet weight (g/m^2). Data are subset to the southeastern Bering Sea south of 60°N. Data courtesy of Mike Levine (Mike.Levine@noaa.gov)

Capelin: Fish were sampled using a surface trawl net towed in the upper 25 m during the fall (Aug/Sept) EMA Eastern Bering Sea Juvenile Fish Fall (BASIS) survey in the southeastern Bering Sea (south of 60°N). Annual indices of relative biomass were estimated using a single-species spatio-temporal model with the sdmTMBpackage version 1.1.0 Data courtesy of Lia Domke (Lia.Domke@noaa.gov)

Herring: see methods for capelin above. Data courtesy of Lia Domke (Lia.Domke@noaa.gov)

Age-0 pollock: see methods for capelin above. Data courtesy of Lia Domke (Lia.Domke@noaa.gov)

Mapping Fish Distributions in the NBS Using eDNA

Contributed by Kimberly Ledger and Diana Baetscher
Auke Bay Laboratories, Alaska Fisheries Science Center, NOAA Fisheries, Juneau, AK
Contact: kimberly.ledger@noaa.gov
Last updated: September 2025

Description of indicator: Environmental DNA (eDNA) consists of scales, skin, cells, and other genetic material released from organisms into the environment. In marine ecosystems, researchers collect and filter water to concentrate the genetic material. DNA is then extracted from the sample. DNA sequencing can provide information on the presence and relative abundance of particular species or groups of species near the sampling location (Thomsen et al., 2012), although eDNA alone cannot distinguish the life stage(s) of individuals contributing to the signal.

We used water samples collected on the Alaska Fisheries Science Center (AFSC) Northern Bering Sea (NBS) surface trawl survey for eDNA analysis. Data collection occurred during late summer/early fall (August-September) in both 2023 and 2024. Water samples were collected using Niskin bottles deployed at 10m depth at 42 stations in 2023 and 41 stations in 2024 spanning approximately 60°N to 64°N and 171°W to 162.5°W. At each station, three 1-L water samples were collected and filtered individually. DNA was then extracted, amplified, and sequenced. We identified eDNA of 54 fish taxa in sample replicates using multi-species metabarcoding of the 12S rRNA gene (Miya et al., 2015). We selected four species (walleye pollock (*Gadus chalcogrammus*), chum salmon (*Oncorhynchus keta*), Pacific herring (*Clupea pallasii*), and saffron cod (*Eleginus gracilis*) for spatio-temporal models because they represent moderate-to-high abundance taxa and play crucial roles in the ecosystem, either as targets for commercial fisheries or essential forage fishes. Detection frequencies from eDNA sample replicates are likely to reflect the true abundance of each species, and persistent sampling and analysis over time can reveal trends in species abundance (Hänfling et al., 2016).

We modeled single-species detection frequencies across space and time using the tinyVAST package version 1.2.0 and R version 4.4.1 (Thorson et al., 2025; Team, 2022). We fit spatio-temporal models with species-specific binomial distributions with a cloglog link to model spatial and spatio-temporal variation in both probability of encounter and detection frequency. Models also accounted for the compositional nature of data collection (i.e., a constraint on the total reads across species) by modelling a random effect for each sample (i.e., approximating the multinomial-to-Poisson treatment of compositional data; Thorson et al., 2022). The fitted models were then used to predict detection frequencies across the survey extent.

Status and trends: Spatial distributions of pollock, chum salmon, Pacific herring, and saffron cod appeared relatively stable between 2023 and 2024. All four species show consistent spatial patterns of high-detection areas across both years (Figure 94), with increases in both range and intensity of detections from 2023 to 2024 (Table 6). Pollock had the highest detection frequencies in both years, with near-100% detection concentrated in the southwestern region of the survey extent in both years. Chum salmon were most frequently detected in the southernmost area of the survey (below 61°N). Pacific herring were detected more often in shallower, nearshore waters in Norton Sound. Saffron cod detections were primarily concentrated in nearshore waters adjacent to the Yukon-Kuskokwim Delta.

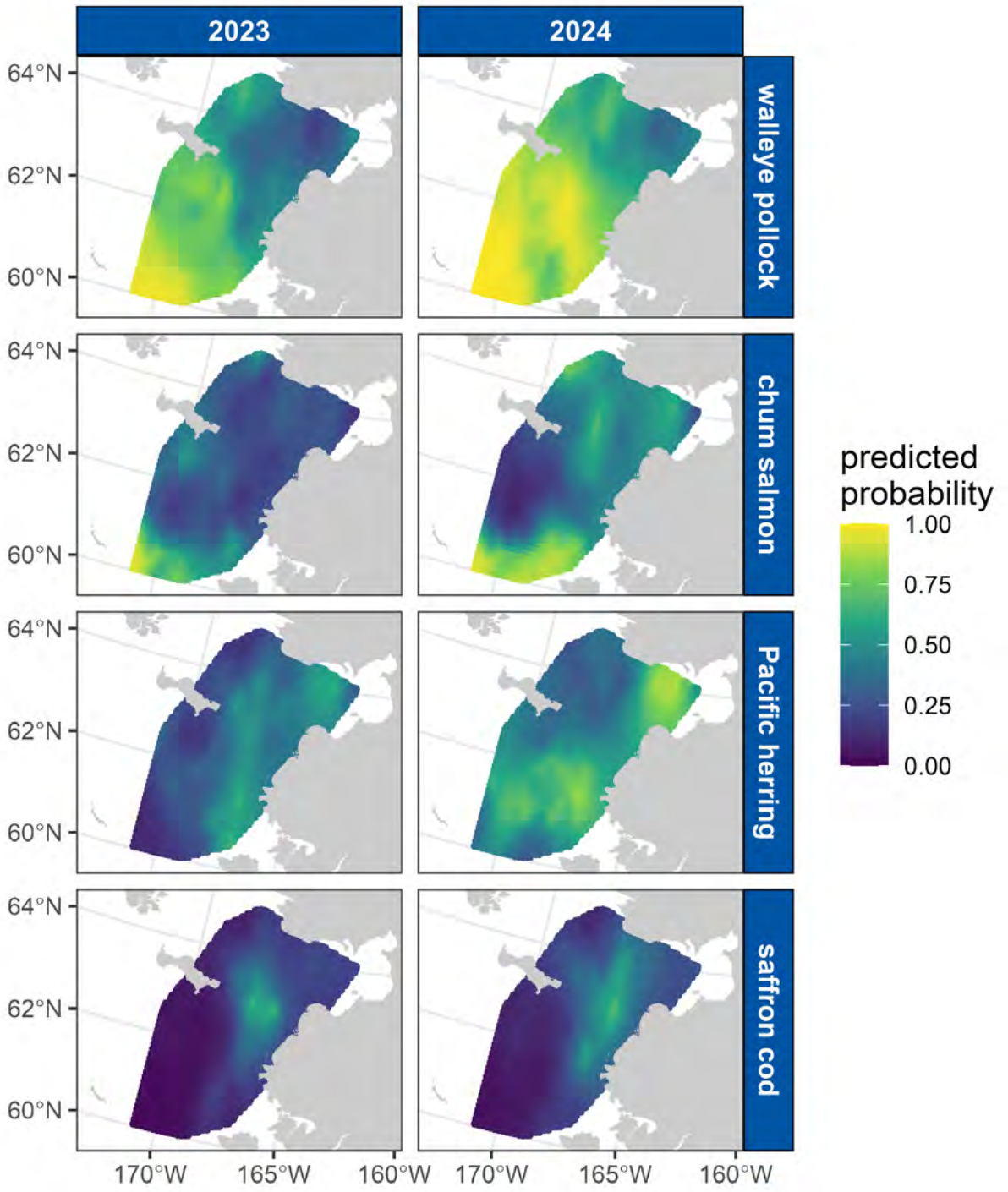


Figure 94: Estimated eDNA detection frequencies of pollock, chum salmon, Pacific herring, and saffron cod in near-surface waters (10m depth) surveyed in the northern Bering Sea during late summer (August-September), 2023-2024.

Table 6: Overall mean eDNA detection frequencies of four fish species in the northern Bering Sea in 2023 and 2024.

Species	2023	2024
Walleye pollock	0.68	0.77
Chum salmon	0.42	0.47
Pacific herring	0.36	0.53
Saffron cod	0.18	0.24

Factors influencing observed trends: The observed spatial and temporal patterns may be influenced by environmental factors. Sea surface temperatures in fall 2023 and 2024 were close to the 30-year baseline period (1985-2014) (Callahan and Lemagie, 2024), and bottom temperatures were similar across most of the survey area, though bottom temperatures in Norton Sound were warmer in 2024 than 2023 (Kearney, 2024), indicating that ocean conditions were neither extreme or substantially different between years. This relative stability likely contributed to similar species distributions and eDNA detection patterns across the two years.

Water samples for eDNA are collected at 10m depth, which could include detections for both adults and juveniles, depending on their location in the water column. Throughout most of the survey extent in the NBS, the bottom depth is relatively shallow such that the full water column is mixed, allowing for eDNA sampled at 10m to detect fishes at both shallower and deeper depths.

Implications: The spatiotemporal patterns in eDNA detection frequencies highlight the potential value of eDNA as a data source for informing species distribution models in marine ecosystems. Although the current dataset is limited to a short time span, continued investment in routine sampling will allow the development of reliable detection-based indices of abundance from eDNA, supporting the assessment of many species' change over time. A longer time series of this data will be especially valuable, as it will enable us to use an eDNA index that can detect changes in species distributions across years with high inter-annual variability or during periods of environmental instability.

Future directions: Although the data presented in this report are eDNA data alone, we are developing joint spatio-temporal models using combined eDNA and trawl data. Joint species distribution models that integrate eDNA and trawl data provide an opportunity to account for their different detection processes and, in doing so, better represent the true species distribution. By leveraging the response variables of trawl catch (e.g., weight or numerical abundance per unit effort), the joint model can estimate a catchability ratio that intercalibrates eDNA densities to expected biomass or abundance. Modeling both data sources together could enable improved estimates of species abundance and distribution.

Age-0 Pollock and Pacific Cod from Surface Trawl Surveys, 2003-2026

Contributed by Alex Andrews[1], Lia Domke[1], Jim Murphy[1], Adam Spear[2], Andrew Dimond[1], and Caroline Lawrence[1]
[1]Auke Bay Laboratories, Alaska Fisheries Science Center, NOAA Fisheries, Juneau, AK
[2]Resource Assessment and Conservation Engineering Division, Alaska Fisheries Science Center, NOAA Fisheries, Seattle, WA
Contact: alex.andrews@noaa.gov
Last updated: September 2026

Description of indicator: See p. 145.

Status and trends: Since 2016, the EMA Eastern Bering Sea Juvenile Fish Fall survey occurred biennially, in even years, while the EMA Northern Bering Sea Ecosystem Surface Trawl Fall survey occurs annually; both surveys were conducted annually prior to 2016. During 2026, age-0 pollock relative biomass estimates were near average or below the time series average in the northern Bering Sea (NBS) and southeastern Bering Sea (SEBS), respectively. However, the 2025 age-0 pollock relative biomass estimate in the NBS region was the highest for the entire time series (2003-2026; Figure 95). Elevated age-0 pollock relative biomass estimates in surface waters (0-25 m deep) tend to occur during warm periods characterized by reduced cold pool extents. In the NBS, relative biomass estimates increased in 2005, 2014, 2015, 2018, and 2025. In the SEBS, relative biomass estimates increased in 2003-2005, 2014, 2016, and 2018.

During 2026, age-0 Pacific cod relative biomass estimates were below the time series average in the SEBS (Figure 96). Although 2026 was below the long-term average, these relative biomass estimates are not as low as 2003, 2007, 2009, 2014, and 2016. Unfortunately, due to multiple years of no catch in the NBS, the NBS regional sdmTMB model did not converge; therefore, we do not present age-0 Pacific cod relative biomass estimates in the NBS.

Factors influencing observed trends: Changes in climate-mediated oceanographic conditions, such as water column temperatures, may influence the vertical and spatial distribution of age-0 pollock and therefore the resulting surface trawl catches. Age-0 pollock were found closer to the surface in warm years supported by combined acoustic-trawl methods (see p. 168, Spear et al., 2023). However, warm periods with increased age-0 pollock relative biomass do not always correlate with strong recruitment, which is likely a result of the lack of high quality prey during warm years (Coyle et al., 2011; Heintz et al., 2013). In 2026, the Bering Sea water temperatures were colder than observed in the last decade. These conditions along with adequate age-0 biomass estimates should be favorable for age-0 pollock winter survival.

These changes in climate-mediated oceanographic conditions are likely impacting age-0 Pacific cod, including distribution and phenology (Hurst et al., 2012; Rogers et al., 2026). Northward shifts in the distribution of adult Pacific cod have been observed in the Bering Sea (Spies et al., 2020). Less is known about shifts in spawning aggregation locations which could influence age-0 Pacific cod abundance and distributions. Furthermore, it's difficult to measure the contribution of specific spawning areas to the abundance of young Pacific cod (Miller et al., 2016).

Implications: In 2025, the large increase in relative biomass estimates of age-0 pollock in the NBS region could reflect stronger advection of age-0 fish into the NBS, northward movement of adult spawning aggregations, or improved juvenile habitat in the NBS. Monitoring changes in relative biomass estimates along with vertical distribution provides a better understanding of biomass throughout the water column and spatial distribution (Figure 97) of age-0 pollock in the EBS. The estimates in 2026 are modestly higher in the SEBS. The relative biomass estimate in the NBS has declined since the record high in 2025, but has moved closer to the time series average. Age-0 pollock are a major source of prey for upper trophic level guilds including fish, birds, and mammals.

In earlier years of the EMA Eastern Bering Sea Juvenile Fish Fall survey (2004-2009), age-0 Pacific cod were rarely encountered in the NBS (Hurst et al., 2012). Frequency of catch of age-0 Pacific cod in the NBS are increasing, with positive encounters at 49% of the stations sampled in 2026. Additional monitoring of age-0 Pacific cod is needed to elucidate changes in abundance and distributional shifts in the EBS.

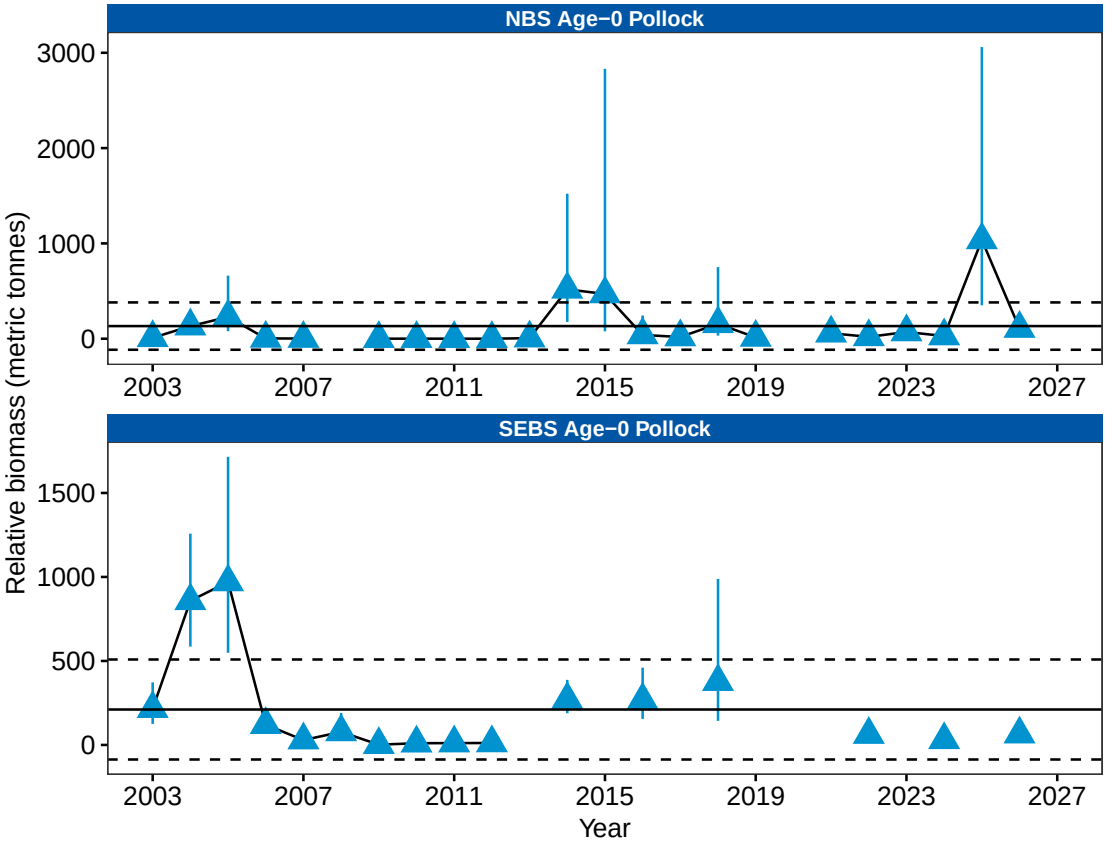


Figure 95: Estimated relative biomass (metric tonnes) of age-0 pollock in surface waters (0-25 m deep) surveyed in the northern Bering Sea (NBS; upper panel) and southeastern Bering Sea (SEBS; lower panel) during late summer, 2003-2026. Solid line is the long term average with the dashed lines representing ± 1 standard deviation around the average.

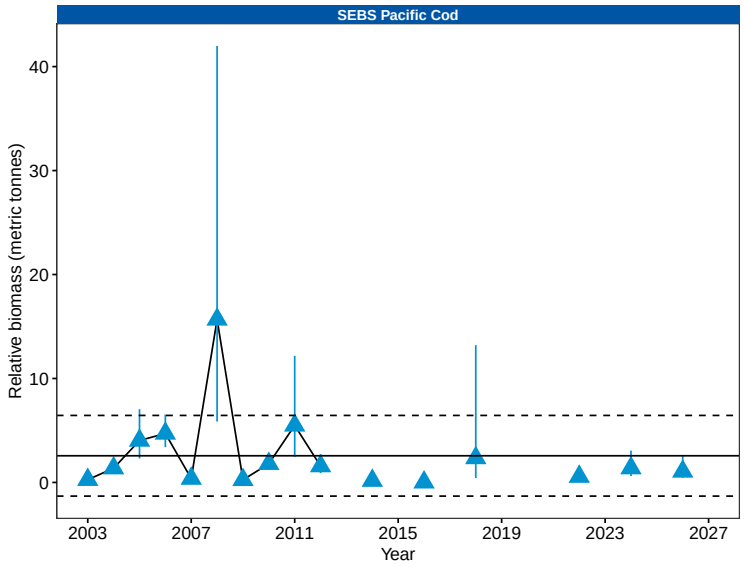


Figure 96: Estimated relative biomass (metric tonnes) of age-0 Pacific cod in surface waters (0-25 m deep) surveyed in the southeastern Bering Sea (SEBS) during late summer, 2003-2026. Solid line is the long term average with the dashed lines representing ± 1 standard deviation around the average.

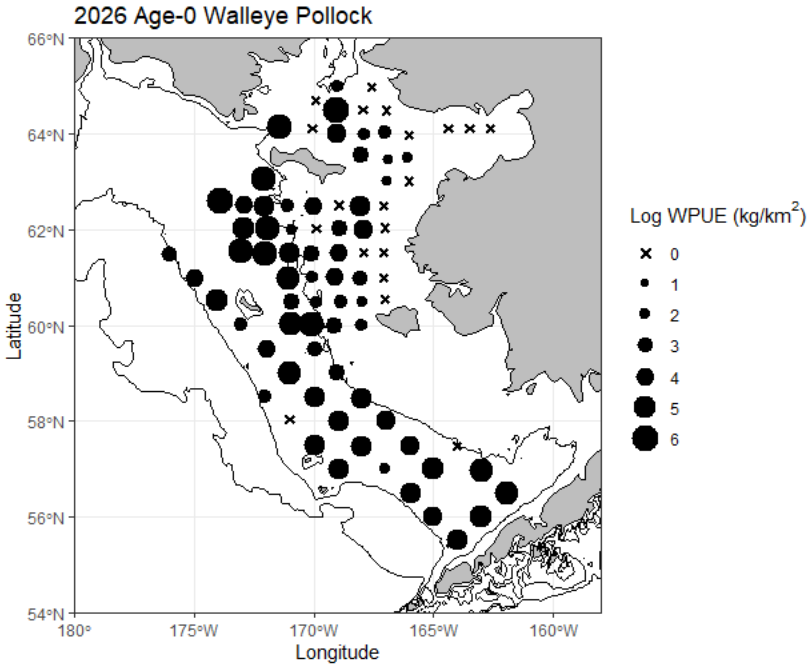


Figure 97: Map of the spatial distribution of age-0 pollock CPUE estimates [log(kg)/km^2] in surface waters (0-25 m deep) surveyed in the eastern Bering Sea during late summer, 2026.

Vertical Distribution of Age-0 Pollock in the Southeastern Bering Sea

Contributed by Adam Spear[1] and Alexander G. Andrews III[2]
[1]Resource Assessment and Conservation Engineering Division, Alaska Fisheries Science Center, NOAA Fisheries, Seattle, WA
[2]Auke Bay Laboratories, Alaska Fisheries Science Center, NOAA Fisheries, Juneau, AK
Contact: adam.spear@noaa.gov
Last updated: October 2026

Description of indicator: Vertical distribution of age-0 pollock was estimated through the calculation of an abundance-weighted mean depth during seven years between 2011-2026. The abundance of age-0 walleye pollock in the southeastern Bering Sea was estimated using acoustic-trawl methods. The process involved assigning trawl-catch data to acoustic backscatter data that were measured along a transect line. The trawl catch information was manually assigned to backscatter from a single surface, oblique, or midwater trawl depending on proximity, tow depth, and backscatter characteristics. Scrutinized backscatter was echo-integrated into 0.5 nautical mile (nmi) by 5 m bins, and output as nautical area scattering coefficient, m^2/nmi^2 (NASC). The species-specific compositions from each catch were used to convert NASC to species-specific abundance (individuals/nmi^2) using published measurements of the acoustic properties of these species. The middle domain (50 to 100 m isobath; Coachman, 1986) was the most consistent region surveyed across all years. Thus, to account for survey bias, values were constrained to those sampled over the middle domain. Age-0 pollock abundance was summed over each depth bin to calculate the weighted mean depth. Here, we show yearly abundance-weighted mean depths during the late summer over the southeastern Bering Sea middle domain.

Status and trends: Abundance weighted mean depths increased from 33 to 40 m during the years 2024 and 2026, respectively (Figure 98). This change coincides with changes in bottom temperatures from average to cold conditions from 2024 to 2026 (see Figure 54).

Factors influencing observed trends: Across the surveyed years bottom temperatures in the southeastern Bering Sea were average (2022 and 2024), warmer than average (2014 and 2016), and colder than average (2011, 2012, and 2026). These changes in temperature phases resulted in a change in the vertical distribution of age-0 pollock (Spear et al., 2023). Energy densities of age-0 pollock collected in trawls from these surveys showed that pollock collected in cold years had higher energy densities than those collected in warm years, suggesting improved feeding and provisioning conditions at depth in colder-than-average thermal conditions. Colder years have greater abundances of larger lipid-rich prey which result in higher dietary percentages of lipid and energy densities of age-0 pollock (Coyle et al., 2011; Heintz et al., 2013; Kimmel et al., 2018). This is partially explained by larger lipid-rich prey vertically migrating deeper in the water column during the day. Deeper age-0 pollock in 2016 is likely attributed to extreme surface temperatures that reached >15°C in the southeastern Bering Sea (Stabeno et al., 2017), which is within the range where they exhibit thermal stress (Laurel et al., 2016).

Implications: Vertical shifts may impact predator-prey overlap between age-0 pollock and their lipid-rich prey, calanoid copepods and euphausiids, resulting in different feeding conditions that ultimately define fish body condition prior to winter onset. As the climate warms further, or these warm phases potentially lengthen in time, there may be a compounding problem of poor condition and recruitment, thus significantly reducing standing stocks.

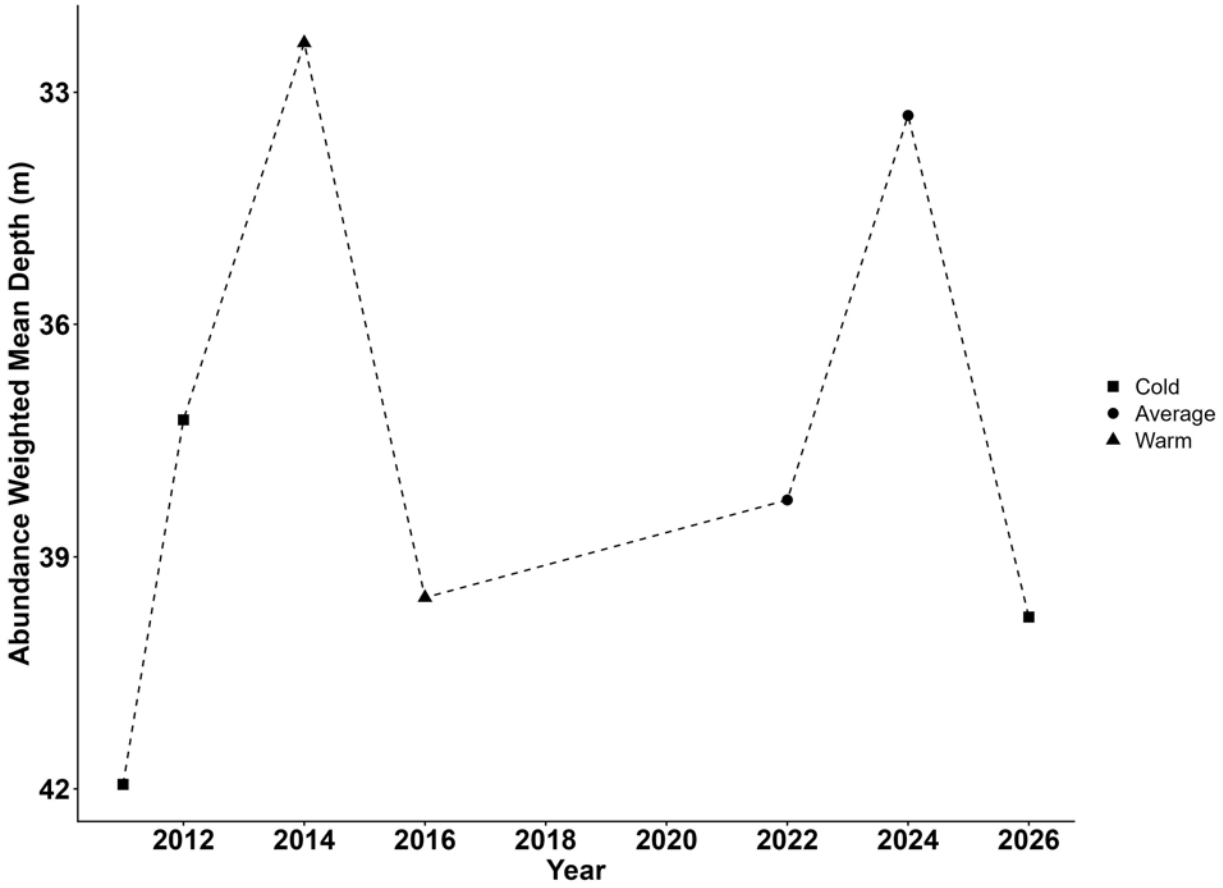


Figure 98: Annual abundance-weighted mean depth of age-0 pollock during late summer in the southeastern Bering Sea.

Fall Condition of Young-Of-The-Year Walleye Pollock in the Northern and Southeastern Bering Sea, 2002-2026

Contributed by Johanna Page, Jacek Maselko, Rob Suryan, Emily Fergusson, and Elizabeth Siddon
Auke Bay Laboratories, Alaska Fisheries Science Center, NOAA Fisheries, Juneau, AK
Contact: johanna.vollenweider@noaa.gov
Last updated: October 2026

Description of indicator: Several body condition metrics of young-of-the-year (YOY) walleye pollock (*Gadus chalcogrammus*) in the northern Bering Sea (NBS) and southeastern Bering Sea (SEBS) are presented, including energy density residuals and length-weight residuals. Fish were sampled primarily by surface trawl from the late-summer BASIS (Bering Arctic Subarctic Integrated Survey) and NBS trawl surveys, with a relatively small number of fish from opportunistic surveys. Fish <110 mm total length were assumed to be YOY (Bailey, 1989). Annual length-weight residuals were calculated from the linear regression of log transformed length (total length, mm) and weight (whole wet mass, g). Energy density (ED) was measured in the analytical chemistry laboratory at Auke Bay Laboratories, Juneau, AK, following standard protocols described in Vollenweider et al., 2011. Length-adjusted weight and ED were based on residuals obtained from the regression of weight and energy density on length, respectively.

Status and trends: Trends in YOY pollock condition diverge at 60°N, with different energetic processes in the NBS and SEBS. In the SEBS, pollock condition fluctuates in response to temperature-mediated processes, with below-average energy density during warm periods with positive sea surface temperature anomalies (2002-2005, 2014-2025), and above-average body condition during cold periods with negative anomalies (2006-2012) (Figure 99). In 2026 with the return of cold ocean temperatures, energy density rebounded and was higher than average. Body weight is less variable and not coupled with ocean temperatures (Figure 100). Length-adjusted weight was above average in 2026 in the SEBS after being relatively low since 2012. In the NBS, YOY pollock body condition is less variable than in the SEBS and is not coupled with regional changes in temperature. In 2026, pollock had low energy density and were of average weight (Figures 99 and 100).

Factors influencing observed trends: The NBS and SEBS are characterized by distinct physical oceanography with consequences on their respective biological communities. The NBS has more stable, colder conditions with extensive sea ice cover while the SEBS undergoes large interannual variability in sea ice cover and ocean temperature (Stabeno et al., 2012*a*). During relatively cool periods in the SEBS, zooplankton assemblages include large, energy-rich *Calanus* spp. and *Thysanoessa raschii* (Coyle et al., 2008; Stabeno et al., 2012*b*). In combination, an abundance of high-quality prey and reduced metabolic demands maximize growth and lipid storage of YOY pollock for winter survival (Andrews et al., 2019; Koenker et al., 2018; Laurel et al., 2016; Siddon et al., 2013). Though similar processes have occurred more recently in the NBS lower trophic level (Kimmel et al., 2023), the stability of ice cover dampens physical and biological variability.

Implications: Summer environmental conditions and the ability of YOY pollock to balance the synonymous energetic demands to grow and store lipid is reflected in their body condition prior to winter in NOAA's autumn surveys. Winter survival is dependent on their ability to grow large enough for predator avoidance while simultaneously having acquired sufficient lipid stores to sustain them through winter when food is relatively scarce. In the Bering Sea, the first winter survival of YOY pollock to age-1 recruits alternates during cold and warm regimes (Heintz et al., 2013, Vollenweider et al., submitted).

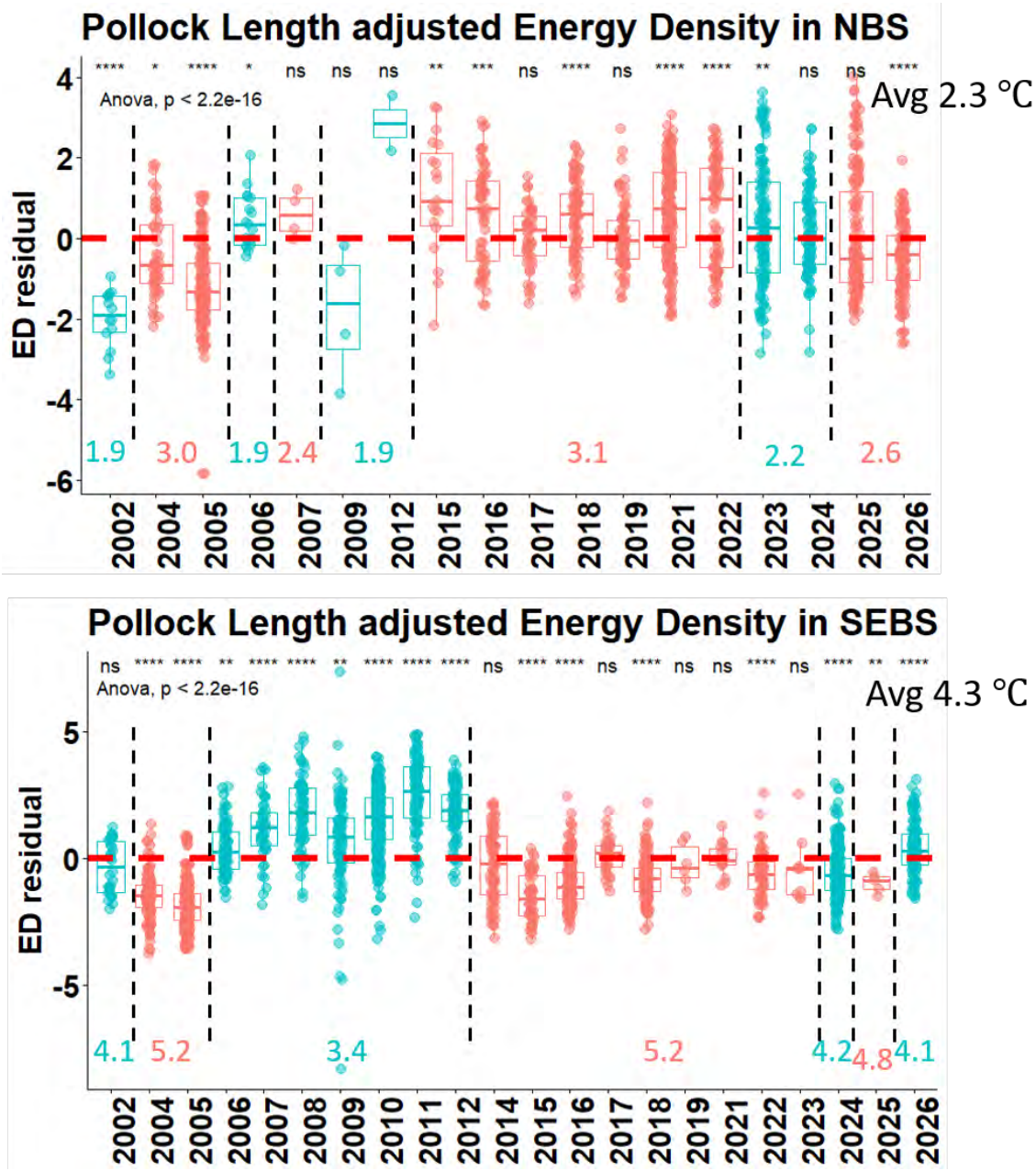


Figure 99: Annual length-adjusted energy density (ED; kJ/gram fish dry mass) of young-of-the-year pollock in the northern Bering Sea (NBS; top) and southeastern Bering Sea (SEBS; bottom). The horizontal dashed red line indicates the mean of all residuals. The significance of deviations from the mean are denoted by asterisks above the given year where ns = not significant. The dashed vertical black lines delineate periods of positive and negative sea surface temperature anomalies (see Figure 54), and the average annual daily temperature for that period is presented.

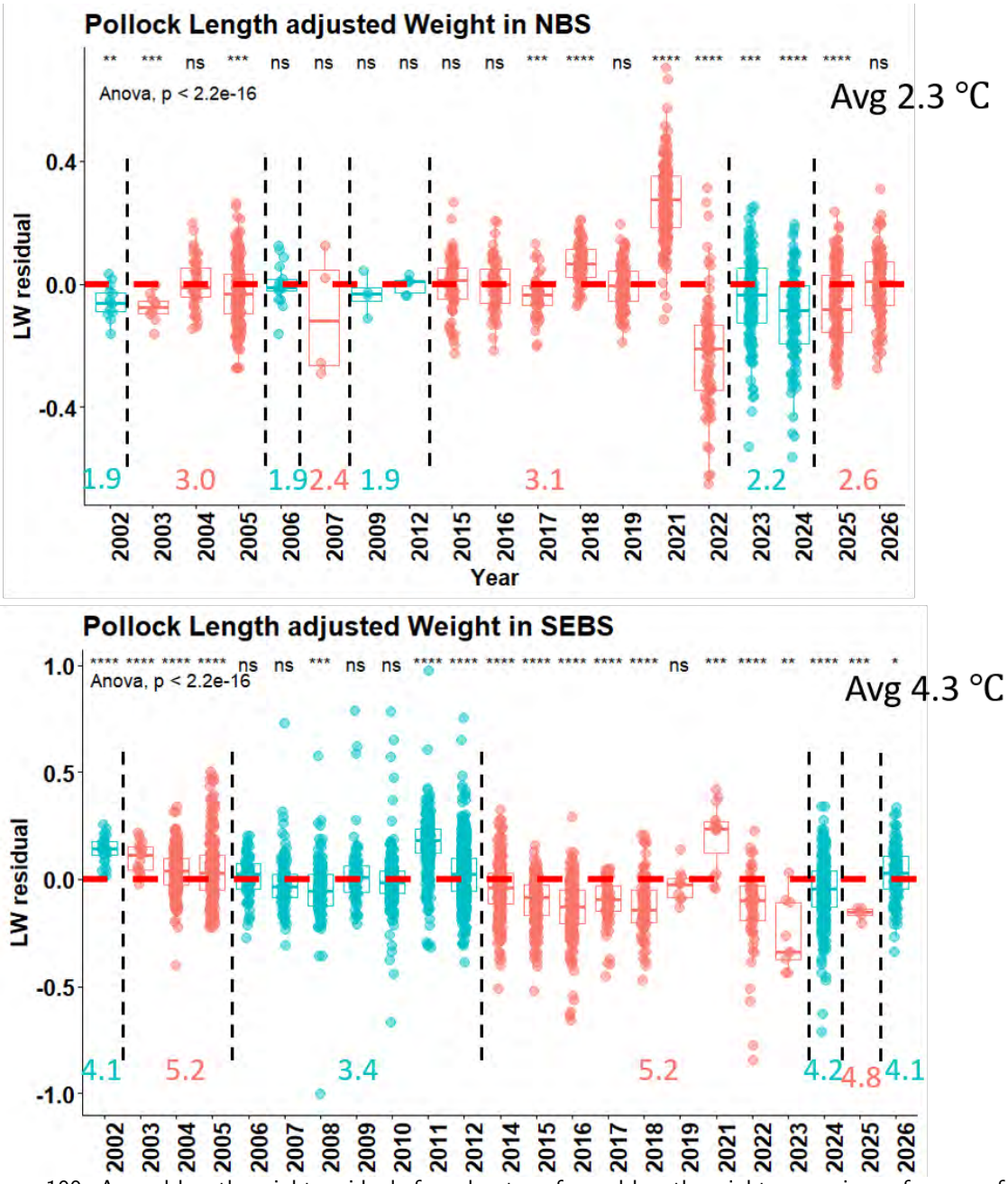


Figure 100: Annual length-weight residuals from log-transformed length-weight regressions of young-of-the-year pollock in the northern Bering Sea (NBS; top) and southeastern Bering Sea (SEBS; bottom). The horizontal dashed red line indicates the mean of all residuals. The significance of deviations from the mean are denoted by asterisks above the given year where ns = not significant. The dashed vertical black lines delineate periods of positive and negative sea surface temperature anomalies (see Figure 54), and the average annual daily temperature for that period is presented.

Pacific Herring and Capelin from Surface Trawl Surveys, 2003-2026

Contributed by Alex Andrews, Lia Domke, Jim Murphy, Andrew Dimond, Caroline Lawrence, and Rob Suryan
Auke Bay Laboratories, Alaska Fisheries Science Center, NOAA Fisheries, Juneau, AK
Contact: alex.andrews@noaa.gov
Last updated: September 2026

Description of indicator: See 'Description of indicator' on p. 145.

Status and trends: Since 2016, the EMA Eastern Bering Sea Juvenile Fish Fall survey occurred biennially, in even years, while the EMA Northern Bering Sea Ecosystem Surface Trawl Fall survey occurs annually; both surveys were conducted annually prior to 2016. Pacific herring (i.e., age-0 and age-1+) are predominantly caught in the northern Bering Sea (NBS) (Andrews et al., 2015). While relative biomass estimates have gradually increased in the NBS from 2021-2026, estimates have remained lower than the time series average in this region. Pacific herring relative biomass estimates remained at low levels in the southeastern Bering Sea (SEBS) in 2022, 2024, and 2026 (Figure 101).

In recent years of the time series, capelin are predominantly caught in the NBS, while historically they were caught in both the SEBS and NBS (Andrews et al., 2015). Although relative biomass estimates from 2021-2023 were lower than previous estimates in the time series, capelin relative biomass estimates increased significantly in the NBS in 2024. In 2025-2026 biomass estimates have returned to below the time series average (Figure 102).

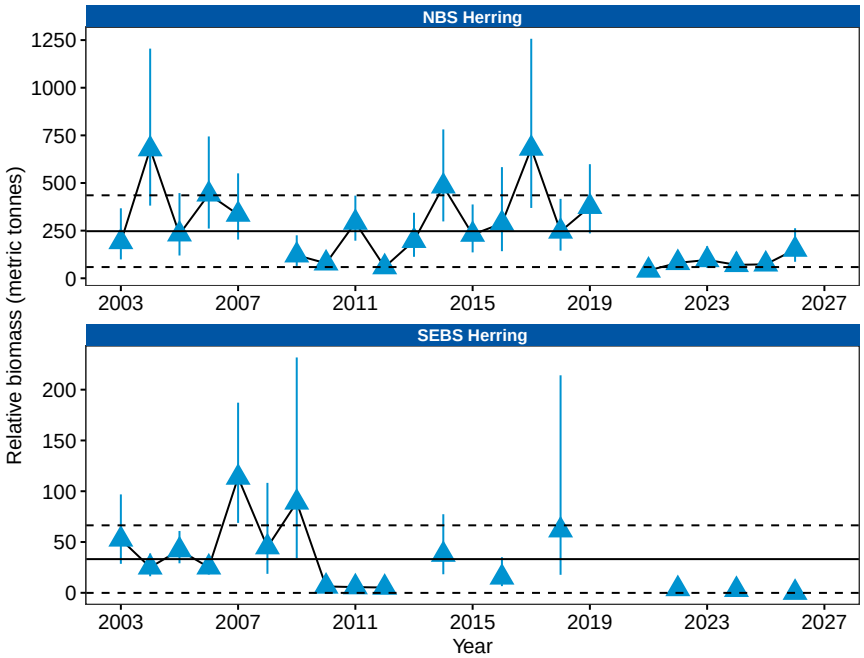


Figure 101: Estimated relative biomass of Pacific herring in surface waters (0-25 m deep) surveyed in the north (upper panel) and southeastern (lower panel) Bering Sea during late summer, 2003-2026. Solid line is the long term average with the dashed lines representing ±1 standard deviation around the average.

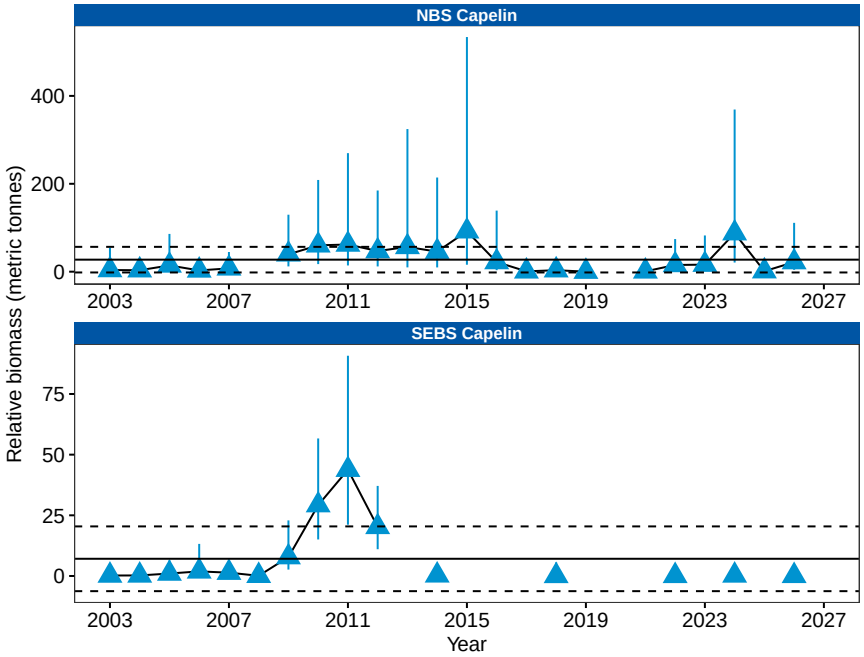


Figure 102: Estimated relative biomass of capelin in surface waters (0-25 m deep) surveyed in the north (upper panel) and southeastern (lower panel) Bering Sea during late summer, 2003-2026. Solid line is the long term average with the dashed lines representing ±1 standard deviation around the average.

Factors influencing observed trends: Favorable conditions for herring recruitment are linked to warm temperatures, favorable wind direction, and prey availability (Dressel et al., 2024; Williams and Quinn, 2000; Wespestad and Gunderson, 1991). High relative biomass estimates in 2014, 2017, and 2019 occurred during a series of warm years in the EBS (Figure 101. In the NBS, catches of herring in the surface trawl are predominantly age-0s and juveniles. Therefore, the high relative biomass estimates in 2017 were likely an early indicator of high age-4 recruit strength in 2021 (Dressel et al., 2024). Thus, relatively low juvenile herring relative biomass estimates in 2022-2026 indicate that age-4 recruits in 2026-2030 may be at or below average.

Estimates of capelin relative biomass are generally higher in the eastern Bering Sea (EBS) during cold periods when the cold pool extends into the SEBS. The highest relative biomass estimates in the time series occurred in the NBS and the SEBS between 2009-2016, either during a cold year or closely following a series of cold years. In 2024 (a cold to average year), biomass estimates in the NBS abruptly rebounded. Despite 2026 having an extensive cold pool in the EBS, capelin catches were below the time series average.

Implications: Pacific herring and capelin are both important forage species for upper trophic level guilds including groundfish (Ciannelli and Bailey, 2005; Aydin and Mueter, 2007), birds, and mammals (Sinclair et al., 2008). In addition, Pacific herring is an important resource for both subsistence and commercial harvesters. Monitoring relative biomass estimates can provide important information for changes in distribution patterns and abundance and the impacts of climate change in the EBS.

Salmon

Salmon Summary and Synthesis

Contributions to the 2026 Eastern Bering Sea Ecosystem Status Report (ESR) provide information on the status of both adult and juvenile salmon (*Oncorhynchus* spp.) of all species. Due to the variable age structure and complex life cycles of Pacific salmon which span multiple habitats, it can be challenging to disentangle the impacts of environmental conditions experienced across different life stages on their population dynamics. However, some salient patterns do emerge from the contributions to the 2026 ESR, with signals of species-specific responses to the near-average to cool temperature conditions that have prevailed recently, in contrast to the acute marine heatwave conditions of earlier years (e.g., 2018/2019).

Adult returns of western Alaska chum salmon (*O. keta*) stocks experienced precipitous declines during the marine heatwave period. Poor juvenile energetic condition driven by dietary shifts to lower quality prey items during this period indicate that negative bottom-up effects associated with warmer conditions were likely responsible for these declines (Farley Jr et al., 2024). Juvenile condition of chum salmon encountered in the NBS survey improved in 2021, and remained above-average through 2023, possibly reflecting the transition to near-average temperatures and associated food web responses during these years. NBS juvenile chum salmon energy density declined to near average values in 2024. More recently, energy density for NBS juvenile chum salmon has been above average (2025) to near average (2026). Juvenile fall chum salmon abundance in the NBS survey was slightly below average in 2025-2026 following the large juvenile year class encountered in 2024. The abundance and energy density patterns in 2025-2026 are consistent with the near-average temperature and ecosystem conditions in recent years, and indicate neither evidence of severe adverse ecosystem conditions, nor strongly favorable conditions for chum salmon. However, it is important to note that a consistent relationship between juvenile chum salmon abundance and future adult returns has not been established.

Western Alaska Chinook salmon (*O. tshawytscha*) runs have been in decline since the early 2000s and remain at low levels. Available evidence points to a complex suite of impacts operating across the life cycle (Cunningham et al., 2018; Howard and von Biela, 2023; Neuswanger et al., 2015; Ohlberger et al., 2020; Feddern et al., 2024). Abundance of juvenile Chinook salmon encountered in the NBS survey improved to slightly below average in 2025-2026 compared to the low levels observed in 2019-2024. Low juvenile abundance may be partially due to depressed spawner abundance in contributing stock complexes like the Yukon River, although environmental factors also strongly influence juvenile recruitment (Cunningham et al., 2018; Feddern et al., 2024; Neuswanger et al., 2015). Like chum salmon, juvenile Chinook salmon encountered in the NBS survey exhibited above average energy density in 2025, and near average levels in 2026. However, the relationship between body condition and survival for NBS Chinook salmon is unclear. There is a consistent relationship between the stock-specific juvenile abundance of Chinook salmon in the NBS survey and subsequent adult returns (Murphy et al., 2017), suggesting that near average run sizes may be expected in the next three to four years (when most juvenile Chinook present in 2026 would be expected to mature and return to freshwater to spawn). Such an outlook is encouraging for stock complexes such as Yukon River Chinook salmon, which have been experiencing improving (but still depressed) run sizes in recent years following severe lows in 2022-2023. However, it should be noted that the juvenile Chinook salmon abundance presented here is not stock-specific, and outlooks will be updated when genetic stock identification information is applied.

While the abundance of many salmon stocks declined during/following the marine heatwave years, Bristol Bay sockeye (*O. nerka*) salmon exhibited an opposite response, exhibiting record-high run sizes instead. The abundance of Bristol Bay sockeye peaked in 2021-2022, likely reflecting favorable ocean entry conditions in 2019-2020. The contrasting response of Bristol Bay sockeye to marine temperature conditions may reflect, to some extent, their freshwater rearing and marine migratory life histories. While other anadromous salmon species may typically rear in riverine habitats or outmigrate directly to sea as juveniles, sockeye typically rear in lakes for 1-2 years before ocean entry. Warming temperatures have been shown to increase the productivity of lake ecosystems in Bristol Bay watersheds (Rogers and Schindler, 2011) with corresponding increases in juvenile size and growth (Cline et al., 2019). As such, juvenile sockeye salmon may be better equipped to survive the size-dependent mortality typically experienced during early marine residency after enjoying better growing conditions in freshwater during warmer years. Moreover, there is evidence that Bristol Bay sockeye salmon modulate their marine migration pathways in response to ocean temperature conditions, migrating offshore more rapidly under warmer conditions (Farley et al., 2007). Consistent with these expectations, the recent return to near-average and cooler temperatures has resulted in smaller (but still above average) adult run sizes. Given these temperature responses, continued Bering Sea temperatures near or below average may be expected to result in more modest Bristol Bay run sizes in the near future.

Compiled by Lukas DeFilippo
Alaska Fisheries Science Center, NOAA Fisheries
Seattle, WA

Southern Bering Sea Nearshore Juvenile Salmon Survey, 2024-2026

Contributed by Sabrina Garcia, Ben Gray, Zoe Munson, and Hillary Thalmann
Alaska Department of Fish & Game, Division of Commercial Fisheries, Anchorage, AK
Contact: sabrina.garcia@alaska.gov
Last updated: October 2026

Description of indicator: The Alaska Department of Fish & Game has been leading a nearshore surface trawl survey in the southern Bering Sea since 2024 (Figure 103). The aim of this survey is to study the early marine life stage, known as the juvenile stage, of salmon originating from southwestern Alaska systems (primarily Kuskokwim River and Bristol Bay). Juvenile salmon surveys provide valuable insights on the early marine ecology (e.g., abundance, distribution, size, diet, and condition) of juvenile salmon, which are needed to understand which parts of the salmon life cycle are most critical for survival. Mixed-stock abundance indices for juvenile salmon are based on catch-per-unit-effort (number of fish/km^2) data from 2024-2026. In addition to juvenile salmon, survey operations also encounter forage fish species. Catch numbers for these species are reported.

Status and trends: Across the three years of the southern Bering Sea juvenile salmon survey, juvenile coho (*Oncorhynchus kisutch*) salmon CPUEs were relatively similar. Chinook (*O. tshawytscha*) salmon CPUE was highest in 2024 and similar in 2025 and 2026. The higher CPUE (and larger standard error) in 2024 was driven by a large catch of juvenile Chinook salmon at a single station. Catches of this magnitude (100+) were not seen in other survey years. The CPUEs for juvenile sockeye (*O. nerka*) and chum (*O. keta*) salmon in 2026 were approximately half the size of those seen in 2025 for both species, and chum salmon CPUEs in 2024 and 2026 were similar. Given that pink salmon (*O. gorbuscha*) runs in western Alaska are predominantly even-year dominant, juvenile pink salmon should be present in larger abundances in odd-numbered years. While pink salmon CPUE trends followed expectations, the CPUE in 2026 was much lower than expected with only two juvenile pink salmon captured throughout survey operations (Figure 104).

Catches of forage fish species have been variable across the three survey years (Table 7). In 2026, the dominant species captured were age-0 walleye pollock (*Gadus chalcogrammus*), Pacific herring (*Clupea pallasii*), sand lance (*Ammodytes* spp.), and Pacific sandfish (*Trichodon trichodon*). Pacific sand lance, Pacific sandfish, and rainbow smelt (*Osmerus mordax*) were all caught in higher numbers in 2026 than in the previous two years of the survey. We also caught 2 saffron cod (*Eleginus gracilis*) in 2026, which is the first time this species has been captured on this survey. Age-0 Pacific cod (*G. macrocephalus*) were captured in low numbers, primarily in the offshore stations in Bristol Bay, while no capelin (*Mallotus villosus*) were caught in 2026. In total, 33 fish species were caught during survey operations.

Factors influencing observed trends: With only three survey years available, the processes influencing inter-annual variation in juvenile salmon CPUE in the southern Bering Sea remain poorly understood, although freshwater survival, early marine survival, and adult spawning escapement are likely key factors influencing abundance. This survey is intended to be a long-term project to assess the early marine ecology of southwestern Alaska stocks, understand factors that influence population dynamics, and make progress towards developing a forecasting tool for southwestern Alaska systems by using juvenile abundance to predict adult returns in future years. Funding has been secured to continue survey operations into 2027 and 2028. Physical oceanographic data, water sample analyses (chlorophyll-a,

nutrients, and environmental DNA), zooplankton abundance and distribution, juvenile salmon genetic stock compositions, and juvenile salmon diet and energetic density results from 2024-2026 should be available in spring 2027.

Implications: Juvenile salmon are competitors and, in some cases, predators of groundfish species, such as age-0 pollock. Diet analyses of juvenile salmonids in previous years of this survey have indicated that age-0 pollock comprise a portion of juvenile Chinook, coho, sockeye, and chum salmon diet in the southeastern Bering Sea. However, juvenile sockeye, pink, and chum salmon were caught in markedly lower numbers in 2026 compared to 2025, and it is unlikely that increased predation or competition from salmon were main drivers in the unusually low age-0 pollock catches seen in 2026.

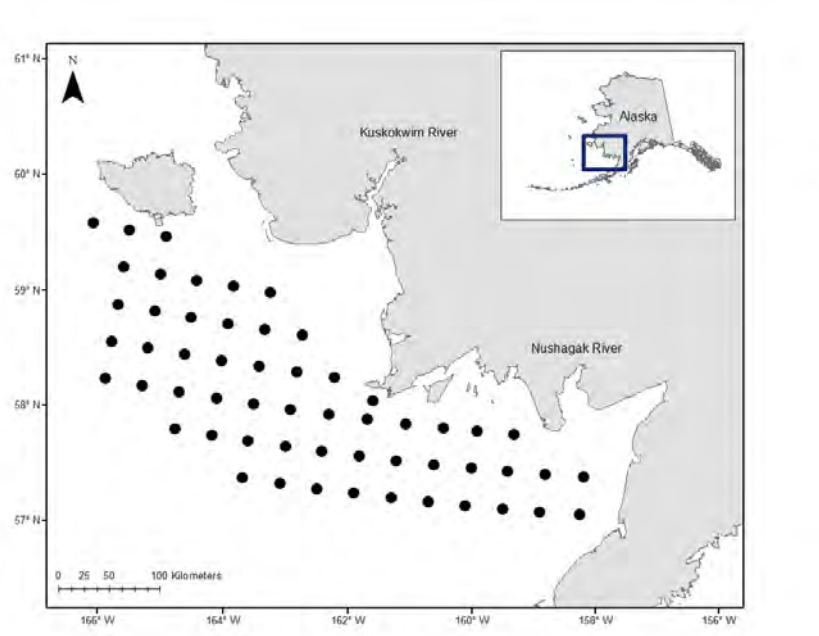


Figure 103: Southern Bering Sea juvenile salmon survey stations. At each station, water column properties, such as temperature and salinity, were measured using a CTD; water samples were collected for eDNA, nutrient, and chlorophyll-a analyses; a Calvet and bongo net were towed to collect zooplankton; and a 1-hr surface trawl was conducted to sample juvenile salmon and other pelagic fish.

Table 7: Salmon and forage fish catch data (all age classes combined) from the southern Bering Sea juvenile salmon survey, 2024-2026. Total catch numbers include a sum of all salmon and forage fishes captured per year, while total number of fish species captured (per year) includes a count of salmon, forage fishes, and other fish species not classified as forage fishes.

	Survey Year		
Group, species	**2024**	**2025**	**2026**
Salmon			
Chinook salmon	316	149	155
Chum salmon	1,349	2,712	1,407
Coho salmon	256	236	228
Pink salmon	84	4,175	2
Sockeye salmon	571	4,064	2,280
Forage fishes			
Capelin	15	0	0
Pacific cod	524	1	11
Pacific herring	324	68,062	6,246
Pacific sandfish	104	304	3,205
Pacific sand lance	2,255	534	5,057
Rainbow smelt	45	3	162
Saffron cod	0	0	2
Walleye pollock	64,668	26,162	7,007
Total salmon plus forage fishes	70,511	106,402	25,761
Total number of fish species captured	27	29	33

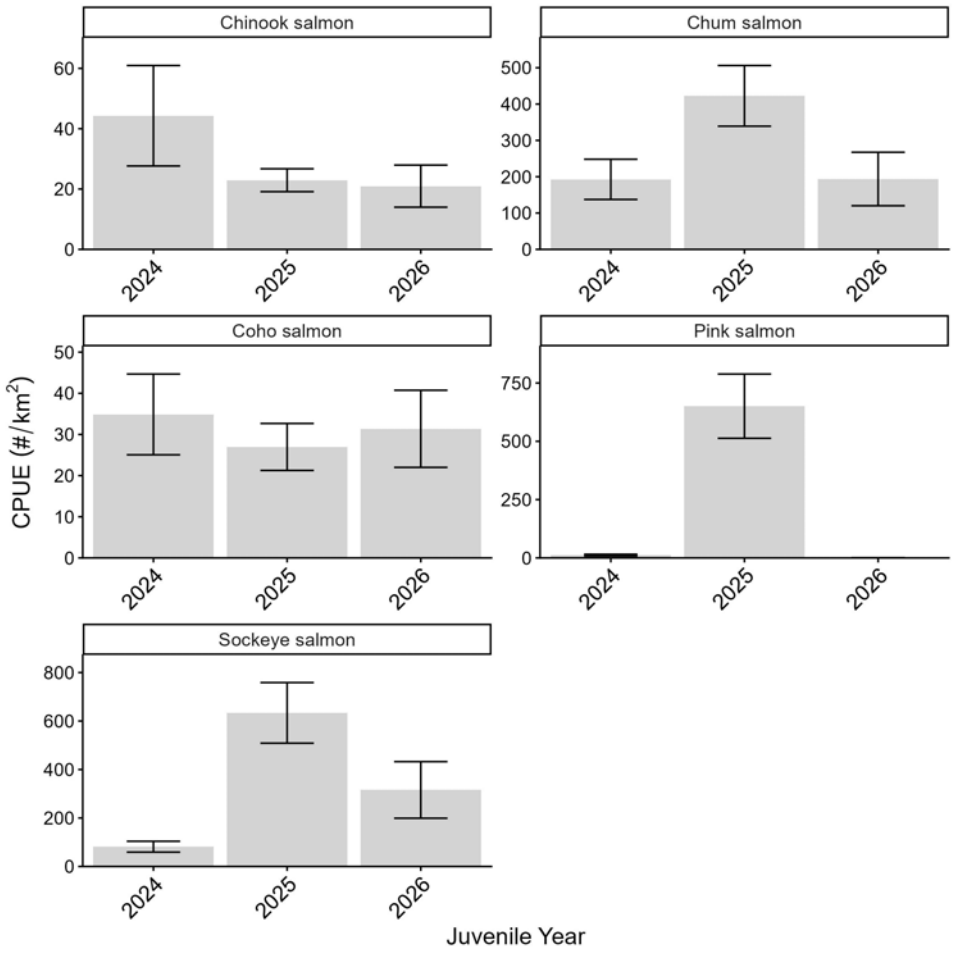


Figure 104: Catch-per-unit-effort (CPUE; number of fish/km^2) of the five species of juvenile salmon caught during surface trawl operations in the southern Bering Sea between 2024-2026. Error bars represent one standard error above and below the average CPUE.

Juvenile Salmon Condition Trends in the Eastern Bering Sea

Contributed by Emily Fergusson, Rob Suryan, Todd Miller, Jim Murphy, and Alex Andrews
Auke Bay Laboratories, Alaska Fisheries Science Center, NOAA Fisheries, Juneau, AK
Contact: emily.fergusson@noaa.gov
Last updated: October 2026

Description of indicator: The eastern Bering Sea surface trawl surveys consist of multidisciplinary research in the northern Bering Sea (NBS) and southeastern Bering Sea (SEBS) that support sampling of fish, zooplankton and lower trophic levels, and oceanographic conditions. The NBS survey occurs annually in late summer (September), and covers the inner domain (bottom depths generally <55 m) waters between 60°N–66.5°N. The SEBS survey occurs biennially in late summer (odd years, August-September) within the middle to outer domains (50-200 m, 55°N–60°N).

Juvenile pink (*Oncorhynchus gorbuscha*), chum (*O. keta*), sockeye (*O. nerka*), coho (*O. kisutch*), and Chinook (*O. tshawytscha*) salmon nutritional condition data were collected from two fisheries-independent surveys. We present 2026 energy density anomalies of juvenile salmon in relation to the time series of fish condition. Energy density trends over time can represent the condition of juvenile salmon and other taxa in response to climate and ocean conditions during early marine residency.

Status and trends: For the NBS in 2026, energy density anomalies (ED, kJ/g dry weight) varied among juvenile salmon species (Figure 105). Pink salmon ED remained above average and consistent with 2025 levels. Chum salmon ED dropped from above-average 2025 levels down to average, while sockeye salmon ED fell from average 2025 levels to below average. Both coho and Chinook salmon ED were above average, though both dropped compared to 2025 levels.

For the SEBS in 2026, ED anomalies were below average for juvenile pink, chum, sockeye, and Chinook salmon, consistent with values since 2022 (Figure 106). No juvenile coho salmon samples were available for ED analysis in the SEBS in 2026.

Factors influencing observed trends: During early marine entry and residency, juvenile salmon must grow quickly to avoid predation while also acquiring enough lipid reserves to survive winter when food is severely limited (Beamish and Mahnken, 2001; Moss et al., 2005). For the NBS, the decrease in energy density indicates a shared functional response to SST values in the Bering Sea. While 2026 SSTs mirrored 2025 levels, cooler bottom temperatures combined with shallow mixed-layer depths forced juvenile salmon into colder waters (NOAA unpublished data). As a mechanism for salmon condition, direct effects of SST on metabolic demands reduce energy available for reserves, while indirect effects alter prey dynamics. Counterintuitively, although the lipids of available prey were higher than in 2025 (see p. 129), the overall energy density of the juvenile salmon was lower. This suggests that despite the presence of more lipid-rich prey, environmental drivers and metabolic constraints further constrained the salmon's capacity to convert prey lipids into energy reserves needed for overwinter survival.

In the SEBS, juvenile salmon energy density has similarly remained low, continuing a persistent downward trend observed since 2022. Despite surface temperatures remaining relatively consistent over this period, zooplankton prey in the SEBS have exhibited higher lipid content compared to previous years. This disconnect mirrors the dynamics seen in the NBS in 2026, where improved prey quality has not translated into higher energy reserves for juvenile salmon, pointing toward broader ecological or bioenergetic constraints across the Bering Sea shelf.

Implications: Juvenile pink, chum, coho, and Chinook salmon entered the NBS in 2026 with average to positive energy stores, which may contribute to higher overwinter survival (when food is limited) and higher adult returns. The juvenile salmon in the SEBS showed ED anomaly values that were more consistent with lower energy stores and a reduced capacity for overwinter survival.

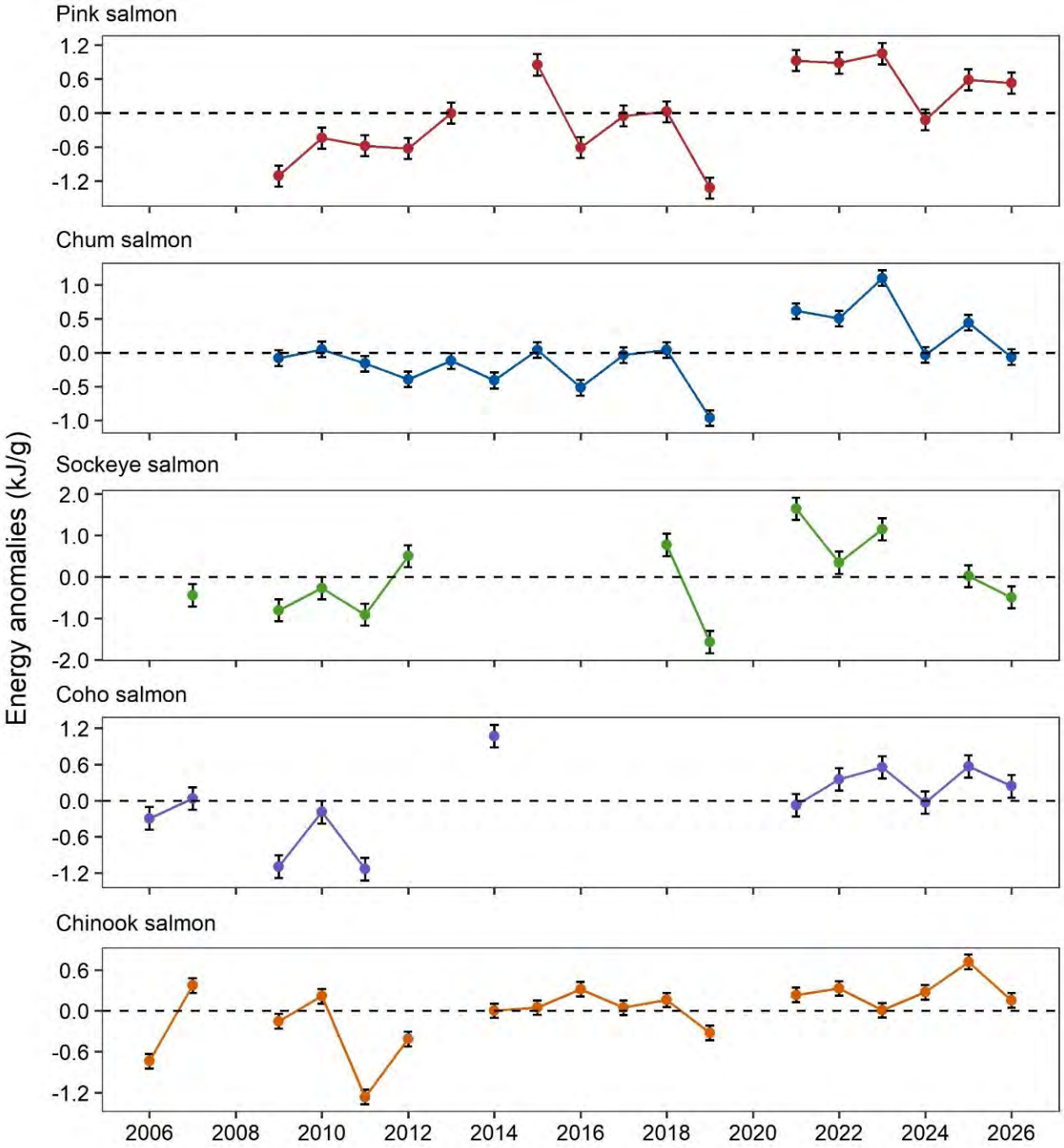


Figure 105: Energy density anomalies (kJ/g, dry weight; ±1 SE) of juvenile salmon captured in the northern Bering Sea, 2006-2026. Time series average is indicated by the dashed line.

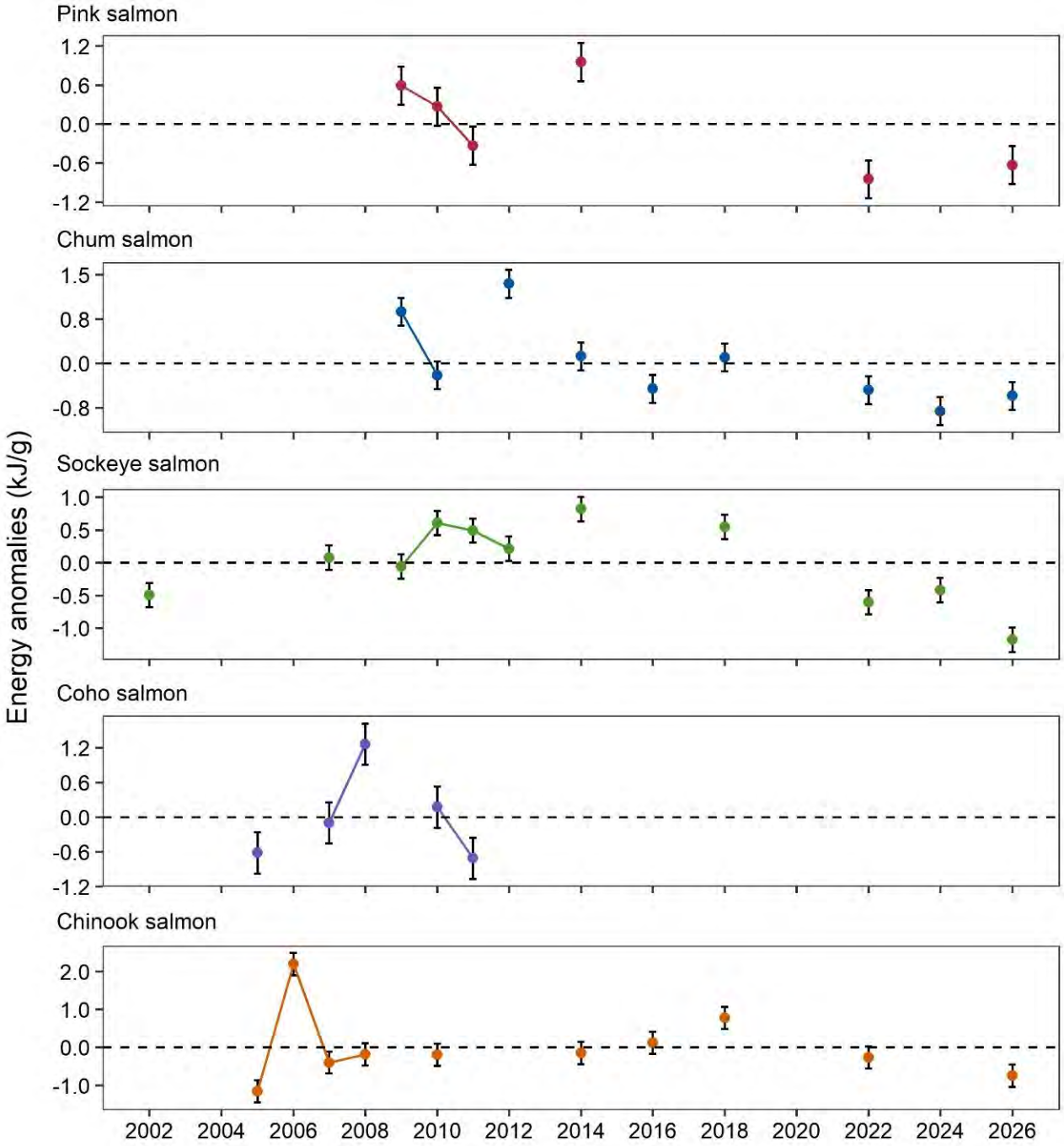


Figure 106: Energy density anomalies (kJ/g, dry weight; ±1 SE) of juvenile salmon captured in the southeastern Bering Sea, 2002-2026. Time series average is indicated by the dashed line.

Northern Bering Sea Juvenile Salmon Abundance Indices

Contributed by Jim Murphy[1], Sabrina Garcia[2], Ben Gray[2], Elizabeth Lee[2], Todd Miller[1], Emily Fergusson[1], Curry Cunningham[3], and Kathrine Howard[1]
[1]Auke Bay Laboratories, Alaska Fisheries Science Center, NOAA Fisheries, Juneau, AK
[2]Alaska Department of Fish & Game, Anchorage, AK
[3]College of Fisheries and Ocean Sciences, University of Alaska Fairbanks, Juneau, AK
Contact: jim.murphy@noaa.gov
Last updated: October 2026

Description of indicator: Mixed-stock juvenile (first year at sea) Chinook salmon (*Oncorhynchus tshawytscha*) abundance indices are estimated from late summer (September) surface trawl catch-per-unit-effort (CPUE) data and adjusted for mixed-layer depth in the northern Bering Sea (NBS). This mixed-stock index provides a rapid assessment of all juvenile Chinook salmon stocks present in the NBS and is different from the stock-specific abundance estimates of Yukon River Chinook salmon that are used to forecast future run sizes.

Abundance indices for Yukon River Fall Chum salmon (*O. keta*)(Upper Yukon River genetic stock group) are based on CPUE data from surveys in both the northern and southern Bering Sea. While NBS surveys occur annually, the southern Bering Sea (SBS) survey occurred annually between 2003-2012 and then even-year only through 2026 (with 2020 missed due to the COVID-19 pandemic). The preliminary 2026 CPUE index was generated using the average genetic stock proportion from 2022 to 2024 and will change once stock compositions from 2025 and 2026 become available.

Juvenile pink salmon (*O. gorbuscha*) abundance indices are calculated similarly to those detailed above for Chinook salmon. Mixed-stock, juvenile pink salmon CPUE data from the NBS survey are ln-transformed by station, adjusted by station-specific mixed-layer depth to depth sampled ratios, and averaged by year to create a yearly abundance index. This index was originally developed with a goal of forecasting adult returns to the NBS region (Yukon River and Norton Sound combined). In recent years, due to data incompleteness issues within the Yukon River region, the focus has shifted to using the juvenile abundance index to forecast an index of adult returns to Norton Sound.

Status and trends: The mixed-stock abundance of juvenile Chinook salmon in the NBS in 2026 is 2.5 million, slightly more than double the record low abundance of 1.04 million in 2024. However, juvenile Chinook salmon abundance has varied from 1.04 million to 5.82 million, and the 2026 index was below the 2003-2025 average of 2.76 million (Figure 107). The 2026 stock-specific CPUE index for the Fall Chum salmon stock is 41.8, below the time series average of 48.1 (Figure 108). The 2026 juvenile pink salmon mixed-stock CPUE index of abundance is 1.14. This value is below the even-year juvenile pink salmon abundance index time series average of 2.18 (Figure 109).

Factors influencing observed trends: Early life-history (freshwater and early marine) survival and adult spawning escapement are the key factors that determine juvenile Chinook salmon abundance in the NBS. The parent year spawning escapement for Yukon River Chinook salmon improved slightly in 2024, and parasitic infections (*Ichthyophonus*) have declined in the adult population (JTC, 2026). Although juvenile abundance still remains below average, these factors are believed to be contributing to the improved abundance of juvenile Chinook salmon. Fall chum salmon abundance indices have been variable over the survey time series. Juvenile chum salmon are believed to disperse out of the northern Bering Sea faster than other species.

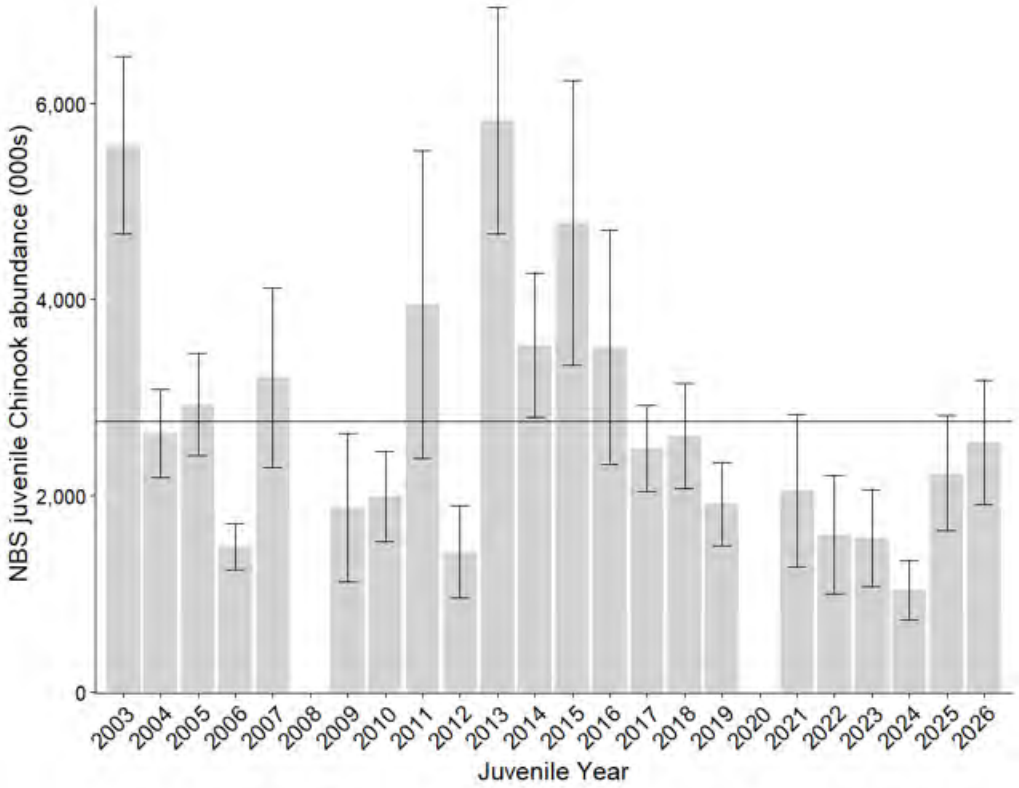


Figure 107: Juvenile Chinook salmon abundance estimates in the northern Bering Sea (NBS), 2003-2026. Error bars are one standard deviation above and below juvenile abundance estimates. The solid black line identifies the average abundance of juvenile Chinook salmon in the NBS across the time series (2.76 million).

Inter-annual differences in abundance may reflect changes in dispersal speeds as well as annual differences in stock composition estimates. However, like other juvenile salmon species, environmental conditions during the early marine life history may also play a role. The observed trends seen for juvenile pink salmon abundance are related in part to spawning escapement, environmental conditions faced during early life-history (freshwater and early marine), and energetic status attained prior to the first winter spent at sea.

Implications: As juvenile Chinook salmon abundance is significantly correlated with adult returns within the Yukon River, fishery managers and subsistence fishers should expect run sizes to recover to near average three to four years in the future (juveniles typically remain at sea for three to four years before returning to freshwater to spawn). Although the condition (energy density) of juvenile Chinook was slightly above average in 2026 (see p. 181) it is unlikely to improve the abundance-based outlook as we have not observed a significant connection between their condition and survival. The condition (energy density) of juvenile chum salmon was average in 2026 (see p. 181), which may contribute to better overwinter survival. A stable relationship between juvenile abundance and adult returns hasn't been established for Yukon River fall chum salmon. The 2022 and 2023 CPUE indices were both below average but returns from the cohorts contributed to an average fall chum salmon return in 2026. Similar to juvenile Chinook salmon, the mixed-stock abundance index for juvenile pink salmon is significantly correlated with adult returns to Norton Sound (Murphy et al., 2025). The below average even-year juvenile pink salmon index in 2026 likely indicates a below average odd-year adult return to Norton Sound in 2027.

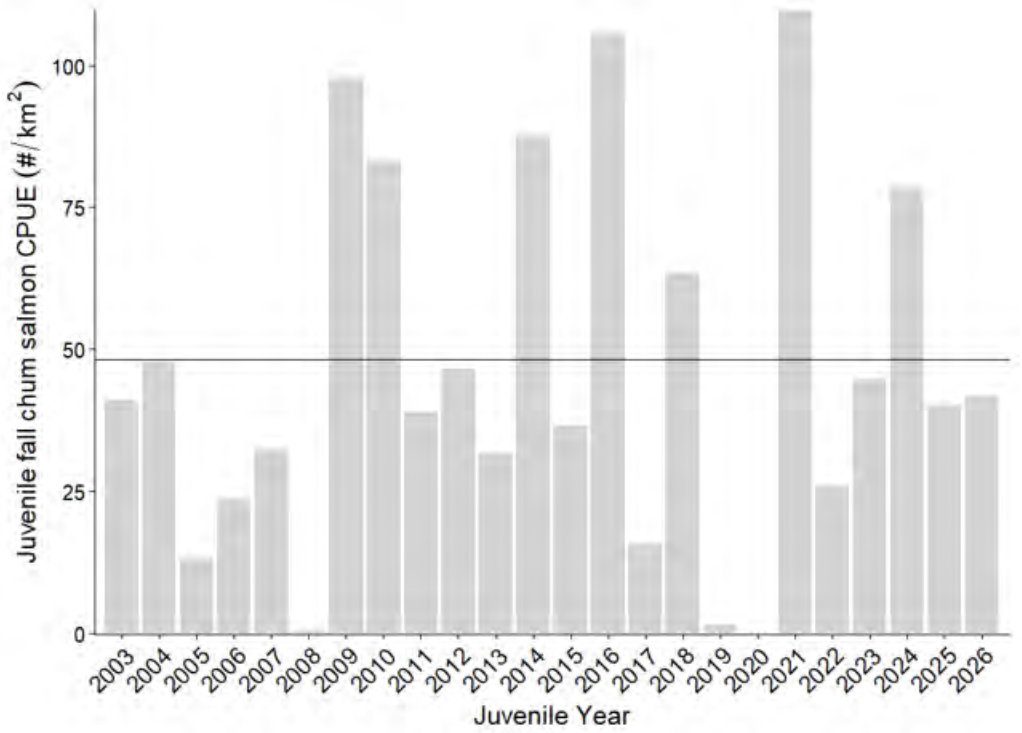


Figure 108: Juvenile chum salmon abundance index (#/km^2) for the Upper Yukon River (fall chum) stock group, 2003-2026. No NBS survey occurred in 2008 and neither survey operated in 2020. The 2025 and 2026 abundance indices were generated using the average genetic stock proportion from 2022 to 2024 and will change once the stock composition from those years becomes available. Dashed line indicates the average juvenile chum salmon index across years 2003-2026 (40.81).

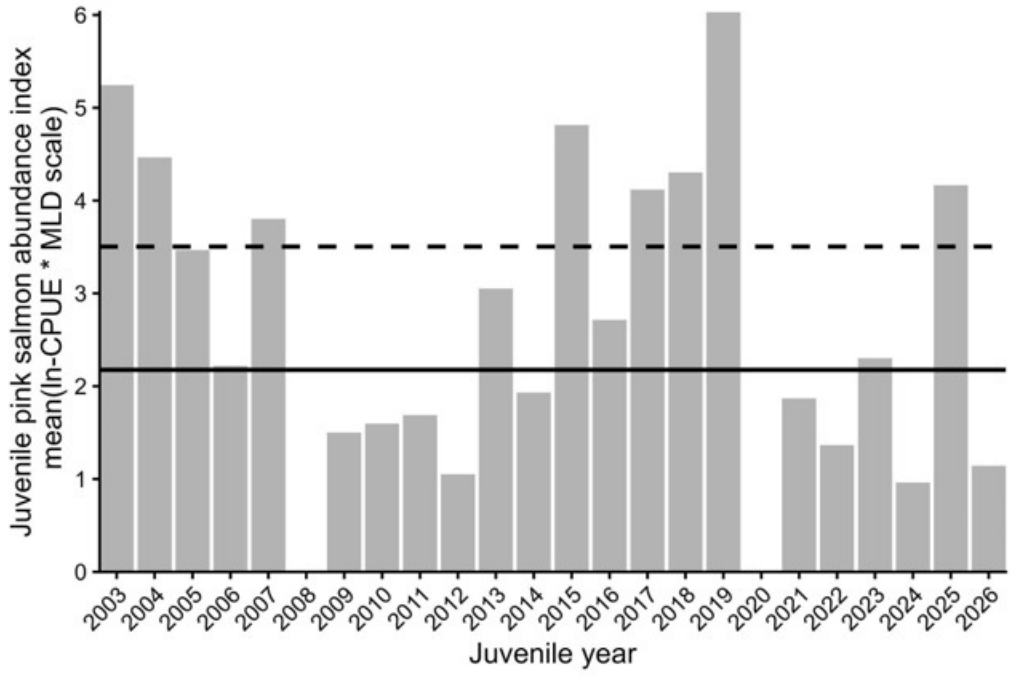


Figure 109: Juvenile pink salmon abundance index in the northern Bering Sea (NBS), 2003-2026 (no survey 2008 and 2020). The abundance index is for mixed stocks of juvenile pink salmon in the NBS and is developed by taking the yearly average of station-specific ln-transformed CPUE ($\#/km^2$) scaled by the station-specific ratio of mixed-layer depth (m) to trawl-footrope depth (m). The dashed line indicates the average odd-year juvenile pink salmon abundance index across years 2003 to 2026, and the solid line indicates the even-year average.

Temporal Trend in the Annual Inshore Run Size of Bristol Bay Sockeye Salmon (Oncorhynchus nerka)

Contributed by Curry J. Cunningham[1], Stacy Vega[2], and Jasmine Terry-Shindelman[2]
[1]College of Fisheries and Ocean Sciences, University of Alaska Fairbanks, Juneau, AK
[2]Alaska Department of Fish & Game, Anchorage, AK
Contact: cjcunningham@alaska.edu
Last updated: October 2026

Description of indicator: The annual abundance of adult sockeye salmon (*Oncorhynchus nerka*) returning to Bristol Bay, Alaska is enumerated by the Alaska Department of Fish and Game (ADF&G). The total inshore run in a given year is the sum of catches in five terminal fishing districts plus the escapement of sockeye to nine major river systems. Total catch is estimated based on the mass of fishery offloads and the average weight of individual sockeye within time and area strata. Escapement is the number of fish successfully avoiding fishery capture and enumerated during upriver migration toward the spawning grounds, or through post-season aerial surveys of the spawning grounds (Elison et al., 2018). Although there have been slight changes in the location and operation of escapement enumeration projects and methods over time, these data provide a consistent index of the inshore return abundance of sockeye salmon to Bristol Bay since 1963.

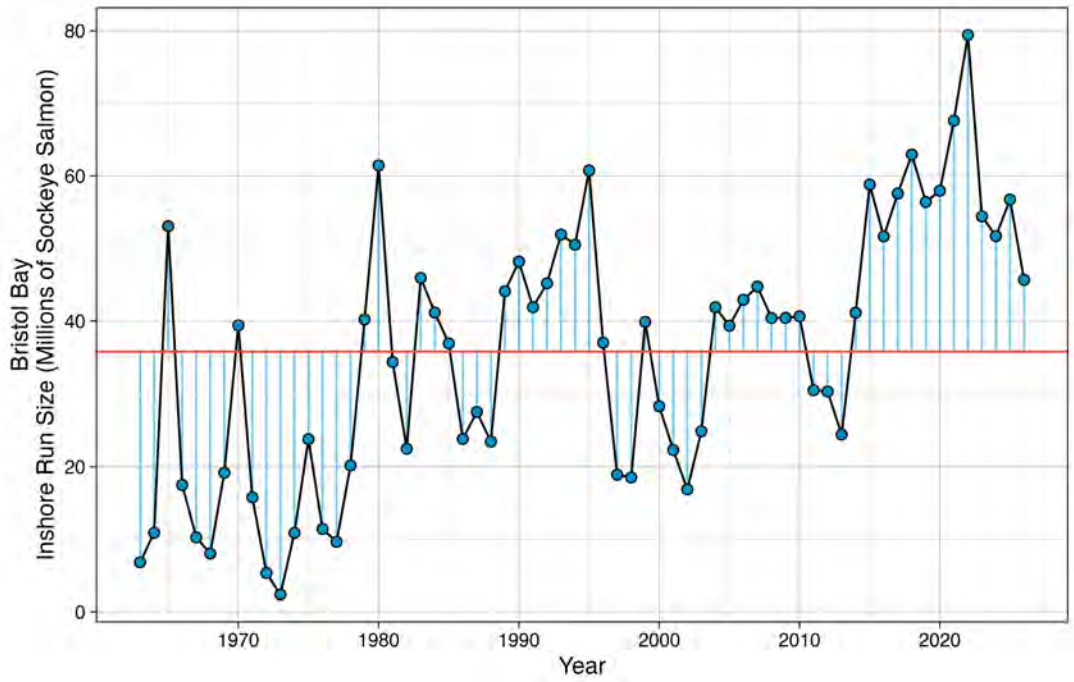


Figure 110: Annual Bristol Bay sockeye salmon inshore run size 1963-2026. Red line is the time series average of 35.8 million sockeye.

Status and trends: The 2026 Bristol Bay preliminary inshore run estimate of 45.7 million sockeye salmon is 23.4% lower than the recent 10-year average of 59.6 million sockeye, and 27.7% higher than the 1963-2025 average of 35.8 million sockeye salmon. The 2026 inshore run represents a continued decrease from the record high Bristol Bay runs sizes observed in 2021-2022, and the first year since 2014 with a run size of less than 50 million sockeye salmon (Figure 110).

Note: *At this time 2026 Bristol Bay inshore run size numbers are preliminary and subject to change.*

Factors influencing observed trends: The return abundance of Bristol Bay sockeye salmon is positively correlated with the Pacific Decadal Oscillation (Hare et al., 1999), specifically with Egegik and Ugashik district run sizes increasing after the 1976/1977 regime shift (Figure 111). However, recent research has highlighted that relationships between salmon population dynamics and the PDO may not be as consistent as once thought, and may in fact vary over time (Litzow et al., 2020*a*,*b*). The abundance and growth of Bristol Bay sockeye salmon has also been linked to the abundance of pink salmon (*Oncorhynchus gorbuscha*) in the North Pacific (Ruggerone and Nielsen, 2004; Ruggerone et al., 2016).

Implications: The record high inshore runs of Bristol Bay sockeye salmon in 2021-2022, and above-average run sizes 2015-2025, indicate overall positive survival conditions for these stocks while in the ocean. Given evidence that the critical period for sockeye salmon survival occurs during the first summer and winter at sea (Beamish and Mahnken, 2001; Farley et al., 2007, 2011) and the predominant age classes observed for Bristol Bay stocks are 1.2, 1.3, 2.2, and 2.3 (European designation: years in freshwater - years in the ocean), the extremely large 2021-2022 inshore run sizes suggests these salmon experienced positive conditions at entry into the eastern Bering Sea in the summers of 2019 and 2020, and winters of 2019-2020 and 2020-2021. However, the lower overall magnitude of the 2026 inshore run, which was predominantly comprised of the 1.2 and 1.3 age classes, suggests lower survival at ocean entry in 2023-2024 for cohorts originating from the 2021-2022 brood years. In considering the impact of immature sockeye salmon as foragers in the eastern Bring Sea, recent inshore runs suggest a progressive reduction in their aggregate consumption potential between 2020 and 2024.

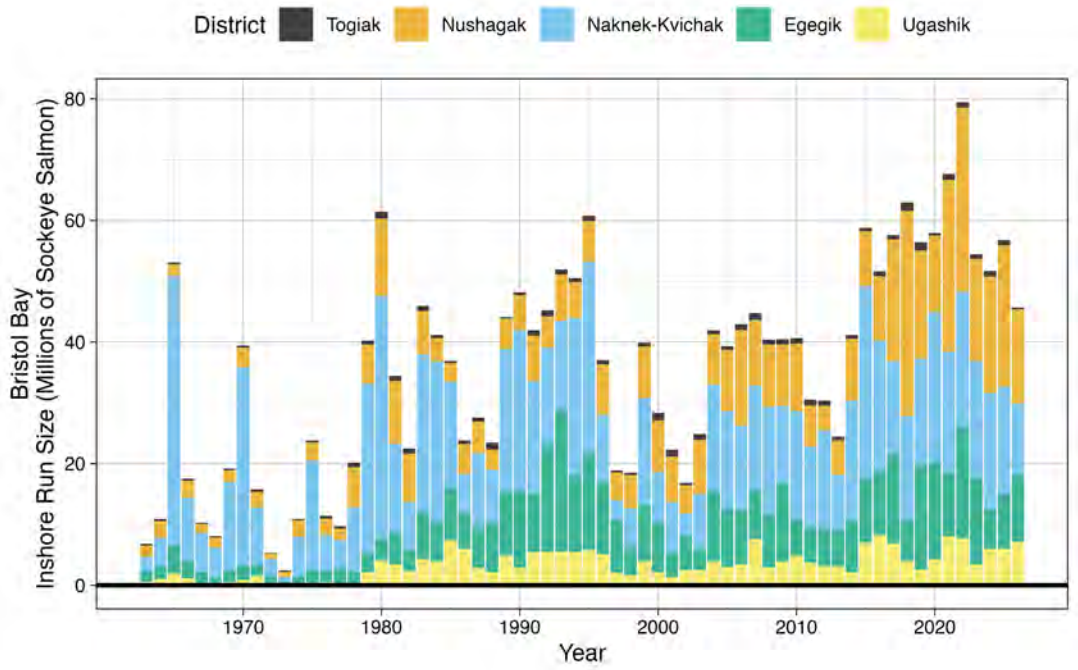


Figure 111: Annual Bristol Bay sockeye salmon inshore run size 1963-2026 by commercial fishing district.

Trends in Alaska Commercial Salmon Catch – Bering Sea

Contributed by George A. Whitehouse
Cooperative Institute for Climate, Ocean, and Ecosystem Studies (CICOES), University of Washington, Seattle, WA
Contact: gaw@uw.edu
Last updated: October 2026

Description of indicator: This contribution provides historic and current commercial catch information for salmon of the Bering Sea. This contribution summarizes data and information available in current Alaska Department of Fish and Game (ADF&G) reports (e.g., Gleason and Munro, 2026) and on their website[22].

Pacific salmon in Alaska are managed in four regions based on freshwater drainage basins[23]: Southeast/Yakutat, Central (encompassing Prince William Sound, Cook Inlet, and Bristol Bay), Arctic-Yukon-Kuskokwim, and Westward (Kodiak, Chignik, and Alaska peninsula). ADF&G prepares harvest projections for all areas rather than conducting run size forecasts for each salmon run. There are five Pacific salmon species with directed commercial fisheries in Alaska; they are sockeye (*Oncorhynchus nerka*), pink (*O. gorbuscha*), chum (*O. keta*), Chinook (*O. tshawytscha*), and coho (*O. kisutch*) salmon.

Status and trends:
Statewide
Combined catches from directed fisheries on the five salmon species have fluctuated over recent decades but in total have been strong statewide (Figure 112). The salmon commercial harvests from 2025 totaled 197 million fish, which was 17 million less than the preseason forecast of 214 million fish. In particular, the 2025 total commercial harvest of 120 million pink salmon was below the harvest projection of 138 million. While the 2026 harvest data are not yet final, preliminary data from ADF&G for 2026 indicates a statewide total commercial salmon harvest of about 83 million fish (as of 25 September), which is below the preseason projection of 125 million fish. Individually, the preliminary statewide sockeye salmon harvest of 33.9 million fish is approximately 16 million below the projected harvest.

Bering Sea
Salmon harvests in the Bering Sea are numerically dominated by the catch of sockeye in Bristol Bay (Figure 113). The 2025 Bristol Bay sockeye salmon run of 56.7 million and the harvest of 41.3 million were both greater than the preseason forecasts. Preliminary data for 2026 from ADF&G shows that the commercial harvest of Bristol Bay sockeye salmon of 30 million fish will be just below the preseason forecast of 33 million. The 2026 preliminary commercial harvest of other species in the Bering Sea were approximately 11,000 Chinook, 457,000 chum, 666,000 pink, and 56,000 coho salmon.

Chinook salmon abundance in the Arctic-Yukon-Kuskokwim region has been low since the mid-2000s and remains low. From 2008 to 2025, no commercial periods targeting Chinook salmon were allowed in the Yukon Management Area. Preliminary data for 2026 indicate that Chinook salmon escapement goals will not likely be met for the Yukon Area. In 2025, Chinook salmon did meet the drainage-wide sustainable escapement goal for the Kuskokwim River.

[22] https://www.adfg.alaska.gov/
[23] https://www.adfg.alaska.gov/index.cfm?adfg=commercialbyfisherysalmon.salmonareas

In 2025, summer and fall chum salmon did not meet the sustainable escapement goals in the Yukon Area. There were no commercial salmon harvests during the summer or fall seasons on the Yukon River in 2025. Preliminary data for 2026 in the Yukon River indicates that fall chum escapement goals are likely to be met.

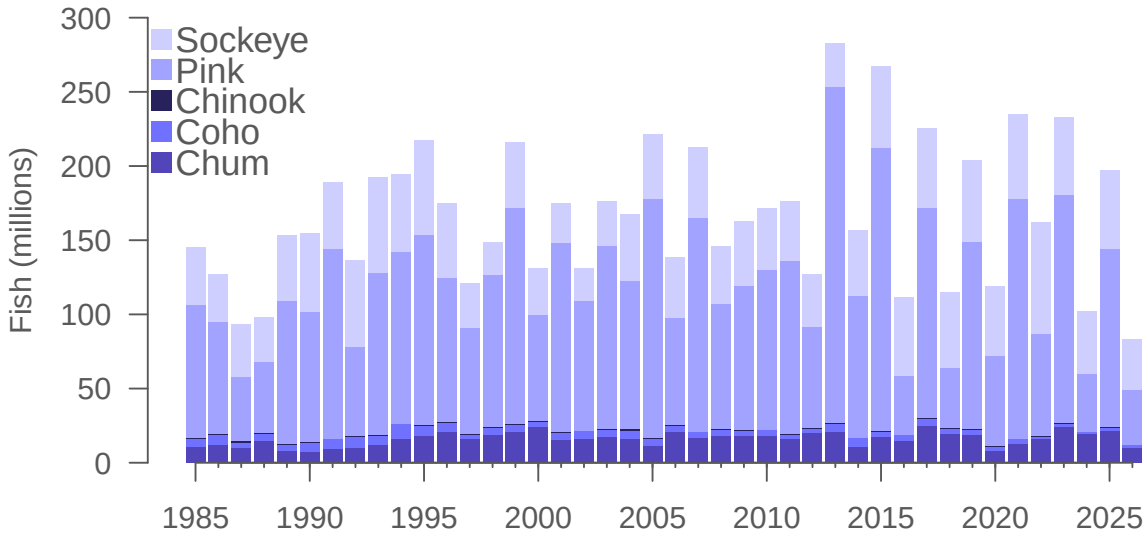


Figure 112: Alaska statewide contemporary commercial salmon catches, 2026 values are preliminary. Source: ADF&G, `http://www.adfg.alaska.gov`. ADF&G is not responsible for errors or deficiencies in the reproduction, subsequent analysis, or interpretation of data.

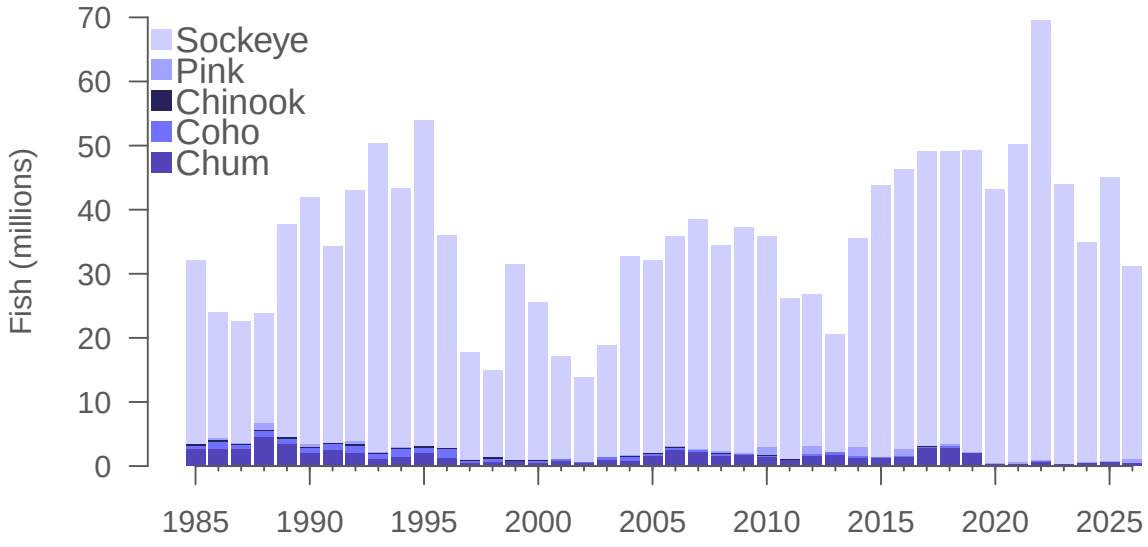


Figure 113: Contemporary commercial salmon catches in the eastern Bering Sea, 2026 values are preliminary. Source: ADF&G, `http://www.adfg.alaska.gov`. ADF&G is not responsible for errors or deficiencies in the reproduction, subsequent analysis, or interpretation of data.

Factors influencing observed trends: Salmon have complex life histories and are subject to stressors in the freshwater and marine environments, as well as anthropogenic pressures. These forces do not affect all species and stocks equally or in the same direction, and resolving what is driving the population dynamics of a particular stock is challenging (Rogers and Schindler, 2011). Interannual variation in Alaska statewide total salmon abundance is partly due to the even-year, odd-year cycle in pink salmon, particularly production from the Prince William Sound stock of pink salmon, which typically have larger runs in odd years. Chinook runs have been declining statewide since 2007. Size-dependent mortality during the first year in the marine environment is thought to be a leading contributor to low Chinook run sizes (Beamish and Mahnken, 2001; Graham et al., 2019). Rising sea temperatures and loss of sea ice may be contributing factors leading to slower growth for juvenile Chinook salmon in the eastern Bering Sea (Yasumiishi et al., 2020). Additionally, warming water temperatures and low stream discharges during adult spawner migrations may reduce Chinook salmon reproductive success (Howard and von Biela, 2023). Warming water temperatures have also been linked to lower quality prey and lower energy density of juvenile chum salmon (Kaga et al., 2013; Farley Jr et al., 2024).

Salmon may also be caught as bycatch in Bering Sea groundfish trawl fisheries, most of which are Chinook and chum salmon. The North Pacific Fishery Management Council has implemented a number of management measures and incentives that have been successful at reducing Chinook salmon bycatch in groundfish trawl fisheries since their peak in 2007 (Stram and Ianelli, 2015). However, the bycatch of non-chinook salmon (i.e., chum) has trended upward since 2012 and in 2021 was at its highest level since 2005[24].

In the Bering Sea, sockeye salmon are the most abundant salmonid and since the early 2000s, they have had consistently strong runs, which have supported large harvests. Bristol Bay sockeye salmon display a variety of life history types and use a diverse range of habitats for spawning (Hilborn et al., 2003). Productivity within these various habitats may be affected differently depending upon varying conditions, such as climate (Mantua et al., 1997), so more diverse sets of populations provide greater overall stability (Schindler et al., 2010). The abundance of Bristol Bay sockeye salmon may also vary over centennial time scales, with brief periods of high abundance separated by extended periods of low abundance (Schindler et al., 2006).

Implications: Salmon have important influences on Alaska marine ecosystems through interactions with marine food webs as predators on lower trophic levels and as prey for other species such as Steller sea lions. In years of great abundance, salmon may exploit prey resources more efficiently than their competitors. In odd years when pink salmon are most abundant, they can initiate pelagic trophic cascades (Batten et al., 2018) which may negatively impact the growth and population dynamics of several other species, including other salmonids, forage fishes, seabirds, and whales (Ruggerone et al., 2023; Rand and Ruggerone, 2024). A biennial pattern in seabird reproductive success has been attributed to a negative relationship with years of high pink salmon abundance (Springer and van Vliet, 2014). Directed salmon fisheries are economically important for the state of Alaska. The trend in total statewide salmon catch in recent decades has been for strong harvests, despite annual fluctuations and lower catches for some species in specific management areas.

Measures to reduce salmon bycatch can affect the spatial distribution of groundfish trawl fisheries through area closures and incentives to avoid bycatch. When the aggregate Chinook salmon run size in the Kuskokwim, Unalakleet, and Upper Yukon Rivers is less than 250,000, a lower limit to Chinook bycatch is imposed on the pollock fishery.

[24] https://www.npfmc.org/wp-content/PDFdocuments/bycatch/BeringSeaSalmonBycatchFlyer.pdf

Synthesizing Indicators of Yukon and Kuskokwim Salmon Health and Abundance for a 2027 Outlook

Contributed by Terese Vicente[1], Vanessa von Biela[2], Janessa Newman[3], Diloola Erickson[4], Jacqueline Muehlbauer[4], Erik Schoen[5], Megan Williams[6], Justin Leon[1], Andrew Magel[1], Patricia Chambers[6], Daniel Auerbach[1], Nicholas Jacuk[6], Craig Chythlook[3], and Jim Simon[3]

[1]Kuskokwim River Inter-Tribal Fish Commission (KRITFC), Bethel, AK
[2]U.S. Geological Survey, Alaska Science Center, Anchorage, AK
[3]Yukon River Inter-Tribal Fish Commission (YRITFC), Fairbanks, AK
[4]Tanana Chiefs Conference, Fairbanks, AK
[5]International Arctic Research Center, University of Alaska Fairbanks, Fairbanks, AK
[6]Arctic & Northern Waters Program, Ocean Conservancy, Anchorage, AK

Contact: terese@kritfc.org
Last updated: October 2026

Description of indicator: Key ecological and anthropogenic factors affect salmon species at different life stages, providing insight into current and projected salmon status. This contribution examines indicators of Yukon and Kuskokwim Chinook and chum and Kuskokwim sockeye salmon health (including disease, body size, and energetic condition) and abundance by life stage, beginning with parent spawners in 2021-2023, for the cohorts rearing in the North Pacific and/or returning to rivers as adult spawners in 2027. While not a predictive forecast for salmon abundance or returns in 2027, this contribution contextualizes recent data on life-stage-specific indicators of Yukon and Kuskokwim salmon status to understand projected trends.

Status and trends: In 2026, Yukon and Kuskokwim watersheds continued to experience below-average Chinook salmon spawner abundance, with significant impacts to regional health and food security, cultures, economies, and ecosystems[25] (KRITFC, 2024). Meanwhile, Yukon summer and fall chum salmon stocks and Kuskokwim chum salmon stocks showed returns closer to historic levels, allowing for limited subsistence harvest opportunities (except for mainstem Yukon fall chum to protect poor-performing Canadian-origin fall chum)[25]. Conditions of chum salmon spawners on both rivers and of Kuskokwim Chinook salmon were reported as healthy and of larger size. However, there were some reports of white-spotted heart tissue and soft flesh in some Yukon Chinook salmon in 2026, indicative of *Ichthyophonus* infection. These observations were generally consistent with the outlook provided in last year's contribution to the 2025 Eastern Bering Sea Ecosystem Status Report (ESR; the 2025 ESR was not produced; the contribution is available upon request). In contrast, Kuskokwim sockeye salmon abundance was below average in 2026[25], which did not align with the outlook for above average adult spawner abundance from last year's contribution.

[25]AYK Database Management System. Alaska Department of Fish and Game: Commercial Fisheries Division. Available at `https://www.adfg.alaska.gov/CF_R3/external/sites/aykdbms_website/Default.aspx`.

The 2027 outlook for each species is as follows:

- Chinook: Anticipated poor abundance and average health.
- Chum: Anticipated poor abundance and below-average health.
- Sockeye: Anticipated average abundance and health.

This outlook does not account for the very strong El Niño forecast for late 2026 to early 2027, which could reduce the 2027 cohorts' health and abundance through food web disruption[26],[27].

Factors influencing observed trends: The outlooks for each species were developed by synthesizing information about life-stage-specific indicators, beginning with the likely parent spawners of the 2027 cohorts (2021 and 2022 for Chinook salmon; 2022 and 2023 for chum and sockeye salmon). Indicators were considered during the river (parent spawners, egg incubation, freshwater rearing, outmigration) and marine (ocean entry, marine rearing) phases. Primary indicators evaluated include physical environmental conditions, drivers of salmon health, species interactions, and anthropogenic factors. Indicators presented in this synthesis are classified as standout (i.e., anomalous or significant events documented during the time frame) or persistent (i.e., consistent patterns or trends). Indicators were identified using Local and Traditional Knowledge in addition to Western science.

Each indicator and its likely effect on the 2027 cohorts is described below and summarized in Figure 114. The absence of a species evaluation indicates that the effect of the indicator on that species is unknown or not applicable.

Parent spawner abundance (standout): The abundance of parent year classes of salmon is correlated with the abundance of recruits (future spawners), especially for chum and sockeye salmon (Gleason and Munro, 2026).

- Chinook: Unfavorable effect due to below average abundance in 2021 and 2022[25], and record-low return of Yukon Chinook in 2022 (JTC, 2023).
- Chum: Unfavorable effect due to below average abundance in 2022 and 2023[25].
- Sockeye: Favorable effect due to near average abundance of river-type spawners in 2022, above-average returns of river-type spawners in 2023, and above-average returns of lake-type spawners in 2022 and 2023[25].

Ichthyophonus (standout): The *Ichthyophonus* pathogen, particularly prevalent in female and large Chinook salmon, is suspected to cause high rates of premature mortality (Kocan et al., 2004; Zuray et al., 2012; Jallen et al., 2023; Wilber et al., 2026)[28].

- Chinook: Unfavorable effect due to high Ichthyophonus prevalence and severity in 2021 and 2022 (Jallen et al., 2023; JTC, 2023).

[26] https://www.cpc.ncep.noaa.gov/products/analysis_monitoring/enso_advisory/ensodisc.pdf.

[27] https://www.usgs.gov/mission-areas/ecosystems/news/what-a-super-el-nino-could-mean-alaskas-seabirds-salmon-and-seas.

[28] https://yukonsalmon.org/yukon-fisheries-news-fall-2020/.

Body size (persistent): Long-term declines in adult salmon body size, particularly for Chinook, are linked to younger age-at-return, smaller and fewer eggs, reduced productivity, and reduced resilience to migration stressors such as streamflow, temperature, and disease (Oke et al., 2020; Feddern et al., 2024; Ohlberger et al., 2020, 2025).

- Chinook: Unfavorable effect due to parent spawner body sizes in 2021 and 2022 at or below the 10-year average at all sampling stations in each watershed[25].
- Chum: Unfavorable effect due to parent spawner body sizes in 2022 and 2023 below the 10-year average at all sampling stations in each watershed[25].
- Sockeye: Mixed effect due to parent spawner body sizes below the 10-year average in 2022 and above the average in 2023[25].

Freshwater temperature (standout): Optimal water temperatures for adult Pacific salmon are typically 7-15°C; warmer temperatures are associated with heat stress and mortality of adults and of eggs still inside females (McCullough, 1999). In the Yukon and Kuskokwim regions heat stress has been confirmed in Chinook salmon beginning at ∼18°C (von Biela et al., 2026). During the 2019 heatwave, mortality observations of Chinook and chum salmon coincided with river temperatures reaching ∼21°C (von Biela et al., 2022).

- Chinook: Favorable effect due to water temperatures primarily <18°C for both rivers in 2021-2022[25],[29].
- Chum: Mixed effect due to water temperatures primarily <18°C in 2022 for both rivers and Kuskokwim River in 2023, but >21°C in the Yukon River in 2023[25],[29].
- Sockeye: Favorable effect due to Kuskokwim River temperatures primarily <18°C in 2022-2023[25].

Pike predation (persistent): Traditional Knowledge holders have observed increasing abundance of Northern pike, a predator of salmon eggs and fry, raising concern for depressed salmon populations.

- Chinook, chum, and sockeye: Unfavorable effect, though extent unknown.

Fall flood events (standout): High streamflows during spawning and egg incubation have been associated with reduced productivity of Chinook salmon in the Yukon River (Feddern et al., 2024).

- Chinook: Unfavorable effect due to record rainfall and high water events across the Yukon in 2021 (JTC, 2022) and high water events in the Kuskokwim in 2022, potentially exacerbated by ex-Typhoon Merbok (KRITFC, 2022; Whitworth et al., 2023)[30].

[29] `https://aktemp.uaa.alaska.edu/`.
[30] `https://akclimate.org/widespread-storm-damage-along-the-west-coast/`

Spring breakup/flood events (standout): Late spring breakup in the smolt outmigration year has been associated with reduced productivity of Yukon River Chinook salmon (Cunningham et al., 2018). High water levels and discharge in the spring may displace newly emerged Chinook and chum fry (JTC, 2022).

- Chinook: Unfavorable effect due to extreme breakup flood events in the Yukon and Kuskokwim drainages in 2023[31] and late spring breakup in both rivers in 2023[32]. Breakup dates in both rivers were average in 2024[32].
- Chum: Unfavorable effect due to extreme breakup flood events in the Yukon and Kuskokwim drainages in 2023[31].

Wildfires (standout): Wildfires and fire suppression may harm freshwater juvenile salmon by raising water temperatures, eroding stream banks, releasing retardant into waterways, and spreading invasive species through lake water used for suppression, as documented in other regions (Roon et al., 2025) and observed by Local and Traditional Knowledge holders.

- Chinook and sockeye: Unfavorable effect due to widespread wildfire instances in 2022 throughout the Yukon-Kuskokwim region[33],[34],[35] and in the Canadian Yukon River drainage in 2023[36].

Juvenile abundance (standout): The first year-at-sea is critical for Chinook salmon survival to adulthood (Murphy et al., 2017). Abundance of juvenile Chinook salmon is correlated with abundance of future returns on the Yukon (Murphy et al., 2017, 2024). There is no established link between juvenile abundance and future adult returns for chum or sockeye salmon.

- Chinook: Unfavorable effect for Yukon salmon due to northern Bering Sea juvenile abundance below average in 2023 and at a record-low in 2024 (Murphy et al., 2024). No southeastern Bering Sea (Kuskokwim) data for 2023 and 2024.

Juvenile condition (standout): Higher energy density in first year-at-sea juvenile salmon is associated with greater stomach fullness, overwinter survival, and health, especially for chum salmon (Farley Jr et al., 2024; Fergusson et al., 2024).

- Chinook: Favorable effect due to above average energy density in the northern Bering Sea (Yukon) in 2023 and 2024 (Fergusson et al., 2024). No southeastern Bering Sea (Kuskokwim) data for 2023 or 2024.
- Chum: Mixed effect due to above average energy density in the northern Bering Sea (Yukon salmon) in 2023 and average in 2024, but below average energy density in the southeastern Bering Sea (Kuskokwim salmon) in 2024 (Fergusson et al., 2024).
- Sockeye: Mixed effect due to above average energy density in the northern Bering Sea (Yukon salmon) in 2023, but below average in the southeastern Bering Sea (Kuskokwim salmon) in 2024 (Fergusson et al., 2024).

[31] https://ready.alaska.gov/Documents/Sitrep/Archive//2023/5.15.2023%20Spring%20Floods%20SITREP.pdf

[32] https://www.weather.gov/aprfc/breakupdb

[33] https://storymaps.arcgis.com/stories/cf12854b0439415cacd19825f291128f

[34] https://akfireinfo.com/2022/04/27/narrated-aerial-surveillance-flight-infrared-footage-of-kwethluk-fire-april-26-2022/

[35] https://akfireinfo.com/2022/07/14/new-start-near-mcgrath-burns-90-acres/

[36] https://yukon.ca/en/fireline-2023-wildfire-season-review

Sea surface temperature (standout): High sea surface temperatures, including marine heat wave events, negatively affect chum and Chinook salmon by reducing prey availability and increasing metabolic pressure (Farley Jr et al., 2024; DeFilippo et al., 2026).

- Chinook and chum: Favorable effect due to near-average and more stable sea surface temperatures in the northern and southern Bering Sea in 2023 and 2024 (Callahan and Lemagie, 2024), as well as 2025 and 2026[37].

Competition at sea (persistent): The abundance of potential competitors in the ocean, including wild and hatchery-origin pink and chum salmon, has been negatively associated with Chinook salmon productivity in the Yukon and Kuskokwim rivers (Cunningham et al., 2018; Murdoch et al., 2023; Feddern et al., 2024), with the body size of Yukon and Kuskokwim chum salmon (Oke et al., 2020; Ruggerone et al., 2023), and with the body size and productivity of sockeye salmon in Bristol Bay and other parts of Alaska (Ruggerone et al., 2016; Cline et al., 2019; Connors et al., 2020; Rand and Ruggerone, 2024). Alaska is currently the largest producer of hatchery salmon in the North Pacific Ocean (Connors et al., 2025)[38] having released record-high numbers of salmon during 2022-2024 (Wilson, 2026).

- Chinook and chum: Mixed effect due to record-high abundance of pink and chum salmon in 2023, driven primarily by high wild and hatchery production of pink salmon in Alaska and Russia, during ocean entry life stages, and below-average abundance of these species in 2024 and 2025 (Connors et al., 2025, G. Ruggerone, pers. comm.). Data for 2026 are not available.
- Sockeye: Favorable effect due to below-average abundance of pink and chum salmon in 2024 and 2025 (Connors et al., 2025, G. Ruggerone, pers. comm.). Data for 2026 are not available.

Bering Sea bycatch (persistent): Annual genetic studies indicate the Bering Sea pollock trawl fishery catches salmon from Western Alaska rivers, including the Yukon and Kuskokwim: 50.3% of Chinook salmon from 2011-2025, and 18.2% of chum salmon from 2011-2024[39],[40].

- Chinook: Mixed effect due to ongoing but below-average bycatch in 2024, 2025, and 2026 (2011-2023 average is 18,316 fish[41]). Preliminary genetic estimates attribute 51.1% (4,112 fish) of the 2024 bycatch and 73.2% (14,505 fish) of 2025 bycatch to Kuskokwim/Bristol Bay and Yukon stocks, indicating high removals, particularly of the Kuskokwim/Bristol Bay reporting group[39]. Approximately 6,044 of the preliminary 2026 bycatch of 12,017 fish may be from these stocks based on the 50.3% stock composition estimate[41].
- Chum: Mixed effect due to ongoing but below-average bycatch in 2024, 2025, and 2026 (2011-2023 average is 268,777 fish[42]). An estimated 13.1% (4,205 fish) of 2024 bycatch and 4.5% (6,764 fish) of 2025 bycatch was from Western Alaska rivers, including the Kuskokwim and Yukon[43],[44].

[37] https://connect.fisheries.noaa.gov/ak-sst-mhw/

[38] https://www.npafc.org/statistics/

[39] https://meetings.npfmc.org/CommentReview/DownloadFile?p=bbad9f76-b42d-4e69-adb4-6e269dd1c528.pdf&fileName=B10%20Chinook%20Bycatch%20Genetics%20Report.pdf

[40] https://meetings.npfmc.org/CommentReview/DownloadFile?p=e7b2483f-4a64-4019-a91a-841249864f35.pdf&fileName=B2%20Chum%20Salmon%20Genetics%20Report%202025.pdf

[41] https://www.fisheries.noaa.gov/sites/default/files/akro/chinook_salmon_mortality2026.html

[42] https://www.fisheries.noaa.gov/sites/default/files/akro/chum_salmon_mortality2026.html

[43] https://meetings.npfmc.org/CommentReview/DownloadFile?p=845933ce-b9c4-41b7-a380-2df22d8c54a3.pdf&fileName=C2%202024%20Chum%20Salmon%20Bycatch%20Report.pdf

[44] https://meetings.npfmc.org/CommentReview/DownloadFile?p=e7b2483f-4a64-4019-a91a-841249864f35.pdf&fileName=B2%20Chum%20Salmon%20Genetics%20Report%202025.pdf

In-season estimates for bycatch specific to the in-shore pollock trawl sector are 6.4% (4,714 fish) in 2025 and 15.7% (13,778 fish) through October 7, 2026[45],[46].

Alaska Peninsula harvest (persistent): Genetic studies indicate the June and post-June South Alaska Peninsula (Area M) fishery harvests salmon from Western Alaska rivers, including the Yukon and Kuskokwim. Recent analyses estimate this composition at 5.6% of Chinook salmon from 2024-2025[47], and 12.5% of chum salmon across the season, though more concentrated at 24% of chum salmon in the month of June, from 2022-2024[48].

- Chinook: Mixed effect due to ongoing but below-average harvest (2011-2023 average is 15,548 fish[47]), including an estimated 1,350 Kuskokwim/Bristol Bay and Yukon Chinook salmon in 2024-2025[47]. Approximately 255 of the preliminary 2026 harvest of 4,545 fish may be from these stocks based on the 5.6% stock composition estimate[49].
- Chum: Mixed effect due to ongoing but below-average harvest (2011-2023 average is 1,004,156 fish[49]), including an estimated 126,127 Coastal Western Alaska and upper Yukon chum salmon in 2024[48]. Approximately 154,128 of the combined June harvests from 2025 (156,136 fish) and preliminary 2026 (486,068 fish) may be from these stocks based on the 24% stock composition estimate for the June fishery[48],[50].

Implications: Trends in salmon health, particularly for chum salmon, can serve as a proxy for conditions faced by other pelagic foragers such as walleye pollock. Additionally, Yukon and Kuskokwim salmon trends directly affect salmon-dependent communities along these rivers, which are connected to the Bering Sea through salmon. Because Chinook and chum salmon from these and other Western and Interior Alaska rivers are encountered as bycatch in Bering Sea groundfish fisheries, these trends can also help industry and managers anticipate salmon Prohibited Species Catch encounters in the following seasons. Kuskokwim sockeye salmon, rarely encountered in these fisheries, are a key source of food and cultural security amid Chinook and chum salmon declines, and more research is needed on what drives their abundance.

[45] https://www.bbsri.org/_files/ugd/bc10d6_f19738b4145b4f319ca638b8f3ffc94c.pdf

[46] https://static1.squarespace.com/static/5afdc3d5e74940913f78773d/t/6a8764c912ae6e0eda0114b8/1787258057489/BBSRI_Chum+Gen_St+Wk+33_Aug+9-15+2026.pdf

[47] https://www.adfg.alaska.gov/FedAidPDFs/RIR.5J.2026.02.pdf

[48] https://www.adfg.alaska.gov/static/regulations/regprocess/fisheriesboard/pdfs/2025-2026/akpen/FDS25-63.pdf

[49] https://www.adfg.alaska.gov/index.cfm?adfg=commercialbyareaakpeninsula.salmonharvestsummary

[50] https://www.adfg.alaska.gov/static/regulations/regprocess/fisheriesboard/pdfs/2025-2026/akpen/rc3-5.pdf.

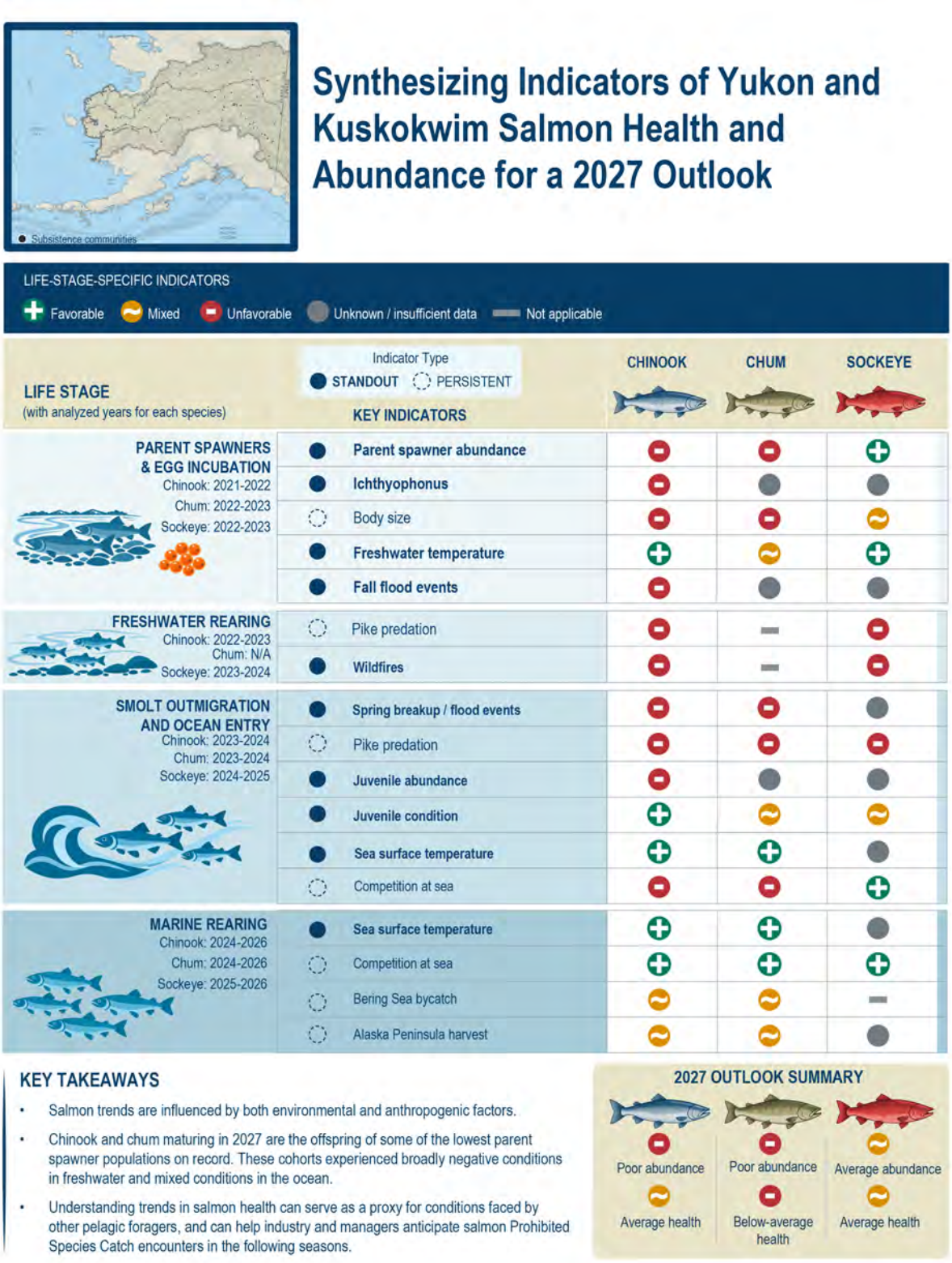


Figure 114: Synthesis of life-cycle stage indicators across the 2027 Chinook, chum, and sockeye salmon cohorts' life history. Colored circles refer to the indicator's effect on salmon for the given time frame, with green/plus sign signifying favorable effects, yellow/tilde signifying mixed effects, and red/minus sign signifying unfavorable effects. Standout indicators are indicated by boldface and solid circles, while persistent indicators are indicated by regular type and open circles.

Groundfish

Summer Food Habits of Walleye Pollock and Pacific Cod

Contributed by Kerim Aydin
Resource Ecology and Fishery Management Division, Alaska Fisheries Science Center, NOAA Fisheries, Seattle, WA
Contact: kerim.aydin@noaa.gov
Last updated: October 2026

Description of indicator: Stomachs of walleye pollock (*Gadus chalcogrammus*) and Pacific cod (*G. macrocephalus*) have been collected on the Alaska Fisheries Science Center's eastern Bering Sea (EBS) shelf survey between 1984-2026; samples were preserved in formalin and prey contents identified to the lowest resolvable taxonomic category and weighed. For key prey items such as snow crab (*Chionoecetes opilio*) or tanner crab (*C. bairdi*), prey size (standard length for fish and carapace width for crabs) was measured when sufficiently intact prey samples were present in predator stomach samples. To estimate diet proportions for the population, samples are stratified by length and survey stratum and weighted by the survey biomass for each length class and stratum and estimated ration for each size class. Collection, analysis, and stratification methods are described in Livingston et al., 2017 while ration estimation is described in Holsman and Aydin, 2015.

Status and trends: Summer pollock diets for the EBS primarily consist of euphausiids, copepods, and other plankton throughout the time series (Figure 115). Euphausiids were lower in importance from 2004-2011 in terms of diet proportion; in particular in 2010-2011 both euphausiids and copepods were low compared to "other" plankton, which was dominated by amphipods in 2010-2011. In 2024, euphausiids declined in region-wide diet compared to copepods, a situation that continued in 2025-2026, when copepods and euphausiids had similar proportions in pollock diets. Cannibalism, as a proportion of overall diet, was a larger component in the 1990s and declined to historic lows in 2018 and 2022-2024; it increased slightly in 2025-2026 but remains low with respect to the long-term average.

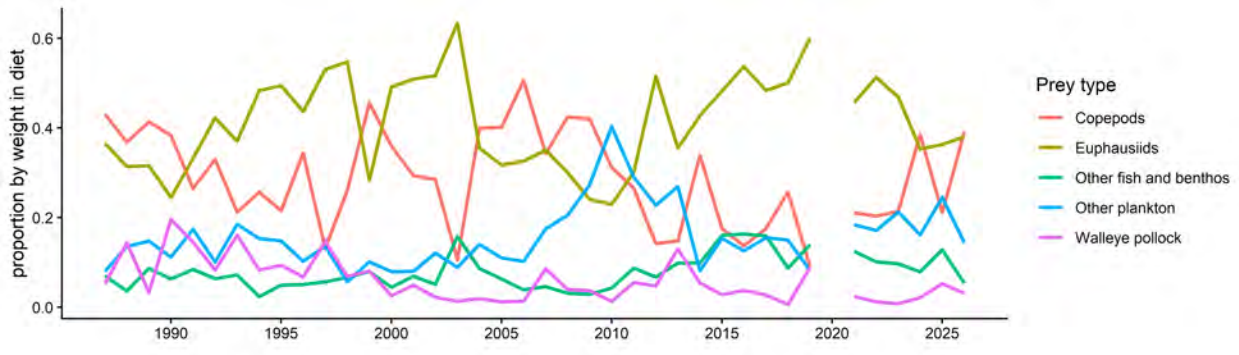


Figure 115: Percent by weight in diet of major prey types of walleye pollock in the eastern Bering Sea, weighted by survey stratum and predator survey biomass in each stratum.

Pacific cod diets included a range of fish and crab species (Figure 116). Feeding on pollock was highest in the late 1980s, declined significantly from 2006-2016, before increasing again in 2019-2026; in 2026 pollock was the largest diet component of cod for the first time since 2005. As a proportion of diet, snow crab feeding was at a high level from 2014-2018; from 2023-2026 snow crab proportion in diet has been stable at a relatively low level.

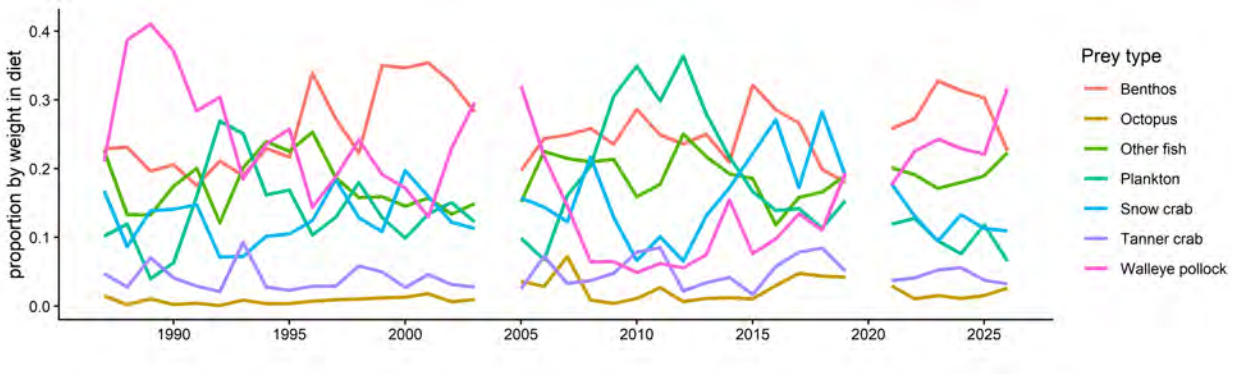


Figure 116: Percent by weight in diet of major prey types of Pacific cod in the eastern Bering Sea, weighted by survey stratum and predator survey biomass in each stratum.

Multiplying the diet proportion of crab in cod stomachs by cod biomass and temperature-adjusted cod ration results in an estimated daily consumption rate of crab during the summer sampling season (Figure 117). The snow crab consumption rate showed particularly high consumption from 2014-2016, and in 2018. Tanner crab consumption shows less variation over the time series and has been nearly constant 2023-2026. The size (carapace width) of snow crab and tanner crab in cod stomachs (Figure 118) show sizes classes corresponding with crab measured directly during the bottom trawl survey, with the addition of potential early signs of crab recruitment showing in cod stomachs before appearing in the survey (e.g., in 2021). In 2026, feeding was spread across multiple crab size classes; 2025 showed a peak of the smallest snow crab sizes for the first time since 2021, while 2026 shows a larger peak of the smallest tanner crab sizes for the first time since 2021.

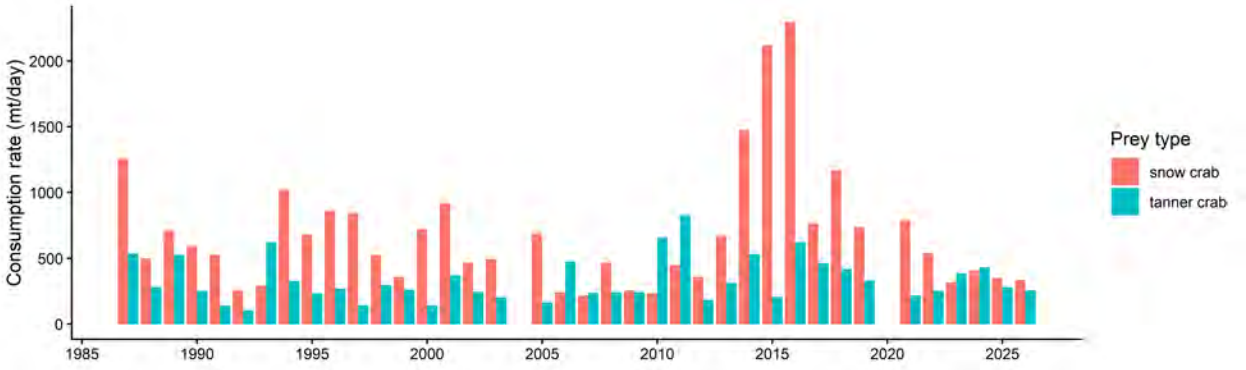


Figure 117: Daily consumption rate of snow crab by Pacific cod, calculated by multiplying the diet proportion in each survey strata with cod biomass-at-length from the survey data and temperature-specific cod daily ration-at-length using methods described in Holsman and Aydin, 2015.

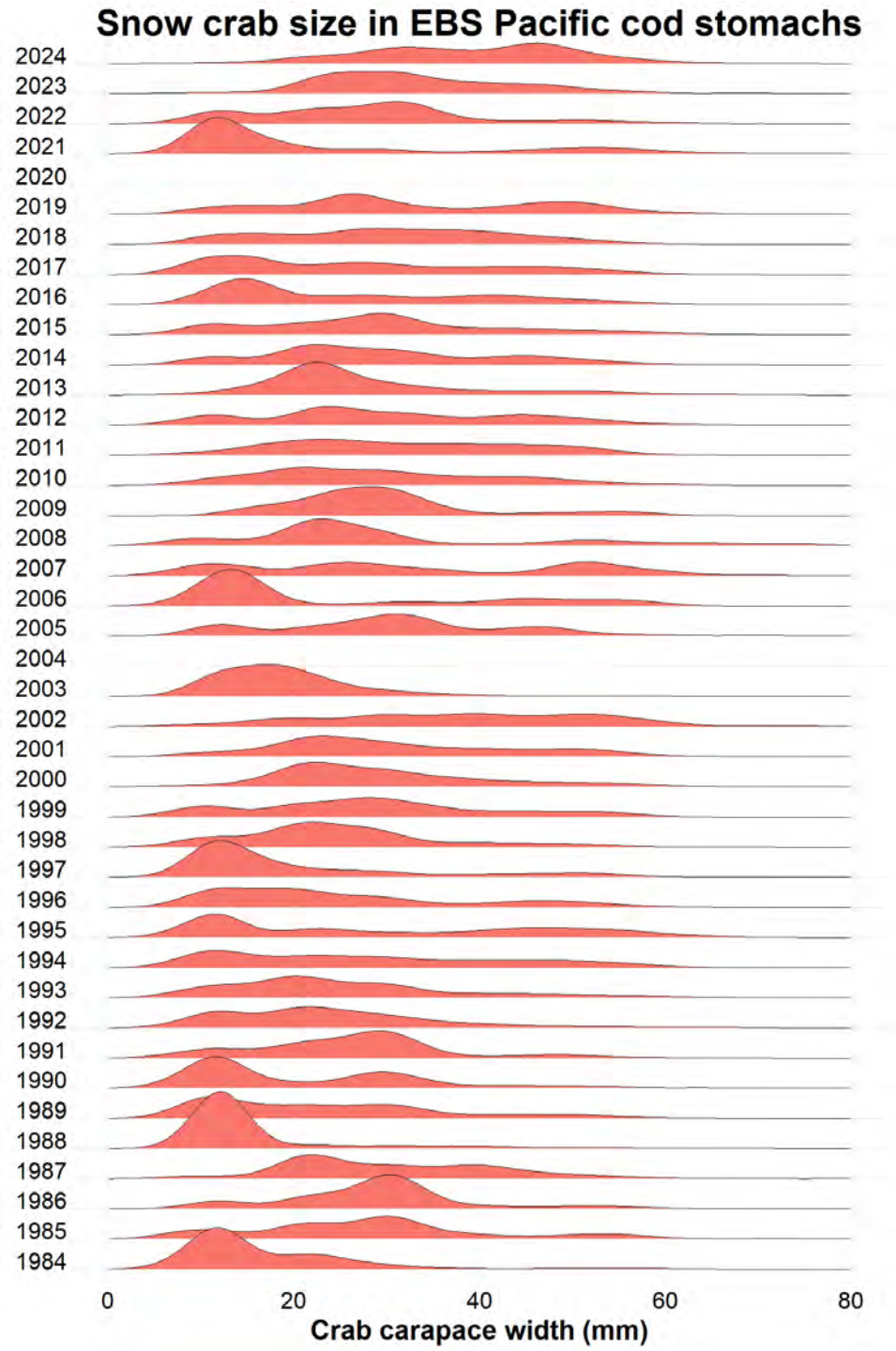


Figure 118: Carapace width frequencies of measurable snow crab (*Chionoecetes opilio*, left panel) and tanner crab (*C. opilio*, right panel) removed from Pacific cod stomachs in the EBS, 1987-2026.

Factors influencing observed trends: When viewing population-level consumption across the entire EBS, shifts in diet proportion may come from changes in prey populations within a single strata; however, the shifts may also be due to changes in predator distribution between strata or differences in the size composition of the predator population as age classes with differing feeding ontogeny move through the ecosystem.

In particular, in 2024-2026 the high proportion of copepods in pollock diets (Figure 115) was due to a larger proportion of the total pollock biomass being distributed on the northwest outer shelf, where larger oceanic copepods from the Bering Sea shelf break and basin form the bulk of diets in most years. It is not known if this distribution shift is due to better-than-typical foraging of copepods on the outer shelf versus poorer production in the middle domain, where euphausiids are the prominent diet item. The other major ecosystem shift visible in the data came in 2009-2011 when both euphausiids and copepods were lower in diets in favor of "other" zooplankton, primarily consisting of amphipods. This shift came with historic highs in the EBS cold pool extent and represents the influence of more Arctic zooplankton species associated with the larger cold pool.

For Pacific cod, there was a notable decline of pollock in diets from 2008-2013, again likely due to the large cold pool limiting overlap between these species (Figure 116). Cod diets showed increased plankton consumption during these years, in particular focusing on colder-water shrimp species. From 2014-2019, the prominence of snow crab in diets (Figure 117) was likely a "bottom-up" effect, as a large cohort of crab were in evidence in both the stomachs and survey data. Similarly, the changes in crab carapace width distribution over time (Figure 118) was likely driven by these crab recruitment events. For 2026, the high pollock consumption may be due to both cod size composition and cod distribution. Since 2018, cod consumption, in terms of total bottom-trawl survey biomass, has been dominated by cod with fork lengths of 60+ cm that have the most piscivorous diets; conversely, between 2010-2017 the majority of cod consumption was by 30-60 cm fork length cod, with a more benthivorous diet. Moreover, in 2026, cod were far more distributed in the northwest outer domain where juvenile pollock are the most prevalent.

Implications: Changes in diet composition of fish may be an indicator of fish health condition, growth, or later recruitment, and may also signal potential changes in productivity that would come with longer-term climate change. For 2026, diet patterns in the EBS do not indicate dependence on unusual prey types for either pollock or cod, and pollock cannibalism is relatively low, suggesting generally normal/good growth conditions. The increase of pollock in cod diets, and corresponding decrease of snow crab in cod diets, is likely due to greater overlap of cod and pollock in the northwest outer domain and out of the middle domain, possibly due to the large cold pool area in the middle domain. This concentration creates a bottom-up effect of more available pollock and does not suggest increased pollock mortality rates at the population level. The peak of small (10-15 mm carapace width) tanner crab in Pacific cod stomachs may be an early indicator of crab recruitment.

Eastern and Northern Bering Sea Groundfish Condition

Contributed by Bianca Prohaska and Sean Rohan
Groundfish Assessment Program, Resource Assessment and Conservation Engineering Division,
Alaska Fisheries Science Center, NOAA Fisheries, Seattle, WA
Contact: bianca.prohaska@noaa.gov
Last updated: September 2026

Description of indicator: Length-weight residuals represent how heavy a fish is per unit body length and are an indicator of somatic growth variability (Brodeur et al., 2004). Therefore, length-weight residuals can be considered indicators of prey availability, growth, general health, and habitat condition (Blackwell et al., 2000; Froese, 2006). Positive length-weight residuals indicate better condition (i.e., heavier per unit length) and negative residuals indicate poorer condition (i.e., lighter per unit length) (Froese, 2006). Fish condition calculated in this way reflects realized outcomes of intrinsic and extrinsic processes that affect fish growth, which can have implications for biological productivity through direct effects on growth and indirect effects on demographic processes, such as reproduction and mortality (e.g., Rodgveller, 2019; Barbeaux et al., 2020).

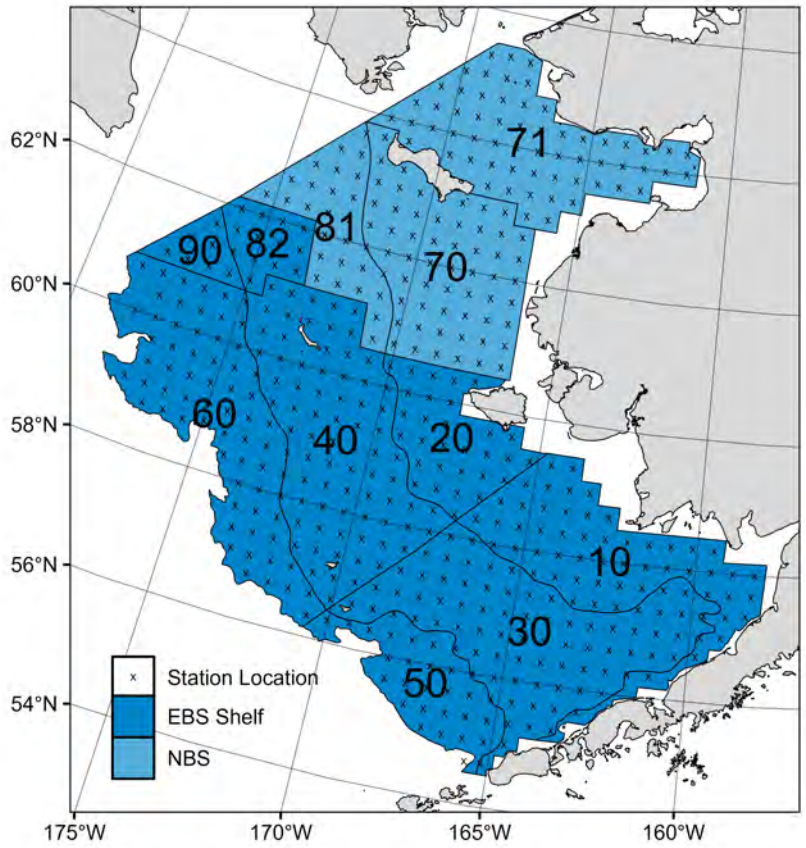


Figure 119: NOAA Alaska Fisheries Science Center summer bottom trawl survey strata (10-90) and station locations (x) in the eastern Bering Sea (EBS) and northern Bering Sea (NBS).

The groundfish morphometric condition indicator is calculated from paired fork lengths (mm) and weights (g) of individual fish that were collected during bottom trawl surveys of the eastern Bering Sea (EBS) shelf and northern Bering Sea (NBS), which were conducted by the Alaska Fisheries Science Center's Resource Assessment and Conservation Engineering (AFSC/RACE) Groundfish Assessment Program (GAP). Fish condition analyses were applied to walleye pollock (*Gadus chalcogrammus*), Pacific cod (*G. macrocephalus*), arrowtooth flounder (*Atheresthes stomias*), yellowfin sole (*Limanda aspera*), flathead sole (*Hippoglossoides elassodon*), northern rock sole (*Lepidopsetta polyxystra*), and Alaska plaice (*Pleuronectes quadrituberculatus*). All species were collected in bottom trawls at standard survey stations (Figure 119). For these analyses and results, survey strata 31 and 32 were combined as stratum 30; strata 41, 42, and 43 were combined as stratum 40; and strata 61 and 62 were combined as stratum 60. Northwest survey strata 82 and 90 were excluded from these analyses.

To calculate indicators, length-weight relationships were estimated from linear regression models based on a log-transformation of the exponential growth relationship, $W = aL^b$, where W is weight (g) and L is fork length (mm) for all areas for the period 1999-2026 (EBS: 1999-2026, NBS: 2010, 2017, 2019, 2021-2023, and 2025). Unique intercepts (a) and slopes (b) were estimated for each species, survey stratum, sex, and interaction between stratum and sex to account for sexual dimorphism and spatial-temporal variation in growth and bottom trawl survey sampling. Length-weight relationships for 100–250 mm fork length walleye pollock (corresponding with ages 1–2 years) were calculated separately from adult walleye pollock ($>$ 250 mm). Residuals for individual fish were obtained by subtracting observed weights from bias-corrected weights-at-length that were estimated from regression models. Length-weight residuals from each stratum were aggregated and weighted proportionally to total biomass in each stratum from area-swept expansion of mean bottom-trawl survey catch per unit effort (CPUE; i.e., design-based stratum biomass estimates). Variation in fish condition was evaluated by comparing average length-weight residuals among years. To minimize the influence of unrepresentative samples on indicator calculations, combinations of species, stratum, and year with a sample size $<$10 were used to fit length-weight regressions, but were excluded from calculating length-weight residuals for both the EBS and NBS. Morphometric condition indicator time series, code for calculating the indicators, and figures showing results for individual species are available through the *akfishcondition* R package and GitHub repository[51].

Methodological Changes: EBS Greenland turbot and Kamchatka flounder condition is presented in 2026 for the first time.

Status and trends:
Eastern Bering Sea: Fish condition, measured by length-weight residuals, has varied over time for all species examined in the EBS (Figures 120 and 121). Changes in condition from 2025 to 2026 differed among species. Condition increased for large walleye pollock ($>$250 mm) and small walleye pollock (100-250 mm), while condition was similar to 2025 observations for Pacific cod, arrowtooth flounder, and flathead sole, and condition decreased for northern rock sole, yellowfin sole, Alaska plaice, Kamchatka flounder, and Greenland turbot. The change in condition from the previous year was approximately one standard deviation or greater for small walleye pollock (100-250 mm) and northern rock sole, and smaller for the remaining species. In 2026, mean condition for all species except small walleye pollock (100-250 mm) and northern rock sole was at or above the time series mean. The mean condition of small walleye pollock (100-250 mm) increased by approximately one standard deviation compared to 2025; however, it remained just below the time series mean. Conversely, large walleye pollock ($>$250 mm) condition was above the time series mean for the first time since 2019. In contrast, northern rock

[51] `https://github.com/afsc-gap-products/akfishcondition`

sole condition decreased to approximately one standard deviation below the time series mean, the lowest level since 2009. Other species remained above the time series mean in 2026: Pacific cod remained at its highest level since 2005, yellowfin sole condition decreased from the highest observed in the time series in 2025 but remained within one standard deviation of the mean, and arrowtooth flounder condition remained the second highest in the time series, behind 2019. Condition of Greenland turbot remained approximately two standard deviations above the time series mean, second only to 2025, and condition of Kamchatka flounder, Alaska plaice, and flathead sole was within approximately one standard deviation above the mean.

In 2026, fish condition was positive across all strata with estimates for yellowfin sole (strata 10, 30, and 40), arrowtooth flounder (strata 30, 40, 50, and 60), Alaska plaice (strata 10 and 40), and Greenland turbot (stratum 60). Condition was negative across all strata with estimates for northern rock sole (strata 10, 20, 30, and 40). For the remaining species, condition differed among strata: large walleye pollock (>250 mm) was positive in strata 20, 40, and 60 but negative in strata 10 and 30; small walleye pollock (100-250 mm) was negative in all strata except the southern middle shelf (stratum 30); Pacific cod was positive in strata 20, 40, 50, and 60 but negative in strata 10 and 30; Kamchatka flounder was positive in strata 40 and 60, but negative in strata 30 and 50; and flathead sole was positive in strata 30 and 40, but negative in strata 10 and 50 (Figure 121).

Northern Bering Sea: The NBS survey was not conducted in 2026; fish condition results through 2025 are presented here. In 2025, positive condition was observed for large walleye pollock (>250 mm), continuing an upward trend observed since 2021. Pacific cod and Alaska plaice exhibited near-average condition, similar to values observed in 2023. Small walleye pollock (100-250 mm) were in below average condition which continued a downward trend since 2021. Yellowfin sole increased slightly from below average condition in 2023 to near-average in 2025 (Figure 122).

In 2025, large walleye pollock (>250 mm) exhibited positive condition in strata 70 and 81, and slightly negative condition in stratum 71. In contrast, small walleye pollock (100-250 mm) and yellowfin sole were in negative condition in all NBS strata in both 2023 and 2025. Pacific cod condition was negative on the outer and inner southern NBS shelf (strata 71 and 81). Alaska plaice condition was positive on the inner southern NBS shelf (stratum 71) and negative in strata 70 and 81 (Figure 123).

Factors influencing observed trends: Bottom and sea surface temperatures during the EBS survey have fluctuated over multidecadal timescales, including a prolonged warm stanza from approximately 2014 through 2019, when both were generally more than one standard deviation above their long-term means (Physical Environment Synthesis, p. 67; Bond et al., 2015; Stabeno and Bell, 2019). Since the 2021 survey, temperatures have generally trended toward or below the long-term mean. Near-average cold pool extent and water temperatures in 2024 were associated with near-average condition (within 1 S.D. of the mean) for all species examined in the EBS that year, while the further warming in 2025 was associated with subsequent increases in fish condition. In the EBS, particularly cold years have historically corresponded with negative condition, while warm years have generally corresponded with positive condition, although this was not the case in 2026, a year featuring the largest survey-observed 2°C cold pool since 2012 and coldest mean bottom temperature since 2013. Spatiotemporal factor analyses suggest the morphometric condition of age-7 walleye pollock is strongly correlated with cold pool extent in the EBS (Grüss et al., 2021). In recent years, warm temperatures across the Bering Sea shelf, following the record low seasonal sea ice extent in 2017-2018 and historical cold pool area minimum in 2018 (Stabeno and Bell, 2019), may have contributed to the positive condition trends observed in several species from 2016 to 2019. However, despite near-average temperatures in 2023, large walleye pollock (>250 mm) condition in the EBS was the second-lowest on record for the time series. In 2024

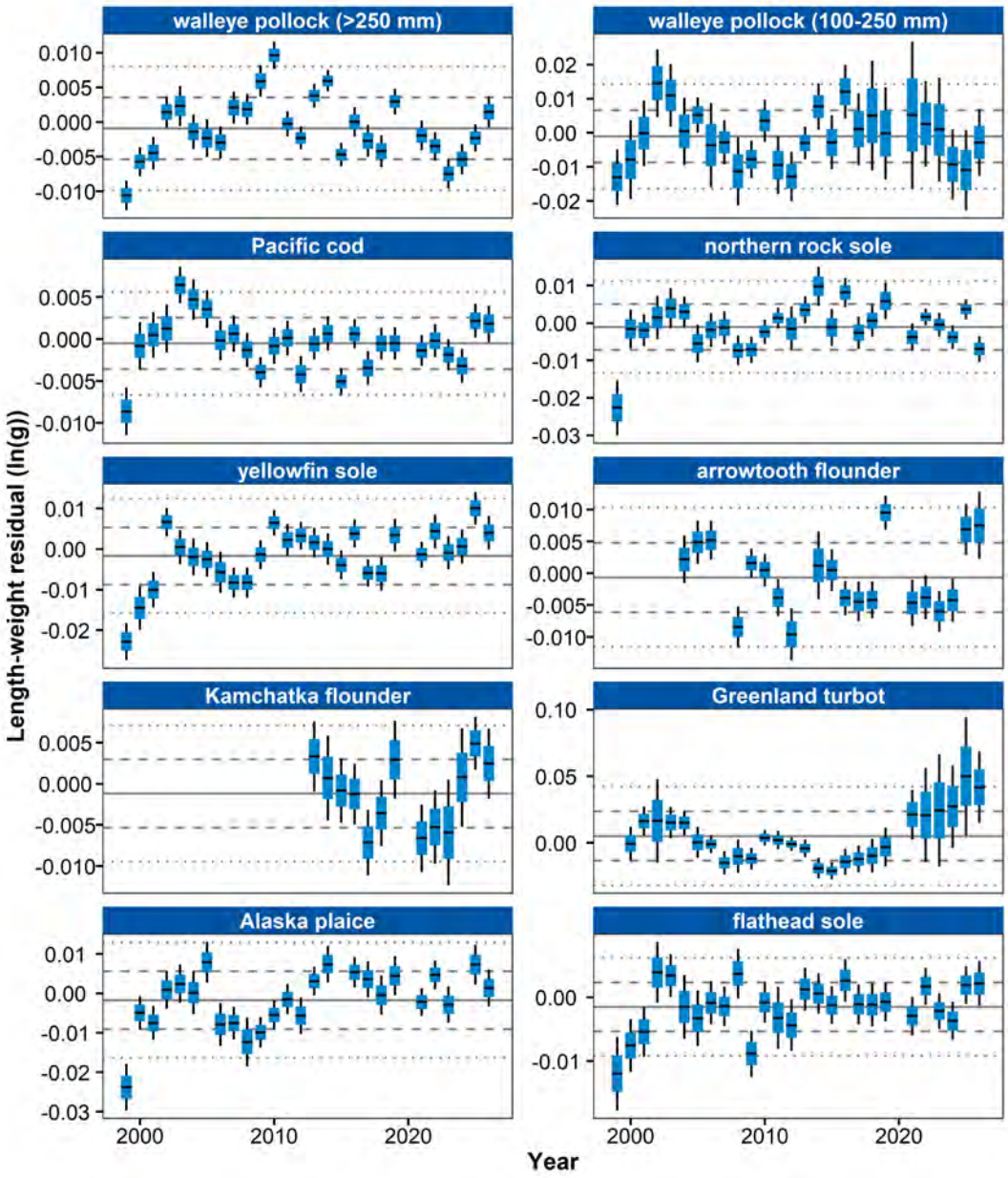


Figure 120: Morphometric condition of groundfish species collected during AFSC/RACE GAP standard summer bottom trawl surveys of the eastern Bering Sea shelf (1999-2026) based on residuals of length-weight regressions. The dash in the blue boxes denotes the mean for that year, the box denotes one standard error, and the lines on the boxes denote two standard errors. Lines on each plot represent the historical mean, dashed lines denote one standard deviation, and dotted lines denote two standard deviations.

and 2025, temperatures again remained near-average, and although large walleye pollock (>250 mm) condition was still negative, it was less so than in 2023. By 2026, with continued near-average water temperature, large walleye pollock (>250 mm) condition improved further and is now slightly above the historical mean for the first time since 2019. Bottom trawl survey biomass estimates for yellowfin sole in the EBS were near their time series minimum for the third consecutive year, although condition reached a record high in 2025 despite near-average temperature conditions. Increasing condition can be

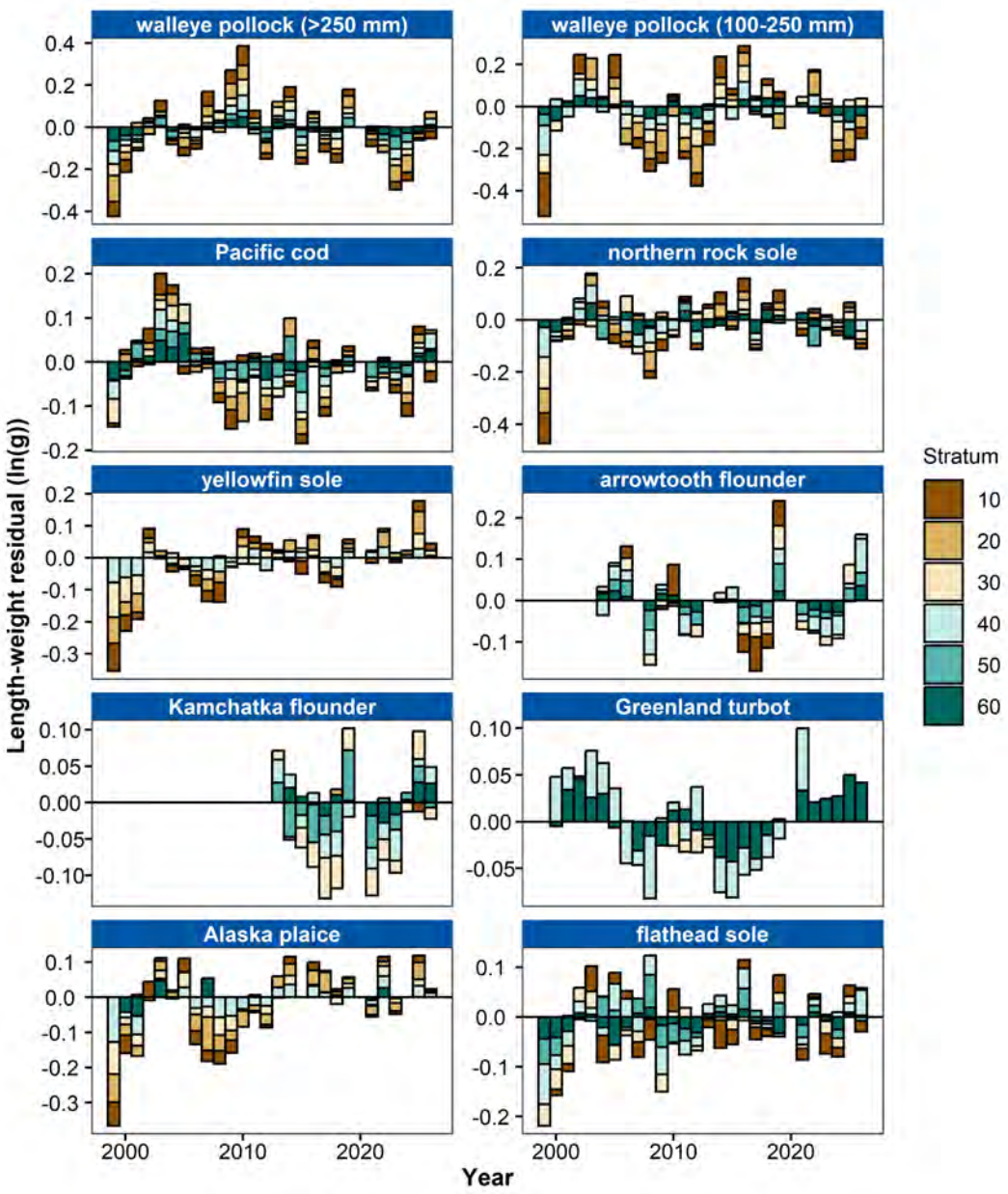


Figure 121: Length-weight residuals by survey stratum (10-60) for seven eastern Bering Sea shelf groundfish species and age 1–2 walleye pollock (100–250 mm) sampled in the AFSC/RACE GAP standard summer bottom trawl survey, 1999-2026. Length-weight residuals are not weighted by stratum biomass.

an indicator of reduced density-dependent competition when populations decline (Haberle et al., 2023), although there is no direct evidence that this is occurring for yellowfin sole in the EBS.

Although warmer temperatures may increase growth rates if there is adequate prey to offset temperature-dependent increases in metabolic demand, growth rates may also decline if prey resources are insufficient to offset temperature-dependent increases in metabolic demand. Therefore, the influence of temperature on growth rates depends on the physiology of predator species, prey availability, and the adaptive capacity of predators to respond to environmental change through migration, changes in behavior, and

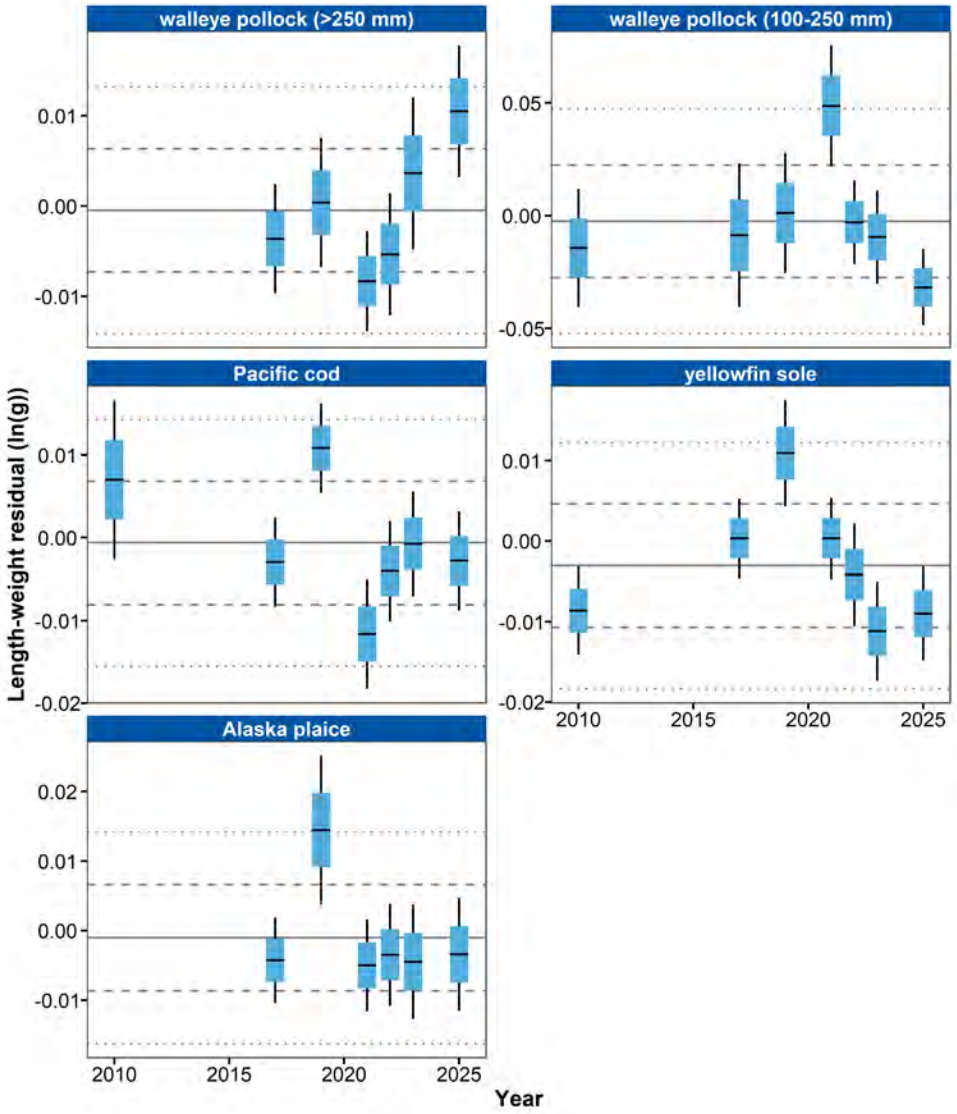


Figure 122: Morphometric condition of groundfish species collected during AFSC/RACE GAP standard summer bottom trawl surveys of the northern Bering Sea shelf (2010, 2017, 2019, 2021-2023, and 2025) based on residuals of length-weight regressions. The dash in the blue boxes denotes the mean for that year, the box denotes one standard error, and the lines on the boxes denote two standard errors. Lines on each plot represent the historical mean, dashed lines denote one standard deviation, and dotted lines denote two standard deviations.

acclimatization. For example, elevated temperatures during the 2014-2016 marine heatwave in the Gulf of Alaska led to lower growth rates and condition of Pacific cod and early life history stages of walleye pollock, because available prey resources did not make up for increased metabolic demand (Barbeaux et al., 2020; Rogers et al., 2021).

Other factors that could affect morphological condition include survey timing, stomach fullness, fish movement patterns, and environmental conditions (Froese, 2006)). The starting date of annual length-weight data collections has varied from late May to early June and ended in late July-early August in the EBS, and mid-August in the NBS. Although stratum-specific coefficients in the length-weight models

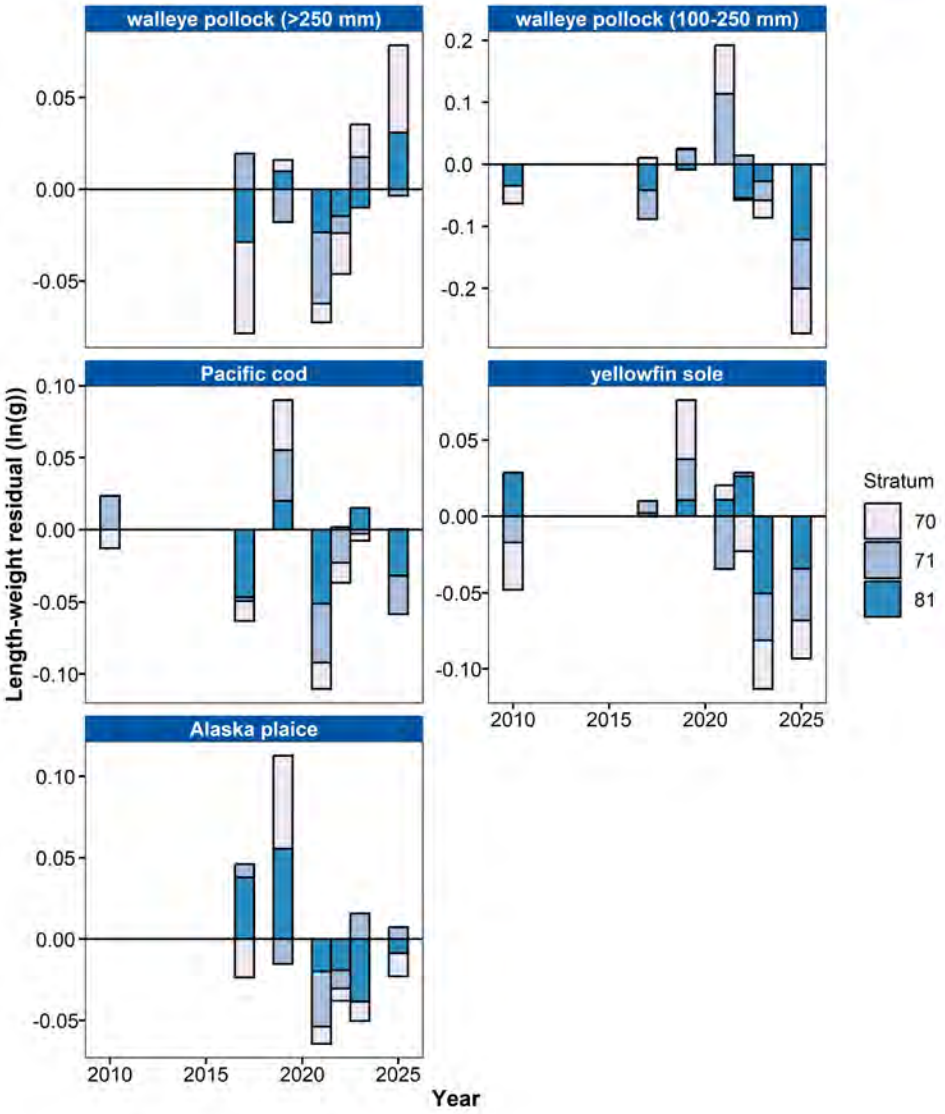


Figure 123: Length-weight residuals by survey stratum (70, 71, and 81) for four northern Bering Sea shelf groundfish species and age 1–2 walleye pollock (100–250 mm) sampled in the AFSC/RACE GAP standard summer bottom trawl survey during 2010, 2017, 2019, 2021-2023, and 2025. Length-weight residuals are not weighted by stratum biomass.

account for some of this variation, condition estimates may still be influenced by survey timing within strata. Survey timing can be further compounded by seasonal fluctuations in reproductive status with the buildup and depletion of energy stores (Wuenschel et al., 2019). In addition, because weights are taken at sea and include gut contents, variation in stomach fullness may influence condition estimates. Since feeding conditions vary over space and time, prey consumption rates and the proportion of total body weight attributable to gut contents may be an important factor influencing the length-weight residuals.

Finally, although the condition indicators characterize temporal variation in morphometric condition for important fish species in the EBS and NBS, they do not inform the mechanisms or processes behind the observed patterns.

Implications: Fish morphometric condition can be considered an indicator of ecosystem productivity with implications for fish survival, maturity, and reproduction. For example, in Prince William Sound, the pre-winter condition of herring may determine their overwinter survival (Paul and Paul, 1999), differences in feeding conditions have been linked to differences in morphometric condition of pink salmon in Prince William Sound (Boldt and Haldorson, 2004), variation in morphometric condition has been linked to variation in maturity of sablefish (Rodgveller, 2019), and lower morphometric condition of Pacific cod was associated with higher mortality and lower growth rates during the 2014-2016 marine heat wave in the Gulf of Alaska (Barbeaux et al., 2020). Condition can also be an indicator of stock status relative to carrying capacity because morphometric condition is expected to be high when the stock is at low abundance and low when the stock is at high abundance because of the effects of density-dependent competition (Haberle et al., 2023). Thus, the condition of EBS and NBS groundfishes may provide insight into ecosystem productivity as well as fish survival, demographic status, and population health. However, survivorship is likely also affected by many factors not examined here.

Another important consideration is that fish condition was computed for all sizes of fishes combined, except in the case of walleye pollock. Examining condition of early juvenile stage fishes separately from the condition of adult fishes could provide further insight into the value of length-weight residuals as an indicator of individual health or survivorship (Froese, 2006), particularly since large and small walleye pollock have shown diverging condition trends in the NBS in recent years, even though both size classes increased in condition in the EBS in 2026.

The above-average condition observed in most species in 2025 and 2026 does not appear to be explained by survey temperature alone, since bottom and surface temperatures were both slightly below the long-term mean in 2026 even as several species, including large walleye pollock, showed improved condition this year. However, trends in recent years such as prolonged warmer water temperatures following the marine heatwave of 2014-2016 (Bond et al., 2015) and reduced sea ice and cold pool areal extent in the eastern Bering Sea (Stabeno and Bell, 2019) may continue to affect fish condition in ways that have not yet been determined. Additionally, periods of high fishing mortality that reduce population biomass are likely to increase body condition because of the compensatory alleviation of density-dependent competition (Haberle et al., 2023). As we continue to add years of length-weight data and expand our knowledge of relationships between condition, growth, production, survival, and the ecosystem, these data may increase our understanding of the health of fish populations in the EBS and NBS.

Research priorities: Research is underway at the AFSC to examine relationships among putatively similar indicators of fish condition (i.e., morphometric, bioenergetic, physiological). This includes an evaluation of hepatosomatic index, microwave energy meter (fatmeter) measurements, and Fourier-transform near-infrared (FT-NIR) spectroscopy as alternative condition indicators, compared against biochemical measurements of liver lipid content (Prohaska et al., in prep.). Depending on the outcome of this work and the feasibility of collecting the required measurements during surveys, these indicators may be incorporated into future Ecosystem Status Reports (ESRs).

Patterns in Foraging and Energetics of Bering Sea Walleye Pollock, Pacific Cod, and Pacific Halibut

Contributed by Kirstin K. Holsman[1], Cheryl Barnes[2], Kerim Aydin[1], Ben Laurel[3], Jon Reum[1], and Anna Sulc[1]
[1]Resource Ecology and Fishery Management Division, Alaska Fisheries Science Center, NOAA Fisheries, Seattle, WA
[2]Coastal Oregon Marine Experiment Station, Oregon State University, Newport, OR
[3]Resource Assessment and Conservation Engineering Division, Alaska Fisheries Science Center, NOAA Fisheries, Newport, OR
Contact: kirstin.holsman@noaa.gov
Last updated: October 2026

Description of indicator: We report trends in metabolic demand from an adult bioenergetics model for groundfish in the eastern Bering Sea (EBS) (Ciannelli et al., 1998; Holsman et al., 2019; Holsman and Aydin, 2015) and patterns in diet composition from the NOAA Fisheries Alaska Fisheries Science Center's Food Habits database of fish diets collected during summer bottom trawl surveys in the SEBS and NBS. Bioenergetics-based indices were calculated for individual predator stomach samples using bioenergetics models. Samples were averaged by 1-cm predator length bins across stations within a stratum and then extrapolated to the population level using annual proportional biomass for each bin in each stratum based on bottom trawl surveys (see Ciannelli et al., 1998; Holsman et al., 2019; Holsman and Aydin, 2015, and Livingston et al., 2017 for more information).

Bioenergetic diet indices collectively indicate changes in foraging and growing conditions; relative foraging rate (RFR) reflects the ratio of observed food consumption (specific consumption rate in grams of prey per grams of predator per day; $C_{g_{\text{prey}}\ g^{-1}d^{-1}}$) to a theoretical temperature and size-specific maximum consumption rate from laboratory feeding experiments. Declines in this index can reflect decreases in prey availability or prey switching to more energetically valuable prey. Therefore, we also present mean diet energy density (j) which reflects the average energetic density of prey in stomachs sampled from across the EBS in a given year. Less favorable foraging patterns would be reflected in declines in RFR when average diet energy density ($\bar{ED}_{Jg^{-1}}$) remains the same or also declines in a given year. Metabolic demand ($R_{g\ g^{-1}d^{-1}}$) generally increases with temperature and indicates the basal energetic requirements of the fish. Finally, specific growth potential ($G_{g\ g^{-1}d^{-1}}$) integrates metabolic demand, prey energy, and relative consumption rates to indicate how changes in temperature and foraging collectively influence (potential) growth (Table 8).

Table 8: Potential processes reflected in high or low RFR under different conditions.

RFR	$\bar{ED}_{Jg^{-1}}$	Interpretation
Low	Low	Low RFR with low energetic density may indicate poor foraging conditions for predator species. If coupled with high or baseline metabolic demand, there may be reduced growth potential ($G_{g\ g^{-1}d^{-1}}$) for predator species.
Low	High	Low RFR with high diet energetic density may indicate prey switching to more valuable prey and lower required foraging rates to satisfy metabolic demand ($R_{g\ g^{-1}d^{-1}}$). If coupled with higher metabolic demand, this may indicate a change in foraging strategies to compensate for increased metabolic demand.
High	High	High RFR with high energetic density may indicate increased foraging rates on highly valuable prey. When coupled with moderate metabolic demand, this could lead to higher (potential) growth.
High	Low	High RFR with low energetic density may indicate reduced access to, or availability of, high-quality prey necessitated increased predator foraging rates to meet metabolic demands.

Status and trends: All six energetic indices suggest that shifting environmental conditions and recent marine heatwaves across the eastern Bering Sea may be impacting foraging and growth conditions for groundfish including, walleye pollock (*Gadus chalcogrammus*; hereafter "pollock"), Pacific cod (*Gadus macrocephalus*; hereafter "P. cod"), and Pacific halibut (*Hippoglossus stenolepis*; hereafter "halibut"). In particular, energetic indices indicate more than a decade of reduced foraging and potential growth conditions that follow from warmer indices of thermal experience and attendant elevated metabolic demands that were first observed in 2010 and had been largely sustained through 2025 (Figures 124 and 125). Overall, thermal experience (species-specific survey biomass weighted mean bottom temperature; 'TempC') of all three groundfish species increased during MHW years (2016-2019), with thermal experience in those years being the highest in the 30+ year time series for all three species (Figure 124). In 2026, cooler conditions in the Bering Sea are reflected in the cooler thermal experience ($TempC$) of juveniles and adults of all three species, with the exception of adult halibut, where thermal experience was well above the long-term 1982-2010 average.

Trends in energetic indices differ among species and lifestage, with consistenly negative anomalies in potential growth largest for adult pollock and P. cod and lower (and more variable) for Pacific halibut and juveniles of each species. For adult pollock and P. cod, protracted negative anomalies in foraging rates (consumption; $C_{g_{\text{prey}}\ g^{-1}d^{-1}}$) were observed until 2025 when cooler thermal experience in 2025 and 2026 resulted in reduced metabolic demand and an associate return from below average to near baseline foraging rates and near average potential growth.

Patterns in juvenile pollock energetic indices are more variable. In 2026, juvenile pollock potential growth indices remain below average, driven by combination of large increases in metabolic demand and relative and absolute consumption rates and prey energy densities near the long-term mean. Juvenile P. cod, and to a lesser extent halibut, appear to have experienced more moderate metabolic demand and more favorable conditions resulting in high and slightly above average growth potential for P. cod and halibut, respectively (Figure 124).

Potential growth ($G_{g\ g^{-1}d^{-1}}$) of juvenile and adult pollock is negatively correlated with bottom temperatures in the Bering Sea (Figure 126), with potential a particular inflection point around 3.5°C after which potential growth rapidly declines with increasing temperature. In contrast, adult halibut potential growth expresses a positive, near-linear correlation with increasing temperatures, with highest growth potential observed at $\sim$5°C. There are no clear trends in potential growth of juvenile halibut and adult and juvenile P. cod with increasing temperature (Figure 126).

Factors influencing observed trends: Metabolic demands for ectothermic fish like pollock, P. cod, and halibut are largely a function of thermal experience and body size and tend to increase exponentially with increasing temperatures. Fish can minimize metabolic costs through behaviors such as movement to thermally optimal temperatures (e.g., movement to climate refugia in the NBS or at depth) or increasing consumption of food energy (quality and/or quantity of prey) to meet increasing metabolic demands. The latter requires sufficient access to abundant or high energy prey resources. By examining patterns in diets of fish across the EBS, we are able to derive indices of metabolic demand, foraging rate, and growth potential (or "scope for growth") that provide insight into ecological changes associated with marine heatwaves and long-term warming in the region.

Implications: For all three species, during recent anomalously warm years, metabolic demands were elevated while foraging rates and potential growth were reduced (Figure 124). Of particular note, from 2010 to 2024 juvenile and adult pollock and P. cod potential growth across the entire EBS generally remained below the long-term average (1982-2010). Synergistic patterns of anomalously low foraging rates and growth potential points to system-wide reductions in foraging conditions during 2010 to 2024.

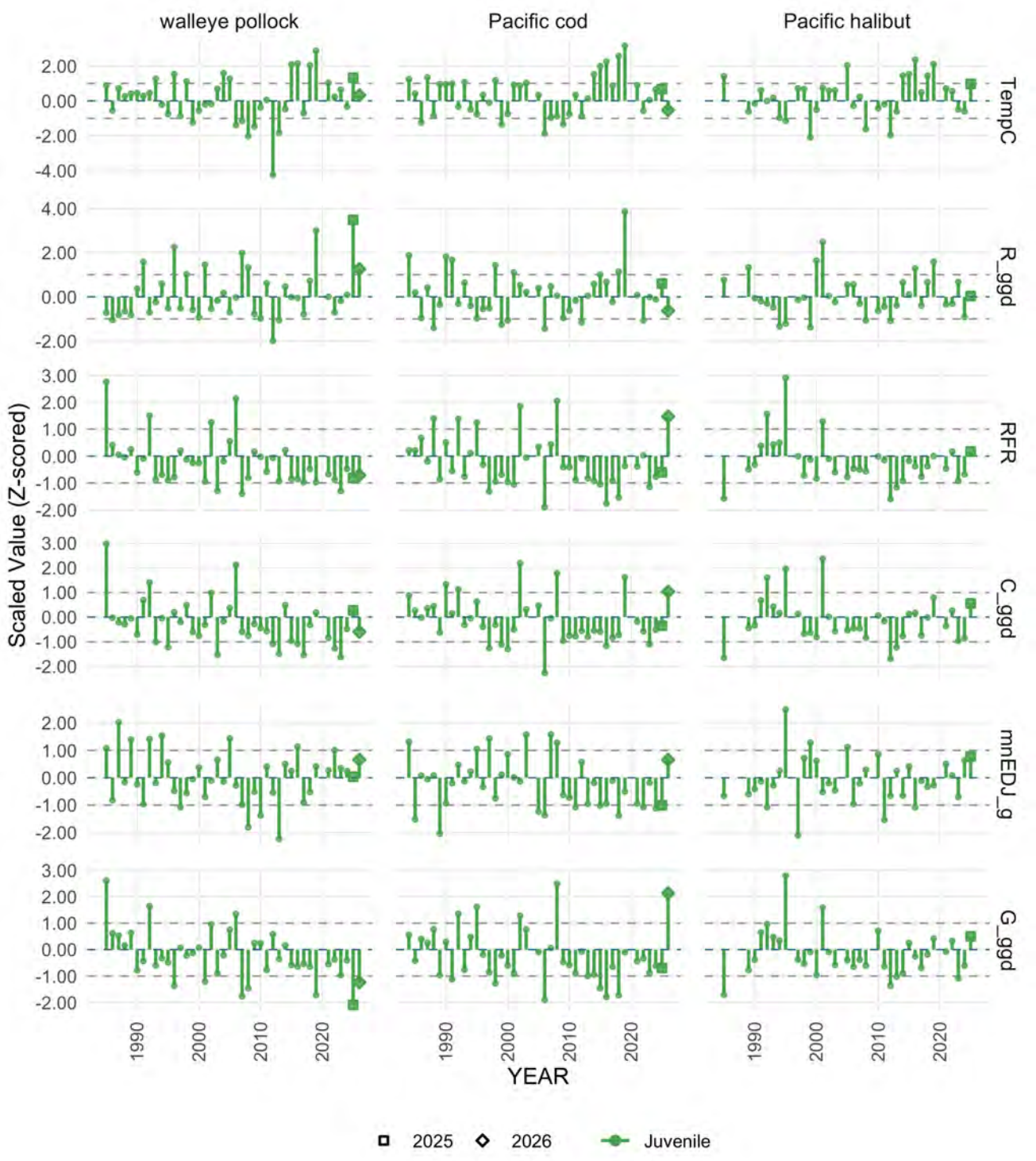


Figure 124: Normalized (i.e., Z-score scaled) bioenergetic diet indices for juvenile (<45 cm) groundfish species over time including thermal experience ('TempC'), metabolic demand ('R_ggd'), Relative Foraging Rate ('RFR'), observed specific consumption rate ('C_ggd'), mean diet energy density '(mnEDJ_g'), and scope for growth ('G_ggd'). Mean values for each year and bin are shown as dots, while recent sampled years are highlighted for reference (large triangles and squares). The spline represents a LOESS smoother. Data is based on biomass-weighted indices for samples collected during NOAA NMFS AFSC bottom-trawl summer surveys.

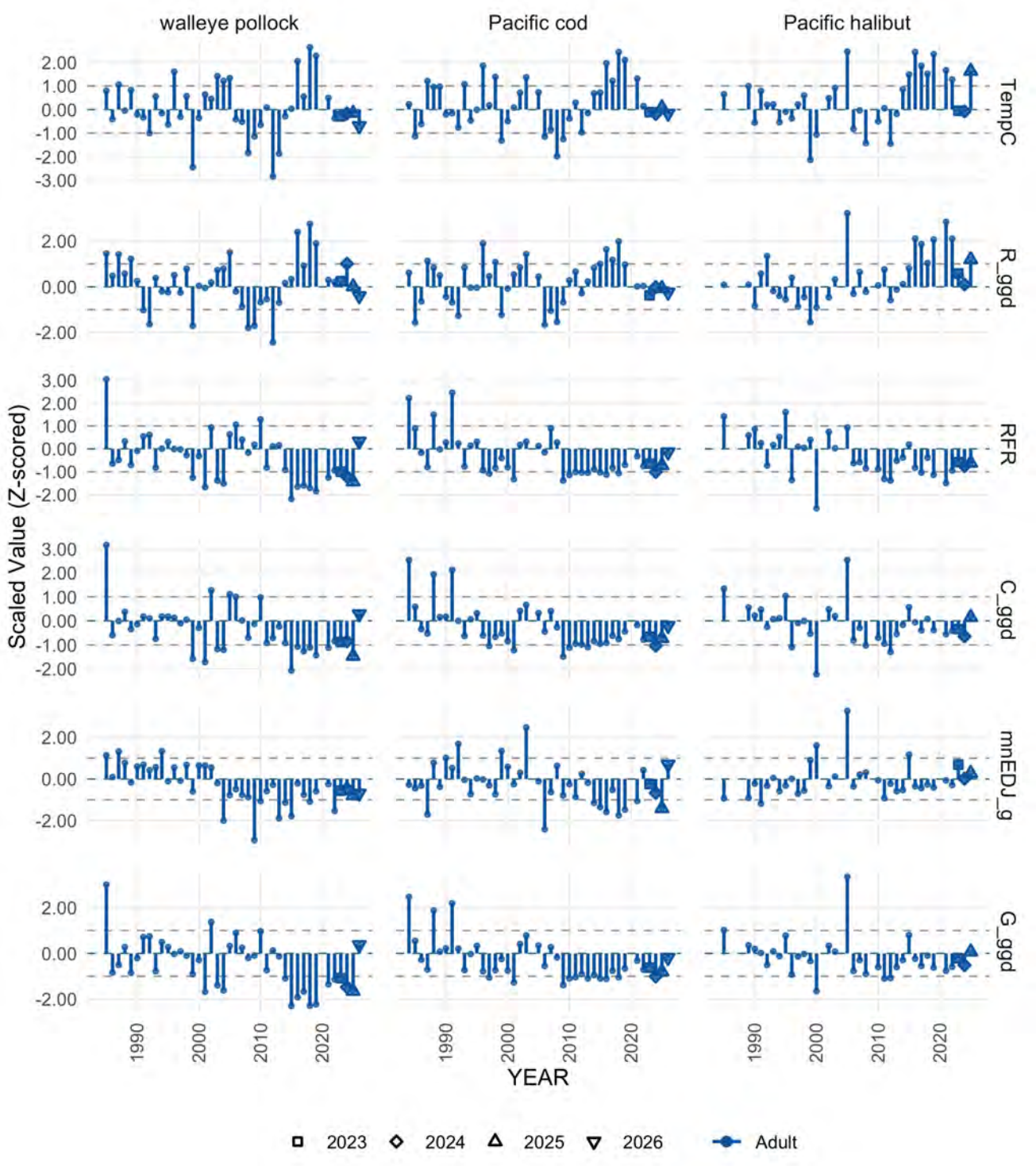


Figure 125: Normalized (i.e., Z-score scaled) bioenergetic diet indices for adult groundfish species over time including thermal experience ('TempC'), metabolic demand ('R_ggd'), Relative Foraging Rate ('RFR'), observed specific consumption rate ('C_ggd'), mean diet energy density '(mnEDJ_g'), and scope for growth ('G_ggd'). Mean values for each year and bin are shown as dots, while recent sampled years are highlighted for reference (large triangles and squares). The spline represents a loess smoother. Data is based on biomass-weighted indices for samples collected during NOAA NMFS AFSC bottom-trawl summer surveys.

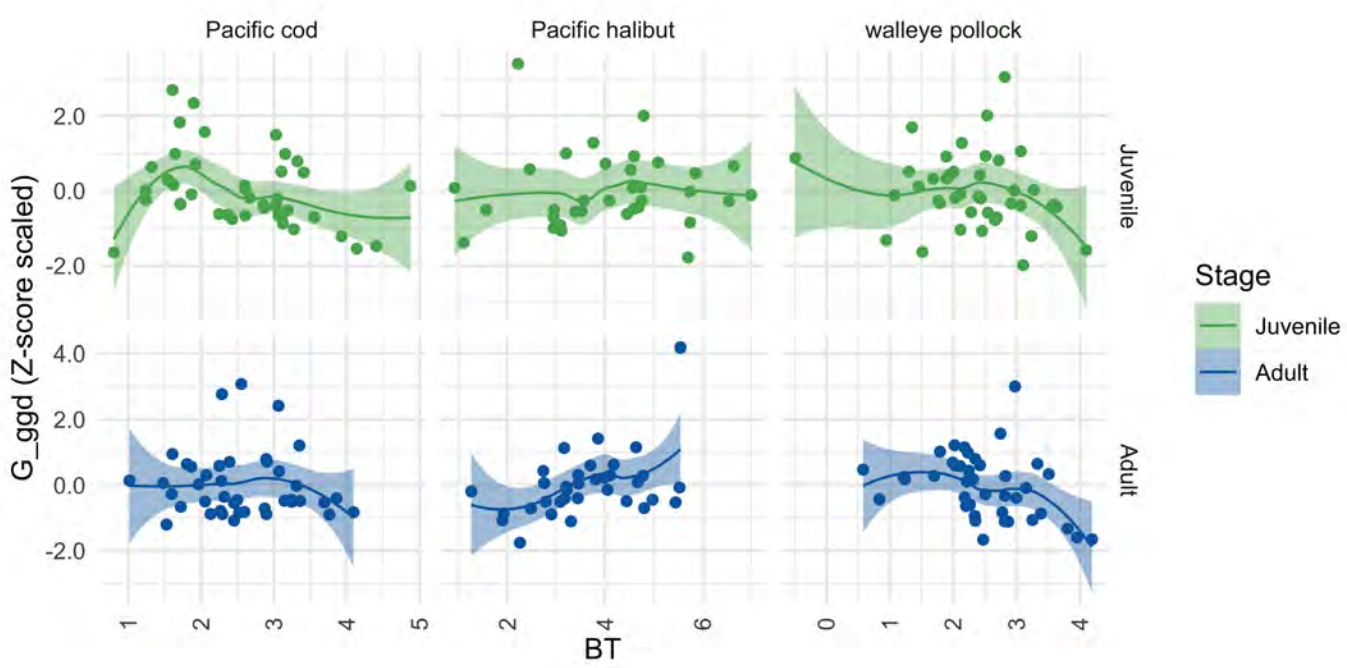


Figure 126: Normalized (i.e., Z-score scaled) bioenergetic (potential) scope for growth ('G_ggd') for juvenile and adult fish as a function of survey bottom temperature (BT; deg. C). Data is based on biomass-weighted indices for samples collected during NOAA NMFS AFSC bottom-trawl summer surveys.

Bering Sea Multispecies Model (CNRG) Estimates of Time-Varying Natural Mortality

Contributed by Kirstin K. Holsman, Jim Ianelli, Kalei Shotwell, Steve Barbeaux, Kerim Aydin, Grant Adams, and Kelly Kearney
Resource Ecology and Fishery Management Division, Alaska Fisheries Science Center, NOAA Fisheries, Seattle, WA
Contact: kirstin.holsman@noaa.gov
Last updated: November 2026

Summary statement:

Cooler water temperatures in 2026 combined with declines in adult groundfish biomass has resulted in net declines in estimates of predation mortality for juvenile groundfish in recent years. This pattern indicates continued favorable top-down conditions for juvenile groundfish survival in 2026 through 2027 via predation release.

Description of indicator:

We report trends in age 1 total mortality for walleye pollock (*Gadus chalcogrammus*), P. cod (*Gadus macrocephalus*) and arrowtooth flounder (*Atheresthes stomias*), from the eastern Bering Sea (USA). Total mortality rates are based on residual mortality inputs (M1) and model estimates of annual predation mortality (M2) produced from the Climate-linked Numbers at age, Recruitment, and Growth model ("CNRG", formerly CEATTLE). See the BSAI climate-linked multispecies stock assessment (Holsman et al. 2026, 2024, 2020, 2016), Adams et al. 2022, Holsman and Aydin 2015, Ianelli et al. 2016, and Jurado-Molina et al. 2005 for more information.

Status and trends:

Estimates of mortality from the CNRG model for walleye pollock (hereafter "pollock"), Pacific cod (hereafter "P. cod"), and arrowtooth flounder continue to remain relatively low. For all three species, age 1 predation mortality rates have declined markedly relative to 2025 (Figure 127). At 1.07 yr^{-1}, age 1 mortality estimated by the model was greatest for pollock and lower for P. cod and arrowtooth, with total age 1 natural mortality at around 0.58 and 0.46 yr^{-1} for P. cod and arrowtooth, respectively.

Cannibalism is the largest source of predation of age 1 pollock over time, followed by arrowtooth flounder (Figure 128). The 2026 predation mortality rate due to cannibalism is slightly below the long-term mean. P. cod is the largest predator on age 1 conspecifics as well as age 1 arrowtooth flounder, although overall predation mortality rates for those species are much lower than that of pollock. P. cod predation on all three species is trending downward and below the long-term mean (Figure 128).

While the rate of predation mortality of cannibalism is below the long-term mean, overall biomass of pollock consumed by conspecifics is markedly higher than previous years, and is the third highest in the timeseries. Cannibalism is greatest on age 1 pollock, slightly above zero on age 2, and not typically observed for older fish. Cannibalism peaked in 2013 and 2018 as large cohorts of older pollock matured and metabolic demand peaked with warmer temperatures (Figure 129).

Patterns in the total biomass of each prey species (typically <3 yr old fish) consumed by all three predators in the model exhibit similar trends to predation mortality in 2026. Pollock biomass consumed

by all predators in the model is below the long-term mean (indicating fewer 1-3 year old pollock were consumed in the last few years than on average), while P. cod and arrowtooth consumed is approximately the mean (just below). Total biomass consumed of each species is slightly trending downward (Figure 130).

Factors influencing observed trends:

Temporal patterns in natural mortality reflect annually varying changes in predation mortality that primarily impact age 1 fish (and to a lesser degree impact ages 2 and 3 fish in the model). Pollock are primarily consumed by older conspecifics, and pollock cannibalism accounts for 63% (on average) of total age 1 predation mortality, with the exception of the years 2006-2010 when predation by arrowtooth marginally exceeded cannibalism as the largest source of predation mortality of age 1 pollock (Figure 128, Figure 129). The relative proportion of age 1 pollock consumed by older pollock decreased in 2026 relative to previous years as did the relative proportion consumed by P. cod and arrowtooth flounder.

Combined annual predation demand (annual ration) of pollock, P. cod, and arrowtooth flounder in 2026 was 5.5 million tons, down 20 % from the 6.89 million t annual average during the warm years and large maturing cohorts of 2014-2018. Walleye pollock represent approximately 0.77% of the model estimates of combined prey consumed with a long-term average of 5 million tons of pollock consumed annually by all three predators in the model. The peak in predation mortality of age 1 pollock in 2015-2016 corresponds to warmer than average conditions and higher than average energetic demand of predators combined with the maturation of the large 2010-2012 year classes of pollock and P. cod (collectively with arrowtooth 13.11 million t per year).From 2015 - 2018,individual annual rations were above average for all three predator species, driven by anomalously warm water temperatures in the Bering Sea during during those years. However, cooler temperatures in 2026 relative to the recent warm years has resulted in annual rations at or below the long-term average (Figure 130).

Implications:

We find evidence of continued declines in predation mortality of age 1 pollock, P. cod and arrowtooth flounder relative to elevated rates earlier in the timeseries. While cooler temperatures reduce metabolic (and energetic) demand of predators, declines in total predator biomass, in particular P. cod, are contributing to a net decrease in total consumption (relative to 2018) and therefore reduced predation rates and mortality in 2024-2026. This pattern indicates continued favorable top-down conditions for juvenile groundfish survival in 2026 through predator release due to declining biomass of groundfish.

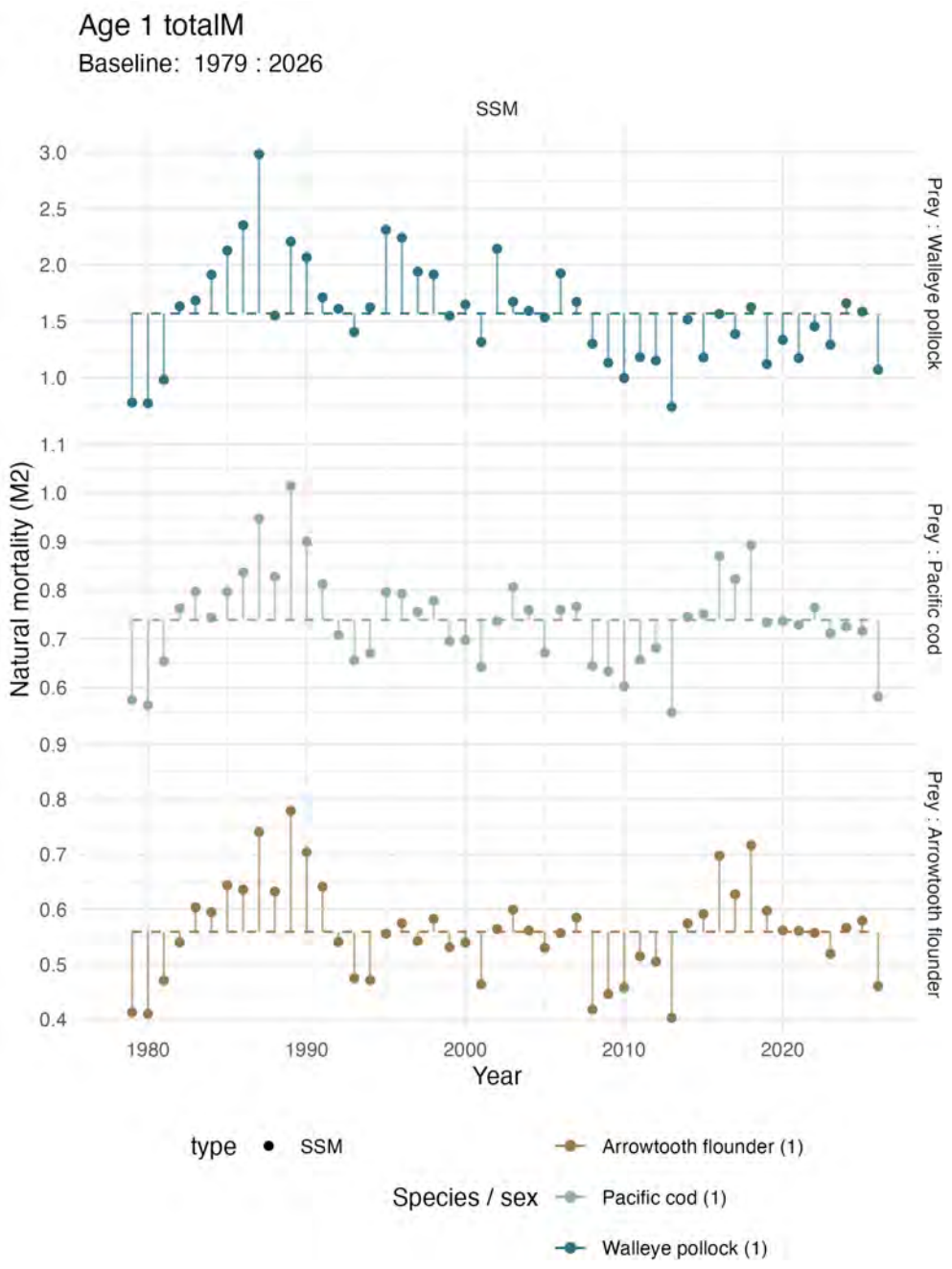


Figure 127: Annual variation in total mortality (M1+M2) of age 1 pollock, Pacific cod, and arrowtooth flounder, comparing single-species and multispecies model estimates.

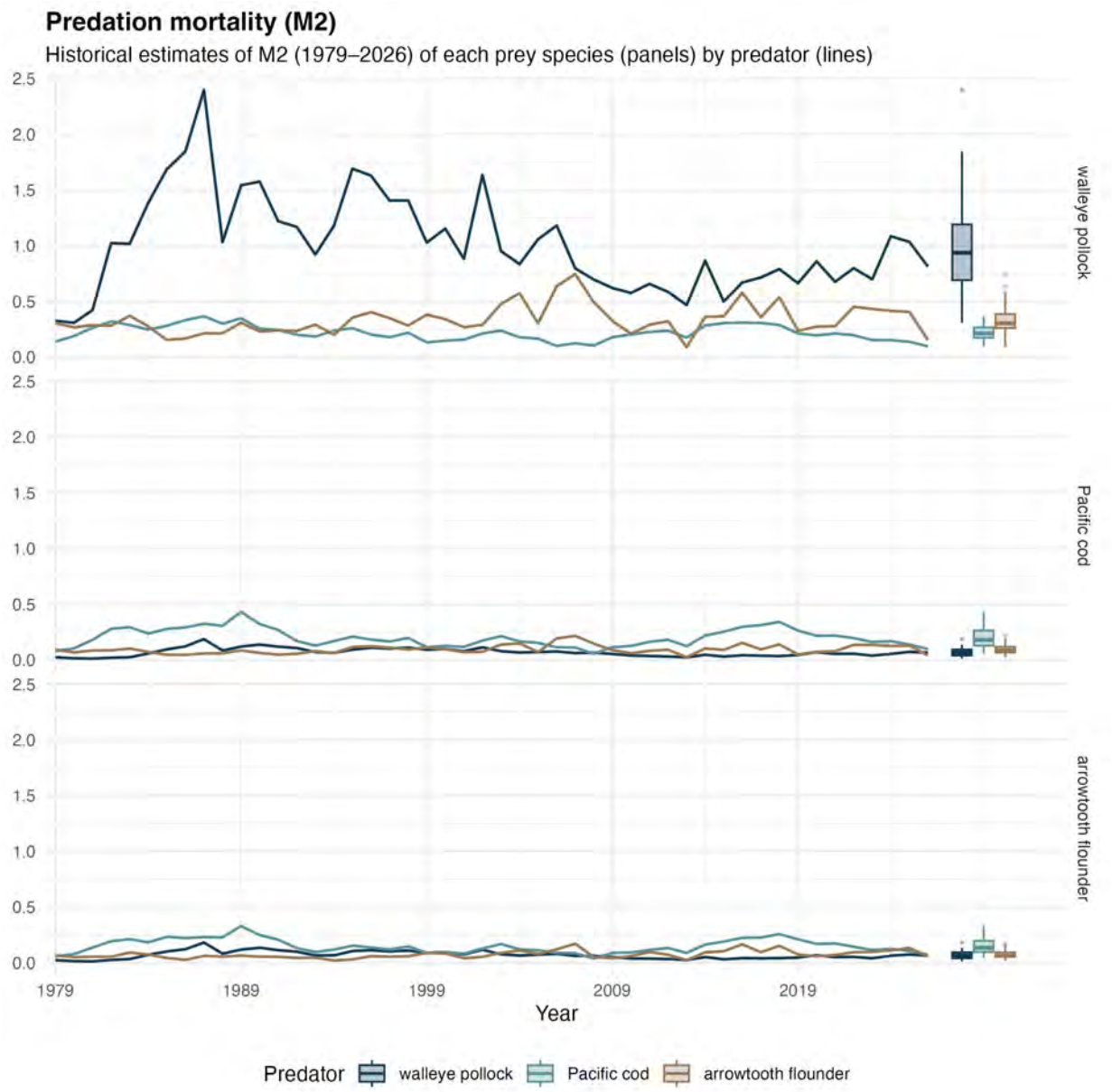


Figure 128: CNRG model estimates of annual predation mortality (M2) for each prey species (panels) by predator species (lines).

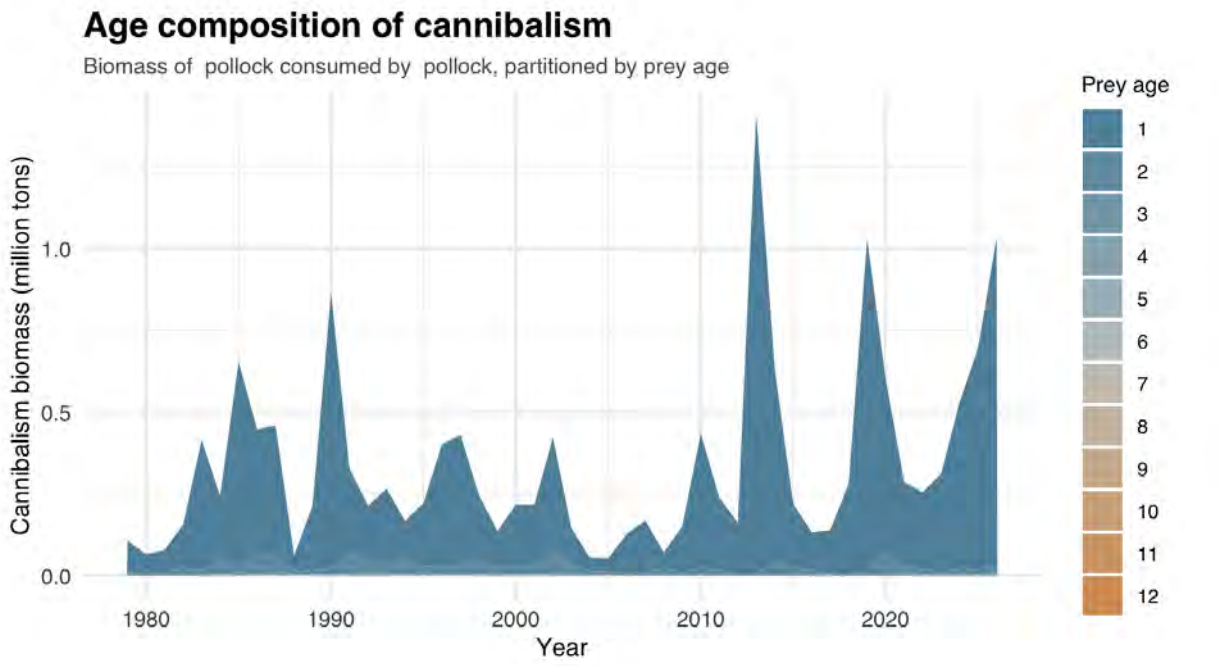


Figure 129: CNRG model estimates of annual pollock biomass consumed by cannibalistic conspecifics.

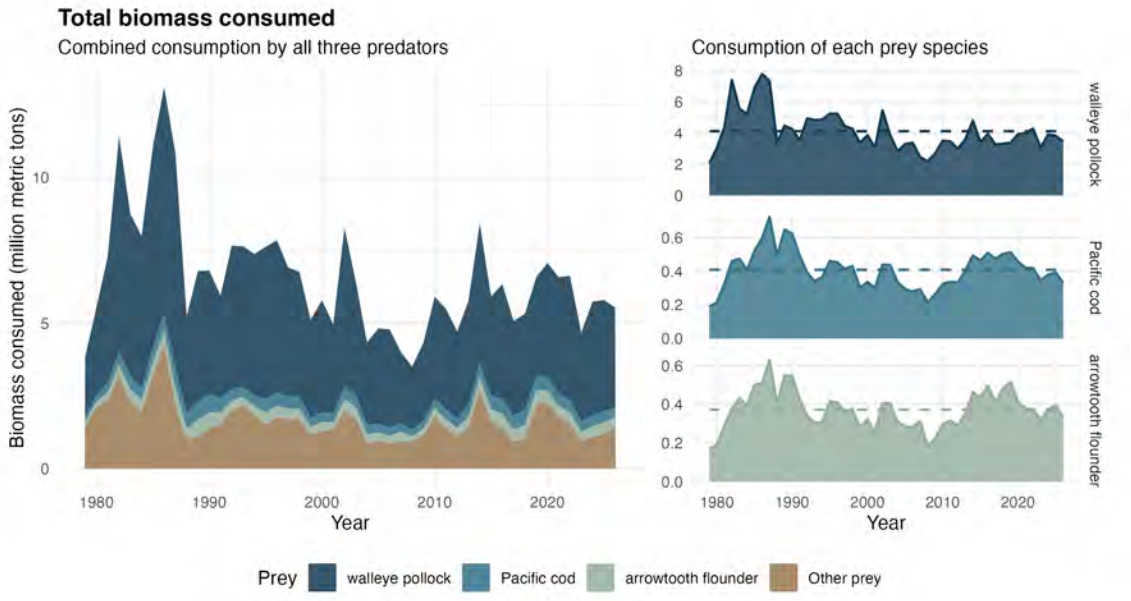


Figure 130: CNRG annual estimates of combined prey biomass consumed by all predators in the model.

Benthic Communities and Non-target Fish Species

Eastern and Northern Bering Sea – Miscellaneous Benthic Fauna

Contributed by Thaddaeus Buser
Groundfish Assessment Program, Resource Assessment and Conservation Engineering Division,
Alaska Fisheries Science Center, NOAA Fisheries, Seattle, WA
Contact: thaddaeus.buser@noaa.gov
Last updated: September 2026

Description of indicator: 'Miscellaneous' benthic fauna fall into three groups: eelpouts (fishes of the Family Zoarcidae), poachers (fishes of the Family Agonidae), and sea stars (Class Asteroidea). The three species comprising the bulk of the eelpout group are the wattled eelpout (*Lycodes palearis*) and shortfin eelpout (*L. brevipes*) and to a lesser extent the marbled eelpout (*L. raridens*). The biomass of poachers is dominated by the sturgeon poacher (*Podothecus acipenserinus*) and to a lesser extent the sawback poacher (*Leptagonus frenatus*). The composition of sea stars is dominated by the purple-orange sea star (*Asterias amurensis*), found primarily in the inner/middle shelf (strata 10–40), and the common mud star (*Ctenodiscus crispatus*), primarily in the outer shelf (strata 50 and 60).

Since 1982, the RACE Groundfish Assessment Program (GAP) and Shellfish Assessment Program (SAP) have conducted annual fishery-independent summer bottom trawl surveys on the EBS shelf using standardized trawl gear and methods. Biomass index trends from the survey are likely to reflect changes in the abundance of species and life history stages that are available to the survey, especially if trends are sustained over time.

Regional and stratum indices of abundance (biomass in kilotons) and confidence intervals were estimated for each taxonomic group by fitting a multivariate random effects model (REM) to stratum-level design-based abundance index time series calculated from AFSC summer bottom trawl survey catch and effort data. Indices were calculated for the standardized survey time series (EBS: 1982-2026, NBS: 2010-2025). Design-based indices of abundance were calculated using the gapindex R package (Oyafuso, 2025) and REM were fitted to survey time series using the rema R package (Sullivan and Balstad, 2022). Code and data used to produce these indicators are provided in the esrindex R package and repository (Rohan, 2025).

Status and trends:
Eastern Bering Sea:
The 2026 biomass estimate for eelpouts is almost identical to that of 2025, maintaining the increased abundance that began in 2021 (Figure 131). The 2026 estimate is >1 standard deviation above the time series mean and represents the largest biomass estimate since 1983. Eelpout biomass is concentrated on the outer shelf in strata 50 and 60 (100-200m bottom depth) and southern middle shelf in stratum 30 (50-100m bottom depth; Figure 132).

Poacher biomass increased from 2025 and is >1 standard deviation higher than the time series average, which is an estimated biomass not seen since 2005 (Figure 131). Poacher biomass is concentrated in inner (<50m) and middle (50-100m) shelf strata (10-40), although lower abundances of deeper species are encountered in strata 50 and 60 (Figure 132).

The biomass for sea stars increased in 2026 compared to 2025, and continues a trend of increasing biomass over the past three years, following a brief decrease in biomass that was observed from 2021 to 2024. The 2026 sea star biomass estimate is at or above the time series average and represents a return to levels last seen in 2019 (Figure 131). Sea stars are observed in all survey strata, although their biomass in stratum 50 is much lower than in other strata (Figure 132).

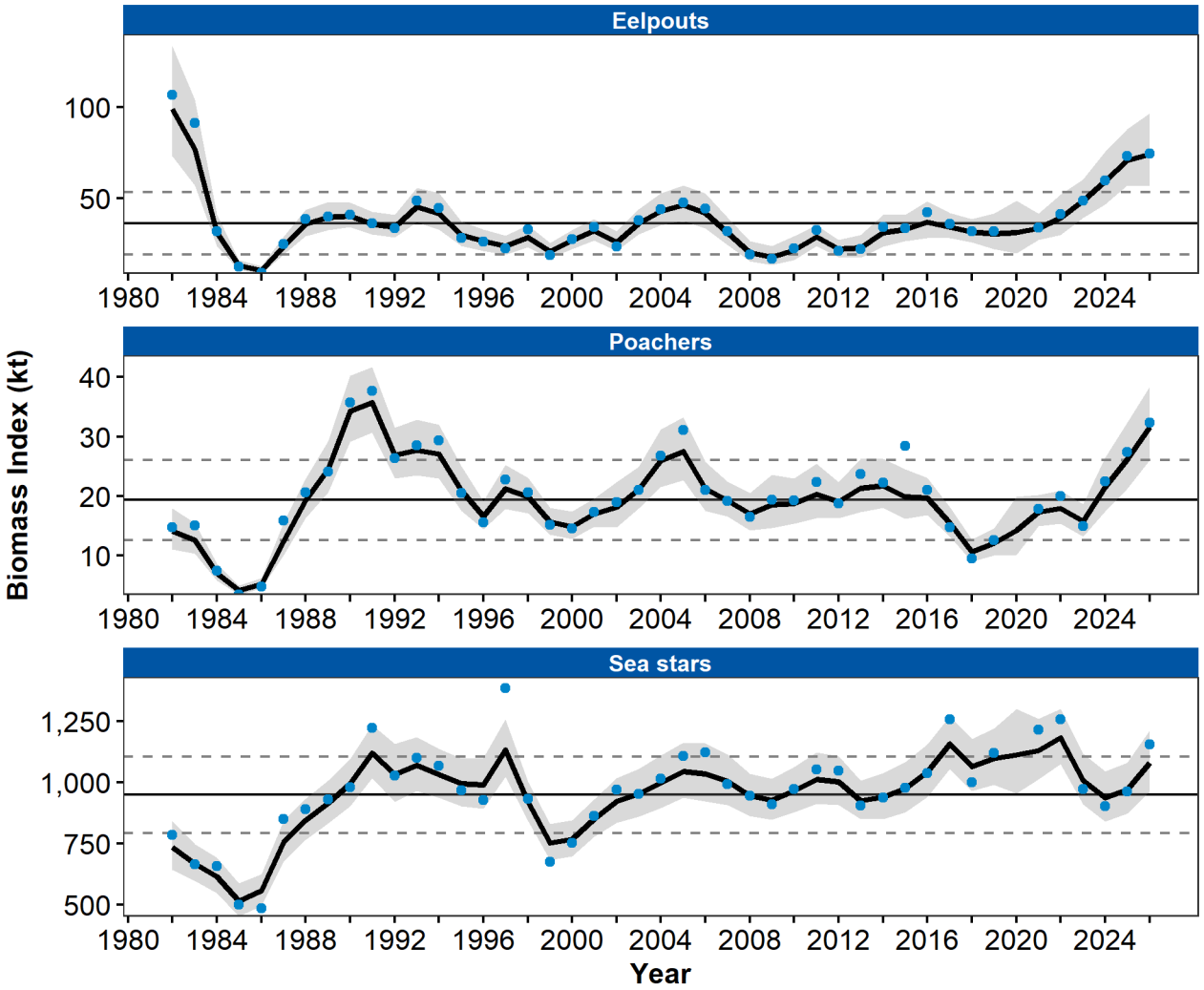


Figure 131: Biomass index of miscellaneous benthic fauna (eelpouts, poachers, sea stars; kilotons) estimated from AFSC/RACE summer bottom trawl surveys of the eastern Bering Sea continental shelf from 1982 to 2026. Panels show the observed survey biomass index mean (blue points), random effects model fitted mean (solid black line), 95% confidence interval (gray shading), time series mean (solid gray line), and horizontal dashed gray lines representing one standard deviation from the mean.

Northern Bering Sea:

The Northern Bering Sea was not sampled in 2026; results from the 2025 survey are presented here. The 2025 biomass estimate of eelpouts is close to the time series average and similar to those estimated since 2019 (Figure 133). These recent year estimates are much lower than those of 2010 and 2017. However, it is unclear whether this indicates a trend given the gaps in sampling years. Eelpouts were predominantly found in strata 71 and 81 (Figure 134).

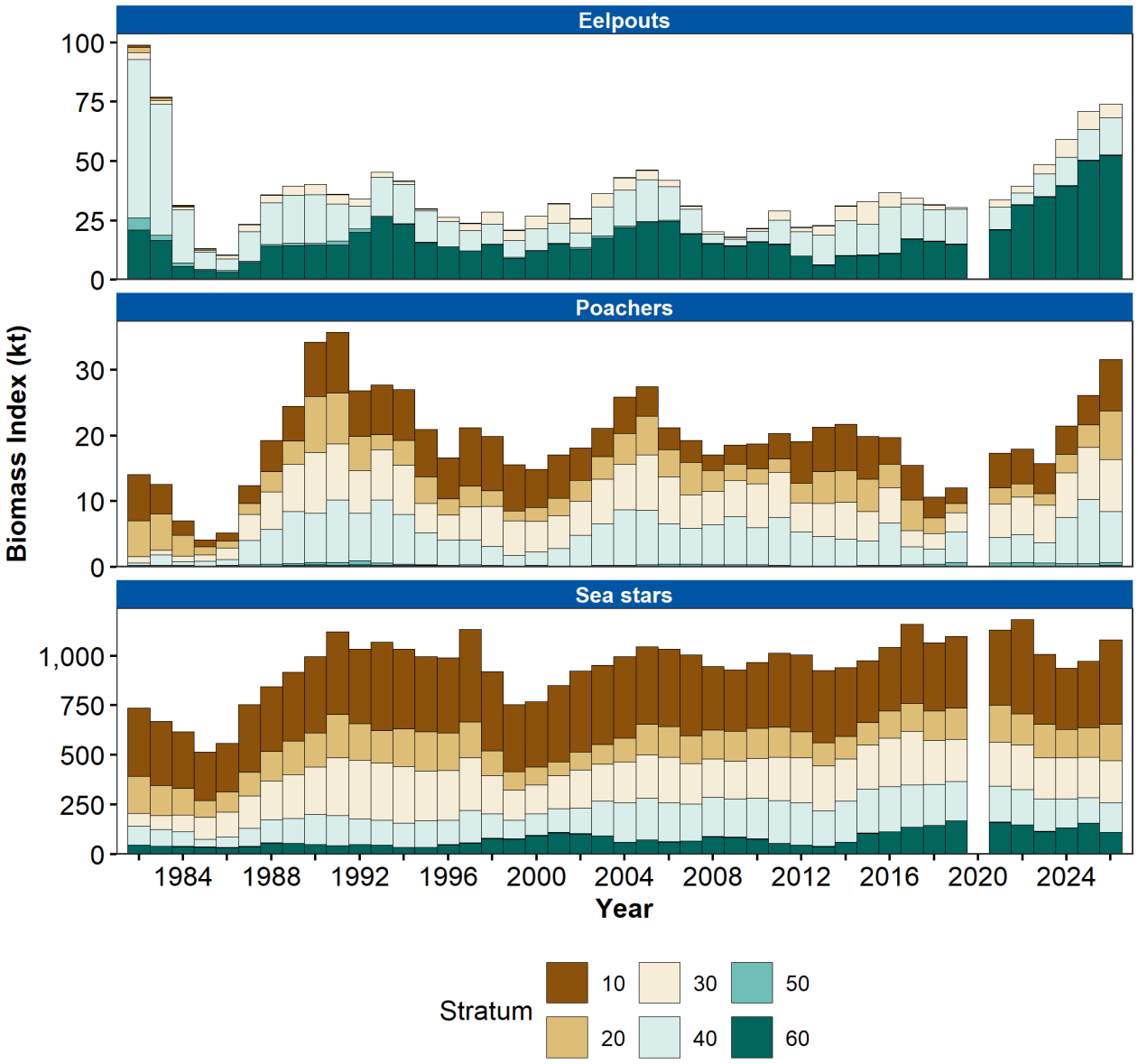


Figure 132: Biomass index of miscellaneous benthic fauna (eelpouts, poachers, sea stars; kilotons) in eastern Bering Sea continental shelf survey strata 10-60 estimated from RACE Groundfish Assessment Program and Shellfish Assessment Program summer bottom trawl survey data from 1982 to 2026.

For poachers, the biomass estimate for 2025 was likewise near the overall time series average (Figure 133). This follows a period of relatively low abundance estimated from 2021-2023. Poacher relative biomass was consistently highest in stratum 70, with lower relative biomass in strata 71 and 81 (Figure 134).

The biomass estimate for sea stars in 2025 is >1 standard deviation lower than the overall time series average and marks an all-time low for sea stars in the NBS (Figure 133). However, the gaps in sampling years make it difficult to confidently identify trends in the data at this point. Sea stars biomass was highest in strata 70 and 71 (Figure 134).

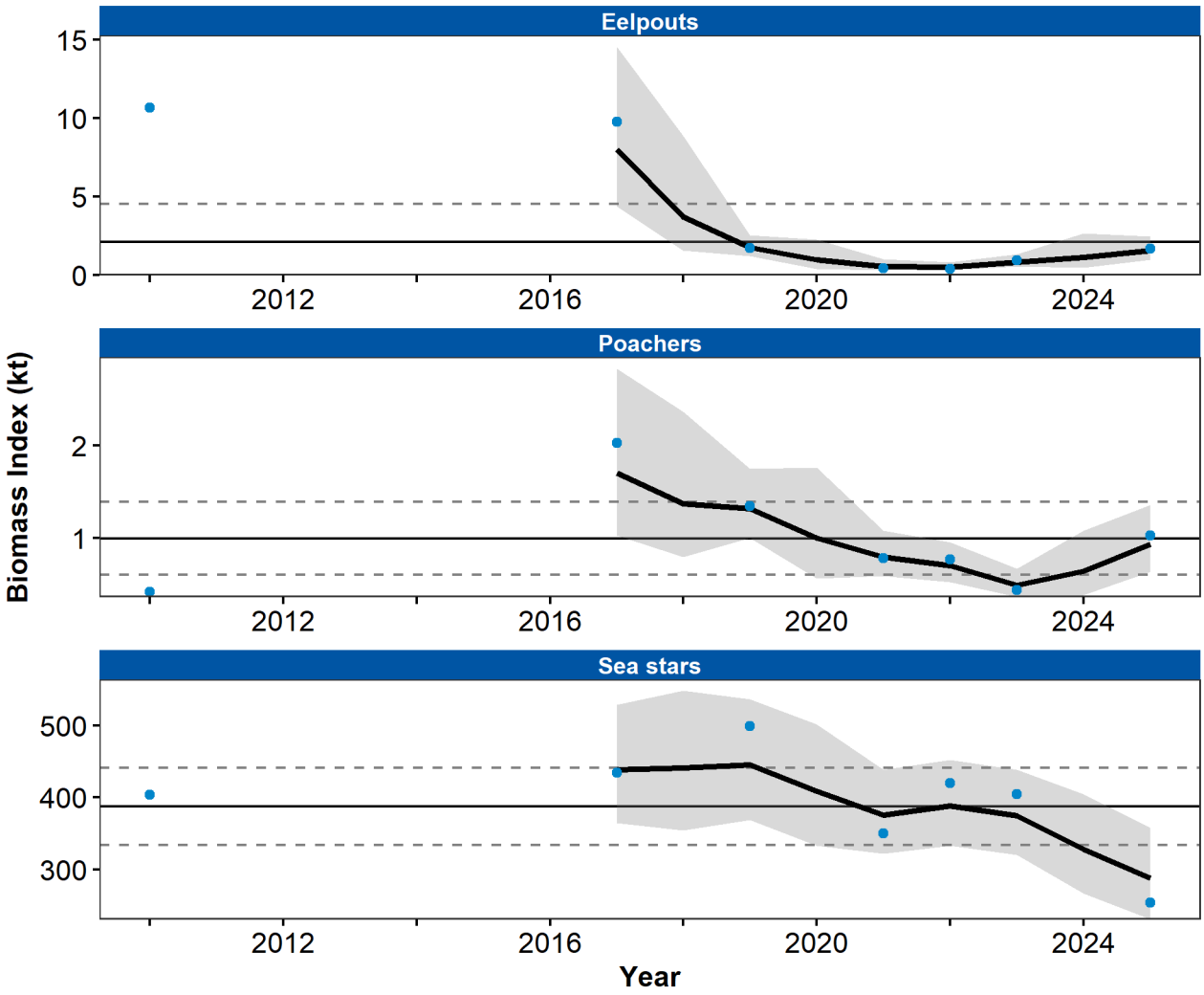


Figure 133: Biomass index of miscellaneous benthic fauna (eelpouts, poachers, sea stars; kilotons) estimated from AFSC/RACE summer bottom trawl surveys of the northern Bering sea from 2010 to 2025. Panels show the observed survey biomass index mean (blue points), random effects model fitted mean (solid black line), 95% confidence interval (gray shading), time series mean (solid gray line), and horizontal dashed gray lines representing one standard deviation from the mean.

Factors influencing observed trends: There are several factors that could influence the observed trends but it is often challenging to identify which one plays the greatest role. For example, the low abundance after 2018 in poachers could be influenced by environmental conditions, representing actual changes in species' abundance and demographic structure. However, distributional changes or selectivity might also influence these results. Parsing out the impact of these potential influences will require more specific research on survey trawl gear selectivity relative to interannual differences in bottom temperatures and on the life history characteristics of these epibenthic species.

Implications: Eelpouts, poachers, and sea stars have important roles in the energy flow within benthic communities. For example, eelpouts are a common prey item of arrowtooth flounder (*Atheresthes stomias*). However, it is not known at present whether these changes in CPUE are related to changes in energy flow.

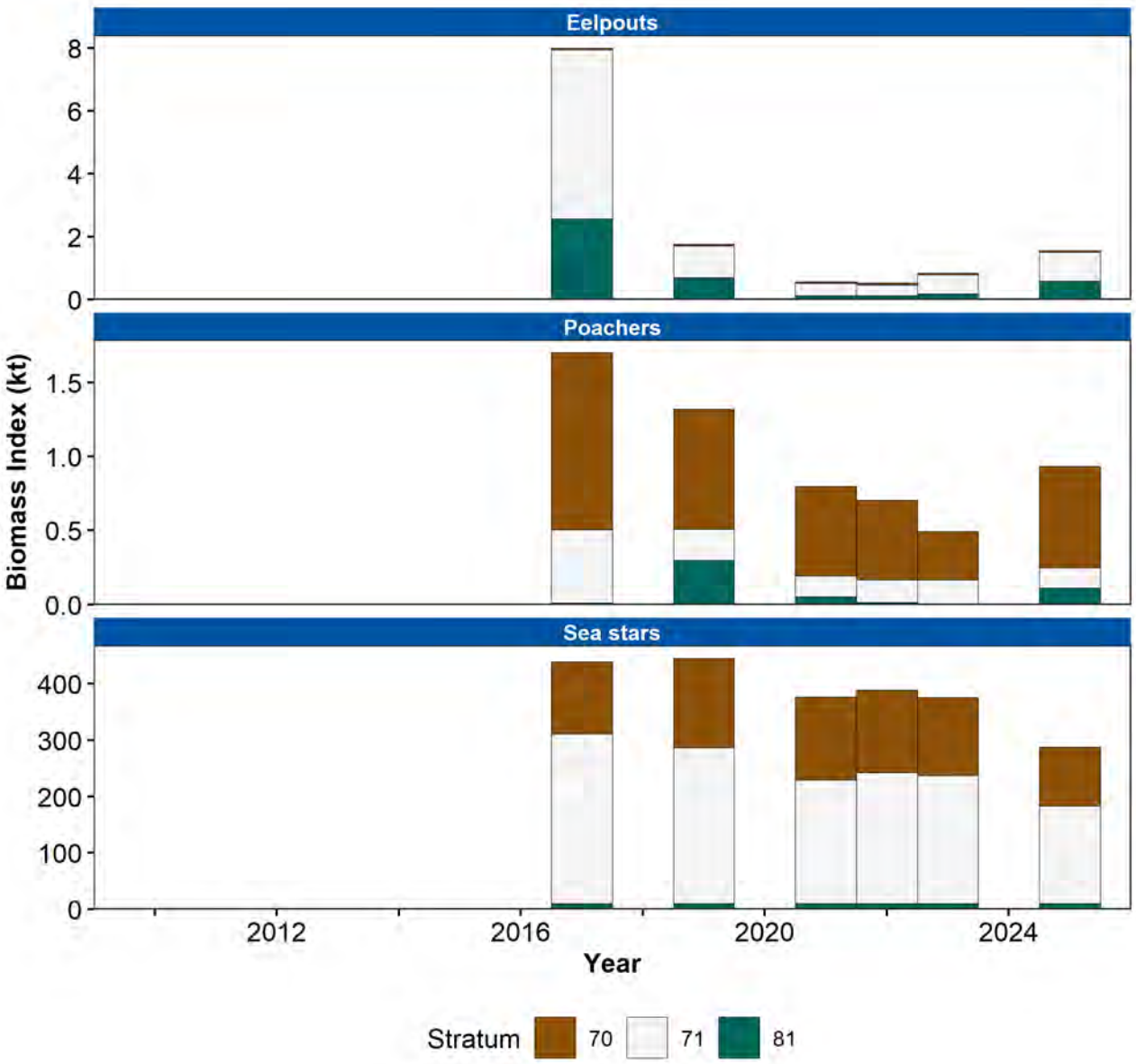


Figure 134: Biomass index of miscellaneous benthic fauna (eelpouts, poachers, sea stars; kilotons) in northern Bering Sea survey strata 70, 71, and 81, estimated from RACE Groundfish Assessment Program and Shellfish Assessment Program summer bottom trawl survey data from 2010 to 2025.

Research priorities: The bottom trawl survey uses standardized survey protocols aimed at ensuring consistent sampling efficiency. However, additional research is needed to better characterize the catchability and selectivity of structural epifauna groups by the bottom trawl survey.

Diet-based Indicators of Benthic Fauna

Contributed by Jonathan Reum
Resource Ecology and Fishery Management Division, Alaska Fisheries Science Center,
NOAA Fisheries, Seattle, WA
Contact: jonathan.reum@noaa.gov
Last updated: August 2026

Description of indicator: Stomach content data are routinely collected for several groundfish predators in the Alaska Fisheries Science Center's eastern Bering Sea (EBS) shelf survey and are available for most years between 1987 and 2025. The data provide a basis for inferring abundance trends for several benthic forage groups that are not otherwise sampled. Specifically, a spatiotemporal modeling framework was developed that permitted synthesis of diet data from multiple predators while controlling for predator species and predator size effects on the prevalence of prey in stomachs. The intent of the approach is to isolate temporal trends related to the relative abundance of forage groups and is analogous to regression-based methods for standardizing fisheries catch-per-unit-effort data across multiple data sources. Details regarding stomach content data collection are available in Livingston et al. (2017); annual forage abundance indices follow methods presented in Reum et al. (2025). Trends are presented for common benthic forage groups in groundfish diets: benthic amphipods (primarily from families Gammeridae and Caprillidae), hermit crabs, nonpandalid shrimp (primarily Crangonidae), and polychaetes. In addition, we provide trends for octopus which are managed as a single species complex and assessed using Tier 6 methods.

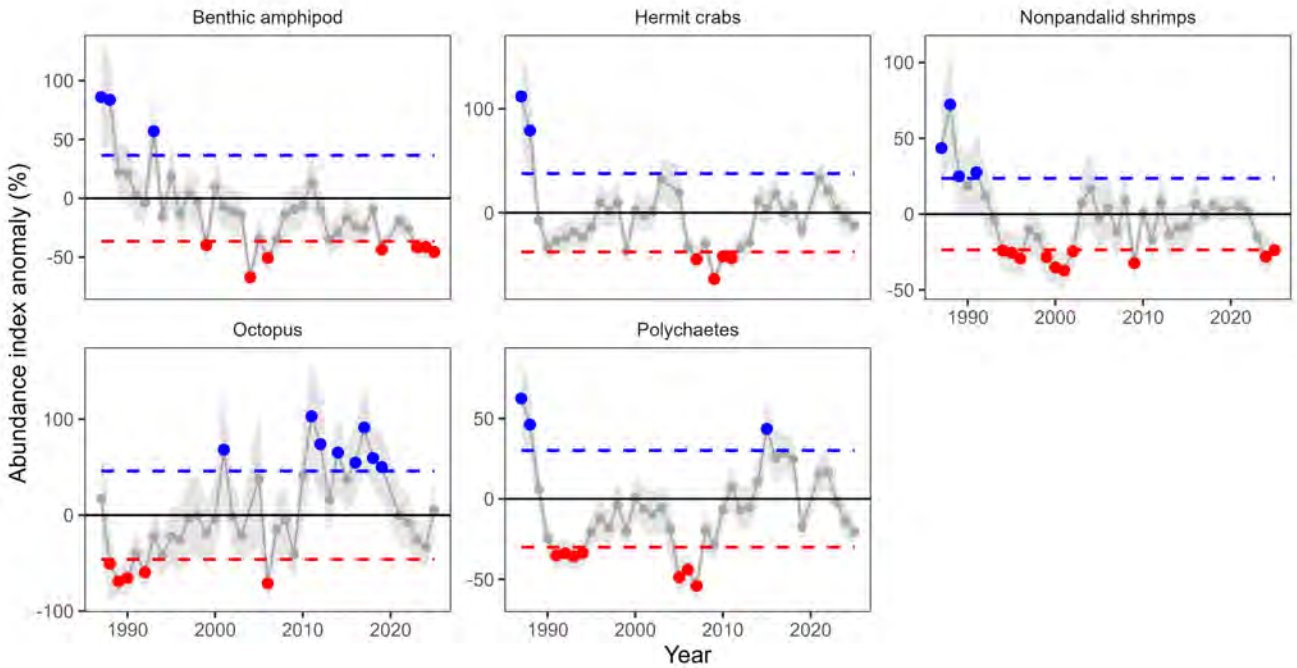


Figure 135: Annual abundance index anomalies for key benthic invertebrate functional groups and species from the southeastern Bering Sea derived from groundfish predator diet data. Error bands indicate 95% confidence intervals; blue and red dashed lines: ±1 standard deviation of the index, respectively. Years falling outside 1 standard deviation are highlighted in blue and red.

Status and trends: Here, anomalies are defined as values exceeding or falling outside 1 standard deviation of the historical mean (1987 to 2025). In 2025, benthic amphipods and nonpandalid shrimps were near or at anomalously low levels but similar to values for 2024. For the remaining forage groups, 2025 values were closer to the historical long-term mean (Figure 135).

Factors influencing observed trends: Currently, the extent to which abundance trends are driven by bottom-up environmental conditions or top-down predation pressure is unknown. We are currently pursuing research to evaluate potential causal linkages with observed interannual abundances.

Implications: Abundance trends in major benthic forage groups help characterize overall system-level patterns in benthic productivity and may relate to feeding conditions, particularly for benthic feeders such as flatfish. For octopus, the diet-based index is the only available indication of potential historical population trends and current relative status.

Eastern Bering Sea Commercial Crab Stock Biomass Indices

Contributed by Jon Richar
Kodiak Laboratory, Alaska Fisheries Science Center, NOAA Fisheries, Kodiak, AK
Contact: jon.richar@noaa.gov
Last updated: September 2026

Description of indicator: The eastern Bering Sea bottom trawl survey has been conducted annually since 1975 by the Resource Assessment and Conservation Engineering Division of the Alaska Fisheries Science Center. The purpose of this survey is to collect data on the distribution and abundance of crab, groundfish, and other benthic resources in the eastern Bering Sea. The data provided here include the time series of results from 1998 to the present. In 2026, 349 standard stations were sampled on the eastern Bering Sea shelf from 1 June to 4 August. This constitutes a continuation of reduced sampling effort relative to the long-term historical norm, and results from the elimination of corner stations near the Pribilofs and St. Matthew Is. since 2024. The observed trends in crab biomass may be indicative of trends in either benthic production, or benthic response to environmental variability. The commercial crab biomass is also indicative of trends in exploited resources over time.

Status and trends: The historical trends of commercial crab biomass and abundance are highly variable (Figure 136). In 2026, Bristol Bay mature male red king crab biomass increased by 30% relative to 2025 estimates, continuing the trend of increasing population seen since 2024. Conversely, mature female red king crab biomass decreased by 12%, while abundance declined by -1.43%, with the discrepancy being due to an increasing proportion of smaller crab. Numbers remain near the historical low points.

The St. Matthew blue king crab adult male biomass increased by 37% relative to 2025 estimates, reversing a declining trend decline observed since 2014. Female blue king crab biomass is not adequately sampled during this survey due to a nearshore distribution around St. Matthew Island.

Mature male Tanner biomass trends were positive, with the eastern district seeing a 169% increase, and a 21% increase occurring in the western district. Although the increase in the eastern district mature male biomass constitutes a reversal in the recent declining trend, biomass remains down by -52% since 2014. Mature female biomass declined in the western district (-29%), but increased in the eastern district (+24%).

Total snow crab biomass decreased by 1.16% relative to 2025. Declines were seen in mature males (-28%), immature males (-16%), immature females (-84%), and industry-preferred males (-29%). Increases were seen in legal males (3%) and mature females (+90%). The substantial changes in female categories were driven by maturation of the pseudocohort seen in previous surveys, coincident with reduced recruitment to the juvenile population

Pribilof Island crab stocks remain extremely depressed with highly variable survey biomass estimates due to trawl survey limitations related to crab habitat and the patchy crab distribution. Although Pribilof blue king crab catches represented the largest catches seen for this stock in a decade or more, these crab were still only encountered at a few stations. Consequently estimates may be an artifact of the net randomly sampling a few aggregations, rather than a genuine significant increase in this population. The Pribilof red king crab stock saw increases of 127% in both mature and legal male stocks, while mature females increased by 684%. Small numbers of both immature males and immature females were caught, this contrasts with 2025 when none were seen.

Factors influencing observed trends: Environmental variability and exploitation affect trends in commercial crab biomass over time. Recent modeling analyses suggest that environmental variability is largely driving inter-annual variability in crab stock recruitment. Additionally, recent trends may be influenced by ongoing changes in survey methodology associated with modernization efforts. Beginning in 2024, estimates are likely to be influenced by the aforementioned reduction in survey effort, particularly those for Pribilof red king crab and blue king crab, and St. Matthew blue king crab. Analyses suggest that impacts on estimates for stocks other than these are likely to be minor ($<<<$10%). Recent reviews of data have suggested that new net mensuration equipment first adopted in 2024 has eliminated the need for a correction factor that had been applied to area swept estimates, leading to post-hoc changes to data for 2024-2026. Finally, finer scale size-binning of crab in updated analysis codes has lead to minor changes in size class estimates ($\sim$1-2%).

Implications: The implications of the observed variability in crab stocks are dramatic inter-annual and inter-decadal variability in benthic predators and ephemeral (seasonal) pelagic prey resources when crab are in larval stages in the water column or as juveniles in the benthos. Although it is unclear at what life stage crab stock variability is determined, it is likely that environmental variability affecting larval survival and changes in predation affecting juvenile survival are important factors. As such, the environmental conditions affecting larval crab may also be important for larval demersal groundfish and the availability of crab as prey may be important for demersal fish distributions and survival. Disease may also be a factor, although this is speculative.

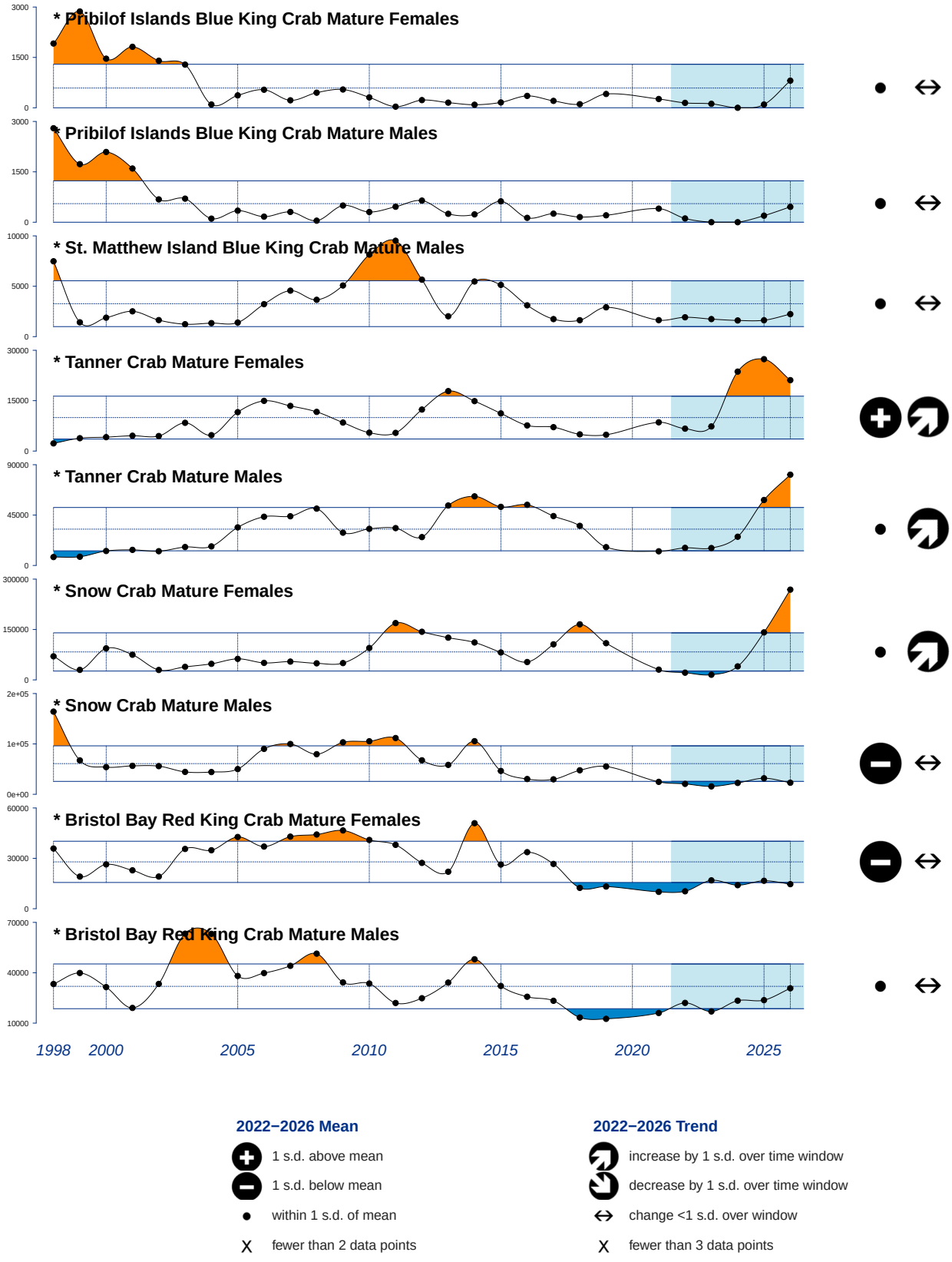


Figure 136: Biomass of commercial crab stocks caught on the NOAA eastern Bering Sea bottom trawl survey, 1998-2026.

Seabirds

Integrated Seabird Information

This integration is in response to ongoing collaborative efforts within the seabird community and contains contributions from (in alphabetical order):

Matthew Rustand – U.S. Fish & Wildlife Service, Alaska Maritime National Wildlife Refuge, Homer, AK
Florence Sullivan – Coastal Observation and Seabird Survey Team [COASST], Seattle, WA
Stephani Zador – Alaska Fisheries Science Center, NOAA Fisheries, Seattle, WA

Last updated: October 2026

Summary Statement
Seabirds at the Pribilof Islands in the southeastern Bering Sea were monitored by the Alaska Maritime National Wildlife Refuge throughout 2026. At the Pribilofs, 2026 was a strong reproductive year for monitored species, including common and thick-billed murres, black-legged and red-legged kittiwakes, and red-faced cormorants. On St. George Island, productivity across monitored species was consistently average, reflecting stable but typical breeding conditions. St. Paul Island experienced above-average productivity for murres, kittiwakes, and red-faced cormorants, indicating particularly favorable foraging conditions and good chick survival. Murres tended to initiate breeding slightly later than average, while kittiwakes bred earlier than average. Colony attendance in 2026 was stable for most species, further supporting the characterization of 2026 as a productive year for seabirds at the Pribilofs.

Introduction
Seabirds can be viewed as indicators of ecosystem changes in productivity therefore population-level responses can signal shifts in prey availability that may similarly affect commercial fish populations. In this Seabird Integration section, we synthesize information and observations from a variety of sources to provide an overview of environmental impacts to seabirds and what that may indicate for ecosystem productivity as it pertains to fisheries management. We merge across information sources to derive a regional summary for the southeastern Bering Sea and interpret changes in seabird dynamics with respect to understanding ecosystem productivity.

Approach
We focused on several attributes of seabirds that may serve as broader ecosystem indicators important to fisheries managers. We interpret these attributes as reflective of seabirds' life history and how they sample the ecosystem, either as fish-eating or plankton-eating species.

1. *Breeding timing* can represent conditions prior to breeding and/or phenological variation in the environment. Birds arriving to breed at an earlier date can reflect favorable winter and/or spring foraging conditions, or earlier peaks in ocean productivity.

2. *Reproductive success* can represent food availability around the colony during the breeding season, with a higher number of fledged chicks generally reflecting an increase in the local abundance of high-quality prey.

3. *Mortality* gives insight into environmental conditions and ecosystem impacts beyond breeding colonies and the breeding season.

Breeding and Reproductive Success

Southeastern Bering Sea (Pribilof Islands)

Common murres had average reproductive success on St. George Island, matching long-term norms, while St. Paul murres performed above average (Figure 137). The mean hatch date was near the long-term average on both St. George and St. Paul.

Thick-billed murres showed average productivity on St. George Island in 2026, remaining close to long-term means, while St. Paul Island saw strongly above-average reproductive success. The mean hatch date was near the long-term average on St. George and St. Paul.

Least auklets mean hatch date in 2026 on St. George Island was four days later than the mean. Least auklets productivity on St. George Island in 2026 was near average, indicating stable breeding performance.

Black-legged and red-legged kittiwake exhibited average productivity on St. George Island in 2026 while St. Paul's productivity was well above average. Kittiwakes hatched earlier than average on both islands.

Red-faced cormorants productivity monitoring indicated mixed results in 2026. On both St. Paul and St. George, boom-bust monitoring, which calculates reproductive success as a measure chicks per nest start, was below the long-term average. However, on St. Paul, where individual nest monitoring is also conducted, productivity measured as chicks fledged per nest start was above average, highlighting a more favorable outcome when using the finer-scale monitoring method.

A multivariate seabird breeding index (Figure 2) indicated that, on the whole, seabird reproductive timing and success at the Pribilof Islands was slightly above average in 2026, although there were minor differences between islands and species that may reflect local-scale processes and/or diversity in foraging strategies. Murres at both islands hatched chicks slightly later than average while kittiwakes were slightly earlier. Reproductive success and/or hatch timing can be influenced by their food supply, therefore above-average productivity or earlier hatch timing may indicate strong recruitment of year classes that seabirds feed on (e.g., age-0 pollock), or abundant forage fish that commercially fished species feed on (e.g., capelin eaten by both seabirds and Pacific cod).

Northern Bering Sea (including Hall Island, St. Lawrence Island, and the Bering Strait region)

A field crew was stationed at Hall Island from 28 July to 16 August 2026. Preliminary results show that colony index counts for black-legged kittiwakes, thick-billed murres, and common murres were comparable to counts from 2021 and 2019, suggesting stable colony attendance during the 2026 breeding season. Boom-bust productivity monitoring, which measures overall reproductive output as total chicks per total nests, yielded values of 0.75 chicks per nest for black-legged kittiwakes, 0.41 for thick-billed

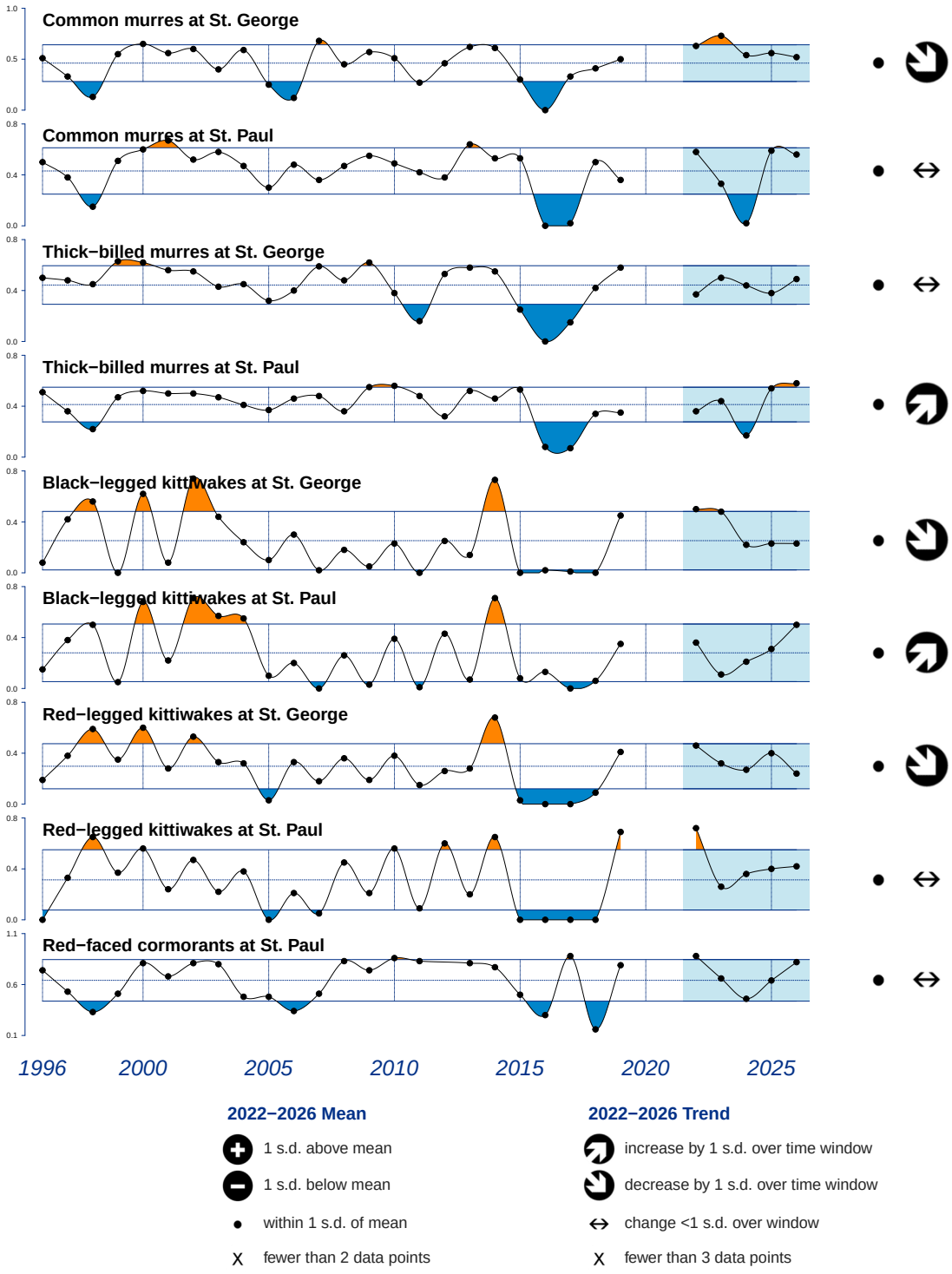


Figure 137: Reproductive success of five seabird species at St. George and St. Paul Islands between 1996-2026.

murres, and 0.64 for common murres. These boom-bust values are coarse but can provide early indicators of shifts in forage conditions: higher ratios often reflect periods of adequate prey availability, while lower ratios may signal years in which chick provisioning was constrained. In this context, the 2026 results suggest generally favorable feeding conditions around Hall Island.

Mortality

Eastern Bering Sea

Monitoring by the Coastal Observation and Seabird Survey Team (COASST) and regional partners provides a standardized measure of relative beached bird abundance. Carcass identifications are verified using collected measurements and photographs. Basic data (carcass count, identity, and condition information) are used to create a baseline (long-term normal) against which unusual events can be compared. Surveys began in the eastern Bering sea in 2006, and since that time, over 1512 surveys have taken place across 26 beaches; in 2026, 38 surveys took place across 11 beaches, mostly concentrated on the Pribilof Islands, but sites in Bristol Bay and near Nome were also surveyed. In 2025, 30 surveys took place across the same 11 beaches. Detailed methods for beached bird surveys can be found in Jones et al., 2019.

In 2026, surveyors reported very few bird carcasses across beaches in the Bering Sea.

In 2025, surveyors reported relatively low numbers of carcasses until an unusual mortality event occurred on St. George Island in August. Unusual mortality events are defined as encounter rates 5 times or more above the established baseline rate; see monthly encounter rates in 2019 and 2025 in Figure 138 for examples of elevated encounter rates indicative of such an event.

There are two COASST beaches monitored on St. George Island during the summer months by AMNWR seasonal biologists: Zapadni Beach and Staraya Artil. Both are 0.9 km in monitored length. Historically, island-wide carcass encounter rates in August on St. George Island were 1.74 $\pm$0.45 (mean, SE, N = 19 years). In August 2025, the single COASST survey (17 August 2025) recorded 52 carcasses on Staraya Artil and 8 on Zapadni. Averaging across these beaches, this translates into a carcass encounter rate $\sim$18 times higher than normal.

Intactness, or the proportion of carcasses found as fresh kills without wounds, is a measure of scavenger satiation, which is an indirect measure of multi-day carcass abundance. This can be another way to quantify die-off events, as greater intactness will be proportional with greater carcass abundance (e.g., scavengers become satiated because more carcasses are deposited than they can eat). Intactness rates between the two beaches in August also varied. Historically rates were low-to-nil (Staraya Artil 0%; Zapadni 37%), with rates increasing $\sim$25% during the August 2025 die-off event (Staraya Artil 27%; Zapadni 62%), indicating a significant increase in carcass deposition rates. For example, during the tufted puffin die-off of 2016-2017 on St. Paul Island, carcass intactness jumped from a historic average of 17% to 75% (Jones et al., 2019).

The species identity of carcasses discovered during August 2025 COASST surveys (N = 53; 17 August 2025) and by community members (N = 55; 4-19 August 2025) also varied relative to long-term trends (Figure 139).

August surveys are traditionally dominated by murres (mainly thick-billed), short-tailed shearwaters, northern fulmars, and least auklets, with a smattering of other species each making up 1-4% of the total. During the August 2025 event, the proportion of murres (thick-billed, common, undesignated) more than doubled to $\sim$57%, dominating the sample. At the same time, the proportion of northern fulmars fell from a historic value of 19.7% down to only 3.7%. Smaller, but notable changes occurred

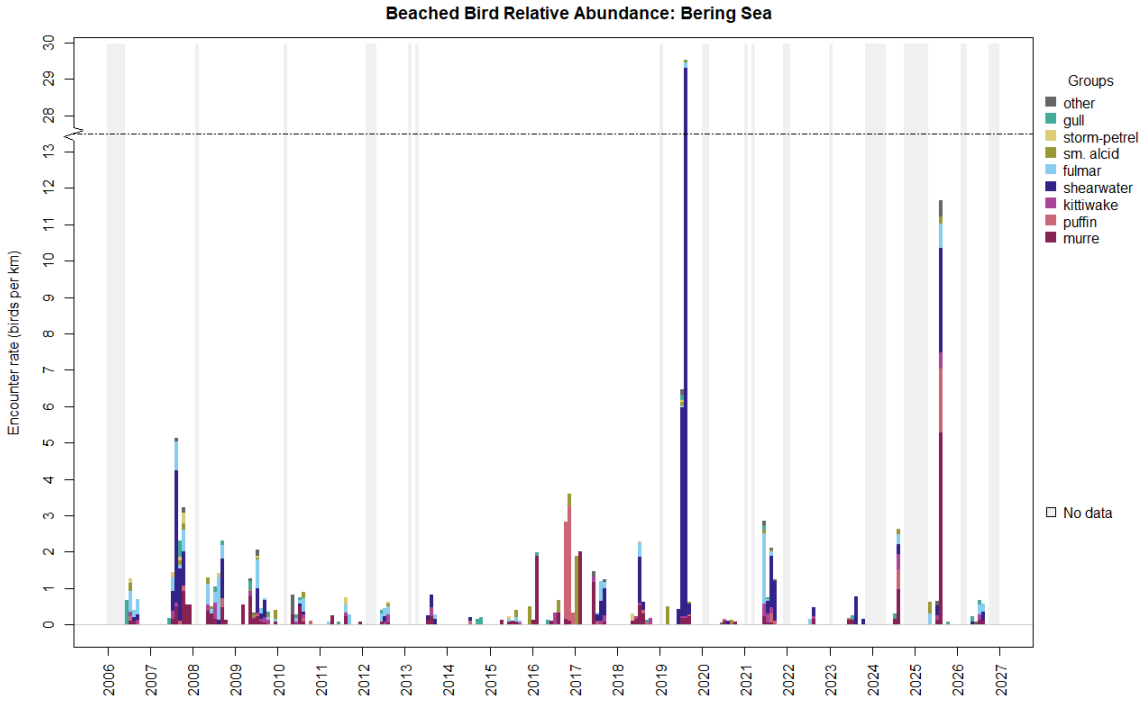


Figure 138: Month-averaged beached bird abundance, standardized per km of survey effort, for the eastern Bering Sea. Species groups (gull, storm-petrel, small alcid, fulmar, shearwater, kittiwake, puffin, murre) are depicted with different colors within each bar, with gray bars indicating months where no survey was conducted. Note that a break in the y-axis between 13 and 28 birds/km, indicated by the dashed line, shows the magnitude of the 2019 die off while still being able to distinguish patterns among other years. Credit: COASST.

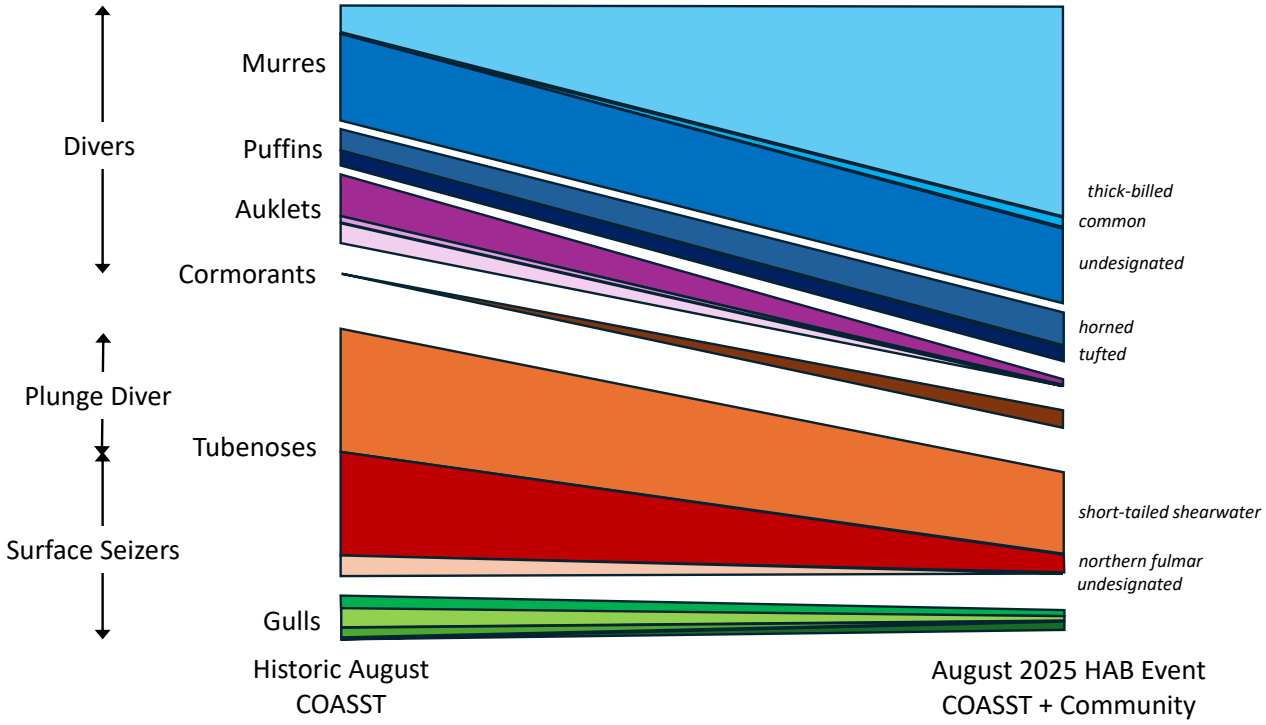


Figure 139: A comparison of the species composition of carcasses documented in August 2025 on St. George Island. On the left, the proportions of each species found during August COASST surveys between 2006-2024 (N = 19 years). On the right, the proportions of species found during COASST surveys with additional community reports from the August 2025 event. Species and species groups are indicated by color and labeled on the y axis. Additionally, foraging guilds are indicated on the far left.

in the auklets (least, parakeet, undesignated) from 13.2% historically to just under 1% in August 2025; and cormorants which were unrepresented in the historic data but made up 3.7% (N = 4 individuals found) in August 2025.

Abstracting to foraging guilds, large-bodied, diving piscivores appeared to be most sensitive to the August 2025 event, whereas small-bodied diving omnivores (i.e., auklets) and surface seizers (northern fulmars, kittiwakes, gulls, terns) were relatively unaffected. Plunge divers (shearwaters), able to access up to 15 m of the upper ocean, were affected.

Implications

Fish-eating, surface feeding seabirds include black-legged kittiwakes who feed on small schooling fish that are available at the surface (e.g., capelin, Arctic cod, juvenile pollock and juvenile herring), making them potential indicators of processes affecting juvenile groundfish that migrate to the surface to feed. Fish eating, diving seabirds include common murres who feed on small schooling fish (age-0 and age-1 pollock) to depths up to 90 m, thus they have access to fish throughout the water column and to the ocean bottom in shallow areas.

Planktivorous seabirds include least and crested auklets, which feed primarily on copepods and euphausiids. Shearwaters and thick-billed murres also consume euphausiids, along with larvae and small fish. All of these species are indicators of feeding conditions for planktivorous groundfish species, including the larvae and juveniles of fish-eating species.

Marine Mammals

Integrated Marine Mammal Information

This synthesis is a collaborative effort and contains contributions from (in alphabetical order by affiliation):
Aaron Lestenkof, Chelsea Campbell, Dallas Melovidov, Paul Melovidov – Ecosystem Conservation Office, Aleut Community of St. Paul Island, AK
Carey Kuhn, Erin Richmond, Jeremy Sterling, Josh London, Katie Luxa, Rod Towell, Rolf Ream, Tom Gelatt, Tonya Zeppelin – Marine Mammal Laboratory, Alaska Fisheries Science Center, NOAA Fisheries, Seattle, WA
Michael Williams – Protected Resources Division, Alaska Regional Office, NOAA Fisheries, Anchorage, AK

Synthesis compiled by **Elizabeth McHuron** – Cooperative Institute for Climate, Ocean, and Ecosystem Studies (CICOES), University of Washington, Seattle, WA

Synthesis Summary
Harbor seals and northern fur seals were monitored at the Pribilof Islands in 2025 and 2026 through collaborations between NOAA researchers and the Aleut Community of St. Paul Island. Population abundance was estimated for harbor seals, who are year-round residents in the nearshore ecosystems of St. Paul, St. George, and Otter Islands. The most recent (2023) population estimate for all three islands was 331 harbor seals, with an 8-year trailing trend (2015-2023) of +1.53% per year. Data collected on northern fur seals, who are seasonally present in summer and fall on St. Paul and St. George Islands, included maternal foraging trip duration, pup mass, and diet samples. Maternal foraging trip durations in 2025 and 2026 were below the long-term St. Paul Island average, with the shortest average trip duration reported at St. Paul Island in 2026 in over a decade of continuous monitoring. Shorter trip durations translated to above-average October female pup masses, with pups at St. Paul Island heavier than those at St. George Island in 2026. Since 2021, observed maternal trip durations and pup masses at St. Paul Island have been more in line with those at St. George Island, and 2025 and 2026 continue this trend. This indicates favorable fur seal feeding conditions in relative proximity to the Pribilof Islands (<150 km) in the past six years, with particularly good conditions within 120 km to the north and northwest of St. Paul Island across the outer and middle shelf regions in 2026. Pacific herring occurred frequently in the September 2025 diet of St. Paul Island fur seals, and preliminary September 2026 observations indicate herring was present in fur seal diets at both islands. Walleye pollock were also frequently consumed in 2025, predominantly age-0 pollock. Fur seal mortalities from saxitoxin were reported in 2025, indicating observed blooms of *Alexandrium catenella* that produce saxitoxin were transferred into the upper trophic levels of the eastern Bering Sea food web. The population implications of recent ecosystem conditions on northern fur seals are unknown because pup production has not been reported since 2022; however, observed pup masses and maternal trip durations at St. Paul Island are more consistent with those measured in populations that have experienced recent growth, including St. George Island.

Introduction

Marine mammals are indicators of ecosystem productivity and health, with different species providing information across different components of the ecosystem. As large mammalian endotherms, they have high energy requirements, are responsive to changes in prey availability, and also play important roles in marine food webs, including through impacts on natural mortality rates of prey species. Indicators derived from marine mammals can provide information on the distribution and availability of resources, the presence of biotoxins, and also inform the ability of local ecosystems to sustain healthy marine mammal populations, which speaks to overall ecosystem health.

Northern Fur Seals

Northern fur seals (*Callorhinus ursinus*) occur seasonally in the eastern Bering Sea where they breed on the Pribilof Islands and Bogoslof Island, collectively managed as the Eastern Pacific Stock. Fur seal pups are dependent on their mothers for milk during the 4-month lactation period, with lactating females alternating foraging trips at sea with nursing visits onshore. Spatial variation in foraging areas among and within islands leads to variation in diet composition (Zeppelin and Ream, 2006; Robson et al., 2004), where sites in close geographical proximity (referred to as 'complexes') tend to exhibit similarities in foraging locations and diet. There are five complexes on the Pribilof Islands, two on St. George Island, and three on St. Paul Island. Primary prey items are generally shared across Pribilof Island complexes, including pollock, salmon, several forage fish species, and squid. Complex-specific diet variation broadly aligns with population trends, where complexes that have the greatest dependence on pollock have experienced negative population growth (Musbach et al., 2024).

Indicator description

We focus on four northern fur seal measurements: maternal trip duration, female pup mass, prey occurrence in the diet, and pup production (the total number of pups born in a given year). The first three measurements reflect within-season conditions, whereas pup production is a lagged index that integrates ecosystem conditions across multiple years.

1. *Maternal trip duration* is influenced by the distribution and availability of prey, with longer trips occurring when females travel further from the rookery to find sufficient resources (Kuhn et al., 2014). Maternal trip duration also tends to fluctuate throughout the season as the environment and pup energy needs change. *Contributors: Jeremy Sterling, jeremy.sterling@noaa.gov, Rolf Ream, and Michael Williams.*

2. *Female pup mass* is inversely related to the duration of maternal foraging trips (Merrill et al., 2021). Pups that experience shorter maternal absences (i.e., more frequent nursing visits) spend less time fasting and grow better than pups that experience longer maternal absences (Springer et al., 2008). Pup mass also may be influenced by maternal condition, prey energy density, and air temperatures. Pup mass at weaning is believed to be positively related to post-weaning survival rates (Baker and Fowler, 1992; Rutishauser et al., 2004; Beauplet et al., 2005). *Contributors: Rolf Ream, rolf.ream@noaa.gov, Chelsea Campbell, Dallas Melovidov, Aaron Lestenkof, Paul Melovidov, Michael Williams, Tom Gelatt, and Jeremy Sterling.*

3. *Prey occurrence* in scat and spew samples provides an index of relative abundance of prey species because fur seals are generalist predators that prey on the most abundant and readily accessible fish and squid species (Kajimura, 1984). Hard parts can also be used to identify the size/age composition of prey species (Harvey et al., 2000). *Contributors: Tonya Zeppelin, tonya.zeppelin@noaa.gov, and Katie Luxa.*

4. *Pup production* is an index of population abundance that is influenced by the number of adult females in the population and pregnancy and birth rates. Pup production is affected by female survival at all life stages, including as pups when foraging conditions in the eastern Bering Sea affect their growth and subsequent survival and recruitment into the population between four to seven years of age. *Contributors: Rolf Ream, Jeremy Sterling, Rod Towell, and Tonya Zeppelin.*

Status and trends

Maternal trip duration

Maternal trip durations are summarized seasonally from June to September 15th using data transmitted and recorded from VHF tags attached to adult females (Figure 140, top). In 2026, St. Paul Island recorded its shortest observed maternal trip durations (mean ±95% CI: 3.9 ±0.2 days). St. George Island was excluded in 2025 due to a VHF recorder malfunction and in 2026 due to low sample size (only two tagged maternal females observed). Since 2020, St. Paul Island trip durations have declined to levels seen on St. George since 2017. In September of 2026, 91 VHF transmitters were attached to adult females on both St. Paul and St. George Islands as part of a long-term population monitoring program and collaboration with the Aleut Community of St. Paul Island (ACSPI).

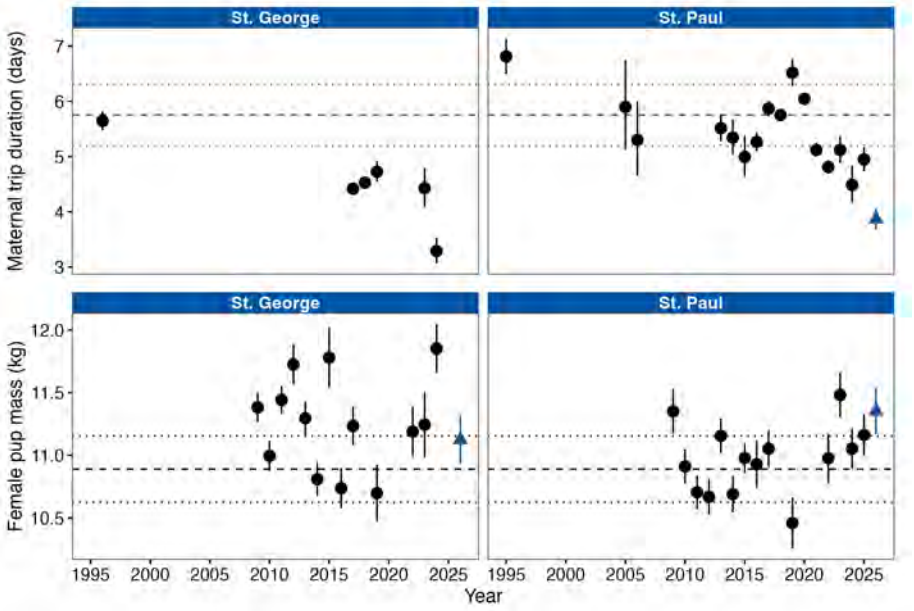


Figure 140: Northern fur seal indicators of maternal trip duration from June to September 15th (top) and female pup mass standardized to October 1 (bottom) at St. George and St. Paul Islands. Error bars are the 95% confidence intervals around the mean, whereas dashed lines indicate the pre-2020 mean and interannual standard deviation at St. Paul Island. Measurements collected in 2026 are shown as a blue triangle.

Female pup mass

Pup masses were collected in September 2025 at St. Paul Island and in 2026 at both islands. In 2026, female pup masses at both islands (standardized to October 1) were above the St. Paul Island 2009-2019 average (Figure 140, bottom). Across the time series, pups from St. George Island are statistically heavier than those from St. Paul, but in 2026 female pups at St. Paul were heavier than those from St. George. The 2026 data continue the several year trend at both islands of female pup masses above the St. Paul average, consistent with the relatively short maternal trip durations during this time.

Prey occurrence

Diet samples were collected on St. Paul Island from two fur seal complexes in late September 2025. Samples were also collected in late September 2026 on St. Paul and St. George Islands but analysis is ongoing. In 2025, there were seven prey species or groups that had greater than 10% frequency of occurrence (FO) at one or more complexes (Figure 141). Pacific herring and pollock were the most frequently occurring prey, though species rankings varied by complex. Age-0 was the dominant age class of pollock consumed, but other age classes, including adult pollock, were also consumed (Figure 141).

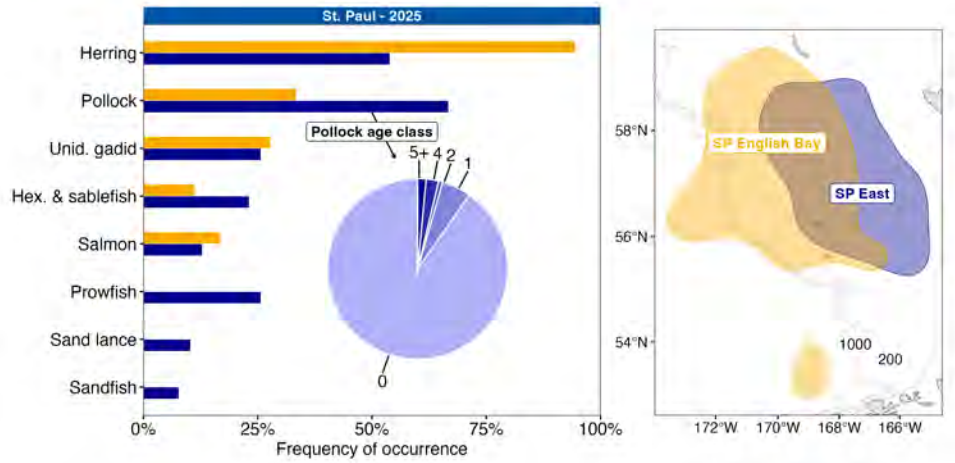


Figure 141: Left: The frequency of occurrence in diet samples collected in September 2025 at two complexes on St. Paul Island (English Bay, n = 18; East, n = 39). The inset pie chart shows the age-composition of pollock consumed from the East complex. Right: The foraging areas used by females at each complex with 200 m and 1000 m isobaths.

Pup production

No data on Pribilof Island pup production have been reported since 2022. Pup production at St. Paul Island declined at an annual rate of 3.95% between 1998 and 2022 (Figure 142). Between the last two full island surveys in 2018 and 2022, pup production at St. Paul Island declined by 11.8%. Pup production at St. George Island saw no significant trend between 1998 and 2022, but it increased at an annual rate of 4.7% since its lowest point in 2012 (Figure 142).

Other observations

The first confirmed northern fur seal mortalities from saxitoxin poisoning occurred in August 2024 and 2025 on St. Paul and St. George Islands, respectively (Lefebvre et al., 2025*a*). Mortalities coincided with the detection of large *Alexandrium catenella* blooms in the southeast Bering Sea (Ostle et al., 2026), the marine dinoflagellate responsible for producing saxitoxin (see p. 267).

Pacific harbor seals

Contributions from Josh London, josh.london@noaa.gov, Erin Richmond, and Aaron Lestenkof

Pacific harbor seals (*Phoca vitulina richardii*) are an important protected species in Alaska that are year-round residents of intertidal shorelines, bays, and estuaries. They are a key upper-trophic predator, a valuable cultural resource for Alaska Native communities, and serve as sentinels of nearshore ecosystems. There are 12 demographically independent Alaska harbor seal management stocks recognized by the National Marine Fisheries Service. Of these stocks, the Pribilof Islands (the smallest) and Bristol Bay (the largest) reside within the eastern Bering Sea, with the Pribilof Islands stock being unique in its geographic isolation. There is limited diet data available for the Pribilof Island harbor seal stock, with

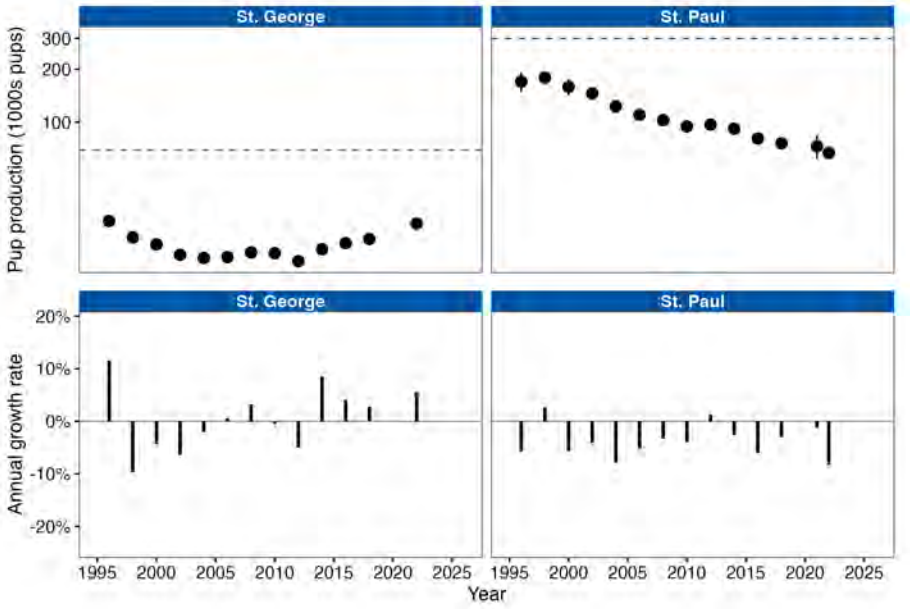


Figure 142: Northern fur seal indicators of total pup production (top) and annual growth rates (bottom) at St. George and St. Paul Islands. Pup production is presented on a log scale with associated standard error estimates. For historical context, the dashed line represents the 1966 estimate of pup production at each island.

scat samples collected from Otter Island in August 2018 containing Pacific cod, northern rock sole, and Irish lord spp. While some dietary overlap with northern fur seals is expected based on harbor seal diets in other parts of Alaska (Geiger et al., 2013; Pitcher and Calkins, 1979), harbor seals are more nearshore and tend to have a greater dependence on demersal species than northern fur seals.

Indicator description

We focus on a single indicator, *population abundance*, which is an integrated measure that reflects the current and previous years influence on survival and reproductive rates. Alaskan stock abundance and trend estimates for harbor seals are largely derived from multi-decadal aerial survey efforts and a two-stage Bayesian hierarchical model that accounts for temporal variation in survey effort (Boveng et al., 2026; Ver Hoef et al., 2025). The Pribilof Island stock requires a different approach because of its small size and remoteness. Sporadic and opportunistic efforts to obtain shore-based counts on the Pribilof Islands occurred between 1974 and 2015. Since September 2018, there have been collaborative efforts among ACSPI, NOAA Alaska Fisheries Science Center, and Duke University to comprehensively survey harbor seals in the Pribilof Island region using small, uncrewed aerial systems.

Status and trends

Population Abundance

Counts from 1974 to 2015 on St. George and Otter Islands ranged widely (100 to 1200 seals) based on sporadic surveys predominately conducted in July. Recent annual survey efforts, largely conducted by ACSPI from June to August, continued on Otter, St. Paul, and St. George Islands through 2026. Counts from these surveys, analyzed through 2023, contribute to a 2023 abundance estimate of 331 (95% CI: 242–449) harbor seals and an 8-year trailing trend (2015-2023) of +1.53% per year.

Marine Mammal Strandings

Contributed by Jenna Malek and Carley Lowe
Protected Resources Division, Alaska Regional Office, NOAA Fisheries
Contact: jenna.malek@noaa.gov
Last updated: September 2026

Description of indicator: Since 1985, members of the NMFS Alaska Marine Mammal Stranding Network (AMMSN) have collected and compiled reports on marine mammal strandings throughout the state. These reports are indices of events witnessed by members of the stranding network, the scientific community, and the general public, with varying degrees of knowledge regarding marine mammal biology and ecology. A marine mammal is considered "stranded" if it meets one of the following criteria: 1) dead, whether found on the beach, ice, or floating in the water; 2) alive on a beach (or ice) but unable to return to the water; 3) alive on a beach (or ice) and in need of apparent medical attention; or 4) alive in the water and unable to return to its natural habitat without assistance. The causes of marine mammal strandings are often unknown but some causes include disease, exposure to contaminants or harmful algal blooms, vessel strikes, and entanglement in or ingestion of human-made gear or debris.

When a stranded marine mammal is reported, information is collected including species, location, age class or size. In some cases, the initial photos and observations reported to AMMSN may be the only opportunity to collect information on the event. When possible, trained and authorized AMMSN members respond and collect life history data and samples as part of a postmortem examination. Photos and carcasses are evaluated for potential human interactions such as entanglement. These responses are conducted under the Marine Mammal Protection Act authorization either under a 112(c) agreement issued by NMFS to AMMSN members through a Stranding Agreement or under 109(h) authority exercised by local, state, federal, or tribal entities. All responses involving ESA-listed species and some enhanced responses (e.g., remote sedation) are authorized under the NOAA Permit No. 24359.

Status and trends: The number of confirmed strandings in Alaska has increased over time. Stranding data was not included in the 2025 Ecosystem Status Report; the current report includes complete 2024 and 2025 stranding data (January 1 - December 31; Table 9), in addition to data from January 1, 2026 through September 30, 2026. Thus far in 2026, 215 confirmed stranded marine mammals were reported within Alaska; 75 occurred in the eastern Bering Sea (Table 9). These numbers do not include entangled pinnipeds with no response or live, entangled baleen whales. The majority of reports were from more populated areas where AMMSN members are located (Figure 143 and 144). Further, increased outreach and dedicated surveys associated with high priority species or events (e.g., northern fur seal entanglement survey and response on St. Paul Island) also contributed to reported strandings in some areas and years. Reported strandings in the eastern Bering Sea region since 2022 varied between years without an overall pattern or consistent increase in reports (Table 9). The data from January 1, 2026 through September 30, 2026 are preliminary and the details may change as we review reports and receive additional information.

Factors influencing observed trends: It is important to recognize that stranding reports represent effort that has varied substantially over time and location. Human population and activity in an area influences the potential for a carcass or stranded marine mammal to be observed and reported. Overall,

[52]For clarity, unidentified baleen whales were grouped together for the map. Please see Table 9 for exact genus or species identification.

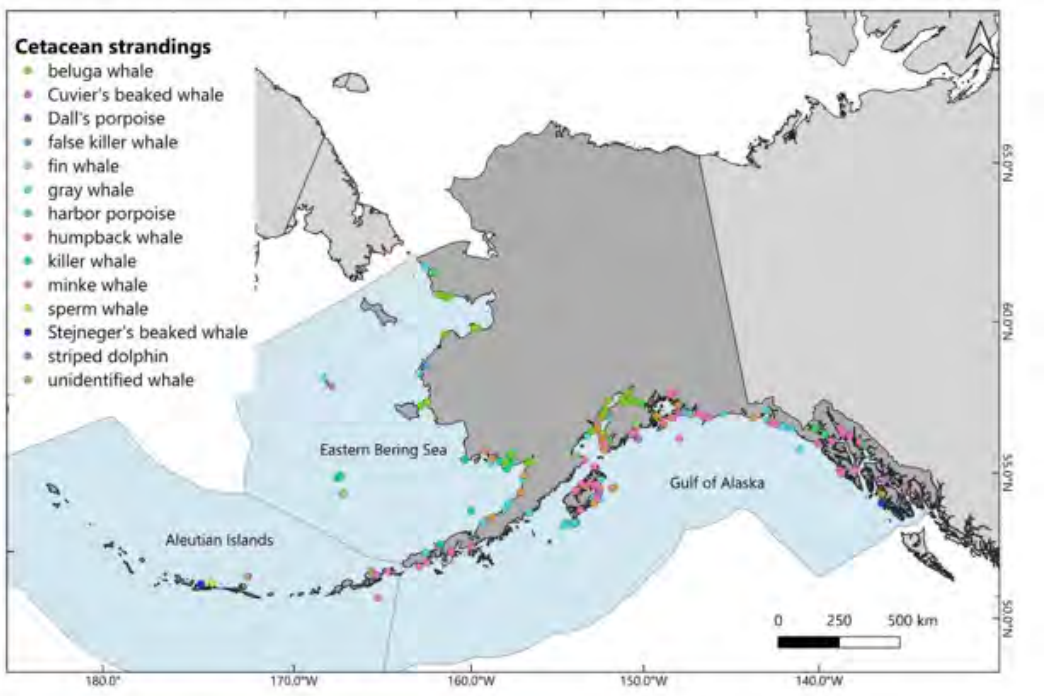


Figure 143: Reported cetacean[52]strandings from Sept 1, 2024 through Sept 30, 2026 in Alaska.

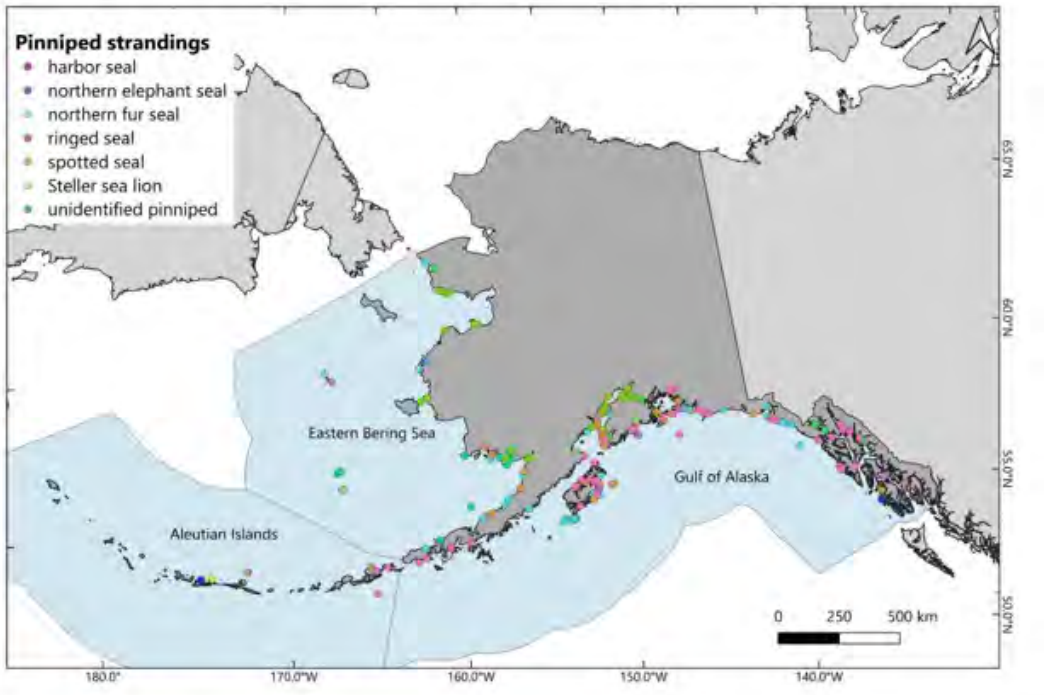


Figure 144: Reported pinniped strandings from Sept 1, 2024 through Sept 30, 2026 in Alaska.

this effort has increased across Alaska and particularly in areas with higher human population densities. Unusual Mortality Events (UME), including the 2019 gray whale UME, can have a large influence on variability between years in this area (Table 9). Under the Marine Mammal Protection Act, an UME is defined as "a stranding that is unexpected; involves a significant die-off of any marine mammal population; and demands immediate response".

Other factors that may influence the number and species of marine mammals being reported include changing populations of some species including the increase in northern fur seals using Bogoslof Island for breeding prior to its most recent eruption. Further, the number of stranded marine mammals in an area can vary due to the potential conflict with fishery resources either directly through prey competition or indirectly through interactions with fishing gear such as increased entanglements (e.g., harbor porpoise caught in subsistence salmon nets). Within the eastern Bering Sea region, there has been a dramatic increase in stranded northern fur seals since 2022 (Table 9). Nearly all of these fur seals were alive and disentangled by the Ecosystem Conservation Office (ECO) of the Aleut Community of St. Paul Island, an AMMSN member. Under the Examiners Guide[53] the Level A and Human Interaction forms are completed for entangled pinnipeds when a response is conducted and the animal is in-hand. Observations of entangled pinnipeds with no response are captured in the Alaska Region dataset and by the ECO database but these observations are not part of the National Stranding Database. In 2021, the Aleut Community of St. Paul Island increased ECO team efforts which allowed entangled northern fur seals observed during their weekly entanglement surveys or subsistence efforts to be captured and disentangled (Table 9, Figure 144). Therefore, the increase in stranded northern fur seals since 2022 in this region is due, at least in part, to reporting requirements and the successful capture and disentanglement of northern fur seals by the Aleut Community of St. Paul Island, rather than solely due to an increase in entanglements.

Implications: Across Alaska, reported marine mammal strandings have varied by year and location. It is important to track and have a sense of the regular number of strandings in an area to provide a context to mass strandings or Unusual Mortality Events. Marine mammal stranding data can be paired with other datasets and may give clues to ecosystem-wide changes or other stressors. For example, in 2019, the increase in gray whale strandings across the migration route between Mexico and Alaska led to the declaration of an UME which continued until November 2023. There were 148 stranded gray whales in Alaska during this UME. The UME Investigative Team concluded that the preliminary cause of this UME was localized ecosystem changes in the whale's subarctic and Arctic feeding areas that led to changes in prey availability, leading to malnutrition, decreased birth rates, and increased mortality. After several years of decreased stranding numbers, there has been an increase in gray whale strandings from 2024 to present, with a total of 67 animals (13 reported in the eastern Bering Sea; Table 9. The factors documented as causes of death during the gray whale UME may also be responsible for the recent increase in strandings, but further assessment is needed. As in the case of the gray whale UME, increases in marine mammal strandings, when paired with other datasets, may signal changes in the environment or other stressors (e.g., human interactions such as entanglements, vessel strikes).

[53] https://media.fisheries.noaa.gov/2021-07/EXAMINERS%20GUIDE_2024%20FINAL.pdf?

[54] 2026 stranding data includes confirmed strandings reported between January 1, 2022 and September 30, 2026.

[55] Most of the northern fur seals in the eastern Bering Sea region in 2022-2026 were alive and entangled in fishing gear or debris. Seals were captured, disentangled, and immediately released by the Aleut Community of St. Paul Island. There was a group event of ten dead northern fur seals and a large number of cod and sole observed on Benson Beach, a known catcher beach on St. Paul Island on August 18, 2024.

Table 9: Reported NMFS marine mammal strandings from 2022-2026[54] in the eastern Bering Sea region by species. The numbers represent combined dead and live strandings.

Species	**2022**	**2023**	**2024**	**2025**	**2026**
Baird's beaked whale		1			
Beluga whale	6	5	3	10	7
Bowhead whale	1				
False killer whale			1		
Fin whale				2	1
Gray whale	4	3	1	6	6
Harbor porpoise	3	3	6	4	1
Humpback whale	3	1		3	1
Killer whale	1	1	2	2	9
Minke whale	1	1			1
Pacific white-side dolphin		1			
Unidentified balaenopterid whale				1	1
Unidentified baleen whale	1	4	1		
Unidentified cetacean	4	2	2		3
Total Cetaceans	**24**	**22**	**16**	**28**	**30**
Harbor seal		5	3	4	
Northern fur seal[55]	49	57	48	87	40
Ringed seal	4	2	1	1	
Spotted seal	2			1	
Steller sea lion	3	5	3	3	3
Unidentified phocid					1
Unidentified pinniped			1	1	1
Total Pinnipeds	**58**	**69**	**56**	**97**	**45**
Total Animals	**82**	**91**	**72**	**125**	**75**

Ecosystem or Community Indicators

Mean Lifespan of the Fish Community

Contributed by George A. Whitehouse
Cooperative Institute for Climate, Ocean, and Ecosystem Studies (CICOES), University of Washington, Seattle, WA
Contact: gaw@uw.edu
Last updated: September 2026

Description of indicator: The mean lifespan of the community is a proxy for the turnover rate of species and communities and reflects the resistance of the community to perturbations (Shin et al., 2010). Lifespan estimates of groundfish species regularly encountered during the NMFS/AFSC annual summer bottom-trawl survey of the eastern Bering Sea were retrieved from the AFSC Life History Database[56]. The groundfish community mean lifespan is weighted by biomass indices calculated from the bottom-trawl survey catch data.

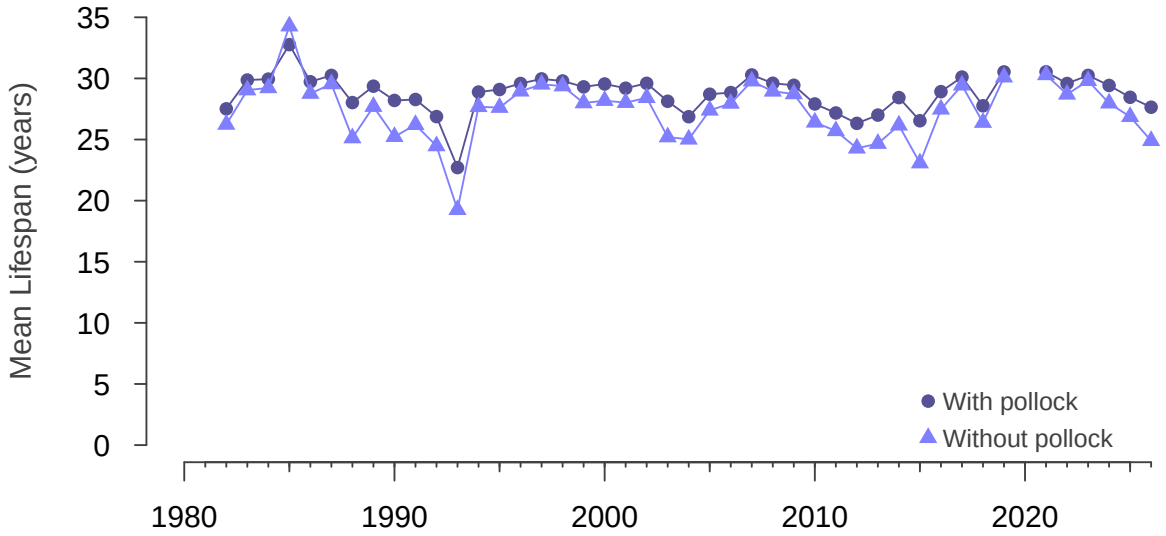


Figure 145: The mean lifespan of the eastern Bering Sea demersal fish community, weighted by biomass indices calculated from the NMFS/AFSC annual summer bottom-trawl survey. The circles are the series with pollock included and the triangles are the series without pollock included.

This indicator specifically applies to the portion of the demersal groundfish community that is efficiently sampled by the trawling gear used by NMFS during this survey at the standard survey sample stations (for survey details see Markowitz et al., 2023). Species that are infrequently encountered or not efficiently caught by the bottom-trawling gear are excluded from this indicator (e.g., sharks, grenadiers, myctophids, pelagic smelts). The survey index used here is the same as that used for foraging guild biomass indices on the report card (Figure 2).

[56] https://apps-afsc.fisheries.noaa.gov/refm/reem/lhweb/index.php

Walleye pollock is a biomass dominant species in the eastern Bering Sea and may drive the value of community indicators. Therefore, this indicator is presented as two series, one with and one without walleye pollock.

Status and trends:
With pollock included: The mean lifespan of the eastern Bering Sea demersal fish community in 2026 is 27.6, down from 28.5 years in 2025, and is below the time series mean of 28.8 years (Figure 145, circles). Mean groundfish lifespan has generally been stable over the time series with only a small amount of year-to-year variation.

Without pollock included: The mean lifespan of the eastern Bering Sea groundfish community without pollock in 2026 is 24.9, down from 26.9 years in 2025. Over the times series, the patterns and trends are similar between the two series with the values being slightly lower for the series without pollock (Figure 145, triangles). The exception to this pattern was 1985 when the mean lifespan was 32.8 with pollock included and 34.3 without pollock.

Factors influencing observed trends: Fishing can affect the mean lifespan of the groundfish community by preferentially targeting larger, older fishes, leading to decreased abundance of longer-lived species and increased abundance of shorter-lived species (Pauly et al., 1998). Interannual variation in mean lifespan can be influenced by the spatial distribution of species and the differential selectivity of species and age classes to the trawling gear used in the survey. Strong recruitment events or periods of weak recruitment could also influence the mean community lifespan by altering the relative abundance of age classes and species. For example, the low value observed in 1993 reflects a year of peak biomass index for capelin, a shorter-lived species. The peak mean lifespan for both series in 1985 was in part elevated by high biomass indices for long-lived species, such as sablefish. The lifespan of pollock is slightly higher than the mean groundfish lifespan without pollock. When pollock are removed from this indicator, there is a small decrease in value, but the same overall trend is followed. The downward trend in both series from 2023 to 2026 coincides with a decreasing trend in the shelf survey biomass index of sablefish, a relatively long-lived species.

Implications: The groundfish mean lifespan has been stable over the time series of the summer bottom-trawl survey. There is no indication longer-lived species have decreased in relative abundance or are otherwise being replaced by shorter-lived species. Species that are short-lived are generally smaller and more sensitive to environmental variation than larger, longer-lived species (Winemiller, 2005). Longer-lived species help to dampen the effects of environmental variability, allowing populations to persist through periods of unfavorable conditions and to take advantage when favorable conditions return (Berkeley et al., 2004; Hsieh et al., 2006).

Mean Length of the Fish Community

Contributed by George A. Whitehouse
Cooperative Institute for Climate, Ocean, and Ecosystem Studies (CICOES), University of Washington, Seattle, WA
Contact: gaw@uw.edu
Last updated: September 2026

Description of indicator: The mean length of the groundfish community tracks fluctuations in the size of groundfish over time. This size-based indicator is sensitive to the effects of commercial fisheries because larger predatory fish are often targeted by fisheries and their selective removal would reduce mean size (Shin et al., 2005). This indicator is also sensitive to shifting community composition of species with different mean sizes. Fish lengths are routinely recorded during the NMFS bottom trawl survey of the eastern Bering Sea, which occurred each year from 1982 to 2026, except in 2020. Mean lengths are calculated for groundfish species (or functional groups of multiple species, e.g., eelpouts) from the length measurements collected during the trawl survey. The mean length for the groundfish community is calculated with the species mean lengths, weighted by biomass indices (Shin et al., 2010) calculated from the bottom-trawl survey catch data.

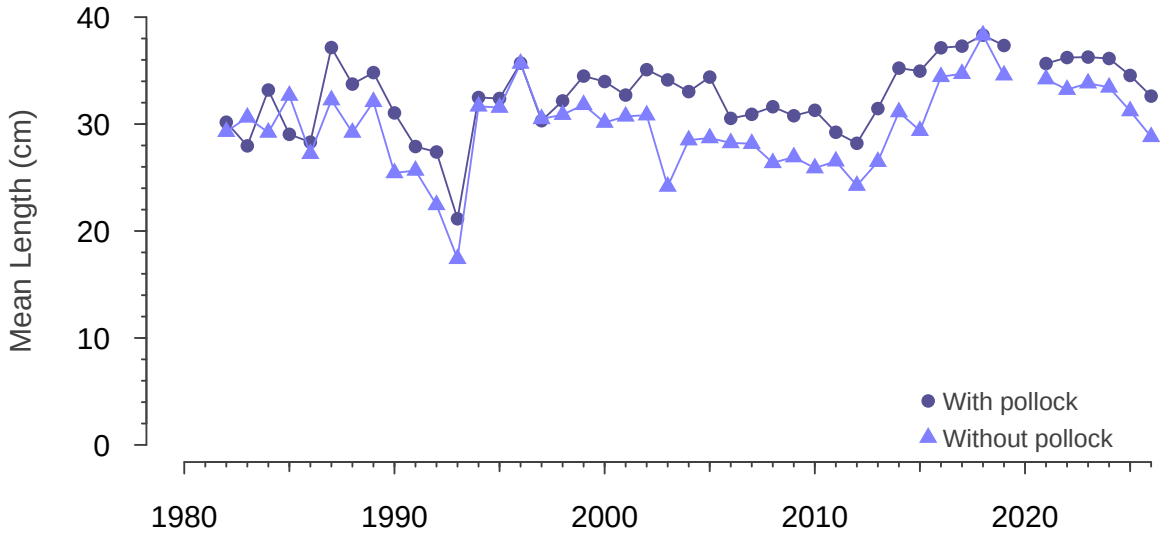


Figure 146: Mean length of the groundfish community sampled during the NMFS/AFSC annual summer bottom-trawl survey of the eastern Bering Sea (1982-2026). The groundfish community mean length is weighted by the relative biomass of the sampled species. The circles are the mean length with pollock included and the triangles are the series without pollock.

This indicator specifically applies to the portion of the demersal groundfish community that is efficiently sampled with the trawling gear used by NMFS during the summer bottom-trawl survey of the EBS at the standard survey sample stations (for survey details see Markowitz et al., 2023). Species that are infrequently encountered or not efficiently caught by the bottom-trawling gear are excluded from this indicator (e.g., sharks, grenadiers, myctophids, pelagic smelts). The survey index used here is the same as that used for foraging guild biomass indices on the report card (Figure 2).

Species (or functional groups) infrequently sampled for lengths (less than five times over the time series) are excluded from this indicator (e.g., capelin, eulachon, greenlings). Twenty-two species are included. Eleven species had their lengths sampled in all 44 years of the survey time series. Another 11 species were sampled between 11 and 41 times over the time series. In years when a species' lengths were not sampled, we replaced with a long-term mean for that species.

Walleye pollock is a biomass dominant species in the eastern Bering Sea and may drive the value of community indicators. Therefore, this indicator is presented as two series, one with and one without pollock included.

Status and trends:
With pollock included: The mean length of the eastern Bering Sea groundfish community in 2026 is 32.6 cm, down from 34.5 in 2025, but nearly equal to the long term mean of 32.7 (Figure 146, circles).

Without pollock included: The mean length of eastern Bering Sea groundfish without pollock is 28.8 cm in 2026, down from 31.2 cm in 2025, and below the long term mean of 29.7 cm (Figure 146, triangles). This series trended upward from 2012 to 2018 but has trended downward in the years since.

Factors influencing observed trends: This indicator is specific to fishes that are routinely caught and sampled during the NMFS summer bottom-trawl survey. The estimated mean length can be biased if specific species-size classes are sampled more or less than others and is sensitive to spatial variation in the size distribution of species. Changes in fisheries management or fishing effort could also affect the mean length of the groundfish community. Modifications to fishing gear, fishing effort, and targeted species could affect the mean length of the groundfish community if different size classes and species are subject to changing levels of fishing mortality. The mean length of groundfish could also be influenced by fluctuations in recruitment, where a large cohort of small forage species could reduce mean length of the community. Environmental factors could also influence fish growth and mean length by affecting the availability and quality of food or by direct temperature effects on growth rate.

Pollock is a biomass dominant component of this ecosystem and year-to-year fluctuations in their mean size and biomass have a noticeable effect on this indicator. In 1993, their biomass index was above average, but their mean size was the fifth lowest of the time series. Additionally, 1993 was a pronounced peak in the biomass index of capelin. This reduced the proportional contribution of other species to total groundfish biomass index, thus reducing the indicator value in 1993. Years where this indicator attained its highest values (1987, 2016-2024) generally correspond to years of above average mean size and/or biomass index for pollock, except 2018, 2021, and 2023 where pollock mean size was above average but their biomass index was below average.

The series without pollock mirrored the overall trends in the series with pollock included, but was generally lower. This was because the mean length of pollock was generally a few cm greater than the mean length of the rest of the groundfish community. Exceptions occurred in 1983, 1985, and 2018 when the mean length of pollock was less than the mean of the rest of the groundfish community.

Implications: The mean length of the groundfish community in the EBS has been stable over the bottom-trawl time series (1982-2026) with some interannual variation. The collective stability of the combined biomass of relatively larger groundfish species has helped to maintain this indicator at its recent high values. Previous dips in this indicator were in part attributable to spikes in abundance of smaller forage species (e.g., capelin) as opposed to a sustained shift in community composition or reductions in species mean length.

Stability of Fish Biomass

Contributed by George A. Whitehouse
Cooperative Institute for Climate, Ocean, and Ecosystem Studies (CICOES), University of Washington, Seattle, WA
Contact: gaw@uw.edu
Last updated: September 2026

Description of indicator: The stability of the groundfish community total biomass is measured with the inverse biomass coefficient of variation (1 divided by the coefficient of variation of total groundfish biomass (1/CV[B])). This indicator provides a measure of the stability of the ecosystem and its resistance to perturbation. The variability of total community biomass is thought to be sensitive to fishing and is expected to increase with increasing fishing pressure (Blanchard and Boucher, 2001). The CV is the standard deviation of the groundfish biomass index over the previous 10 years divided by the mean biomass over the same time span (Shin et al., 2010). The biomass index for groundfish species was calculated from the catch of the NMFS/AFSC annual summer bottom-trawl survey of the eastern Bering Sea (EBS). Ten years of data are needed to calculate this metric, so the indicator values start in 1991, the tenth year in the trawl survey time series (1982-2026). This metric is presented as an inverse, so as the CV increases the value of this indicator decreases, and if the CV decreases the value of this indicator increases.

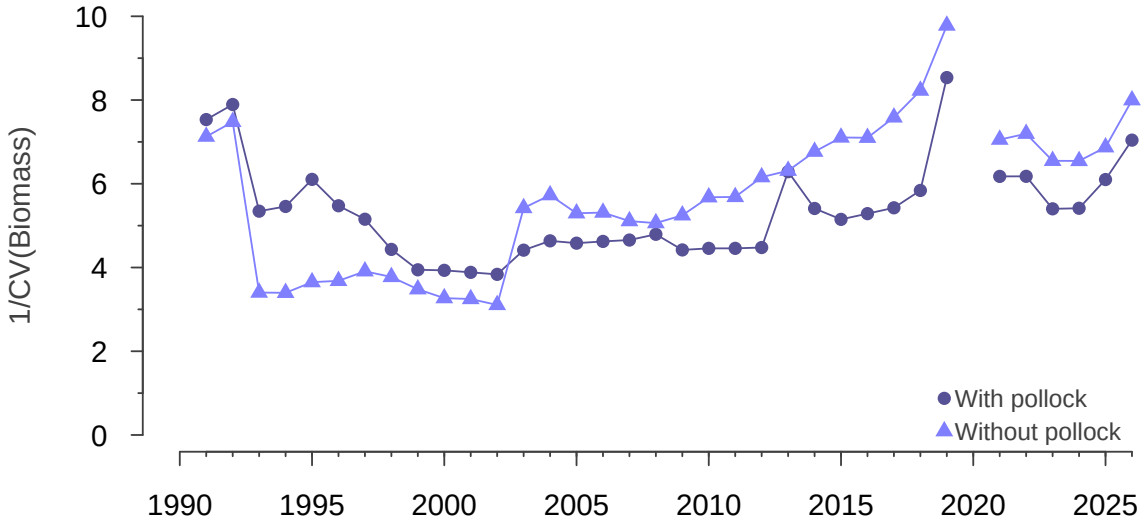


Figure 147: The stability of groundfish in the eastern Bering Sea represented with the inverse biomass coefficient of variation of total groundfish biomass (1/CV[B]). The circles are the series with pollock included in the index, and the triangles are the same series but without pollock.

This indicator specifically applies to the portion of the demersal groundfish community that is efficiently sampled by the trawling gear used by NMFS during the annual summer survey at the standard survey sample stations (for survey details see Markowitz et al., 2023). Species that are infrequently encountered or not efficiently caught by the bottom-trawling gear are excluded from this indicator (e.g., sharks, grenadiers, myctophids, pelagic smelts). The survey index used here is the same as that used for foraging guild biomass indices on the report card (Figure 2).

Walleye pollock is a biomass dominant species in the eastern Bering Sea and may drive the value of this community indicator. Therefore, this indicator is presented as two series, one with and one without pollock.

Status and trends:
With pollock included: The state of this indicator in 2026 is 7.04 (Figure 147, circles), which is above its time series mean of 5.36. An earlier peak of 7.9 was observed in 1992, which was followed by a steady decrease to a low of 3.84 in 2002. Since then, it gradually increased to a value of 5.84 in 2018 before sharply increasing to a recent high in 2019.

Without pollock included: This indicator decreased from 7.19 in 2022 to 6.55 in 2023 and increased to 8.0 in 2026 (Figure 147, triangles). This indicator dropped sharply from 7.48 in 1992 to 3.40 in 1993, and remained below four until 2003, when the value increased to 5.42. The indicator remained relatively stable until 2010, when the indicator began a steady upward trend to the series high value in 2019.

Factors influencing observed trends: Fishing is expected to influence this metric as fisheries can selectively target and remove larger, long-lived species affecting population age structure (Berkeley et al., 2004; Hsieh et al., 2006). Larger, longer-lived species can become less abundant and be replaced by smaller shorter-lived species (Pauly et al., 1998). Larger, longer-lived individuals help populations to endure prolonged periods of unfavorable environmental conditions and can take advantage of favorable conditions when they return (Berkeley et al., 2004). A truncated age-structure could lead to higher population variability (CV) due to increased sensitivity to environmental dynamics (Hsieh et al., 2006). Interannual variation in this metric could also be influenced by interannual variation in species abundance in the trawl survey catch, patchy spatial distribution for some species, or species distribution shifts (Stevenson and Lauth, 2019; Thorson, 2019). This metric, as calculated here with trawl-survey data, reflects the stability of the portion of the groundfish community that is represented in the catch data of the annual summer bottom-trawl survey. Both sharp increases or decreases in species index values can increase variability and reduce the indicator value. In general, as total biomass decreases species spatial distribution may contract or have increasingly isolated patches, both of which may lead to increased CV (Shin et al., 2010).

The high values for this indicator in 2019 and at the start of the time series were indicative of stable groundfish biomass with a relatively low CV during the previous ten years. The CVs for both time series (with and without pollock) in 2019 were the lowest over their respective time series resulting in their highest indicator values. The sharp drop in total biomass in 2021, particularly for pollock, increased the CV resulting in lower indicator values in 2021. Previously, both series dropped sharply from 1992 to 1993. This was because the index for capelin in 1993 was anomalously high, which increased variability and reduced the indicator value. In 2003, both series increased, which was in part due to the high capelin value in 1993 no longer being a part of the most recent 10 years.

In 2009, the series without pollock begins a steady increase towards its high value in 2019. The series with pollock included has a more modest positive trend over the same span, with high values in 2013 and 2019. Pollock is a biomass dominant species in the EBS and interannual fluctuations in their biomass are sufficient to increase variability for the total groundfish community and thus, reduce the indicator value. The series without pollock is more sensitive to fluctuations of other species, such as capelin. The sharp increase in the capelin index in 1993 kept this series lower than the series with pollock included from 1993-2002.

Implications: This measure indicates that the EBS groundfish community has been generally stable over the period examined here, particularly since 2003. While the indicator value dropped from 2022 to 2023 for both indicators (with and without pollock), both series remain above their long term means in 2026, indicating a maintenance of community biomass stability.

Emerging Stressors

Ocean Acidification

Contributed by Darren Pilcher[1,2], Natalie Monacci[3], Elizabeth Siddon[4], W. Christopher Long[5], Jessica Cross[6], and Esther Kennedy[3]
[1]Cooperative Institute for Climate, Ocean, and Ecosystem Studies, University of Washington, Seattle, WA
[2]NOAA Pacific Marine Environmental Laboratory, Seattle, WA
[3]University of Alaska Fairbanks, College of Fisheries and Ocean Sciences, Ocean Acidification Research Center, Fairbanks, AK
[4]Auke Bay Laboratories, Alaska Fisheries Science Center, NOAA Fisheries, Juneau, AK
[5]Kodiak Laboratory, Alaska Fisheries Science Center, NOAA Fisheries, Kodiak, AK
[6]Pacific Northwest National Laboratory, Seattle, WA

Contact: darren.j.pilcher@noaa.gov
Last updated: October 2026

Description of indicator: The oceanic uptake of anthropogenic CO_2 is decreasing ocean pH and carbonate mineral saturation states in a process known as ocean acidification (OA). The cold, carbon rich waters of the Bering Sea are already naturally more corrosive than other regions of the global ocean, making this region more vulnerable to rapid changes in ocean chemistry. The projected areal expansion and shallowing of corrosive waters with continued absorption of anthropogenic CO_2 from the atmosphere poses a direct threat to marine calcifiers and an indirect threat to other species through trophic interactions. These OA risks demonstrate a clear need to track and forecast the spatial extent of acidified waters in the Bering Sea.

Here, we present updated carbonate chemistry output from the MOM6-COBALT-NEP10k model (Drenkard et al., 2025), which currently spans 1993-August 14, 2026. We note that our OA indicator for previous years has used a different model, the ROMS Bering10K (Pilcher et al., 2025). The transition to MOM6 is part of a broader effort within the Changing Ecosystems and Fisheries Initiative (CEFI) and was further motivated by limitations in the forcing used for the ROMS Bering10K model. Additional details of this transition are described in a Noteworthy contribution (see p. 31) and we offer a comparison between the two models specific to our OA indicator at the end of this section.

Figure 148 shows spatial plots for modeled Bering Sea bottom water pH, including both the conditions in 2026 as well as the 2026 detrended anomaly. The detrended anomaly removes the impact of ocean acidification (otherwise a slow, consistent process) and highlights the role of natural processes, which generate most of the interannual variability in the carbon system. It is calculated as the residual after removing the linear trend over the entire 1993-2026 hindcast, similar to removing the global warming trend from a long-term temperature timeseries. Thus, the anomaly reflects deviations from average conditions, after detrending. We focus on bottom waters and the late summer timeframe because this is where and when we expect the most acidic waters to develop, due to the combination of ocean acidification pressures and natural seasonal biological respiration. This is also when bottom temperatures typically reach seasonal highs. Late summer is, therefore, the time most likely for synergistic negative effects of temperature and OA on crabs to emerge (Swiney et al., 2017).

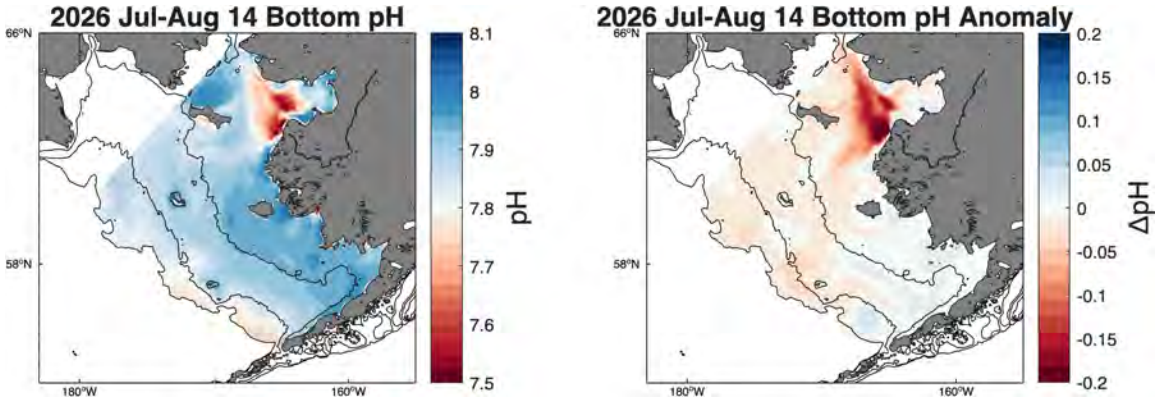


Figure 148: Model spatial maps of July-August 14 averaged bottom water pH for (left) 2026 hindcast and (right) the 2026 detrended anomaly. Contour lines denote the 50m (inner shelf), 100m (middle shelf), and 200m (outer shelf) isobaths. Regions that are outside of the eastern Bering Sea management region are omitted. Impacts of ocean acidification on fisheries are understood to be a combination of the temporal duration, biogeochemical intensity, and spatial extent. This visualization shows both the intensity and extent of acidified conditions over the Bering Sea shelf.

Model outputs are used to develop indices for both pH and the aragonite saturation state (Ω_{arag}) using threshold values of biological significance (Figures 149 and 150). The growth and survival of red king and Tanner crab are negatively affected at pH$\leq$7.8 (Long et al., 2013), and bivalve larvae are negatively affected at $\Omega_{arag}<1$ (Waldbusser et al., 2015). The goal of this index, along with the spatial anomaly plot, is to provide a quick assessment of the summer water conditions compared to previous years.

Status and trends: Modeled bottom water pH and Ω_{arag} values in 2026 are generally lower compared to 2025, with shelf wide averaged values for both variables at minimum values over our model simulation. Detrended bottom water pH anomalies are negative throughout most of the shelf, with especially low anomalies near the Yukon River delta (Figure 148). Some portions of the southeastern shelf display weak positive anomalies. This year saw a notable increase in the spatial extent of bottom waters with $\Omega_{arag}<1$, following a reduction in these conditions during the previous year (Figure 150). Bottom waters with pH$\leq$7.8 increased slightly.

Factors influencing observed trends: Modeled bottom water pH and Ω_{arag} averaged over the shelf decreased compared to 2025, reaching the lowest values for both variables over our model timeframe. The low values are partly driven by very anomalously low pH and Ω_{arag} values near the Yukon River delta (Figure 148). These conditions are likely driven by changes in freshwater runoff, which can decrease pH and Ω_{arag} due to freshening and high carbon loading from terrestrial carbon sources. Outside the Yukon River delta, large portions of the outer and middle shelf are also somewhat lower in pH and Ω_{arag} compared to 2025. Lower Ω_{arag} in the southeastern shelf (figure not shown) is likely driven by the thermal solubility effect due to the relatively colder water conditions in 2026. The relatively greater change in the Ω_{arag} index compared to shelf-averaged Ω_{arag} (i.e., Figure 149 compared to Figure 150) is due to middle and outer shelf waters that had a decrease in Ω_{arag}, pushing them below the $\Omega_{arag} = 1$ threshold (figure not shown). Because most of the outer and middle shelf has been near the $\Omega_{arag} = 1$ threshold in recent years, we expect to see relatively large interannual swings in the Ω_{arag} index, compared to both the shelf-wide Ω_{arag} value and the pH index. We anticipate that natural variability will continue to be the dominant source of interannual variability such as that illustrated between 2025-2026, and that over decadal timeframes, pH and Ω_{arag} will continue to decline with ocean acidification.

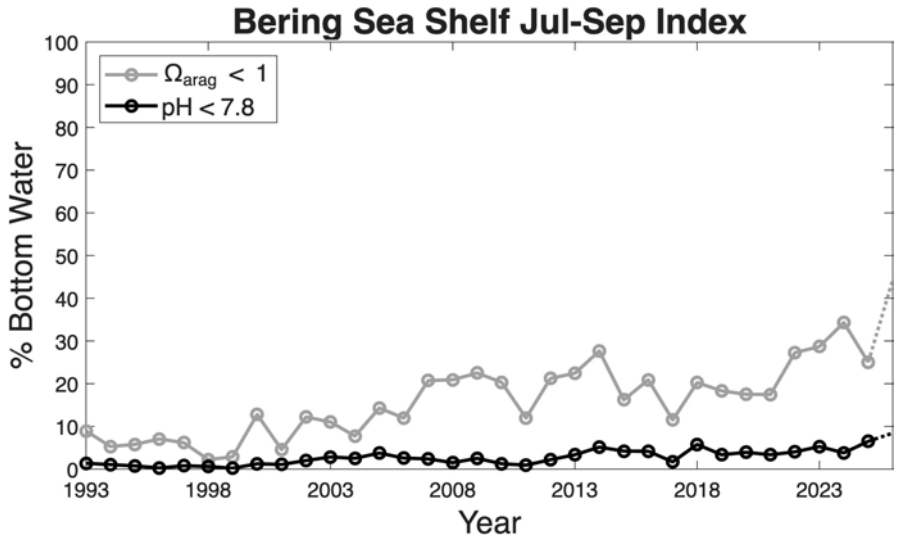


Figure 149: Model timeseries of the July-September (black line) pH index and (grey line) Ω_{arag} undersaturation index. Each index is calculated as the percent of spatial area of the eastern Bering Sea region (see Figure 148) where bottom waters have a July-September average below the denoted value. The dotted portion at the end represents the incomplete 2026 value, which is run through August 14 at the time of writing. Impacts of ocean acidification on fisheries are a function of the temporal duration, biogeochemical intensity, and spatial extent. This visualization shows the percent area (spatial extent) of the shelf that is exposed to potentially harmful biogeochemical conditions.

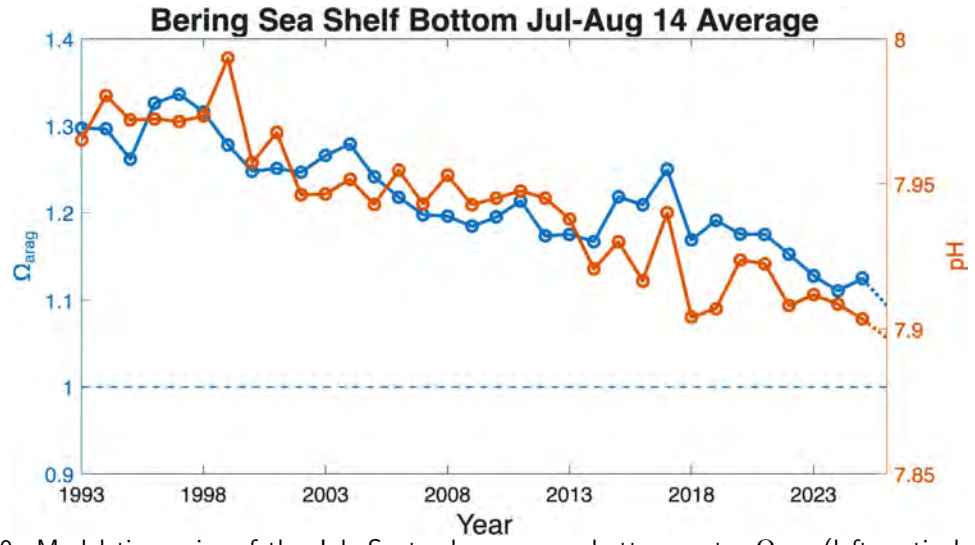


Figure 150: Model timeseries of the July-September average bottom water Ω_{arag} (left vertical axis, blue) and pH (right vertical axis, orange). The dashed line represents the Ω_{arag}saturation horizon, below which dissolution of Ω_{arag} (e.g., for calcifier shells) can occur. The dotted portion at the end represents the incomplete 2026 value, which is run through August 14 at the time of writing. Impacts of ocean acidification on fisheries are understood to be a combination of the temporal duration, biogeochemical intensity, and spatial extent. Visualizing the net shelf-wide average, rather than scaling these variables spatially (see Figure 149), helps show the intensity of aggregate conditions. However, it is important to consider this figure in context with Figures 148 and 149, as a shelf-wide average may disguise some areas of resilience (e.g., cool colors, Figure 148) and ocean acidification hotspots (e.g., warmer colors, Figure 148).

Implications: Based on the sensitivity of red king crab to pH, previous work suggests that OA may have significant negative impacts to the red king crab fishery (Seung et al., 2015; Punt et al., 2016). Indeed, recent work suggests that OA has negatively impacted red king crab recruitment in Bristol Bay, though additional research is required (Litzow et al., 2025). In 2026, modeled pH conditions in Bristol Bay are slightly higher than the detrended average conditions and the shallower inner shelf waters that serve as habitat for juvenile red king crab are relatively well buffered. However, the anomalously low pH off the Yukon extends well up into Norton Sound and may negatively affect the red king crab there. Conversely, Ω_{arag} conditions are anomalously lower, likely due to colder water temperatures decreasing Ω_{arag} through thermal solubility. An experimental study suggests that snow crab embryos and larvae are resilient to a pH of 7.5, at least at a temperature of 3°C (Long et al., 2023), however, juveniles suffer higher mortality at that pH (Long, 2026). Fortunately, there is currently no substantial overlap between snow crab and pHs that low this year.

Indicator Updates: The model output used for our indicators this year is from the recently developed MOM6-COBALT-NEP10k model (Drenkard et al., 2025), while previous OA indicators in the ESR used model output from the ROMS Bering10K model (Pilcher et al., 2025). The switch in model output was motivated both by long-term plans to integrate the MOM6 output and logistical bottlenecks on the model forcing used for ROMS Bering10K. The model switch has reduced the length of the historical model hindcast, from 1970-2024 with ROMS Bering10K to 1993-2026 for MOM6-COBALT-NEP10k. The shorter timeframe for the NEP10k output is due to the timeframe of the historical atmospheric reanalysis product used to force the NEP10k model. We may explore adding an additional forcing product to expand the NEP10k model hindcast to earlier years, though combining forcing products can introduce biases that make longterm trend analysis more challenging (Pilcher et al., 2025).

A preliminary analysis suggests that there are several key differences between the MOM6-COBALT-NEP10k and ROMS Bering10K carbonate chemistry output over the overlapping timeframe of 1993-2024 that impact our OA indicators. First, NEP10k bottom water pH and Ω_{arag} tends to be slightly higher (i.e., less acidic and less corrosive) than Bering10K when averaging over the eastern Bering Sea shelf (Figure 151). Conversely, surface water values of pH and Ω_{arag} for NEP10k tend to be lower (figure not shown), which combined with the difference in bottom waters, suggests that NEP10k simulates less summer productivity than Bering10K. Next, the magnitude of interannual variability for bottom pH and Ω_{arag} is greater in Bering10K compared to NEP10k (Figure 151). However, the models strongly agree on the phasing of this variability, indicated by strong correlation coefficients between the two timeseries ($R>0.9$). Lastly, while shelf-average values are comparable, spatial patterns over the shelf are significantly different between the two models (Figure 152). Bering10K inner shelf waters have much higher pH, but middle and outer shelf bottom waters have much lower pH. This leads to a sharper cross-shelf gradient in bottom pH for Bering10K compared to NEP10k. The lower pH and Ω_{arag} values for middle and outer shelf bottom waters in Bering10K also leads to a much larger spatial extent of bottom waters that are acidic/corrosive to red king crab and pteropods (Figure 153). This leads to substantially greater differences between the models for the OA index (Figure 153) compared to shelf-wide averaged pH and Ω_{arag} (Figure 151). It is currently unclear whether one model is performing "better" than the other, and a more complete model skill assessment with recently collected bottom water data is in development.

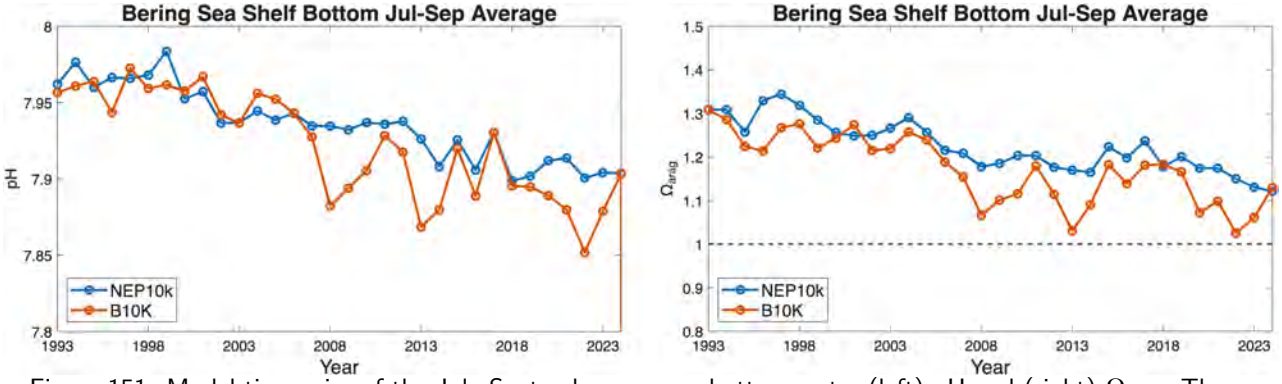


Figure 151: Model timeseries of the July-September average bottom water (left) pH and (right) Ω_{arag}. The blue line is MOM6-COBALT-NEP10k and the orange line is ROMS Bering10K. The dashed line represents the Ω_{arag} saturation horizon, below which dissolution of Ω_{arag} (e.g., for calcifier shells) can occur. The timeseries is constrained to the 1993-2024 timeframe when the two models overlap.

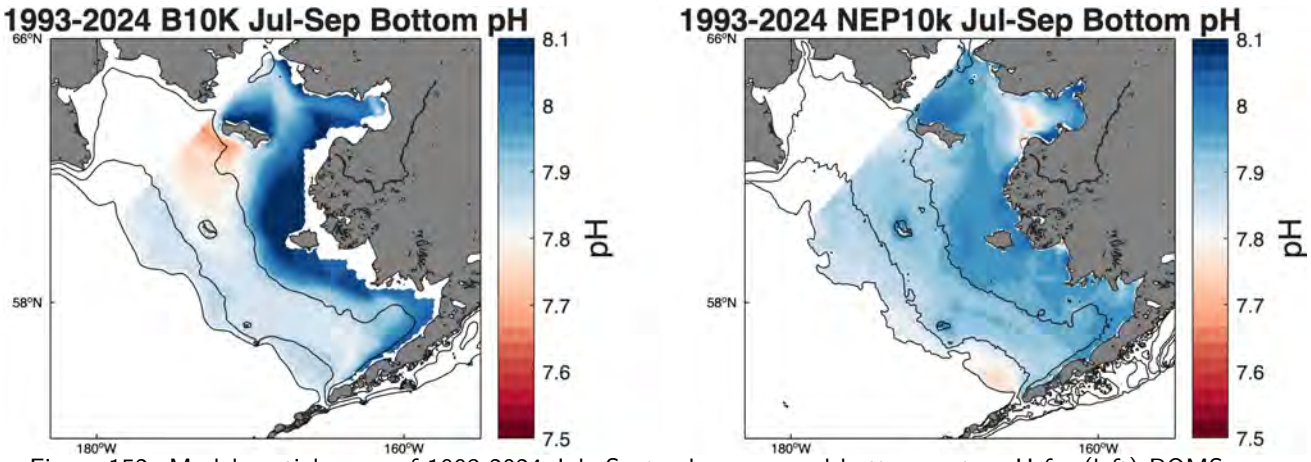


Figure 152: Model spatial maps of 1993-2024 July-September averaged bottom water pH for (left) ROMS Bering10K and (right) MOM6-COBALT-NEP10k. Contour lines denote the 50m, 100m, and 200m isobaths. Regions that are outside of the eastern Bering Sea management region are omitted.

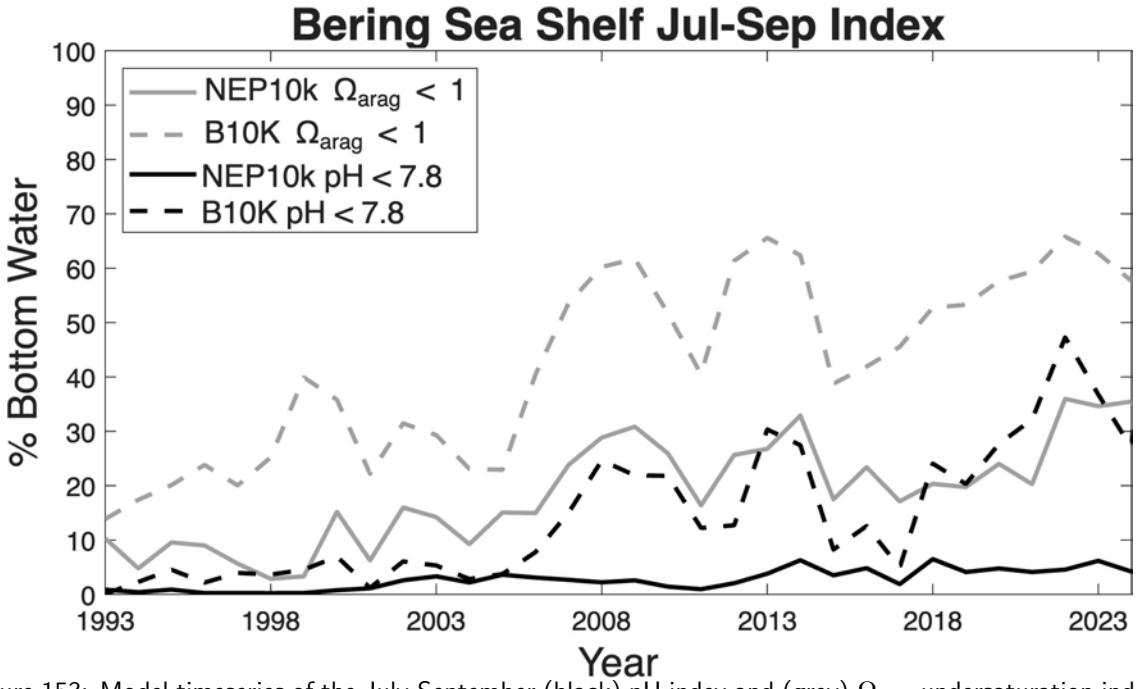


Figure 153: Model timeseries of the July-September (black) pH index and (grey) Ω_{arag} undersaturation index shown for the (solid) MOM6-COBALT-NEP10k model and the (dashed) ROMS Bering10K model. Each index is calculated as the percent of spatial area of the eastern Bering Sea region (Figure 148) where bottom waters have a July-September average below the denoted value.

Harmful Algal Blooms

Contributed by Thomas Farrugia
Alaska Ocean Observing System, Anchorage, AK
Contact: farrugia@aoos.org
Last updated: October 2025

Description of indicator: Alaska's most well-known and toxic harmful algal blooms (HABs) are caused by phytoplankton in the genera of *Alexandrium* and *Pseudo-nitzschia*. *Alexandrium* produces paralytic shellfish toxins (PST) which can cause paralytic shellfish poisoning (PSP) and has been responsible for five deaths and over 100 cases of PSP in Alaska since 1993[57]. Analyses of paralytic shellfish toxins are commonly reported as µg of toxin/100 g of tissue, where the FDA regulatory limit is 80 µg/100 g. Toxin levels between 80 µg - 1000 µg/100 g are considered to potentially cause non-fatal symptoms, whereas levels above 1000 µg/100g (∼12x regulatory limit) are considered potentially fatal. Testing for PSTs is done for all commercial species by regulation, whereas for marine subsistence food items, testing is done as funding allows.

Another harmful algal species, *Pseudo-nitzschia* produces domoic acid which can cause amnesic shellfish poisoning and inflict permanent brain damage. Domoic acid has been detected in 13 marine mammal species in Alaska and has the potential to impact the health of marine mammals and birds. No human health impacts of domoic acid have been reported in Alaska, although both acute and chronic amnesic shellfish poisoning has been reported in several states, including Washington and Oregon.

Another organism, *Dinophysis* spp., produces okadaic acid which can lead to diarrhetic shellfish poisoning. This primarily impacts the gastrointestinal system and is not usually life-threatening but can lead to nausea, vomiting, abdominal cramping, and diarrhea. Although there have not been recorded cases of diarrhetic shellfish poisoning in Alaska, *Dinophysis* has been detected throughout Alaska, and okadaic acid is at times detected in shellfish.

As a way of detecting these harmful species in Alaska and using them as an ecosystem status indicator, we have started to develop a monitoring program using Imaging FlowCytoBots (IFCBs). IFCBs are connected to the flow-through seawater system of research vessels and sample 5 mL approximately every 20 minutes. These samples are run through a flow cell and images are taken of individual particles up to 150 μm in size. To learn more about IFCBs in Alaska, see p. 57 in this report. In 2026, the Alaska Ocean Observing System (AOOS) deployed three IFCBs on research vessels that transited through Alaskan waters between Seattle, Prince William Sound, and the Chukchi Sea (Figure 154). When a bloom of a potentially toxic species is detected by the IFCBs, a HAB advisory is drafted and sent to nearby communities to alert them of the situation.

The State of Alaska tests all commercial shellfish harvest, however there is no state-run shellfish testing program for recreational and subsistence shellfish harvest. Regional programs, run by Tribal, agency, and university entities, have expanded over the past five years to provide test results to inform harvesters and researchers and reduce human health risk. All of these entities are partners in the Alaska Harmful Algal Bloom Network (AHAB) which was formed in 2017 to provide a statewide approach to HAB awareness, research, monitoring, and response in Alaska. More information can be found on the AHAB

[57]State of Alaska. Epidemiology Bulletin. 2022. Available at: `http://www.epi.alaska.gov/bulletins/docs/b2022_05.pdf`

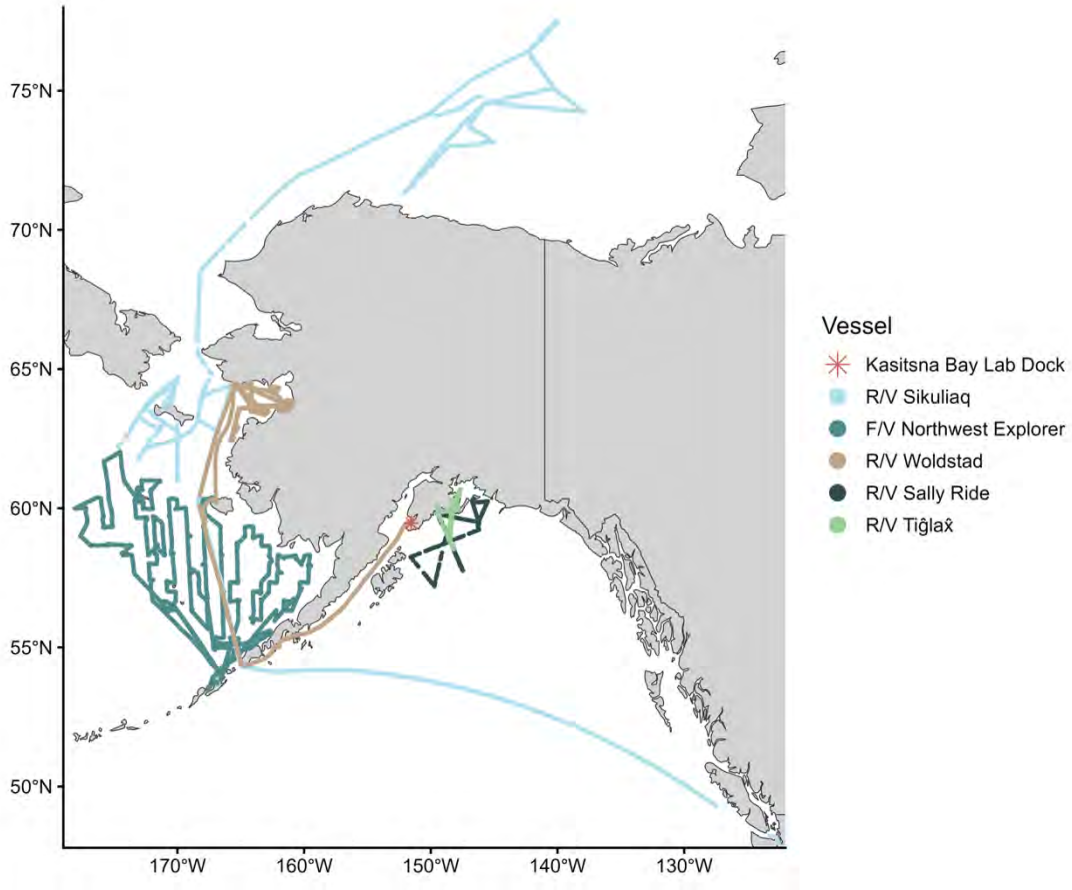


Figure 154: Tracks of the three IFCBs deployed on research vessels or onshore during May-October 2026. Colors represent different deployments (see text for details and links to the data dashboards for each deployment).

Network website[58]. For a summary of HAB events and testing results once they are available, visit the HAB Alerts page.

The Alaska Department of Health, Section of Epidemiology (SOE) continues to partner with the AHAB network. Nurse consultants join in on the monthly meetings and collaborate with stakeholders so they can be made aware of reportable illness such as Paralytic shellfish Poisoning (PSP). SOE published an Epidemiology Bulletin describing cases of PSP from 1993-2021[59]. More information about PSP and other shellfish poisoning can be found on the SOE website[60].

Status and trends:
Alaska Region:
The three IFCBs sampled for over 270 days in Alaska waters (Figure 154) and results from the IFCB monitoring in 2026 showed a generally similar picture of phytoplankton from 2024 and 2025. However, detection of HAB species seemed to have been slightly lower, especially in the Gulf of Alaska.

[58] https://ahab.aoos.org
[59] https://epi.alaska.gov/bulletins/docs/b2022_05.pdf
[60] https://health.alaska.gov/en/education/shellfish-poisoning/

The only bloom of a harmful algal species detected by IFCBs this summer happened in the Bering Sea, where an *Alexandrium* bloom seemed to have started at low levels at the end of June east of the Pribilof Islands, and by the end of August there was a widespread and fairly dense bloom covering much of the southeastern Bering Sea. This is now the third year in a row that this *Alexandrium* bloom has been detected in this general area, suggesting that this may be a perennial feature of the southeastern Bering Sea. Unlike 2024 and 2025, no mortalities of northern fur seals were linked to paralytic shellfish toxins in 2026 (see p. 267 for more information on those events).

Although low levels of *Pseudo-nitzschia* and *Dinophysis* were also detected throughout the season, and showed occasional slight upticks, nothing that would be categorized as a bloom was detected. 2026 seemed to have been an overall cooler year in terms of sea surface temperatures, and this likely accounted for the slight decrease in bloom events. Over the last few years, the dinoflagellate *Dinophysis* has become more common and abundant in water samples, and 2026 continued that trend. We are also seeing a geographic expansion of areas that are sampling for phytoplankton species.

Eastern Bering Sea:
Three vessels spent much of the 2026 season in the eastern Bering Sea, between Unimak Pass and the Bering Strait (Figure 155). The F/V Northwest Explorer covered much of the southeastern Bering Sea during the NOAA bottom trawl survey. The R/V Woldstad spent a lot of time in Norton Sound, and the R/V Sikuliaq transited up to St Lawrence Island, and then eventually through the Bering Strait into the Chukchi Sea. In general, the phytoplankton patterns showed higher abundance and diversity closer to shore, decreasing as the vessels moved further offshore.

A large *Alexandrium* bloom was detected in the southeastern Bering Sea that seemed to have started at the end of June. On June 21-22, the IFCB on the R/V Woldstad and the IFCB on the F/V Northwest Explorer transited the same area and detected an uptick in *Alexandrium* cells, above the expected background level. The cell concentrations peaked at around 800 cells/L about 130 miles east of St. Paul Island. This concentration was not high enough to trigger a HAB advisory, but the information was shared for informational purposes.

At the end of August, a sampling effort by biologists on board the R/V Oscar Dyson detected very high concentrations of *Alexandrium*. This was communicated to the AHAB Network, and a few days later, the IFCB on the R/V Sikuliaq also transited the area and detected the same bloom (Figure 156). Data from both sampling efforts showed that cell concentrations reached an estimated 50,000 cells/L. These concentrations of *Alexandrium* are considered very high and potentially dangerous. A HAB Advisory was drafted by a group of experts and sent to communities, managers, and researchers in the region to alert them of the potential impacts of this bloom.

This area of the southeastern Bering Sea has been surveyed with IFCBs since 2024, and every year since then an *Alexandrium* bloom in the same area seems to develop. In 2024, the bloom was detected in early July, and in early August a die-off of northern fur seals and fish was detected on St. Paul Island. This die-off was connected to the *Alexandrium* bloom detected in July (Lefebvre et al., 2025*a*). In 2025, high *Alexandrium* concentrations were found in the same area, this time in early August, and about 2 weeks later, a die-off of northern fur seals, seabirds, and fish was detected on St. George Island. In 2026, the bloom started setting up in June, but seemed to have reached peak concentrations later in August. Although no mortalities of northern fur seals were detected in 2026 on the Pribilof Islands, the United States Geological Survey tested dead seabirds found on Round Island on August 9, 2026 and found toxicosis from paralytic shellfish toxins to be one of the causes of death[61]. We are still investigating

[61] `https://whispers.usgs.gov/event/205412`

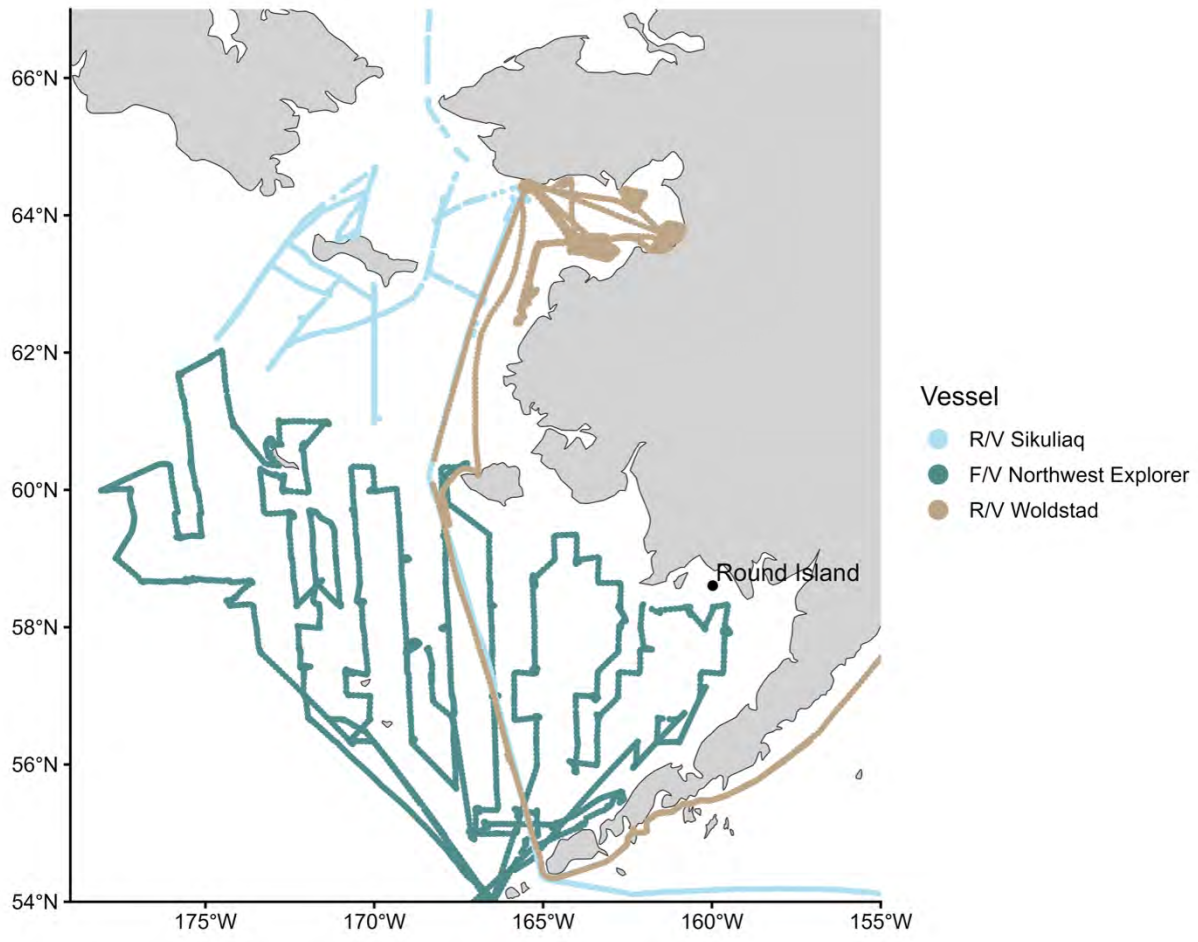


Figure 155: Tracks of IFCB deployments in the eastern Bering Sea. The location of Round Island is highlighted because of the seabird die-off detected there in August 2026. Colors represent different deployments (see text for details and links to the data dashboards for each deployment).

whether this mortality event may be linked to the *Alexandrium* bloom detected by the IFCBs.

Details about each IFCB deployment, as well as images taken by the IFCBs and maps of sampled locations, can be accessed through the following Woods Hole Oceanographic Institution (WHOI) dashboards (dates indicate the date range for which the IFCB collected data in the Bering Sea):

- F/V Northwest Explorer (May 31 - August 14)[62]
- R/V Woldstad (June 21 - August 25)[63]
- R/V Sikuliaq (August 28 - September 23)[64]

[62] https://habon-ifcb.whoi.edu/timeline?dataset=NWexplorer2026
[63] https://habon-ifcb.whoi.edu/timeline?dataset=Woldstad2026
[64] https://habon-ifcb.whoi.edu/timeline?dataset=Sikuliaq2026

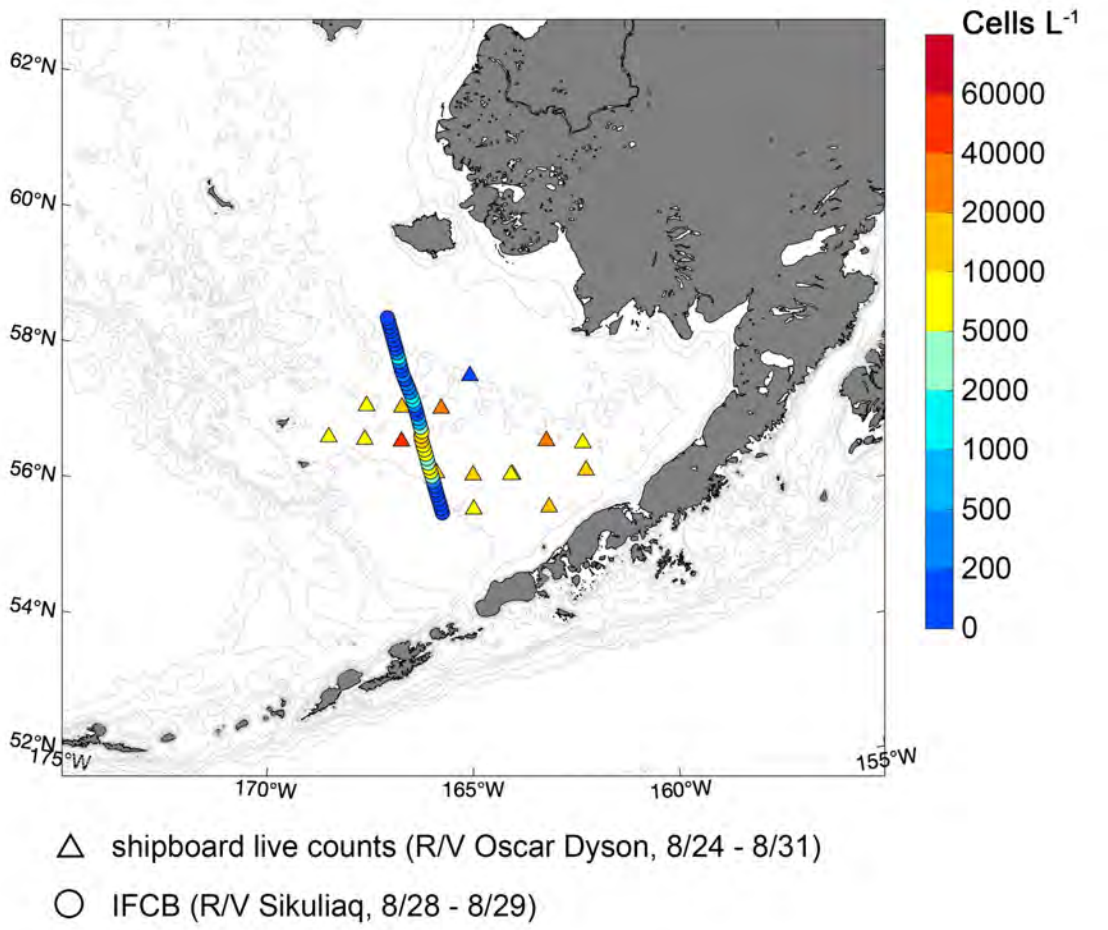


Figure 156: Map of the *Alexandrium* cell concentration estimates from the R/V Oscar Dyson (live microscopy counts) and from the R/V Sikuliaq (IFCB counts). The peak of the blooms seems to be about 70 nautical miles east of the Pribilof Islands, but covers the area from the Pribilofs to the north side of the Alaska Peninsula. (R/V Oscar Dyson data from Nata Spada, map by Evie Fachon, WHOI).

Factors influencing observed trends: HABs are likely to increase in intensity and geographic distribution in Alaska waters with warming water temperatures. Observations in Southeast and Southcentral Alaska suggest *Alexandrium* blooms occur at temperatures above 10°C and salinities above 20 (Vandersea et al., 2018; Tobin et al., 2019; Harley et al., 2020). As waters warm throughout Alaska, blooms may increase in frequency and geographic extent.

Implications: HABs pose a risk to human health when present in wildlife species that people consume, including shellfish, birds and marine mammals. Research across the state is attempting to better understand the presence and circulation of HABs in the food web. HAB toxins have been detected in stranded and harvested marine mammals from all regions of Alaska in past years (Lefebvre et al., 2016). A multi-disciplinary statewide study funded by NOAA's ECOHAB program (see p. 267) is underway and encompasses ship-based sediments samples, water samples, zooplankton samples, krill samples, copepod samples, multiple species of fish, bivalves, and the continuation of sampling subsistence-harvested and dead stranded marine mammals.

ECOHAB: Harmful Algal Bloom (HAB) Toxins in Arctic Food Webs

Contributed by Kathi Lefebvre[1], Don Anderson[2], Gay Sheffield[3], Raphaela Stimmelmayr[4], Evangeline Fachon[2], Patrick Charapata[1], Robert Pickart[2], and Emily Bowers[1]
[1]Environmental and Fisheries Science, Northwest Fisheries Science Center, NOAA Fisheries, Seattle, WA
[2]Woods Hole Oceanographic Institution, Woods Hole, MA
[3]University of Alaska Fairbanks, Alaska Sea Grant, Nome, AK
[4]North-Slope Borough Department of Wildlife Management, Utqiagvik, AK
Contact: kathi.lefebvre@noaa.gov
Last updated: September 2026

Description of indicator: *Alexandrium* and *Pseudo-nitzschia* are two common harmful algal bloom (HAB) species in Alaskan waters that produce neurotoxic compounds such as saxitoxin (STX; generated by *Alexandrium* species; causes Paralytic Shellfish Poisoning PSP) and domoic acid (DA; generated by *Pseudo-nitzschia* species; causes Amnesic Shellfish Poisoning ASP). Monitoring the presence and abundance of HAB cell (i.e., *Alexandrium* and *Pseudo-nitzschia*) densities and toxin (STX and DA) prevalence and concentrations in marine food webs are useful indicators of ecosystem health and potential threats to wildlife and human health. Multiple years of sampling via the ECOHAB: Arctic Food Webs study confirm that HAB toxins are present in Arctic and Subarctic food webs on a regular basis and at varying concentrations (Figure 157). The risks of these toxins include human illness and death associated with seafood consumption as well as health impacts to marine wildlife at multiple trophic levels. Many commercially valuable shellfish and finfish are impacted by these toxins, as well as marine mammals, invertebrates, seabirds, and filter-feeding fishes that are harvested for subsistence purposes and consumed by Alaska's coastal communities. Using HAB toxins as an indicator of ecosystem change over the last two decades, we have confirmed that warming ocean conditions are increasing the presence of HAB toxins in Arctic and Subarctic food webs and thereby risks to the Bering Sea marine ecosystem (Lefebvre et al., 2025*b*). Figure 157 shows HAB toxin concentrations in Bowhead fecal samples over 19 years are directly linked to ocean heat flux (higher heat flux = higher toxin concentrations). Bowheads migrate annually from the Bering Sea to the Beaufort Sea linking these ecosystems.

Status and trends: As the climate has warmed over the past few decades, the Pacific sector of the Arctic Ocean has warmed with dramatic consequences. The quality, quantity, and duration of sea ice has decreased markedly due to earlier melting and a delayed freeze-up (Frey et al., 2014). The input of Pacific water northwards through the Bering Strait has increased, warmed, and freshened (Woodgate et al., 2012). Warmer air temperatures are peaking earlier in the season and have led to increased summer ocean warming (Pickart et al., 2013). Stronger summertime northeasterly winds have led to upwelling-favorable conditions along the western Alaskan coast (Pickart et al., 2011). Combined, these physical changes have made conditions more favorable for HAB species, particularly the dinoflagellate *Alexandrium catenella*, as cyst germination and cell growth rates increase with warmer bottom and surface water temperatures (Anderson et al., 2021, 2022). Increased HAB activity results in increased toxin presence in the food web.

A recent northern fur seal mortality event occurred during summer 2024 on St. Paul Island, AK in the Southeast Bering Sea (Figure 158). Investigations confirmed that the deaths were caused by saxitoxin poisoning (Lefebvre et al., 2025*a*). High saxitoxin concentrations were detected in multiple tissues in

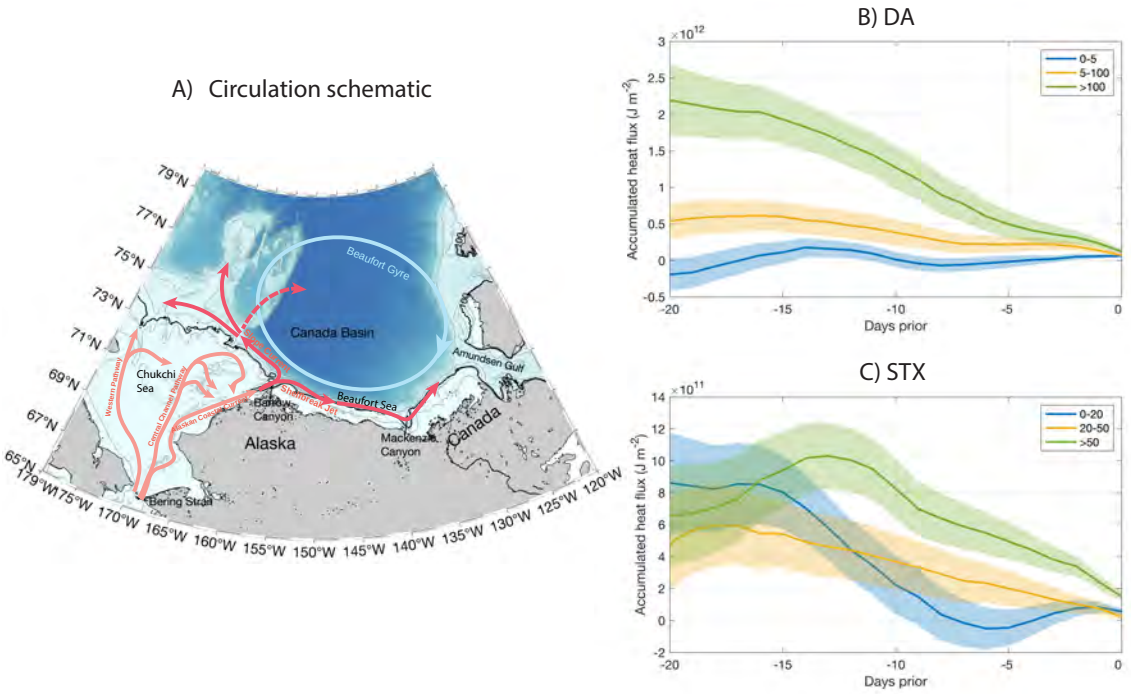


Figure 157: Algal toxins and accumulated heat flux. (a) Map of currents and location of the long-term oceanographic mooring (gold star). (b) Composites of accumulated heat flux (Jm^{-2}) measured at the mooring over the 20 days before bowhead whale fecal sampling for the three domoic acid (DA) concentration groups (ng/g): low (n = 90, blue), medium (n = 73, yellow), and high (n = 42, green). (c) Same as (b) except with saxitoxin (STX) concentration groups (ng/g): low (n = 80, blue), medium (n = 63, yellow), and high (n = 62, green). The shading represents the standard error (standard deviation/$\sqrt{N}$) of the average heat flux for each composite. Figure taken from Lefebvre et al., 2025*a*.

all seals sampled. Exceptionally high saxitoxin concentrations detected in seal urine samples indicated lethal toxin exposure when compared to previous known urine STX concentrations from other paralytic shellfish poisoning mortality events in humans (Llewellyn et al., 2002). This was the first ever confirmed marine mammal saxitoxin poisoning event in northern and western Alaska and was followed by another northern fur seal mortality event in late summer 2025 on St. George Island, AK just south of St. Paul Island.

Implications: The impacts of increased biotoxin exposure include increased risks to ecosystem, wildlife, and public health in Northern Arctic regions. As ocean temperatures continue to rise, algal growth and cyst germination rates of toxic *Alexandrium* will continue to increase. Recurrent detection of saxitoxin in Bering Sea food webs confirms the regular occurrence of toxic *Alexandrium* blooms and continued increase in toxin exposure risks to wildlife. Impacts also include food security concerns to Arctic coastal peoples as well as conservation concerns for many species of marine resources, including several marine mammals currently listed under the Endangered Species Act (ESA). Arctic coastal people sampling efforts are being developed, but consistent funding is needed to sustain temporal and spatial monitoring coverage of HAB activity in the Alaskan ecosystem.

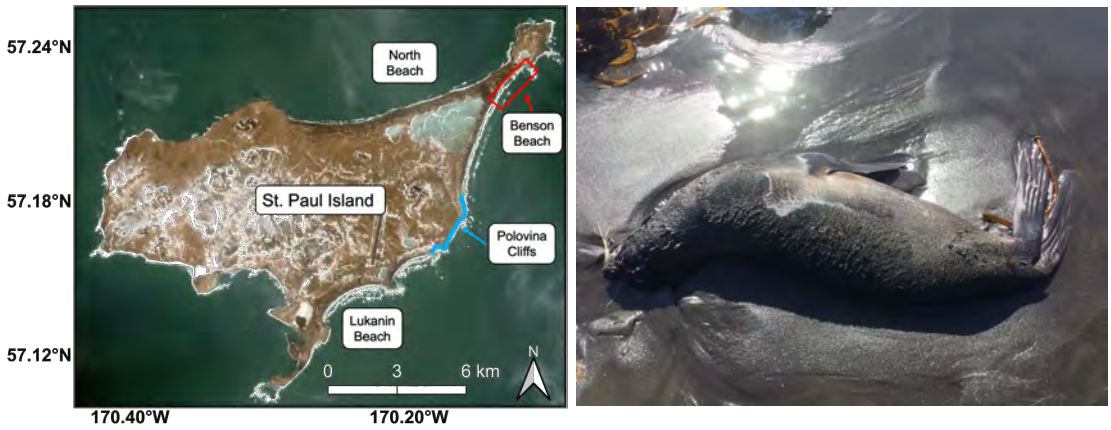


Figure 158: Deaths of Northern Fur Seals linked to saxitoxin poisoning. (a) Map of St. Paul Island, AK with the location of Benson Beach were dead seals washed ashore in August 2024 (red square). (b) photo of dead seal taken from Lefebvre et al., 2025*a*.

Future Steps:
This ECOHAB team has received another five-year grant to continue research projects to develop continuous monitoring of *Alexandrium* and *Pseudo-nitzschia* within Alaskan waters and their biotoxins among marine trophic levels. Innovative technology such as the Imaging FlowCytobot (IFCB; see p. 57) allows continuous 24/7 underway sampling during extended research cruises (>1 month). The IFCB can identify *Alexandrium* and *Pseudo-nitzschia* cells and provide cell densities using machine learning based algorithms. This has continued to be useful for providing real time updates on bloom activity in sampled areas. Currently, models for quantifying toxin exposure risks in Arctic marine ecosystems are being developed. Thus, cruises will continue to collect samples from organisms throughout different components of the food web (phytoplankton, zooplankton, invertebrates, fish, and marine mammals) to develop toxin trophic transfer models that will estimate biotoxin exposure to commercially important marine resources and Native Alaskan food resources during HABs of different intensities. Data are available from 2019-2024 and various analyses relating to HAB species abundances and trophic transfer models are underway. The implementation of continuous HAB monitoring efforts such as IFCB deployments are needed to provide early warning and ensure future ecosystem and Native Alaskan community health. Close collaborations with Native Alaska communities reliant on marine resources for subsistence are being strengthened to develop capacity to monitor for HABs and toxins locally.

Maintaining Diversity: Discards and Non-Target Catch

Time Trends in Groundfish Discards

Contributed by Anna Abelman
Resource Ecology and Fisheries Management Division, Alaska Fisheries Science Center, NOAA Fisheries
Alaska Fisheries Information Network, Pacific States Marine Fisheries Commission
Contact: anna.abelman@noaa.gov
Last updated: October 2026

Description of indicator: Estimates of groundfish discards for 1993-2002 are sourced from NMFS Alaska Region's blend data, while estimates for 2003 and later come from the Alaska Region's Catch Accounting System. These sources, which are based on observer data in combination with industry landing and production reports, provide the best available estimates of groundfish discards in the North Pacific. Discard rates as shown in Figure 159 below are calculated as the weight of groundfish discards divided by the total (i.e., retained and discarded) catch weight for the relevant area gear-target sector. Where rates are described below for species or species groups, they represent the total discarded weight of the species/species group divided by the total catch weight of the species/species group for the relevant area-gear-target sector. These estimates include only catch of FMP-managed groundfish species within the FMP groundfish fisheries. Discards of groundfish in the halibut fishery and discards of forage fish and species managed under prohibited species catch limits, such as halibut, are not included.

Status and trends: Since 1993, discard rates of groundfish in federally-managed Alaskan groundfish fisheries have generally declined in the trawl pollock and non-pollock trawl fisheries in the eastern Bering Sea (EBS) (Figure 159). Annual discard rates in the EBS pollock trawl sector declined from 10% to about 1% in 1999 and have since remained below this level. The large increase in discard rate in 2021 is likely due to an overall decrease in total catch in NBS for pollock trawl. Rates in the non-pollock trawl sector have declined from a high of 50% in 1994 and have remained at 10% or lower since 2010. Discard rates and volumes in the fixed gear (hook-and-line and pot) sector trended upward from 2010 to 2016, reaching the highest annual discard biomass (26.7K metric tons) over the entire time series before declining from 2017 to 2021. Fixed gear discards in the northern Bering Sea trended upward from 2016 to 2018 as some vessels targeting Pacific cod moved their fishing activity northward, but these increases were offset by declines in discard biomass in the southern subregion. Through week 42 of 2026, discard biomass through week 42 is lower in all three sectors relative to the preceding 5-year (2021-2025) period (Figure 160).

Factors influencing observed trends: Fishery discards may occur for economic or regulatory reasons. Economic discards include discarding of lower value and unmarketable fish, while regulatory discards are those required by regulation (e.g., upon reaching an allowable catch limit for a species). Minimizing discards is recognized as an ecological, economic, and moral imperative in various multilateral initiatives and in National Standard 9 of the Magnuson-Stevens Fishery Conservation and Management Act (Alverson et al., 1994; FAO, 1995; Karp et al., 2011). In the North Pacific groundfish fisheries, mechanisms to reduce discards include:

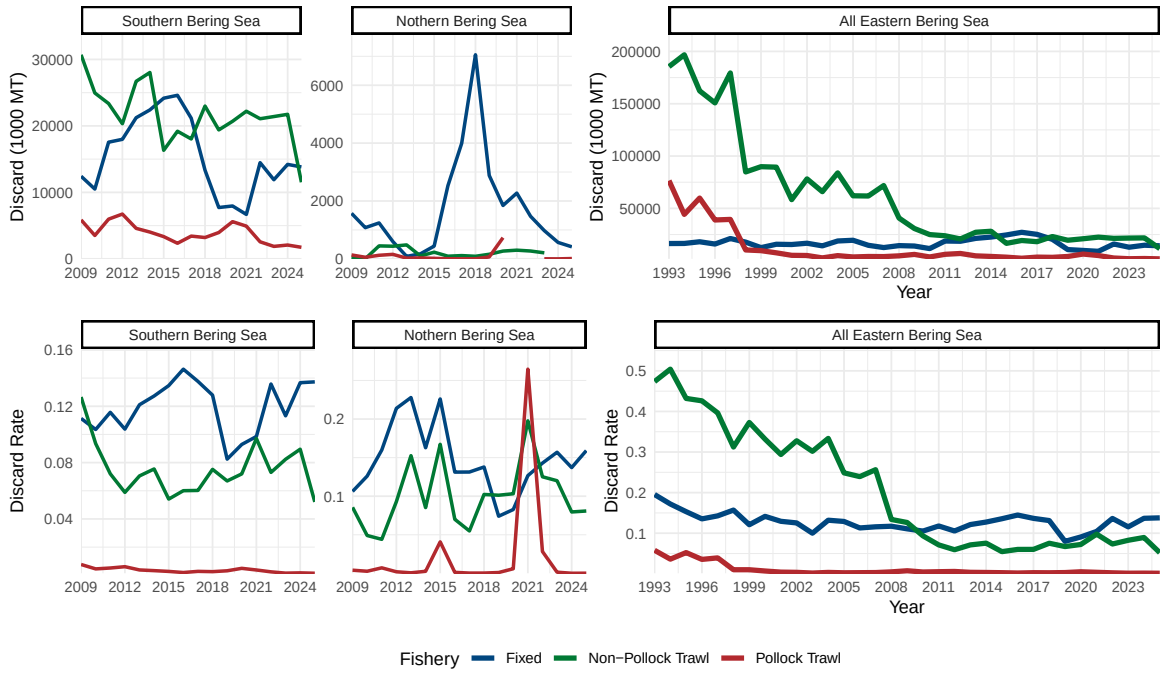


Figure 159: Total biomass and percent of total catch biomass of FMP groundfish discarded in the fixed gear, pollock trawl, and non-pollock trawl sectors for the eastern Bering Sea (EBS) region, 1993-2025; and for northern (NBS) and southern (SBS) subregions, 2009-2025. Discard rates are calculated as total discard weight of FMP groundfish divided by total retained and discarded weight of FMP groundfish for the sector (includes only catch counted against federal TACs).

- Limited access privilege programs (LAPPs), which allocate catch quotas and may reduce economic discards by slowing down the pace of fishing
- In-season closure of fisheries once target or bycatch species quotas are attained
- Minimum retention and utilization standards for certain fisheries
- Maximum retainable amounts (MRAs), which allow for limited retention of species harvested incidentally in directed fisheries.

In the eastern Bering Sea, management and conservation measures aimed at reducing bycatch have contributed to an overall decline in groundfish discards since the early 1990s (NPFMC, 2016, 2017). Pollock roe stripping, wherein harvesters discard all but the highest value pollock product, was prohibited in 1991 (56 Federal Register 492). Throughout the 1990s, declines in total catch and discard of non-pollock groundfish in the pollock fishery coincided with the phasing out of bottom trawl gear in favor of pelagic gear, which allows for cleaner pollock catches (Graham et al., 2007). Full retention requirements for pollock and Pacific cod were implemented in 1998 for federally-permitted vessels fishing for groundfish (62 Federal Register 63880). Between 1997 and 1998 annual discard rates for cod fell from 13% to 1% in the non-pollock trawl sector and from 50% to 3% in the trawl pollock sector; pollock discards also declined significantly across both trawl gear sectors. In the trawl pollock fishery, discards of pollock have remained at nominal levels since passage of the American Fisheries Act, which established a sector-based LAPP and implemented more comprehensive observer requirements for the fishery in 2000. As of March

2020, the regulations 50 CFR 679.20(j) and 50 CFR 679.7(a)(5) were implemented to require operators of catcher vessels using hook-and-line, pot, or jig gear (fixed gear) to fully retain rockfish landings in the BSAI or GOA. These regulations also limits the amount of rockfish that can enter into the market with the overall purpose of limiting total catch of rockfish.

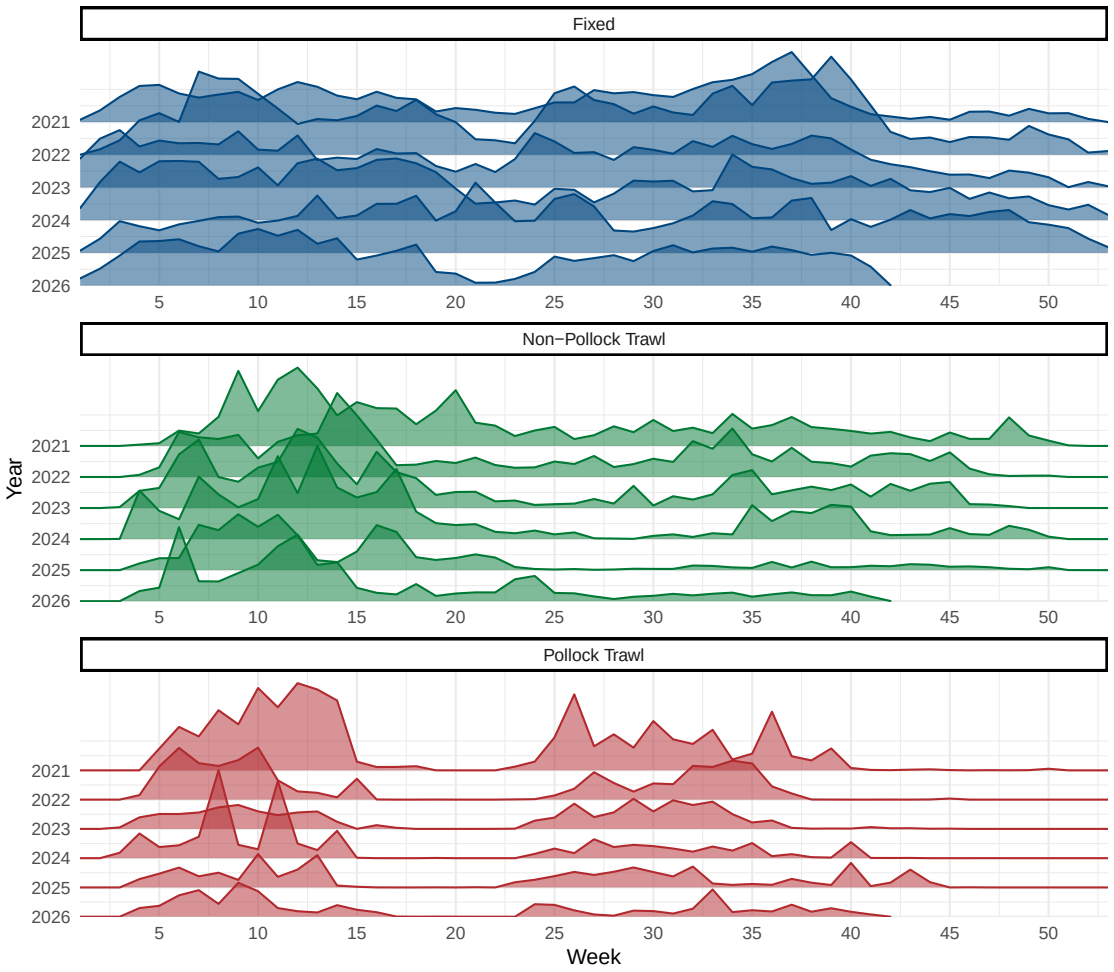


Figure 160: Total biomass of FMP groundfish discarded in the eastern Bering Sea region by sector and week, 2021-2026 (data for 2026 is shown through week 42). Plotted heights are not comparable across sectors.

Low retention rates in the non-AFA trawl catcher processor (head and gut) fleet prompted Amendments 79 and 80 to the BSAI Groundfish FMP in 2008 (NPFMC, 2016). Amendment 79 established a Groundfish Retention Standard (GRS) Program with minimum retention and utilization requirements for vessels at least 125 feet LOA; industry-internal monitoring of retention rates has since replaced the program. Amendment 80 expanded the GRS program to all vessels in the fleet and established a cooperative-based LAPP with fixed allocations of certain non pollock groundfish species. In combination with the GRS program, these allocations are intended to remove the economic incentive to discard less valuable species caught incidentally in the multi-species fishery. In 2013, NMFS revised MRAs for groundfish caught in the BSAI Arrowtooth flounder fishery, including an increase from 0 to 20 percent for pollock, cod, and flatfish (78 Federal Register 29248). Groundfish discard rates in the trawl flatfish fishery fell from 23% to 12% between 2007 and 2008 and have continued on a gradual decline since then.

Since 2003 across all Bering Sea sectors combined, discard rates for species groups historically managed together as the "other groundfish" assemblage (skate, sculpin, shark, squid, and octopus) have ranged from 65% to 80%, with skates representing the majority of discards by weight. In the fixed gear sector other groundfish typically account for at least 70% of total groundfish discards annually. Fluctuations in discard volumes and rates for these species may be driven by changes in market conditions and in fishing behavior within the directed fisheries in which these species are incidentally caught. For example, low octopus catch from 2007-2010 may be attributable to lower processor demand for food-grade octopus and decreases in cod pot-fishing effort stemming from declines in cod prices (Conners et al., 2016).

In April 2025, the North Pacific Fishery Management Council (NPFMC) recommended allowing economically undesirable small sablefish to be discarded[65]. While this is still pending NMFS rulemaking, the Advisory Panel is urging implementation in time for the 2027 season[66]. Later, in October 2025, the Council recommended updating the Maximum Retainable Amounts (MRA) for groundfish in the BSAI and GOA. This change could reduce regulatory discards without increasing overall harvest limits, though it is also currently pending rulemaking[67].

Implications: Fishery bycatch adds to the total human impact on biomass without providing a benefit to the Nation and as such perceived as "contrary to responsible stewardship and sustainable utilization of marine resources" (Kelleher, 2005). Bycatch may constrain the utilization of target species and increases the uncertainty around total fishing-related mortality, making it more difficult to assess stocks, define overfishing levels, and monitor fisheries for overfishing (Alverson et al., 1994; Clucas, 1997; Karp et al., 2011). Although ecosystem effects of discards are not fully understood, discards of whole fish and offal have the potential to alter energy flow within ecosystems and have been observed to result in changes to habitat (e.g., oxygen depletion in the benthic environment) and community structure (e.g., increases in scavenger populations) (Queirolo et al., 1995; Alverson et al., 1994; Catchpole et al., 2006; Zador and Fitzgerald, 2008). Monitoring discards and discard rates provides a means of assessing the efficacy of measures intended to reduce discards and increase groundfish retention and utilization.

[65] https://www.npfmc.org/april-2025-newsletter/

[66] https://meetings.npfmc.org/CommentReview/DownloadFile?fileName=F+AP+Report.pdf&p=6fa31f15-8c66-49ec-9ba3-bcb1bd2ed6b1.pdf

[67] https://www.npfmc.org/october-2025-newsletter/

Time Trends in Non-Target Species Catch

Contributed by George A. Whitehouse[1] and Sarah Gaichas[2]
[1]Cooperative Institute for Climate, Ocean, and Ecosystem Studies (CICOES), University of Washington, Seattle, WA
[2]Hydra Scientific LLC, Falmouth, MA
Contact: gaw@uw.edu
Last updated: August 2026

Description of indicator: This indicator reports the catch of non-target species in groundfish fisheries in the eastern Bering Sea (EBS). Catch since 2003 has been estimated using the Alaska Region's Catch Accounting System (Cahalan et al., 2014). This sampling and estimation process does result in uncertainty in catches, which is greater when observer coverage is lower and for species encountered rarely in the catch. Since 2013, the three categories of non-target species tracked here are:

1. Scyphozoan jellyfish
2. Structural epifauna (seapens/whips, sponges, anemones, corals, tunicates)
3. Assorted invertebrates (bivalves, brittle stars, hermit crabs, miscellaneous crabs, sea stars, marine worms, snails, sea urchins, sand dollars, sea cucumbers, and other miscellaneous invertebrates).

The catch of non-target species/groups from the Bering Sea includes the reporting areas 508, 509, 512, 513, 514, 516, 517, 521, 523, 524, and 530[68].

Status and trends: The catch of jellyfish more than doubled from 2020 to 2021 (Figure 161, top). Previous high catches of jellyfish occurred in 2011, 2014, and 2018 and were each followed by a sharp decrease in jellyfish catch the following year. The catch of jellyfish has trended downward trend from 2021 to 2025. Jellyfish are primarily caught in the pollock fishery.

The catch of structural epifauna trended downward from 2015 to 2020 and has remained low from 2021 to 2025 (Figure 161, middle). Benthic urochordate caught in non-pelagic trawls were the dominant component of the structural epifauna catch in 2012 and 2015-2023. In 2013, 2014, 2024, and 2025 anemones caught in the Pacific cod fishery were the dominant part of the structural epifauna catch. Sponge were the dominant component of the structural epifauna catch in 2011 and were primarily caught in non-pelagic trawls.

Sea stars make up more than 85% of the assorted invertebrate catch in all years (2011-2025) and are primarily caught in flatfish fisheries. The catch of assorted invertebrates generally trended upward from 2011 to 2015, then declined from 2015 to 2025 (Figure 161, bottom).

Factors influencing observed trends: The catch of non-target species may change if fisheries change, if ecosystems change, or both. Because non-target species catch is unregulated and unintended, if there have been no large-scale changes in fishery management in a particular ecosystem, then large-scale signals in the non-target catch may indicate ecosystem changes. Catch trends may be driven by changes

[68]https://www.fisheries.noaa.gov/alaska/sustainable-fisheries/alaska-fisheries-figures-maps-boundaries-regulatory-areas-and-zones

in biomass or changes in distribution (overlap with the fishery) or both. Fluctuations in the abundance of jellyfish in the EBS are influenced by a suite of biophysical factors affecting the survival, reproduction, and growth of jellies including temperature, sea ice phenology, wind-mixing, ocean currents, and prey abundance (Brodeur et al., 2008). The lack of a clear trend in the catch of scyphozoan jellies may reflect interannual variation in jellyfish biomass and/or changes in the overlap with fisheries.

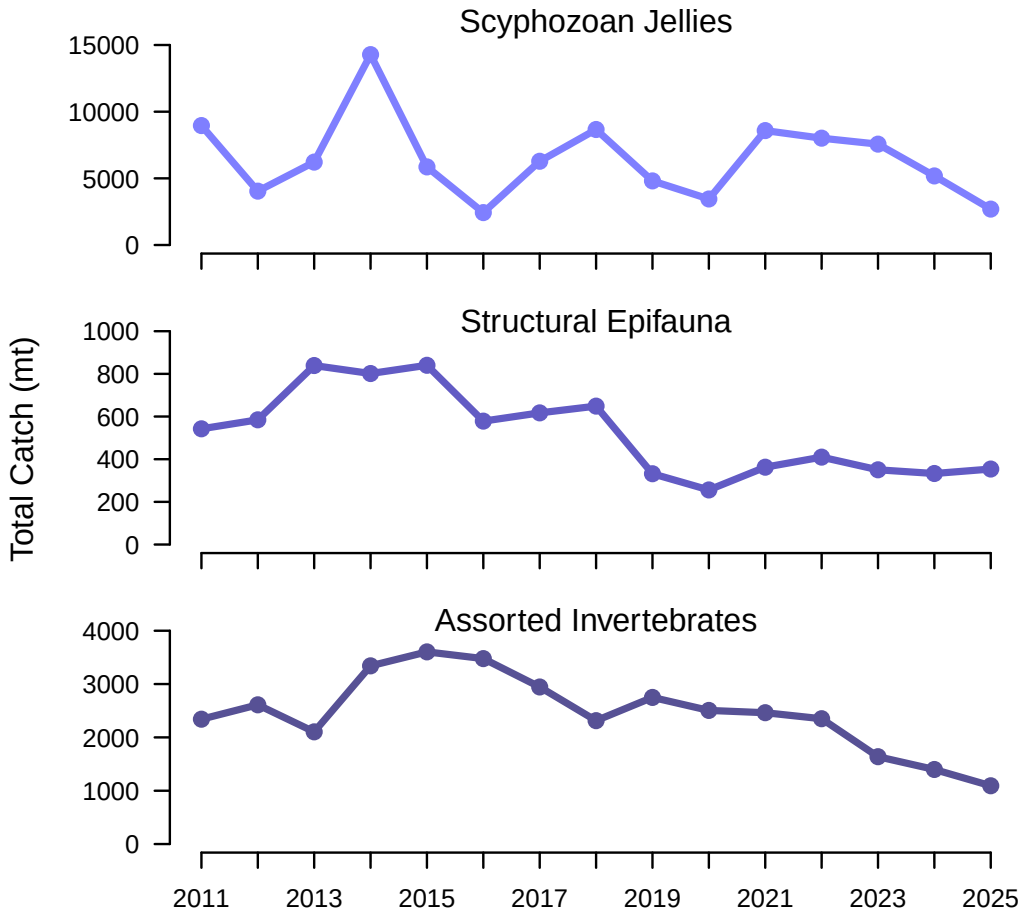


Figure 161: Total catch of non-target species (tons) in EBS groundfish fisheries (2011-2025). **Please note the different y-axis scales** between the species groups.

Implications: The catches of structural epifauna species and assorted invertebrates are very low compared with the catch of target species. Structural epifauna species may have become less available to the EBS fisheries or the fisheries avoided them more effectively. Abundant jellyfish may have a negative impact on fishes as they compete with planktivorous fishes for prey resources (Purcell and Arai, 2001; Ruzicka et al., 2020), and may prey upon the early life history stages (eggs and larvae) of fishes (Purcell and Arai, 2001; Robinson et al., 2014). Additionally, jellyfish may be an important prey resource for predators, including commercially important groundfishes (Brodeur et al., 2021).

Seabird Bycatch Estimates for Groundfish and Halibut Fisheries in the Eastern Bering Sea, 2016-2025

Contributed by Jessica Beck[1], Maggie Chan[2], and Cathy Tide[2]
[1]Resource Ecology and Fisheries Management Division, Alaska Fisheries Science Center, NOAA Fisheries, Seattle, WA
[2]Sustainable Fisheries Division, Alaska Regional Office, NOAA Fisheries, Juneau, AK
Contact: jessica.beck@noaa.gov
Last updated: September 2026

Description of indicator: This report provides estimates of the numbers of seabirds caught as bycatch in commercial groundfish and halibut fisheries operating in waters off Alaska in the eastern Bering Sea (EBS) for 2016 through 2025. Estimates of seabird bycatch from earlier years using different methods are not included here, nor are estimates prior to the start of data collection in the Pacific halibut longline fishery (see previous Ecosystem Status Reports for these estimates). Fishing gear types represented are demersal longline, pot, pelagic trawl, and non-pelagic trawl. These numbers do not apply to jig, gillnet, seine, or troll fisheries[69].

The NOAA Fisheries Alaska Regional Office Catch Accounting System (CAS) produces the estimates (Cahalan et al., 2010, 2014) and provides near real-time delivery of accurate groundfish and prohibited species catch and bycatch information for inseason management decisions. These estimates are based on three sources of information: (1) data provided by NMFS-certified fishery observers deployed to vessels and floating or shoreside processing plants, (2) video review of electronically monitored (EM) fixed gear vessels, and (3) industry reports of catch and production. CAS also estimates non-target species (such as invertebrates) and seabird bycatch in the groundfish and halibut fisheries. The data sets used by CAS are subject to change over time. Each year, an Annual Deployment Plan (ADP) describes the science-driven method for deployment of observers and EM on vessels in the partial coverage component of the North Pacific Observer Program (50 CFR 679.51(a))[70]. The ADP specifies the scientific deployment design for the partial coverage fisheries and the selection rate - the portion of trips that are sampled by observers and EM. Deployment rates can differ by gear type, location, or other factors. In the full coverage category of the North Pacific Observer Program every trip is monitored by 1 or 2 observers. In 2025, 61.6% of the demersal longline fishing trips were in the partial coverage category in the BSAI and 38.4% were in full coverage (Table 4-1 in the North Pacific Observer Program 2025 Annual Report[71]).

This report delineates and separately discusses estimates of seabird bycatch in the southeastern Bering Sea (SEBS) and the northern Bering Sea (NBS). Estimates of seabird bycatch from the SEBS include the reporting areas 508, 509, 512, 513, 514, 516, 517, 521, part of 523, and 524 (estimates for 514 and 524 only include data south of 60°N). Estimates from the NBS include areas north of 60°N and south of 65°N in reporting areas 514 and 524. Estimates of seabird bycatch north of 65°N are not included in the NBS summaries or discussed in the trends as they are outside the scope of the ESR regions, but

[69]This report does not include estimates of seabird bycatch in fisheries using jig, gillnet, seine, or troll gear because NOAA Fisheries does not have independent observer data from these fisheries. These estimates also do not apply to State of Alaska-managed salmon, herring, shellfish (including crab), or dive fisheries.

[70]`https://www.fisheries.noaa.gov/tags/north-pacific-observer-program?title=annual%20deployment&field_species_vocab_target_id=&sort_by=created`

[71]Alaska Fisheries Science Center and Alaska Regional Office. 2026. North Pacific Observer Program 2025 Annual Report. Alaska Fish. Sci. Cent., NOAA, Natl. Mar. Fish. Serv., 7600 Sand Point Way N.E., Seattle, Washington 98115.

are provided as a separate table (Table 12) for readers' reference. In previous versions of this report, bycatch estimates in the SEBS, NBS, and waters north of 65°N were all included as the EBS summaries, but bycatch estimates from area 523 were not[72]. The areas included in this version of the ESR were updated to more accurately reflect the ecoregions.

Status and trends:

Southeastern Bering Sea

In the SEBS, overall estimated takes of seabirds in 2025 increased 22% from the 2016-2024 average (4750 and 3883 takes, respectively; Figure 162, Table 10). This increase was primarily driven by estimated takes of Laysan albatross (*Phoebastria immutabilis*) and Northern fulmars (*Fulmarus glacialis*) in the region. High numbers of Laysan albatross were caught in SEBS in both 2024 and 2025. The number of estimated Laysan takes in 2025 was 214 birds, which is a 229% increase over 2016-2024 average (65 birds) and a 449% increase over the 2016-2023 average (39 birds) when 2024 estimates are excluded. There was also a modest increase of 30% in Northern fulmar estimated takes in the SEBS in 2025, with 2825 individuals estimated caught versus the 2016-2024 average of 2163 birds. Shearwater estimated bycatch also increased between 2024 (482 birds) and 2025 (792 birds) but the 2025 estimates actually decreased 22% from the 2016-2024 average (1012 birds). Shearwater bycatch is predominantly made up of Short-tailed shearwaters (*Ardenna tenuirostris*) along with some Sooty shearwaters (*A. grisea*), but are lumped together into Shearwater spp. due to the difficulty of distinguishing between the two in fishery samples.

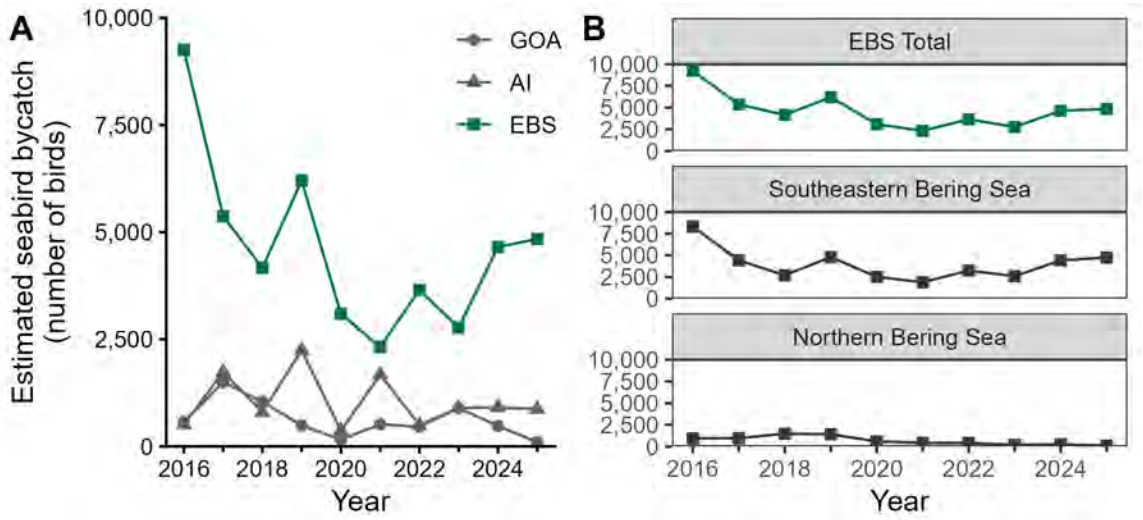


Figure 162: (A) Total estimated seabird bycatch in Gulf of Alaska (GOA), Aleutian Islands (AI), and Eastern Bering Sea (EBS) groundfish and halibut fisheries, all gear types combined, 2016 through 2025. (B) Total estimated seabird bycatch in the Eastern Bering Sea (EBS Total), Southeastern Bering Sea, and Northern Bering Sea groundfish and halibut fisheries, all gear types combined, 2016 through 2025.

[72]Alaska Fisheries Figures, Maps, Boundaries, Regulatory Areas, and Zones: `https://www.fisheries.noaa.gov/alaska/sustainable-fisheries/alaska-fisheries-figures-maps-boundaries-regulatory-areas-and-zones`

Table 10: Estimated seabird bycatch in southeastern Bering Sea groundfish and halibut fisheries for all gear types, 2016 through 2025. Note that these numbers represent extrapolations from observed bycatch, not direct observations. See text for estimation methods.

Species Group	**2016**	**2017**	**2018**	**2019**	**2020**	**2021**	**2022**	**2023**	**2024**	**2025**
Unidentified Albatross	0	0	0	0	0	0	0	0	0	0
Short-tailed Albatross	0	0	0	0	11	0	0	0	0	0
Laysan Albatross	12	19	151	14	7	27	45	34	276	214
Black-footed Albatross	0	0	0	0	0	0	63	0	0	0
Northern Fulmar	4,473	2,840	1,943	1,988	1,822	966	1,515	1,508	2,416	2,825
Shearwaters	2,946	885	147	2,507	243	677	496	723	482	792
Storm Petrels	0	0	0	0	0	7	0	0	0	1
Gull	582	320	364	141	169	107	664	135	785	645
Kittiwake	0	22	37	16	21	13	6	21	6	3
Murre	52	10	0	0	6	1	0	0	0	0
Puffin	7	0	0	0	0	0	0	0	0	0
Auklets	1	25	0	0	0	0	4	0	11	0
Other Alcid	0	0	6	6	0	0	0	0	0	0
Cormorant	0	0	0	0	0	0	0	0	0	0
Other	0	63	0	0	7	0	48	0	0	0
Unidentified	257	242	52	136	233	106	408	175	443	270
Grand Total	8,330	4,426	2,700	4,807	2,520	1,905	3,249	2,595	4,419	4,750

Table 11: Estimated seabird bycatch in northern Bering Sea groundfish and halibut fisheries for all gear types, 2016 through 2025. Note that these numbers represent extrapolations from observed bycatch, not direct observations. See text for estimation methods.

Species Group	2016	2017	2018	2019	2020	2021	2022	2023	2024	2025
Unidentified Albatross	0	0	0	0	0	0	0	0	0	0
Short-tailed Albatross	0	0	0	0	0	0	0	0	0	0
Laysan Albatross	0	10	27	0	1	10	0	0	4	0
Black-footed Albatross	0	0	0	0	0	0	6	0	0	0
Northern Fulmar	615	760	875	672	302	40	263	99	135	56
Shearwaters	257	104	398	661	128	254	92	31	77	5
Storm Petrels	0	0	0	0	0	0	0	0	0	2
Gull	20	51	140	15	5	45	10	43	11	29
Kittiwake	5	0	0	2	3	0	18	0	0	0
Murre	0	0	0	0	0	7	0	0	0	0
Puffin	3	0	0	0	0	0	0	0	0	0
Auklets	0	0	0	0	0	0	0	0	0	0
Other Alcid	0	0	0	0	0	0	0	0	0	0
Cormorant	0	0	0	0	0	0	0	0	0	0
Other	0	0	0	0	0	0	0	0	0	0
Unidentified	25	22	25	50	133	60	15	2	6	0
Grand Total	925	948	1,465	1,399	571	415	403	175	233	93

Northern Bering Sea

In the NBS, 2025 estimated seabird bycatch (93 birds) decreased 87% from 2016-2024 average (726 birds; Figure 162,Table 11). Contributing to this decrease was a 87% decline in 2025 estimated Northern fulmar bycatch when compared to the 2016-2024 average (56 and 418 birds, respectively). Shearwater estimated takes also decreased 98% compared to the 2016-2024 average, with 5 birds taken in 2025 and 222 birds being the average previous years.

Factors influencing observed trends: There are many factors that may influence annual variation in bycatch rates, including seabird distribution, population trends, prey supply, and fisheries activities.

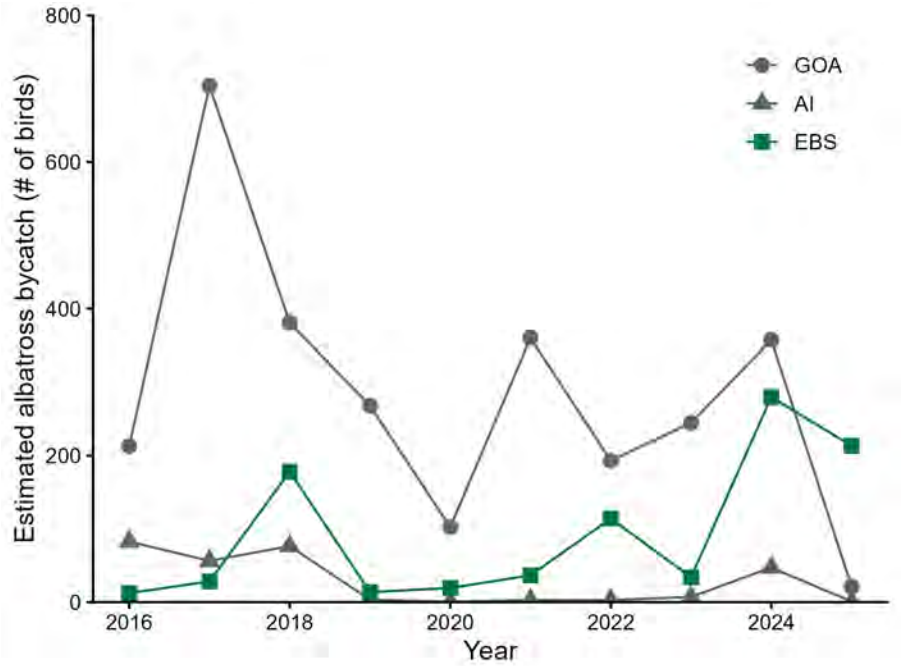


Figure 163: Total estimated albatross bycatch in Gulf of Alaska (GOA), Aleutian Islands (AI), and Eastern Bering Sea (EBS) groundfish and halibut fisheries, all gear types combined, 2016 through 2025.

Increased Laysan Albatross Takes in the SEBS:

The number of increased seabird takes in the SEBS is primarily driven by two species: Laysan albatross and Northern fulmars. These patterns are likely driven by a combination of fleet and species-specific factors.

The SEBS has consistently been the region with the highest estimates of seabird bycatch of any ESR region. This is in large part due to the presence of the Pacific cod hook-and-line fishery, which annually average an estimated 4,816 seabird takes per year (2007-2015) and for which 90% of the fishery occurs in the Bering Sea/Aleutian Islands region (Eich et al., 2016). The number of birds caught per 1,000 hooks for cod catcher vessels is low in comparison with sablefish and turbot fisheries in Alaska, and also moderately low for cod catcher processors (Eich et al., 2016). These bycatch rates are even lower when calculated specifically for albatross species. However, while seabird bycatch rates are low, the total number of hooks deployed in cod fisheries (particularly by catcher processors) are magnitudes higher than in the sablefish and turbot fisheries (Dietrich and Fitzgerald, 2010), resulting in fleets with high fishing effort and low bycatch rates, overlapped with core areas of Northern fulmar distributions.

For Laysan albatross takes in the eastern Bering Sea in 2024, 100% of Laysan specimens recorded by NMFS-certified fishery observers in their fishery samples were from catcher processor vessels targeting cod. In 2025, 96% of Laysan specimen records from observer samples were from catcher processor vessels targeting cod in the SEBS. In these samples, observers recorded that the vessel was using paired streamers during 56% and 52% of the samples (in 2024 and 2025, respectively). For the remainder of the samples with Laysan specimens, observers were not able to check seabird bycatch deterrent type (likely due to conflicting workload demands). Temporally, these specimens were all documented between January-June of both years, with 72% of 2024 specimens recorded in April and 78% of 2025 specimens recorded in March and April. Note that observer provided data are not the sole sources of data used for CAS estimates.

While the number of hook-and-line vessels in the 60-124 ft and 125-230 ft. categories targeting Pacific cod did increase between 2020 and 2024 (Abelman et al., 2026), vessel participation does not directly measure hooks deployed or the spatial and temporal overlap between fishing and Laysan albatross. The available evidence therefore does not yet establish how much fishing effort contributed to increased estimated Laysan albatross bycatch in 2024 and 2025. Other potential fleet-related explanations include changes in the location and timing of fishing, target and vessel composition, vessel-specific operating practices, and observer coverage and sampling.

Laysan albatross are the most prevalent albatross species in the Bering Sea, according to fisheries independent survey data, with seasonal increases in early spring. This species frequently forages offshore of the shelf break, utilizing waters across the outer and middle shelf regions (Suryan and Kuletz, 2018). Albatross are long-distance fliers, and rely on low-altitude winds to access foraging grounds across their ranges. A possible factor in increased bycatch patterns could be interannual spatial and temporal changes of localized and north Pacific Basin wind currents, and the possibility that the currents funneled more Laysan albatross into the SEBS region in both years. However, fishery-independent albatross distribution data is not currently available to investigate this possibility. Another factor to consider is that several of the catcher processor vessels that observed Laysan takes originated from in both years were fishing in moderate to high winds on the days the birds were incidentally caught. Even when vessels are properly using streamers as seabird bycatch mitigation methods, the effectiveness of these methods can be greatly decreased in high winds and crosswinds if the streamers no longer cover the hookline.

While there are likely various factors influencing Laysan albatross bycatch patterns in the SEBS, a single factor that can clearly explain increased takes of Laysan albatross in 2024 and 2025 has not yet been identified. A more in-depth analysis is needed to better understand underlying variables and their interactions.

ESA species

There were no takes of ESA-listed seabirds in the eastern Bering Sea in 2024 or 2025 in federally-managed groundfish fisheries. Observers are trained to retain any specimens that they suspect could be ESA-listed species, even if they cannot positively identify the specimen to species in the field[73].

[73] https://www.fisheries.noaa.gov/resource/document/north-pacific-observer-sampling-manual

Implications: Estimated seabird bycatch in the SEBS fisheries off of Alaska in 2025 increased, while NBS seabird bycatch estimates decreased compared to the 2016-2024 average.

It is difficult to determine how seabird bycatch estimates and trends are linked to changes in ecosystem components. Many seabirds caught in groundfish and halibut fisheries in Alaska are wide-ranging and can fly hundreds of miles per day, resulting in less restricted foraging areas. Of the species caught as bycatch in the Bering Sea regions, only gulls, storm petrels, kittiwakes, and Northern fulmars breed in the region. Changes in fleet dynamics also affect seabird bycatch estimates, further complicating direct links with ecosystem components.

Fisheries bycatch can also affect seabird populations directly. In Alaska, bycatch of ESA-listed species is tightly regulated, and NOAA works in conjunction with outside agencies and partners to assess and manage the risk of bycatch to unlisted seabird species, including requiring seabird bycatch mitigation tools in hook-and-line groundfish and halibut fisheries[74].

[74] https://www.fisheries.noaa.gov/alaska/bycatch/seabird-avoidance-gear-and-methods

Table 12: Estimated seabird bycatch in groundfish and halibut fisheries outside the ESR ecoregions (i.e., north of the NBS reporting area) for all gear types, 2016 through 2025. Note that these numbers represent extrapolations from observed bycatch, not direct observations. See text for estimation methods.

Species Group	2016	2017	2018	2019	2020	2021	2022	2023	2024	2025
Unidentified Albatross	0	0	0	0	0	0	0	0	0	0
Short-tailed Albatross	0	0	0	0	0	0	0	0	0	0
Laysan Albatross	0	0	0	0	0	0	0	0	0	0
Black-footed Albatross	0	0	0	0	0	0	0	0	0	0
Northern Fulmar	0	0	0	22	0	0	0	0	0	0
Shearwaters	0	0	0	4	0	0	0	0	0	0
Storm Petrels	0	0	0	0	0	0	0	0	0	0
Gull	0	0	0	0	1	0	0	0	0	0
Kittiwake	0	0	0	0	0	0	0	0	0	0
Murre	0	0	0	0	0	0	0	0	0	0
Puffin	0	0	0	0	0	0	0	0	0	0
Auklets	0	0	0	0	0	0	0	0	0	0
Other Alcid	0	0	0	0	0	0	0	0	0	0
Cormorant	0	0	0	0	0	0	0	0	0	0
Other	0	0	0	0	0	0	0	0	0	0
Unidentified	0	0	0	5	0	0	0	0	0	0
Grand Total	0	0	0	31	1	0	0	0	0	0

Sustainability (for consumptive and non-consumptive uses)

Fish Stock Sustainability Index – Bering Sea and Aleutian Islands

Contributed by George A. Whitehouse
Cooperative Institute for Climate, Ocean, and Ecosystem Studies (CICOES), University of Washington, Seattle, WA
Contact: gaw@uw.edu
Last updated: August 2026

Description of indicator: The Fish Stock Sustainability Index (FSSI) is a performance measure for the sustainability of fish stocks selected for their importance to commercial and recreational fisheries[75]. The FSSI will increase as overfishing is ended and stocks rebuild to the level that provides maximum sustainable yield. The FSSI is calculated by awarding points for each stock based on the following rules:

1. Stock has known status determinations:
   (a) overfishing level is defined = 0.5
   (b) overfished biomass level is defined = 0.5
2. Fishing mortality rate is below the "overfishing" level defined for the stock = 1.0
3. Biomass is above the "overfished" level defined for the stock = 1.0
4. Biomass is at or above 80% of the biomass that produces maximum sustainable yield (B_{MSY}) = 1.0 (this point is in addition to the point awarded for being above the "overfished" level)

The maximum score for each stock is 4.

In the Alaska Region, there are 35 FSSI stocks and an overall FSSI of 140 would be achieved if every stock scored the maximum value, 4. Over time, the number of stocks included in the FSSI has changed as stocks have been added and removed from Fishery Management Plans (FMPs). To keep FSSI scores for Alaska comparable across years we report the FSSI as a percentage of the maximum possible score.

Additionally, there are 33 non-FSSI stocks in Alaska, three ecosystem component species complexes, and Pacific halibut which are managed under an international agreement. Two of the non-FSSI crab stocks are overfished but are not subject to overfishing. The Pribilof Islands blue king crab stock is in year twelve of a rebuilding plan, and the Saint Matthews Island blue king crab stock is in year six of a 26-year rebuilding plan. None of the other non-FSSI stocks are known to be subject to overfishing, are overfished, or known to be approaching an overfished condition. For more information on non-FSSI stocks see the Status of U.S. Fisheries webpage[1].

[75] https://www.fisheries.noaa.gov/national/population-assessments/fishery-stock-status-updates

Status and trends: The statewide Alaska FSSI generally trended upwards from 80% in 2006 to a high of 94% in 2018, then trended downward to 88.2% in 2022. It increased incrementally to 89% in 2023 and 90.3% in 2024 and 2025. The statewide Alaska FSSI has decreased slightly to 90.0% in 2026 (Figure 164).

As of June 30, 2026, no BSAI groundfish stock or stock complex is subject to overfishing, is known to be overfished, or known to be approaching an overfished condition (Table 13). The BSAI groundfish FSSI score is 60.5 out of a maximum possible 64. The Aleutian Islands Pacific cod stock FSSI increased from 1.5 to 3 due to establishing that the stock is not overfished, is not approaching an overfished condition, and for the stock biomass being above the overfished level. The Bogoslof walleye pollock stock FSSI score is of 1.5 due to not having known overfished status or known biomass relative to their overfished levels or to BMSY. All other BSAI groundfish FSSI stocks received the maximum possible score of four points.

The BSAI king and tanner crab FSSI is 17 out of a possible 20. Two points were deducted for the Bering Sea snow crab being overfished and for the stock's biomass being below 80% of B_{MSY}. Another point was lost for the biomass of Aleutian Islands golden king crab being less than 80% of B_{MSY}.

The overall BSAI FSSI score is 77.5 out of a maximum possible score of 84 (Table 13). The BSAI FSSI trended upward from 74% in 2006 to a peak of 95.5% in 2019. It dropped to 92.9% in 2020 and has generally been stable since then (Figure 165).

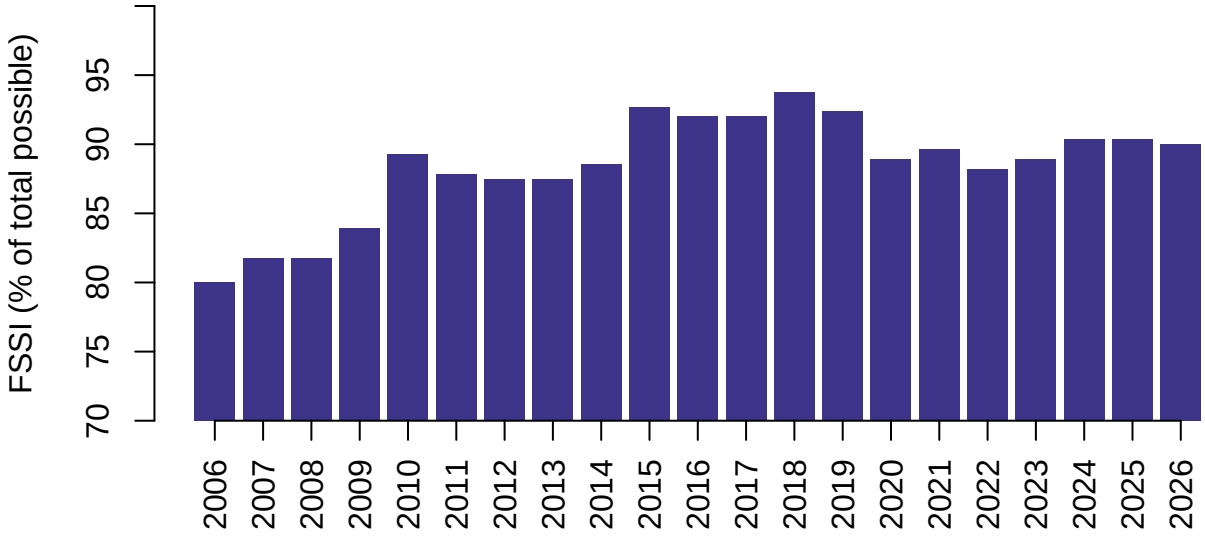


Figure 164: The trend in Alaska statewide FSSI from 2006 through 2026, as a percentage of the maximum possible FSSI. The maximum possible FSSI was 140 from 2006 to 2014, 144 from 2015 to 2019, and 140 since 2020. All scores are reported through the second quarter (June) of each year and are retrieved from the Status of U.S. Fisheries website: `https://www.fisheries.noaa.gov/national/population-assessments/fishery-stock-status-updates`.

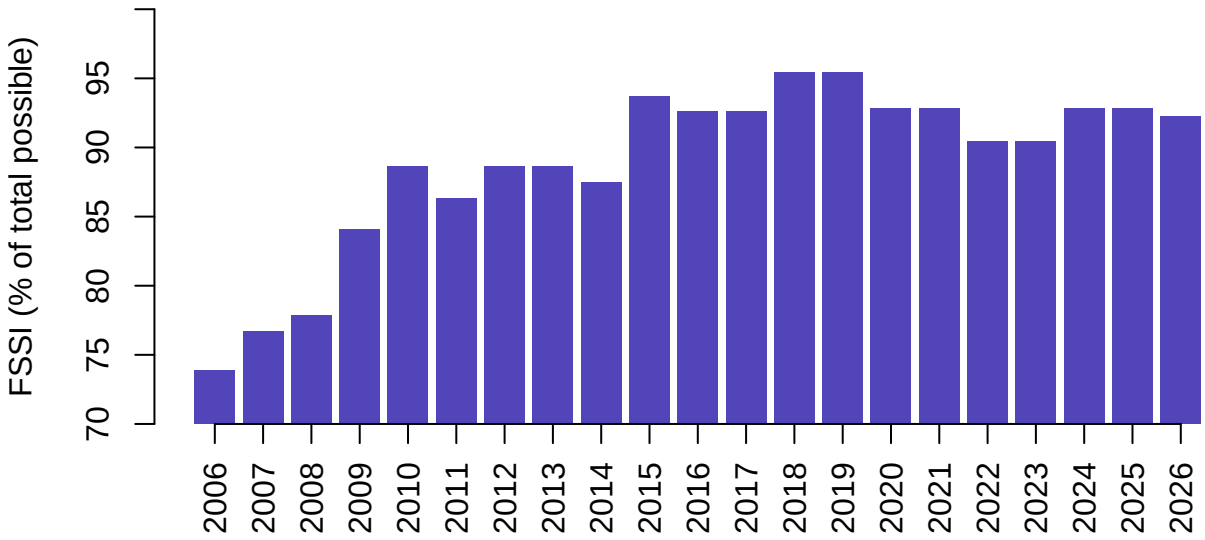


Figure 165: The trend in BSAI FSSI from 2006 through 2026 as a percentage of the maximum possible FSSI. All scores are reported through the second quarter (June) of each year and are retrieved from the Status of U.S. Fisheries website: `https://www.fisheries.noaa.gov/national/population-assessments/fishery-stock-status-updates`.

Factors influencing observed trends: The overall trends in the Alaska statewide FSSI and the BSAI FSSI were positive between 2006-2015, and both have remained generally flat from 2016-2026. There was a net loss of 0.5 points in the Alaska statewide FSSI due to one point each lost for Aleutian Islands golden king crab and Bering Sea snow crab and a 1.5 point gain for Aleutian Islands Pacific cod.

Implications: The majority of Alaska groundfish and crab fisheries appear to be sustainably managed. Bering Sea snow crab is the only FSSI groundfish or crab stock in the BSAI known to be overfished and is presently in year 3 of a 6 year rebuilding plan.

Table 13: BSAI FSSI stocks under NPFMC jurisdiction updated through June 2026 adapted from the NOAA Fishery Stock Status Updates webpage: https://www.fisheries.noaa.gov/national/population-assessments/fishery-stock-status-updates. *See FSSI and Non-FSSI Stock Status Table on the Fishery Stock Status Updates webpage for definition of stocks, stock complexes, and notes on rebuilding.

Stock	Overfishing	Overfished	Approaching	Progress	B/Bmsy	FSSI Score
Golden king crab - Aleutian Islands*	No	No	No	NA	1.094, 0.788	3
Red king crab - Bristol Bay	No	No	No	NA	1.066	4
Red king crab - Norton Sound	No	No	No	NA	1.097	4
Snow crab - Bering Sea*	No	Yes	No	Year 3 of 6 year plan	0.421	2
Southern Tanner crab - Bering Sea	No	No	No	NA	2.302	4
BSAI Alaska plaice	No	No	No	NA	1.578	4
BSAI Atka mackerel	No	No	No	NA	1.164	4
BSAI Arrowtooth Flounder	No	No	No	NA	2.583	4
BSAI Kamchatka flounder	No	No	No	NA	1.504	4
BSAI Flathead Sole Complex*	No	No	No	NA	2.077	4
BSAI Rock Sole Complex*	No	No	No	NA	1.612	4
BSAI Skate Complex*	No	No	No	NA	2.065	4
BSAI Greenland halibut	No	No	No	NA	1.489	4
BSAI Northern rockfish	No	No	No	NA	2.095	4
BS Pacific cod	No	No	No	NA	1.075	4
AI Pacific cod	No	No	No	NA	0.704	3
BSAI Pacific Ocean perch	No	No	No	NA	1.600	4
Walleye pollock - Aleutian Islands	No	No	No	NA	1.309	4
Walleye pollock - Bogoslof	No	Unknown	Unknown	NA	not estimated	1.5
Walleye pollock - Eastern Bering Sea	No	No	No	NA	1.373	4
BSAI Yellowfin sole	No	No	No	NA	1.699	4

References

Abelman, A., A. Abolhassani, M. Dalton, R. Dame, R. Felthoven, B. Garber-Yonts, J. Lee, C. Seung, M. Szymkowiak, and S. Wise. 2026. Stock Assessment and Fishery Evaluation Report of the Groundfish Fisheries of the Gulf of Alaska and Bering Sea/Aleutian Islands Area: Economic Status of the Groundfish Fisheries off Alaska, 2025. Report, NOAA Fisheries, 7600 Sand Point Way N.E., Seattle, WA 98115.

Adams, G. D., K. K. Holsman, S. J. Barbeaux, M. W. Dorn, J. N. Ianelli, I. Spies, I. J. Stewart, and A. E. Punt. 2022. An ensemble approach to understand predation mortality for groundfish in the Gulf of Alaska. Fisheries Research **251**:106303.

Alverson, D. L., M. H. Freeberg, S. A. Murawski, and J. Pope. 1994. A global assessment of fisheries bycatch and discards (Vol. 339). Food Agriculture Organization.

Amakasu, K., T. Mukai, and M. Moteki. 2017. Measurement of the volume-backscattering spectrum from an aggregation of Antarctic krill and inference of their length-frequency distribution. Polar Science **12**:79–87.

Anderson, D. M., E. Fachon, R. S. Pickart, P. Lin, A. D. Fischer, M. L. Richlen, V. Uva, M. L. Brosnahan, L. McRaven, and F. Bahr. 2021. Evidence for massive and recurrent toxic blooms of *Alexandrium catenella* in the Alaskan Arctic. Proceedings of the National Academy of Sciences **118**.

Anderson, S. C., E. J. Ward, P. A. English, and L. A. Barnett. 2022. sdmTMB: an R package for fast, flexible, and user-friendly generalized linear mixed effects models with spatial and spatiotemporal random fields. BioRxiv page 2022.03. 24.485545 .

Andrews, A., M. A. Cook, E. Siddon, and A. Dimond. 2019. Prey Quality Provides a Leading Indicator of Energetic Content for Age-0 Walleye Pollock. Stock Assessment and Fishery Evaluation Report, North Pacific Fishery Management Council 605 W. 4th Avenue, Suite 306, Anchorage, AK 99301.

Andrews, A. G., W. W. Strasburger, E. V. Farley, J. M. Murphy, and K. O. Coyle. 2015. Effects of warm and cold climate conditions on capelin (*Mallotus villosus*) and Pacific herring (*Clupea pallasii*) in the eastern Bering Sea. Deep Sea Research Part II: Topical Studies in Oceanography .

Aydin, K., and F. Mueter. 2007. The Bering Sea - a dynamic food web perspective. Deep Sea Research Part II: Topical Studies in Oceanography **54**:2501–2525.

Bailey, K. M. 1989. Interaction between the vertical distribution of juvenile walleye pollock Theragra chalcogramma in the eastern Bering Sea, and cannibalism. Mar. Ecol. Prog. Ser **53**:205–213.

Baird, P. 2022. Diatoms and fatty acid production in Arctic and estuarine ecosystems—a reassessment of marine food webs, with a focus on the timing of shorebird migration. Marine Ecology Progress Series **688**:173–196.

Baker, J. D., and C. W. Fowler. 1992. Pup weight and survival of northern fur seals Callorhinus ursinus. Journal of Zoology **227**:231–238.

Baker, M. R., K. K. Kivva, M. N. Pisareva, J. T. Watson, and J. Selivanova. 2020. Shifts in the physical environment in the Pacific Arctic and implications for ecological timing and conditions. Deep Sea Research Part II: Topical Studies in Oceanography **177**:104802.

Barbeaux, S. J., K. Holsman, and S. Zador. 2020. Marine heatwave stress test of ecosystem-based fisheries management in the Gulf of Alaska Pacific Cod Fishery. Frontiers in Marine Science **7**:703.

Batten, S. D., G. T. Ruggerone, and I. Ortiz. 2018. Pink salmon induce a trophic cascade in plankton populations in the southern Bering Sea and around the Aleutian Islands. Fisheries Oceanography **27**:548–559.

Beamish, R. J., and C. Mahnken. 2001. A critical size and period hypothesis to explain natural regulation of salmon abundance and the linkage to climate and climate change. Progress in Oceanography **49**:423–437.

Beauplet, G., C. Barbraud, M. Chambellant, and C. Guinet. 2005. Interannual variation in the post-weaning and juvenile survival of subantarctic fur seals: influence of pup sex, growth rate and oceanographic conditions. Journal of Animal Ecology **74**:1160–1172.

Berkeley, S. A., M. A. Hixon, R. J. Larson, and M. S. Love. 2004. Fisheries sustainability via protection of age structure and spatial distribution of fish populations. Fisheries **29**:23–32.

Blackwell, B. G., M. L. Brown, and D. W. Willis. 2000. Relative weight (Wr) status and current use in fisheries assessment and management. Reviews in fisheries Science **8**:1–44.

Blanchard, F., and J. Boucher. 2001. Temporal variability of total biomass in harvested communities of demersal fishes. Fisheries Research **49**:283–293.

Boldt, J. 2007. Ecosystem Considerations for 2008. Stock Assessment and Fishery Evaluation Report for the Groundfish Resources of the Bering Sea/Aleutian Islands and Gulf of Alaska. North Pacific Fishery Management Council, 605 W. 4th Ave., Suite 306, Anchorage, AK 99501.

Boldt, J. L., and L. J. Haldorson. 2004. Size and condition of wild and hatchery pink salmon juveniles in Prince William Sound, Alaska. Transactions of the American Fisheries Society **133**:173–184.

Bond, N. A., M. F. Cronin, H. Freeland, and N. Mantua. 2015. Causes and impacts of the 2014 warm anomaly in the NE Pacific. Geophysical Research Letters **42**:3414–3420.

Bouchard, C., and L. Fortier. 2020. The importance of Calanus glacialis for the feeding success of young polar cod: a circumpolar synthesis. Polar Biology **43**:1095–1107.

Boveng, P. L., G. M. Brady, M. F. Cameron, C. L. Christman, S. P. Dahle, L. M. Hiruki-Raring, J. K. Jansen, S. M. Koslovsky, J. M. London, B. T. McClintock, R. A. Montgomery, E. E. Moreland, E. L. Richmond, M. A. Simpkins, J. M. Ver Hoef, S. M. Walcott, D. E. Withrow, J. N. Womble, K. M. Yano, and H. L. Ziel. 2026. Abundance and trends of harbor seals (¡em¿Phoca vitulina richardii¡/em¿) in Alaska, 1996–2023. bioRxiv page 2026.09.02.748977 .

Brodeur, R. D., T. W. Buckley, G. M. Lang, D. L. Draper, J. C. Buchanan, and R. E. Hibpshman. 2021. Demersal fish predators of gelatinous zooplankton in the Northeast Pacific Ocean. Marine Ecology Progress Series **658**:89–104.

Brodeur, R. D., M. B. Decker, L. Ciannelli, J. E. Purcell, N. A. Bond, P. J. Stabeno, E. Acuna, and G. L. Hunt. 2008. Rise and fall of jellyfish in the eastern Bering Sea in relation to climate regime shifts. Progress in Oceanography **77**:103–111.

Brodeur, R. D., R. L. Emmett, J. P. Fisher, E. Casillas, D. J. Teel, and T. W. Miller. 2004. Juvenile salmonid distribution, growth, condition, origin, and environmental and species associations in the Northern California Current. Fishery Bulletin **102**:25–46.

Brodeur, R. D., M. T. Wilson, L. Ciannelli, M. Doyle, and J. M. Napp. 2002. Interannual and regional variability in distribution and ecology of juvenile pollock and their prey in frontal structures of the Bering Sea. Deep Sea Research Part II: Topical Studies in Oceanography **49**:6051–6067.

Buckley, T. W., I. Ortiz, S. Kotwicki, and K. Aydin. 2016. Summer diet composition of walleye pollock and predator–prey relationships with copepods and euphausiids in the eastern Bering Sea, 1987–2011. Deep Sea Research Part II: Topical Studies in Oceanography **134**:302–311.

Cahalan, J., J. Gasper, and J. Mondragon. 2014. Catch sampling and estimation in the Federal groundfish fisheries off Alaska, 2015 edition. Report, U.S. Dep. Commer., NOAA Tech. Memo. NMFS-AFSC-286, 46 p.

Cahalan, J., J. Mondragon, and J. Gasper. 2010. Catch sampling and estimation in the Federal groundfish fisheries off Alaska. Report, U.S. Dep. Commer., NOAA Tech. Memo. NMFS-AFSC-205, 42 p.

Callahan, M., and E. Lemagie. 2024. Bering Sea SST Anomalies. Water Temperature sub-section. In: Physical Environment Synthesis. In Siddon, E. 2024. Ecosystem Status Report 2024: Eastern Bering Sea. Report, North Pacific Fishery Management Council, 1007 W 3rd Ave, Suite 400, Anchorage, AK 99501.

Campbell, J., D. Antoine, R. Armstrong, K. Arrigo, W. Balch, R. Barber, M. Behrenfeld, R. Bidigare, J. Bishop, and M. Carr. 2002. Comparison of algorithms for estimating ocean primary production from surface chlorophyll, temperature, and irradiance. Global biogeochemical cycles **16**:9–1–9–15.

Catchpole, T., C. Frid, and T. Gray. 2006. Resolving the discard problem - A case study of the English *Nephrops* fishery. Marine Policy **30**:821–831.

Ciannelli, L., and K. M. Bailey. 2005. Landscape dynamics and resulting species interactions: the cod-capelin system in the southeastern Bering Sea. Marine Ecology Progress Series **291**:227–236.

Ciannelli, L., R. Drodeur, and T. Buckley. 1998. Development and application of a bioenergetics model for juvenile walleye pollock. Journal of Fish Biology **52**:879–898.

Clement Kinney, J., W. Maslowski, R. Osinski, Y. J. Lee, C. Goethel, K. Frey, and A. Craig. 2022. On the variability of the Bering Sea Cold Pool and implications for the biophysical environment. PLoS One **17**:e0266180.

Cline, T. J., J. Ohlberger, and D. E. Schindler. 2019. Effects of warming climate and competition in the ocean for life-histories of Pacific salmon. Nature Ecology Evolution **3**:935–942.

Clucas, I. 1997. A study of the options for utilization of bycatch and discards from marine capture fisheries. FAO fisheries circular **928**:1–59.

Coachman, L. 1986. Circulation, water masses, and fluxes on the southeastern Bering Sea shelf. Continental Shelf Research **5**:23–108.

Cochrane, N., D. Sameoto, A. Herman, and J. Neilson. 1991. Multiple-frequency acoustic backscattering and zooplankton aggregations in the inner Scotian Shelf basins. Canadian Journal of Fisheries and Aquatic Sciences **48**:340–355.

Conners, M. E., K. Y. Aydin, and C. L. Conrath. 2016. Assessment of the octopus stock complex in the Bering Sea and Aleutian Islands. Report, North Pacific Fishery Management Council.

Connors, B., M. J. Malick, G. T. Ruggerone, P. Rand, M. Adkison, J. R. Irvine, R. Campbell, and K. Gorman. 2020. Climate and competition influence sockeye salmon population dynamics across the Northeast Pacific Ocean. Canadian Journal of Fisheries and Aquatic Sciences **77**:943–949.

Connors, B., G. T. Ruggerone, and J. R. Irvine. 2025. Adapting management of Pacific salmon to a warming and more crowded ocean. ICES Journal of Marine Science **82**:fsae135.

Cooney, R., and K. Coyle. 1982. Trophic implications of cross-shelf copepod distributions in the southeastern Bering Sea. Marine Biology **70**:187–196.

Cooper, D. W., and D. G. Nichol. 2016. Juvenile northern rock sole (Lepidopsetta polyxystra) spatial distribution and abundance patterns in the eastern Bering Sea: spatially dependent production linked to temperature. ICES Journal of Marine Science **73**:1138–1146.

Coyle, K. O., L. B. Eisner, F. J. Mueter, A. I. Pinchuk, M. A. Janout, K. Cieciel, E. V. Farley, and A. G. Andrews. 2011. Climate change in the southeastern Bering Sea: impacts on pollock stocks and implications for the oscillating control hypothesis. Fisheries Oceanography **20**:139–156.

Coyle, K. O., A. Pinchuk, L. Eisner, and J. M. Napp. 2008. Zooplankton species composition, abundance and biomass on the eastern Bering Sea shelf during summer: the potential role of water column stability and nutrients in structuring the zooplankton community. Deep-Sea Research Part II **55**:1755–1791.

Cunningham, C. J., P. A. Westley, and M. D. Adkison. 2018. Signals of large scale climate drivers, hatchery enhancement, and marine factors in Yukon River Chinook salmon survival revealed with a Bayesian life history model. Global Change Biology **24**:4399–4416.

De Robertis, A., D. R. McKelvey, and P. H. Ressler. 2010. Development and application of an empirical multifrequency method for backscatter classification. Canadian Journal of Fisheries and Aquatic Sciences **67**:1459–1474.

de Souza, J. M. A. C., and C. d. G. R. Costa. 2026. An Assessment of the Moana Operational Forecast System Assimilating Innovative Mangopare Fishing Vessel Observations in Aotearoa, New Zealand. Journal of Marine Science and Engineering **14**.

Decker, M. B., R. D. Brodeur, L. Ciannelli, L. L. Britt, N. A. Bond, B. P. DiFiore, and G. L. Hunt Jr. 2023. Cyclic variability of eastern Bering Sea jellyfish relates to regional physical conditions. Progress in Oceanography **210**:102923.

Decker, M. B., and G. L. Hunt Jr. 1996. Foraging by murres (Uria spp.) at tidal fronts surrounding the Pribilof Islands, Alaska, USA. Marine Ecology Progress Series **139**:1–10.

DeFilippo, L. B., K. G. Howard, C. J. Cunningham, R. M. Suryan, P. D. Barry, J. M. Murphy, and W. A. Larson. 2026. Shifting stage-specific constraints on productivity shape recovery potential for Yukon River Chinook salmon. Ecological Applications **36**:e70229.

DeFilippo, L. B., J. T. Thorson, C. A. O'Leary, S. Kotwicki, J. Hoff, J. N. Ianelli, V. V. Kulik, and A. E. Punt. 2023. Characterizing dominant patterns of spatiotemporal variation for a transboundary groundfish assemblage. Fisheries Oceanography .

Dickman, E. M., J. M. Newell, M. J. González, and M. J. Vanni. 2008. Light, nutrients, and food-chain length constrain planktonic energy transfer efficiency across multiple trophic levels. Proceedings of the National Academy of Sciences **105**:18408–18412.

Dietrich, K. S., and S. M. Fitzgerald. 2010. Analysis of 2004-2007 vessel-specific seabird bycatch data in Alaska demersal longline fisheries. Alaska Fisheries Science Center, Resource Ecology and Fisheries Management Division.

Drenkard, E. J., C. A. Stock, A. C. Ross, Y.-C. Teng, T. Cordero, W. Cheng, A. Adcroft, E. Curchitser, R. Dussin, and R. Hallberg. 2025. A regional physical–biogeochemical ocean model for marine resource applications in the Northeast Pacific (MOM6-COBALT-NEP10k v1. 0). Geoscientific Model Development **18**:5245–5290.

Dressel, S., S. Miller, C. Brown, and J. Erickson. 2024. Togiak Herring Population Trends. Stock Assessment and Fishery Evaluation Report, North Pacific Fishery Management Council, 1007 West 3rd Ave., Suite 400, Anchorage, Alaska 99501.

Duffy-Anderson, J. T., P. Stabeno, A. G. Andrews III, K. Cieciel, A. Deary, E. Farley, C. Fugate, C. Harpold, R. Heintz, and D. Kimmel. 2019. Responses of the northern Bering Sea and southeastern Bering Sea pelagic ecosystems following record-breaking low winter sea-ice. Geophysical Research Letters **46**:9833–9842.

Eich, A. M., K. R. Mabry, S. K. Wright, and S. M. Fitzgerald. 2016. Seabird bycatch and mitigation efforts in Alaska Fisheries: summary report, 2007 through 2015 .

Eisner, L., K. Cieciel, J. Gann, and C. Ladd. 2017. Phytoplankton biomass and size structure during the late summer to early fall in the eastern Bering Sea. Stock Assessment and Fishery Evaluation Report, North Pacific Fishery Management Council, 605 W. 4th Avenue, Suite 306, Anchorage, AK 99301.

Eisner, L. B., J. C. Gann, C. Ladd, K. D. Cieciel, and C. W. Mordy. 2016. Late summer/early fall phytoplankton biomass (chlorophyll a) in the eastern Bering Sea: Spatial and temporal variations and factors affecting chlorophyll a concentrations. Deep Sea Research Part II: Topical Studies in Oceanography **134**:100–114.

Eisner, L. B., J. M. Napp, K. L. Mier, A. I. Pinchuk, and A. G. Andrews III. 2014. Climate-mediated changes in zooplankton community structure for the eastern Bering Sea. Deep Sea Research Part II: Topical Studies in Oceanography **109**:157–171.

Eisner, L. B., E. M. Yasumiishi, A. G. Andrews III, and C. A. O'Leary. 2020. Large copepods as leading indicators of walleye pollock recruitment in the southeastern Bering Sea: Sample-Based and spatio-temporal model (VAST) results. Fisheries Research **232**:105720.

Elison, T., P. Salomone, T. Sands, G. Buck, K. Sechrist, and D. Koster. 2018. 2017 Bristol Bay area annual management report. Report, Alaska Department of Fish and Game, Fishery Management Report No. 18-11.

Fachon, E., R. S. Pickart, G. Sheffield, E. Pate, M. Pathare, M. L. Brosnahan, E. Muhlbach, K. Horn, N. N. Spada, and A. Rajagopalan. 2025. Tracking a large-scale and highly toxic Arctic algal bloom: Rapid detection and risk communication. Limnology and Oceanography Letters **10**:62–72.

Falk-Petersen, S., P. Mayzaud, G. Kattner, and J. R. Sargent. 2009. Lipids and life strategy of Arctic Calanus. Marine Biology Research **5**:18–39.

FAO. 1995. Code of Conduct for Responsible Fisheries. Food and Agriculture Organization, Rome.

Farley, E., J. Moss, and R. Beamish. 2007. A Review of the critical size, critical period hypothesis for juvenile Pacific salmon. North Pacific Anadromous Fish Commission Bulletin **4**:311–317.

Farley, E. V., R. A. Heintz, A. G. Andrews, and T. P. Hurst. 2016. Size, diet, and condition of age-0 Pacific cod (*Gadus macrocephalus*) during warm and cool climate states in the eastern Bering Sea. Deep Sea Research Part II: Topical Studies in Oceanography **134**:247–254.

Farley, E. V., A. Starovoytov, S. Naydenko, R. Heintz, M. Trudel, C. Guthrie, L. Eisner, and J. R. Guyon. 2011. Implications of a warming eastern Bering Sea for Bristol Bay sockeye salmon. ICES Journal of Marine Science **68**:1138–1146.

Farley Jr, E. V., E. M. Yasumiishi, J. M. Murphy, W. Strasburger, F. Sewall, K. Howard, S. Garcia, and J. H. Moss. 2024. Critical periods in the marine life history of juvenile western Alaska chum salmon in a changing climate. Marine Ecology Progress Series **726**:149–160.

Feddern, M. L., R. Shaftel, E. R. Schoen, C. J. Cunningham, B. M. Connors, B. A. Staton, A. von Finster, Z. Liller, V. R. von Biela, and K. G. Howard. 2024. Body size and early marine conditions drive changes in Chinook salmon productivity across northern latitude ecosystems. Global Change Biology **30**:e17508.

Fergusson, E., R. Suryan, T. Miller, J. Murphy, and A. Andrews. 2024. Juvenile salmon condition trends in the eastern Bering Sea. *In*: Siddon, E. 2024. Ecosystem Status Report 2024: Eastern Bering Sea. Stock Assessment and Fishery Evaluation Report, North Pacific Fishery Management Council, 1007 West Third, Suite 400, Anchorage, Alaska 99501.

Ferriss, B. 2026. Gulf of Alaska Ecosystem State Analyses. *In*: Ferriss, B.E. 2026. Ecosystem Status Report 2026: Gulf of Alaska. Stock Assessment and Fishery Evaluation Report, North Pacific Fishery Management Council, 1007 West Third, Suite 400, Anchorage, Alaska 99501.

Fetterer, F., K. Knowles, W. N. Meier, M. Savoie, and A. K. Windnagel. 2017. Sea Ice Index, Version 3. Regional Daily Data. Report, Boulder, Colorado USA. NSIDC: National Snow and Ice Data Center.

Frey, K. E., J. A. Maslanik, J. C. Kinney, and W. Maslowski. 2014. Recent variability in sea ice cover, age, and thickness in the Pacific Arctic region, pages 31–63 . Springer.

Froese, R. 2006. Cube law, condition factor and weight–length relationships: history, meta-analysis and recommendations. Journal of Applied Ichthyology **22**:241–253.

Gann, J. C., D. G. Kimmel, F. J. Mueter, M. W. Lomas, L. B. Eisner, and S. L. Mincks. 2026. Phytoplankton communities respond to environmental shifts in the eastern Bering Sea: Low abundances of Calanus copepods correlate with larger but potentially adverse phytoplankton taxa during warm stanzas. Limnology and Oceanography **71**:e70439.

Geiger, G. L., S. Atkinson, J. N. Waite, G. M. Blundell, J. R. Carpenter, and K. Wynne. 2013. A new method to evaluate the nutritional composition of marine mammal diets from scats applied to harbor seals in the Gulf of Alaska. Journal of experimental marine biology and ecology **449**:118–128.

Gerace, S. D., J. Yu, J. K. Moore, and A. C. Martiny. 2025. Observed declines in upper ocean phosphate-to-nitrate availability. Proceedings of the National Academy of Sciences **122**:e2411835122.

Gleason, C., and A. Munro. 2026. Run forecasts and harvest projections for 2026 Alaska salmon fisheries and review of the 2025 season. Report, Alaska Department of Fish and Game, Special Publication No. 26-08, Anchorage, AK.

Glover, D. M., W. J. Jenkins, and S. C. Doney. 2011. Modeling methods for marine science. Cambridge University Press.

Graham, C. J., T. M. Sutton, M. D. Adkison, M. V. McPhee, and P. J. Richards. 2019. Evaluation of growth, survival, and recruitment of Chinook salmon in southeast Alaska rivers. Transactions of the American Fisheries Society **148**:243–259.

Graham, N., R. S. Ferro, W. A. Karp, and P. MacMullen. 2007. Fishing practice, gear design, and the ecosystem approach—three case studies demonstrating the effect of management strategy on gear selectivity and discards. ICES Journal of Marine Science **64**:744–750.

Grüss, A., J. T. Thorson, C. C. Stawitz, J. C. Reum, S. K. Rohan, and C. L. Barnes. 2021. Synthesis of interannual variability in spatial demographic processes supports the strong influence of cold-pool extent on eastern Bering Sea walleye pollock (*Gadus chalcogrammus*). Progress in Oceanography **194**:102569.

Guo, S., Y. Feng, L. Wang, M. Dai, Z. Liu, Y. Bai, and J. Sun. 2014. Seasonal variation in the phytoplankton community of a continental-shelf sea: the East China Sea. Marine Ecology Progress Series **516**:103–126.

Haberle, I., L. Bavčević, and T. Klanjscek. 2023. Fish condition as an indicator of stock status: Insights from condition index in a food-limiting environment. Fish and Fisheries .

Hare, C. E., K. Leblanc, G. R. DiTullio, R. M. Kudela, Y. Zhang, P. A. Lee, S. Riseman, and D. A. Hutchins. 2007. Consequences of increased temperature and CO2 for phytoplankton community structure in the Bering Sea. Marine Ecology Progress Series **352**:9–16.

Hare, S. R., N. J. Mantua, and R. C. Francis. 1999. Inverse production regimes: Alaska and west coast Pacific salmon. Fisheries **24**:6–14.

Harley, J. R., K. Lanphier, E. G. Kennedy, T. A. Leighfield, A. Bidlack, M. O. Gribble, and C. Whitehead. 2020. The Southeast Alaska Tribal Ocean Research (SEATOR) Partnership: Addressing Data Gaps in Harmful Algal Bloom Monitoring and Shellfish Safety in Southeast Alaska. Toxins **12**:407.

Harvey, J. T., T. R. Loughlin, M. A. Perez, and D. S. Oxman. 2000. Relationship between fish size and otolith length for 63 species of fishes from the eastern North Pacific Ocean. US. Department of Commerce. NOAA Technical Report NMFS **150**.

Heintz, R. A., E. C. Siddon, E. V. Farley Jr, and J. M. Napp. 2013. Correlation between recruitment and fall condition of age-0 pollock (*Theragra chalcogramma*) from the eastern Bering Sea under varying climate conditions. Deep Sea Research Part II: Topical Studies in Oceanography **94**:150–156.

Hennon, T., and S. Danielson. 2026. Predicted Ocean Temperatures in Northern Gulf of Alaska. *In*: Ferriss, B.E. 2026. Ecosystem Status Report 2026: Gulf of Alaska. Stock Assessment and Fishery Evaluation Report, North Pacific Fishery Management Council, 1007 West Third, Suite 400, Anchorage, Alaska 99501.

Hersbach, H., B. Bell, P. Berrisford, S. Hirahara, A. Horányi, J. Muñoz-Sabater, J. Nicolas, C. Peubey, R. Radu, and D. Schepers. 2020. The ERA5 global reanalysis. Quarterly journal of the royal meteorological society **146**:1999–2049.

Hilborn, R., T. P. Quinn, D. E. Schindler, and D. E. Rogers. 2003. Biocomplexity and fisheries sustainability. Proceedings of the National Academy of Sciences of the United States of America **100**:6564–6568.

Holliday, D. V., and R. Pieper. 1995. Bioacoustical oceanography at high frequencies. ICES Journal of marine Science **52**:279–296.

Holsman, K., A. Haynie, A. Hollowed, J. Reum, K. Aydin, A. Hermann, W. Cheng, A. Faig, J. Ianelli, and K. Kearney. 2020. Ecosystem-based fisheries management forestalls climate-driven collapse. Nature communications **11**:4579.

Holsman, K. K., and K. Aydin. 2015. Comparative methods for evaluating climate change impacts on the foraging ecology of Alaskan groundfish. Marine Ecology Progress Series **521**:217–235.

Holsman, K. K., K. Aydin, J. Sullivan, T. Hurst, and G. H. Kruse. 2019. Climate effects and bottom-up controls on growth and size-at-age of Pacific halibut (*Hippoglossus stenolepis*) in Alaska (USA). Fisheries Oceanography **28**:345–358.

Holsman, K. K., J. Ianelli, K. Aydin, A. E. Punt, and E. A. Moffitt. 2016. A comparison of fisheries biological reference points estimated from temperature-specific multi-species and single-species climate-enhanced stock assessment models. Deep Sea Research Part II: Topical Studies in Oceanography **134**:360–378.

Holsman, K. K., J. Ianelli, K. Shotwell, S. Barbeaux, K. Aydin, G. Adams, K. Kearney, A. Sulc, and S. Wassermann. 2024. Climate-enhanced multispecies stock assessment for walleye pollock, Pacific cod, and arrowtooth flounder in the eastern Bering Sea. Report, North Pacific Fisheries Management Council.

Howard, K. G., and V. von Biela. 2023. Adult spawners: A critical period for subarctic Chinook salmon in a changing climate. Global Change Biology **29**:1759–1773.

Hsieh, C.-H., C. S. Reiss, J. R. Hunter, J. R. Beddington, R. M. May, and G. Sugihara. 2006. Fishing elevates variability in the abundance of exploited species. Nature **443**:859–862.

Hunt, G. L., P. H. Ressler, G. A. Gibson, A. De Robertis, K. Aydin, M. F. Sigler, I. Ortiz, E. J. Lessard, B. C. Williams, and A. Pinchuk. 2016. Euphausiids in the eastern Bering Sea: A synthesis of recent studies of euphausiid production, consumption and population control. Deep Sea Research Part II: Topical Studies in Oceanography **134**:204–222.

Hunt, G. L., P. Stabeno, G. Walters, E. Sinclair, R. D. Brodeur, J. M. Napp, and N. A. Bond. 2002. Climate change and control of the southeastern Bering Sea pelagic ecosystem. Deep-Sea Research Part II-Topical Studies in Oceanography **49**:5821–5853.

Hunt, J., George L., K. O. Coyle, L. B. Eisner, E. V. Farley, R. A. Heintz, F. Mueter, J. M. Napp, J. E. Overland, P. H. Ressler, S. Salo, and P. J. Stabeno. 2011. Climate impacts on eastern Bering Sea foodwebs: a synthesis of new data and an assessment of the Oscillating Control Hypothesis. ICES Journal of Marine Science **68**:1230–1243.

Hunt Jr, G. L., C. Baduini, and J. Jahncke. 2002. Diets of short-tailed shearwaters in the southeastern Bering Sea. Deep Sea Research Part II: Topical Studies in Oceanography **49**:6147–6156.

Hunt Jr, G. L., D. G. Kimmel, L. B. Eisner, K. Aydin, N. Bond, A. G. Andrews III, M. F. Sigler, E. C. Siddon, J. Ianelli, and P. Ressler. 2025. Testing hypotheses to explain a surprisingly large year-class of walleye pollock in an ice-free subarctic southeastern Bering Sea; a review of available data. Progress in Oceanography page 103531 .

Hurst, T. P., J. H. Moss, and J. A. Miller. 2012. Distributional patterns of 0-group Pacific cod (Gadus macrocephalus) in the eastern Bering Sea under variable recruitment and thermal conditions. ICES Journal of Marine Science **69**:163–174.

Hänfling, B., L. Lawson Handley, D. S. Read, C. Hahn, J. Li, P. Nichols, R. C. Blackman, A. Oliver, and I. J. Winfield. 2016. Environmental DNA metabarcoding of lake fish communities reflects long-term data from established survey methods. Molecular ecology **25**:3101–3119.

Ianelli, J., K. K. Holsman, A. E. Punt, and K. Aydin. 2016. Multi-model inference for incorporating trophic and climate uncertainty into stock assessments. Deep Sea Research Part II: Topical Studies in Oceanography **134**:379–389.

Ianelli, J., T. Honkalehto, S. Wassermann, A. McCarthy, S. Steinessen, C. McGillard, and E. Siddon. 2024. Stock assessment for eastern Bering Sea walleye pollock. In Stock Assessment and Fishery Evaluation Report for the Groundfish Resources of the Bering Sea/Aleutian Islands. Report, North Pacific Fishery Management Council, Anchorage, AK.

Jallen, D. M., C. M. Gleason, B. M. Borba, F. W. West, S. K. Decker, and S. R. Ransbury. 2023. Yukon River salmon stock status and salmon fisheries, 2022: a report to the Alaska Board of Fisheries, January 2023. Fisheries .

Jones, T., L. M. Divine, H. Renner, S. Knowles, K. A. Lefebvre, H. K. Burgess, C. Wright, and J. K. Parrish. 2019. Unusual mortality of Tufted puffins (*Fratercula cirrhata*) in the eastern Bering Sea. PloS one **14**:e0216532.

JTC. 2022. Joint Technical Committee of the Yukon River U.S./Canada Panel: Yukon River salmon 2021 season summary and 2022 season outlook. Report, Alaska Department of Fish and Game, Division of Commercial Fisheries, Regional Information Report No. 3A22-01, Anchorage.

JTC. 2023. Joint Technical Committee of the Yukon River U.S./Canada Panel: Yukon River salmon 2022 season summary and 2023 season outlook. Report, Alaska Department of Fish and Game, Division of Commercial Fisheries, Regional Information Report No. 3A23-01, Anchorage.

JTC. 2026. Joint Technical Committee of the Yukon River Panel: Yukon River salmon 2025 season summary and 2026 seasonal outlook. Yukon JTC (26)-01. Report.

Jurado-Molina, J., P. A. Livingston, and J. N. Ianelli. 2005. Incorporating predation interactions in a statistical catch-at-age model for a predator-prey system in the eastern Bering Sea. Canadian Journal of Fisheries and Aquatic Sciences **62**:1865–1873.

Jónasdóttir, S. H. 2019. Fatty acid profiles and production in marine phytoplankton. Marine drugs **17**:151.

Kaga, T., S. Sato, T. Azumaya, N. D. Davis, and M.-a. Fukuwaka. 2013. Lipid content of chum salmon Oncorhynchus keta affected by pink salmon O. gorbuscha abundance in the central Bering Sea. Marine Ecology Progress Series **478**:211–221.

Kajimura, H. 1984. Opportunistic feeding of the northern fur seal, Callorhinus ursinus, in the eastern North Pacific Ocean and eastern Bering Sea.

Karp, W. A., L. L. Desfosse, and S. G. Brooke. 2011. US National bycatch report. Report, U.S. Dep. Commer., NOAA Tech. Memo., NMFS-F/SPO-117E, 508 p.

Kearney, K. 2024. Cold Pool Extent - ROMS. Cold Pool Extent sub-section. In: Physical Environment Synthesis. In Siddon, E. 2024. Ecosystem Status Report 2024: Eastern Bering Sea. Report, North Pacific Fishery Management Council, 1007 W 3rd Ave, Suite 400, Anchorage, AK 99501.

Kearney, K., A. Hermann, W. Cheng, I. Ortiz, and K. Aydin. 2020. A coupled pelagic–benthic–sympagic biogeochemical model for the Bering Sea: documentation and validation of the BESTNPZ model (v2019. 08.23) within a high-resolution regional ocean model. Geoscientific Model Development **13 (2)**.

Kearney, K. A., P. J. Stabeno, A. J. Hermann, and C. W. Mordy. 2025. An updated regional model skill assessment for seasonal and interannual variability of bottom temperature across the eastern Bering Sea shelf. Frontiers in Marine Science **12**:1483945.

Kelleher, K. 2005. Discards in the world's marine fisheries: an update. Report 9251052891, Food Agriculture Org., Vol. 470.

Kerry, C., M. Roughan, and J. M. Azevedo Correia de Souza. 2024. Assessing the impact of subsurface temperature observations from fishing vessels on temperature and heat content estimates in shelf seas: a New Zealand case study using Observing System Simulation Experiments. Frontiers in Marine Science **11**:1358193.

Kimmel, D. G., D. C. Crouser, C. E. Harpold, J. F. Lamb, and A. H. Spear. 2025. Rapid Zooplankton Assessment: Evaluating a Tool for Ecosystem-Based Fisheries Management in the Large Marine Ecosystems of Alaska. Fisheries Oceanography **34**:e12707.

Kimmel, D. G., L. B. Eisner, and A. I. Pinchuk. 2023. The northern Bering Sea zooplankton community response to variability in sea ice: evidence from a series of warm and cold periods. Marine Ecology Progress Series **705**:21–42.

Kimmel, D. G., L. B. Eisner, M. T. Wilson, and J. T. Duffy-Anderson. 2018. Copepod dynamics across warm and cold periods in the eastern Bering Sea: Implications for walleye pollock (*Gadus chalcogrammus*) and the Oscillating Control Hypothesis. Fisheries Oceanography **27**:143–158.

Kiorboe, T., and M. Sabatini. 1995. Scaling of fecundity, growth and development in marine planktonic copepods. Marine ecology progress series. Oldendorf **120**:285–298.

Kocan, R., P. Hershberger, and J. Winton. 2004. Ichthyophoniasis: an emerging disease of Chinook salmon in the Yukon River. Journal of Aquatic Animal Health **16**:58–72.

Koenker, B. L., B. J. Laurel, L. A. Copeman, and L. Ciannelli. 2018. Effects of temperature and food availability on the survival and growth of larval Arctic cod (Boreogadus saida) and walleye pollock (Gadus chalcogrammus). ICES Journal of Marine Science **75**:2386–2402.

Koslow, J., S. Brault, J. Dugas, R. Fournier, and P. Hughes. 1985. Condition of larval cod (Gadus morhua) off southwest Nova Scotia in 1983 in relation to plankton abundance and temperature. Marine Biology **86**:113–121.

Kotwicki, S., and R. R. Lauth. 2013. Detecting temporal trends and environmentally-driven changes in the spatial distribution of bottom fishes and crabs on the eastern Bering Sea shelf. Deep Sea Research Part II: Topical Studies in Oceanography **94**:231–243.

KRITFC. 2022. Kuskokwim River Salmon Situation Report. Report, Kuskokwim River Inter-Tribal Fish Commission. https://static1.squarespace.com/static/5afdc3d5e74940913f78773d/t/6359792089ec3e15693c80dd/1666808118921/Salmon+Sit+Report+2022_10-03-22_FINAL.pdf

KRITFC. 2024. 2023 Kuskokwim River Salmon Situation Report. Report, Kuskokwim River Inter-Tribal Fish Commission. Bethel, Alaska. https://static1.squarespace.com/static/5afdc3d5e74940913f78773d/t/66e4bb2dfcc5d24880434ff7/1726266166559/2023+Kusko+Situation+Report_4.19.24+final.pdf

Kuhn, C. E., J. D. Baker, R. G. Towell, and R. R. Ream. 2014. Evidence of localized resource depletion following a natural colonization event by a large marine predator. Journal of Animal Ecology **83**:1169–1177.

Ladd, C., and P. J. Stabeno. 2012. Stratification on the Eastern Bering Sea shelf revisited. Deep Sea Research Part II: Topical Studies in Oceanography **65**:72–83.

Lang, G. M., P. A. Livingston, and K. A. Dodd. 2005. Groundfish food habits and predation on commercially important prey species in the eastern Bering Sea from 1997 through 2001 .

Lange, P. K., E. Fachon, J. M. Nielsen, M. Brosnahan, J. Zhang, C. W. Mordy, J. C. Gann, M. W. Lomas, E. Pate, and G. Sheffield. 2025. Application of dinoflagellate-specific satellite models to aid Alexandrium catenella bloom monitoring in the Bering and Chukchi seas. Journal of Environmental Management **380**:125042.

Large, W., and S. Yeager. 2009. The global climatology of an interannually varying air–sea flux data set. Climate dynamics **33**:341–364.

Laurel, B. J., M. Spencer, P. Iseri, and L. A. Copeman. 2016. Temperature-dependent growth and behavior of juvenile Arctic cod (Boreogadus saida) and co-occurring North Pacific gadids. Polar Biology **39**:1127–1135.

Lefebvre, K. A., C. M. Campbell, L. M. Divine, P. Melovidov, H. Hellen, K. B. Huntington, E. K. Bowers, N. Rouse, E. Fachon, and T. J. Farrugia. 2025*a*. Saxitoxin Linked to Deaths of Northern Fur Seals in the Southeast Bering Sea. Marine Mammal Science page e70028 .

Lefebvre, K. A., P. Charapata, R. Stimmelmayr, P. Lin, R. S. Pickart, K. A. Hubbard, B. D. Bill, G. Sheffield, E. K. Bowers, and D. M. Anderson. 2025*b*. Bowhead whale faeces link increasing algal toxins in the Arctic to ocean warming. Nature **644**:693–698.

Lefebvre, K. A., L. Quakenbush, E. Frame, K. B. Huntington, G. Sheffield, R. Stimmelmayr, A. Bryan, P. Kendrick, H. Ziel, and T. Goldstein. 2016. Prevalence of algal toxins in Alaskan marine mammals foraging in a changing arctic and subarctic environment. Harmful Algae **55**:13–24.

Lellouche, J., E. Greiner, R. Bourdallé Badie, G. Garric, A. Melet, M. Drévillon, C. Bricaud, M. Hamon, O. Le Galloudec, and C. Regnier. 2021. Global Ocean Physics Reanalysis, Copernicus [data set].

Levine, M., and A. De Robertis. 2025. Making do with less: Extending an acoustic-based time series of euphausiid abundance using an uncrewed surface vehicle with fewer frequencies. Fisheries Research **282**:107270.

Levine, M., A. De Robertis, P. Ressler, and B. Lucca. 2026. A revised time series of euphausiid density and distribution from acoustic-trawl surveys of the Eastern Bering Sea shelf. NOAA Technical Memorandum NMFS-AFSC **525**:86.

Levine, M., and P. H. Ressler. 2024. Eastern Bering Sea euphausiids ('krill'). *In*: Siddon, E. Ecosystem Status Report 2024: Eastern Bering Sea. Stock Assessment and Fishery Evaluation Report, North Pacific Fishery Management Council, 1007 West Third, Suite 400, Anchorage, Alaska 99501.

Levine, M., K. Williams, and P. H. Ressler. 2018. Measuring the in situ tilt orientation of fish and zooplankton using stereo photogrammetric methods. Limnology and Oceanography: Methods **16**:390–399.

Levine, R. M., A. De Robertis, D. Grünbaum, S. Wildes, E. V. Farley, P. J. Stabeno, and C. D. Wilson. 2023. Climate-driven shifts in pelagic fish distributions in a rapidly changing Pacific Arctic. Deep Sea Research Part II: Topical Studies in Oceanography **208**:105244.

Lindgren, F., H. Rue, and J. Lindström. 2011. An explicit link between Gaussian fields and Gaussian Markov random fields: the stochastic partial differential equation approach. Journal of the Royal Statistical Society Series B: Statistical Methodology **73**:423–498.

Litzow, M. A., M. E. Hunsicker, N. A. Bond, B. J. Burke, C. J. Cunningham, J. L. Gosselin, E. L. Norton, E. J. Ward, and S. G. Zador. 2020*a*. The changing physical and ecological meanings of North Pacific Ocean climate indices. Proceedings of the National Academy of Sciences **117**:7665–7671.

Litzow, M. A., W. C. Long, K. J. Palof, and D. J. Pilcher. 2025. Ocean acidification may contribute to recruitment failure of Bering Sea red king crab. Canadian Journal of Fisheries and Aquatic Sciences **82**:1–7.

Litzow, M. A., M. J. Malick, N. A. Bond, C. J. Cunningham, J. L. Gosselin, and E. J. Ward. 2020*b*. Quantifying a Novel Climate Through Changes in PDO-Climate and PDO-Salmon Relationships. Geophysical Research Letters **47**:e2020GL087972.

Liu, H., M. Chen, F. Zhu, and P. J. Harrison. 2016. Effect of diatom silica content on copepod grazing, growth and reproduction. Frontiers in Marine Science **3**:89.

Livingston, P. A., K. Aydin, T. W. Buckley, G. M. Lang, M.-S. Yang, and B. S. Miller. 2017. Quantifying food web interactions in the North Pacific–a data-based approach. Environmental Biology of Fishes **100**:443–470.

Llewellyn, L., M. Dodd, A. Robertson, G. Ericson, C. De Koning, and A. Negri. 2002. Post-mortem analysis of samples from a human victim of a fatal poisoning caused by the xanthid crab, Zosimus aeneus. Toxicon **40**:1463–1469.

Long, W. C. 2026. Ocean acidification reduces juvenile snow crab, Chionoecetes opilio, survival but does not affect growth or morphometrics. Journal of Experimental Marine Biology and Ecology **594**:152153.

Long, W. C., K. M. Swiney, and R. J. Foy. 2023. Direct, carryover, and maternal effects of ocean acidification on snow crab embryos and larvae. Plos one **18**:e0276360.

Long, W. C., K. M. Swiney, C. Harris, H. N. Page, and R. J. Foy. 2013. Effects of ocean acidification on juvenile red king crab (*Paralithodes camtschaticus*) and Tanner crab (*Chionoecetes bairdi*) growth, condition, calcification, and survival. PloS one **8**:e60959.

Lucca, B. M., P. H. Ressler, H. R. Harvey, and J. D. Warren. 2021. Individual variability in sub-Arctic krill material properties, lipid composition, and other scattering model inputs affect acoustic estimates of their population. ICES Journal of Marine Science **78**:1470–1484.

Malecha, P., and J. Heifetz. 2017. Long-term effects of bottom trawling on large sponges in the Gulf of Alaska. Continental shelf research **150**:18–26.

Mantua, N. J., S. R. Hare, Y. Zhang, J. M. Wallace, and R. C. Francis. 1997. A Pacific Interdecadal Climate Oscillation with Impacts on Salmon Production. Bulletin of the American Meteorological Society **78**:1069–1079.

Maritorena, S., O. H. F. d'Andon, A. Mangin, and D. A. Siegel. 2010. Merged satellite ocean color data products using a bio-optical model: Characteristics, benefits and issues. Remote Sensing of Environment **114**:1791–1804.

Markowitz, H., E. Dawson, C. Anderson, S. Rohan, E. Charriere, B. Prohaska, and D. Stevenson. 2023. Results of the 2022 Eastern and Northern Bering Sea Continental Shelf Bottom Trawl Survey of Groundfish and Invertebrate Fauna .

Marsh, J. M., F. J. Mueter, and T. J. Quinn. 2020. Environmental and biological influences on the distribution and population dynamics of polar cod (Boreogadus saida) in the US Chukchi Sea. Polar Biology **43**:1055–1072.

Martinelli, M., C. Castro Muniain, E. Cecapolli, F. Domenichetti, G. Giuliani, N. Hirose, S. Kida, K. Kohama, F. Kudo, V. Lago, G. Maynard, P. Penna, P. Polidori, M. Roughan, L. Stoltz, K. Takiguchi, T. Takikawa, T. Tanaka, L. Zacchetti, A. Taylor, and C. Van Vranken. 2026. FVON Instrument Intercomparison Experiments Phase 1. Report, https://doi.org/10.5281/zenodo.19354290.

McCullough, D. A. 1999. A review and synthesis of effects of alterations to the water temperature regime on freshwater life stages of salmonids, with special reference to Chinook salmon. US Environmental Protection Agency, Region 10, Seattle, WA, USA.

Merrill, G. B., J. W. Testa, and J. M. Burns. 2021. Maternal foraging trip duration as a population-level index of foraging and reproductive success for the northern fur seal. Marine Ecology Progress Series **666**:217–229.

Metting Jr, F. 1996. Biodiversity and application of microalgae. Journal of industrial microbiology **17**:477–489.

Meyer, B., X. Irigoien, M. Graeve, R. Head, and R. Harris. 2002. Feeding rates and selectivity among nauplii, copepodites and adult females of Calanus finmarchicus and Calanus helgolandicus. Helgoland Marine Research **56**:169–176.

Michael, K., L. A. Suberg, W. Wessels, S. Kawaguchi, and B. Meyer. 2021. Facing Southern Ocean warming: Temperature effects on whole animal performance of Antarctic krill (Euphausia superba). Zoology **146**:125910.

Miller, J. A., R. A. DiMaria, and T. P. Hurst. 2016. Patterns of larval source distribution and mixing in early life stages of Pacific cod (Gadus macrocephalus) in the southeastern Bering Sea. Deep Sea Research Part II: Topical Studies in Oceanography **134**:270–282.

Miya, M., Y. Sato, T. Fukunaga, T. Sado, J. Poulsen, K. Sato, T. Minamoto, S. Yamamoto, H. Yamanaka, and H. Araki. 2015. MiFish, a set of universal PCR primers for metabarcoding environmental DNA from fishes: detection of more than 230 subtropical marine species. Royal Society open science **2**:150088.

Moal, J., V. Martin-Jezequel, R. Harris, J.-F. Samain, and S. Poulet. 1987. Interspecific and intraspecific variability of the chemical-composition of marine-phytoplankton. Oceanologica acta **10**:339–346.

Monnahan, C. C., D. W. McGowan, J. Ianelli, B. E. Ferriss, and L. Rogers. 2026. Proceedings of the 2025 workshop on walleye pollock biology and ecology .

Montero-Serra, I., C. Linares, D. F. Doak, J. Ledoux, and J. Garrabou. 2018. Strong linkages between depth, longevity and demographic stability across marine sessile species. Proceedings of the Royal Society B: Biological Sciences **285**:20172688.

Moss, J. H., D. A. Beauchamp, A. D. Cross, K. W. Myers, E. V. Farley Jr, J. M. Murphy, and J. H. Helle. 2005. Evidence for size-selective mortality after the first summer of ocean growth by pink salmon. Transactions of the American Fisheries Society **134**:1313–1322.

Moyano, M., B. Illing, P. Peschutter, K. B. Huebert, and M. A. Peck. 2016. Thermal impacts on the growth, development and ontogeny of critical swimming speed in Atlantic herring larvae. Comparative Biochemistry and Physiology Part A: Molecular Integrative Physiology **197**:23–34.

Mueter, F. J., and M. A. Litzow. 2008. Sea ice retreat alters the biogeography of the Bering Sea continental shelf. Ecological Applications **18**:309–320.

Murdoch, A., B. Connors, N. Lapointe, J. Mills Flemming, S. Cooke, and C. Mantyka-Pringle. 2023. Multiple environmental drivers across life stages influence Yukon River Chinook salmon productivity. Canadian Journal of Fisheries and Aquatic Sciences **81**:97–114.

Murphy, J., D. Cooper, J. Dimond, S. Garcia, E. Lee, S. Decker, E. Labunski, C. Wright, J. Ferguson, and D. Kimmel. 2025. Northern Bering Sea Ecosystem and Surface Trawl Survey Cruise Report, 2022. Report, AFSC Processed Rep. 2025-05, 124 p. Alaska Fish. Sci. Cent., NOAA, Natl. Mar. Fish. Serv., 7600 Sand Point Way NE, Seattle WA 98115.

Murphy, J., S. Garcia, D. Cooper, A. Dimond, E. Lee, L. DeFilippo, and K. Howard. 2024. Northern Bering Sea juvenile salmon abundance indices. *In*: Siddon, E. 2023. Ecosystem Status Report 2023: Eastern Bering Sea. Stock Assessment and Fishery Evaluation Report, North Pacific Fishery Management Council, 1007 West 3rd Ave., Suite 400, Anchorage, Alaska 99501.

Murphy, J. M., K. G. Howard, J. C. Gann, K. C. Cieciel, W. D. Templin, and C. M. Guthrie. 2017. Juvenile Chinook Salmon abundance in the northern Bering Sea: Implications for future returns and fisheries in the Yukon River. Deep-Sea Research Part II-Topical Studies in Oceanography **135**:156–167.

Musbach, J., B. Brost, L. Divine, B. Easley-Appleyard, K. Gibson, H. Hellen, L. Kleine, C. Kuhn, K. Luxa, and J. Malek. 2024. Conservation plan for the Eastern Pacific stock of northern fur seal (*laaqudax*). U.S. Department of Commerce, National Oceanic and Atmospheric Adminstration, National Marine Fisheries Service, Alaska Region, Juneau, AK. NOAA Technical memorandum NMFS-F/AKR **27**.

Neuswanger, J. R., M. S. Wipfli, M. J. Evenson, N. F. Hughes, and A. E. Rosenberger. 2015. Low productivity of Chinook salmon strongly correlates with high summer stream discharge in two Alaskan rivers in the Yukon drainage. Canadian Journal of Fisheries and Aquatic Sciences **72**:1125–1137.

Nielsen, J. M., M. F. Sigler, L. B. Eisner, J. T. Watson, L. A. Rogers, S. W. Bell, N. Pelland, C. W. Mordy, W. Cheng, and K. Kivva. 2024. Spring phytoplankton bloom phenology during recent climate warming on the Bering Sea shelf. Progress in Oceanography **220**:103176.

Nishizawa, B., K. Matsuno, E. A. Labunski, K. J. Kuletz, A. Yamaguchi, and Y. Watanuki. 2017. Seasonal distribution of short-tailed shearwaters and their prey in the Bering and Chukchi seas. Biogeosciences **14**:203–214.

NPFMC. 2016. Bering Sea/Aleutian Islands Groundfish Fishery Management Plan Amendment Action Summaries. Report, North Pacific Fishery Management Council, 605 W 4th Ave Suite 306, Anchorage, Alaska 99501.

NPFMC. 2017. Fishery Management Plan for Groundfish of the Bering Sea and Aleutian Islands Management Area. Report, North Pacific Fishery Management Council, 605 W 4th Ave Suite 306, Anchorage, Alaska 99501.

Ohlberger, J., D. E. Schindler, R. J. Brown, J. M. Harding, M. D. Adkison, A. R. Munro, L. Horstmann, and J. Spaeder. 2020. The reproductive value of large females: consequences of shifts in demographic structure for population reproductive potential in Chinook salmon. Canadian Journal of Fisheries and Aquatic Sciences **77**:1292–1301.

Ohlberger, J., D. E. Schindler, and B. A. Staton. 2025. Accounting for salmon body size declines in fishery management can reduce conservation risks. Fish and Fisheries **26**:113–130.

Oke, K., C. Cunningham, P. Westley, M. Baskett, S. Carlson, J. Clark, A. Hendry, V. Karatayev, N. Kendall, and J. Kibele. 2020. Recent declines in salmon body size impact ecosystems and fisheries. Nature communications **11**:1–13.

Olson, R. J., A. Shalapyonok, D. J. Kalb, S. W. Graves, and H. M. Sosik. 2017. Imaging FlowCytobot modified for high throughput by in-line acoustic focusing of sample particles. Limnology and Oceanography: Methods **15**:867–874.

Ortiz, I., F. Weise, and A. Greig. 2012. Marine regions boundary data for the Bering Sea shelf and slope. UCAR/NCAR—Earth Observing Laboratory/Computing, Data, and Software Facility. Dataset. doi **10**:D6DF6P6C.

Ostle, C., K. C. Lawlor, S. D. Batten, M. Brunetta, M. Cunliffe, C. H. Davies, G. M. Harper, D. G. Johns, H. Robinson, and F. Loro. 2026. Mega-blooms of the harmful alga Alexandrium catenella in the Bering Sea recorded by the Continuous Plankton Recorder Survey. Harmful Algae page 103194 .

Oyafuso, Z. 2025. gapindex: Standard AFSC GAP Product Calculations. R package version 3.0.2, https://github.com/afsc-gap-products/gapindex .

Paul, A., and J. Paul. 1999. Interannual and regional variations in body length, weight and energy content of age-0 Pacific herring from Prince William Sound, Alaska. Journal of fish biology **54**:996–1001.

Pauly, D., V. Christensen, J. Dalsgaard, R. Froese, and F. Torres. 1998. Fishing down marine food webs. Science **279**:860–863.

Pebesma, E. J. 2004. Multivariable geostatistics in S: the gstat package. Computers geosciences **30**:683–691.

Perrette, M., A. Yool, G. Quartly, and E. E. Popova. 2011. Near-ubiquity of ice-edge blooms in the Arctic. Biogeosciences **8**:515–524.

Petitgas, P. 1993. Geostatistics for fish stock assessments: a review and an acoustic application. ICES Journal of Marine Science: Journal du Conseil **50**:285–298.

Pickart, R., G. Moore, T. Weingartner, S. Danielson, and K. Frey. 2013. Physical Drivers of the Chukchi, Beaufort, and Northern Bering Seas. Developing a Conceptual Model of the Arctic Marine Ecosystem **2**.

Pickart, R. S., M. A. Spall, G. W. Moore, T. J. Weingartner, R. A. Woodgate, K. Aagaard, and K. Shimada. 2011. Upwelling in the Alaskan Beaufort Sea: Atmospheric forcing and local versus non-local response. Progress in Oceanography **88**:78–100.

Pilcher, D. J., J. N. Cross, N. Monacci, L. Mu, K. A. Kearney, A. J. Hermann, and W. Cheng. 2025. Amplified bottom water acidification rates on the Bering Sea shelf from 1970–2022. Biogeosciences **22**:3103–3125.

Pilcher, D. J., D. M. Naiman, J. N. Cross, A. J. Hermann, S. A. Siedlecki, G. A. Gibson, and J. T. Mathis. 2019. Modeled effect of coastal biogeochemical processes, climate variability, and ocean acidification on aragonite saturation state in the Bering Sea. Frontiers in Marine Science **5**:508.

Pinger, C., L. Copeman, M. Stowell, B. Cormack, C. Fugate, and M. Rogers. 2022. Rapid measurement of total lipids in zooplankton using the sulfo-phospho-vanillin reaction. Analytical Methods **14**:2665–2672.

Pitcher, K. W., and D. G. Calkins. 1979. Biology of the harbor seal, *Phoca vitulina richardsi*, in the Gulf of Alaska. Outer Continental Shelf Environmental Assessment Program, U.S. Department of Interior, Bureau of Land Management.

Platt, T., C. Fuentes-Yaco, and K. T. Frank. 2003. Marine ecology: spring algal bloom and larval fish survival. Nature **423**:398–399.

Polovina, J. J., and E. A. Howell. 2005. Ecosystem indicators derived from satellite remotely sensed oceanographic data for the North Pacific. ICES Journal of Marine Science **62**:319–327.

Porter, S. 2025. Condition of larval walleye pollock (Gadus chalcogrammus) in the southeastern Bering Sea in relation to their environment and size. Fishery Bulletin **123**:207–220.

Punt, A. E., R. J. Foy, M. G. Dalton, W. C. Long, and K. M. Swiney. 2016. Effects of long-term exposure to ocean acidification conditions on future southern Tanner crab (*Chionoecetes bairdi*) fisheries management. ICES Journal of Marine Science **73**:849–864.

Purcell, J. E., and M. N. Arai. 2001. Interactions of pelagic cnidarians and ctenophores with fish: a review. Hydrobiologia **451**:27–44.

Queirolo, L. E., L. Fritz, P. Livingston, M. Loefflad, D. Colpo, and Y. DeReynier. 1995. Bycatch, utilization, and discards in the commercial groundfish fisheries of the Gulf of Alaska, eastern Bering Sea, and Aleutian Islands. NOAA Tech. Memo. NMFS-AFSC **58**:148.

Rand, P. S., and G. T. Ruggerone. 2024. Biennial patterns in Alaskan sockeye salmon ocean growth are associated with pink salmon abundance in the Gulf of Alaska and the Bering Sea. ICES Journal of Marine Science **81**:701–709.

Ressler, P., A. De Robertis, and S. Kotwicki. 2014. The spatial distribution of euphausiids and walleye pollock in the eastern Bering Sea does not imply top-down control by predation. Marine Ecology Progress Series **503**:111–122.

Ressler, P. H., A. De Robertis, J. D. Warren, J. N. Smith, and S. Kotwicki. 2012. Developing an acoustic survey of euphausiids to understand trophic interactions in the Bering Sea ecosystem. Deep Sea Research Part II: Topical Studies in Oceanography **65–70**:184–195.

Reum, J. C., J. T. Thorson, P. H. Ressler, and M. Levine. 2026. Eastern Bering sea krill abundance trends and climate response inferred from predator stomach contents and joint spatiotemporal models. Progress in Oceanography page 103830 .

Reum, J. C., J. T. Thorson, C. Yeung, and K. Aydin. 2025. Assessing benthos through predator stomach contents: spatiotemporal modeling of abundance and habitat use. Ecography page e07723 .

Richardson, A., A. Walne, A. John, T. Jonas, J. Lindley, D. Sims, D. Stevens, and M. Witt. 2006. Using continuous plankton recorder data. Progress in Oceanography **68**:27–74.

Robinson, K. L., J. J. Ruzicka, M. B. Decker, R. Brodeur, F. Hernandez, J. Quiñones, E. Acha, S. Uye, H. Mianzan, and W. Graham. 2014. Jellyfish, forage fish, and the world's major fisheries. Oceanography **27**:104–115.

Robson, B. W., M. E. Goebel, J. D. Baker, R. R. Ream, T. R. Loughlin, R. C. Francis, G. A. Antonelis, and D. P. Costa. 2004. Separation of foraging habitat among breeding sites of a colonial marine predator, the northern fur seal (Callorhinus ursinus). Canadian Journal of Zoology **82**:20–29.

Rodgveller, C. J. 2019. The utility of length, age, liver condition, and body condition for predicting maturity and fecundity of female sablefish. Fisheries Research **216**:18–28.

Rodionov, S., and J. E. Overland. 2005. Application of a sequential regime shift detection method to the Bering Sea ecosystem. Ices Journal of Marine Science **62**:328–332.

Rodionov, S. N., N. A. Bond, and J. E. Overland. 2007. The Aleutian Low, storm tracks, and winter climate variability in the Bering Sea. Deep Sea Research Part II: Topical Studies in Oceanography **54**:2560–2577.

Rogers, L. A., K. E. Axler, and J. S. Bigman. 2026. Widespread Phenological Shifts With Temperature in Alaska's Marine Fishes. Global Change Biology **32**:e70708.

Rogers, L. A., and D. E. Schindler. 2011. Scale and the detection of climatic influences on the productivity of salmon populations. Global Change Biology **17**:2546–2558.

Rogers, L. A., M. T. Wilson, J. T. Duffy-Anderson, D. G. Kimmel, and J. F. Lamb. 2021. Pollock and "the Blob": Impacts of a marine heatwave on walleye pollock early life stages. Fisheries Oceanography **30**:142–158.

Rohan, S. 2025. esrindex: Abundance index products for Alaska ESRs. R package version 1.2.4, https://github.com/afsc-gap-products/esrindex .

Rohan, S., L. Barnett, and N. Charriere. 2022. Evaluating approaches to estimating mean temperatures and cold pool area from Alaska Fisheries Science Center bottom trawl surveys of the eastern Bering Sea .

Roon, D. A., J. R. Bellmore, J. R. Benjamin, F.-N. Robinne, R. L. Flitcroft, J. E. Compton, J. L. Ebersole, J. B. Dunham, and K. D. Bladon. 2025. Linking fire, food webs, and fish in stream ecosystems. Ecosystems **28**:1.

Rooper, C. N., P. Goddard, and R. Wilborn. 2019. Are fish associations with corals and sponges more than an affinity to structure? Evidence across two widely divergent ecosystems. Canadian Journal of Fisheries and Aquatic Sciences **76**:2184–2198.

Rooper, C. N., I. Ortiz, A. J. Hermann, N. Laman, W. Cheng, K. Kearney, and K. Aydin. 2021. Predicted shifts of groundfish distribution in the Eastern Bering Sea under climate change, with implications for fish populations and fisheries management. ICES Journal of Marine Science **78**:220–234.

Rooper, C. N., M. F. Sigler, P. Goddard, P. Malecha, R. Towler, K. Williams, R. Wilborn, and M. Zimmermann. 2016. Validation and improvement of species distribution models for structure-forming invertebrates in the eastern Bering Sea with an independent survey. Marine Ecology Progress Series **551**:117–130.

Ruggerone, G. T., B. A. Agler, B. M. Connors, E. V. Farley Jr, J. R. Irvine, L. I. Wilson, and E. M. Yasumiishi. 2016. Pink and sockeye salmon interactions at sea and their influence on forecast error of Bristol Bay sockeye salmon. North Pacific Anadromous Fish Commission Bulletin **6**:349–361.

Ruggerone, G. T., and J. L. Nielsen. 2004. Evidence for competitive dominance of pink salmon (*Oncorhynchus gorbuscha*) over other salmonids in the North Pacific Ocean. Reviews in Fish Biology and Fisheries **14**:371–390.

Ruggerone, G. T., A. M. Springer, G. B. van Vliet, B. Connors, J. R. Irvine, L. D. Shaul, M. R. Sloat, and W. I. Atlas. 2023. From diatoms to killer whales: impacts of pink salmon on North Pacific ecosystems. Marine Ecology Progress Series **719**:1–40.

Rutishauser, M. R., D. P. Costa, M. E. Goebel, and T. M. Williams. 2004. Ecological implications of body composition and thermal capabilities in young Antarctic fur seals (Arctocephalus gazella). Physiological and Biochemical Zoology **77**:669–681.

Ruzicka, J., R. D. Brodeur, K. Cieciel, and M. B. Decker. 2020. Examining the ecological role of jellyfish in the Eastern Bering Sea. ICES Journal of Marine Science **77**:791–802.

Saha, S., S. Moorthi, H.-L. Pan, X. Wu, J. Wang, S. Nadiga, P. Tripp, R. Kistler, J. Woollen, and D. Behringer. 2010. The NCEP climate forecast system reanalysis. Bulletin of the American Meteorological Society **91**:1015.

Saha, S., S. Moorthi, X. Wu, J. Wang, S. Nadiga, P. Tripp, D. Behringer, Y.-T. Hou, H.-y. Chuang, and M. Iredell. 2014. The NCEP climate forecast system version 2. Journal of climate **27**:2185–2208.

Schindler, D. E., R. Hilborn, B. Chasco, C. P. Boatright, T. P. Quinn, L. A. Rogers, and M. S. Webster. 2010. Population diversity and the portfolio effect in an exploited species. Nature **465**:609–613.

Schindler, D. E., P. R. Leavitt, S. P. Johnson, and C. S. Brock. 2006. A 500-year context for the recent surge in sockeye salmon (*Oncorhynchus nerka*) abundance in the Alagnak River, Alaska. Canadian Journal of Fisheries and Aquatic Sciences **63**:1439–1444.

Seung, C. K., M. G. Dalton, A. E. Punt, D. Poljak, and R. Foy. 2015. Economic impacts of changes in an Alaska crab fishery from ocean acidification. Climate Change Economics **6**:1550017.

Shelton, A. O., J. T. Thorson, E. J. Ward, and B. E. Feist. 2014. Spatial semiparametric models improve estimates of species abundance and distribution. Canadian Journal of Fisheries and Aquatic Sciences **71**:1655–1666.

Shin, Y.-J., M.-J. Rochet, S. Jennings, J. G. Field, and H. Gislason. 2005. Using size-based indicators to evaluate the ecosystem effects of fishing. ICES Journal of marine Science **62**:384–396.

Shin, Y.-J., L. J. Shannon, A. Bundy, M. Coll, K. Aydin, N. Bez, J. L. Blanchard, M. d. F. Borges, I. Diallo, and E. Diaz. 2010. Using indicators for evaluating, comparing, and communicating the ecological status of exploited marine ecosystems. Part 2. Setting the scene. ICES Journal of Marine Science **67**:692–716.

Siddon, E. C., R. A. Heintz, and F. J. Mueter. 2013. Conceptual model of energy allocation in walleye pollock (*Theragra chalcogramma*) from age-0 to age-1 in the southeastern Bering Sea. Deep Sea Research Part II: Topical Studies in Oceanography **94**:140–149.

Sigler, M. F., F. J. Mueter, B. A. Bluhm, M. S. Busby, E. D. Cokelet, S. L. Danielson, A. De Robertis, L. B. Eisner, E. V. Farley, and K. Iken. 2017. Late summer zoogeography of the northern Bering and Chukchi seas. Deep Sea Research Part II: Topical Studies in Oceanography **135**:168–189.

Sigler, M. F., J. M. Napp, P. J. Stabeno, R. A. Heintz, M. W. Lomas, and G. L. Hunt Jr. 2016. Variation in annual production of copepods, euphausiids, and juvenile walleye pollock in the southeastern Bering Sea. Deep Sea Research Part II: Topical Studies in Oceanography **134**:223–234.

Sigler, M. F., P. J. Stabeno, L. B. Eisner, J. M. Napp, and F. J. Mueter. 2014. Spring and fall phytoplankton blooms in a productive subarctic ecosystem, the eastern Bering Sea, during 1995–2011. Deep Sea Research Part II: Topical Studies in Oceanography **109**:71–83.

Simonsen, K. A., P. H. Ressler, C. N. Rooper, and S. G. Zador. 2016. Spatio-temporal distribution of euphausiids: an important component to understanding ecosystem processes in the Gulf of Alaska and eastern Bering Sea. ICES Journal of Marine Science: Journal du Conseil page fsv272 .

Sinclair, E. H., L. S. Vlietstra, D. S. Johnson, T. K. Zeppelin, G. V. Byrd, A. M. Springer, R. R. Ream, and G. L. Hunt. 2008. Patterns in prey use among fur seals and seabirds in the Pribilof Islands. Deep-Sea Research Part II-Topical Studies in Oceanography **55**:1897–1918.

Smart, T., E. Siddon, and J. Duffy-Anderson. 2013. Vertical distributions of the early life stages of walleye pollock (Theragra chalcogramma) in the Southeastern Bering Sea. Deep Sea Research Part II: Topical Studies in Oceanography **94**:201–210.

Smith, J. N., P. H. Ressler, and J. D. Warren. 2013. A distorted wave Born approximation target strength model for Bering Sea euphausiids. ICES Journal of Marine Science: Journal du Conseil **70 (1)**:204–214.

Spear, A., A. G. Andrews III, J. Duffy-Anderson, T. Jarvis, D. Kimmel, and D. McKelvey. 2023. Changes in the vertical distribution of age-0 walleye pollock (Gadus chalcogrammus) during warm and cold years in the southeastern Bering Sea. Fisheries Oceanography **32**:177–195.

Spencer, P. D. 2008. Density-independent and density-dependent factors affecting temporal changes in spatial distributions of eastern Bering Sea flatfish. Fisheries Oceanography **17**:396–410.

Spencer, P. D., K. K. Holsman, S. Zador, N. A. Bond, F. J. Mueter, A. B. Hollowed, and J. N. Ianelli. 2016. Modelling spatially dependent predation mortality of eastern Bering Sea walleye pollock, and its implications for stock dynamics under future climate scenarios. ICES Journal of Marine Science **73**:1330–1342.

Spies, I., K. M. Gruenthal, D. P. Drinan, A. B. Hollowed, D. E. Stevenson, C. M. Tarpey, and L. Hauser. 2020. Genetic evidence of a northward range expansion in the eastern Bering Sea stock of Pacific cod. Evolutionary Applications **13**:362–375.

Springer, A., R. Ream, and S. Iverson. 2008. Seasonal Foraging Strategies and Consequences for Northern Fur Seals at Colonies with Opposite Population Trends—Year 2, North Pacific Research Board Final Project Report. North Pacific Research Board Final Project Report page 79 .

Springer, A. M., and G. B. van Vliet. 2014. Climate change, pink salmon, and the nexus between bottom-up and top-down forcing in the subarctic Pacific Ocean and Bering Sea. Proceedings of the National Academy of Sciences **111**:E1880–E1888.

Stabeno, P., S. Danielson, D. Kachel, N. Kachel, and C. Mordy. 2016. Currents and transport on the eastern Bering Sea shelf: An integration of over 20 years of data. Deep Sea Research Part II: Topical Studies in Oceanography **134**:13–29.

Stabeno, P., J. Duffy-Anderson, L. Eisner, E. Farley, R. Heintz, and C. Mordy. 2017. Return of warm conditions in the southeastern Bering Sea: Physics to fluorescence. PloS one **12**:e0185464.

Stabeno, P. J., and S. W. Bell. 2019. Extreme conditions in the Bering Sea (2017–2018): record-breaking low sea-ice extent. Geophysical Research Letters **46**:8952–8959.

Stabeno, P. J., J. Farley, E. V., N. B. Kachel, S. Moore, C. W. Mordy, J. M. Napp, J. E. Overland, A. I. Pinchuk, and M. F. Sigler. 2012*a*. A comparison of the physics of the northern and southern shelves of the eastern Bering Sea and some implications for the ecosystem. Deep-Sea Research Part II-Topical Studies in Oceanography **65-70**:14–30.

Stabeno, P. J., N. B. Kachel, S. E. Moore, J. M. Napp, M. Sigler, A. Yamaguchi, and A. N. Zerbini. 2012*b*. Comparison of warm and cold years on the southeastern Bering Sea shelf and some implications for the ecosystem. Deep Sea Research Part II: Topical Studies in Oceanography **65**:31–45.

Stevenson, D. E., and R. R. Lauth. 2019. Bottom trawl surveys in the northern Bering Sea indicate recent shifts in the distribution of marine species. Polar Biology **42**:407–421.

Stoecker, D. K., A. C. Weigel, D. A. Stockwell, and M. W. Lomas. 2014. Microzooplankton: Abundance, biomass and contribution to chlorophyll in the Eastern Bering Sea in summer. Deep Sea Research Part II: Topical Studies in Oceanography **109**:134–144.

Stone, R. P., H. Lehnert, and G. R. Hoff. 2019. Inventory of the eastern Bering Sea sponge fauna, geographic range extensions and description of Antho ridgwayi sp. nov. Zootaxa **4567**:zootaxa. 4567.2. 2–zootaxa. 4567.2. 2.

Stram, D. L., and J. N. Ianelli. 2015. Evaluating the efficacy of salmon bycatch measures using fishery-dependent data. ICES Journal of Marine Science **72**:1173–1180.

Strasburger, W. W., N. Hillgruber, A. I. Pinchuk, and F. J. Mueter. 2014. Feeding ecology of age-0 walleye pollock (Gadus chalcogrammus) and Pacific cod (Gadus macrocephalus) in the southeastern Bering Sea. Deep Sea Research Part II: Topical Studies in Oceanography **109**:172–180.

Suchman, C. L., E. A. Daly, J. E. Keister, W. T. Peterson, and R. D. Brodeur. 2008. Feeding patterns and predation potential of scyphomedusae in a highly productive upwelling region. Marine Ecology Progress Series **358**:161–172.

Sullaway, G. H., C. Cunningham, D. G. Kimmel, J. M. Nielsen, D. Pilcher, A. I. Pinchuk, and P. J. Stabeno. 2025. Impacts of climate change on Bering Sea copepod phenology and reproductive strategy. Marine Ecology Progress Series **755**:45–61.

Sullivan, J., and L. Balstad. 2022. rema: A generalized framework to fit the random effects (RE) model, a state-space random walk model developed at the Alaska Fisheries Science Center (AFSC) for apportionment and biomass estimation of groundfish and crab stocks. R package version 1.2.0, https://github.com/afsc-assessments/rema .

Suryan, R. M., and K. J. Kuletz. 2018. Distribution, habitat use, and conservation of albatrosses in Alaska. Iden **72**:156–164.

Suryan, R. M., J. Maselko, E. A. Fergusson, F. Sewall, J. J. Vollenweider, A. G. Andrews III, J. M. Murphy, and E. M. Yasumiishi. 2026. Capelin Size, Condition, and Abundance Through Multiple Heatwaves in Alaska. Fisheries Oceanography **35**:413–429.

Svantemann, M. M., B. A. Krafft, F. F. Thompson, G. Zhang, and L. A. Krag. 2025. Automated krill body length estimation based on stereo camera images. ICES Journal of Marine Science **82**:fsaf058.

Swiney, K. M., W. C. Long, and R. J. Foy. 2017. Decreased pH and increased temperatures affect young-of-the-year red king crab (*Paralithodes camtschaticus*). ICES Journal of Marine Science **74**:1191–1200.

Szuwalski, C. S., K. Aydin, E. J. Fedewa, B. Garber-Yonts, and M. A. Litzow. 2023. The collapse of eastern Bering Sea snow crab. Science **382**:306–310.

Team, R. C. 2022. R: a language and environment for statistical computing and graphics. Foundation for Statistical Computing .

Theilacker, G. H., K. M. Bailey, M. F. Canino, and S. M. Porter. 1996. Variations in larval walleye pollock feeding and condition: a synthesis. Fisheries Oceanography **5**:112–123.

Thomsen, P. F., J. Kielgast, L. L. Iversen, P. R. Møller, M. Rasmussen, and E. Willerslev. 2012. Detection of a Diverse Marine Fish Fauna Using Environmental DNA from Seawater Samples. PLOS ONE **7**:e41732.

Thorson, J., M. Fossheim, F. Mueter, E. Olsen, R. Lauth, R. Primicerio, B. Husson, J. Marsh, A. Dolgov, and S. Zador. 2019. Comparison of near-bottom fish densities show rapid community and population shifts in Bering and Barents Seas. Arctic Report Card .

Thorson, J. T. 2019. Measuring the impact of oceanographic indices on species distribution shifts: the spatially varying effect of cold-pool extent in the eastern Bering Sea. Limnology and Oceanography **64**:2632–2645.

Thorson, J. T., S. C. Anderson, P. Goddard, and C. N. Rooper. 2025. tinyVAST: R Package With an Expressive Interface to Specify Lagged and Simultaneous Effects in Multivariate Spatio-Temporal Models. Global Ecology and Biogeography **34**:e70035.

Thorson, J. T., A. G. Andrews III, T. E. Essington, and S. I. Large. 2024. Dynamic structural equation models synthesize ecosystem dynamics constrained by ecological mechanisms. Methods in Ecology and Evolution **15**:744–755.

Thorson, J. T., M. L. Arimitsu, T. Levi, and G. H. Roffler. 2022. Diet analysis using generalized linear models derived from foraging processes using R package mvtweedie. Ecology **103**:e3637.

Thorson, J. T., L. Ciannelli, and M. A. Litzow. 2020. Defining indices of ecosystem variability using biological samples of fish communities: A generalization of empirical orthogonal functions. Progress in Oceanography **181**:102244.

Thorson, J. T., J. N. Ianelli, E. A. Larsen, L. Ries, M. D. Scheuerell, C. Szuwalski, and E. F. Zipkin. 2016. Joint dynamic species distribution models: a tool for community ordination and spatio-temporal monitoring. Global Ecology and Biogeography **25**:1144–1158.

Tobin, E. D., C. L. Wallace, C. Crumpton, G. Johnson, and G. L. Eckert. 2019. Environmental drivers of paralytic shellfish toxin producing *Alexandrium catenella* blooms in a fjord system of northern Southeast Alaska. Harmful algae **88**:101659.

Trenberth, K., and J. W. Hurrell. 1994. Decadal atmosphere-ocean variations in the Pacific. Climate Dynamics **9**:303–319.

Van Vranken, C., J. Jakoboski, J. W. Carroll, C. Cusack, P. Gorringe, N. Hirose, J. Manning, M. Martinelli, P. Penna, and M. Pickering. 2023. Towards a global Fishing Vessel Ocean Observing Network (FVON): state of the art and future directions. Frontiers in Marine Science **10**:1176814.

Van Vranken, C., B. M. Vastenhoud, J. P. Manning, K. S. Plet-Hansen, J. Jakoboski, P. Gorringe, and M. Martinelli. 2020. Fishing gear as a data collection platform: Opportunities to fill spatial and temporal gaps in operational sub-surface observation networks. Frontiers in Marine Science **7**:485512.

Vandersea, M. W., S. R. Kibler, P. A. Tester, K. Holderied, D. E. Hondolero, K. Powell, S. Baird, A. Doroff, D. Dugan, and R. W. Litaker. 2018. Environmental factors influencing the distribution and abundance of *Alexandrium catenella* in Kachemak bay and lower cook inlet, Alaska. Harmful algae **77**:81–92.

Ver Hoef, J. M., B. T. McClintock, P. L. Boveng, J. M. London, and J. K. Jansen. 2025. An integrated data model to estimate abundance from counts with temporal dependence and imperfect detection. Ecology **106**:e70073.

Vollenweider, J. J., R. A. Heintz, L. Schaufler, and R. Bradshaw. 2011. Seasonal cycles in whole-body proximate composition and energy content of forage fish vary with water depth. Marine biology **158**:413–427.

von Biela, V. R., A. M. Regish, S. D. McCormick, J. Spaeder, K. Whitworth, J. Leon, D. Gillikin, Z. Liller, R. Ivanoff, and J. Bell. 2026. Migration water temperature and heat stress assessments in western Alaska Chinook salmon overlapping the 2019 heatwave. Canadian Journal of Fisheries and Aquatic Sciences **83**:1–14.

von Biela, V. R., C. J. Sergeant, M. P. Carey, Z. Liller, C. Russell, S. Quinn-Davidson, P. S. Rand, P. A. Westley, and C. E. Zimmerman. 2022. Premature mortality observations among Alaska's Pacific Salmon during record heat and drought in 2019. Fisheries **47**:157–168.

Waga, H., H. Eicken, T. Hirawake, and Y. Fukamachi. 2021. Variability in spring phytoplankton blooms associated with ice retreat timing in the Pacific Arctic from 2003–2019. Plos one **16**:e0261418.

Waldbusser, G. G., B. Hales, C. J. Langdon, B. A. Haley, P. Schrader, E. L. Brunner, M. W. Gray, C. A. Miller, and I. Gimenez. 2015. Saturation-state sensitivity of marine bivalve larvae to ocean acidification. Nature Climate Change **5**:273–280.

Ward, E. J., and S. C. Anderson. 2025. Approximating spatial processes with too many knots degrades the quality of probabilistic predictions. bioRxiv page 2025.11. 14.688354 .

Wespestad, V., and D. Gunderson. 1991. Climatic induced variation in Eastern Bering Sea herring recruitment. Report, Proceedings of the International Herring Symposium, Anchorage, AK. Alaska Sea Grant.

Whitworth, K. L., W. R. Bechtol, and A. Magel. 2023. 2022 Takotna River salmon run timing and abundance. Report for the Alaska Department of Fish & Game, Anchorage, AK .

Wilber, M. Q., J. A. Ferguson, D. J. Páez, and Z. W. Liller. 2026. Disease-associated mortality drives reduction in Yukon River Chinook salmon escapement: A novel method for quantifying the negative impacts of 'misfit'parasites to improve fisheries management. Journal of Applied Ecology **63**:e70456.

Williams, E. H., and T. J. Quinn. 2000. Pacific herring, *Clupea pallasii*, recruitment in the Bering Sea and north-east Pacific Ocean, I: relationships among different populations. Fisheries Oceanography **9**:285–299.

Wilson, L. I. 2026. Alaska salmon fisheries enhancement annual report 2025. Alaska Department of Fish and Game, Division of Commercial Fisheries, Regional Information Report No. 5J26-04, Juneau, AK.

Winder, M., and U. Sommer. 2012. Phytoplankton response to a changing climate. Hydrobiologia **698**:5–16.

Winemiller, K. O. 2005. Life history strategies, population regulation, and implications for fisheries management. Canadian Journal of Fisheries and Aquatic Sciences **62**:872–885.

Witteveen, B. H., A. De Robertis, L. Guo, and K. M. Wynne. 2015. Using dive behavior and active acoustics to assess prey use and partitioning by fin and humpback whales near Kodiak Island, Alaska. Marine Mammal Science **31**:255–278.

Woodgate, R. A., T. J. Weingartner, and R. Lindsay. 2012. Observed increases in Bering Strait oceanic fluxes from the Pacific to the Arctic from 2001 to 2011 and their impacts on the Arctic Ocean water column. Geophysical Research Letters **39**.

Wuenschel, M. J., W. D. McElroy, K. Oliveira, and R. S. McBride. 2019. Measuring fish condition: an evaluation of new and old metrics for three species with contrasting life histories. Canadian Journal of Fisheries and Aquatic Sciences **76**:886–903.

Xiao, W., E. A. Laws, Y. Xie, L. Wang, X. Liu, J. Chen, B. Chen, and B. Huang. 2019. Responses of marine phytoplankton communities to environmental changes: New insights from a niche classification scheme. Water Research **166**:115070.

Yasumiishi, E. M., K. Cieciel, A. G. Andrews, J. Murphy, and J. A. Dimond. 2020. Climate-related changes in the biomass and distribution of small pelagic fishes in the eastern Bering Sea during late summer, 2002–2018. Deep Sea Research Part II: Topical Studies in Oceanography **181**:104907.

Zador, S. G., and S. Fitzgerald. 2008. Seabird attraction to trawler discards. Report, Alaska Fisheries Science Center, NOAA, NMFS, 7600 Sand Point Way NE, Seattle WA 98115.

Zeppelin, T., and R. Ream. 2006. Foraging habitats based on the diet of female northern fur seals (Callorhinus ursinus) on the Pribilof Islands, Alaska. Journal of Zoology **270**:565–576.

Zuray, S., R. Kocan, and P. Hershberger. 2012. Synchronous cycling of Ichthyophoniasis with Chinook Salmon density revealed during the annual Yukon River spawning migration. Transactions of the American Fisheries Society **141**:615–623.

Appendix

History of the Ecosystem Status Reports

Since 1995, staff at the Alaska Fisheries Science Center have prepared a separate Ecosystem Status (formerly Considerations) Report within the annual Stock Assessment and Fishery Evaluation (SAFE) report. Each new Ecosystem Status Report provides updates and new information to supplement the original report. The original 1995 report presented a compendium of general information on the Gulf of Alaska, Bering Sea, and Aleutian Island ecosystems as well as a general discussion of ecosystem-based management. The 1996 edition provided additional information on biological features of the North Pacific, and highlighted the effects of bycatch and discards on the ecosystem. The 1997 edition provided a review of ecosystem-based management literature and ongoing ecosystem research, and provided supplemental information on seabirds and marine mammals. The 1998 edition provided information on the precautionary approach, essential fish habitat, effects of fishing gear on habitat, El Niño, local knowledge, and other ecosystem information. The 1999 edition again gave updates on new trends in ecosystem-based management, essential fish habitat, research on effects of fishing gear on seafloor habitat, marine protected areas, seabirds and marine mammals, oceanographic changes in 1997/98, and local knowledge.

In 1999, a proposal came forward to enhance the Ecosystem Status Report by including more information on indicators of ecosystem status and trends and more ecosystem-based management performance measures. The purpose of this enhancement was to accomplish several goals:

1. Track ecosystem-based management efforts and their efficacy
2. Track changes in the ecosystem that are not easily incorporated into single-species assessments
3. Bring results from ecosystem research efforts to the attention of stock assessment scientists and fishery managers
4. Provide a stronger link between ecosystem research and fishery management
5. Provide an assessment of the past, present, and future role of climate and humans in influencing ecosystem status and trends

Each year since 1999, the Ecosystem Status Reports have included some new contributions and will continue to evolve as new information becomes available. Evaluation of the meaning of observed changes should be in the context of how each indicator relates to a particular ecosystem component.

For example, particular oceanographic conditions, such as bottom temperature increases, might be favorable to some species but not for others. Evaluations should follow an analysis framework such as that provided in the draft Programmatic Groundfish Fishery Environmental Impact Statement that links indicators to particular effects on ecosystem components.

In 2002, stock assessment scientists began using indicators contained in this report to systematically assess ecosystem factors such as climate, predators, prey, and habitat that might affect a particular stock. Information regarding a particular fishery's catch, bycatch, and temporal/spatial distribution can be used to assess possible impacts of that fishery on the ecosystem. Indicators of concern can be highlighted within each assessment and can be used by the Groundfish Plan Teams and the Council to justify modification of allowable biological catch (ABC) recommendations or time/space allocations of catch.

We initiated a regional approach to the ESR in 2010 and presented a new ecosystem assessment for the eastern Bering Sea. In 2011, we followed the same approach and presented a new assessment for the Aleutian Islands based on a similar format to that of the eastern Bering Sea but with regional report cards for the western, central, and eastern Aleutian Islands. In 2012, we provided a preliminary ecosystem assessment on the Arctic. Our intent was to provide an overview of general Arctic ecosystem information that may form the basis for more comprehensive future Arctic ecosystem assessments. In 2015, we presented a new Gulf of Alaska report card and assessment, which was further divided into Western and Eastern Gulf of Alaska report cards beginning in 2016. This was also the year that the previous Alaska-wide ESR was split into four separate reports, one for the Gulf of Alaska, Aleutian Islands, eastern Bering Sea, and the Arctic[76].

The eastern Bering Sea and Aleutian Islands ecosystem assessments were based on additional refinements contributed by Ecosystem Synthesis Teams. For these assessments, the teams focused on a subset of broad, community-level indicators to determine the current state and likely future trends of ecosystem productivity in the EBS and ecosystem variability in the Aleutian Islands. The teams also selected indicators that reflect trends in non-fishery apex predators and maintaining a sustainable species mix in the harvest as well as changes to catch diversity and variability. Indicators for the Gulf of Alaska report card and assessment were also selected by a team of experts, via an online survey first, then refined in an in-person workshop.

Originally, contributors to the Ecosystem Status Reports were asked to provide a description of their contributed indicator, summarize the historical trends and current status of the indicator, and identify potential factors causing those trends. Beginning in 2009, contributors were also asked to describe why the indicator is important to groundfish fishery management and implications of indicator trends. In particular, contributors were asked to briefly address implications or impacts of the observed trends on the ecosystem or ecosystem components, what the trends mean and why are they important, and how the information can be used to inform groundfish management decisions. Answers to these types of questions will help provide a "heads-up" for developing management responses and research priorities.

In 2018, a risk table framework was developed for individual stock assessments as a means of documenting concerns external to the stock assessment model, but relevant to setting the Acceptable Biological Catch (ABC) value for the current year. These concerns could be categorized as those reflecting the assessment model, the population dynamics of the stock, and environmental and ecosystem concerns—including those based on information from Ecosystem Status Reports. In the past, concerns used to justify an ABC below the maximum estimated by the assessment model were documented in an ad-hoc

[76]The Arctic Report has not been regularly produced.

manner in the stock assessment report or in the minutes of the Groundfish Plan Teams or Scientific and Statistical Committee (SSC) reviews. With the risk table, formal consideration of concerns—including ecosystem—are documented and ranked, and the stock assessment author presents a recommendation for the maximum ABC as specified by the stock assessment model or a lower value. The recommended ABC (whether at maximum or lower) from the lead stock assessment author is subsequently reviewed and adjusted or accepted by the Groundfish Plan Team and the Scientific and Statistical Committee. Five risk tables were completed in 2018 as a test case. After review, the Council requested risk tables to be included in all full stock assessments in 2019. The SSC also requested a fourth category of concern to be added to the risk tables. The fishery performance category serves to represent any concerns related to the recommended ABC that can be inferred from commercial fisheries performance. Importantly, these concerns refer to indications of stock status, not economic performance.

In Briefs were started in 2018 for the Eastern Bering Sea, 2019 for the Gulf of Alaska, and 2020 for the Aleutian Islands. These more public-friendly succinct versions of the full ESRs have since been produced annually in tandem with the ESRs.

In 2019, risk tables were completed for all full assessments. Ecosystem scientists collaborated with stock assessment scientists to use the Ecosystem Status Reports to help inform the ecosystem concerns in the risk tables. Some ecosystem information can also be used to inform concerns related to the population dynamics of the stock. Initially, there were 4 levels of concern from no concern to extreme. In 2023 (and revised in 2024), based on a recommendation from the SSC, the levels of risk were reduced to 3: Level 1 (Normal), Level 2 (Increased concern), and Level 3 (Extreme concern). For stock assessments which include an Ecosystem and Socioeconomic Profile (ESP), the ESP is also used to inform the ecosystem risk column as well as the population dynamics and fisheries performance columns.

ESPs were initiated in 2017 (sablefish) and ESR editors began working closely with ESP teams in 2019 (starting with GOA walleye pollock). These complimentary annual status reports inform groundfish management and alignment in research that feeds these reports increases efficiency and collaboration between ecosystem and stock assessment scientists.

Full ESRs were not produced in 2025 due to the lapse in government appropriations that fall, though, an Abbreviated Gulf of Alaska ESR was published.

This report represents much of the first three steps in Alaska's IEA: defining ecosystem goals, developing indicators, and assessing the ecosystems (Figure 166). The primary stakeholders in this case are the North Pacific Fishery Management Council. Research and development of risk analyses and management strategies is ongoing and will be referenced or included as possible.

It was requested that contributors to the Ecosystem Status Reports provide actual time series data or make them available electronically. The Ecosystem Status Reports and data for many of the time series presented within are available online at: `https://alaskaesr.psmfc.org`. These reports and data are also available through the NOAA-wide IEA website at: `https://www.integratedecosystemassessment.noaa.gov/regions/alaska`.

Past reports and all groundfish stock assessments are available at: `https://www.fisheries.noaa.gov/alaska/population-assessments/north-pacific-groundfish-stock-assessments-and-fishery-evaluation`.



Figure 166: The IEA (integrated ecosystem assessment) process.

Responses to SSC Comments From December 2024

C1 BSAI and C2 GOA Ecosystem Status Reports[77]
General Comments Applicable to all three ESRs

The SSC thanks the authors for their responses to SSC comments, in particular the development of integrated metrics to track changes in ecosystem state, modeling approaches to help discern linkages among indices affecting individual species, and references to how conditions will affect different groundfish species depending on spawn timing, larval ecology, and varying responses to temperature changes. The SSC encourages continued efforts along these lines.

The ESR team appreciates this line of encouragement. Examples in the 2026 ESRs include updated Ecosystem State metrics in Ferriss, 2026 and updated DSEM analyses connecting ecosystem conditions to groundfish population dynamics (see pages 42 and 154).

The SSC looks forward to the continued consideration of socioeconomic metrics that could be included in ESRs.

The ESR team continues to engage with NOAA's Alaska Fisheries Science Center to advance the development of socioeconomic metrics that could be used in ESRs.

The SSC requests that for report cards, contributors not connect time series points in figures if there is a gap greater than the standard survey interval to avoid indicating a trend between missing years.

Starting in 2026, ESR Report Cards no longer connect timeseries points when there is a gap greater than the standard survey interval. ESR editors have also requested a similar approach from contributors and will continue to update figures in future ESR editions.

The SSC notes the value of continuing dynamic structural equation modeling (DSEM) modeling efforts, but recommends including the full model for comparison with the final most parsimonious model to clearly identify which hypothesized links were not supported by the data. The SSC appreciates the five-month lead climate forecasts.

The 2026 EBS ESR includes two applications of DSEM modeling: "Forage Fish Dynamics in the Eastern Bering Sea" (see p. 154) and "Eastern Bering Sea Walleye Pollock Early Survival Pathways" (see p. 42).

In 2026, the ESRs all include NMME five-month climate forecasts. The Gulf of Alaska and Aleutian Islands ESRs also include forecasts from MOM6 NEP10k.

The SSC appreciates the confirmation that satellite-derived chlorophyll-a metrics are routinely validated with in-situ measurements to ensure accuracy. To this end, the ESR authors noted inconsistencies in 2024 satellite-derived chlorophyll-a values and decided to postpone updating these contributions until 2025.

The 2026 ESRs include satellite-derived chlorophyll-a metrics based on OC-CCI, a merged product that combines information from Visible-Infrared Imaging Radiometer Suite (VIIRS), MODerate resolution Imaging Spectroradiometer (MODIS), Sea-viewing Wide Field-of-view Sensor (SeaWiFS), and the Ocean

[77] https://meetings.npfmc.org/CommentReview/DownloadFile?p=dc61bc73-be5c-492f-89b3-a723ea14311d.pdf&fileName=SSC%20Report%20Dec%202024_FINAL.pdf

and Land Color Instrument (OLCI), using 8-day composites at a 4 km x 4 km resolution. For more information, see p. 115.

BSAI Ecosystem Status Reports

Eastern Bering Sea

The SSC appreciates the addition of the NBS report card and highlights the important contrasts between the two regions throughout the report. There was no bottom trawl survey in the NBS this year, so apex predator and pelagic forager metrics were not available. However, portions of the SEBS bottom trawl do extend into the NBS, beyond latitude 60°N. The SSC recommends that contributors evaluate whether annual metrics for the NBS can be produced from sampling at these stations.

The EBS ESR editor conveyed this recommendation to AFSC's Groundfish Assessment Program. Below is their response:

"For the bottom trawl survey...we exclude strata 82 and 90 from...indicators because there aren't enough stations to produce reliable stratum-level indicators for those strata using design-based indices and specimen samples. I don't feel there are enough stations (or samples) north of 60°N to produce a separate time series for that area. The data issues become more problematic the further back in the survey time series we go because our sampling methods used to be less spatially balanced. However, dividing at 60°N would mean calculating indicators for areas that do not align with groundfish and crab strata. I think there would also be the matter of how to approach the calculations since we have 16 stations at approximately 60°N that can fall north or south of the line depending on the exact tow placement each year. More broadly, I'm wondering if stations just north of the line could be interpreted as indicative of the NBS - we just really don't get that far north of 60°N - especially at depths $<$70 m."

The SSC supports the continued application of DSEM to explore mechanisms driving changes in forage and juvenile groundfish populations as in this ESR and recruitment as explored in the GOA pollock assessment. The SSC recommends pollock as a focus of further exploration of DSEM for the EBS given the wealth of data for this species and as an attempt to understand the contrasting patterns of indicators. The SSC supports further investigation into why previous recruitment relationships for pollock in the EBS appear to have broken down.

The 2026 EBS ESR includes a DSEM modeling exploration for age-0 pollock: "Eastern Bering Sea Walleye Pollock Early Survival Pathways" (see p. 42).

The SSC also requests that the pollock cannibalism index include an extrapolation to quantify the biomass of pollock consumed by other pollock in order to better understand the effect of both rate and scale of predation.

The EBS ESR editor conveyed this recommendation to AFSC's Resource Ecology and Fishery Management Division. New indices of cannibalism are included in the "Bering Sea Multispecies Model (CNRG) Estimates of Time-Varying Natural Mortality" (see p. 219).

Responses to Crab Plan Team Comments from September 2025

September 2025 Crab Plan Team Report[78]
Ecosystem Status Report - EBS

There were no suggestions or recommendations from the Crab Plan Team.

Responses to Joint Groundfish Plan Team Comments from September 2025

September 2025 Joint Groundfish Plan Team Report[79]
ESR climate update
While the presentation was focused on climate and physical oceanography, there was much discussion on whether to expand on some of the hypothesized ecosystem impacts during the September report (such information is typically presented in November).

The Teams recommended that in future September reports, the ESR team continue working to link climate trends to ecosystem and groundfish community processes (e.g., recruitment, phenology across groups of species).

Responses to SSC Comments From October 2025

C3 BSAI Crab[80]
Ecosystem Status Report Preview
The SSC recommends the authors work with ESR contributors to evaluate composite metrics of physical and biological indices that provide leading indicators of overall conditions or potential change. The SSC further recommends authors articulate uncertainty in metrics to the extent possible and identify which products are validated versus which are under development, description of base models and skill, and clearly identify modeled products.

The ESR team continues to work with our contributors to develop and evaluate composite metrics and leading indicators of ecosystem conditions. Examples include the revised spatially resolved borealization index in the EBS ESR (see p. 64), and Ferriss, 2026 and Hennon and Danielson, 2026 in the Gulf of Alaska ESR. New this year for the Aleutian Islands is the contribution on summer groundfish diets which includes the total estimated daily consumption by prey type for indicator species Aydin and Ortiz (2026)

[78] https://meetings.npfmc.org/CommentReview/DownloadFile?p=3506263a-4da3-4d77-aafb-ffbc694b69ef.pdf&fileName=C3%20CPT%20Report.pdf

[79] https://meetings.npfmc.org/CommentReview/DownloadFile?p=1d6600e8-c5cb-48a3-9d13-e0a0a39217a8.pdf&fileName=C5a%20Joint%20GFPT%20Report.pdf

[80] https://meetings.npfmc.org/CommentReview/DownloadFile?p=bb3958b1-c8ca-42ab-9391-c5673c6e9872.pdf&fileName=SSC%20Report%20Oct%202025_FINAL.pdf

and an extended contribution for apex predators and pelagic foragers Ortiz et al. (2026). We will strive to improve communication of uncertainty and skill in these and future metrics.

Responses to Joint Groundfish Plan Team Comments from September 2026

September 2026 Joint Groundfish Plan Team Report[81]
ESR Climate Update
There were no suggestions or recommendations from the Crab Plan Team.

Responses to Crab Plan Team Comments from September 2026

BSAI Crab Plan Team Report[82]
EBS Ecosystem Status Report
A question was asked about whether hybrid consumption due to Pacific cod predation should be included in ESPs, but it was recommended that predation on hybrid crab remain in the Ecosystem Status Report presentation.

The October ESR presentation to the SSC will continue to include information on Pacific cod consumption of hybrid crabs.

Responses to SSC Comments From October 2026

C3 BSAI Crab[83]
Ecosystem Status Report Preview
The report, links, and summarized metrics were very helpful, and the SSC particularly appreciates the ongoing development of tailorable, regionally specific climate indices. The SSC hopes to see the extensions of similar tools for biological features.

The ESR editors will continue to work with contributors to develop tailorable, regionally specific indices.

[81] https://meetings.npfmc.org/CommentReview/DownloadFile?p=c82250d2-16bb-40d2-a404-8f420396055a.pdf&fileName=C3%20Joint%20Groundfish%20Plan%20Team%20Report.pdf

[82] https://meetings.npfmc.org/CommentReview/DownloadFile?p=45c09c86-69c3-4473-bf2d-2261a23ed8fa.pdf&fileName=Sept%202026%20CPT%20Report.pdf

[83] https://meetings.npfmc.org/CommentReview/DownloadFile?p=72476d9c-c900-4f64-8e25-bb9dc7842c26.pdf&fileName=SSC%20Report%20October%202026%20FINAL.pdf

Description of the SEBS Report Card Indicators

1. The North Pacific Index (NPI) winter average (Nov-Mar): The NPI index (Trenberth and Hurrell, 1994) was selected as one of the key indicators for characterizing the large-scale atmospheric circulation variability over the North Pacific and plays an important role in regulating climate conditions of the Bering Sea. The NPI is a measure of the strength of the Aleutian Low, specifically the area-weighted sea level pressure (SLP) for the region of 30°N to 65°N, 160°E to 140°W. Above (below) average winter (November-March) NPI values imply a weak (strong) Aleutian Low and generally calmer (stormier) conditions.

The advantages of the NPI include its systematic relationship to the primary causes of climate variability in the Northern Hemisphere, especially the El Niño-Southern Oscillation (ENSO) phenomenon, and to a lesser extent the Arctic Oscillation (AO). It may also respond to North Pacific SST and high-latitude snow and ice cover anomalies, but it is difficult to separate cause and effect.

The NPI also has some drawbacks: (1) it is relevant mostly to the atmospheric forcing in winter, (2) it relates mainly to the strength of the Aleutian Low rather than its position, which has also been shown to be important to the seasonal weather of the Bering Sea (Rodionov et al., 2007; see Figure 26), and (3) it is more appropriate for the North Pacific basin as a whole than for a specific region (i.e., Bering Sea shelf).

Implications: For the Bering Sea, the strength of the Aleutian Low relates to wintertime temperatures, with a deeper low (negative SLP anomalies) associated with a greater preponderance of maritime air masses and hence warmer conditions.

Contact: Muyin Wang
Muyin.Wang@noaa.gov

2. Borealization index: To evaluate the spatiotemporal progression of borealization, a Spatial Dynamic Factor Analysis (SDFA) was used to estimate a single shared spatial latent factor across seven environmental variables from 1958 through 2026. Negative factor loadings correspond to Arctic-like conditions (e.g., increased sea ice cover), while positive loadings indicate boreal conditions (e.g., elevated temperatures). Regional trends were summarized by calculating the annual median index across the Bering Sea and other sub-regions of interest including the SEBS. *Implications:* This index tracks the broad ecosystem reorganization from an Arctic physical state supporting a cold-adapted assemblage to a subarctic (boreal) state supporting a warm-adapted assemblage. Upgrading from a domain-aggregated DFA to an SDFA resolves spatial heterogeneity across the shelf, enabling the identification of localized borealization hotspots, sub-regional boundaries, and persistent Arctic refugia previously masked by spatial averaging. Following a peak during the 2018-2019 marine heatwave, SEBS index values have trended back toward the 69-year long-term average and sit slightly below average in 2026.

Contact: Kaitlyn O'Brien
kaobrien4@alaska.edu

3. Bering Sea ice extent: Annual sea ice extent for the southeastern Bering Sea was calculated using National Snow and Ice Data Center (NSIDC) daily sea ice concentration data at a 25 km resolution with a 0.15 concentration threshold. Monthly sea ice extent values were first computed from the daily data for each region, defined by marine ecosystem management boundaries, and then averaged to obtain the annual sea ice extent. The Python code used to compute the extent is available at `https://psmfc-fin.github.io/alaska-seaice/`. *Implications:* Seasonal sea-ice coverage impacts, for example, the extent of the cold pool, bloom strength and timing, and bottom-up productivity

Contact: Sunny Bak-Hospital
sun.bak-hospital@noaa.gov

4. Cold pool extent: Area of the cold pool in the eastern Bering Sea (EBS) shelf bottom trawl survey area (including strata 82 and 90) from 1982-2026. The cold pool is defined as the area of the EBS continental shelf with bottom temperature <2°C, in square kilometers (km^2). *Implications:* The cold pool has a strong influence on the thermal stratification and influences the spatial structure of the demersal community (Spencer, 2008; Kotwicki and Lauth, 2013; Thorson et al., 2020), trophic structure of the eastern Bering Sea food web (Mueter and Litzow, 2008; Spencer et al., 2016), and demographic processes of fish populations (Grüss et al., 2021).

Contact: Sean Rohan and Lewis Barnett
Sean.Rohan@noaa.gov and Lewis.Barnett@noaa.gov

5. Proportion of open water blooms: The timing of ice retreat[84] and bloom peak was used to estimate bloom type over the southeastern Bering Sea shelf (<60°N). Bloom type differentiates between open-water blooms (i.e., ice retreat occurred $\geq$21 days prior to bloom peak) and ice-associated blooms (i.e., ice retreat occurred $<$21 days prior to bloom peak) for each year (Perrette et al., 2011). Timing of sea-ice retreat was determined as the date when ice coverage remained below 15% based on the 15-day running mean of the daily sea-ice fraction data. Bloom peak timing was estimated using standardized merged ocean color satellite data of 8-day satellite chlorophyll-a (chl-a, μg/L) at a 4 km-resolution from The Hermes GlobColour website[85] covering the years 1998-2024. *Implications:* Bloom type provides a metric of the bloom dynamics related to sea ice; increased ice-associated blooms tend to correlate positively with higher abundances of large zooplankton and have been suggested to favor pollock recruitment (Hunt et al., 2011).

Contact: Matt Callahan
Matt.Callahan@noaa.gov

[84] `https://coastwatch.pfeg.noaa.gov/erddap/griddap/NOAA_DHW.html`
[85] `http://hermes.acri.fr/`, Maritorena et al., 2010

6. Large copepod abundance: Large copepods (predominantly *Calanus* spp.) are quantified from 505 μm mesh, 60 cm bongo net samples taken during the fall (Aug/Sept) 70 m isobath survey over the southeastern Bering Sea shelf. Detailed information on sampled taxa is provided after in-lab processing protocols have been conducted (1 year post survey). The current year value is an estimate of relative abundance derived from an at-sea Rapid Zooplankton Assessment (RZA). RZA abundance estimates may not closely match historical estimates of abundance as methods differ between laboratory processing and ship-board RZA. *Implications:* Large copepods are an important prey and trophic link between primary production and fish, marine mammals, and seabirds.

Contact: David Kimmel
David.Kimmel@noaa.gov

7. Euphausiid biomass: In the absence of direct measurements of secondary production in the eastern Bering Sea, we rely on estimates of biomass. We use an estimate of euphausiid biomass as determined by acoustic backscatter and midwater trawl data collected during biennial pollock surveys. Since the previous update to this index, euphausiid backscatter observations from the 2020 acoustic-only Saildrone uncrewed surface vehicle survey as well as the 2024 acoustic-trawl survey of pollock were added to the time series. *Implications:* The data presented here suggest that euphausiid prey availability increased in 2026, though remained below the timeseries mean. Euphausiids form a key, large group of macrozooplankton that function as intermediaries in the trophic transfer from primary production to living marine resources (commercial fisheries and protected species). Understanding the mechanisms that control secondary production is an obvious goal toward building better ecosystem syntheses.

Contact: Mike Levine
Mike.Levine@noaa.gov

8. Pelagic forage fish biomass: This index represents the relative biomass of small fishes captured in the BASIS surface trawl (upper 25 m) survey in the southeastern Bering Sea during late summer. Primary fish caught and included in the forage fish species aggregate are age-0 pollock, age-0 Pacific cod, capelin, Pacific herring, juvenile Chinook, sockeye, chum, pink, and coho salmon, rainbow smelt, and saffron cod. *Implications:* When this index is higher (lower), it indicates there may be more (less) food available to upper trophic predators (e.g., fish, seabirds, and mammals).

Contact: Lia Domke
Lia.Domke@noaa.gov

9., 10., 11., 12. Description of the fish and invertebrate guilds: We present four guilds to indicate the status and trends for fish and invertebrates in the eastern Bering Sea: motile epifauna, benthic foragers, pelagic foragers, and apex predators. Each is described in detail below. The full guild analysis involved aggregating all eastern Bering Sea species included in a food web model (Aydin and Mueter, 2007) into 18 guilds by trophic role, habitat, and physiological status (Table 14). For the four guilds included here, time trends of biomass are presented for 1982-2024. Foraging guild biomass is based on catch data from the NMFS-AFSC annual summer bottom trawl survey of the EBS shelf ($<$200 m), modified by an Ecopath-estimated catchability coefficient that takes into account the minimum biomass required to support predator consumption (see Appendix 1 in (Boldt, 2007) for complete details). This survey index is specific to the standard bottom trawl survey area in the southeastern Bering Sea (does

not include strata 82 and 90) and does not include the northern Bering Sea. The foraging guild biomass is weighted by strata area (km^2) which has resulted in a minor shift in the biomass values from reporting in previous years but the trends and patterns remain the same. Also, we no longer include species that lack time series and were previously represented by a constant biomass equal to the mid-1990s mass balance level estimated in (Aydin and Mueter, 2007).

Contact: Kerim Aydin or George A. Whitehouse
Kerim.Aydin@noaa.gov or Andy.Whitehouse@noaa.gov

Table 14: Composition of foraging guilds in the eastern Bering Sea.

Motile Epifauna	Benthic Foragers	Pelagic Foragers	Apex Predators
Eelpouts	Yellowfin sole	W. pollock	P. cod
Octopuses	Flathead sole	P. herring	Arrowtooth
Tanner crab	N. rock sole	Atka mackerel	Kamchatka fl.
King crab	Alaska plaice	Misc. fish shallow	Greenland turbot
Snow crab	Dover sole	Salmon returning	P. halibut
Sea stars	Rex sole	Capelin	Alaska skate
Brittle stars	Misc. flatfish	Eulachon	Other skates
Other echinoderms	Greenlings	Sandlance	Sablefish
Snails	Other sculpins	Other pelagic smelts	Large sculpins
Hermit crabs		Other managed forage	
Misc. crabs		Scyphozoid jellies	

9. Motile epifauna (fish and benthic invertebrates): This guild includes both commercial and non-commercial crabs, sea stars, snails, octopuses, other mobile benthic invertebrates, and eelpouts. There are ten commercial crab stocks in the current Fishery Management Plan for Bering Sea/Aleutian Islands King and Tanner Crabs; we include seven on the eastern Bering Sea shelf: two red king crab *Paralithodes camtschaticus* (Bristol Bay, Pribilof Islands), two blue king crab *P. platypus* (Pribilof District and St. Matthew Island), one golden king crab *Lithodes aequispinus* (Pribilof Islands), and two Tanner crab stocks (southern Tanner crab *Chionoecetes bairdi* and snow crab *C. opilio*). The three dominant species comprising the eelpout group are marbled eelpout (*Lycodes raridens*), wattled eelpout (*L. palearis*), and shortfin eelpout (*L. brevipes*). The composition of seastars in shelf trawl catches is dominated by the purple-orange seastar (*Asterias amurensis*), which is found primarily in the inner/middle shelf regions, and the common mud star (*Ctenodiscus crispatus*), which is primarily an inhabitant of the outer shelf. *Implications:* Trends in the biomass of motile epifauna indicate benthic productivity and/or predation pressure, although individual species and/or taxa may reflect shorter or longer time scales of integrated impacts of bottom-up or top-down control.

10. Benthic foragers (fish only): The species which comprise the benthic foragers group are the Bering Sea shelf flatfish species, greenlings, and small sculpins. *Implications:* Trends in the biomass of benthic foragers indirectly indicate availability of infauna (i.e., prey of these species).

11. Pelagic foragers (fish and Scyphozoid jellies only): This guild includes adult and juvenile walleye pollock (*Gadus chalcogrammus*), other forage fish such as Pacific herring (*Clupea pallasi*), capelin (*Mallotus villosus*), eulachon (*Thaleichthys pacificus*), and sandlance, salmon, Atka mackerel (*Pleurogrammus monopterygius*), and scyphozoid jellies. *Implications:* Trends in the biomass of pelagic foragers largely track walleye pollock which is an important component of the Bering Sea ecosystem, both as forage and as a predator.

12. Apex predators (shelf fish only): This guild includes Pacific cod (*Gadus macrocephalus*), arrowtooth flounder, Kamchatka flounder (*Atheresthes evermanni*), Pacific halibut (*Hippoglossus stenolepis*), Greenland turbot (*Reinhardtius hippoglossoides*), sablefish (*Anoplopoma fimbria*), Alaska skate, and large sculpins. *Implications:* Trends in the biomass of apex predators indicate relative predation pressure on zooplankton and juvenile fishes within the ecosystem.

13. Multivariate seabird breeding index: This index represents the dominant trend among 17 reproductive seabird data sets from the Pribilof Islands that include diving and surface-foraging seabirds. The trend of the leading principal component (PC1) explains 49% of the variance among the data sets and represents all seabird hatch timing and the reproductive success of murres and cormorants, defined as loadings $>|0.2|$. *Implications:* Above-average index values reflect high reproductive success and/or early breeding (assumed to be mediated through food supply) and indicate better than average recruitment of year classes that seabirds feed on (e.g., age-0 pollock), or better than average supply of forage fish that commercially-fished species feed on (e.g.,capelin eaten by both seabirds and Pacific cod).

Contact: Stephani Zador
Stephani.Zador@noaa.gov

Description of the NBS Report Card Indicators

1. The North Pacific Index (NPI) winter average (Nov-Mar): Please see 'Description of the SEBS Report Card indicators' (p. 320).

Contact: Muyin Wang
Muyin.Wang@noaa.gov

2. Borealization index: Please see 'Description of the SEBS Report Card indicators' (p. 320).

Contact: Kaitlyn O'Brien
kaobrien4@alaska.edu

3. Bering Sea ice extent: Annual sea ice extent for the northern Bering Sea was calculated using NSIDC daily sea ice concentration data. Please see 'Description of the SEBS Report Card indicators' (p. 320) for more information.

Contact: Sunny Bak-Hospital
sun.bak-hospital@noaa.gov

4. Proportion of open water blooms: The timing of ice retreat[86] and bloom peak was used to estimate bloom type over the northern Bering Sea shelf (>60°N). Please see 'Description of the SEBS Report Card indicators' (p. 320) for more information.

Contact: Matt Callahan
Matt.Callahan@noaa.gov

5. Large copepod abundance: Large copepods (predominantly *Calanus* spp.) are quantified from 505 μm mesh, 60 cm bongo net samples taken during the fall (Aug/Sept) surface trawl survey over the northern Bering Sea shelf. Please see 'Description of the SEBS Report Card indicators' (p. 320) for more information.

Contact: David Kimmel
David.Kimmel@noaa.gov

6. Pelagic forage fish biomass: This index represents the relative biomass of small fishes captured in the surface trawl (upper 25 m) survey in the northern Bering Sea during late summer. Please see 'Description of the SEBS Report Card indicators' (p. 320) for more information.

Contact: Lia Domke
Lia.Domke@noaa.gov

[86] `https://coastwatch.pfeg.noaa.gov/erddap/griddap/NOAA_DHW.html`

7. Juvenile snow crab: The estimated biomass (metric tons) of juvenile snow crab sampled during the northern Bering Sea bottom trawl survey (strata 70, 71, and 81) in 2010, 2017-2019, 2021-2023, and 2025. *Implications:* Trends in the biomass of juvenile snow crab, an important component of the benthic community, reflect broad scale benthic production and indicate the strength of crab recruitment as these crabs mature and likely move south into the eastern Bering Sea.

Contact: Shannon Hennessey
shannon.hennessey@noaa.gov

8. Yellowfin sole: The estimated biomass index (metric tons) of yellowfin sole sampled during the northern Bering Sea bottom trawl survey (strata 70, 71, and 81) in 2010, 2017, 2019, 2021-2023, and 2025. *Implications:* Trends in the biomass of yellowfin sole indicate relative predation pressure on small infaunal prey (e.g., polychaete worms, bivalves, small crustaceans).

Contact: Sean Rohan
sean.rohan@noaa.gov

9. Walleye pollock: The estimated biomass index (metric tons) of walleye pollock sampled during the northern Bering Sea bottom trawl survey (strata 70, 71, and 81) in 2010, 2017, 2019, 2021-2023, and 2025. *Implications:* Trends in the biomass of walleye pollock indirectly indicate relative predation pressure on zooplankton and forage fish.

Contact: Sean Rohan
sean.rohan@noaa.gov

10. Pacific cod: The estimated biomass index (metric tons) of Pacific cod sampled during the northern Bering Sea bottom trawl survey (strata 70, 71, and 81) in 2010, 2017, 2019, 2021-2023, and 2025. *Implications:* Trends in the biomass of Pacific cod, a generalist apex predator, indicate relative predation pressure on forage fish and crab within the ecosystem.

Contact: Sean Rohan
sean.rohan@noaa.gov

Methods Description for the Report Card Plots

For each plot, the mean (dashed line) and ±1 standard deviation (SD; solid lines) are shown as calculated for the entire time series. Time periods for which the time series was outside of this ±1 SD range are shown in orange (for high values) and blue (for low values).

The shaded blue window shows the most recent 5 years prior to the date of the current report. The symbols on the right side of the graph are all calculated from data inside this 5-year moving window (maximum of 5 data points). The first symbol represents the "2022-2026 Mean" as follows: '+ or -' if the recent mean is outside of the ±1 SD long-term range, '.' if the recent mean is within this long-term range, or 'x' if there are fewer than 2 data points in the moving window. The symbol choice does not take into account statistical significance of the difference between the recent mean and long-term range. The second symbol represents the "2022-2026 Trend" as follows: if the magnitude of the linear slope of the recent trend is greater than 1 SD/time window (a linear trend of >1 SD in 5 years), then a directional arrow is shown in the direction of the trend (up or down), if the change is <1 SD in 5 years, then a double horizontal arrow is shown, or 'x' if there are fewer than 3 data points in the moving window. Again, the statistical significance of the recent trend is not taken into account in the plotting.

The intention of the figure is to flag ecosystem features and the magnitude of fluctuations within a generalized "fisheries management" time frame (i.e., trends that, if continued linearly, would go from the mean to ±1 SD from the mean within 5 years or less) for further consideration, rather than serving as a full statistical analysis of recent patterns.